



Oncolytic Adenoviral Therapy for the Treatment of Multiple Myeloma

A thesis submitted in fulfilment of the requirements for the degree of Doctor
of Philosophy



By

Georgia Rose Stewart

September 2021

Department of Oncology and Human Metabolism

Faculty of Medicine, Dentistry and Health

The University of Sheffield

'Life's swinging hard, but I'm swinger harder...♪'

Table of Contents

Table of Contents	2
Abbreviations	7
Declaration.....	11
Acknowledgements.....	12
Reviews Submitted	14
Manuscripts in Preparation	14
Conference Papers.....	15
Awards	16
List of Tables	17
List of Figures	18
Abstract.....	22
Chapter 1 : Introduction	23
1.1 Multiple myeloma	24
1.1.1 Clinical Manifestations.....	25
1.1.2 Mutations Associated with Multiple Myeloma	27
1.1.3 Treatment of Multiple Myeloma	31
1.2 Oncolytic Virotherapy	33
1.2.1 Classes of Oncolytic Viruses	37
1.2.2 Clinical Experience and Safety of Oncolytic Viruses	40
1.3 Oncolytic Virotherapy in Multiple Myeloma	42
1.3.1 Preclinical Studies with Vaccinia Virus in Multiple Myeloma	43
1.3.2 Preclinical studies with Myxoma Virus in Multiple Myeloma.....	44
1.3.3 Preclinical Studies with Reovirus in Multiple Myeloma.....	45
1.3.4 Preclinical Studies with Measles Virus in Multiple Myeloma	46
1.3.5 Preclinical Studies with Vesicular Stomatitis Virus in Multiple Myeloma.....	47
1.3.6 Clinical Trials with Oncolytic Viruses in Multiple Myeloma	48
1.4 Adenovirus	50
1.4.1 History.....	50
1.4.2 Adenovirus Life Cycle	52
1.4.3. Oncolytic Adenoviruses as Therapeutic Tools	58
1.4.4 Oncolytic Adenoviruses and Multiple Myeloma.....	63
1.4.5 Targeting Multiple Myeloma with a Selective Adenovirus.....	66
1.5 The Future of Oncolytic Virotherapy for Multiple Myeloma	72
1.6 Oncolytic viruses in combination with MM standard of care.....	75

1.6.1 Bortezomib and Proteasome Inhibitors.....	75
1.6.2 Melphalan and Alkylating Agents	81
1.6.3 Panobinostat and HDACIs	87
1.6.4 IMiDs	92
1.6.5 Summary	93
1.7 Conclusion.....	94
1.8 Hypothesis and Aims.....	95
Chapter 2 : Materials and Methods.....	96
2.1 General Cell Culture Methods.....	97
2.1.1 Cell Lines	98
2.1.2 Cell Counting and Maintaining Cell Stocks.....	101
2.1.3 Primary Cells and Culture Techniques	103
2.2 Adenoviruses.....	106
2.2.1 Recombinant Adenoviruses	106
2.2.2 Adenoviral Amplification, Purification, and Quantification.....	108
2.3 Cell Biology.....	112
2.3.1 Adenoviral Infection and Replication.....	112
2.3.2 Viability, Cytotoxicity, Proliferation and Apoptosis	114
2.3.3 Cell Labelling	123
2.3.4 Flow Cytometry.....	123
2.3.5 Fluorescent Microscopy.....	130
2.4 Molecular Biology	130
2.4.1 RNA Extraction	130
2.4.2 Reverse Transcription	131
2.4.3 Real Time PCR	133
2.5 Developing Dormancy/MRD Models of Multiple Myeloma <i>in vitro</i>	136
2.5.4 Assessment of PolyHIPE Scaffolds for Ad[CE1A] Treatment.	138
2.6 Animals.....	139
2.6.1 Animal Models	139
2.6.2 <i>In vivo</i> Imaging of Tumour	143
2.6.3 Primary Animal Cells and Tissues <i>ex vivo</i>	144
2.7 Histology	145
2.7.1 Preparation of Soft Tissue and Bones.....	145
2.7.2 Immunohistochemistry Staining.....	146
2.8 Bone Parameter Analysis	150
2.8.1 <i>Ex vivo</i> Micro-computed Tomography.....	150

2.9 Proteome Profiler Mouse Cytokine array	151
2.10 Statistics	151
Chapter 3 : Efficacy and Cell Death Mechanisms of Ad[CE1A] in Human Multiple Myeloma	153
3.1 Introduction	154
3.1.1 Adenovirus in Multiple Myeloma.....	154
3.1.2 Hypothesis, Aims and Objectives	157
3.2 Results	158
3.2.1 Human Myeloma Cell Lines Express Primary and Secondary Adenovirus Entry Receptors	158
3.2.2 Human Myeloma Cell Lines have Increased CS1 Expression Compared to Non-myeloma cells	160
3.2.3 Human Myeloma Cell Lines have High Adenovirus Infection Efficiency.....	163
3.2.4 Ad[CE1A] Replicates in Human Myeloma Cell Lines	166
3.2.4 Ad[CE1A] Causes Oncolysis in Human Myeloma Cell Lines.	168
3.2.5 Ad[CE1A] Oncolysis in Myeloma Cell Lines when Cocultured with BMSC.....	173
3.2.6 Patient-derived Primary Multiple Myeloma Cells Highly Express Primary and Secondary Adenovirus Receptors	175
3.2.7 Patient-derived Primary Multiple Myeloma Cells Highly Express CS1 Compared to Healthy Donor Plasma Cells and BMMC <i>Ex vivo</i>	176
3.2.8 Oncolysis of Ad[CE1A] in Patient-derived Primary Multiple Myeloma Cells <i>ex vivo</i>	178
3.2.9 Adenovirus Infection in Patient-derived Primary MM Cells and Healthy Donor CD138 ⁺ BMMCs.....	180
3.2.10 The Involvement of Apoptosis in Ad[CE1A] Cytotoxicity	182
3.2.11 The Involvement Necroptosis in Ad[CE1A] Cytotoxicity	186
3.2.12 The Expression of Immunogenic Cell Death Markers following Ad[CE1A] Treatment. ...	193
3.3 Discussion.....	202
3.4 Chapter conclusion	213
Chapter 4 : Ad[CE1A] Treatment to Target Minimal Residual Disease and Prevent Relapse	215
4.1 Introduction	216
4.1.1 Hypothesis, Aims and Objectives	217
4.2 Results	218
4.2.1 Ad[CE1A] Prevents Myeloma Cell Regrowth after Bortezomib Treatment.	218
4.2.2 Ad[CE1A] Causes Oncolysis of Bortezomib Insensitive Cells.	220
4.2.3 Efficacy of Ad[CE1A] Against MRD/relapse in the <i>in vivo</i> Low Tumour Burden Model. ...	222
4.2.4 Developing <i>in vitro</i> Models of MRD/dormancy	225

4.3 Discussion.....	235
4.4 Chapter Conclusion	241
Chapter 5 : The Efficacy of Ad[CE1A] in 5TGM1 Murine Myeloma.....	242
5.1 Introduction	243
5.1.1 Adenovirus Serotype 5 in Murine Cells.....	243
5.1.2 Hypothesis, Aims and Objectives.....	245
5.2 Results.....	246
5.2.1 The 5TGM1 Murine Myeloma Cell Line Expresses CS1.....	246
5.2.2 The 5TGM1 Murine Myeloma Cell Line has High Adenovirus Infection Efficiency.....	246
5.2.3 Ad[CE1A] Replicates in the 5TGM1 Murine Myeloma Cell Line.	248
5.2.4 Ad[CE1A] Causes Oncolysis in the 5TGM1 Murine Myeloma Cell Lines.	249
5.2.5 The Involvement of Apoptosis in Ad[CE1A]-induced Cytotoxicity in the 5TGM1 Cell Line.....	250
5.2.6 The Involvement Necroptosis in Ad[CE1A] Cytotoxicity in 5TGM1 Cell Line.....	252
5.2.7 The Expression of Immunogenic Cell Death Markers in Ad[CE1A] Infection.....	254
5.2.8 Efficacy of Ad[CE1A] against 5TGM1 in a Syngeneic Model.	256
5.3 Discussion.....	266
5.4 Chapter Conclusion	271
Chapter 6 : Preclinical Investigation of Ad[CE1A] in Combination with Anti-myeloma Therapies	272
6.1 Introduction	273
6.1.1 Adenovirus in combination in Multiple Myeloma	273
6.1.7 Hypothesis, Aims and Objectives.....	275
6.2 Results.....	276
6.2.1 Dose Response to Ad[CE1A] and Anti-myeloma Chemotherapies.	276
6.2.2 Augmenting Ad[CE1A] Suppression of MPC Line Viability with Anti-Myeloma Chemotherapies.....	278
6.2.3 Augmenting Ad[CE1A]-induced MPC Cytotoxicity with Anti-myeloma Chemotherapies .	289
6.2.4 Mechanisms of Synergy	293
6.2.4.4 Augmenting Ad[CE1A] E1A Expression after Anti-Myeloma Chemotherapies	303
6.2.4.5 Augmenting Ad[CE1A] Viral Progeny Production after Anti-myeloma Chemotherapies .	305
6.2.5.6 Augmenting ICD following Ad[CE1A] in Combination with Anti-myeloma Therapies.....	308
6.3 Discussion	312
6.4 Chapter Conclusion	335
Chapter 7 : Final Conclusions and Future Directions	336
7.1 Final Conclusions.....	337
7.2 Future directions.....	339

7.3 Overall Conclusion	341
Chapter 8 : Appendices	342
References	371

Abbreviations

Ad	Adenovirus
Ad5	Adenovirus Serotype 5
ADP	Adenovirus Death Protein
AE	Adverse Event
APC	Antigen Presenting Cell
ASCT	Autologous Stem Cell Transplant
BLIMP-1	B Lymphocyte-Induced Maturation Protein 1
BM	Bone Marrow
BMMC	Bone Marrow Mononuclear Cell
BMSC	Bone Marrow Stromal Cell
BTZ	Bortezomib
CALR	Calreticulin
CAR	Coxsackie Adenovirus Receptor
CAR-T	Chimeric Antigen Receptor T
CI	Combination Index
CM	Conditioned Media
CPA	Cyclophosphamide
CRAD	Conditionally Replicating Adenovirus
CS1	CD-Subset-1
DAMP	Danger Associated Molecular Pattern
DC	Dendritic Cell
DMSO	Dimethylsulfoxide
EAT-2	Ewing's Sarcoma-Associated Transcript 2
FBS	Foetal Bovine Serum
FGF3	Fibroblast Growth Factor 3
GM-CSF	Granulocyte-Macrophage Colony-Stimulating Factor
HD	Healthy Donor
HDACI	Histone Deacetylase Inhibitor
HMGB1	High Mobility Group Box 1

HPC	Hematopoietic Progenitor Cell
HSP	Heat Shock Protein
HSP70	Heat Shock Protein 70
HSP90	Heat Shock Protein 90
HSPG	Heparin Sulphate Proteoglycan
HSV-1	Herpes Simplex Virus Type-1
hTERT	Human Telomerase Reverse Transcriptase
I.P	Intraperitoneal
I.V	Intravenous
IFM	Intergroupe Francophone du Myelome.
IFN	Interferon
Ig	Immunoglobulin
IGH	Immunoglobulin Heavy-Chain
IHC	Immunohistochemistry
IKZF	Ikaros Family
IKZF1	Ikaros
IKZF3	Aiolos
IMiD	Immunomodulatory Drug
IMWG	International Myeloma Working Group
JAM-1	Junctional Adhesion Molecule 1
Len	Lenalidomide
LOAd	Lokon Oncolytic Adenovirus
Luc	Luciferase
mAb	Monoclonal Antibody
MAC	Magnetic Activated Cell Sorting
MAPK	Mitogen-Activated Protein Kinase
MDSC	Myeloid-Derived Suppressor Cell
Melph	Melphalan
MFI	Mean Fluorescent Intensity
MGUS	Monoclonal Gammopathy of Undetermined Significance
MLKL	Mixed Lineage Kinase Domain-Like

MLP	Major Late Promoter
MM	Multiple Myeloma
MMSET	Multiple Myeloma SET domain
MPC	Myeloma Plasma Cell
MRD	Minimal Residual Disease
mSMART	Stratification for Myeloma and Risk-Adapted Therapy.
MTD	Maximum Tolerated Dose
MV	Measles Virus
MYXV	Myxoma Virus
NDV	Newcastle Disease Virus
Nec-1	Necrostatin-1
NF-κB	Nuclear Factor Kappa B
NIS	Sodium Iodide Symporter
NK	Natural Killer
NSA	Necrosulfonamide
OB	Osteoblast
OC	Osteoclast
OV	Oncolytic Virus
Pan	Panobinostat
PBMC	Peripheral Blood Mononuclear Cell
PCL	Plasma Cell Leukaemia
PD-1	Programmed Cell Death Protein-1
PD-L1	Programmed Death-Ligand 1
PI	Propidium Iodide
PKR	Protein Kinase R
Pom	Pomalidomide
pRb	Retinoblastoma Protein
PRDM1	Positive Regulatory Domain Zinc Finger Protein 1
PS	Phosphatidylserine
RANKL	Receptor Activator of Nuclear Factor Kappa-B Ligand
RIPK1	Receptor-Interacting Serine/Threonine-Protein Kinase 1

RIPK3	Receptor-Interacting Serine/Threonine-Protein Kinase 3
ROS	Reactive Oxygen Species
RV	Reovirus
SLAM	Signalling Lymphocytic Activation Molecule
SLAMF7	Signalling Lymphocytic Activation Molecule F7
SMaRT	Sheffield Myeloma Research Team
SMM	Smouldering Myeloma
STR	Short Tandem Repeat
TAA	Tumour-Associated Antigen
TAM	Tumour-Associated Macrophages
TK	Thymidine Kinase
TMZ	Temozolomide
TP53	Tumour Protein P53
T-reg	T-Regulatory Cell
VSV	Vesicular Stomatitis Virus
VV	Vaccinia Virus
WT	Wild Type

Declaration

I confirm that I shall abide by the University of Sheffield's regulations on plagiarism and that all written work shall be my own and will not have been plagiarised from other paper-based or electronic sources.

Where used, material gathered from other sources will be clearly cited in the text.

Acknowledgements

Firstly, I would like to thank Dr Andrew Chantry and Dr Michelle Lawson who have been my primary supervisors during my PhD project for their continued support. I would like to thank them for allowing me to be part of the Sheffield Myeloma Research Team in the first instance, by allowing me to undertake my one-year research placement as part of my undergraduate degree, and then accepting me as a PhD candidate to pursue this research project and be involved in multiple research projects within the group. I would like to thank Dr Michelle Lawson for 'adopting' me as her PhD student after Dr Andrew Chantry pursued clinical work full time. I would also like to thank Dr Andrew Chantry for continuing to have input in my PhD project whilst working for the NHS full time. I would like to express my gratitude for allowing me to travel with my research (San Diego was the highlight of my PhD!), support me to write grants, contribute to charity lab tours and events and just as importantly, all the afterwork pub sessions that always resulted in Andy talking about his missed opportunity at being a rock star.

I would like to express my utmost gratitude to Sheffield Hospitals Charity for funding this project, which was crowd funded, such an amazing achievement. I also must thank Sheffield Hospitals Charity further for funding my project for another year following the delays due to the COVID-19 pandemic.

I would like to express my gratitude to my co-supervisor Dr Munitta Muthana, for her in-depth knowledge of oncolytic viruses and cancer research, for her help and continued support throughout my PhD. I want to thank Darren Lath and Jenifer Down for their technical help with patient samples and *in vivo* methodology and their general uplifting chitchats. I would also like to thank Sue Clarke and the flow cytometry team for their technical help with the machines. I would like to thank all the undergraduate and masters' students I have helped supervise for helping me learn to be a better teacher.

I would like to thank all the patients and donors who have given their time for the samples used in this work, in the hope that we will help others with multiple myeloma.

Lastly, I would like to thank my parents, who are so proud of their northern working class, Sheffield born-and-bred daughter, that has managed to peruse an education in their lifelong passion they could only dream of whilst growing up. Last of all, I would like to thank my partner Omari, for picking me up when times got tough and always being the calm to my storm.

Reviews Submitted

Georgia Stewart, Andrew D. Chantry and Michelle A. Lawson (2021). The Use of Oncolytic Viruses in the Treatment of Myeloma. *Cancers* **13**(22). doi: 10.3390/cancers13225687.

Manuscripts in Preparation

Georgia Stewart, Simon Tazzyman, Darren Lath, Jenny Down, Michelle A. Lawson, Munitta Muthana, Andrew. D. Chantry. Anti-myeloma effect of conditionally replicating oncolytic Adenovirus utilizing CS1-promoter alone and in combination with myeloma standard of care.

Conference Papers

Oral

- 'The use of oncolytic virus therapy for myeloma shows considerable promise in pre-clinical models' UK myeloma forum scientific workshop on immunotherapy and myeloma microenvironment 2018, London, UK.

Poster

- Molecular pharmacology and cancer and bone society 2018, Oxford, UK.
- 60th American society of haematology conference 2018, San Diego, USA. Abstract publication: Georgia Stewart *et al.* (2018) Myeloma-specific oncolytic adenovirus induces significant tumour oncolysis *in vitro* and *in vivo* and prevents cell line regrowth, *Blood*. **132**(S1)
- 59th British society of haematology annual scientific meeting 2019, Glasgow, UK. Abstract publication. Georgia Stewart *et al.* (2018) Myeloma-specific oncolytic adenovirus induces significant tumour oncolysis *in vitro* and *in vivo* and prevents cell line regrowth, *British Journal of Haematology*. **185**(S1).
- Poster and snap poster presentation at the European Society of Calcified tissue society congress, 2019, Budapest, Hungary.

Awards

Learned society fund travel scholarship

2018

Travel scholarship fund from the University of Sheffield for researchers presenting at national or international conferences, £650.

British Society of Haematology Scientific Meeting Abstract award

2019

Travel scholarship offered to presenters of high-scoring abstracts to facilitate attendance to the conference, £500.

List of Tables

Table 1.1: International staging system for myeloma	26
Table 1.2: IMWG Myeloma diagnostic Criteria (adapted from IMWG)	26
Table 1.3: Prognosis for each cytogenetic abnormality according to the risk stratification models for MM (25).	27
Table 1.4: MM genetic abnormalities with genetic alterations and related prognosis (26).	28
Table 1.5: Comparison of Oncolytic Viruses (Table adapted with permission from 63).....	38
Table 1.6: Severe Adverse Events reported with OVs.....	41
Table 1.7: Oncolytic viruses used preclinically for myeloma treatment	43
Table 1.8: Subgroups of Human adenovirus (Table reproduced with permission from 163).....	50
Table 1.9: Ad5 proteins and their function	54
Table 1.10: Oncolytic adenoviruses in clinical trials (Table reproduced with permission from 256). 62	
Table 1.11: Combining OVs with proteasome inhibitors (469).....	77
Table 1.12: Combining OVs with alkylating agents (469)	82
Table 1.13: Combining OVs with HDACI	88
Table 2.1: Reagents required for tissue culture	97
Table 2.2: Medium required for tissue culture	98
Table 2.3 Buffers required for tissue culture	98
Table 2.4: MPC lines origin and characteristics (331,332).	99
Table 2.5: Materials and reagents required for adenoviral purification.....	108
Table 2.6: Solutions and buffers required for adenoviral purification.....	109
Table 2.7: Concentrations used to generate dose response curves.	115
Table 2.8: Buffers required for flow cytometry	123
Table 2.9: Laser, absorbance, emission, and detector information for fluorochromes used in flow cytometry	124
Table 2.10: Antibodies used in flow cytometry	126
Table 2.11: Reagents required for RT for one sample	132
Table 2.12: Thermocycler Conditions for RT	132
Table 2.13: Reagents and quantities required for one real-time qPCR samples	133
Table 2.14: Primers used for RT-qPCR	135
Table 2.15: RT-qPCR conditions	136
Table 2.16: Features of NSG Model	140
Table 2.17: Buffers, reagents and antibodies used in IHC	149
Table 6.1: Suboptimal dose range for synergy experiments	277
Table 6.2: Summary of CI data from cell viability experiments in MPC lines	289
Table 6.3: Summary of CI data for highest dose concentration	290
Table 6.4: Summary of viral infection data following anti-MM chemotherapies.	300
Table 6.5 Summary of viral replication data following anti-MM chemotherapies.	307
Table 6.6 Summary of Bortezomib in combination with Ad[CE1A].	313
Table 6.7 Summary of Melphalan in combination with Ad[CE1A].	319
Table 6.8 Summary of Panobinostat in combination with Ad[CE1A].	324
Table 6.9 Summary of Pomalidomide in combination with Ad[CE1A].	330
Appendix Table 8.1:STR profile of human cell lines.....	343

List of Figures

Figure 1.1: The development of monoclonal gammopathies:.....	30
Figure 1.2: Intrinsic mechanisms of action of oncolytic viruses:	34
Figure 1.3: Immunogenic cell death by oncolytic viruses:	36
Figure 1.4: Virion structure and schematic representation of Ad 5 genome:.....	51
Figure 1.5: The cell entry pathway of adenovirus:.....	53
Figure 1.6 Schematic representation of E1A-mediated regulation of the cell cycle:.....	59
Figure 1.7: Ad[CE1A] induces cell death specifically in MPC lines in vitro and in vivo but has no effect on MM-induced bone disease:.....	71
Figure 2.1: Percentage of CD138 ⁺ and CD138 ⁻ populations isolated from MM patients and HDs. .	105
Figure 2.2: Plasmid schematics used in the construction of Ad[CE1A].	107
Figure 2.3: Representative images of adenoviral banding after CsCl ultracentrifugation:.....	110
Figure 2.4: Representative images of Adeno-X™ Rapid titre kit in HEK293A cells at two serial dilutions.	111
Figure 2.5: Schematic of study design of Ad[CE1A] survival study in U266 xenograft low tumour burden model of myeloma.	141
Figure 2.6: Expression of Luc and CD138 in 5TGM1-Luc cells.	142
Figure 2.7: Schematic of study design of Ad[CE1A] proof of concept study in 5TGM1 model.....	143
Figure 2.8: Representative bioluminescent images showing ROI analysis in hind limbs (anterior) and vertebra (posterior) in Living image software.	144
Figure 2.9: A schematic diagram demonstrating a sandwich IHC technique.	146
Figure 2.10: An example image using the Aperio Scan Scope slide scanner and analysis of tumour burden using QuPath software.	150
Figure 3.1: Flow cytometric analysis of CAR, $\alpha\beta_5$ and $\alpha\beta_3$ expression in human MPC lines compared to Ad5 susceptible cell line HEK293A:.....	159
Figure 3.2: Flow cytometric analysis of CS1 cell surface expression in human MPC lines compared to control non-MM cells:	161
Figure 3.3: SLAMF7 mRNA Expression in human MPC cell lines:	162
Figure 3.4: Correlation between CS1 cell surface protein expression and mRNA expression:	163
Figure 3.5: Representative images of live fluorescent microscopy of Ad-GFP expression in human MPC lines:	164
Figure 3.6: Flow cytometric analysis of the percentage of human MPC lines infected with Ad-GFP after 24 and 48 hours:.....	165
Figure 3.7: E1A mRNA expression in MPC lines at 4 and 24 hours:.....	166
Figure 3.8: Correlation between SLAMF7 mRNA expression and E1A mRNA expression:.....	167
Figure 3.9: Infectious virion production in human MPCs lines:.....	168
Figure 3.10: Dose and time response Ad[CE1A] toxicity in human MPCs:.....	169
Figure 3.11: Cytotoxicity of Ad[CE1A] compared to Ad[PSA] in human MPCs:	170
Figure 3.12: Cytotoxicity of Ad[CE1A] in human MPC lines compared to control cancer cell lines:	171
Figure 3.13: Correlation between CS1 cell surface expression and cell death after Ad[CE1A] treatment:	172
Figure 3.14: Flow cytometric analysis of KI-67 expression after Ad[CE1A] treatment at 24 and 48 hours in JJN-3 and OMP-2 cell lines:.....	173
Figure 3.15: Cytotoxicity of Ad[CE1A] in JJN-3, U266 and OMP-2 cells in the presence or absence of BMSC line HS-5:	174

Figure 3.16: Flow cytometric analysis of CAR, $\alpha\beta_5$ and $\alpha\beta_3$ expression in patient derived PCL cells:	175
Figure 3.17: CS1 expression in primary cells ex vivo:	177
Figure 3.18: Cytotoxicity of Ad[CE1A] in patient-derived MM cells compared to non-malignant cell populations:	179
Figure 3.19: Percentage of patient-derived primary MM CD138 ⁺ cells and primary HD CD138 ⁻ BMMC infected with Ad-GFP after 24 and 48 hours:	181
Figure 3.20: Percentage Annexin V ⁺ TO-PRO-3 ⁻ after Ad[CE1A] treatment:	183
Figure 3.21: mRNA expression of apoptotic markers in JJN-3 after Ad[CE1A] incubation at indicated times:	184
Figure 3.22: Ad[CE1A] response in MPCs in the presence of the pan caspase inhibitor Z-VAD-FMK:	185
Figure 3.23 Ad[CE1A] response in MPCs in the presence of the RIPK1 inhibitor Nec-1.	188
Figure 3.24 Ad[CE1A] response in MPCs in the presence of the RIPK3 inhibitor GSK-872:	190
Figure 3.25 Ad[CE1A] response in MPCs in the presence of the MLKL inhibitor NSA:	192
Figure 3.26: Cell surface calreticulin exposure in MPCs following Ad[CE1A] treatment:	194
Figure 3.27: Cell surface CD47 expression in MPCs following Ad[CE1A] treatment:	196
Figure 3.28: Extracellular release of ATP in MPCs following Ad[CE1A] treatment:	197
Figure 3.29 Cell surface HLA-ABC expression in MPCs following Ad[CE1A] treatment:	199
Figure 3.30 Cell surface HLA-DR expression in MPCs following Ad[CE1A] treatment:	200
Figure 3.31 Cytokine-induced bystander killing of MM cells:	201
Figure 4.1: Percentage of MPC line death after incubation with BTZ \pm indicated doses of Ad[CE1A] over time:	219
Figure 4.2: Percentage of JJN-3 and U266 BTZ insensitive and parental cells dead after Ad[CE1A] (MOI 10) incubation at 72 hours:	221
Figure 4.3: Analysis and quantification of in vivo tumour burden in U266 bearing NSG mice by bioluminescent imaging over time:	223
Figure 4.4: Kaplan-Meier survival curves of U266 bearing NSG mice treated with vehicle, Ad[CE1A], or with BTZ \pm early Ad[CE1A] treatment to target MRD or late Ad[CE1A] treatment to target relapse:	225
Figure 4.5: Representative flow cytometry dot plots over time of DID fluorescence in U266-GFP expressing cell lines:	226
Figure 4.6: Percentage of Vybrant TM DID populations over time in JJN-3, U266 and OPM-2 GFP expressing cell lines:	227
Figure 4.7: Representative flow cytometry plots of DID fluorescence in JJN-3 cells in cultured in HS-5 or Saos-2 conditioned media at Day 0, 10 and 21 post staining:	228
Figure 4.8: Percentage of Vybrant TM DID ^{High} population over time in JJN-3, U266 and OPM-2 GFP expressing cells after culture in HS-5 or Saos-2 CM compared to control:	229
Figure 4.9: Proliferation of U266 MPCs, Saos-2 osteoblast like cells, and U266-Saos-2 cocultures in polyHIPE scaffolds:	231
Figure 4.10 Scanning Electron Microscopy images of 3D polyHIPE scaffolds with MPC mono- or cocultures with Saos-2 Cells:	232
Figure 4.11: Cell viability of U266 cells after BTZ or Ad[CE1A] or combination treatment in polyHIPE scaffolds:	233
Figure 4.12 Percentage of Live/Dead Vybrant TM DID populations JJN-3, U266 and OPM-2 following Ad[CE1A] treatment:	234
Figure 5.1: CS1 cell surface protein expression in 5TGM1 cells:	246
Figure 5.2 Percentage of 5TGM1 cells infected with Ad-GFP:	247

Figure 5.3: E1A mRNA expression in 5TGM1 cell lines compared to JJN-3 and U266 human MPCs:	248
Figure 5.4: Infectious virion production in 5TGM1 cells compared to JJN-3 and U266 cells:	249
Figure 5.5: Percentage of 5TGM1 cells dead after incubation with Ad[CE1A]:	250
Figure 5.6: Percentage Annexin V positive 5TGM1 cells after Ad[CE1A] treatment:	251
Figure 5.7 Ad[CE1A] response in 5TGM1 cells in the presence of the pan caspase inhibitor Z-VAD-FMK:	252
Figure 5.8 Ad[CE1A] response in 5TGM1 cells in the presence of RIPK1 inhibitor Nec-1:	253
Figure 5.9 Ad[CE1A] response in 5TGM1 cells the presence of the RIPK3 inhibitor GSK-872:	254
Figure 5.10 Cell surface calreticulin exposure following Ad[CE1A] treatment in 5TGM1 cells:	255
Figure 5.11 Extracellular release of ATP following Ad[CE1A] treatment in 5TGM1 cells:	256
Figure 5.12: Analysis and quantification of in vivo tumour burden in 5TGM1 bearing C57BL/KaLwRij mice treated with vehicle or Ad[CE1A] at two doses by two routes of admission:	258
Figure 5.13: Percentage of BM cells expressing CD138 in 5TGM1 bearing C57BL/KaLwRij mice following treatment with vehicle or Ad[CE1A] at two doses by two routes of admission:	260
Figure 5.14: Kappa IHC staining in the tibiae of 5TGM1 bearing C57BL/KaLwRij mice following treatment with vehicle or Ad[CE1A] at two doses by two routes of admission:	261
Figure 5.15 Micro-CT analysis of tibiae in 5TGM1 bearing C57BL/KaLwRij mice following treatment with vehicle or Ad[CE1A] at two doses by two routes of admission:	262
Figure 5.16 Analysis of E1A expression in 5TGM1-bearing C57BL/KaLwRij mice following treatment with vehicle or Ad[CE1A] at two doses by two routes of admission:	263
Figure 5.17 Proinflammatory cytokine secretion from serum in 5TGM1 bearing C57BL/KaLwRij mice following treatment with vehicle or Ad[CE1A] at two doses by two routes of admission:	265
Figure 6.1: Dose response curves of Ad[CE1A] and anti-MM chemotherapies in MPC lines:	277
Figure 6.2: Ad[CE1A] in combination with BTZ in MPCs cell lines:	279
Figure 6.3: Heatmap of CI of Ad[CE1A] in combination with BTZ in MPC lines:	281
Figure 6.4: Ad[CE1A] in combination with Melph in MPC cell lines:	282
Figure 6.5: Heatmap of CI of Ad[CE1A] in combination with Melph in MPC lines:	283
Figure 6.6: Ad[CE1A] in combination with Pan in MPC lines:	284
Figure 6.7: Heatmap of CI of Ad[CE1A] in combination with Pan in MPC lines:	286
Figure 6.8: Ad[CE1A] in combination with Pom in MPC lines:	287
Figure 6.9: Heatmap of CI of Ad[CE1A] in combination with Pom in MPC lines:	288
Figure 6.10: Percentage of total Annexin V positive cells after A[CE1A] and anti-MM chemotherapy combination therapy in MPC lines:	292
Figure 6.11: CAR expression after 48 hours of anti-MM chemotherapy treatment:	294
Figure 6.12: Percentage of Ad-GFP expression after anti-MM therapies compared to untreated control:	296
Figure 6.13: Percentage of Ad-GFP expression after anti-MM therapies compared to untreated control:	298
Figure 6.14: CS1 receptor expression after 48 hours of anti-MM chemotherapy treatment:	302
Figure 6.15 E1A expression after 24 hours of anti-MM chemotherapy treatment:	304
Figure 6.16 Anti-MM chemotherapies increase viral titre in MPC lines:	306
Figure 6.17: Cell surface CALR expression after 24 hour treatment of Ad[CE1A] ± anti-MM chemotherapy:	309
Figure 6.18: Extracellular release of ATP following 24 hour treatment of Ad[CE1A] ± anti-MM chemotherapy:	311
Appendix Figure 8.1: Example of results from Mycoplasma PCR kit.	345

Appendix Figure 8.2 Patient and healthy donor information sheets and consent forms	346
Appendix Figure 8.3 Time required to UV inactivate Ad[CE1A] in CM.....	354
Appendix Figure 8.4 Percentage Annexin V positive after Ad[CE1A] treatment in a primary patient-derived PCL cells, CB1.....	355
Appendix Figure 8.5 Dose response to Nec-1 to determine non-toxic dose.....	356
Appendix Figure 8.6 Dose response to GSK-872 to determine non-toxic dose.	356
Appendix Figure 8.7 Dose response to NSA to determine non-toxic dose.	357
Appendix Figure 8.8 Percentage of GFP positive U266 cells from BM flush of left femora in U266 low tumour burden model of myeloma.	358
Appendix Figure 8.9 Body weight of mice in U266 low tumour burden model over time.....	359
Appendix Figure 8.10 U266 cells within the ovary of NSG mice in the U266 low tumour burden model of MM.....	360
Appendix Figure 8.11 Proliferation of MPCs following different percentages of CM from either HS-5 cells or Saos-2 cells	361
Appendix Figure 8.12 Examples of bioluminescent signal fluctuating over time in two vehicle treated mice and two BTZ treated mice in the U266 low tumour burden model of MM.....	362
Appendix Figure 8.13 Dose response to GSK-872 to determine non-toxic dose in 5TGM1 cells. ...	363
Appendix Figure 8.14 Histological analysis of Ad hexon or E1A staining from Ad[CE1A] treated 5TGM1-bearing mice.....	364
Appendix Figure 8.15 Dose response to Len.	365
Appendix Figure 8.16 Percentage of Annexin V positive cells after A[CE1A] and anti-MM chemotherapy combination therapy in MPC lines.	366
Appendix Figure 8.17 Correlation between CAR relative fold change after treatment and synergy CI score.....	367
Appendix Figure 8.18 Mean fluorescent intensity of Ad-GFP in combination anti-MM therapies compared to untreated control.	368
Appendix Figure 8.19 Mean fluorescent intensity of Ad-GFP after anti-MM therapies compared to untreated control.	369
Appendix Figure 8.20 Correlation between CS1 relative fold change after treatment and synergy CI score.....	370

Abstract

Multiple myeloma (MM) is a bone marrow cancer of differentiated B-lymphocytes known as plasma cells. Although MM usually responds initially to chemotherapy regimens, unfortunately, after periods of remission of variable duration, successive relapses and the emergence of treatment-refractory disease typically manifest. Therefore, new approaches are required that not only reduce tumour load, but also prevent tumour recrudescence i.e. relapse from foci of minimal residual disease (MRD).

One such approach is the use of oncolytic viruses (OVs), which preferentially infect, replicate, and kill cancer cells. A novel *SLAMF7*-promoter driven oncolytic adenovirus (Ad[CE1A]) was genetically engineered to target MM. Previously, preliminary results showed Ad[CE1A] to have efficacy against MM, however, did not remove all tumour. Therefore, to progress Ad[CE1A] into clinical trials, the aim of this project was to determine Ad[CE1A] efficacy alone or in combination with standard anti-MM chemotherapies, and to determine if Ad[CE1A] can control/eradicate MRD.

Ad[CE1A] was found to have efficacy in myeloma plasma cells (MPCs) and most importantly in patient-derived MM cells. Unfortunately, *in vivo* in a U266 low tumour burden xenograft murine model of MM, results were inconclusive and further investigation is needed to determine if Ad[CE1A] can prevent MRD regrowth. However, when Ad[CE1A] was assessed in the 5TGM1 syngeneic murine model of MM, it showed efficacy. Ad[CE1A] was also investigated in combination with MM standard of care drugs (Bortezomib, Melphalan, Panobinostat or Pomalidomide). Ad[CE1A] combinations showed enhanced anti-MM effects. Mechanistically, Melphalan was found to increase Ad[CE1A] replication, for the other drugs it was not clear whether they were augmenting Ad[CE1A] life cycle, indicating other mechanisms.

The results reported here outline a promising role for Ad[CE1A] against MM. They provide a foundation for continued investigation into the mechanisms of Ad[CE1A] alone and in combination with other MM standard of care drugs, which will provide a better understanding of Ad[CE1A] therapy as well as the clinical setting in which they have the greatest efficacy.



Chapter 1 : Introduction



1.1 Multiple myeloma

Multiple myeloma (MM) is a haematological malignancy of immunoglobulin-secreting terminally differentiated B lymphocytes, known as plasma cells, which undergo clonal proliferation in their primary resident site, the bone marrow (BM). In the UK, approximately 5,500 people are diagnosed with MM each year. MM is the nineteenth most common cancer in the UK, accounting for 2% of all new cases of cancer, and is the second most common haematological malignancy (1). There are racial disparities that exist with MM and its premalignant conditions, with both having higher incidence rates in Afro-Caribbean populations (2). MM has no known environmental aetiological factors that play a major role in MM pathogenesis, with the exception of petrochemical exposure in a small minority of cases (3). MM incidence increases sharply with age, and is generally considered a cancer of the elderly, with only 16% of patients <60 years; 59% of patients >70 years, with a median age of presentation 69 years (4,5). The global population of elderly people is rapidly increasing, with people over the age of 80 expected to quadruple by 2050, therefore, MM incidence appears to be increasing in parallel (1,4,6).

MM is a disease that evolves through several progressive stages (7). One of the unique features of MM is the presence of a well-defined asymptomatic pre-malignant state, called monoclonal gammopathy of undetermined significance (MGUS) (7), which is present in around 2-3% of adults over the age of 50, and around 5% of adults over the age of 70 (8–11). Over time, MGUS can progress to malignancy, but it is still largely asymptomatic, called smouldering MM (SMM), with a 1% annual risk of progression from MGUS to SMM (8–10). Eventually, disease progresses to symptomatic MM, where rapid proliferation of these malignant plasma cells occurs in the BM, causing localised sites of tumour known as plasmacytomas. Some patients present with a solitary plasmacytoma (12) but most develop systemic disease characterised by multiple distinct tumours. The risk of patients progressing from asymptomatic disease to symptomatic disease is 10% per year for the first five years. After 5 years, this risk diminishes (13).

1.1.1 Clinical Manifestations

MM is characterised primarily by the overproduction of non-functional intact monoclonal immunoglobulins (Igs); also known as M proteins, paraproteins and Bence-Jones proteins in the urine. However, 15-20% of patients secrete monoclonal Ig light chains, and <3% of patients no monoclonal protein is secreted (7,9,14). MM is also the second most common cancer to involve the skeleton, with 80-90% of patients developing bone lesions throughout the course of their disease (15). This is due to the malignant cells in the BM secreting a variety of factors, such as Receptor activator of nuclear factor kappa-B ligand (RANKL), interleukin-6 (IL-6) and interleukin-3 (IL-3), that cause remodelling of local bone structure (16). Therefore, clinical manifestations are driven by the accumulation of plasma cells and the secretion of paraproteins, which cause hyperCalcaemia, Renal insufficiency, Anaemia, and/or Bone disease with lytic lesions and/or pathological fractures, known collectively as CRAB features (17). MM is an extremely heterogeneous disease, with some patients surviving decades without requiring therapy, whilst others succumb to disease within weeks from aggressive progressive disease. Consequently, developing reliable diagnostic and prognostic systems has been highly important. Therefore, the international myeloma working group (IMWG) have established MM diagnostic criteria and MM prognostic criteria called the international staging system (ISS) (Table 1.1), that is regularly updated with the advent of new diagnostic biomarkers (Table 1.2) (18).

Table 1.1: International staging system for myeloma

Stage	Criteria
I	Serum β 2 microglobulin <3.5 mg/L Serum albumin \geq 3.5 g/dL Low-risk chromosomal abnormalities Normal Lactate Dehydrogenase (LDH)
II	Serum β 2 microglobulin between 3.5 mg/L and 5 mg/L with any serum albumin level OR Serum β 2 microglobulin <3.5 mg/mL and serum albumin <3.5 mg/dL Low risk cytogenetics Normal LDH
III	Serum β 2 microglobulin between >5.5 mg/L High LDH High risk cytogenetics

Table 1.2: IMWG Myeloma diagnostic Criteria (adapted from IMWG)

<p>Clonal bone marrow plasma cells \geq10% (clonality should be established)</p> <p>Or</p> <p>Histology proven bony or extramedullary plasmacytoma on abnormal scans (clonality should be established)</p> <p>And require</p> <p>Any one of the following myeloma-defining events (must be attributed to underlying clonal proliferative disorder)</p>
1. Bone lesions on skeletal radiography, low dose CT, FDG, PET-CT scan: One or more osteolytic lesions. If bone marrow has <10% clonal plasma cells, more than one bone lesion is required to distinguish from solitary plasmacytoma with minimal marrow involvement.
2. Bone lesions on MRI: \geq 2 foci (bone and/or marrow) lesions with each focal lesion \geq 5 mm.
3. Involved/uninvolved serum free light chain ratio >100 , uninvolved serum-free light chain concentration \geq 10 mg/dL
4. Hypercalcaemia: Serum calcium >0.25 mmol/L (>1 mg/dL) higher than the upper limit of normal or >2.75 mmol/L (>11 mg/dL).
5. Anaemia: Haemoglobin value of >2.0 g/dL below the lower limit of normal or a haemoglobin value <10.0 g/dL.
6. Renal insufficiency: Creatine clearance <40 mL/minute (reliable) and/or serum creatine >173 mmol/L (>2 mg/dL; less reliable)
<p>Or</p> <p>None of the above</p> <p>But</p>
<p>Presence of \geq60% clonal bone marrow plasma cells (clonality should be established)</p>

1.1.2 Mutations Associated with Multiple Myeloma

MM is a genetically complex and biologically heterogeneous disease that results from multiple genomic events that lead to tumour development and progression (Figure 1.1) (19). A dichotomy of genetic aberrations account for the large majority, if not all of myeloma initiating events, also known as primary genomic events. Firstly, ~50% of myeloma cases contain an aneuploidy of several odd numbered chromosomes including 3, 5, 7, 9, 11, 15, 19 and 21, this is known as hyperdiploidy (20). The mechanism behind hyperdiploidy is still unknown, however one hypothesis is that the gain of multiple whole chromosomes occurs during a single catastrophic mitosis, as opposed to serial gain of chromosomes over time, which is what has also been suggested to occur in hyperdiploid acute lymphocytic leukaemia (21,22).

The second genetic aberration heavily involved in a myeloma initiating event are translocations involving the Ig heavy-chain (*IGH*) genes, which is mutually exclusive with hyperdiploid myeloma (20). IgH translocations juxtapose the IgH enhancers to one of several oncogenes, which include any of the three Cyclin D genes (*CCND1-3*), *WHSC1* (also known as MM SET domain (MMSET)), *MAF* or *MAFB* (23). These translocations include t(4;14), t(14;16), t(11;14), t(6;14) and t(14;20)(24). Each translocation and copy number variation is associated with its own genetic risk and prognosis outlined in Table 1.3 and 1.4.

Table 1.3: Prognosis for each cytogenetic abnormality according to the risk stratification models for MM (25).

	mSMART	IFM	IMWG
t(11;14)	Standard Risk		
t(4;14)	Intermediate Risk	High Risk	High Risk
t(14;16)	High Risk		High Risk
Del17p	High Risk	High Risk	High Risk
Del13q	Intermediate Risk		
Gain1p	High Risk		

mSMART: Stratification for Myeloma and Risk-Adapted Therapy. IFM: Intergroupe Francophone du Myelome. IMWG: International Myeloma Working Group.

Table 1.4: MM genetic abnormalities with genetic alterations and related prognosis (26).

Cytogenetics	Genetic Event	Frequency	Prognosis
t(11:14)(q13;q32)	<i>CCND1</i>	20%	Good Prognosis
t(4:14)(p16.3;q32)	<i>FGFR3, MMSET</i>	15%	Negative impact on PFS and OS
t(14;16)(q32;q23)	<i>CMAF</i>	2-3%	Controversial
Del17p13	<i>TP53</i>	5-15%	Negative impact on PFS and OS
Del1p32 Del1p22	<i>CDKN2C</i>	7-17%	Negative impact on PFS and OS
Gain1q21	<i>CKS1B</i>	34-40%	Negative impact on PFS and OS

PFS: Progression Free Survival. OS: Overall Survival. FGFR3: Fibroblast Growth Factor Receptor 3. MMSET: MM SET Domain. CKS1B: CDC28 protein kinase regulatory subunit 1B. CDKN2C: Cyclin-dependent kinase 4 inhibitor C. CCND1: Cycline-D1. MAF: musculoaponeurotic fibrosarcoma.

Secondary genomic events, such as chromosomal translocations, copy-number variations and single-nucleotide variants occur which provide a fitness advantage to a particular subclone over other populations and are required for disease progression. This clonal heterogeneity and evolution was recently accepted as a Darwinian selection process. Additionally, copy-number variations, translocations involving *MYC*, and somatic mutations affecting mitogen-activated protein kinase (MAPK), nuclear factor kappa B (NF-κB), and DNA-repair pathways are observed during MM, and less frequently in pre-malignant stages, therefore, these events are likely to be secondary driver events (19).

Some of these secondary genomic events are linked to worse prognosis, Del(13q) occurs in ~50% of newly diagnosed MM. Del(13q) co-occurs with t(4:14) and t(14:16) and was once considered to be a marker of poor prognosis, but since the introduction of proteasome inhibitors in the treatment of MM, it appears the outcome of poor prognosis with Del(13q) has changed (SUMMIT and APEX trials) (23). Amp(1q) occurs in 40% of MM and is associated with worse prognosis (24,25). The poor prognosis associated with Amp(1q) appears to be dose-dependent, as patients with 4 or more copies of chromosome 1q do worse than those with 3 copies (26). The additional copies of 1q likely have a proportional effect on 1q gene expression, as a gene signature of high-risk myeloma is composed of a large number of 1q genes (27). Del(1p) occurs in 20-25% of patients and often co-occurs with

hypodiploidy (loss of chromosomes), which is associated with worse prognosis, as it del(1p) (22,28). The risk and prognosis of these secondary genetic events are outlined and summarised in Table 1.3 and 1.4.

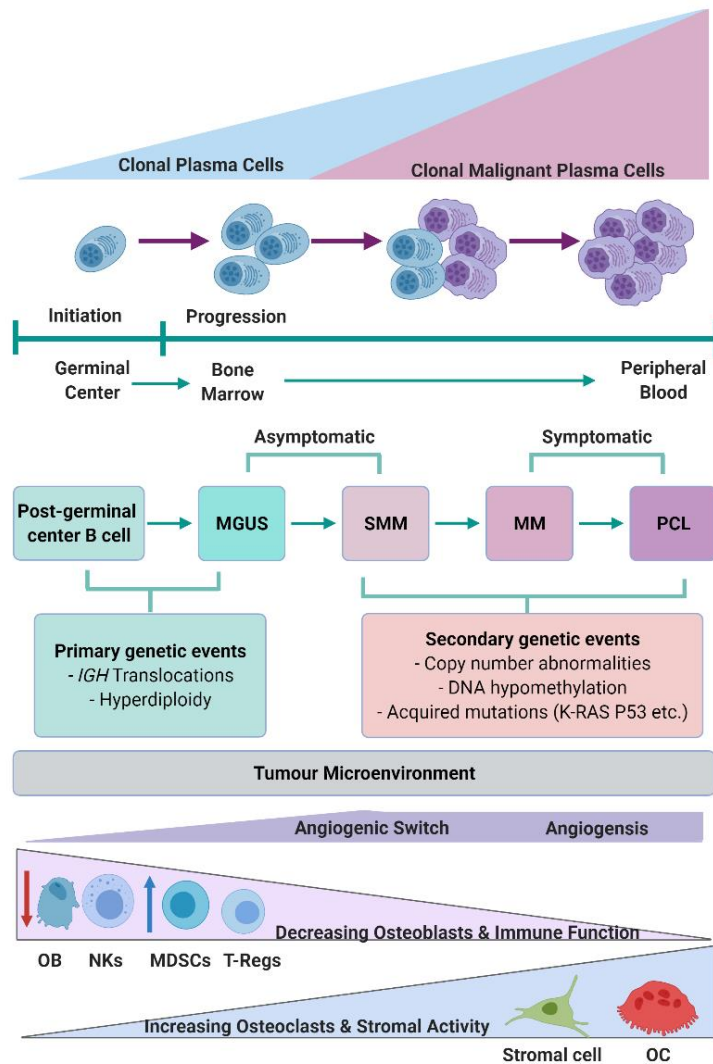


Figure 1.1: The development of monoclonal gammopathies:

The development of multiple myeloma (MM) is a multistep process, starting with precursor states such as monoclonal gammopathy of undetermined significance (MGUS) and smouldering MM (SMM). MM can progress to bone marrow-independent diseases, such as extramedullary MM and plasma cell leukaemia (PCL). MM progression involves clonal evolution and heterogeneity, which is not just cell autonomous, but is also dependent on interactions with the tumour microenvironment, which includes an increase in T-regulatory cells (T-regs), myeloid-derived suppressor cells (MDSCs) osteoclasts (OCs), angiogenesis, and mesenchymal stem cells but a decrease in natural killer cells (NK), and osteoblasts (OBs). Primary genetic events in the development of MGUS, SMM and MM include chromosomal translocations involving the immunoglobulin (Ig) heavy-chain genes (IGH) and aneuploidy (with hyperdiploidy being most frequent). The number of secondary genomic alterations increases from MGUS to SMM and then to MM which include copy number abnormalities, DNA hypomethylation and acquired mutations such as fibroblast growth factor 3 (FGF3), N-Ras, K-Ras and tumour protein P53 (TP53). Figure reproduced and adapted with permission from (7,21) created using BioRender.

1.1.3 Treatment of Multiple Myeloma

Historically, MM treatment involved combinations of chemotherapy, either with or without radiation. Frequently, these therapies were able to induce at least partial remissions; unfortunately, there were high rates relapse, typically within 2-3 years (22). The reasons for relapse are complicated and probably involve a variety of factors, including the high degree of genomic variability (23–25), phenotypic plasticity (26,27), the undefined nature of tumorigenic MM stem cells (28,29), chemotherapeutic resistance (30,31) and the interplay between MM cells and the tumour microenvironment (32). Because of this poor prognosis, MM patients that were eligible, typically younger, biologically fit patients, were treated with aggressive myeloablative chemotherapy combined with autologous stem-cell transplants (ASCT) (33). Whilst this strategy has improved prognosis, which has been supported by evidence from many randomised control trials (reviewed in (34)), there are severe treatment-related morbidities associated with myeloablative regimes, including increased risk of infection and neutropenia. Sadly, even with the use of ASCT, patients often relapse within 3-5 years. Relapse following an ASCT was thought to be caused primarily by minimal residual disease (MRD) persisting within treated patients (22,35,36). However, it was found that almost all ASCT samples were contaminated with MM cells that were reintroduced to the patient during transplant (22,37). It remains controversial as to what impact these contaminating MM cells have on disease relapse, however, their reintroduction back into patients seems unlikely to be beneficial. Unfortunately, ASCT regime is not suited for a large cohort of patients, as discussed above, MM is predominantly a disease of the elderly, therefore many patients are insufficiently fit for this treatment approach (34).

From 2000 onwards, novel chemotherapeutics including, first- and second-generation proteasome inhibitors, such as Bortezomib (BTZ), and immunomodulatory drugs (IMiDs) such as Thalidomide and Lenalidomide (Len) began to improve patient outcomes of both MM patient cohorts. Use of these drugs have improved MM patients 5-year survival from 30% in 2000-2003 to the current 5-year

survival rate of 52.3% (38). However, this is low compared to other haematological cancers such as non-Hodgkin's lymphoma (75%) and for solid cancers such as breast cancer (85%) (39,40).

A better understanding of MM pathobiology and the role of the immune system has led to the discovery of novel targets and pathways that affect survival and proliferation of the malignant clone. Therefore, since 2010, a variety of new drugs have also been approved for use in MM, including Carfilzomib (second generation proteasome inhibitor) (41), Pomalidomide (Pom) (Thalidomide analogue) (42), Panobinostat (Pan) (histone deacetylase inhibitor)(43), Daratumumab or Isatuximab (CD38 monoclonal antibody (mAb)) (44,45), Ixazomib (second generation proteasome inhibitor) (46), Selinexor (selective inhibitor of nuclear export) (47), Belantamab Mafoditin (antibody-drug conjugate against B cell maturation antigen) (48), and Idecabtagene Vicleucel (a B cell maturation antigen-directed chimeric antigen receptor T cell (CAR-T)) (49). Mechanisms of how some of these therapies work will be discussed later in section 1.6. Additionally, antibodies that augment the host immune response through immune checkpoint inhibitors targeting programmed cell death protein-1 (PD-1) and PD ligand-1 (PD-L1) are also in development for MM (50). These drugs promise to improve prognosis even further. It is due to these advances, that the long-held belief that MM is an incurable, but treatable disease is gradually being challenged. Nonetheless, MM remains incurable for the vast majority of patients, even with the advent of new treatment options. Generally, the clinical course of MM is characterised by ever-shortening cycles of remission and relapse after sequential therapies due to MRD and various factors mentioned previously. Additionally, a high proportion of patients present with advanced disease, therefore, there continues to be a need for effective and minimally toxic new treatment modalities for MM.

1.2 Oncolytic Virotherapy

Novel therapies that do not rely on the use of generic chemotherapies with their inevitable toxicities are highly desirable for MM. This is because two of the major factors contributing to therapeutic failure in MM are tumour heterogeneity and plasticity leading to the emergence of resistant clones (22). One such therapy being studied is oncolytic virotherapy, which is an emerging form of anticancer therapy that aims to treat cancer with live, replicating viruses. Anecdotal evidence emerged in the 20th century that viral infection could induce remission in various cancer types (51,52), including MM (53). Since these first observations, several viruses have been investigated and developed as therapeutic agents for cancer. The first oncolytic virus (OV), a second-generation herpes simplex virus type 1 (HSV-1) armed with granulocyte-macrophage colony-stimulating factor (GM-CSF), obtained FDA approval in 2015 in the USA and Europe for melanoma (54). A paradigm shift has occurred where OVs are now practiced in clinic in some cancers, and it is likely that they will be accepted into mainstream clinical use in combination with other anticancer drugs.

OVs can infect both normal and malignant cells, however, they show a tropism toward malignant cells due to the presence of aberrant signalling pathways, abnormal homeostasis, and response to stress, which are advantageous for viral replication (55,56). These aberrant signalling pathways activated during malignant transformation clearly antagonise host antiviral responses, creating cancer cells that are hypersensitive to viral infection and replication (Figure 1.2), for example cancer cells that have a defective Type I interferon (IFN) response to virus infection can result in prevention of viral clearance. This is because IFN shuts down protein synthesis, rendering the cell unfit for viral replication, therefore healthy cells with intact IFN response can abort virus replication, whilst cancer cells with a defective IFN response cannot (69). The therapeutic efficacy of OVs depends on two main modes of action. Firstly, by direct oncolysis, OVs can inhibit protein synthesis and destroy infected tumour cells by viral replication until the cell lyses. This type of cell death is passive with no reliance on active cell death mechanisms, such as apoptosis, which could degrade intracellular virions halting OV anticancer efficacy (57,58). Despite this, some OVs appear to stimulate cellular apoptotic pathways (59,60), whilst

other viruses mediate other active cell death processes (61,62). One possible advantage of cell death that is independent or not reliant on apoptosis, may be the ability to evade apoptosis-related pathways of acquired drug resistance (58).

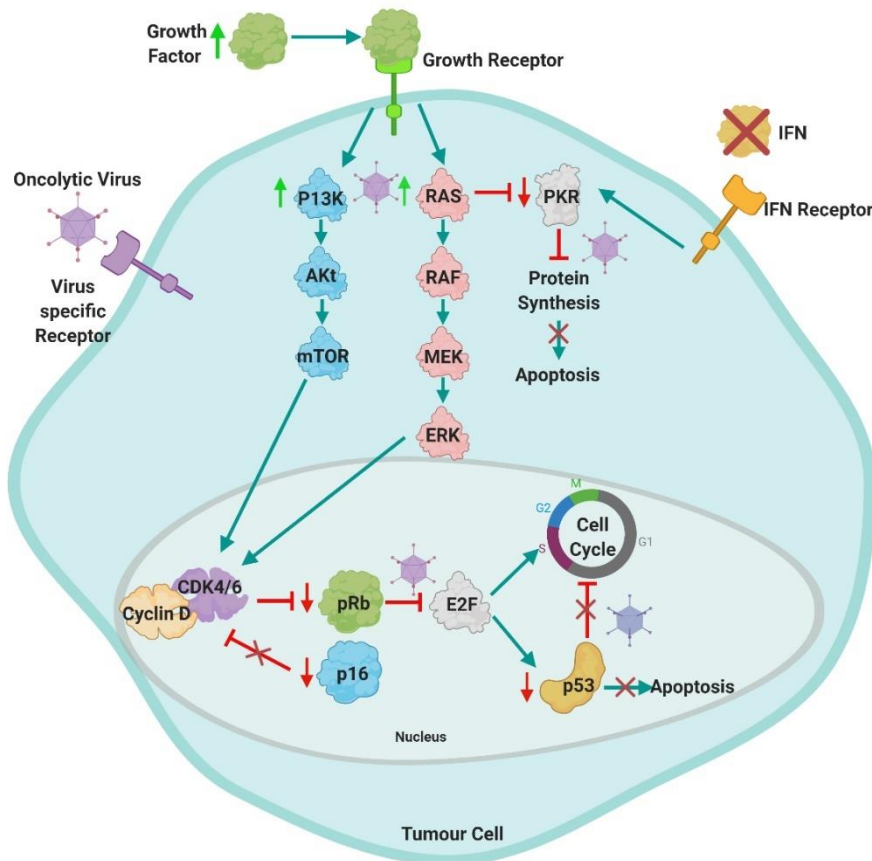


Figure 1.2: Intrinsic mechanisms of action of oncolytic viruses:

Oncolytic viruses (OVs) preferentially select cancer cells due to the presence of aberrant signalling pathways or targeted molecules (such as RAS, PKR, P13K/Akt/mTOR, IFN, p53 or Rb/E2F/p16). Hyperactivation of P13K/Akt/mTOR and RAS pathways and consequent activation of their downstream cascade results in an increase of cell proliferation and inhibition of apoptosis. OVs can exploit this to replicate efficiently. Additionally, hyperactivation of RAS blocks protein kinase R (PKR), which prevents cells from detecting stress, thus allowing the cells to continue protein translation and aberrant proliferation. Consequently, OVs can selectively replicate as cancer cells cannot terminate protein translation in response to infection. Interferon (IFN) signalling may also be abnormal in malignant cells, thus viral clearance is prevented. Malignant cells with mutated p53 cannot undergo abortive apoptosis, therefore some OVs preferentially target p53 mutant cells. Likewise, aberrant expression of cell cycle regulatory components such as retinoblastoma protein (pRb) and p16, can render cancer cells sensitive to OVs. Furthermore, oncolytic viruses have a natural tropism for receptors expressed abnormally in cancer cells (56). Figure reproduced and altered with permission from (56) created using BioRender.

Secondly, oncolysis is widely accepted to be highly immunogenic as viral antigens known as pathogen-associated molecular pattern (PAMPs), such as dsRNA, ssRNA, dsDNA and ssDNA, tumour-associated antigens (TAAs), damage-associated molecular patterns (DAMPs), such as high-mobility group box 1 (HMGB1), heat shock protein (HSP) 60 and 70 and cytokines are released from dying cancer cells (Figure 1.3) (57,58). This can recruit and activate immune cells to infiltrate the tumour, such as cells of the innate immune response, natural killer cells (NKs), dendritic cells (DCs) and macrophages (63). These cells further destroy infected tumour cells and secrete proinflammatory cytokines. An adaptive T-cell mediated immune response can be initiated when the cells of the innate immune system uptake viral and TAAs and present them for T cell activation, which then exert their effector functions against cancer cells. This adaptive immunity is critical for durable cancer control in systemic/metastatic disease (64–66). This immunogenic process of cell death is termed immunogenic cell death (ICD) and will be discussed in more detail in chapter 3. Furthermore, OVs can be armed with additional transgenes that either enhance cell death or antitumour response (67).

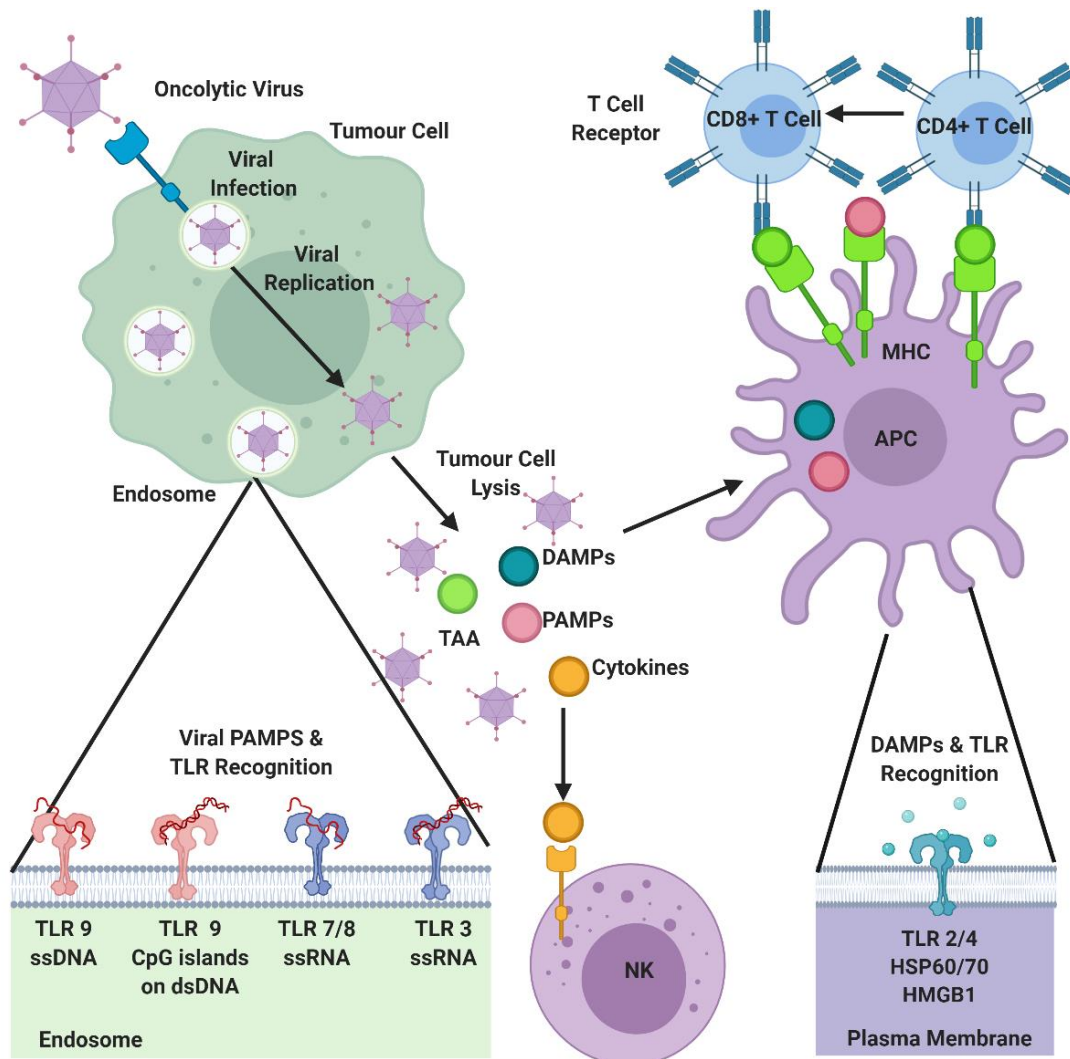


Figure 1.3: Immunogenic cell death by oncolytic viruses:

Systemic innate and tumour specific adaptive immune responses are activated after oncolytic virus infection and subsequent lysis of tumour cells. Oncolysis releases cytokines, tumour-associated antigens (TAAs), and other danger signals, such as damage-associated molecular patterns (DAMPs) molecules and pathogen-associated molecular pattern (PAMPs) molecules which are recognised by specific toll like receptors (TLRs). Viral PAMPs include dsDNA, ssDNA, dsRNA and ssRNA and are recognised by intracellular TLRs on the endosome surface. The release of TAAs, in combination with the local cytokines and DAMPs such as heat shock proteins (HSP) and high mobility group box 1 (HMGB1) which are recognised by cell surface TLRs, activates natural killer (NK) cells and stimulates antigen presenting cell (APC) maturation, which in turn, triggers both CD4⁺ and CD8⁺ T Cells in the adaptive immune response by cross-presentation (56). Figure reproduced and adapted with permission from (56) created using BioRender.

Both cell death mechanisms as a result of OV infection are beneficial; however, they are also linked to some therapeutic hurdles. For example, intrinsic cell death is rapid and efficient in some settings, but elimination occurs only in cells directly infected with a virus. Therefore, delivering the virus to sites of tumour is of huge importance, and is a challenge that remains unsolved in the field. On the other hand, immunotherapy can entirely sterilize the tumour site, but it is much slower than intrinsic methods, and frequently, only shows clinical benefit in a small percentage of patients. Therefore, successful oncolytic virotherapy requires a fine balance between the two mechanisms of tumour cell death (22).

1.2.1 Classes of Oncolytic Viruses

There are a wide range of OVs in preclinical and clinical trials (Table 1.5). OVs can be characterised into three broad categories which consist of 1) wild-type (WT) viruses, which have natural oncotropism; 2) genetically modified viruses that have deletions within their genome, typically deletions within virulence genes, or tropism modifications; and 3) genetically modified viruses that express therapeutic transgenes.

Table 1.5: Comparison of Oncolytic Viruses (Table adapted with permission from 63)

Virus	Virus Type	Benefits	Limitations
Herpes Simplex virus	DNA	<ol style="list-style-type: none"> 1. Wide host-cell range. 2. Large number of nonessential genes that can be replaced with foreign DNA to enhance cytotoxicity. 3. Clinically available antiviral agents. 	<ol style="list-style-type: none"> 1. Systemic delivery may be limited by pre-existing immunity and hepatic adsorption.
Adenovirus	DNA	<ol style="list-style-type: none"> 1. Wide host-cell range. 2. Large amount of nonessential genes that can be replaced with foreign DNA to enhance cytotoxicity. 3. Possible to be produced at high titre (10^{12}). 4. Clinically available antiviral agents. 	<ol style="list-style-type: none"> 1. Coxsackie Adenovirus receptor variability in humans. 2. Systemic delivery may be limited by pre-existing immunity, hepatic adsorption, and toxicity.
Reovirus	RNA	<ol style="list-style-type: none"> 1. Wild-type virus causes mild to no disease. 2. Systemic delivery possible. 3. No clinically available antiviral agents due to its lack of definitive association with human disease. 	<ol style="list-style-type: none"> 1. Inability to enhance infection with foreign DNA/large transgenes.
Vaccinia Virus	DNA	<ol style="list-style-type: none"> 1. Wide host-cell range. 2. Large amount of nonessential genes that can be replaced with foreign DNA to enhance cytotoxicity. 3. Clinically available antiviral agents. 	<ol style="list-style-type: none"> 1. Inefficient systemic delivery. 2. Systemic delivery may be limited by pre-existing immunity, hepatic adsorption, and toxicity.
Myxoma virus	DNA	<ol style="list-style-type: none"> 1. Non-pathogenic in humans. 2. No clinically available antiviral agents due to its non-pathogenic nature in humans. 	<ol style="list-style-type: none"> 1. Infection relies on altered Akt signaling.
Measles virus	RNA	<ol style="list-style-type: none"> 1. Natural preference for tumour cells. 2. No specific clinically available antivirals. 	<ol style="list-style-type: none"> 1. Highly pathogenic. 2. Narrow tropism. 3. Systemic delivery may be limited by pre-existing immunity via vaccination.
Vesicular stomatitis virus	RNA	<ol style="list-style-type: none"> 1. Targets cancer cells with loss of interferon (IFN) responsiveness. 2. No specific clinically available antivirals. 	<ol style="list-style-type: none"> 1. Uncertain tumour-selective oncolytic effect. 2. Effects Cattle
Coxsackie Virus	RNA	<ol style="list-style-type: none"> 1. Natural preference for tumour cells 2. No specific clinically available antivirals. 	<ol style="list-style-type: none"> 1. Infection depends on the presence of specific receptor molecules.

Virus	Virus Type	Benefits	Limitations
Seneca Valley Virus	RNA	1. Non-pathogenic in humans 2. No clinically available antiviral agents due to its non-pathogenic nature in humans.	1. Mechanism of infection unclear. 2. Inability to enhance infection with foreign DNA.
Newcastle Disease Virus	RNA	1. Non-pathogenic in humans. 2. Targets cancer cells with loss of interferon responsiveness.	1. Unclear mechanism. 2. Not well studied.
Poliovirus	RNA	1. Oncolytic. 2. Clinically available antivirals.	1. Narrow tropism. 2. Pathogenic. 3. Difficult manipulation. 4. Systemic delivery may be limited by pre-existing immunity via vaccination.

1.2.1.1 Wild-type Viruses

Native or naturally occurring OV are replication-competent viruses that selectively infect and kill tumour cells without requiring genomic alteration, this is either due to the virus not causing clinical disease in humans or that strain of virus is weakly pathogenic and does not require genomic alteration for safety. Some WT OV include the Reovirus (RV), Newcastle Disease virus (NDV), and Vesicular Stomatitis virus (VSV). As discussed earlier, these viruses specifically target cancer by exploiting cellular phenotypic aberrations that occur in tumour cells, such as overexpressed surface attachment receptors, activated RAS or Akt, or via defective IFN pathways. One example is Reolysin, a WT RV that preferentially replicates in RAS-transformed cells. Reolysin has been in multiple clinical trials, including MM (69), malignant glioma (70), prostate cancer (71), metastatic melanoma (72) and solid tumours (71,73,74). In 2015, Reolysin was granted an orphan drug status by the US FDA for the treatment ovarian cancer, malignant glioma, pancreatic cancer, and fallopian tube cancer.

1.2.1.2 Genetically Modified Oncolytic Viruses

The development of molecular biology techniques and genetic editing technology has been used to optimise WT OV strains, this is normally performed to weaken viral pathogenicity, increase tumour selective infection and/or improve immunogenicity (75,76). OV can also be modified to insert exogenous therapeutic genes, most commonly this is either immune-stimulatory molecules to enhance immunotherapy, or delivery of therapeutic payloads (77). One example is Pexa-Vec, which is

a replication-competent Vaccinia virus (VV) which has a deletion in the thymidine kinase (TK) gene and has been modified to express granulocyte macrophage-colony stimulation factor (GM-CSF) (78). Pexa-Vec was studied in a phase IIb clinical trial in combination with best supportive care (TRANSVERESE Trial) in patients with advanced, unresectable hepatocellular carcinoma. Unfortunately, the trial failed as there was no difference between the two treatment arms and there was a high drop-out rate in the control arm which confounded assessment of response-based endpoints. Despite this, Pexa-Vec was generally well tolerated (79).

1.2.2 Clinical Experience and Safety of Oncolytic Viruses

Several viral families are being developed as OV's for a range of cancers, many of which have been investigated in early clinical trials (80). Concerns surrounding safety have always been associated with the use of viruses both WT and genetically modified, however numerous phase I/II clinical trials have been undertaken and have shown good safety profiles (80,81). All viruses used in the clinical trials are manufactured according to Good Manufacturing Practice (GMP), with the majority of clinical trials never reaching maximum tolerated dose (MTD). Reasons for this could be due to technical restrictions on producing high quantity virus titres or unclear dosing regimens, with no evident correlation between dose and efficacy or toxicity. For this reason, the majority of clinical trials focus on their primary outcome measure of safety and MTD (80). Common adverse events (AEs) are known to be mild flulike symptoms and local reaction at the injection site (81). Flulike symptoms manifested as fever, chills, myalgia, fatigue, nausea, diarrhoea, vomiting and headache (82–84), which can be managed with non-steroidal anti-inflammatories or by a pre-dose of paracetamol before OV delivery (85). Local reactions often manifest as pain, rash, erythema, peripheral oedema etc. (86,87). Other common AEs include anaemia, leukopenia, lymphopenia, neutropenia, thrombocytopenia, liver dysfunction and haematological abnormalities (88–91). Few OV's have caused severe AEs that harm patients' health (Table 1.6), and those that were induced could be managed by symptomatic treatment or treatment withdrawal, rarely causing severe damage to patients (reviewed in (92)).

Table 1.6: Severe Adverse Events reported with OV_s

Oncolytic Virus	Severe Adverse Events
HSV (93–97)	Severe hypotension Tachycardia Pleural Effusion Herpes virus infection Central nervous system symptoms (brain oedema, encephalitis, speech disorder) Severe liver dysfunction Pleural effusion Dyspnoea
Adenovirus (98–100)	Pleural Effusion Dehydration Hypokalaemia Severe liver dysfunction Sepsis
Pox Virus (85,101–103)	Severe haematological abnormalities Hypokalaemia Pancreatitis
Reovirus (104)	Severe neutropenia Severe diarrhoea Elevated liver enzymes Dehydration
Measles Virus (86,105)	Arthralgia Neutropenia Leukopenia Anaemia

Although some current clinical OV trials have led to severe AE in a few patients, which eventually subside after treatment withdrawal or pharmacological management, the long-term AEs and potential safety issues of OV_s remain unclear. One speculated long-term potential safety issue relates to viruses that remain latent in tissues, such as HSV-1 which remain latent in nerve tissue during natural infection, which has been proposed may induce severe neurological HSV infection long-term after oncolytic HSV administration (94). However, oncolytic HSV_s have the neurovirulent latency gene (ICP34.5) deleted so should not be able to grow within neurons or mediate a latent infection. To support this, there have been no preclinical or clinical reports of reactivation of latent HSV (106). Another issue is shedding and transmission of OV_s during therapy, which has been found with several OV_s, including HSV Adenovirus (Ad), RV and Poxvirus (reviewed in (107)).

Currently, there are only two genetically engineered OV_s approved for clinical use, Talimogene laherparepvec (T-Vec), a second-generation oncolytic HSV-1 armed with GM-CSF, which was approved in 2015 in the USA and Europe for melanoma (54); and H101, an *E1B*-deleted Ad, which was approved in 2005 in China for head and neck cancer and oesophagus cancer (66,108). Therefore, it is now abundantly clear that OV_s have shown antitumour efficacy. Despite rare severe AEs and/or mild AEs which disappear spontaneously or can be controlled, OV_s are considered generally safe. As a result, a paradigm shift has now occurred where their use has been accepted in clinical practice in some cancers. Therefore, it is now more likely that OV_s will be investigated and if found efficacious, they will be approved, and eventually accepted into mainstream clinical use for a wider range of cancers.

1.3 Oncolytic Virotherapy in Multiple Myeloma

OV_s have been exploited for their antitumour effects across a range of solid and haematological malignancies. In MM specifically, anecdotal evidence of viruses reducing MM tumour burden in a human patient was first reported in a single case study in 1987 that suggested VV can (at least transiently) reduce systemic tumour burden in a MM patient (52). Since then, pre-clinical studies have focused on a range of RNA and DNA viruses which have shown pre-clinical efficacy in MM, with infection resulting in the rapid elimination of MM cells through a variety of mechanisms (Table 1.7).

Table 1.7: Oncolytic viruses used preclinically for myeloma treatment

Virus	Mechanism of MM Specificity	Mechanism of MM-cell killing	Potential toxicity	Potential therapeutic uses
Measles Virus (109–113)	Overexpression of viral receptor CD46	Lytic viral replication	Low	Treatment of established disease
Vesicular Stomatitis Virus (114–119)	Defects in interferon responses	Lytic viral replication Inhibition of DNA synthesis	Moderate	Treatment of established disease
Reovirus (120–124)	Overexpression of viral receptor (JAM-1)	Lytic viral replication Apoptosis Autophagy Unfolded protein response	Low	Treatment of established disease Purging of ASCT samples
Adenovirus (125–129)	Unknown	Lytic Viral Replication	Low	Treatment of established disease
Vaccinia Virus (130–133)	Engineered	Lytic viral replication	Moderate	Treatment of established disease
Myxoma virus (134–139)	MM-specific binding (unknown receptor)	Induction of apoptosis	Low	Treatment of established disease Purging of ASCT samples
Bovine Viral Diarrhoea Virus (140)	Overexpression of viral receptor CD46	Induction of apoptosis	Low	Treatment of established disease
Newcastle Disease Virus (71)	Unknown	Lytic viral replication Induction of apoptosis	Low	Treatment of established disease
Rotavirus (141)	Unknown	Lytic viral replication	Low	Treatment of established disease

1.3.1 Preclinical Studies with Vaccinia Virus in Multiple Myeloma

VV is a large dsDNA virus that belongs to the *Poxviridae* family, derived from the original cowpox or horsepox virus. The historical use of VV as a smallpox vaccine has proven clinical safety in humans. Therefore, attenuated VV (TK and vaccinia growth factor deleted) has been investigated preclinically in MM. VV was found to infect and replicate in a range of myeloma plasma cell (MPC) lines resulting in decreased viability and apoptosis *in vitro*. In disseminated tumour xenografts treated with intravenous (I.V) VV, resulted in significant tumour reduction and improved survival compared to controls. This suggests future clinical potential (131). More recently, a TK-deleted VV strain was engineered to express one of two antitumour factors, miR-34a (VV-miR-34a) and Smac (VV-Smac),

with the former inhibiting several oncogenic processes and the later involved in apoptosis induction. Both viruses showed increased efficacy *in vitro* and *in vivo* compared to parental virus, but combination of both viruses showed the most efficacy showing synergy and induction of apoptosis through the expression of the caspase pathway (132). The same group also modified a TK-deleted VV virus to express beclin-1 (OVV-BECN1), an essential autophagy protein linked to multiple processes including tumour suppression. OVV-BECN1 showed efficacy *in vitro* and *in vivo* in a MPC line and a leukemic cell line but did not cause cytotoxicity in peripheral blood mononuclear cells (PBMCs). OVV-BECN1 induced autophagy and not apoptosis in MM cells, through activation on sirtuin1 (SIRT1), a member of class III histone deacetylases, which following OVV-BECN1 infection, deacetylated LC3, contributing to the induction of autophagy (133).

1.3.2 Preclinical studies with Myxoma Virus in Multiple Myeloma

Myxoma virus (MYXV) is a non-segmented dsDNA and has a strict tropism for rabbits and hares, therefore, does not cause human disease. Whilst MYXV does not infect healthy non-malignant human cells, MYXV has been shown to infect a variety of cancer cell types. Therefore, MYXV has been investigated preclinically in MM. MYXV has been found to induce rapid oncolysis in MPC lines, this is dependent on caspase-8 mediated apoptosis by inhibiting ATF4 expression during the unfolded protein response (134,136,142). *In vivo* in a disseminated xenograft model of MM, I.V injection of MYXV resulted in rapid debulking of tumour (70-90%) within 24 hours, whilst sparing the haematopoietic BM niche, it's important to note that mice had a low level of tumour burden (~20%) and these effects may not have been as pronounced in a more advanced stage of disease. Additionally, MYXV induced an anti-MM CD8⁺ T cell response which resulted in a significant but small increase in overall survival by approximately 3 days (134). Due to MYXV rapid induction of oncolysis, it has been proposed that MYXV may be an effective purging strategy for ASCTs. Arming murine allogeneic BM containing a mouse MM cell line with MYXV and transplanting into recipient mice dramatically ablated pre-seeded residual MM *in vivo* (138). Additionally, MYXV was able to eliminate CD138 positive (+) MM cells from patient BM samples within 24 hours of treatment. However, only 3 patients were used

in this experiment, whether the same effects are seen across a wider range of heterogeneous patients' needs to be explored (142). More recently, autologous murine BM carrier leukocytes, pre-armed with MYXV were therapeutically superior to MYXV armed murine PBMCs or free virus. Additionally, when survivor mice were rechallenged with the same MPC line, the mice did not develop tumour as the mice had acquired immunity against the MPC line due to previous MYXV treatment (139).

1.3.3 Preclinical Studies with Reovirus in Multiple Myeloma

RV is a dsRNA virus of the *Reoviridae* family, with the human type 3 Dearing strain being developed for oncolytic virotherapy. RV showed sensitivity in MPC lines and *ex vivo* tumour specimens (120,122). Mechanistically, this has been shown to occur via apoptosis (143), however, upregulation of autophagy genes is also seen *in vitro* (120). *In vivo*, RV established no effect on human CD34⁺ stem cells, and demonstrated complete eradication of MM cells, preventing relapse and improved survival in mice (144). Reolysin; a proprietary formulation of WT reovirus; combined with BTZ decreased tumour burden and bone disease in xenografts with no AEs (145). Disappointingly, the above authors did not show viral specificity in the tumour or surrounding healthy tissue, immunohistological analysis of fixed tissues would be needed.

More recently, RV has been shown to increase PD-L1 expression in MPC lines *in vitro* and *in vivo*, this increase wasn't observed when UV-inactivated RV was used, therefore, live replicating RV was needed to increase PD-L1 expression. When RV was given in conjunction with anti-PD-L1 therapy in the syngeneic 5TGM1 murine model of MM, combination therapy enhanced anti-MM efficacy by decreased tumour burden and enhanced survival compared to monotherapies. Therefore, RV and PD-1/PD-L1 targeted therapy could be beneficial for MM patients (146). RV has also been combined with BTZ preclinically for MM therapy. *In vitro* RV and BTZ showed synergistic interactions in BTZ-resistant cell lines. *In vivo*, in a syngeneic Vk*MYC BTZ resistant immunocompetent transplantable MM murine model, enhanced anti-MM activity such as decreased tumour burden and improved overall survival was observed when RV was used in combination with BTZ. Mechanistically, BTZ augmented RV replication in MM cells and tumour-associated endothelial cells as assessed by increased RV protein

levels resulting in enhanced viral delivery and subsequently enhanced anti-MM activity. The study also showed enhanced anti-MM immune responses following combination treatment such as increased CD3⁺ T cell tumour infiltration, increased NK cell tumour infiltration, increased PD-L1 expression in tumour and decreased tumour infiltrated T-regs and tumour-associated macrophages (TAMs) (124). RVs was also shown to reduce MM tumour burden and MM bone disease *in vivo* and augment anti-MM immune responses *in vitro*. In a 5TGM1 syngeneic MM murine model, RV treatment increased NK and CD8⁺ T Cells numbers and activation, and upregulated effector-memory CD8⁺ T cells. Additionally, the study found that coculture of MM cells with bone-marrow stromal cell (BMSC) lines (HS-5 and HS-27) were able to induce resistance to MPC RV oncolysis and bystander cytokine killing in some cell lines. However, BMSC lines were not able to protect MPCs from RV-activated NK cells and MM-specific cytotoxic T cells (147). This suggests that induction of anti-MM immune responses can overcome BMSC-mediated resistance, therefore may be a useful treatment modality against relapsed/refractory MM or during plateau/remission phase to target MRD that may be protected from conventional therapy by BMSCs.

1.3.4 Preclinical Studies with Measles Virus in Multiple Myeloma

Measles virus (MV) is an enveloped negative-sense ssRNA virus in the family *Paramyxoviridae*. The most studied strain is the attenuated Edmonston strain (MV-Edm), which has mutations in two accessory proteins (C and V) leading to tumour selectivity, genetic stability and is non-transmissible (148). MV-Edm effectively lysed MPCs, whilst having no effect on peripheral blood lymphocytes *in vitro*. *In vivo*, intratumoral MV-Edm treatment of subcutaneous MM xenograft mice resulted in all tumours regressing. Following I.V administration, there was significant tumour response and 1 mouse had complete tumour regression (109). MV-Edm was further modified to encode human thyroidal sodium iodine symporter (MV-NIS). Infection of MPC lines with MV-NIS showed similar oncolysis and were shown to take up radioiodine *in vitro*. Three subcutaneous xenograft murine models of MM were tested, two MV-sensitive and one MV-resistant. The two MV-sensitive xenografts regressed completely after one I.V dose of MV-NIS. The MV-resistant xenograft was unresponsive to MV-NIS

infection alone, but when combined with iodine-123 (123I), resulted in enhanced tumour regression compared to MV-NIS alone, as well as non-invasively tracking MV spread *in vivo*, a major advantage (111). To better target MV to MM, researchers mutated the H protein of a MV variant, so it lacks the ability to bind to its receptors CD46 and SLAM, which is also expressed on B cells, T cells and monocytes. Hummel *et al.*, (2009) attached a single chain variable fragment (scFV) based on a mouse mAb known as Wue-1. Wue-1 binds to CD138 which is expressed on healthy plasma cells, primary MM cells and lymphoblastic lymphoma cells. MV-Wue propagated efficiently in primary MM cells and specifically infected and killed primary MPCs by apoptosis while CD138 negative (-) cells were untouched. Normal MV was shown to infect and kill both CD138⁺ and CD138⁻ cells, however this contradicts the previous research. MV-Wue was found to bound to mature, healthy or malignant B cells and plasma cells without discrepancy. MV-Wue infecting healthy plasma cells could be a concern. However, in lymphoma patients, the widespread use of the well tolerated anti-CD20 mAb Rituximab causes long lasting B cell depletion after administration. Therefore, eradicating plasma cells after MV-Wue administration should not generate toxicity problems (149).

1.3.5 Preclinical Studies with Vesicular Stomatitis Virus in Multiple Myeloma

VSV is a member of the family *Rhabdoviridae*, VSV is an enveloped negative-sense ssRNA virus. VSV commonly infects livestock animals, but can infect humans causing flu-like illnesses, however, infection is limited to those in direct contact with infected animals. Therefore, there is a lack of a human reservoir for VSV, making it an attractive candidate as the majority of the population will be negative for VSV anti-viral antibodies (150). Preclinically, VSV has demonstrated effectiveness against MM *in vitro* and *in vivo*. VSV was engineered to express NIS, allowing for treatment with radioactive iodine and to track virus via imaging. VSV-NIS was able to replicate to high titres in MPC lines and cause oncolysis in MPC lines and primary MM cells *in vitro*. *In vivo* in subcutaneous xenograft MM model, VSV-NIS showed high intratumoral viral replication which resulted in tumour regression. In the 5TGM1 syngeneic murine model, with either subcutaneous or orthotopic MM tumours, VSV-NIS had enhanced tumour regression and survival when it was combined with radioactive iodine (151). To

enhance VSV oncolysis and improve safety, VSV-NIS was engineered to express IFN- β . VSV-IFN- β -NIS significantly improved anti-MM responses and prolonged survival compared to treatment with control VSV in subcutaneous and disseminated 5TGM1 syngeneic models of MM (118,152).

1.3.6 Clinical Trials with Oncolytic Viruses in Multiple Myeloma

Thus far, pre-clinical success to date with MV, RV and VSV has led to early-phase clinical trials in MM.

The first clinical trial to be completed and published using an OV in MM was a phase I clinical trial with systemically delivered RV (Reolysin) in patients with relapsed MM. The clinical trial identified no dose-limiting toxicities; however, only modest efficacy was seen, with the best clinical outcomes being stable disease (observed in 25% of patients) (69). Consequently, RV does not seem to be effective as a monotherapy, therefore, combination treatments might be needed to increase efficacy. Interestingly, correlative studies from this trial demonstrated that patients' MM cells did not significantly express JAM-1 (RV entry receptor), therefore, it was hypothesised that there was insufficient viral entry to mediate tumour cell killing. JAM-1 expression has been shown to determine response to RV in MM, with low JAM-1 expression conferring RV resistance (123). Research has shown histone deacetylase inhibitors (HDACIs) or the proteasome inhibitor BTZ, can sensitise MM cells to RV infection by increasing the expression of the viral receptor JAM-1 (123,153). Currently, there are two active clinical trials using RV for MM therapy; NCT03015922, a phase I trial in which Reolysin is being tested in combination with IMiDs Len or Pom in relapsed MM, and NCT02514382, a phase Ib trial in which Reolysin is being tested in combination with BTZ and Dexamethasone in relapsed/refractory MM. Interim results from the latter have demonstrated that whilst no dose limiting toxicities occurred, only half of evaluable patients (n=3) had stable disease after treatment (154).

A phase I clinical trial with systemically delivered MV (MV-NIS) in patients with recurrent or refractory MM was published in 2017. The trial identified some grade III and IV haematological toxicities, despite this, whilst this study was not powered for analysis of efficacy, some impressive results were obtained. One patient underwent complete disease regression following therapy, whilst other patients in the study had variable and transient drops in their serum free light chains (105). However, the existence

of anti-MV antibodies in large proportion of patients who have been vaccinated against the virus potentially negates its oncolytic potential and limits its clinical use. In agreement with this, further investigation was done post clinical trial which found that the patient who achieved complete remission following MV-NIS had a low baseline titre of anti-MV antibodies, high baseline counts of both MV-reactive and TAA-reactive T cells and a high mutational burden. At the time of this study being published the authors state the patient has remained disease free having no systemic MM. However, the patient has had two focal relapses at 9- and 30-months post MV therapy, which were successfully treated with radiotherapy. Therefore, the authors speculate that the long-term remission observed in this patient is as a consequence of sustained immune control of residual MM, driven by their high mutational burden, causing more expression of TAAs that were targeted by cytotoxic T cells (155). A phase II clinical trial is being conducted with MV-NIS in combination with cyclophosphamide in MM patients (NCT02192775). The trial involves administering a single I.V dose of MV-NIS followed by a 4-day course of cyclophosphamide. The trial has been completed but data has not been published yet. Preclinical results with VSV have led to the establishment of an early phase clinical trial (NCT03017820) with VSV-IFN β -NIS in patients with haematological malignancies, including relapsed MM. The trial is currently active and recruiting.

It is clear that a large number of viruses have been shown to specifically eliminate MM cells preclinically, however, the couple of clinical trials performed to date do not seem to translate this efficacy to a large cohort of patients. Therefore, if the preclinical efficacy of OV is to translate to clinical trials, more preclinical work needs to be performed to better understand viral-host interactions, this will be discussed in section 1.5. With no single OV standing out as a clear front runner for virotherapy for MM, our research group hypothesises oncolytic Ads could be a useful treatment modality for MM therapy, the reasons for this are described in section 1.4.

1.4 Adenovirus

1.4.1 History

Ads were first identified in the 1950s and ever since have been intensively studied for oncolytic virotherapy (156). The Adenoviridae family can be divided into 4 genera and 6 species (157), and thus far, 84 serotypes of human Ads have been identified (158,159). Ads have a wide range of hosts and are found across all vertebrates, from fish to humans (160). Generally, Ads are endemic in most parts of the world and have low pathogenicity in humans. However, Ads can cause clinical disease (Table 1.8), but most occur in children younger than the age of 5 years and are generally self-limiting illnesses. (158,161).

Table 1.8: Subgroups of Human adenovirus (Table reproduced with permission from 163).

Subgroup	Serotype	Disease
A	12, 18, 31	Meningoencephalitis
B	3, 7, 11, 14, 16, 21, 34, 35, 50	Acute Respiratory Disease
C	1, 2, 5, 6	Acute febrile pharyngitis
D	8, 9, 13, 15, 17, 19, 20, 22-30, 32, 33, 36-39, 42-49, 51	Epidemic Keratoconjunctivitis
E	4	Pneumonia
F	40, 41	Gastroenteritis
G	52	Gastroenteritis

The most widely studied Ad is serotype 5 (Ad5). Ad5 has been extensively used as a platform for gene therapy and oncolytic virotherapy (160), therefore, the following literature review will be focused on Ad5. Ad5s are large, non-enveloped, icosahedral viruses approximately 70-100 nm containing dsDNA genome of approximately 36KBP. The Ad5 virion is composed of a protein capsid made up of 252 capsomeres, and a nucleoprotein core that contains the linear dsDNA viral genome and internal proteins (Figure 1.4) (158).

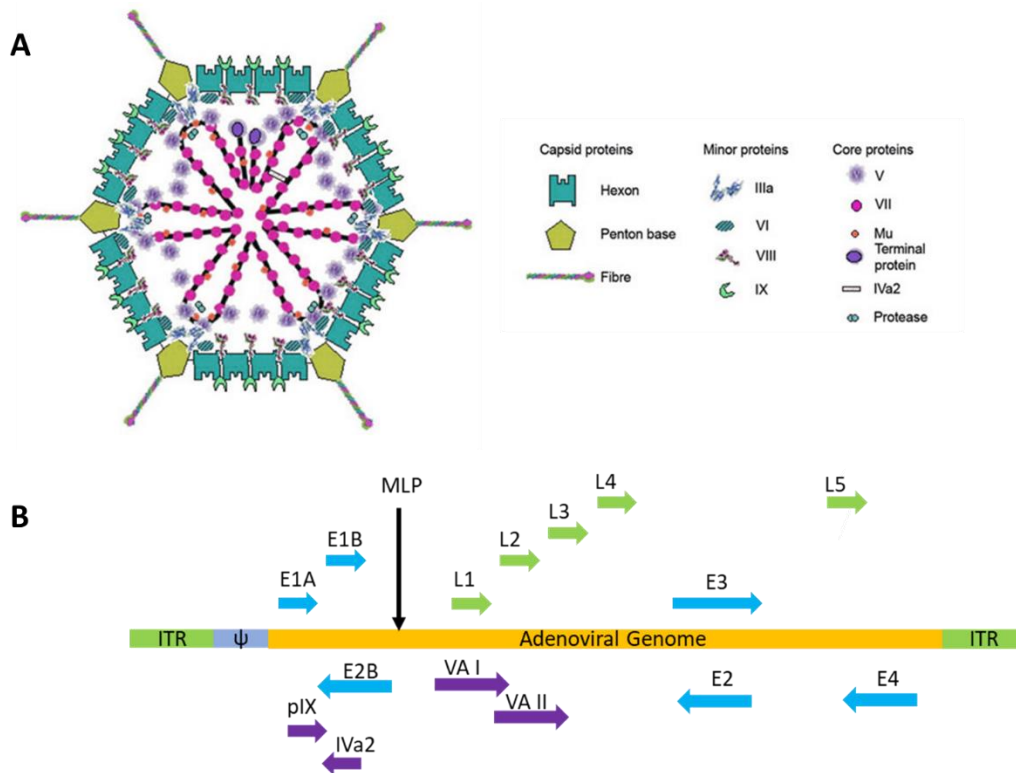


Figure 1.4: Virion structure and schematic representation of Ad 5 genome:

(A) Virion Structure (Figure reproduced from 165) The virion is composed of a protein capsid made up of 252 capsomeres, and a nucleoprotein core that contains the linear dsDNA viral genome and internal proteins (158). The linear dsDNA is associated with three virus coded polypeptides V, VII and Mu (164,165), as well as a 55kDa terminal protein that is attached at the 5' end of the linear dsDNA (166). The capsid has an icosahedral shape, consisting of 240 hexon components and 12 pentons per virus particle. Each penton contains a base plate with a projecting fiber containing arginine-glycine-aspartic acid (RGD) motif, and a knob domain at each penton base (167,168). **(B) Ad5 Genome** (Figure reproduced from 171). The diagram represents the Ad5 genome with arrows illustrating the location and orientation of gene transcription. The genome termini are comprised of inverted terminal repeat (ITR) sequences incorporating the viral origin of replication. Also shown is the packing domain (ψ) involved in virus genome packing into capsids. There are six early RNA polymerase II transcription units, E1A, E1B, E2A, E2B, E3 and E4, which generate several mRNA transcripts by differential splicing and alternative start codon usage. The major late promoter (MLP) drives expression of a long transcript that produces the late mRNAs L1-L5 through alternative splicing and differential polyadenylation. pIX and IVa2 are intermediate genes. The small virus-associated (VA) I and II RNAs are synthesised by RNA Pol III and act to regulate mRNA translation (169,170).

1.4.2 Adenovirus Life Cycle

The Ad5 life cycle is in two phases, separated by the onset of viral DNA replication. The early phase, which lasts 5-6 hours, starts with initial attachment to host cells and is mediated by a high affinity interaction of the fibre knob domain with the Coxsackie Adenovirus receptor (CAR) (171). This triggers secondary lower affinity interaction with RGD motif and cellular $\alpha\beta$ -integrins (Figure 1.5) (172). In combination, these interactions lead to a cooperative, irreversible interaction of the capsid with the cell surface (173). Additionally, interaction between Ad5 capsids and heparin sulphate proteoglycan (HSPG) has also been reported (174). Once bound to the cell surface, integrin-mediated endocytosis occurs, resulting in the detachment of the viral fibres into clathrin-coated vesicles. The acidic environment of the endosome causes the virion to dissociate and release vertex proteins including pVI (172). Once in the cytosol, the partially disassembled virion is transported along microtubules and interacts with the motor protein, dynein, to facilitate translocation into the nucleus (175). When the capsid reaches the nucleus, it forms a stable interaction with the nucleus resulting in capsid uncoating (176,177). Once the Ad genome enters the nucleus and the components for adenoviral DNA replication are ready, the late phase can start. Ad5 expresses at least 36 major proteins (Table 1.9), which ultimately results in the assembly of progeny virions (170). Virions are released by viral induced cell lysis, which is facilitated by Ad death protein (ADP) which promotes lysis of the infected cell (178). This lytic replication life cycle is favourable for oncolysis, when compared to some enveloped viruses, which complete replication by budding from intact, live, host cells (179).

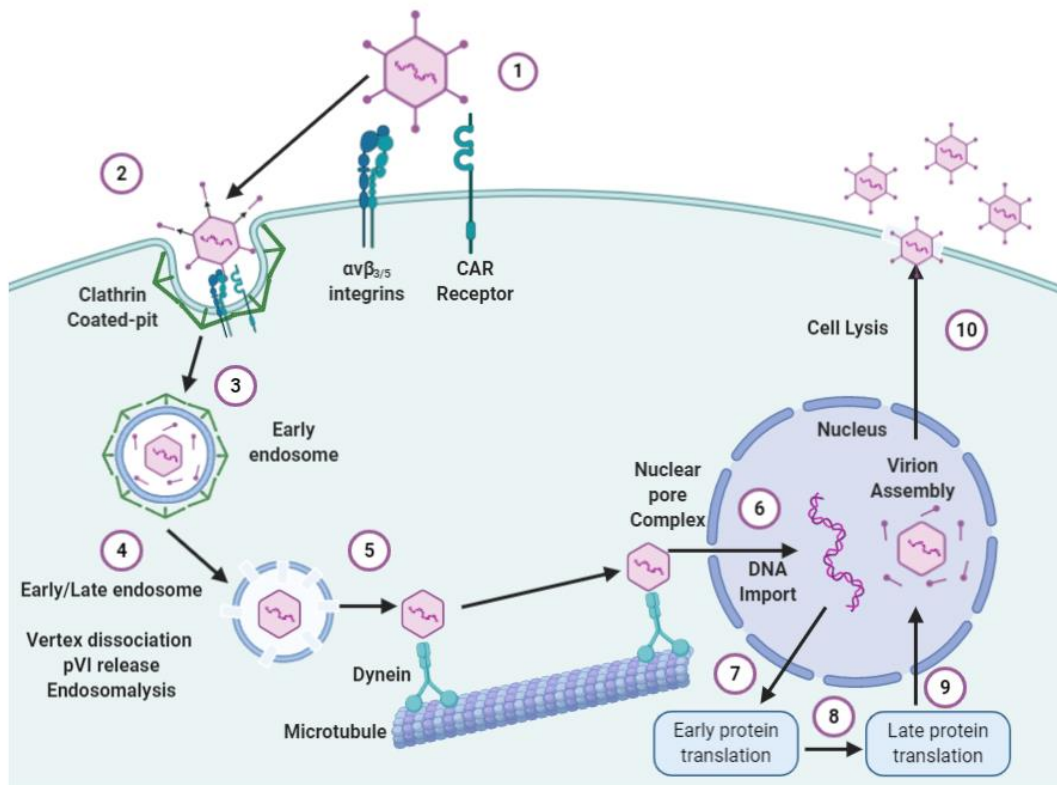


Figure 1.5: The cell entry pathway of adenovirus:

(1) The Ad5 fibre attaches to the primary receptor, which for most cell types is the Coxsackie-adenovirus receptor (CAR). (2) After attachment clathrin-mediated endocytosis occurs, which is facilitated by the interaction of the penton base with α_v integrins. (3) The virion enters the cell and is contained within the early endosome, (4) the low pH environment of the endosome makes the virion start to dissociate and release the vertex proteins, including pVI, which has been implicated in endosomal membrane disruption, which releases the virion from the endosome (5). The partially disassembled virion is transported along microtubules via the microtubule motor protein dynein to the nuclear pore complex. Intracellular trafficking towards the nucleus is also mediated by activation of the cAMP-dependent protein kinase A (PKA) and p38/MAPK signalling pathways (180). (6) At the nuclear pore the viral DNA is imported into the nucleus with the help of hexon, viral core protein VII, histone H1, import receptor transportin 1, HSP70 and importin- α (172,173,176) (7). Adenoviral replication occurs inside the nucleus. First, early viral genes are transcribed and translated. This starts with the E1A gene, which is constitutively transcribed, followed in order by E1B, E2, E3 and E4. Viral DNA synthesis activates three delayed early viral promoters IX, IVa2 and E2 late (8) This results in the transcription and translation of late genes, L1-L5 which are alternative splice units from a single transcription unit from the major late promoter (MLP). Late proteins are involved in the production and assembly of the virion capsid (181). (9) Virion assembly occurs within the nucleus (10) which are then released by viral induced cell lysis. Figure created using biorender.

Table 1.9: Ad5 proteins and their function

Protein	Gene	Function(s) during infection	References
E1A12S	E1A	<ul style="list-style-type: none"> • Induction of host DNA synthesis • Transcriptional regulation of genes involved in cell-cycle, apoptosis, inflammation, protein translation • Regulation of protein stability through interaction with the 26S proteasome • Induction of apoptosis 	(182–184)
E1A13S	E1A	<ul style="list-style-type: none"> • Transcriptional activation of host and viral genes 	(182)
E1B19K	E1B	<ul style="list-style-type: none"> • Inhibition of extrinsic and intrinsic apoptosis 	(184,185)
E1B55K	E1B	<ul style="list-style-type: none"> • Inhibition of DNA-damage and response • Inhibition of p53-dependent apoptosis • Late viral mRNA nuclear export and translation • Blocking of host mRNA nuclear export and protein synthesis 	(183,184)
DBP	E2A	<ul style="list-style-type: none"> • Replication and elongation • Transcriptional regulation • DNA recombination • Virus assembly 	(170,183)
Pol	E2B	<ul style="list-style-type: none"> • DNA polymerisation/replication 	(170)
pTP	E2B	<ul style="list-style-type: none"> • DNA replication (serves as primer) 	(170)
E3-12.5K	E3	<ul style="list-style-type: none"> • Unknown 	
E3-11.6K (ADP)	E3	<ul style="list-style-type: none"> • Cell Lysis 	(186)
E3gp19K	E3	<ul style="list-style-type: none"> • Inhibition of MHC class I cell surface expression by binding and retaining the heavy chain in endoplasmic reticulum (ER) • Inhibition of the processing of peptides presented by class I MHC • Sequestration of natural killer cell ligands 	(170,187,188)
E3-6.7K (CR1α)	E3	<ul style="list-style-type: none"> • Inhibition of extrinsic apoptosis through TRAIL-R2 internalisation and degradation in lysosomes • Directs E3gp19K to ER 	(189–191)

Protein	Gene	• Function(s) during infection	References
E3-10.3K (RIDα)	E3	<ul style="list-style-type: none"> • Inhibition of extrinsic apoptosis through death receptor internalisation and degradation in lysosomes • Inhibition of TNF-induced secretion of arachidonic acid, production of chemokines and NF-κB signal transduction 	(163,187)
E3-14.9K (RIDβ)	E3	<ul style="list-style-type: none"> • Inhibition of extrinsic apoptosis through death receptor internalisation and degradation in lysosomes • Inhibition of TNF-induced secretion of arachidonic acid, production of chemokines and NF-κB signal transduction 	(163,187)
E3-14.7K	E3	<ul style="list-style-type: none"> • Inhibition of TNFα-induced secretion of arachidonic acid 	(163,187)
E4orf1	E4	<ul style="list-style-type: none"> • Growth induction through PI3K/mTOR pathway activation 	(183)
E4orf2	E4	<ul style="list-style-type: none"> • Unknown 	
E4orf3	E4	<ul style="list-style-type: none"> • Re-organisation of PML bodies • Inhibition of DNA-damage and repair response • Facilitation of S-phase DNA replication 	(183)
E4orf4	E4	<ul style="list-style-type: none"> • Growth induction through PI3K/mTOR pathway activation • Disruption of PP2A functions 	(183)
E4orf6/7	E4	<ul style="list-style-type: none"> • E4 Inhibition of DNA-damage and repair response • Inhibition of NHEJ DNA repair • Late viral mRNA nuclear export and translation • Blocking of host mRNA nuclear export and protein synthesis Viral DNA replication 	(183)
E4-34K	E4	<ul style="list-style-type: none"> • Unknown 	
pIVa2	IVa2	<ul style="list-style-type: none"> • DNA encapsidation/packing • Activation of late viral gene transcription 	(157,170)
pIX	IX	<ul style="list-style-type: none"> • Cementing of virion structure Stabilization of capsid 	(170)
Hexon (pII)	L3	<ul style="list-style-type: none"> • Formation and structure of the virion Binding of coagulation factors 	(157,166)

Protein	Gene	• Function(s) during infection	References
Penton (pIII)	L4	<ul style="list-style-type: none"> • Cell Attachment via integrins • Virus internalisation and release from endosome • Formation and structure of the virion • Stabilisation of the capsid 	(170)
Fiber (pIV)	L5	<ul style="list-style-type: none"> • Cell attachment via CAR and HSGAG • Blood factor attachment • Formation and structure of the virion 	(166,170)
23K protease	L3	<ul style="list-style-type: none"> • Cleavage of precursors to produce the mature structural proteins • Virion assembly Capsid uncoating Facilitation of cell lysis 	(166,170)
22K	L4	<ul style="list-style-type: none"> • DNA encapsidation/packaging 	(166)
33K	L4	<ul style="list-style-type: none"> • Formation and structure of the virion 	(157)
100K	L4	<ul style="list-style-type: none"> • Formation and structure of the virion • Blockage of protein translation initiation 	(157,183)
Protein IIIa	L1	<ul style="list-style-type: none"> • Cementing of Virion structure 	(157,170)
Protein V	L2	<ul style="list-style-type: none"> • Bridging of viral core and capsid • Possible role in revealing viral DNA for replication and transcription 	(166)
Protein VI	L3	<ul style="list-style-type: none"> • Cementing of virion structure • Disruption of endosomal membrane Virus maturation 	(157,166,170)
Protein VII	L2	<ul style="list-style-type: none"> • Formation and structure of the virion DNA encapsidation • Nuclear import of viral DNA Reduction of early transcription 	(157,166,170)
Protein VIII	L4	<ul style="list-style-type: none"> • Cementing virion structure 	(157,170)
μ or Mu (polypeptide X)	L2	<ul style="list-style-type: none"> • Cementing of virion structure • Precursor in modulating expression from E2 DNA packaging 	(157,170)
52/55K	L1	<ul style="list-style-type: none"> • DNA encapsidation 	(166,170)

Typically, infection of epithelial cells results in a lytic life cycle, however, Ad5 and other group C Ads, can cause persistent and latent infections in lymphocytes (192–194). Therefore, infection with subgroup C Ads appears to be a two-step process characterised by acute replication in epithelial cells, followed by persistent nonlytic infection of lymphocytes. This has been reported to occur mainly in mucosal-associated lymphoid tissues, in particular the T-lymphocyte population (193,195). It is not clear whether latent infection can occur in B cells, particularly plasma cells, which could hinder the use of Ads for MM. Latent infection has been found *in vitro* in B cell lines (Ramos & BJAB: Epstein bar virus negative Burkitt's lymphoma) (195) and in a B cell lymphoma patient (196). A possible mechanism for latent infection has been proposed which implicates ADP. A study showed lymphocytic cell lines with productive lytic infection had high ADP expression levels, whilst lymphocytic cell lines with latent infection had low-level ADP expression. Deletion of ADP converted lytic infection to a persistent infection in lymphocytes, however overexpression of ADP did not convert persistent infection to lytic infection, the authors suggested the latter may be due to levels of ADP not being sufficient to induce cell death, or that ADP death-promoting activity is inhibited in these cells (197). However, the former indicates that the downregulation allows for the virus to persist in some cells that typically exhibit lytic infection, but this was not the case in A549 cells (lung carcinoma epithelial cells). Therefore, it seems there are additional factors which contribute to the switch between lytic infection and persistent infection, and many oncolytic Ads have a deletion in ADP (E3) to be able to insert transgenes and are able to cause lytic infection (discussed below in section 1.4.3).

1.4.3. Oncolytic Adenoviruses as Therapeutic Tools

1.4.3.1. Tumour Specificity

Ad5s make good candidates for oncolytic virotherapy due to several characteristics, including a naturally lytic life cycle, highly efficient replication which can produce high titres (up to 10^{13} pfu/mL), easy to engineer genome, ability to retarget cell tropism, and lastly can infect a broad range of cell types including both dividing and quiescent cells (198,199). The latter is due to the Ads promoting the host cell into the G₁ phase of the cell cycle by binding to Rb via the immediate-early protein E1A and releasing the transcriptional factor E2F (200,201). To improve the safety of oncolytic Ads, multiple tumour targeting strategies have been identified (198).

Ad5 vectors for transgene delivery are usually modified in specific regions, such as E1, E2A, E3 and E4 genes (202). E1, E2A and E4 genes are essential for vector replication. Vectors with deletions in the above genes are replication-defective, however, they can still induce a strong host immune response. To increase vector capacity, the dispensable E3 gene is deleted. In first generation adenoviral vectors, the E1 gene is deleted and replaced with the transgene, but the packaging capacity is limited (8.2kb) (203). Second generation adenoviral vectors have deletions in E1, E2 and E3 or E4 genes, accommodating larger transgenes (up to 10kb) and reducing the possibility of reversion to replication competent Ad (202).

However, for cancer therapy, unlike gene therapy, conditionally replicating Ads (CRAds) are engineered to allow Ads to selectively replicate in malignant cells. One of the first strategies was the generation of a E1B-55K deleted Ad mutant, Onyx-015 (204,205). E1B-55K, is a potent inactivator of p53, thus prevents premature apoptosis (206). Therefore, infection of E1B-55K deleted Ads in healthy cells should allow for p53 activation and apoptosis, stopping the virus life cycle. In contrast, in tumour cells harbouring dysfunctional p53, the virus life cycle should be supported (205). Despite p53 being mutated or deleted in almost every cancer type (207), the rates vary among different cancer types (208,209). For MM, p53 mutation is a rare occurrence in newly diagnosed MM, around 3% (210–213), however, the rate of p53 mutation increases as disease progresses (214). Therefore, the

efficacy of E1B-55K deleted Ads may be low in MM. However, E1B-55k deleted Ads have been shown to be independent from the p53 tumour status (215,216), replicating in tumour cells that can compensate for those functions of E1B-55K required for effective virus production, such as viral mRNA nuclear export (217).

Another strategy is to delete the retinoblastoma-binding site in E1A (referred to as Delta-24) (218). The replication essential E1A protein inactivates retinoblastoma protein (pRB) leading to the release of the transcription factor E2F, resulting in cell cycle activation and viral replication (Figure 1.6). Therefore, replication of Delta-24 in healthy cells is halted, because of its inability to release E2F. However, in tumour cells with impaired pRb function, Delta-24 can replicate. Approximately 25% of tumours have pRb mutations, but pRb can be functionally inactivated by overactivation of D-type cyclins (219,220). Another mutation in the E3/19K protein (truncating insertion, T1), allows E3/19K to transfer to the plasma membrane which enhances virus release (221). Therefore, the T1 mutation may be a useful addition to a tumour-selective Ad-based therapy (222,223).

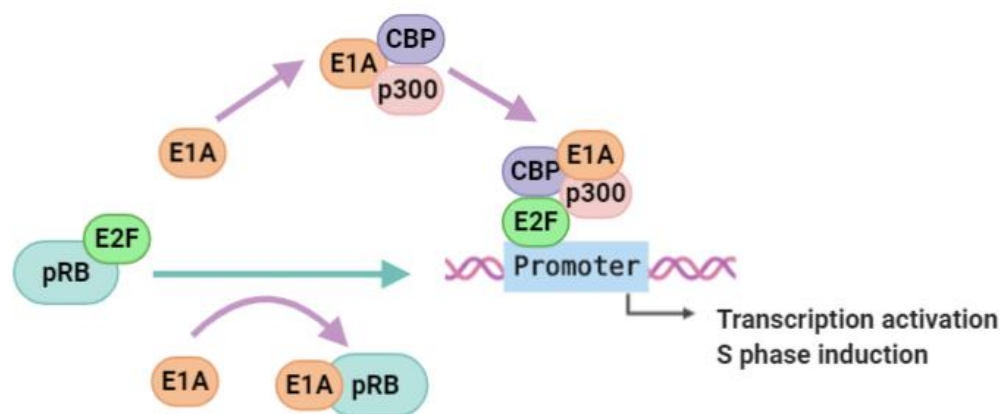


Figure 1.6 Schematic representation of E1A-mediated regulation of the cell cycle:

The E1A adenoviral protein promotes S-phase induction by binding to pRb to release E2F so that viral DNA can be replicated. E1A also induces S-phase induction by binding to p300 and CBP which activates transcription by binding to transcription factors (224). Figure created using biorender.

A different approach is to utilise tumour-selective transcriptional control of E1A (205,225). Various mechanisms of such transcriptional retargeting have been successfully established using tumour specific promoters including α -fetoprotein (226), prostate-specific antigen (PSA) (227–229), and MUC₁/DF (230). Therefore, viral gene expression and replication can only be achieved in those tumours which activate these transgenic promoters (199). These tumour-selective replicating Ads showed efficient lysis of various cancer cell lines *in vitro* and were able to inhibit the growth of corresponding tumours in xenograft models *in vivo*. Disadvantages of this approach are heterogeneity of tumour tissue with regard to the transcriptional activity of the used promoters and significant promoter background activity in healthy cells providing E1A levels sufficient for the onset of viral replication (205). Therefore, to address this issue, attempts have been made to exploit pan-cancer gene expression using promoters for human telomerase reverse transcriptase (hTERT) which is expressed in >90% of cancers (205,231–236), or cyclooxygenase-2 (237). Alternatively, promoters containing hypoxia-responsive elements have been employed (238–240). Clearly, restriction of Ad replication to tumour tissues facilitates safe application but has also been shown to reduce antiviral immune responses after systemic injection in syngeneic mice. Using a nonselective Ad, there was strong stimulation of innate immune response genes and severe liver toxicity, whilst the selective Ad did not trigger innate immunity and prevented liver toxicity (241).

The ability to transcriptionally control the genome is an advantage Ads have over other viruses. All RNA viruses except orthomyxoviruses (e.g., influenza viruses) and retroviruses replicate in the cytoplasm, therefore, these viruses cannot use nuclear transcriptional control elements, such as tissue/tumour promoters. In contrast, DNA viruses, except poxviruses (e.g. VV), replicate in the nucleus and can use nuclear transcriptional control elements. However, viruses such as Picornavirus, RV and Parvovirus, have small compact genomes that do not have room for large transgenes. Genetic modification of small dsRNA viruses, such as RV, has proved to be challenging, however recently, RV has been genetically modified to insert small transgenes due to the development of plasmid-based reverse genetic systems, so limited genetic modification is possible (244,245). Importantly, Ads have

highly regulated temporal sequence of viral gene expression starting with *E1A* which allows tuning transgene expression, unlike other transgene carrying viruses (VSV, MV, NDV, HSV and VV). Therefore, it is clear Ads have advantages over other viruses (242).

Other than engineering the adenoviral genome to restrict replication to tumour cells, the tropism of Ads can be changed to increase infection specificity to tumour cells, by genetically altering or conjugating ligands to the hexon or fibre proteins that target cell surface proteins that are uniquely expressed or overexpressed in cancer cells (reviewed in (243)). It is clear there are numerous ways to genetically modify oncolytic Ads, therefore, the following sections will focus on preclinical and clinical experience with Ads that are modified to control replication to tumour cells.

1.4.3.2. Clinical Experience with Oncolytic Adenovirus

In the early 2000s, multiple phase I and II clinical trials with Onyx-015 showed good safety profiles (244–247), however, only moderate clinical responses were observed, which were more significant when combined with chemotherapy or radiotherapy (246,248). This was related to limited tumour infection and the development of antiviral immunity, which limits efficacy (249–253). Despite this, Onyx-015 was approved in China for the treatment of head and neck squamous cell carcinoma (108), which in phase III clinical trials demonstrated response rates of nearly 80% in combination with cisplatin, with mild side effects such as flu-like symptoms (254). However, it is important to highlight that the Chinese Regulatory Agency approved Onyx-015 without any data regarding patient survival. Although no Ads have yet been approved by any Western country, there is currently a plethora of Ads in clinical trials for the treatment of a range of cancers (Table 1.10), although the majority of them are focussed on the evaluation of safety rather than efficacy of the treatment. Data from these will no doubt emerge over the next few years.

Table 1.10: Oncolytic adenoviruses in clinical trials (Table reproduced with permission from 256).

Name	Modification	Result of modification	Tumour type
ONYX-015	E1B-55kDa	Lyse p53 deficient cells	Head and Neck, glioma, ovary
Oncorine	Ad-E1B ^{-/-}	Promotes cell lysis	Head and Neck, liver, lung, pancreas, solid tumours
CGTG-102	Ad-GM-CSF	Immune cell recruitment	Glioma
DNX-2401	Ad-D24RGD	Preferentially binds and lyses glioma	Melanoma
ICOVIR-5	Ad-DM-E2F-K-D24RGD	Selects cells with E2F-Rb deregulation	Bladder
CG0070	Ad-GM-CSF	Immune cell recruitment	
Colo Ad1	Ad3:Ad1 1P Hybrid	Hybrid virus, boosts potency	Colorectal, ovary
VCN-01	PH20 hyaluronidase	Degrade tumour ECM	Pancreatic
Telomelysin	Ad-hTERT	hTERT promoter-controlled Ad	Solid Tumours
Abbreviations: Ad, adenovirus; ECM, extracellular matrix; GM-CSF, granulocyte-macrophage			

As an example, a phase I clinical trial using a conditionally replicating Ad5 driven by hTERT (Telomelysin) promoter was assessed in patients with advanced solid tumours. Intratumoural injection of Telomelysin was well tolerated at all dose levels, with common grade 1 and 2 toxicities including fever and chills. Biopsies showed hTERT expression in 9 of 12 patients. Viral DNA was transiently detected in the plasma of 13 out of 16 patients, and in four patients, viral DNA was detected in plasma or sputum at days 7 and 14 post treatment, despite below detectable levels at 24 hours, suggesting viral replication. With regards to clinical efficacy, one patient had a partial response in the injected malignant lesion. Seven patients fulfilled Response Evaluation Criteria in Solid Tumours (RECIST), which is a set of published rules to define when solid tumours respond, stabilise or progress during treatment, according to the RECIST criteria seven patient met the definition for stable disease at day

56 after treatment (256). However, it must be taken into account that the RECIST criteria could be underestimating the effectiveness of the treatment, because tumour pseudoprogression has been commonly reported in virotherapy (199,257).

1.4.4 Oncolytic Adenoviruses and Multiple Myeloma

An early study demonstrated that transduction with Ad vectors using a tumour-selective *DF3* promoter to drive the expression of TK were able to efficiently transduce MPC lines (~80% transduction efficiency). This resulted in expression of TK, which with the addition of ganciclovir, was able to significantly reduce MPC lines proliferation (OCI-My5 and RPMI-8226) that were cultured with γ -irradiated BM mononuclear cells (BMMCs) from healthy donors *ex vivo*, without affecting haematopoietic progenitor cells (HPCs) or normal lymphocytes, suggesting their potential utility in MM cells within autografts (258). Fernandes *et al.*, (2009) examined MM targeted delivery of CD40L by a conditionally replicative oncolytic Ad, AdEHCD40L. First, they demonstrated that MM cells were susceptible to AdEHCD40L-mediated apoptosis, and subsequently in an RPMI 8226 subcutaneous xenograft murine model tumour burden was reduced by 50% by AdEHCD40L treatment (127).

Given that most haematological malignancies do not express high levels of CAR, Ad5 has not generally been considered as an oncolytic agent for malignancies such as MM (125,259). Therefore, one study suggests that subgroup D viruses may have efficacy against MM and lymphoma. In this study, two best performing species D viruses, Ad26 and Ad45 were compared to Ad5 for *in vivo* efficacy against lymphoma xenografts. A single intratumoural injection of 3×10^6 virions slowed tumour growth significantly and improved survival of these animals, whilst Ad5 was ineffective (260). However, this may not be the case for MM. Senac *et al.*, (2010) showed that Ad5 can infect and kill most MM cell lines and *ex vivo* patient samples, evidenced by reporter gene expression, viral DNA replication, viral titring, and cell death assays, suggesting a significant therapeutic potential (125). Whilst Drouin *et al.*, (2010) compared Ad5 against a chimeric Ad 5/F35 in B lymphocytes, the latter substitutes Ad5-based vector fibres with those of Ad serotype 35, which uses CD46 as a receptor. This study found that adenoviral transduction efficiencies varied between B-cell lines corresponding to distinct stages of B-

cell lymphogenesis. Cell lines of plasma origin were efficiently transduced with both Ads, with Ad5 having a slightly higher transduction efficiency than Ad5/F35. Interestingly, plasma cell lines with high transduction efficacy, had the lowest CAR expression (e.g. U266 plasma cell line with 100% transduction efficiency only had 15% CAR expression), whilst cells with high CAR expression had low Ad5 transduction efficiency (e.g. mature B lymphocyte cell line which had 85% CAR expression but only had 20% transduction efficiency). Moreover, CD46 was shown to be ubiquitously expressed, yet some cells remained poorly permissive to Ad5/F35 (261). Collectively, these results showed that there is no direct correlation between transduction efficiency and cellular receptor expression for both viruses, as formerly thought (262).

One study showed that $\alpha\beta 5$ integrin is the primary receptor for Ads in CAR-negative cells. This study used CAR-negative human melanoma cell line (WM278) and CAR-negative human breast cancer cell lines (MCF7 and MDA-MB-435). Ad binding was shown not to be dependent on fibre binding to cells but rather the penton base binding to cellular integrins. Additionally, blocking with a specific mAb to $\alpha\beta 5$ integrin in low CAR expressing cells inhibited Ad infection, demonstrating $\alpha\beta 5$ integrin is required for adenoviral attachment in these cells, and not CAR. The binding to $\alpha\beta 5$ integrin was also shown to be extremely high affinity, in the picomolar range (263). This could explain the high transduction efficiencies in low CAR expressing cells.

Early work showed that WT Ad5 infects MM cell lines, however, the life cycle is delayed compared to that of permissive HeLa cells (125,264). This slow or low-level replication appears to be related to repression of the E1 transcripts in MM cells (264,265). This suggests that modifying E1 transcripts to evade RNA destabilisation will enhance the efficacy of oncolytic Ads in MM (125). Furthermore, Senac *et al.*, (2010) showed that Ad5 infected CD138⁺ primary MM cells 10- to 70-fold more efficiently than normal CD138⁻ BM cells. This specificity could be enhanced by applying transcriptional or replication targeting to oncolytic Ad5 to restrict its replication to MM cells (125). Despite the preclinical activity

of Ads in MPC lines and mouse models, clinical investigation has not yet been realised, and their efficacy and safety profile needs to be defined in phase I/II clinical trials.

More recently, a study has investigated the use of Lokon oncolytic Ad (LOAd) therapy for MM treatment (129). Firstly, the virus used an *E1A* deleted chimeric Ad Ad5/F35, this means the adenoviral fibre and knob are switched to serotype 35, which retargets the virus to infect CD46⁺ cells, this is to overcome the apparent lack of CAR expression in MM cells. LOAds are also further modified to express immunomodulatory transgenes, in this study, two LOAds were used, both LOAd700 and LOAd703 encode for CD40L, but LOAd703 also encodes for 4-1BBL. A panel of MPC lines were sensitive to both LOAds, resulting in replication and elimination of MM cells *in vitro*. LOAds replicated much faster than Ad5/F35 alone, in cell viability assays, LOAds appeared to perform better than Ad5/F35 alone, but it was not stated whether significance was reached. Transgene expression was also detected in all MPC lines post LOAd infection.

The authors then wanted to explore the effects of the transgenes on MM cells as well as cocultured immune cells. MM cells treated with LOAds had altered cell phenotypes with a downregulation of markers connected to MM progression (ICAM-1, CD70, CXCL10 etc.) and an upregulation of Fas. When MM cells were cocultured with healthy donor (HD) PBMCs and treated with LOAds, LOAds promoted activation of cytotoxic T cells, and IFN γ expression. However, it would be interesting to see if these increases also occur in MM patients PBMCs or BMMCs, who are typically immunosuppressed. Next, they investigated the efficacy of LOAds *in vivo*. A subcutaneous xenograft MM model was used, mice were treated with either vehicle (PBS), LOAd703 or an unarmed LOAd (LOAd-) (1×10^9 FFU) intratumorally or intravenously. As neither transgene would have activity in this model, they were investigating whether the oncolytic function would be affected *in vivo* if LOAds were armed, hence selecting only one of the LOAds for this study (LOAd703). Only intratumorally injected mice had a significant reduction in tumour burden compared to control (PBS), with both LOAd703 and LOAd- having no significant difference in the amount of tumour burden reduction, however, LOAd703-

treated mice had significantly longer overall survival. As the oncolytic effects of LOAds only showed efficacy *in vivo* intratumorally in a plasmacytoma model, this would be hard to translate to MM patients. Until the immunostimulatory effects can be investigated *in vivo* in systemic disease and administered systemically, it is hard to say whether LOAd efficacy can translate into a potential treatment for MM patients.

Most *in vivo* experiments using Ads have been performed with human cancer xenografts in immunodeficient mice. To fully test the potential therapeutic activity of OV, studies should be performed in immunocompetent animals that can support active viral infection (266). However, the stringent species selectivity of adenoviridae only permits human Ad to infect human cells, therefore, does not permit replication in most rodent cells including mice and rats (267–270). Consequently, researchers have turned to the Syrian hamster model (271), whilst this model system is effective for studying human Ads, it is limited by the accessibility of reagents to study immunological parameters (266). Despite this, some groups have found mouse cell lines that are permissive of Ad infection and replication, these include the mouse glioma cell line, GL261, the mouse mammary epithelial cell line, NMuMG, and the lung adenocarcinoma cell line, ADS-12 (266,272,273).

1.4.5 Targeting Multiple Myeloma with a Selective Adenovirus

It is clear there are numerous ways to genetically modify oncolytic Ads for cancer therapy, in view of previous research discussed in section 1.4.4, the Sheffield Myeloma Research Team (SMaRT) developed an Ad by utilising selective transcriptional control of E1A, using the promoter for signalling lymphocytic activation molecule F7 (SLAMF7), also known as CD-subset-1 (CS1). The reasons for selecting CS1 will be discussed in the following sections.

1.4.5.1 CS1 Expression

CS1(SLAMF7) is one of the nine SLAMF receptors belonging to the CD2 subset of the immunoglobulin superfamily. CS1 is often overexpressed on MM cells (274–277), which has resulted in it being an attractive therapeutic target. In one study, CS1 mRNA was expressed in >90% of 532 MM cases, regardless of cytogenetic abnormalities. CS1 protein was also strongly detected in MM cells in all

plasmacytomas and BM biopsies by immunohistochemistry (IHC). By flow cytometry, CS1 showed specific staining in CD138⁺ MM cells, NK cells, NK-like T cells and CD8⁺ T cells, but no detection on CD34⁺ haematopoietic stem cells (275). In another study, CS1 mRNA and protein was highly expressed in CD138 purified primary MM cells in >97% of patients (n=101), with low levels of circulating CS1 detectable in MM patient sera, but not detectable in HDs (274). In another study, ~87% of MM patients (n=39) showed strong CS1 expression independent of disease stage or treatment history. These studies all corroborate high expression levels of CS1 in the majority of MM patients. Whilst these studies indicate cytogenetic abnormalities are not indicative of CS1 expression, it has been shown that MM cells with t(4:14) translocations (found in about 15% of MM patients) express higher levels of CS1 mRNA and surface protein, which has been found to be linked to MMSET overexpression (278).

Gene expression data have also confirmed high CS1 expression on tumours in patients with myelodysplastic syndrome, chronic lymphocytic leukaemia and diffuse large B cell lymphoma (279). This might mean CS1 therapeutic targets might be useful in other haematological cancers, but the role of CS1 in the pathogenesis of these tumours has not been evaluated. It is important to add that CS1 is expressed in HDs on almost all CD56^{dim} NK cells, most CD56^{bright} NK cells and non-classical CD14^{low}CD16⁺ monocytes and many CD56⁺ T cells, mature dendritic cells, and small subsets of CD4⁺ T cells, B cells and CD14⁺CD16⁺ monocytes (275,280,281). CS1 is also increased in NK cells and B cells in response to various stimuli (281–284). For example, primary resting B cells express minimal levels of CS1, but upon activation with CD40, CS1 is upregulated. Plasma cells, as well as memory B cells, express higher levels of CS1 compared to resting primary B cells (284).

1.4.5.2 CS1 Signalling

CS1 is a homophilic receptor that recognises and binds to CS1 on other cells, this CS1-CS1 interaction results in activation of NK cell natural toxicity (285). NK cells express two splice variants of CS1, one which lacks the intracellular domain for activation (CS1-S) and one which contains the intracellular domain (CS1-L), thus capable of activating NK cytotoxicity (286). Activation of NK cytotoxicity occurs

due to CS1s two signalling motifs, immunoreceptor tyrosine-based switch motif (ITSM) which mediates interaction with Ewing's sarcoma-associated transcript 2 (EAT-2) and activates the receptor. CS1 may also function as an inhibitory receptor in the absence of EAT-2 (287). In B cells, signalling through CS1 induced B cell proliferation and autocrine secretion of cytokines such as IL-14 (284), this suggests CS1 may have growth promoting activity in B cells. In T cells, CS1 is expressed but EAT-2 is not, therefore, CS1 functions as an inhibitory receptor in T cells (287).

In MM, the biological relevance of CS1 is obscure because the expression of EAT-2 and other CS1 proteins are defective in MM cells (288). However, CS1 upregulation in MM cells has been implicated to cause uncontrolled proliferation (289). The extracellular domain of CS1 can be cleaved by unidentified enzyme(s) and detected in the serum of MM patients. Recently, this soluble CS1 has been shown to act as a growth factor for MM, which can be neutralised with antibodies targeting CS1 (290).

1.4.5.3 CS1 Regulation

Transcriptional regulation of CS1 in NK and B cells is regulated by Ying Yang 1 (YY1) in mice (291) and B lymphocyte-induced maturation protein-1 (BLIMP-1) in humans (292). *BLIMP-1*, encoded by positive regulatory domain zinc finger protein 1 (PRDM1), was originally thought to be a transcriptional repressor but has been shown to positively regulate the human CS1 gene. BLIMP-1/PRDM1 is not required for basal expression of human CS1, BLIMP-1/PRDM1 binding leads to increased transcription and expression of human CS1. However, the mechanism of CS1 upregulation is unknown in human MM. In mice YY1 represses murine CS1 in murine MM cell line Sp2/O, as mutating the YY1 binding site on the murine CS1 promoter resulted in an increase in promoter activity (291). Currently, the mechanism behind CS1 upregulation is still unclear.

Recently, it has been shown that IMiDs (Len and Pom) can downregulate CS1 protein and mRNA expression (290). The authors found the human CS1 promoter segment to contain three putative-binding sites for the Ikaros family (IKZF) flanking the BLIMP-1 binding site. This is important as Ikaros (IKZF1) and Aiolos (IKZF3) are target molecules for Len and Pom in MM cells. Because of these findings

the authors investigated the regulation of Ikaros and Aiolos on CS1 expression. A strong correlation was found in the expression levels of CS1 and Ikaros, but not Aiolos, after Len treatment, whilst BLIMP-1 expression was not consistently associated with Len induced changes in CS1 expression levels. CHIP assays showed Len treatment readily decreased the abundance of Ikaros on the CS1 promoter. When Ikaros was knocked down in MM cells, CS1 decreased to the same extent, conversely, when Ikaros was overexpressed, CS1 expression increased. Additionally, in Len resistant MM cell lines, simultaneous upregulation of Ikaros and CS1 expression is observed. Therefore, this suggests Ikaros is a critical transactivator of CS1 in MM cells and transcriptional control is different in MM cells compared to B and NK cells.

1.4.5.4 CS1 Therapeutic Targeting

Due to the upregulation of CS1 in MM cells and its role in increasing MM cell growth and proliferation, CS1 is an attractive therapeutic target. This has resulted in a mAb being generated against it, Elotuzumab, which has been approved in combination with Len and Dexamethasone for relapsed/refractory MM based on the findings from the phase III randomised ELOQUENT-2 trial (293). The mechanism of action of Elotuzumab is mediated through antibody-dependent cell cytotoxicity (ADCC) (294,295). Elotuzumab is unable to directly suppress the growth of MM cells due to MM cells lacking EAT-2 and other molecules, but Elotuzumab does not induce proliferation of MM cells (288). Elotuzumab has a dual mechanism of action, firstly, it can directly activate NK cells by binding to CS1 on the surface of NK cells and activating them, and secondly, by ADCC, whereby Elotuzumab binds to CS1 on MM cells, which targets it for granzyme B destruction via CD16-mediated ADCC by NK cells. CS1 has also been targeted using a CS1-antibody drug conjugate. The results of the first in human phase 1 clinical trial of this CS1-antibody drug conjugate (ABBV-838) was announced in early 2020 (296). This trial showed ABBV-838 to be safe and well tolerated in relapsed/refractory MM but had very limited efficacy, with an overall response rate of 10.7%, with very good partial responses, and partial responses were achieved in 2.7% and 8% of patients' respectively.

Preclinically, CS1 has been targeted by CAR-T cell therapy, which has resulted in MM cell eradication *in vitro* and *in vivo* (297,298). However, anti-CS1 CAR-T cells caused cell death in CS1^{high} B cells, T cells and NK cells, but the CS1^{low} fraction in each cell subset are spared and preserved functional lymphocytes (298). Despite this, phase I clinical trials are currently underway (NCT03710421). From everything described above, it is clear that targeting CS1 expressing MM cells results in anti-MM effects and depending on how it is targeted, seems to have minimal toxicity.

1.4.5.5 CS1 Transcriptionally Controlled Adenovirus

For the reasons discussed above, CS1 was an attractive target to drive the replication of an oncolytic Ad for MM, so a CS1 promoter driven Ad was engineered, called Ad[CE1A]. Prior to the start of this thesis, the ability of Ad[CE1A] to induce cell death was tested in a small panel of MM cell lines (JJN-3, U266 and OPM-2), a melanoma cell line (MDA-MB-435) (Figure 1.7.a), in primary osteoblasts (Figure 1.7.b) and in primary macrophage-differentiated osteoclasts (Figure 1.7.c). Ad[CE1A] was shown to induce cell death only in the MPC lines, and this level of cell death was highly significant (data not published). Ad[CE1A] was also tested *in vivo* in a U266 xenograft model of MM. Ad[CE1A] treatment started when tumour burden was high, and Ad[CE1A] managed to significantly reduce tumour burden (Figure 1.7.e) but had no effect on the bone disease (Figure 1.7.f; Figure 1.7.a) (results unpublished). Unfortunately, Ad[CE1A] did not manage to reduce all the tumour burden as a monotherapy, when Ad[CE1A] therapy was initially administered, tumour burden was well established. Therefore, this leads to the rationale of this PhD project (discussed in detail further in later sections). Briefly, to better understand adenoviral-MM interactions and to further enhance adenoviral-mediated MM cell death. Whether combining with standard chemotherapy to increase anti-MM outcomes in active disease, or by using Ad[CE1A] not as a tumour debulking agent, but to remove MRD following standard of care in the low tumour burden model of MM. If successful, this treatment could be curative for MM patients, especially the latter. Most importantly, these proposed regimes are what would most likely be performed clinically.

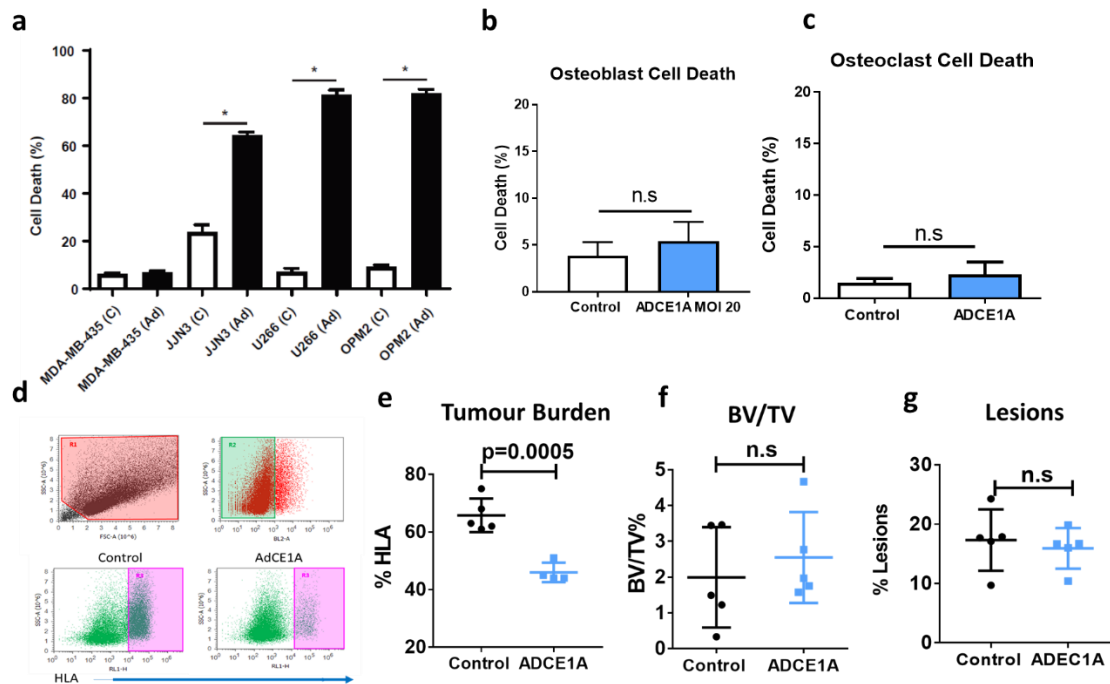


Figure 1.7: Ad[CE1A] induces cell death specifically in MPC lines *in vitro* and *in vivo* but has no effect on MM-induced bone disease:

(a) JLN-3, U-266, OPM-2 and MDA-MB-435 cells were infected with Ad[CE1A] at a multiplicity of infection (MOI) 20. Cell death was analysed 4 days post infection by flow cytometric analysis using propidium iodide staining (PI). n=3 Data is the mean + SEM. p values are for 2-way ANOVA with multiple comparisons with Šidák's correction, where * = p < 0.05. (b) Primary murine osteoblasts and (c) primary macrophage differentiated osteoclasts were infected with Ad[CE1A] at a MOI of 20. Cell death was analysed by flow cytometry 4 days post infection by flow cytometric analysis with PI staining. n=3 Data is the mean + SEM. p values are for students T-test. (d) Left femurs of vehicle (PBS) and Ad[CE1A] treated mice from a U266 xenograft murine model were flushed and stained with anti-HLA and labelled with 2 µg/mL TO-PRO-3 and analysed. (e) The average percentage tumour burden was calculated for each group and plotted. (f) Trabecular bone volume in the left tibiae of each mouse were analysed and the percentage bone volume for control and Ad[CE1A] treated mice calculated. (g) Osteolytic lesions were analysed by Osteolytica software (299) and percentage of lesion analysis for control and Ad[CE1A] treated mice was calculated. All *in vivo* data are mean ± SEM, n=5. P values are for students T-test.

1.5 The Future of Oncolytic Virotherapy for Multiple Myeloma

MM poses considerable therapeutic challenges to be overcome if oncolytic virotherapy is to translate to an effective treatment strategy. The field suffers from several obvious issues, which must be addressed. Firstly, the impact of disease heterogeneity needs to be examined in the context of oncolytic virotherapy. A review of the literature showed that preclinical results derive more from tests on MPC lines than on patient-derived primary MM cells (56). This is related to the well-known difficulties with maintaining primary MM cells outside the functional BM (300–302). However, studies have shown that OVs in primary MM patient samples can infect and typically kill a high percentage of cells. Unfortunately, these studies used small numbers of patient samples (typically only data from one to three patients) (22), with the exception of one more recent paper (n=31) (140). The field would therefore profit from a comprehensive study of the efficacy of oncolytic virotherapy on a large amount of MM patient samples.

Secondly, most of the *in vivo* studies and clinical trials administer virotherapy intratumorally. Most of the work studying OVs in MM has been conducted in immunodeficient models of a single subcutaneous plasmacytoma with intratumoral injection of virus. These studies represent an easy starting point; however, these are not clinically relevant MM models, and fail to recapitulate the clinical realities in two ways. First, due to the nature of OVs, there are different treatment challenges associated with systemic vs localised disease. In particular, delivery of a virus through the circulation to sites of systemic disease is a major translational hurdle (22). This is because once injected systemically, OVs are faced with the inactivating effects of complement, erythrocyte 'virus traps' and antiviral antibodies, all of which targets them for rapid elimination (55,57,303,304). Since MM is typically a systemic disease, this should be addressed in preclinical models. Therefore, OVs need to be assessed for their circulation kinetics, first pass hepatic clearance, and the ability to infect extravascular tumour cells (57,305). It is because of these reasons; the development of intralesional virotherapy approaches for solid tumours has seen more progress.

Additionally, the immune system is recognised to have a significant positive and negative impact on OV. For example, as mentioned previously, complement, erythrocyte 'virus traps' and antiviral antibodies can inhibit viral infectivity (306–309). On the other hand, much of OV efficacy is thought to be mediated through the induction of antitumour T-cell-mediated immunotherapy (21,310). However, MM patients have a high degree of immune dysregulation, either due to the immunosuppressive effects of the disease, or chemotherapy (311,312). MM and its immunosuppressive environment, makes it problematic to achieve sufficient immune responses with OV alone (311). Therefore, OV should be studied in immunocompetent systemic disease models, however this poses an issue with some viruses, which cannot replicate in mouse cells, such as the Ad (as discussed in section 1.4.4), and MV (313). It must be noted that the lack of immunocompetent mouse models has not stopped the MV progressing into clinical trials in MM. This may therefore, not be a hindrance for Ad[CE1A] progressing onto clinical trials. Nonetheless, even recently, subcutaneous solitary plasmacytoma models are still used over systemic disease models for oncolytic virotherapy (129,140).

There have been several strategies to overcome immune clearance and/or successfully systemically deliver OV by a 'trojan horse' method. One strategy has been to deplete/inhibit antiviral immune responses with low dose immunosuppressive chemotherapy (cyclophosphamide) or TGF- β treatment, which resulted in enhanced viral replication, T-reg inhibition resulting in decreased viral clearance, which ultimately resulted in improved antitumour outcomes (314–319). Another strategy is modification of the viral coat through conjugation of polymers like polyethylene glycol (320–322) or lipid encapsulation (323), which can shield OV from neutralising serum factors and prevent the generation of new antiviral antibodies. Alternatively, cell carrier-based methods have been used as a 'trojan horse' which have demonstrated the ability to guide viruses to tumour cells. Many cell types have been used as carriers, including T cells, DCs, macrophages, and mesenchymal stem cells (324). Whilst attempts are still ongoing to retarget viral infection to cancer cells using chemical modification, adaptor proteins or cell carriers, these attempts may be potentially hindered as these modifications

are non-heritable, therefore, progeny virions will not be modified. In the case of modifications to enhance cell death, there will be reduced oncolytic properties in progeny virions. Moreover, modifications to target/shield the virus will also be lost in progeny virions, which raises the possibility that unwanted off target infection and subsequent toxicities may be caused by progeny virions (325). Clearly, the systemic delivery of OV's is still a major challenge in the field, which remains unsolved.

Lastly, combining oncolytic virotherapy with more typical MM standards of care, such as chemotherapy, radiation or mAbs is lacking but may be the best approach to increase efficacy. Results from the first completed clinical trial utilizing oncolytic RV in MM support this notion (326). Enhanced antitumour immune responses have been demonstrated preclinically and clinically in other tumours when combining chemotherapy and oncolytic virotherapy (90,246,254,327–330). This is critical in determining oncolytic virotherapy in context of other MM therapies, for example should OV's be used as a frontline therapy? Or are they better suited to relapsed/refractory patients? Is there any synergism with OV's and other existing MM treatments? As discussed earlier, one of the main issues with patients relapsing is the existence of MRD, so can OV's remove MRD once tumour has been debulked by existing MM chemotherapies? This is a novel and more clinically relevant strategy to target these remaining cells that persist in MRD. Therefore, if the field is to advance from preclinical work to successful clinical trials will largely depend on the ability to use synergistic treatment approaches along with administering OV's at the most clinically relevant time to eliminate MRD, which, if successful, could be curative for MM patients.

1.6 Oncolytic viruses in combination with MM standard of care

Combinational approaches to treat cancers are predominant in the oncolytic virotherapy field (177 trials out of 206 57%). These OV combination trials are using radiotherapy/chemotherapy/surgery (n=80), immunomodulatory agents such as checkpoint inhibitors that target the PD-1/PDL-1 axis (n=39) or CTLA-4 (n=1), immunomodulatory factors such as GM-CSF (n=3), IFN- α (n=3) and IL-2 (n=3) and antigens such as autologous tumour cells (n=14) and MAGE-A3 (n=3). Additionally, OVs are armed with payloads that are integrated into their genome (52%) with the predominant payloads being GM-CSF (n=49) or TK (n=24) (reviewed in (460)). Improved clinical outcomes have been discovered when OVs are used in combination with other treatments (461–463), suggesting that oncolytic virotherapy can be potentiated by combination therapies. Combining OVs with approved therapies has the added benefit that there is a known safety profile, which helps when determining possible adverse interactions. At present, very little is known about OVs and their interactions with anti-MM standard of care drugs/drug classes in MM, these drug/drug classes are BTZ (proteasome inhibitor), Melphalan (Melf) (alkylating agent), Pan (HDAC inhibitor) and Len or Pom (IMiDs), below is a review of the literature of the discussed drugs/drug classes in combination OVs, which will be discussed in greater detail in Chapter 6.

1.6.1 Bortezomib and Proteasome Inhibitors

BTZ (PS-341, Velcade®) is a first-generation proteasome inhibitor, is FDA approved and EMA approved either as a single agent or in combination with other chemo-/radio-therapeutic agents for MM. It is a boronic dipeptide which specifically and reversibly inhibits the threonine residue of the 26S proteasome, an enzyme complex that plays a key role in regulating protein degradation in a controlled manner. Proteins that are no longer required, including proteins involved in control of the cell cycle, apoptosis, and cell signalling, are tagged with ubiquitin, which directs them to the proteasome for subsequent degradation. This process maintains the balance of inhibitory and stimulatory proteins involved in several processes, which results in loss of the tight control of these processes and a build-up of cell cycle and regulatory proteins leading to cell death (465). Therefore, BTZ induces ER stress

and apoptosis in a wide variety of cancer cell lines, including MM (466,467). Cancer cells have increased metabolic demands, this is particularly true of MM cells that are producing large numbers of Igs, therefore, are thought to constantly be on the edge of ER stress, BTZ has also been shown to generate reactive oxygen species (ROS) (468), increasing cellular stress. Additionally, BTZ is one of the few classes of drugs classed as an inducer of ICD. BTZ-treated MM cells, including primary cells, induced an adaptive immune response *in vitro* (increased DC uptake of MM cells) in a HSP90 dependent manner (483). Carfilzomib, a second-generation proteasome inhibitor, has also been shown to increase the ICD DAMP calreticulin (CALR), on MM cell lines (484).

Several proteasome inhibitors (BTZ, PS-341, MG132) have been found to synergise with oncolytic Ads, VSV, and HSV-1 (Table 1.11). The combinations of proteasome inhibitors with OVIs have been found to enhance oncolytic activity of OVIs by enhancing viral infection, viral replication, and tumour cytotoxicity.

Table 1.11: Combining OVVs with proteasome inhibitors (469)

Inhibitors of the proteasome complex				
OVs	Combination Treatment	Tumour Type	Study Phase	Ref
rAd-p53	MG132	Colon	Preclinical Phase. Human colon cell lines and primary patient material.	(470)
oHSV-1	Bortezomib	glioma, head and neck and ovarian	Preclinical phase. Human glioma, head and neck and ovarian cancer cell lines. Subcutaneous xenograft models in athymic nude mice.	(471)
hTERT-Ad	Bortezomib	HCC	Preclinical Phase. Subcutaneous syngeneic model in immunocompetent mice.	(472)
oHSV-1	Bortezomib	Ovarian, head and neck, glioma, and malignant peripheral nerve sheath	Preclinical phase. Human Tumour cell lines. Subcutaneous xenograft models in athymic nude mice. Intracranial xenograft model in nude mice.	(473)
VSV	Bortezomib	MM	Preclinical Phase. Subcutaneous syngeneic model in immunocompetent mice.	(119)
VSV	PS-341	Lung	Preclinical phase. Human lung adenocarcinoma cell lines. Primary HD lung bronchial epithelial cells.	(474)

With regards to proteasome inhibitors enhancing viral infection, there are observations to suggest that the localisation of cell surface levels of CAR may be regulated by ubiquitylation. The proteasome inhibitor MG132 has been shown to upregulate CAR in colon cancer cells, resulting in enhanced Ad infection and oncolysis (470). CAR also associates with LNX, a protein known to act as an E3-ubiquitin ligase (475). There is evidence that the ubiquitination proteasome system (UPS) may also be involved in the regulation of other Ad receptors, regulating their cell surface expression and intracellular trafficking. For example, a PpxY motif on Ad pVI recruits Nedd4 E3 ubiquitin ligases to bind and Ubiquitylate protein VI. The PpxY motif on pVI was found to be involved in rapid, microtubule-dependent intracellular movement. Mutating the PpxY motif or depleting Nedd4 ligases attenuated

the nuclear accumulation of Ad particles. Therefore, there is a role for Nedd4 in Ad entry, however, how ubiquitylation of pVI or interaction with Nedd4 ligases directs accumulation of Ads at the microtubule organising centre remains unknown (476). Therefore, blocking the proteasome may affect how Ads traffic around the cell.

Regarding proteasome inhibitors increasing viral replication in certain OV, BTZ increased oncolytic HSV replication in glioma, head and neck and ovarian cancer cells *in vitro* due to a BTZ induced increase in HSP90, which supported increased viral replication via enhanced nuclear location of the viral polymerase *in vitro*. There was also enhanced viral replication *in vivo* (471). Additionally, proteasome inhibitors indirectly block NF- κ B, as a result NF- κ B cannot be released from the IKK β complex. NF- κ B and IKK β regulate many cellular responses to stimuli, such as innate and adaptive immunity, inflammation and cell death. Therefore, NF- κ B and IKK β play key roles in regulating the innate immune response against OVs (477) which may result in antiviral immune suppression allowing increased viral replication within tumour cells *in vivo* causing increased tumour cytotoxicity or consequently could suppress anti-tumour immune responses resulting in decreased tumour cytotoxicity.

Proteasome inhibitors in combination with OVs have been shown to enhance tumour cytotoxicity, amplifying ER stress or apoptosis due to abnormal unfolded protein response (UPR) increasing cytotoxicity. As discussed above, cancer cells, particularly MM cells, are sensitive to disruption of ER homeostasis due their high protein synthesis levels (478), virally infected cells are also sensitive (479), therefore, OV-infected MM cells would be particularly sensitive to disruption of ER homeostasis. ER stress has been induced by inhibiting the UPR using various inhibitors (Valosin-containing protein, Eeyarastatin I, Golgi-specific brefeldin A-resistant guanine nucleotide exchange factor 1 and golgicide A) in combination with either an oncolytic Ad or an M1 strain of Getah-like alphavirus (GLV). These combinations resulted in significantly enhanced anticancer efficacy (480,481). Indirect effects of ER stress inducers such as Thapsigargin and Ionomycin, were shown to enhance the activity of oncolytic Ads through alteration of Ca²⁺ flux and protein kinase C signalling (482).

More importantly, ER stress has been induced using BTZ in combination with OVs. Preclinically, BTZ has been used in combination with a hTert-Ad in hepatocellular carcinoma (HCC). Both hTert-Ad and BTZ triggered ER stress, which resulted in enhanced apoptosis and oncolysis *in vitro* and *in vivo*. In an HCC syngeneic model, the combination enhanced anti-tumoral immune responses (increased IFN- γ and CD8⁺ T cells), contributing to effective elimination of non-infected HCC lung metastases (472). Additionally, oHSV-1 was used in combination with BTZ in ovarian, head and neck, glioma, and malignant peripheral nerve sheath tumour cells. The combination was synergistic, increased viral replication and enhanced necroptotic tumour cell death as inhibition or knockdown of RIPK1 significantly reduced the synergistic cell killing. The combination also induced ER stress as increased cellular ROS and mitochondrial ROS levels were present, pre-treatment with a JNK inhibitor (JNK signalling contributes to necroptotic cell death) or knockdown of RIPK1 reversed this increase. The combination treatment also activated pro-inflammatory pathways, as an increase of IL-1 α , IFN- γ , TNF α cytokines *in vitro* and *in vivo* were observed. Furthermore, an increase of NK cell activating markers on the tumour cell surface (CD58, CD112 and CD155) and NK activation markers on NK cells (CD69 and TRAIL) in the combination was observed, which lead to enhanced NK cell-mediated tumour cell killing when NK cells were cocultured with tumour cells (473).

In contrast, when BTZ was combined with VSV in MM *in vitro*, a reduction in replication and spread was seen and the combination was antagonistic despite NF- κ B activation being blocked. However, *in vivo* the combination did improve antitumour efficacy compared to monotherapy (119). Likewise, the PS-341 proteasome inhibitor prevented the replication of VSV in human A549 lung adenocarcinoma cells (474).

The use of proteasome inhibitors in combination with OVAs confirm that the interactions between OVAs with the UPS system and ER stressors needs to be explored, however, these conflicting studies make the combination of OVAs with proteasome inhibitors a treatment option that needs further investigation. There is no research on the combination of a proteasome inhibitor with an oncolytic Ad in MM. The one study using VSV in combination with BTZ in MM showed detrimental interactions in vitro but improved efficacy in vivo. There needs to be more research on the effect of proteasome inhibition on Ad life cycle, as proteasome inhibition increased CAR expression resulting in increased Ad infection and tumour oncolysis in colon cells. Therefore, it would be interesting to see if BTZ and Ad[CE1A] combinations result in beneficial outcomes in MM. Additionally, BTZ is one of the few classes of drugs classed as an inducer of ICD. Therefore, it would be interesting to see if combining Ad[CE1A] with proteasome inhibitors increases ICD in MPCs.

1.6.2 Melphalan and Alkylating Agents

Melph (Alkeran™), a nitrogen mustard, is an alkylating agent, alkylating agents transfer alkyl groups to DNA leading to the formation of cytotoxic and mutagenic adducts, leading to tumour cell death. Melph has been used for MM therapy for over fifty years, despite novel agents being introduced, Melph maintains its role in the treatment of MM acting as a cytotoxic agent through DNA damage and as an immunostimulatory drug (485). Melph induces the expression of ROS that results in apoptosis by activation of caspases and subsequent DNA damage that leads to cell death (486–488). Melph, is also an immunostimulatory drug, and is able to induce ICD in tumour cells *in vitro* and *in vivo* (489), and induces proinflammatory cytokines/chemokines, resulting in increased levels of cytokines including IFN- γ , IL-22, IL-10, IL-5, IL-18, and IL-27, and chemokines including CCL2, CCL7, CXCL1, and CXCL10 (486). Despite Melph being classed as an old therapy, it remains crucial in the treatment MM, due to its manageability, safety profile, efficacy, and economic sustainability. These characteristics make Melph treatment critical for new regimens in combination with novel agents (485).

Several alkylating agents (temozolomide (TMZ), cyclophosphamide (CPA) and Melph) have been found to synergise with numerous OVs such as Ads, NDV, MYXV, RV and Seneca Valley virus (Table 1.12). The combination of alkylating agents and OVs have been found to enhance oncolytic activity of OVs by enhancing tumour cytotoxicity, viral replication (490–494) and altering immune cells/activity.

Table 1.12: Combining OV's with alkylating agents (469)

Alkylating agents				
OVs	Combination Treatment	Tumour Type	Study Phase	Ref
CRAAdRGDflt-IL24	TMZ	Glioma	Preclinical Phase. Subcutaneous xenograft model in athymic nude mice.	(490)
Adhz60	TMZ	Lung Cancer	Preclinical Phase. Subcutaneous xenograft model in athymic nude mice.	(491)
NDV-LaSota	TMZ	Glioblastoma	Preclinical Phase. Orthotopic syngeneic model in rats.	(492)
vMyx-M011L-KO	TMZ	Glioblastoma	Preclinical Phase. Orthotopic syngeneic model in immunocompetent mice.	(493)
VV	CPA	Glioma	Preclinical phase. Rat and human glioma cell lines. Subcutaneous xenografts in athymic nude mice. Syngeneic model in immunocompetent rats.	(494)
oHSV-1	CPA	Glioma	Preclinical phase. Syngeneic model in immunocompetent rats.	(495)
VSV or MV	CPA	N/A	Preclinical phase. Immunocompetent model in mice.	(496)
VRX-007 (oAd)	CPA	Renal	Preclinical phase. Syngeneic model in immunocompetent Syrian hamsters.	(497)
GLV-1 h68 (VV)	CPA	Lung	Preclinical phase. Human lung cancer cell lines. Subcutaneous xenograft model in athymic nude mice.	(498)
Ad5-D24-GMCSF	CPA	Advanced solid tumours refractory to and progressing after conventional therapies	Clinical Phase. 43 patients.	(317)
Reolysin (reovirus)	CPA	Advanced or metastatic solid tumours refractory to conventional treatment	Clinical Phase. 36 patients.	(499)

Table 1.12 continued.

OVs	Combination Treatment	Tumour Type	Study Phase	Ref
NTX-010 (Seneca Valley Virus)	CPA	Relapsed or refractory neuroblastoma, rhabdomyosarcoma or rare tumours with neuroendocrine features	Clinical Phase. 22 Paediatric Patients.	(500)
VSV	CPA	Mesothelioma	Preclinical phase. Human mesothelioma cell lines.	(501)
VV	Melphalan plus TNF- α \pm Radiotherapy \pm surgery \pm PDL-1 via isolated limb perfusion	Soft tissue sarcoma	Preclinical phase. Syngeneic immunocompetent rat models.	(502–504)
ONYX-015	Melphalan	Squamous cell and colon	Preclinical phase. Human tumour cell lines.	(505)
HYPER-Ad	BCNU	Glioma	Preclinical phase. Human glioma cell lines. Subcutaneous xenograft model in athymic nude mice.	(506)

With regards to enhancing tumour cytotoxicity and viral replication several studies have shown this preclinically, predominantly using TMZ in combination with oncolytic Ads. In glioblastoma models, a VEGFR-1 promoter-regulated Ad encoding IL-24 (CRaDRGDfl-IL24) was combined with TMZ. The combination increased cytotoxicity against human glioma cells *in vitro*. *In vivo* in intracranial glioma xenografts, the combination inhibited tumour growth and prolonged survival of the mice compared to monotherapy (490). In a similar study, an *E1B*-deleted oncolytic Ad (Adhz60) was used in combination with TMZ in lung cancer (491). The combination of Adhz60 and TMZ synergistically enhanced cytotoxicity, increased apoptosis (increased Annexin V staining and cleaved caspase 3), increased viral production (increased viral titre and E1A protein), and increased autophagy (increased LC3-II and decreased p62). Additionally, the combination downregulated expression of MGMT, which

confers resistance to many alkylating agents, such as TMZ, this was thought to be due to E1A binding to CBP/P300, which has been shown to strongly inhibit MGMT promoter activity (507). Lastly, *in vivo* the combination significantly suppressed the growth of subcutaneous lung cancer xenografts in nude mice, and an increase in Ad hexon and cleaved caspase 3 was observed histologically (491).

TMZ has been used in combination with other viruses. In combination with NDV in glioblastoma models the combination extended survival in rat xenografts, the authors rationale behind the extended survival was thought to be due NDV increasing apoptosis and suppressing AKT signalling which blocks TMZ induction of endogenous AKT kinase activity (492). Additionally, an oncolytic MYXV defective in an anti-apoptotic protein MO11L, has been used in combination with TMZ in glioblastoma. Combination treatment of tumour bearing mice significantly prolonged survival in an immunocompetent brain-tumour bearing glioblastoma model (493).

Regarding altering immune cells/activity, studies suggest that alkylating agents transiently cause beneficial immunosuppression resulting in increased OV propagation and survival within infected tumours. CPA was combined with a double-deleted-VV in glioma syngeneic rat models. The combination enhanced viral replication and prolonged survival (494). When CPA was pre-administered before intratumoural oncolytic HSV in a syngeneic rat glioma model, there was a rapid increase in NK cells, microglia/macrophages and IFN- γ . This also increased HSV replication and tumour oncolysis (495). In another study pre-treatment with either oral or systemic CPA regimen partially or completely suppressed primary antibody responses to I.V administered oncolytic MV or VSV, respectively (496). In an immunocompetent Syrian hamster model, CPA was combined with an oncolytic Ad. CPA treatment allowed intratumoral virus levels to remain elevated for prolonged periods with improved replication and oncolysis whilst CPA alone had no effect on tumour growth (497). CPA in combination with an oncolytic VV (GLV-1 h68) was evaluated in a lung carcinoma model. The combination significantly enhanced the efficacy of intravenously injected VV, resulting in a significant up-regulation of pro-inflammatory cytokines and down-regulation of anti-inflammatory cytokines. Expression of

VCAM-1 on endothelial cells and coagulation factors (fibrinogen and vWF) were significantly decreased, which led to a complete loss of the haemorrhagic phenotype of tumours (498). In a clinical trial in patients with advanced solid refractory tumours, patients were treated with intertumoral oncolytic Ad alone or in combination with three different regimens of low dose CPA (oral and/or I.V). CPA was found to have no effect on antibody formation or viral replication but decreased T-regs without compromising induction of antiviral or antitumour T cell responses. CPA in combination with an oncolytic Ad increased cytotoxic T cells and induced Th1 type immunity on a systemic level in all patients with higher rates of disease control than virus only and the best PFS and overall survival was seen in combination with oral and I.V CPA (317).

In contrast, a phase I dose escalation clinical trial in patients with advanced or metastatic solid cancers refractory to standard treatment received different doses of CPA 3 days before I.V injection of RV with the primary objective of reducing neutralising antibody titre. The combinations were found to be safe but only one patient maintained a neutralising antibody titre below the predefined threshold. No changes in T cell subsets including T-regs occurred with dose escalation. Viable virus was detected in 14% of patients 10 days after the last RV treatment (499). In agreement with the previous study, the Seneca Valley virus (NTX-010) was used in combination with CPA to reduce neutralising antibodies in a phase II trial in children with refractory neuroblastoma, rhabdomyosarcoma, or rare neuroendocrine tumours. The combination was safe but had no influence on antiviral activity (17/18 patients developed neutralising antibodies) (500). In another study VSV had potent oncolytic activity *in vitro* in mesothelioma, but *in vivo* VSV had no effect. Therefore, VSV was combined with CPA to suppress the VSV-targeted innate immune reactions. The combination of VSV and CPA resulted in reduced therapeutic efficacy *in vivo* despite increased intratumoral VSV titres. The authors thought this was due to VSV increasing TGF- β -dependent immune suppressive activity that inhibited CPA NK-dependent killing of tumour cells (501), this is in contrast with Peng *et al.*, (2013) who found pre-treatment of CPA suppressed antibody responses to VSV.

Minimal studies have been conducted with the use of Melph and OV. Predominantly Melph has been used as a standard of care alongside TNF α (biochemotherapy) in isolated limb perfusion in soft tissue sarcoma to test in combination with an oncolytic VV (502), oncolytic VV plus radiotherapy and surgery (503) or oncolytic VV plus PD-L1 (504). It appears in each study that the full combination offered the best treatment/disease control. The only other study combining Melph with an OV was using an oncolytic Ad (ONYX-015). This small preclinical study showed that ONYX-015 was found to have synergistic cytotoxicity, which was greatest when treatment was simultaneous. Pre-treatment with Melph resembled simultaneous treatment, however, in one cell line (HN-5a squamous cell carcinoma), Melph pre-treatment was more effective than virus pre-treatment, the opposite was true for the other cell line (HT-29 colon adenocarcinoma). The authors showed upregulated CAR mRNA expression following 24-hour Melph treatment, and upregulated protein expression by 48 hours, although protein expression was assessed by western blot, it would have been beneficial to do flow cytometry or fluorescent microscopy to determine cell surface expression of CAR (505).

The use of alkylating agents in combination with OVs so far confirm that the interactions of OVs with alkylating agents needs to be further explored. It appears *in vitro* and *in vivo* the combination enhances tumour cytotoxicity and viral replication, however the studies performed with CPA in particular show that the combinations can induce either a positive or negative influence on the immune system and on the antitumour immune response. There is also no research on the combination of an alkylating agent in combination with an OV in MM, so it would be interesting if similar beneficial effects are observed in MM. Additionally, Melph is one of the few classes of drugs classed as an inducer of ICD. Therefore, it would be interesting to see if combining Ad[CE1A] with Melph increases ICD in MPCs.

1.6.3 Panobinostat and HDACIs

Pan is a potent inhibitor of histone deacetylase, which is responsible for the regulation of gene transcription, cellular differentiation, cell-cycle progression, and apoptosis (509). In MM, the inhibition of histone deacetylation damages DNA (as chromatin remodelling can result in dsDNA breaks), upregulates proteins that promote apoptosis and cell-cycle arrest (510). Despite this, Pan lacks therapeutic activity as a monotherapy in patients with MM (511), but has shown synergy with other anti-MM agents when combined with BTZ and Dexamethasone (512,513). In addition to HDACIs anti-neoplastic effects, they are also known to weaken the cellular anti-viral immune response by impairing the expression of IFN and IFN-inducible genes (514–516). Interestingly HDACIs have been shown to have some ICD mechanisms in MM and other cancers (197,540–544). HDACI Quisinostat has been shown to increase cell surface ICD DAMP CALR and decrease CD47 expression in tumour cells, increased DC maturation, and transiently increased the amount of memory and naïve T cells in the BM in 5T33MM models of MM, however, in *in vivo* vaccination assays, Quisinostat did not provide 100% protection (545).

Initially, HDACIs were found to rescue viral replication in resistant cells (517–519), which led to several investigations into their potential to enhance OV replication. Several HDACIs (Vorinostat, Trichostatin A (TSA) and Valproic Acid (VPA)) have been found to synergise with numerous OVs such as Ads, HSV-1, VSV, VV and RV (Table 1.13) (520). The combination of HDACIs and OVs has been found to enhance the oncolytic activity of the OVs by increasing viral infection, replication and tumour cytotoxicity and decreasing type I IFN and IFN stimulated genes (ISGs), further enhancing viral replication and spread in tumour tissues (521). The mechanism by which this specificity occurs in malignant cells and not healthy cells remains unclear, but it is thought to be due to either an inherent preference of OVs for tumour cells or an enhanced susceptibility of tumour cells for HDACIs (522). Additionally, the enhanced susceptibility could be caused by the aberrant activity of HDACs, which has been documented for several tumour types (523–525).

Table 1.13: Combining OV's with HDACI

Histone Deacetylase Inhibitors (HDACI)				
OVs	Combination Treatment	Tumour Type	Study Phase	Ref
OBP-301	FR901228	NSCLC	Preclinical Phase. Human NSCLC cell lines.	(526)
dl520	TSA	Glioblastoma	Preclinical phase. Human glioblastoma cell lines.	(527)
Delta24-RGD	TSA & irinotecan (topoisomerase I inhibitor)	Glioblastoma	Preclinical phase. Patient-derived glioblastoma cells.	(528)
Δ24-luc	SK7041, SBHA and Vorinostat	Lung	Preclinical phase. Human lung cancer cell lines. Subcutaneous xenograft model in nude BALB/c mice.	(529)
FFIG	VPA	Prostate	Preclinical phase. Human prostate cancer cell lines Subcutaneous xenograft model in athymic nude mice.	(530)
dl24	TSA	Ovarian	Preclinical phase. Human cisplatin sensitive and resistant ovarian cancer cell lines.	(531)
ZD55-TRAIL	SAHA	Cervical	Preclinical phase. Human cervical cancer cell lines. Subcutaneous xenograft model in BALB/c nude mice.	(532)
Reovirus	AR-42, SAHA and LBH	MM	Preclinical Phase. Human MM cell lines. Systemic xenograft model in NOD/SCID mice.	(533)
oHSV1	VPA	Glioma	Preclinical Phase. Subcutaneous xenograft model in athymic nude mice.	(534)
HSV ^{GM-CSF}	VPA	Melanoma	Preclinical phase. Human melanoma cell lines. PBMCs from patients or HDs.	(535)
H1 parvovirus	VPA	Pancreatic and Cervical	Preclinical phase. Human pancreatic and cervical cancer cell lines. Subcutaneous xenograft rat model in athymic nude rats. Subcutaneous xenograft of patient derived material in NOD/SCID mice.	(536)
VSV	MS-275	Melanoma	Preclinical Phase. Intracranial syngeneic model in immunocompetent mice.	(537)

With regards to HDACIs increasing viral infection, HDACIs have been found to increase Ad infection by upregulation of CAR (526,527,529), and $\alpha\beta_3$ integrins (528) and RV infection by upregulating JAM-A increasing RV infection (533), which increases RV killing of MM cells *in vitro* and *in vivo*. Concerning the upregulation of Ad infection following HDACI treatment, it was found that HDACI FR901228 upregulated CAR expression in human lung cancer cell lines which increased infection efficiency of oncolytic Ad OBP-301. The combination also resulted in a synergistic antitumour effect *in vitro* (526). In another study TSA upregulated CAR expression, and when combined with Irinotecan (topoisomerase I inhibitor), replication and cell lysis of oncolytic Ad (dl520) was enhanced further (527). In further support of HDACI increasing Ad infection, HDACIs Scriptaid and LBH589 were combined with oncolytic Ad Delta24-RGD (24 base pair deletion in *E1A*, and fibre knob modification to include RGD peptide allowing binding to integrin $\alpha\beta_{3/5}$), which resulted in synergistic interactions in ~50% of glioblastoma stem cells. Both HDACIs increased $\alpha\beta_3$ integrin levels resulting in increased viral infection in responding glioblastoma stem cells, but not in non-responding glioblastoma stem cells. LBH589 moderately increased late viral gene expression (as assessed by GFP expression controlled by the *E3* promoter), but both HDACIs decreased viral titre. Both HDACIs were shown to enhance necrosis, but Scriptaid also enhanced apoptosis (increased caspase 3/7 activity) and autophagy (LC3B conversion, p62 and phosphor-p70S6K consumption) (528). In contrast, *in vitro* treatment of HDACIs (SK7041, SBHA and Vorinostat) at pre- and post-transductional periods were found to increase CAR expression in human lung cancer cell lines resulting in increased transduction of Luc from a Luc expressing oncolytic Ad ($\Delta 24$ -luc). However *in vivo* in a subcutaneous xenograft lung cancer model, the combination suppressed Luc expression from $\Delta 24$ -luc injected tumours, additionally drug interaction analysis *in vitro* showed an antagonistic interaction likely due to suppressed Ad replication. It was found that HDACI increased cell-cycle related protein p21, suppression of p21 expression with siRNA reversed the HDACI-induced Ad replication but failed to reverse antagonistic interaction. However, treatment with HDACI at the pre-transductional period only, revealed an improvement in the transduction efficiency of $\Delta 24$ -luc and induced a synergistic interaction between

$\Delta 24$ -luc and Vorinostat *in vitro*. This was thought to be due to Vorinostat suppressing Ad replication if given post-transduction (529). This study supports the decreased viral titre found following Scriptaid and LBH589 treatment by Pont *et al.*, 2015. Another earlier study supports that HDACIs decrease Ad replication by increased p21. Briefly, VPA was shown to increase E1A and E1B production but decreased late Ad protein production (fibre knob) which resulted in decreased Ad replication late in the viral life cycle and inhibited viral burst and cell cytotoxicity in prostate cancer cells. The authors hypothesised that VPA induced cell-cycle-regulating protein p21 which may be partially responsible for the increased E1A. The authors found a positive correlation with p21 and viral E1A levels. p21 expression limited Ad replication in different cancer cell models (as determined by overexpression and knockout experiments), therefore, suggesting that p21-induced increases in E1A result in dysfunctional E1A or that p21 inhibits downstream effectors of E1A action (530).

The mechanism for downregulated Ad replication following HDACI appears to be p21 mediated, but the mechanism may be more complex as other studies still report enhanced cytotoxicity following HDACI treatment. In contrast, HDACIs have been shown to increase viral infection of other OVs. VPA was shown to increase viral replication of oncolytic HSV-GM-CSF in melanoma cell lines, along with increasing GM-CSF expression and increased cytotoxicity (535). The mechanism of this finding is unknown, but the authors propose that VPA alteration of chromatin structure prevents HSV-GM-CSF from 'hiding' within DNA, making it more accessible for viral replication. Another example of HDACIs increasing viral replication come after treatment of VPA in combination with H1 parvovirus, which enhances tumour cytotoxicity and replication in pancreatic ductal adenocarcinoma and cervical cancer by increasing the acetylation of the viral NS-1 protein (536).

With regards to HDACIs increasing tumour cytotoxicity, it appears the combination with OVs increases apoptosis (528,532) and cell cycle growth arrest (532). TSA was used in combination with an oncolytic Ad (dl24) in ovarian cancer. A cisplatin-resistant ovarian cancer cell line, which upregulate HDAC2 and to a lesser extent HDAC1, showed diminished Ad-mediated cytotoxicity with increasing doses of

cisplatin compared to cisplatin-sensitive cell lines. However, when dl24 was combined with HDACI TSA in cisplatin-resistant cells there was significantly enhanced Ad-mediated cytotoxicity in the presence of cisplatin, whilst TSA monotherapy did not reduce cell viability, suggesting an Ad-dependent effect (531). In another study in cervical cancer, an oncolytic Ad containing the tumour necrosis factor-related apoptosis-inducing ligand (TRAIL) gene (ZD55-TRAIL) was combined with HDACI suberoylanilide hydroxamic acid (SAHA). This combination synergistically killed HELA cells by inducing G2 growth arrest and apoptosis. In a subcutaneous cervical xenograft model, the combination inhibited tumour growth (532).

Some HDACIs decrease type I IFN and IFN stimulated genes (ISGs), butyrate and TSA can indirectly inhibit the innate immune signalling through inhibition of NF- κ B activation by reducing proteasome subunit expression (538). In addition, the adaptive immune response has also been reported to be beneficially influenced by HDACIs. Treatment with Entinostat resulted in prolonged lymphopenia and depletion of T-regs (537,539), in glioblastoma models, VPA was shown to suppress IFN- γ production, and immune infiltration including lymphocytes, NK cells and macrophages, which helped increase oncolytic HSV-1 replication, but has the potential to reduce antitumour immune responses (534). In contrast, the addition of VPA in combination with HSV-GM-CSF in melanoma augmented the development of antitumour immunity by increased expression of activating ligands for NK cell recognition and induced expression of TAAs, whilst supporting innate NK cell killing and CTL priming rather than suppressing it (535). Some of the discrepancy in modulating the adaptive immune response may be related to the differences in HDAC targets of the different HDACIs, whether they target class I and/or II HDACs or are pan-HDACI, but this does not explain the differences above as VPA was used in both papers, therefore, it is probably due to tumour and OV dependent differences.

HDACIs in combination with OVs appears promising but to date, this therapeutic approach has not been initiated in clinical trials. There has been previous research of HDACI in combination with oncolytic Ads, but none have been in MM or any other haematological malignancy, it would be

interesting to determine if HDACi augment Ad[CE1A] infection and cytotoxicity. Additionally, Pan has been shown to induce some markers of ICD. Therefore, it would be interesting to see if combining Ad[CE1A] with Pan increases ICD in MPCs.

1.6.4 IMiDs

IMiDs such as the Thalidomide and its derivatives Len and Pom, have a well-established role as anti-MM agents, they have substantially improved outcomes seen in MM patients over the past decade (546). IMiDs play an important role in modulating the inherently immunosuppressive environment of MM. Specifically, they have been shown to co-stimulate partially active T cells (547), enhance NK cell proliferation (548), inhibit proliferation and function of T-reg cells (549) and downregulate the PD-L1/PD-1 pathway in MM (311,550). Additionally, IMiDs have a well understood role in abrogating MM angiogenesis, altering adhesion between MM cells and the BM environment and mediating direct cell death through induction of apoptosis (313,553). Their established use in the clinic and their immunomodulatory effects make IMiDs a rational candidate for treatment in combination with oncolytic virotherapy.

There are many preclinical and clinical studies investigating a range of immune modulating agents in combination with OVs (reviewed in (460)), however, there are only three preclinical studies using ImiDs in combination with OVs and one clinical trial that is currently underway with RV in combination with Len or Pom in MM (MUK eleven; NCT03015922) with no results published to date. Firstly, Thalidomide was combined with HSV-1 OncdSyn in mouse breast cancer cell line 4T1. In a subcutaneous syngeneic mouse model, Thalidomide was given orally in the food, and virus was administered intratumorally. The combination showed the most significant decrease in primary tumour volume and number of metastatic nodes in the lung compared to monotherapy. Splenocytes derived from mice were treated *ex vivo* with Thalidomide and HSV-1 OncdSyn and incubated with 4T1 cells, TNF- α levels were highest from splenocytes derived from mice treated with Thalidomide and HSV-1 OncdSyn. Therefore, the combination treatment resulted in increased co-stimulation of cellular synthesis of TNF- α to further suppress growth of tumours (552). Len was combined with oHSV-1 in MM. The combination

significantly increased cytotoxicity in all Len-sensitive cell lines compared to monotherapy. Len did not augment oHSV-1 replication; therefore, the enhanced cytotoxicity was found to be Len independent. *In vivo* in a subcutaneous MM xenograft model, mice were treated with oHSV-1 (I.T), Len (I.P) or the combination. The combination suppressed tumour growth the most. The authors conclude that the combination may be an effective therapy for plasma cell neoplasms that are accessible to intratumoral injections (553). Lastly, a pre-clinical study using oncolytic RV in combination with Len in MM was performed. The combination augmented antitumour efficacy against *ex vivo* primary patient MM cells and MPC lines. Additionally, they found that coculture of human MPC lines with human BMSC lines protected against Len and Dexamethasone-induced MM cell death, however, treatment with RV overcame this cytoprotection (554).

The combination of IMiDs and OVAs may represent a rational therapeutic option based on the minimal research thus far that exploits direct cytotoxic as well as indirect immune-mediated mechanisms. Obviously, more research is needed to explore this combination, particularly for oncolytic Ads.

1.6.5 Summary

The number of combination studies with OVAs signifies the increasing interest toward this therapeutic approach. So far, many studies have demonstrated potential of OVAs in combination with the discussed drug class types, augmenting antitumour responses. However, most studies are preclinical, and some drug classes only had a limited number of studies (IMiDs) and only 3 of the studies discussed were in MM. Whilst understanding of how to obtain OVAs full potential evolves, it appears that release of TAAs and activation of the immune system is crucial for OVAs. As discussed in section 1.6, clinical trials of OVAs in combination with immunomodulatory agents are a large section of the clinical trial landscape. However, chemotherapy or targeted therapies can address some of the limitations of OVAs such as improving viral infection, replication, tumour cytotoxicity as well as improving the antitumour immune responses by improving antigen processing and regulation of immune cell populations. Combinations with more traditional chemotherapy/targeted therapies are still a large part of the clinical trial

landscape. The studies discussed contribute to the understanding of how these drug classes may interact with OV_s, and this will help guide Ad[CE1A] combinations in MM.

1.7 Conclusion

We have entered a new era in the treatment of MM with the promising use of OV_s. Although there is insufficient data to support their use in the clinical area as a monotherapy, the next logical step is to combine these OV_s with other synergistic therapies to increase their efficacy and to use OV_s to target and eliminate MRD and activate antitumour immunity after standard chemotherapy.

1.8 Hypothesis and Aims

The efficacy of OVVs against MM remains largely underexplored compared to that of solid malignancies.

This is reflected in the limited translation of OVVs in the haematological setting. Our novel engineered CS1-promoter driven oncolytic Ad (Ad[CE1A]), developed at the University of Sheffield, has shown efficacy *in vitro* and *in vivo* in a late-stage disease xenograft model. Ad[CE1A], like other OVVs, as a monotherapy in late-stage disease is unlikely to induce longer and/or deeper remission periods and may just stabilise or slow down disease progression. Therefore, in my PhD research, I hypothesise that Ad[CE1A] can control or eradicate MRD and when combined with MM standard of care therapies will result in enhanced anti-MM efficacy. With the overall aim to translate Ad[CE1A] therapy to more meaningful patient outcomes. To do this, the following aims were devised.

1. Characterise Ad[CE1A] efficacy and cell death mechanism in human MPC lines and *ex vivo* patient samples (Chapter 3)
2. Investigate Ad[CE1A] treatment of MM MRD *in vivo* in a U266 xenograft model (Chapter 4).
3. Evaluate Ad[CE1A] efficacy in a 5TGM1 syngeneic model of MM (Chapter 5)
4. Evaluate Ad[CE1A] in combination with current anti-MM therapies to find combinations that enhance MM efficacy, and to determine the mechanism(s) responsible for enhanced efficacy (Chapter 6).



Chapter 2 : Materials and Methods



2.1 General Cell Culture Methods

All buffers, reagents and media used in tissue culture are outlined in Tables 2.1, 2.2, and 2.3. All Cell lines were genetically profiled by the genomics core facility at the University of Sheffield using short tandem repeat (STR) analysis to confirm their identity and were routinely tested for mycoplasma, examples are shown in the Appendix (Table 8.1 and Figure 8.1).

Table 2.1: Reagents required for tissue culture

Item	Catalogue number	Source:
Foetal Bovine Serum (FBS), Heat Inactivated	16140071	Gibco™, UK
Penicillin (10,000 units/mL) & Streptomycin (10,000 µg/mL)	15140122	Gibco™, UK
Amphotericin B	15290018	Gibco™, UK
Non-essential Amino Acids x100	11140050	Gibco™, UK
Sodium Pyruvate (100 mM)	11360070	Gibco™, UK
Phosphate Buffered Saline (PBS) (pH 7.4)	10010023	Gibco™, UK
Dimethylsulfoxide (DMSO)	D8418-500ML	Sigma-Aldrich, UK
Trypsin-EDTA (0.05%) with Phenol Red	25300054	Gibco™, UK
Trypan Blue Solution (0.4%)	15250061	Gibco™, UK
Histopaque®-1077	10771-500ML	Sigma-Aldrich, UK
Auto-MACS® Rinsing Solution	130-091-222	Miltenyl Biotech
MACS BSA Stock Solution	130-091-376	Miltenyl Biotech
Magnetic CD138 Beads	130-051-301	Miltenyl Biotech
MS Columns	130-042-201	Miltenyl Biotech
AlamarBlue® Cell Viability Reagent	DAL1100	Invitrogen™

Table 2.2: Medium required for tissue culture

Cell lines	Medium	Supplement(s)
All MPC lines & Primary CD138 ⁺ cells	Roswell Park Memorial Institute (RPMI) 1640 with GlutaMAX™ (Gibco, by Life Technologies, UK)	10% FBS, 1% penicillin & streptomycin, 1% amphotericin B, 1% non-essential amino acids; 1% sodium pyruvate
HEK293, HS-5, LNCaP & Primary CD138 ⁻ cells	Dulbecco's Modified Eagle Medium (DMEM) with GlutaMAX™, no sodium pyruvate (Gibco, by Life Technologies, UK)	10% FBS, 1% penicillin & streptomycin, 1% amphotericin B
Saos-2	Alpha Minimum Essential Media (αMEM) with GlutaMAX™ and sodium pyruvate (Gibco, by Life Technologies, UK)	10% FBS, 1% penicillin & streptomycin, 1% amphotericin B
All Cell Lines	Freezing Medium	90% FBS 10% DMSO

Table 2.3 Buffers required for tissue culture

Solution	Component
Auto-MACS® Buffer	Auto-MACS® Rinsing Solution with 5% MACS BSA stock solution
Erythrocyte lysis Buffer (Ammonium Chloride Potassium)	155mM Sodium Chloride, 10mM Potassium Bicarbonate, 0.1mM EDTA, pH 7.3

2.1.1 Cell Lines

2.1.1.1 Myeloma Cell Lines and Culture

Human MPC lines, JJN-3, RPMI-8226, OPM-2, KMS-11, KMS-12-BM (DSMZ, Germany), U-266 (LGC Standards, UK), L363, RMPI-8226, NCI H929 (kind gift from Dr Khanim, University of Birmingham, Birmingham, UK) and murine 5TGM1 and 5TGM1-Luciferase (Luc) (kind gift from Dr Oyajobi, University of Texas, San Antonio, USA, via Dr Ryan Bishop, Moffitt Cancer Centre, Tampa, Florida, USA) are summarised in Table 2.4. MPC lines were maintained in complete RPMI media (Table 2.2). Cells were incubated in at 37°C in a humidified atmosphere containing 5% CO₂ which were routinely passaged when cells had reached an appropriate density ~80% confluency. The panel of MPC lines above are used in initial experiments in chapter 3, but only JJN-3, U266, OPM-2 and 5TGM1 cells are used throughout the rest of the thesis as these cell lines have more established *in vivo* models.

Table 2.4: MPC lines origin and characteristics (331,332).

Cell line	Origin	Cell Surface Markers	Cytogenetics	Molecular abnormalities	Notes
JJN-3	PCL in 57-year-old female, IgAk. Established from BM.	CD138 ⁺ HLA-DR ⁺	hypotriploid 58-67, XX t(14;16) 9% polyploidy	TP53 homo deletion	2 copies of t(14;16) associated with c-maf activation
L-363	PCL in 36-year-old female, IgG. Established from peripheral blood.	CD138 ⁺ HLA-DR ⁺	Hyperdiploid 11% polyploidy Del(17)(p12) 11q13, 14q32		11q13 and 14q32 breakpoints recurrent in PCL
OPM-2	PCL in 56-year-old female, IgGλ. Established from peripheral blood.	CD138 ⁺ CD38 ⁺ HLA-DR ⁻	Hypertriploid/ hypotetraploid 77-82, XX t(4;14)*	CDKN2C homo del FGFR3 K650E het TP53 R175H homo	Cryptic t(4;14) associated with IgHFGFR3 fusion
U266	PCL in 53-year-old male, IgEλ. Established from peripheral blood.	CD38 ⁺ CD138 ⁺ HLA-DR ⁺	Hypodiploid 6.5% polyploidy t(11;14) 11q13	BRAF K601N het TP53 A161T homo TRAF3 K550IfsX3 homo RB1 E419X homo RB1 K228R homo	Secretes IL-6, IgE and λ light chains. 11q13 breakpoint recurrent in MM
RMPI-8226	PCL in 61-year-old male, IgGλ. Established from peripheral blood.	CD38 ⁺ CD138 ⁺ HLA-DR ⁺	Hypotriploid 7.5% polyploidy 62-67, XXY t(14;16)	CDKN2C homo del KRAS G12A het TP53 E285K homo TRAF3 homo del	Secretes λ light chains only. 14q+ and 22q-associated with multiple myeloma - identified by disomic 14q+
NCI-H929	MM in 62-year-old Caucasian female, IgAk. Established from pleural effusion.	CD38 ⁺ CD138 ⁺ HLA-DR ⁻	Hypodiploid 16% polyploidy 43-46, X t(4;14)*	c-myc rearranged myc RNA expressed, NRAS G13D het	Secretes large amounts of IgA
KMS-11	MM in 67-year-old female, IgGκ. Established from a pleural effusion.	CD138 ⁺	t(4;14)*, t(14;16) hypertriploid	FGFR3 het TP53 homo del TRAF3 homo del	κ light chain secretor
KMS-12-BM	MM in 64-year-old women, non-secretory. Established from the BM.	CD38 ⁺ CD138 ⁺ HLA-DR ⁻	Hypertriploid 3% polyploidy t(11;14)		Carries semi-cryptic t(11;14) with IGH-CCND1 rearrangement
5TGM1	Established from inbred C57BL/KaLwRij mice that spontaneously developed MM	CD138 ⁺	t(14 ;16)		κ light chain secretor

* Associated with increased expression of SLAMF7 mRNA (281). PCL: Plasma Cell Leukaemia.

2.1.1.2 BMSC Line and Culture

HS-5 is a human BMSC line of fibroblast morphology isolated from a healthy 30-year-old Caucasian male which have been HPV-16 E6/E7 transformed (ATCC). HS-5 cells are used as feeder layers as they secrete significant levels of growth factors (438), these cells were maintained in complete DMEM media (Table 2.2) (348). HS-5 cells were used in coculture assays in chapter 3 and to induce dormancy in chapter 4. Cells were incubated at 37°C in a humidified atmosphere containing 5% CO₂ which were routinely passaged with 0.05% trypsin-EDTA when cells had reached 80-90% confluency.

2.1.1.3 Osteosarcoma Cell Line and Culture

Saos-2 are a human bone osteosarcoma cell line of epithelial morphology isolated from an 11-year-old Caucasian female with osteosarcoma. Saos-2 cells have a mature osteoblast phenotype, they have a similar cytokine and growth factor expression profile to human osteoblast cells and have the ability to mineralise matrix (333). Saos-2 cells were maintained in complete α MEM media (Table 2.2). Saos-2 cells were used in coculture assays to induce dormancy in chapter 4. Cells were incubated in at 37°C in a humidified atmosphere containing 5% CO₂ which were routinely passaged with 0.05% trypsin-EDTA when cells had reached 80-90% confluency.

2.1.1.4 Prostate Cancer Cell Line and Culture

LNCaP are a prostate cancer cell line of epithelial morphology isolated from a 50-year-old Caucasian male (441). LNCaP cells were used as a CS1-negative control in experimental assays with MM cells. LNCaP cells were maintained in complete DMEM medium (Table 2.2). Cells were incubated in at 37°C in a humidified atmosphere containing 5% CO₂ which were routinely passaged with 0.05% trypsin-EDTA when cells had reached 80-90% confluency.

2.1.1.5 HEK293A Cell Line and Culture

A Human embryonic kidney cell line (HEK293A) (ATCC, Rockville, US) derived from primary human embryonic kidney cells has been transformed with a fragment of the Ad5 genome including the E1A gene. HEK293A cells are highly permissive for the generation and replication of Ads. HEK293A cells are packaging cells and have been used for the generation and amplification of non-replicative E1-deleted adenoviral vectors, and for the generation and functional titration of oncolytic adenoviruses (442). The HEK293A cell line was cultured in complete DMEM medium (Table 2.2) incubated at 37°C in a humidified atmosphere containing 5% CO₂ which were routinely passaged with 0.05% trypsin-EDTA when cells had reached 80-90% confluency.

2.1.1.6 Developing Bortezomib Insensitive Cell Lines

JJN-3 and U266 human MPC lines were exposed to increasing concentrations of BTZ (0.1 nM-5 nM; increments initially 0.15 nM until 1.5 nM then 0.25 nM thereafter) in complete RPMI medium (Table 2.2) to develop BTZ insensitivity. During this time, BTZ was added for 72 hours, BTZ was then washed off via centrifugation and the cell lines resuspended in fresh complete RPMI medium until viability was recovered, the cycle then began again with increasing concentrations of BTZ.

2.1.2 Cell Counting and Maintaining Cell Stocks

2.1.2.1 Cell Counting

To determine viable cell numbers, manual counting methods were performed using trypan blue exclusion and a haemocytometer. 10 µL of cell suspension was mixed with 10 µL trypan blue and thoroughly mixed. 10 µL of this solution was placed onto a clean haemocytometer chamber. Viable cells in each quadrant were counted and the mean was calculated. The number of cells per mL was calculated using the following formula:

$$\text{Cells per mL} = \text{mean number of cells per quadrant} \times \text{dilution factor} \times 10^4$$

Cells with <90% viability were not used in assays.

2.1.2.2 Cell Passage

For suspension cells, cells were passaged around 80% confluency and were passaged 1:2 to 1:4 every 2-3 days or 1:8 to 1:10 every 5-7days with complete RPMI media. For adherent cells, cells would be passaged around 80-90% confluency. Medium would be removed from the tissue culture flask and the adhered cells would be washed with PBS to remove remaining media containing FBS. To detach cells, pre-warmed (37°C) trypsin-EDTA (0.05%) solution would be added to the flask which would then be incubated at 37°C until cells have detached or for no more than 5 minutes. Once cells have detached, appropriate medium containing FBS for each cell line was added to the flask to stop the trypsin-EDTA reaction. The solution containing the cells, medium and trypsin-EDTA would be collected into a falcon tube and centrifuged at 400g for 5 minutes to remove remaining trypsin. Cells would then be resuspended in media appropriate for the cell line being passaged and were passaged 1:2 to 1:4 every 2-3 days or 1:8 to 1:10 every 5-7days.

2.1.2.3 Cell Freezing and Cryopreservation

Cells were counted as described (section 2.1.2.1) and resuspended in freezing medium (Table 2.2) at a concentration of $1-5 \times 10^6$ cells/mL depending on the cell line. Cell suspension was distributed in cryovials at 1 mL/tube and placed in a container filled with 2-propanol at -80°C for 24 hours (Mr Frosty). The cryovials were then stored in a liquid nitrogen tank. This method allowed for uniform slow freezing of the cells and prevented ice crystal formation.

2.1.2.4 Cell Thawing

Each vial of cells was removed from liquid nitrogen and rapidly thawed by partial emersion in a 37°C water bath. The thawed cells were transferred to a 15 mL falcon tube containing 4 mL of pre-warmed appropriate media, centrifuged (400g x 5 minutes) and washed in 5 mL of media. This wash step was to remove dimethylsulfoxide (DMSO). The cells were then seeded in a T25 cm² flask in 5 mL of medium.

2.1.3 Primary Cells and Culture Techniques

2.1.3.1 Sample Collection from Healthy Volunteers and Multiple Myeloma Patients

Approval was granted by the Yorkshire & The Humber-Sheffield Research Ethics Committee and National NHS ethical approval for collection of samples from patients and healthy volunteers (REC reference:05/Q2305/96). Informed consent was given by all patients and HD. Patients were recruited from the MM clinic at Sheffield Hallamshire hospital and gave written informed consent for peripheral blood (PB) and BM sample collection (Appendix Figure 8.2). HD BM samples were obtained from residual waste in a collection bag after BM stem cell harvests from allogenic stem cell donations. Patient and donor data such as age, sex, date of diagnosis, and clinical parameters were obtained and stored in a secure, anonymous manner according to 'good clinical practice' and the University of Sheffield information governance policies.

BM samples and samples from other sites (pleural cavity) from patients were collected into DMEM medium plus heparin (100 units/mL). For PB samples, venous blood samples were collected in tubes containing SST gel and clot activator K₂EDTA to prevent coagulation. For serum, venous blood samples were collected in tubes containing SST gel and clot activator, collection tubes were centrifuged at 500g for 5 minutes and serum was collected and rapidly frozen and stored at -80°C.

2.1.3.2 Isolation of Mononuclear Fractions

BM and PB samples were filtered through a 100 µm filter and diluted in an equal volume of Auto-MACS[®] rinsing solution and slowly layered over 15 mL of Histopaque[®] and centrifuged 400g for 35 minutes at room temperature with no brake. The mononuclear interface was aspirated using a sterile pasture pipette and the mononuclear cells were washed twice in ice-cold Auto-MACS[®] rinsing solution centrifuging at 400g for 10 minutes, then once again at 400g for 10 minutes. The supernatant was removed and cells were resuspended in residual volume in Auto-MACS[®] rinsing solution. At this step mononuclear cells were counted. 10 µL of mononuclear cells was added to 90 µL of acetic acid to lyse erythrocytes and manually counted as described in section 2.1.2.1.

2.1.3.3 Magnetic Assisted Cell Sorting of CD138 Positive Plasma Cells

CD138, also known as syndecan-1, is expressed on normal and malignant human plasma cells. CD138 magnetic microbeads have been developed for the isolation of plasma cells from PBMCs or BMMCs. Mononuclear cells from section 2.1.3.2 were resuspended in 1 mL of Auto-MACS[®] rinsing solution and then centrifuged at 400g for 5 minutes at 4°C. Supernatant was discarded and resuspended in 80 µL of ice-cold Auto-MACS[®] buffer. Twenty µL of CD138 magnetic microbeads per 1×10^8 cells was added and then incubated on ice for 30 minutes. Mononuclear cells were washed by adding 900 µL of ice-cold Auto-MACS[®] buffer to the cell suspension and centrifuged at 400g for 5 minutes at 4°C. The supernatant was then discarded, and cells were resuspended in 1 mL of ice-cold Auto-MACS[®] buffer. The Auto-MACS[®] MS column and magnet apparatus (Miltenyi Biotec, UK) was assembled and 500 µL of ice-cold Auto-MACS[®] buffer was added to equilibrate the column. Mononuclear cells were added to the column and CD138⁺ cells were collected. The column was washed three times with 500 µL of ice-cold Auto-MACS[®] buffer. The column was then removed from the magnet and 1 mL of ice-cold Auto-MACS[®] buffer was added to elute the CD138⁺ cells. CD138⁺ Cells were counted as described in 2.1.2.1. Percentage of CD138⁺ cells was on average 96.4% in the CD138⁺ population and 4.28% in the CD138⁻ population as determined by flow cytometry (section 2.3.4). Figure 2.1. shows representative flow cytometry plots of CD138⁺ and CD138⁻ staining in respective populations.

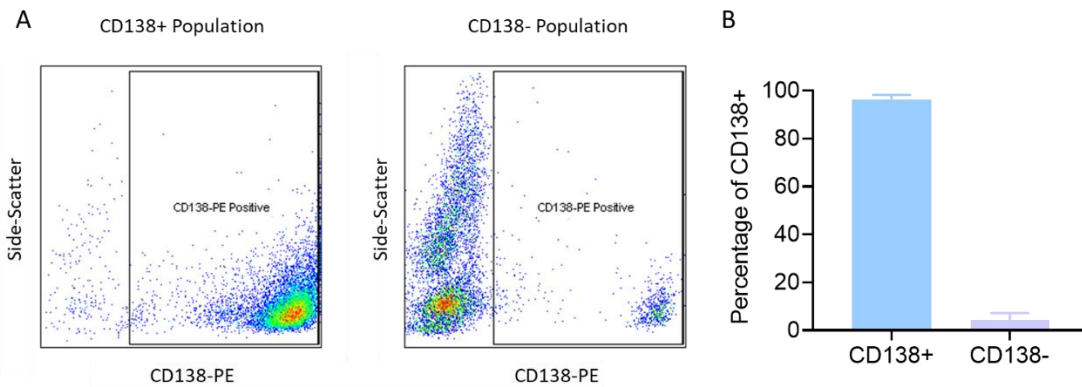


Figure 2.1: Percentage of CD138⁺ and CD138⁻ populations isolated from MM patients and HDs.

(a) Representative flow cytometry dot plots showing CD138 (FL2-H PE) against side scatter in CD138⁺ and CD138⁻ populations from BMMCs obtained from MM patients or HDs after MACs cell sorting acquired by a BD FACS caliber flow cytometer. **(b)** Percentage of CD138 population purity in CD138⁺ and CD138⁻ populations after MACs cell sorting from BMMCs obtained from MM patients or HDs (n=5). Data is the mean \pm SD.

2.1.3.4 Culture of CD138⁺ and CD138⁻ BM cells

CD138⁺ cells were maintained in complete RPMI at ~70% confluency. CD138⁻ cells were maintained in complete DMEM (Table 2.2), at ~80% confluency cells were passaged. Cells were incubated in at 37°C in a humidified atmosphere containing 5% CO₂.

2.1.3.5 Patient-derived PCL cells

The SMaRT has managed to successfully culture PCL cells from two patients for prolonged periods of time. These patient-derived cells are termed ADC1 and CB1. These PCL cells proliferate, unlike most patient cells that are extracted from PB or BM. Therefore, these ADC1 and CB1 cells were used in studies that could not be performed on most non-proliferative patient cells. These cells were kept below passage 15 to try to preserve the genetic and phenotypic similarities to when they were first extracted from patients.

2.1.3.6 Production of Ad[CE1A]-BMMCs Conditioned Media

BMMCs from HDs or MM patients were seeded at 2×10^6 cells/mL and treated with Ad[CE1A] MOI 20 or vehicle PBS. After 48 hours, conditioned media (CM) was collected by removing cells via centrifugation. CM was then sterile filtered using a 0.2 μ m syringe filter and Ad[CE1A] virions were UV inactivated using a UV crosslinker. CM was UV treated for 1 hour in 500 μ L aliquots in an open 24 well plate in a cell culture hood. UV inactivation was confirmed by viral titre assays (Appendix Figure 8.3).

2.2 Adenoviruses

2.2.1 Recombinant Adenoviruses

2.2.1.1 Ad[CE1A]

The conditionally replicating oncolytic Ad used in this thesis, Ad[CE1A], was generated previously by Dr Simon Tazzyman for Sheffield Myeloma Research Team. Figure 2.2 shows plasmid maps used for the production of Ad[CE1A]. This virus was engineered using the AdEasy system so that the E1A gene was placed downstream of the CS1 promoter (unpublished data). This was done by using the E1/E3-deleted AdEasy system according to the manufacturer's instructions. The CS1 promoter sequence was isolated from a CS1 Luc reporting plasmid (SwitchGear, Belgium) using KpnI and HindIII and ligated into pShuttle using the same enzymes. In order to place E1A under the control of the CS1 promoter the pShuttle-CS1 plasmid was digested with Sall and the E1A gene was PCR amplified using primers. The digested plasmids and PCR products were ligated together, and the insert checked for orientation using a digest with AhdI and XbaI. The pShuttle-CS1:E1A combined with the pAdeasy vector. The recombined vector was transfected into HEK293A cells and the virus isolated using Adeno-X Maxi Purification Kit (Clonetechn, France).

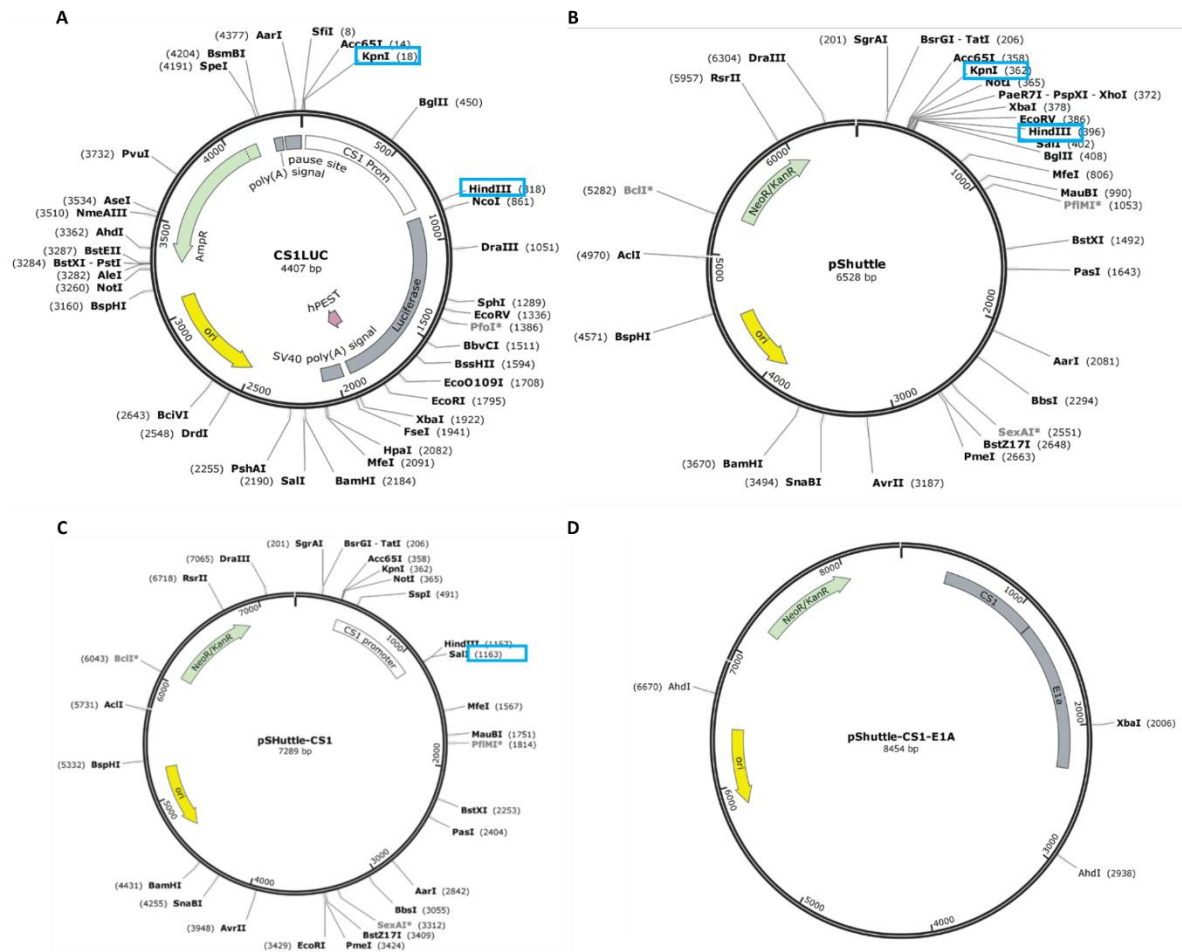


Figure 2.2: Plasmid schematics used in the construction of Ad[CE1A].

(a) Plasmid map of CS1:Luc reporting plasmid with restriction enzymes (KpnI and HindIII) used to cut out the CS1 promoter. (b) plasmid map of the destination vector pShuttle showing the same enzymes. (c) Plasmid map of pShuttle-CS1 following ligation showing locations of the SalI restriction site used to insert amplified E1A. (d) Plasmid map of complete pShuttle-CS1-E1A.

2.2.1.2 Ad-GFP

This recombinant non-replicative E1A/E1B deleted human Ad5 expresses green fluorescent protein (GFP) under the control of a CMV promoter. This virus was used to study infection efficiency of MPCs and as a control against Ad[CE1A] as it has no replicative capacity.

2.2.1.3 Ad[PSA]

This conditionally replicating oncolytic Ad5's replication is restricted to prostate cells. Prostate-specific promoter elements from T-cell receptor γ alternative reading protein (TARP), prostate specific antigen (PSA) and prostate specific membrane antigen (PSMA) genes control *E1A* expression. This virus was used as a replicative Ad5 control.

2.2.2 Adenoviral Amplification, Purification, and Quantification

2.2.2.1 Adenoviral Amplification

HEK293A cells were seeded onto 10-25 T175 flasks at $1-3 \times 10^6$. Once cells reached 70-80% confluency, adenoviral stocks were added at a multiplicity of infection (MOI) of 1-5. After 24 to 72 hours when roughly 50% of cells were showing cytopathic effects, cells and medium were harvested and spun at 400g for 5 minutes. Medium was aspirated, and the cell pellet was resuspended in 10 mL of cold PBS. The cells were centrifuged again at 400g for 5 minutes and resuspended in 1-2 mL of complete DMEM medium. The cells were subject to repeated freeze-thawing using a dry ice/ethanol bath and 37°C water bath four times to release viral particles before centrifuging at 13,000g for 10 minutes to obtain clarified cell extract. The clarified viral lysate was collected and stored at -80°C until required.

2.2.2.2 Adenoviral Purification

All buffers, reagents and materials used in adenovirus purification are outlined in Table 2.5 and Table 2.6

Table 2.5: Materials and reagents required for adenoviral purification

	Catalogue number	Source:
Caesium Chloride (>98%)	C4036-50G	Sigma-Aldrich
Mineral Oil	M5904-500ML	Sigma-Aldrich
Beckman thin wall ultracentrifuge tubes (14x89 mm)	331372	Beckman Coulter
Amicon® ultra-4 centrifugal filter units with a 50 KDa filter	UFC805008	Merk Millipore

Table 2.6: Solutions and buffers required for adenoviral purification

Solution	Components
10x TD Buffer	80 g Sodium Chloride, 3.8 g Potassium Chloride, 2.5 g Sodium phosphate Dibasic and 30 g Tris Base in 1 L ddH ₂ O pH 7.4
1x TD Buffer	100 mLs 10x TD Buffer & 900 mLs ddH ₂ O
Caesium Chloride 1.25 g/mL	36.16 g Caesium Chloride dissolved in 100 mL 1x TD buffer
Caesium Chloride 1.34 g/mL	51.20 g Caesium Chloride dissolved in 100 mL 1x TD buffer
Caesium Chloride 1.40 g/mL	62.00 g Caesium Chloride dissolved in 100 mL 1x TD buffer

Adenoviral purification was performed to obtain a viral stock with the appropriate formulation and concentration to be administered to mice by systemic injection. The method used in this thesis is based on caesium chloride (CsCl) density gradients (1.4 g/mL-1.25 g/mL) combined with ultracentrifugation to separate viral particles from cellular debris and empty viral capsids. The buffer exchange was performed using Amicon® ultra-4 centrifugal filter units with a 50 KDa filter.

The clarified cell extract containing Ad was loaded onto CsCl gradients. The CsCl gradients were prepared in Beckman thin wall ultracentrifuge tubes (14x89 mm). The first CsCl gradient was achieved by adding 2.5 mL of 1.4 g/mL of CsCl solution followed by the addition 2.5 mL of 1.25 g/mL (Buoyant density) of CsCl solution without disturbing the interface. The clarified viral lysate was then carefully loaded on top of the CsCl gradient. Mineral oil was then added on top to approximately 2 mm from the top of the tube to prevent virus aerosolization. The tubes were ultracentrifuged at 210,000g (r_{max}) (35,000 rpm) for 1.5 hours at 15°C in a Beckman L-100 ultracentrifuge with a SW41 swinging bucket rotor. After centrifugation three distinct layers were visible as shown in Figure 2.3. The bottom layer contained properly packaged virions which were removed by puncturing the tube with a 5 mL syringe and 20-gauge needle.

For further purification, a second ultracentrifuge step using a continuous CsCl gradient was necessary. The solution containing the virus was layered on top of 5 mL of 1.34 g/mL CsCl solution in a new ultracentrifuge tube. If clarified viral lysate had to be layered into multiple tubes, due to the volume in the first ultracentrifugation step, needle extracted virus was pooled together and layered onto one continuous gradient. Mineral oil was added on top to approximately 2 mm from the top of the tube.

The virus was centrifuged at 210,000g (r_{max}) (35,000 rpm) for 18 hours at 15°C Beckman L-100 ultracentrifuge with a SW41 swinging bucket rotor. After centrifugation, the lowest band, which contains the intact virions was aspirated using a 5 mL syringe and a 20-gauge needle. Figure 2.3 shows representative images of adenovirus banding after both ultracentrifugation steps. The final viral solution then underwent a buffer exchange in Amicon® ultra-4 centrifugal filter units with a 50 KDa filter to remove the toxic CsCl solution and the virus was placed into an appropriate formulation (PBS) for systemic injection. The purified adenovirus was separated into aliquots and stored at -80°C.

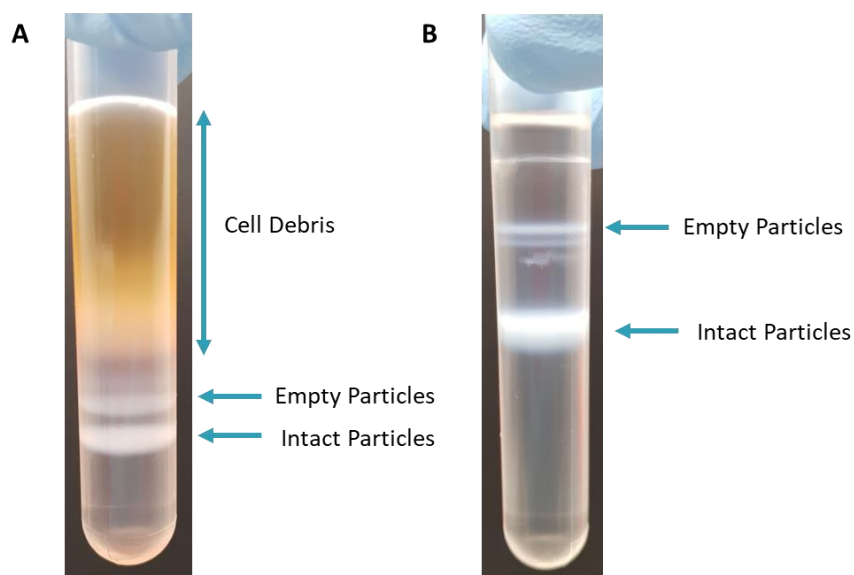


Figure 2.3: Representative images of adenoviral banding after CsCl ultracentrifugation:

(a) Image shows the ultracentrifuge tube following the first round of banding using the crude viral lysate, therefore, cellular protein and lipid is visible in a diffuse band at the first CsCl interphase. Below this, two more distinct bands are present. The lower larger band corresponds to complete virus particles at the 1.4 g/mL:1.25 g/mL CsCl interphase, whilst the upper band is formed by the empty viral particles. **(b)** Image shows the ultracentrifugation tube following the second round of banding after extraction of the lower band from image a. The lowest largest band is found at the CsCl interphase 1.34 g/mL contains the purified intact virus particles. The upper band, which is further away in distance than in image (a), contains empty viral particles that did not separate/were accidentally collected during the first round of collection.

2.2.2.3 Quantification of Adenoviral Stocks

The Adeno-X™ rapid titre kit (Clontech, UK) is based on the detection of virus positive cells for the immunostaining of the viral hexon protein in monolayers of HEK293A cells infected with serial dilutions of the virus. This technique allows the determination of functional infectious units (ifu).

HEK293A cells were seeded at 2.5×10^5 in 24 well plates in 1 mL complete DMEM media. Ten-fold serial dilutions of viral stocks were produced and 50 μ L of viral serial dilutions were added to HEK293A cells and left for 48 hours in a 37°C in a 5% CO₂ humidified incubator. Medium was aspirated, and cells were fixed by gently adding 0.5 mL of ice-cold methanol, the plate was then incubated at -20°C for 10 minutes. Cells were then washed with 0.5 mL PBS with 1% BSA three times. Cells were then stained with 0.25 mL mouse anti-hexon antibody (1:1000 dilution in PBS with 1% BSA) and incubated at 37°C on an orbital shaker for 1 hour. Cells were then washed with 0.5 mL PBS with 1% BSA three times. 0.25 mL of rat anti mouse horse radish peroxidase conjugated antibody was added (1:500 dilution in PBS with 1% BSA) and incubated at 37°C on an orbital shaker for 1 hour. Cells were then washed with 0.5 mL PBS with 1% BSA three times. 0.25 mL of 1X 3, 3'-Diaminobenzidine (DAB) substrate was added to cells and incubated at room temperature for 10 minutes. DAB was aspirated and 0.5 mL of PBS added to wells. Figure 2.4 shows representative images of Adeno-X™ hexon stain in HEK293A cells.

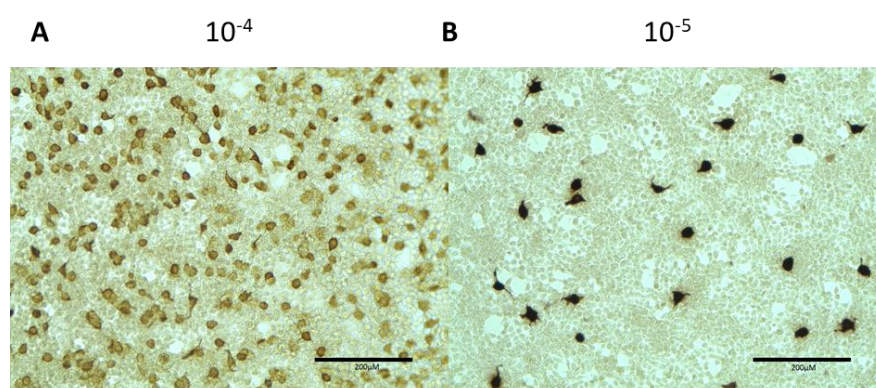


Figure 2.4: Representative images of Adeno-X™ Rapid titre kit in HEK293A cells at two serial dilutions.

Representative images of a) adenoviral hexon staining of viral stocks at a serial dilution of 10^{-4} in HEK293A cells and b) adenoviral hexon staining of viral stocks at a serial dilution of 10^{-5} in HEK293A cells. Clearly the staining in B is easier to accurately count and quantify than in A. Images taken on brightfield channel using EVOS® FL auto imaging microscope scale bar 200 μ m).

A minimum of three fields were counted using a brightfield microscope, and the following equation was used as per instructions.

$$\text{Infectious units per mL} = \frac{(\text{infected cells per field}) \times (\text{fields per well})}{(\text{volume of virus added} \times \text{dilution factor})}$$

2.3 Cell Biology

2.3.1 Adenoviral Infection and Replication

2.3.1.1 Adenoviral Infection

2.3.1.1.1 Adenoviral Infection Assay

To determine the infection efficiency of cells, a recombinant non-replicative E1A/E1B deleted human Ad5 virus that expresses GFP under the CMV promoter (Ad-GFP) was used. Human MPCs lines (JJN-3, L363, U266, OPM-2, NCI-H929, KMS-11 and KMS-12-BM), murine MPC line (5TGM1) and primary-patient derived cells were seeded at 1×10^5 cells in 500 μL complete media in a 48 well plate. Cells were infected with Ad-GFP MOI 2 or 20 or uninfected PBS control. After 24 and 48 hours, live cell imaging of GFP expression was used to qualitatively visualise infection using fluorescent microscopy (EVOS™ FL Auto) (section 2.3.5), GFP expression was then quantified using flow cytometry (section 2.3.4).

2.3.1.1.2 Adenoviral Infection following Anti-myeloma Treatment Assay

To determine if anti-MM therapies effect adenoviral infection, 1×10^5 JJN-3, U266, OPM-2 and 5TGM1 cell lines were seeded per well into a 48 well plate in 1 mL of complete media. Cells were plated in triplicate. Cells were infected with Ad-GFP MOI 2 alone or Ad-GFP and an anti-MM chemotherapy (BTZ, Melph, Pan or Pom). Doses of drugs were decided from previous dose response experiments and doses of Ad-GFP were decided based on previous assays. After 24 and 48 hours, cells were stained with TO-PRO-3 as a dead cell indicator and GFP expression was determined by flow cytometry (section 2.3.4). Additionally, cells were treated with anti-MM chemotherapy (BTZ, Melph, Pan or Pom) 24 hours prior to Ad-GFP infection. Doses of drugs were decided from previous experiments. After 24 hours Ad-GFP was added at MOI 0.2 or 2 and GFP expression was determined by flow cytometry after a further 24 hours (section 2.3.4).

2.3.1.2 Adenoviral Replication

2.3.1.2.1 Adenoviral Replication by *E1A* mRNA Expression

To determine adenoviral gene expression, *E1A* mRNA expression was assessed in a panel of human MPC lines (JJN-3, L363, U266, OPM-2, RMPI-8226, NCI-H929, KMS-11 and KMS-12-BM) and murine MPC line (5TGM1). Cells were seeded at 2×10^6 in a 24 well plate in triplicate in 1 mL of complete media and infected with Ad[CE1A] MOI 20 or with vehicle (PBS) control. Four and twenty-four hours later cells were harvested, total RNA was extracted, converted to cDNA and RT-qPCR was performed to assess *E1A* mRNA expression (section 2.4).

2.3.1.2.2 Adenoviral Virion Production

To assess differences in Ad[CE1A] replication in MPC lines, the production of infectious virus particles was assessed in a panel of human MPC lines (JJN-3, L363, U266, OPM-2, RMPI-8226, NCI-H929, KMS-11) and murine MPC line (5TGM1). Cells were seeded at 1×10^6 in a 24 well plate in 0.5 mL of complete medium and infected with Ad[CE1A] at a MOI 2 or with vehicle (PBS) control. 24 hours later medium was removed from cells by centrifugation (400g x 5 minutes), washed in PBS, recentrifuged again and resuspended in 0.5 mL of complete medium and incubated at 37°C in a humidified atmosphere containing 5% CO₂. 72 hours later cells were collected. The cells were subject to repeated freeze-thawing four times to release viral particles before centrifuging at 13,000g for 10 minutes to remove any cell debris. The supernatant of the cell lysate containing Ad[CE1A] was collected and stored at -80°C until required. Viral titre was determined (section 2.2.2.3).

2.3.1.2.3 Adenoviral Replication by *E1A* mRNA Expression following Anti-myeloma Chemotherapies

To determine if anti-MM therapies increased adenoviral gene expression, *E1A* mRNA expression was assessed in JJN-3, U266, OPM-2 and 5TGM1 MPC lines. Cells were seeded at 2×10^6 in a 24 well plate in triplicate in 1 mL of complete media and infected with Ad[CE1A] MOI 10 alone or Ad[CE1A] MOI 10 and an anti-MM chemotherapy (BTZ, Melph, Pan or Pom). Doses of drugs were decided from previous dose response experiments and doses of Ad[CE1A] were decided based on previous assays. 24 hours later cells were harvested, total RNA was extracted, converted to cDNA and RT-qPCR was performed to assess *E1A* mRNA expression (section 2.4).

2.3.1.2.4 Adenoviral Virion Production following Anti-myeloma Chemotherapies.

To determine if anti-MM therapies effect adenoviral virion production, 1×10^6 JIN-3, U266, OPM-2 and 5TGM1 cell lines were seeded per well into a 24 well plate in 1.5 mL of complete media. Cells were plated in triplicate. Cells were infected with Ad[CE1A] (MOI 2) or Ad[CE1A] and an anti-MM chemotherapy (BTZ, Melph, Pan or Pom). Doses of drugs were decided from previous dose response experiments and doses of Ad[CE1A] were decided based on previous assays. 72 hours later cells were collected in CM. The cells were subject to repeated freeze-thawing four times to release viral particles before centrifuging at 13,000g for 10 minutes to remove any cell debris. The supernatant of the cell lysate containing Ad[CE1A] was collected and stored at -80°C until required. Viral titre was determined (section 2.2.2.3).

2.3.2 Viability, Cytotoxicity, Proliferation and Apoptosis

2.3.2.1 Cell Viability: AlamarBlue® assay

Cell viability was measured using the AlamarBlue® assay (Invitrogen, UK), a fluorescent and colorimetric assay. AlamarBlue® contains a cell permeable, non-toxic weakly fluorescent blue indicator dye called resazurin. Resazurin undergoes colorimetric change in response to cellular metabolic reduction. The reduced form of resorufin is pink and highly fluorescent, the intensity of the fluorescence is proportional to the number of living cells respiring. Through detecting the level of oxidation during respiration, AlamarBlue® acts as a indirect indicator to quantitatively measure cell viability.

For AlamarBlue® assays, cells were seeded at 1×10^4 /well in 100 μL complete media in a 96 well plate, unless stated otherwise. Cells were either infected with vehicle, virus, and/or treated with anti-MM therapies and/or inhibitors. Cell viability was assessed at indicated time points by adding AlamarBlue® at a 10% concentration to each well and incubating for 4 hours at 37°C in a humidified atmosphere containing 5% CO_2 . The plates were read on a SpectrMax5e (molecular devices) plate reader using a fluorescence excitation wavelength of 540-570 nm, and a fluorescence emission wavelength of 580-590 nm. To assess proliferation, data was plotted as relative fluorescent units (RFU), to assess cell

viability, RFU were converted into a viability percentage of treated cells compared to untreated control using the following formula. All data was normalised to blank reagent controls.

$$\text{Percentage Viability} = \frac{\text{Normalised fluorescent reading of untreated controls}}{\text{Normalised fluorescent reading of treated controls}}$$

2.3.2.1.1 Dose Response to Ad[CE1A], Anti-myeloma Chemotherapies and Inhibitors

To determine the dose-response range of various treatments and their effect on cell viability, 1×10^4 cells were seeded per well into a 96 well plate in 100 μ L of complete RPMI media. Cells were seeded in quadruplicate. Experiments involving treatment of cells with virus, anti-MM therapies or inhibitors, appropriate dilutions were made in complete medium. The list of anti-MM therapies/inhibitors and the doses used to generate dose response curves are listed in Table 2.7. After 72 hours incubation, cells viability was assessed by AlamarBlue[®] assay. Sigmoidal dose response curves were generated in GraphPad.

Table 2.7: Concentrations used to generate dose response curves.

Virus/Drug/Inhibitor	Drug class/Target	Concentrations used to generate dose response curves	Company (Catalogue number)
Ad[CE1A]	OV	0.00, 0.10, 1.00, 10.0, 100, 1000 MOI	N/A
Bortezomib	Proteasome Inhibitor	0.0, 0.5, 1.0, 2.0, 2.5, 4.0, 6.0, 12, 24 nM	Selleckchem (#S1013)
Melphalan	Alkylating agent	0.00, 1.00 nM, 10.0 nM, 100 nM 1.0 μ M, 10.0 μ M, 100 μ M	Selleckchem (#S8266)
Panobinostat	HDACI	0.00 nM, 2.50, 5.00, 7.50, 10.0, 12.5, 15.0, 17.5, 20.0, 22.5, 25.0, 27.5, 30.0 nM	Selleckchem (#S1030)
Pomalidomide	IMiD	0.00 nM, 1.00 nM, 10.0 nM, 100 nM, 1.00 μ M, 10.0 μ M, 100 μ M	Selleckchem (#S1567)
Z-VAD-FMK	Pan-caspase inhibitor	N/A dose decided from literature	Selleckchem (#S7023)
Necrostatin-1	RIPK1 inhibitor	0.00, 1.00, 10.0, 25.0, 50.0, 75.0, 100 μ M	Selleckchem (~S8037)
GSK-872	RIPK3 inhibitor	0.00, 1.00, 10.0, 25.0, 50.0, 75.0, 100 μ M	Selleckchem (#S8465)
Necrosulfonamide	MLKL inhibitor	0.00, 1.00, 10.0, 25.0, 50.0, 75.0, 100 μ M	Selleckchem (#S8251)

2.3.2.1.2 Ad[CE1A] in Combination with Anti-myeloma Chemotherapies: Effect on Cell Viability

To determine the effect on cell viability of Ad[CE1A] in combination with anti-MM treatments, 1×10^4 JJN-3, U266, OPM-2 and 5TGM1 cells were seeded per well into 96 well plates in 100 μ L of complete RPMI media. Cells were seeded in quadruplicate. Cells were treated with suboptimal doses of Ad[CE1A] and/or anti-MM chemotherapies (BTZ, Melph, Pan or Pom) based on previous dose response curves. After 72 hours, cell viability was assessed by AlamarBlue[®] assay.

2.3.2.1.3 Dose Response of Ad[CE1A] in the Presence of Inhibitors: Effect on Cell Viability

To determine if inhibiting various proteins involved in distinct cell death pathways has an effect on the dose-response of Ad[CE1A], 1×10^4 JJN-3, U266, OPM-2 and 5TGM1 cells were seeded per well into 96 well plates in 100 μ L of complete RPMI media. Cells were seeded in quadruplicate. Cells were treated with concentrations of Ad[CE1A] to generate a dose-response curve and treated with \pm inhibitors listed in Table 2.7. Concentrations of inhibitors determined by previous dose-response curves. After 72 hours, cell viability was assessed by AlamarBlue[®] assay.

2.3.2.1.4 Bystander Cytokine Killing

To determine if Ad[CE1A] induced bystander cytokine killing, 1×10^4 JJN-3, U266 and OPM-2 cells were seeded per well into 96 well plates in 50 μ L of complete RPMI media. Cells were treated with 50 μ L of UV-inactivated control or Ad[CE1A] CM from BMMCs from HDs or MM patients (as described in section 2.1.3.6). Cells were seeded in quadruplicate. After 96 hours, cell viability was assessed by AlamarBlue[®] assay.

2.3.2.2 Calculation of Synergy using CompuSyn Software

The synergistic effects of Ad[CE1A] and anti-MM therapies were calculated using the combination index (CI) using CompuSyn software (ComboSyn, Inc., Paramus, NJ, USA) (334). To determine synergism or antagonism, the 'potency' and the 'shape' of the dose-effect curve for each drug must be known. The dose-effect parameters of each drug alone, as well as in combination were calculated, and the CI determined. CompuSyn software calculates the dose-effect parameters and CI determined using the median-effect equation by inputting the growth inhibition data for Ad[CE1A] and anti-MM drug alone and in combination. Synergism was indicated by CI where CI= <0.3 strong synergism; CI=0.3-0.7 synergism; CI=0.7-0.9 moderate synergism; CI=0.9-1.1 additive; CI=1.1-1.45 slight antagonism; 1.45-2 antagonism.

2.3.2.3 Flow Cytometry Cell Death Assays

Propidium iodide (PI) is a non-membrane-permeable fluorescent nucleic acid dye, therefore, PI will only be present in the DNA of cells where the plasma membrane has been compromised/permeabilised, making it useful to determine between necrotic, apoptotic and viable cells based on membrane integrity. PI binds to double stranded DNA by intercalating between the bases. Once PI has bound to DNA the excitation/emission spectra is shifted to 535 nm (green)/617 nm (orange-red). TO-PRO-3, similar to PI, but is a far-red fluorescent dye (excitation 642 nm/emission 661 nm), binds to double stranded DNA and is not membrane permeable. TO-PRO-3 was used instead of PI if other fluorophores such as fluorescein isothiocyanate (FITC)/GFP were used in the same assay due to the separation of far-red channel to FITC. Cells were seeded at indicated cell numbers and treated with indicated treatments depending on the assay. Cell cytotoxicity was assessed at indicated time points by staining cells with 2 μ L of PI or TO-PRO-3 as indicated and determining cell cytotoxicity with flow cytometry as described in section 2.3.4.

2.3.2.3.1 Cytotoxicity of Ad[CE1A], Ad[PSA] and Anti-myeloma Chemotherapies.

To determine cytotoxicity of various agents, cells were seeded at 1×10^5 cells in 500 μ L complete RPMI media in a 48 well plate, unless stated otherwise. Cells were seeded in triplicate. Cells were treated with vehicle, virus and/or anti-MM chemotherapies (BTZ, Melph, Pan or Pom) as described based off previous assays. After the indicated time (24-72 hours) cytotoxicity was assessed by PI staining using flow cytometry (section 2.3.4).

2.3.2.3.2 Ad[CE1A] Cytotoxicity in Patient Derived Primary Cells.

To determine the cytotoxicity of Ad[CE1A] in patient derived primary cells, primary CD138⁺ plasma cells from patients (MGUS, newly diagnosed MM and PCL) and HDs were seeded at a range of densities (5×10^4 - 2×10^5 cells/well) as varying amounts CD138⁺ cells were obtained from the samples. To adjust for the difference in cell numbers, the cell density was kept the same at 200,000 cells/mL of media. CD138⁻ BMSCs from patient's and HDs were seeded at 200,000 cells/mL. Both cell populations were treated with Ad[CE1A] MOI 20 or vehicle (PBS) control in the presence of 10% autologous serum. Cells were assessed in duplicate or triplicate depending on number of cells acquired. After 96 hours, cytotoxicity was assessed by PI staining using flow cytometry (section 2.3.4). A longer time period of 96 hours was selected over 72 hours in case of delayed Ad[CE1A] replication kinetics in freshly isolated primary cells.

2.3.2.3.3 Ad[CE1A] Cytotoxicity in MPCS in Coculture with BMSCs

To determine if coculture with BMSCs effects Ad[CE1A]-induced cytotoxicity, HS-5 BMSC line was seeded at 5×10^4 cells/well in triplicate in a 48 well plate in 1 mL of complete DMEM media. Cells were incubated for 24 hours. Following this, media was aspirated to remove non-adherent cells, and 5×10^4 JJN-3-GFP, U266-GFP, OPM2-GFP or RPMI-8226-GFP cells which were labelled with Vybrant™ DiD (section 2.3.3.1), were seeded onto the HS-5 cells in 1 mL of complete RPMI media. Cocultures were treated with vehicle (PBS) or Ad[CE1A] MOI 2 or 10. After 48 hours, cell viability was determined by PI staining using flow cytometry (section 2.3.4).

2.3.2.3.4 Assessment of Ad[CE1A] Efficacy in Preventing Myeloma Cell Regrowth after Bortezomib Treatment

To determine if Ad[CE1A] can keep viability of cells low over a longer period of time following BTZ treatment compared to BTZ treatment alone, 1×10^5 JJN-3 and U266 cells were seeded in triplicate in 48 well plates with 500 μ L of media and treated with 2.5 nM of BTZ. After 24 hours BTZ was washed off and cells were resuspended in fresh complete media. Cells were then treated with Ad[CE1A] at varying concentrations (1, 2.5, 5, 7.5 and 10 MOI) or vehicle (PBS) control. After 1, 3, 7, 14, 18, 21 and 25 days Ad[CE1A] treatment, viability was assessed by PI staining using flow cytometry (section 2.3.4).

2.3.2.3.5. Cytotoxicity of Ad[CE1A] in the Presence of Inhibitors

To determine if inhibiting various proteins involved in distinct cell death pathways had an effect on Ad[CE1A] cytotoxicity, cells were seeded at 1×10^5 cells in 500 μ L complete RPMI media in a 48 well plate. Cells were seeded in triplicate. Cells were treated with Ad[CE1A] as described \pm inhibitors listed in Table 2.7. Concentrations of inhibitors determined by previous dose response assays. After the indicated time (24 to 72 hours) cytotoxicity was assessed by PI staining using flow cytometry (section 2.3.4).

2.3.2.4 Assessment of Proliferation

KI-67 is a widely used marker of cell proliferation. It is highly expressed in cycling cells but strongly downregulated in resting (G0) cells (335).

2.3.2.4.1 KI-67 Expression Analysis following Ad[CE1A] Treatment

2.5×10^5 JJN-3 and OPM-2 cells were seeded in 24 well plates in 1 mL of complete RPMI media and incubated with Ad[CE1A] at a MOI of 2, 10 and 20 or with vehicle (PBS) control. After 24- and 48-hours incubation cells were harvested and stained with KI-67-APC or isotype matched control. Cells were analysed by flow cytometry (section 2.3.4).

2.3.2.5 Assessment of Apoptosis

2.3.2.5.1 Annexin V Assay

Phosphatidylserine (PS) is a phospholipid component of the plasma membrane which normally localises to the inner leaflet of the plasma membrane. During apoptosis, PS translocates from the inner leaflet of the plasma membrane to the outer leaflet of the plasma membrane. It is hypothesised that PS translocates to the outer leaflet to allow recognition for phagocytosis by macrophages. The human vascular anticoagulant Annexin V has a high affinity for PS. Therefore, fluorescent conjugates of Annexin V are commonly used as a marker for apoptosis (336).

Cells were seeded onto 48 well plates at 1×10^5 in 500 μ L of complete media, unless otherwise stated. After indicated time points and treatments cells were stained with Annexin V conjugated to FITC or APC (BD Biosciences, UK) according to the manufacturers protocol. Briefly, cells were centrifuged (400g x5 minutes) and resuspended in 100 μ L of 1x Annexin binding buffer containing 2.5 μ L of Annexin-V-FITC and incubated for 15 minutes at room temperature in the dark. Cells were then centrifuged (400g x5 minutes) and washed with 500 μ L Annexin binding buffer twice and resuspended in a varying volume of Annexin binding buffer depending on cell density, between 400 μ L and 1 mL. Immediately prior to flow cytometric analysis 2 μ L of TO-PRO-3 or PI (stock Concentration 50 μ M) was added and the cell samples were analysed on a flow cytometer as described in section 2.3.4.

2.3.2.5.2 Annexin V Expression following Ad[CE1A] Treatment

1×10^5 human MPC lines (JJN-3 & U266) and murine MPC line (5TGM1) were seeded in triplicate in 48 well plates in 500 μ L of complete RPMI media and treated with Ad[CE1A] at a MOI of 20 or vehicle (PBS) control. At 6- and 24-hours incubation, cells were collected, and apoptosis was assessed by staining cells with Annexin V conjugated to APC or FITC (BD Biosciences, UK) and TOPRO-3 or PI was added and analysed by flow cytometry (section 2.3.4).

2.3.2.5.3 Annexin V Expression of Ad[CE1A] in Combination with Anti-myeloma Chemotherapies

1x10⁵ JJN-3 and OPM-2 cells were seeded per well in 1 mL of complete RPMI media in a 48 well plate. Cells were plated in triplicate. Cells were treated with a single dose of Ad[CE1A] ± anti-MM chemotherapy (BTZ, Melph, Pan or Pom). Doses were decided from best performing dose across all cell lines as previously assessed by cell viability assays. After 72, cells were stained with Annexin V-FITC and TO-PRO-3 and analysed by flow cytometry (section 2.3.4).

2.3.2.5.4 Analysis of Apoptotic Gene Expression following Ad[CE1A] Treatment

To determine mRNA expression of apoptosis related markers after Ad[CE1A] infection, RT-qPCR was performed. 2x10⁶ JJN-3 cells were treated with Ad[CE1A] MOI 20 or vehicle (PBS) control. Total RNA was collected at 4 and 24 hours post treatment using the ReliaPrep™ RNA Miniprep Systems (Promega, UK) kit (section 2.4.1). Total RNA was reverse transcribed using the High-Capacity cDNA to RNA kit (Applied Biosystems, UK) (section 2.4.2). mRNA expression was determined by RT-qPCR (section 2.4.3). Briefly, SYBR™ green primers were used for the housekeeping gene GAPDH and Caspase 3, Caspase 8, Caspase 9, BCL2, FASL, BAX and BID and SYBR™ green master mix was used.

2.3.2.6 Assessment of Immunogenic Cell Death Markers

2.3.2.6.1 Cell Surface Expression of Calreticulin

To analyse the surface expression of calreticulin (CALR) following Ad[CE1A] and/or anti-MM therapy treatment, 2.5x10⁵ cells were seeded into a 24 well plate in 1 mL of media. Cells were treated with Ad[CE1A] and/or anti-MM chemotherapy (BTZ, Melph, Pan or Pom) as described. 24 hours after treatment cells were collected and stained with a primary rabbit polyclonal CALR antibody or dose matched isotype control followed by a fluorescently labelled secondary FITC Donkey anti rabbit IgG as described (section 2.3.4). Fluorescence was determined by flow cytometry. Dead cells were gated out using TO-PRO-3 and only viable cells were used to assess CALR expression.

2.3.2.6.2 Cell Surface Expression of CD47

To analyse the surface expression of CD47 following Ad[CE1A] treatment, 2.5×10^5 cells were seeded into a 24 well plate in 1 mL of media. Cells were treated with Ad[CE1A] as described. 24 and 48 hours after treatment cells were collected and stained with an APC-conjugated anti-human CD47 antibody or dose matched isotype control as described (section 2.3.4). Fluorescence was determined by flow cytometry. Dead cells were gated out using PI and only viable cells were used to assess CD47 expression.

2.3.3.6.2 Luminescent Detection of Extracellular ATP

Secretion of extracellular ATP following Ad[CE1A] and/or anti-MM chemotherapy (BTZ, Melph, Pan or Pom) treatment was determined by a luminescence-based assay (Enlighten[®] ATP assay, Promega). For this, 1×10^5 cells were seeded in triplicate in 48 well plates in 1 mL of complete RPMI media. Cells were treated with Ad[CE1A] and/or anti-MM therapies. Concentrations of treatments determined by previous assays. After 24 hours cells were collected and centrifuged (400g x5 minutes). Meanwhile a standard curve dilution series of the ATP standard (10^{-7} M- 10^{-13} M) was made in complete RPMI media. After samples were centrifuged, 100 μ L of cell culture supernatant was collected per sample and placed a sterile clear bottom black walled 96 well plate. This was performed at low light to allow the plates and samples to dark adapt. 100 μ L of rL/L reagent reconstituted in reconstitution buffer was added to each column of the plate individually and read instantly on SpectrMax5e plate reader (Molecular Devices) using endpoint luminescence (integration time 1000ms).

2.3.2.6.1 Cell Surface Expression of MHC Class I and II

To analyse the surface expression of MHC class I and class II following Ad[CE1A], 2.5×10^5 cells were seeded into a 24 well plate in 1 mL of media. Cells were treated with Ad[CE1A] as described. 48 hours after treatment cells were collected and stained with an APC-conjugated anti-human HLA-ABC antibody or an APC-conjugated HLA-DR antibody or dose matched isotype control as described (section 2.3.4). Fluorescence was determined by flow cytometry. Dead cells were gated out using PI and only viable cells were used to assess HLA-ABC/HLA-DR expression.

2.3.3 Cell Labelling

2.3.3.1 Vybrant™ DiD

Vybrant™ DiD is a fluorescent lipophilic dye that binds to the plasma membrane. Vybrant™ DiD is used for dye-retention studies, where membrane dyes are shared with daughter cells during cell division, which can mark long-term, nondividing, dormant MM cells (337). MPC lines were labelled with Vybrant™ DiD (Invitrogen™) to track proliferation and to distinguish MPCs in cocultures by flow cytometry as described in section 2.3.4. 1×10^6 MPCs were suspended in 1 mL of serum free RPMI media. Five μL of Vybrant™ DiD cell labelling solution was added to the cell suspension and incubated for 15 minutes at 37°C in a humidified atmosphere containing 5% CO_2 . Following this, the cell solution was centrifuged (400g x5minutes) and washed in 1 mL of warm complete RPMI media, this was repeated three times to remove residual Vybrant™ DiD. After the last wash, labelled cells were resuspended in warm serum free media and seeded in well plates or tissue culture flasks depending on the experiment.

2.3.4 Flow Cytometry

All buffers, reagents used in flow cytometry are outlined in Table 2.8.

Table 2.8: Buffers required for flow cytometry

Solution	Component
FACs Buffer	4% FBS in PBS
1x Mouse Red Cell Lysis buffer	M-Lyse Buffer Concentrate (10X) (R&D systems)
1x Mouse wash buffer	Wash Buffer Concentrate (10X) (R&D systems)
Permeabilization buffer	1% FBS, 0.1% Sodium Azide, 0.1% Saponin in PBS, pH to 7.4, filter with 0.2 μM filter.

2.3.4.1 General Principles of Flow Cytometry

Flow cytometry is a technique which allows for the quantification of protein on a single cell basis. Briefly, a cell is labelled with a fluorescently labelled antibody or has been manipulated to express a fluorescently labelled protein. A cell with fluorescence or a cell absent of fluorescence moves through a pressurised system passing through beams of light and subsequent detectors, which detect the forward scatter (cell size) and side scatter (cell granularity) giving information about general cell structure. Additionally, a series of lasers excite the fluorochromes attached to the bound

antibodies/expressed by the cell and the light reflected passes through dichromic mirrors to the detectors, which detect specific wavelengths dependent on the fluorochrome used (all fluorophores used in this thesis are summarised in Table 2.9). The results are then analysed computationally, if a fluorescent signal is detected, this implies an antibody is bound/cell is expressing fluorescent protein.

Table 2.9: Laser, absorbance, emission, and detector information for fluorochromes used in flow cytometry

	Laser excitation (nm)	Absorbance Max (nm)	Emission Max (nm)	Detector
GFP	488	488	510	FL-1
FITC	488	490	525	FL-1
Phycoerythrin (PE)	488	496	578	FL-2
Allophycocyanin (APC)	633	650	660	FL-4
Vybrant™ DiD	633	644	665	FL-4
PI	488	535	617	FL-2
TO-PRO-3	633	642	666	FL-4

2.3.4.2 General Flow Cytometry Methodology

Flow cytometry was used to detect fluorescent cell surface, intracellular proteins, dyes and to detect cell death (all antibodies used are listed in Table 2.10). Briefly cells were collected and centrifuged (400g x5minutes) and resuspended in fluorescent activated cell sorting (FACS) buffer. If cells were obtained directly from mice, erythrocytes were lysed using mouse erythrocyte lysis kit (R&D systems) according to the kits instructions, or from humans, erythrocytes were lysed using erythrocyte lysis buffer described in section 2.1.3. If antibody staining was not needed (e.g GFP expression, DiD labelling, cell death) samples were resuspended in 400 µL FACS buffer and were then ready for flow cytometry.

If antibody staining was needed, cells were resuspended 100 µL of FACS buffer unless otherwise stated. Fluorescently conjugated antibodies were added to cell solution at optimum concentration

described in Table 2.10 or with a matched concentration of isotype control. Antibody concentration was adjusted for cell density when needed. Samples were incubated at 4°C for 45 minutes (unless stated otherwise) in the dark. After incubation, the samples were centrifuged (400g x 5 minutes) and washed three times in 200-500 µL FACS buffer depending on if staining was performed in round bottom 96 well plates or 1.5 mL Eppendorf's. After the final wash, the samples were resuspended in 300-500 µL FACS buffer. Fluorescently conjugated secondary antibodies were used when using unconjugated primary antibodies. For this, after the final wash, cells were resuspended in 100 µL and a host matched fluorescently conjugated secondary antibody was added. Samples were then incubated at 4°C for 45 minutes (unless stated otherwise) in the dark. After incubation, the samples were centrifuged (400g x 5 minutes) and washed three times in 200-500 µL FACS buffer. After the final wash, the samples were resuspended in 300-500 µL FACS buffer. If cells were obtained directly from mice or humans, cells were passed through a 70 µm cell strainer to remove large debris and aggregates before being transferred to flow cytometry tubes. Cell viability was detected using either PI or TO-PRO-3 as described in section 2.3.2.3.

All flow cytometry was performed using a FACSCalibur machine (Becton Dickinson, Oxford, UK) or LSR II (BD Biosciences, Oxford, UK) and data analysed using the FlowJo™ software package (v.10.5.0) (FlowJo LLC, Oregon, USA). Cells were acquired at 10^4 - 10^5 events depending on the experiment. The light scatter parameters were configured so that there was a clear cellular population to eliminate aggregates and cellular debris. For each experiment negative unstained controls were used, alongside isotype and single stain controls to properly set the appropriate voltage and fluorescent compensation and to set up the correct gating strategy for analysis i.e to ensure <1% of staining was evident in the isotype control samples. The setting for the gates then remained the same throughout each experiment. FlowJo™ software allows you to analyse percentage cell populations and/or mean fluorescent intensity (MFI), i.e to determine the percentage of a cell population expressing a certain marker and/or the intensity of the marker in that population.

Table 2.10: Antibodies used in flow cytometry

Antibody Specificity	Clone	Host	Isotype	Fluorochrome	Cell density & Amount of Antibody used (stock conc)	Supplier
Human Anti-CD138	44F9	Mouse	IgG1 κ	PE	5x10 ⁵ cells 1 μ L used. (concentration not stated)	Miltenyi Biotech
Human CD138 Isotype	MOPC-21	Mouse	IgG1 κ	PE	5x10 ⁵ cells 0.5 μ g (200 μ g/mL)	Biolegend
Mouse Anti-CD138	281-2	Rat	IgG2a κ	APC	5x10 ⁵ cells 0.5 μ g (200 μ g/mL)	Biolegend
Mouse CD138 Isotype	RTK2758	Rat	IgG2a κ	APC	5x10 ⁵ cells 0.5 μ g (200 μ g/mL)	Biolegend
Human Anti-CD319	162.1	Mouse	IgG2b κ	PE	5x10 ⁵ cells 1 μ g (200 μ g/mL)	Biolegend
Human CD319 isotype	MPC-11	Mouse	IgG2b κ	PE	5x10 ⁵ cells 1 μ g (200 μ g/mL)	Biolegend
Mouse Anti-CD319	4G2	Rat	IgG1 κ	APC	0.5 μ g (200 μ g/mL)	Biolegend
Mouse CD319 Isotype	RTK2071	Rat	IgG1 κ	APC	0.5 μ g (200 μ g/mL)	Biolegend
Human Anti-CAR	RmcB	Mouse	IgG1	PE	5x10 ⁵ cells 1 μ L used. (concentration not stated)	Merk Millipore
Human CAR Isotype	MOPC-21	Mouse	IgG1	PE	5x10 ⁵ cells 0.5 μ g (200 μ g/mL)	Biolegend
Human Anti-CD51/61 (α v β 3)	23C6	Mouse	IgG1 κ	FITC	5x10 ⁵ cells 0.5 μ g (200 μ g/mL)	Biolegend
Human Anti-CD51/61 (α v β 3) isotype	MOPC-21	Mouse	IgG1 κ	FITC	5x10 ⁵ cells 0.5 μ g (200 μ g/mL)	Biolegend

Antibody Specificity	Clone	Host	Isotype	Fluorochrome	Cell density & Amount of Antibody used (stock conc)	Supplier
Human Anti- $\alpha\beta_5$	NKI-M9	Mouse	IgG2a κ	APC	5x10 ⁵ cells 0.5 μ g (200 μ g/mL)	Biolegend
Human Anti- $\alpha\beta_5$ isotype	MOPC-173	Mouse	IgG2a κ	APC	5x10 ⁵ cells 0.5 μ g (200 μ g/mL)	Biolegend
Human Anti-Ki-67	Ki-67	Mouse	IgG1 κ	APC	2.5x10 ⁵ cells 0.5 μ g (200 μ g/mL)	Biolegend
Human Ki-67 Isotype	MOPC-21	Mouse	IgG1 κ	APC	2.5x10 ⁵ cells 0.5 μ g (200 μ g/mL)	Biolegend
Human Anti-CD47	CC2C6	Mouse	IgG1 κ	APC	2.5x10 ⁵ cells 0.5 μ g (200 μ g/mL)	Biolegend
Human Anti-CD47 Isotype	MOPC-21	Mouse	IgG1 κ	APC	2.5x10 ⁵ cells 0.5 μ g (200 μ g/mL)	Biolegend
Unconjugated polyclonal calreticulin	PA3-900	Rabbit	IgG	N/A	2.5x10 ⁵ cells Concentration not stated. 1 μ L used per 250,000 cells in 100 μ L buffer	Invitrogen
Calreticulin Isotype	Poly29108	Rabbit	IgG	N/A	2.5x10 ⁵ cells 10 μ g (1 mg/mL)	Biolegned
Calreticulin Secondary (Donkey anti-rabbit IgG (minimal x-reactivity))	Poly4064	Donkey	Donkey Polyclonal Ig	FITC	2.5x10 ⁵ cells 5 μ g (0.5 mg/mL)	Biolegend
Anti-human HLA-ABC	W6/32	Mouse	IgG2a κ	APC	2.5x10 ⁵ cells 0.5 μ g (200 μ g/mL)	Biolegend
Human Anti-HLA-ABC isotype	MOPC-173	Mouse	IgG2a κ	APC	5x10 ⁵ cells 0.5 μ g (200 μ g/mL)	Biolegend

Antibody Specificity	Clone	Host	Isotype	Fluorochrome	Cell density & Amount of Antibody used (stock conc)	Supplier
Anti-human HLA-DR	LN3	Mouse	IgG2a κ	APC	5x10 ⁵ cells 0.5 µg (200 µg/mL)	Biolegend
Anti-human HLA-DR isotype	MG2b-57	Mouse	IgG2a κ	APC	5x10 ⁵ cells 0.5 µg (200 µg/mL)	Biolegend

2.3.4.2.1 Assessment of Cell Surface Adenovirus Entry Receptors

Human MPCs lines (JJN-3, L363, U266, OPM-2, RPMI-8226 NCI-H929, KMS-11 and KMS-12-BM), primary-patient derived PCL cells (CB1 and ADC1) and HEK293A cells were assessed for CAR, αβ₅ and αβ₃ cell surface expression. 5x10⁵ cells were stained with either PE-conjugated CAR, APC-conjugated αβ₅, FITC-conjugated αβ₃ or dose matched isotype control for 45 minutes at 4°C in the dark. 2 µL of PI or TO-PRO-3 was added immediately prior to flow cytometry to identify and exclude dead cells. Dead cells were gated out and only viable cells were used to assess Ad receptors expression.

2.3.4.2.2 Assessment of Coxsackie Adenovirus Receptor Expression after Anti-myeloma Chemotherapies.

1x10⁵ JJN-3, U266 and OPM-2 cell lines were seeded per well into a 48 well plate in 1 mL of complete media. Cells were plated in triplicate. Cells were treated with an anti-MM chemotherapy (BTZ, Melph, Pan or Pom). Doses were decided from previous dose response experiments. After 48 hours, cells were stained with PE-conjugated anti-CAR antibody or with PE-conjugated mouse IgG1 isotype control for 45 minutes at 4°C. 2 µL of TO-PRO 3 was added prior to flow cytometry to identify and exclude dead cells, described in section 2.3.2.3. Dead cells were gated out and only viable cells were used to assess Ad receptors expression.

2.3.4.2.3 Assessment of CS1 Cell Surface Expression

Human MPCs lines (JJN-3, L363, U266, OPM-2, RPMI-8226 NCI-H929, KMS-11 and KMS-12-BM), murine MPC line (5TGM1), primary-patient derived cells and control cell lines (HEK293A and human prostate cancer cell line, LNCaP) were assessed for CS1 cell surface expression. For cell lines 5x10⁶ cells

per test were used, for primary cells 1×10^5 cells were labelled with PE-conjugated mouse anti-human CS1 (CD319) or APC-conjugated rat anti-mouse CS1 (CD319) or dose matched isotype control for 45 minutes at 4°C in the dark. Antibody concentration was adjusted for cell density ($2 \mu\text{L}/5 \times 10^5$). $2 \mu\text{L}$ TO-PRO-3 was added immediately prior to analysis on flow cytometry to identify dead cells. Dead cells were gated out and only viable cells were used to assess CS1 expression.

2.3.4.2.4 Assessment of CS1 Receptor expression after Anti-myeloma Chemotherapies.

1×10^5 JJN-3, U266, OPM-2 and 5TGM1 cell lines were seeded per well into a 48 well plate in 1 mL of complete media. Cells were plated in triplicate. Cells were treated with an anti-MM chemotherapy (BTZ, Melph, Pan or Pom). Doses were decided from previous dose response experiments. After 48 hours, JJN-3, U266, OPM-2 and 5TGM1 cells were stained with PE-conjugated mouse anti-human CS1 (CD319)/ APC-conjugated rat anti-mouse CS1 (CD319) or a dose matched isotype control. Cells were stained for 45 minutes at 4°C . $2 \mu\text{l}$ PI or TO-PRO 3 was added prior to analysis on flow cytometry to identify dead cells. Dead cells were gated out and only viable cells were used to assess CS1 expression.

2.3.4.2.5 Assessment of CD138 Cell Surface Expression

The mouse MPC line, 5TGM1 *in vitro* and *ex vivo* from BM flushes, and primary-patient derived cells were assessed for CD138 cell surface expression. For 5TGM1 *in vitro* 5×10^5 cells per test were used, for primary cells 1×10^5 cells per test was used, for 5TGM1 cells *ex vivo* from BM flushes, the BM was divided into two and were labelled with either APC-conjugated anti-mouse CD138 or PE-conjugated anti-human CD138 or dose matched isotype control for 45 minutes at 4°C in the dark. $2 \mu\text{L}$ of PI or TO-PRO-3 was added immediately prior to flow cytometry to identify and exclude dead cells. Dead cells were gated out and only viable cells were used to assess CD138 expression.

2.3.4.2.6 Assessment of KI-67 Expression

For intracellular protein detection (KI-67) an intracellular staining technique was required, whereby the cells were collected, centrifuged (400g x5minutes), and washed twice in PBS. After the final wash cells were fixed by adding 1 mL of 70% ethanol dropwise whilst vortexing. Cells were then incubated for 2 hours at -20°C . Following this, cells were centrifuged (400g x5 minutes) and washed in 1 mL of

permeabilization buffer, described in Table 2.8. After the last wash cells were resuspended in 100 μ L of permeabilization buffer. APC-conjugated anti-KI-67 antibody or dose matched isotype control was added to the samples. Samples were incubated at 4°C for 45 minutes in the dark. After incubation, the samples were centrifuged (400g x5 minutes) and washed three times in 500 μ L FACS buffer. After the final wash the samples were resuspended in 500 μ L FACS buffer. Viable cells were determined and gated by size and granularity using forward and side scatter parameters.

2.3.5 Fluorescent Microscopy

Fluorescent microscopy was used to visualise GFP expression within MPCs and HD CD138⁺ BMMCs. This was performed using the EVOS[®] FL auto imaging microscope with GFP light cube selected (470/22 nm excitation; 510/42 nm emission). After visualisation, images were taken the pictures were exported as tagged image file format files (TIFFs). Images were used as visualisation aids.

2.4 Molecular Biology

2.4.1 RNA Extraction

2.4.1.1 RNA Extraction Methodology

To detect gene expression from the desired tissue or cell type total RNA was extracted from samples using the ReliaPrep[™] RNA Miniprep Systems (Promega, UK). 2×10^6 cells were centrifuged (400g x 5 minutes) and resuspended in 1 mL of ice-cold sterile PBS. Cells were centrifuged again (400g x 5 minutes) and resuspended in 250 μ L of BL+1-Thioglycerol (TG) buffer (provided in the ReliaPrep[™] kit), the cell pellet was dispersed by vigorous pipetting and vortexing. 85 μ L of isopropanol was added and vortexed for 5 seconds and the mixture was transferred to a ReliaPrep[™] Minicolumn with a 2 mL collection tube and centrifuged at 14,000g for 30 seconds. The flow-through was discarded and 500 μ L of RNA wash solution was added to the column and centrifuged for 14,000g for 30 seconds. The flow-through was discarded. In a sterile tube, 24 μ L of yellow core buffer, 3 μ L of 0.09M of $MnCl_2$, 3 μ L of DNase I enzyme was added per reaction. 30 μ L of this solution was added to the membrane of the column and incubated at room temperature for 15 minutes. After the incubation, 200 μ L of column wash was added to the column and centrifuged at 14,000g for 15 seconds. 500 μ L of RNA wash is then

added and centrifuged at 14,000g for 30 seconds. The column was placed into a new collection tube. 300 µL of RNA wash was added and centrifuged at 14,000g for 2 minutes. The column was placed in 1.5 mL elution tubes and 30 µL of nuclease-free water was added to the membrane. The eluted RNA was then stored at -80°C until required.

2.4.1.2 Quantification of RNA

The purity and concentration of all RNA samples were determined using a NanoDrop 2000 and its dedicated software. The purity of each sample was determined using the 260/280 nm and 260/230 absorption ratios. RNA absent of protein contamination (260/280 nm) had a value above 2.0 and RNA which did not contain impurities such as phenol or ethanol (260/230 nm) had a value of 2.0-2.2. The concentration of the RNA (ng/µL) was also calculated using the NanoDrop 2000 software.

2.4.2 Reverse Transcription

2.4.2.1 Reverse Transcription Methodology

Reverse transcription (RT) was conducted to convert mRNA into complementary DNA (cDNA), for subsequent PCR experiments. To remove any contamination before conduction of RT, the required number of 0.5 mL RNase and DNase free tubes for RT reaction and nuclease free water were irradiated for 30 minutes in an ultraviolet (UV) hood (SCIE-PLAS Ltd.). For RT the High-Capacity cDNA to RNA kit (Applied Biosystems, UK) was used for reverse transcribing total RNA. 1 µg of RNA was required per sample. The volume of RNA required to get 1 µg was calculated using the following equation and the volume given (up to 9 µL) placed in 0.5 mL RNase and DNase free tubes.

$$\text{Volume of RNA } (\mu\text{L}) = \frac{\text{RNA concentration desired}}{\text{Sample concentration}}$$

RT was conducted by combining 2x RT buffer mix, 20x RT enzyme mix and nuclease free water to in 0.5 mL RNase and DNase free tubes with the RNA. The volumes required for each reagent for one sample is shown in Table 2.11. For each RNA sample, a RT enzyme negative (RT-) replicate was also prepared, to control for genomic contamination. Samples were mixed gently before centrifuging. Tubes were placed on ice until they were ready to load onto the thermocycler. Samples were run on a thermal cycler using the stated conditions shown in Table 2.12. The cDNA samples were then removed from the thermocycler, diluted to 200 ng/ μ L using nuclease free water and stored at -20°C until required for PCR.

Table 2.11: Reagents required for RT for one sample

Component	Volume per Reaction	
	RT ⁺	RT ⁻
2x RT Buffer Mix	10 μ L	10 μ L
20x RT Enzyme mix	1 μ L	-
RNA Sample	Up to 9 μ L	Up to 9 μ L
Nuclease Free H ₂ O	Q.S* to 20 μ L	Q.S* to 20 μ L
Total per Reaction	20 μ L	20 μ L

*Quantity sufficient

Table 2.12: Thermocycler Conditions for RT

	Step 1	Step 2	Step 3
Temperature (°C)	37	95	4
Time (min)	60	5	∞

2.4.3 Real Time PCR

2.4.3.1 Principles of Real-Time Quantitative PCR

Real-time quantitative PCR (RT-qPCR) uses the basic principles of PCR, but the results are assessed quantitatively in 'real-time'. Intercalating dye or fluorescent hydrolysis probes are used. Intercalating dyes bind directly to the DNA, whilst fluorescent probes, bind to complementary nucleotide on the cDNA template. Intercalating dyes, such as SYBR® green emit fluorescence upon DNA amplification, which increases with increased gene copy repeats for each primer, allowing the reaction to be quantified in RT. Whilst fluorescent probes are made of DNA oligonucleotides with a 5 prime end (5') bound to a reporter molecule and a 3 prime end (3') bound to a quencher molecule, such as minor groove binder (MGB).

2.4.3.2 Real-Time Quantitative PCR Methodology

The cDNA was used to analyse levels of mRNA expression from MPCs, primary CD138⁺ and CD138⁻ cells, LNCAP cells and HEK293A cells. To reduce contamination, a 384 well plate, 0.5 mL RNase and DNase free tubes, RT-PCR H₂O, a micro seal adhesive cover and tips were placed in a UV hood and UV irradiated for 30 minutes. For each reaction, a mix containing RT-PCR H₂O, master mix and probes were made using the volumes for one sample demonstrated in Table 2.13.

Table 2.13: Reagents and quantities required for one real-time qPCR samples

SYBR® Green Assays	
Reagent	Volume (µL)
2x SYBR® green select master mix	5 µL
RT-PCR H ₂ O	3 µL
SYBR® green Forward Primer	0.5 µL
SYBR® green Reverse Primer	0.5 µL
TaqMan™ Assay	
Reagent	Volume (µL)
TaqMan™ Universal PCR mastermix	5 µL
RT-PCR H ₂ O	3 µL
TaqMan™ Primer	1 µL

The entire 9 μ L mix was transferred into a well of the 384 well plate and to this, 1 μ L of cDNA (200 ng) was added. The plate was covered using the micro-seal adhesive cover and centrifuged at 400g for 30 seconds to ensure all liquid was combined at the bottom of the well. The probes were designed to bind to complementary nucleotides on the cDNA template for the gene of interest (GOI) and housekeeping (HK) genes which included *B2M* and *GAPDH*. The list of primers used and their reference numbers are shown in Table 2.14. The plate was analysed by Applied Biosystems HT 7900 real-time PCR machine and SDS 2.3 software. Cycle conditions, which were standard for real-time PCR machines per Applied Biosystems, are described in Table 2.15.

Table 2.14: Primers used for RT-qPCR

Gene	Sequence
Human <i>GAPDH</i>	F 5'-TGCACCACCAACTGCTTAGC R 5'-GGCATGGACTGTGGTCATGAG
Mouse <i>B2M</i>	F 5'-TTCACCCCCACTGAGACTGAT R 5'-GTCTTGGGCTCGGCCATA
<i>E1A</i>	F 5'-ATGGGCAGTCGGTGATAGAGT R 5'-CTCAGGCTCAGGTTCCAGAC
Human <i>Caspase 3</i>	F 5'-AAAGCACTGGAATGACATC R 5'-CGCATCAATTCCACAATTC
Human <i>Caspase 8</i>	F 5'-CTACAGGGTCATGCTCTATC R 5'-ATTTGGAGATTTCTCTTGC
Human <i>Caspase 9</i>	F 5'-CCTACTCTACTTTCCAGGTTTT R 5'-GTGAGCCCACTGCTCAAAGAT
Human <i>BCL2</i>	F 5'-GGAAGTGAACATTTCCGGTGAC R 5'-GCCTCTCCTCACGTTCCC
Human <i>Fas Ligand</i>	F 5'-ATCCCTCTGGAATGGGAAGA R 5'-CCATATCTGTCCAGTAGTGC
Human <i>Bax</i>	F 5'-CAAACCTGGTGCTCAAGGCC R 5'-GCACTCCCGCCACAAAGAT
Human <i>BID</i>	F 5'-GAGGATTGTGGCCTTCTTTG R 5'-CTCAGCCCAGACTCACATCA
Gene	Assay ID
Human <i>GAPDH</i>	Hs00266705_g1 (Thermofisher Scientific)
Human <i>SLAMF7</i>	Hs00904275_m1 (Thermofisher Scientific)

Table 2.15: RT-qPCR conditions

Total cycles	Reaction Step	Length	Temperature
X1	Enzyme activation	10 minutes	95°C
X50	Denaturation	15 seconds	95°C
	Data collection	1 minute	60°C

Gene expression of each molecule was analysed using the $2^{-\Delta\Delta Ct}$ method for relative quantification. Genes which were not expressed and had a Ct value of greater than 35 were referred to as not determined (N.D).

2.4.3.3 Assessment of CS1 (*SLAMF7*) mRNA Expression

CS1 mRNA expression was assessed in a panel of human MPC lines (JJN-3, L363, U266, OPM-2, RPMI-8226, NCI-H929, KMS-11 and KMS-12-BM) and control cell lines (HEK293A and human prostate cancer cell line, LNCaP). CS1 mRNA expression was also assessed in primary MM cells, MM BMMCs and HD BMMCs. Total RNA was extracted using the ReliaPrep™ RNA Miniprep Systems (Promega, UK) kit from 2×10^6 cells for each cell line and 5×10^5 cells for each primary sample. CS1 mRNA expression was determined by RT-qPCR (section 2.4.3). Briefly, TaqMan® primers were used for the housekeeping gene, GAPDH (Cat# 4331182) and CS1 (*SLAMF7*) (Cat# 4331182) and TaqMan® master mix was used.

2.5 Developing Dormancy/MRD Models of Multiple Myeloma *in vitro*.

To be able to test efficacy of Ad[CE1A] and other therapeutics against dormancy/MRD, a quicker, cheaper, and more high throughput method than the low tumour burden *in vivo* model is required.

2.5.1. Assessment of Dormancy Levels in Human Myeloma Cell Lines.

In order to determine the baseline levels of dormancy in human MPC lines JJN-3-GFP, U266-GFP and OPM-2-GFP cells were stained with Vybrant™ DID (section 2.3.3) and monitored for the retainment of fluorescence over a 25-day period by flow cytometry (section 2.3.4).

2.5.2 Assessment of Dormancy Levels following Culture in Conditioned Media from BMSCs or Osteoblast Like Cells.

In order to determine whether BMSCs or osteoblast-like cells secrete cytokines that induce dormancy, CM from HS-5 BMSC line and Saos-2 osteoblast-like cell line was collected after 48 hours growth. To determine the right concentration of CM that will sustain cell viability and not be toxic, AlamarBlue® cellular proliferation experiments were performed. 1×10^4 JIN-3-GFP, U266-GFP and OPM-2-GFP cell lines were seeded into 96 well plates and cultured in varying ratios of CM to complete RPMI media up to 100 μ L (0%, 10%, 20%, 30% 40% and 50%). After 24, 48, 72 and 96 hours, cellular proliferation was determined by AlamarBlue® (section 2.3.2.1). Once the optimum concentration of CM that would not cause cytotoxicity in the cell lines was determined, JIN-3-GFP, U266-GFP and OPM-2-GFP were stained with Vybrant™ DID and cultured in either 100% complete RPMI media, or 50% complete RPMI media with either 50% DMEM media, 50% HS-5 conditioned DMEM media, 50% α -MEM media, or 50% Saos-2 conditioned α -MEM media. Cells were monitored for the retainment of Vybrant™ DID over a 25-day period by flow cytometry (section 2.3.3 & 2.3.4).

2.5.3 Assessment of PolyHIPE Scaffolds for Multiple Myeloma Cell Culture.

In collaboration with Dr Frederick Claeys and his PhD student Betül Aldemir Dikici, the use of 3D polyHIPE scaffolds (4PCLMA) were first assessed for their ability to allow MPCs to proliferate within the scaffold either alone or in culture with osteoblast like cells Saos-2. 3×10^4 Saos-2 cells were seeded onto polyHIPE scaffolds in 20 μ L of complete RPMI media in 48 well plates. Scaffolds were incubated at 37°C 5% CO₂. After one-hour 1 mL of complete media was added. After 24 hours, scaffolds were moved to a fresh well plate to remove any non-adhered cells. For Saos-2 monocultures, 1 mL of fresh media was placed into the well containing the scaffold. For cocultures and U266 monocultures 3×10^4 U266 MPCs were either seeded onto Saos-2 polyHIPE scaffolds or onto fresh polyHIPE scaffolds in 20 μ L of complete RPMI media. Scaffolds were incubated at 37°C 5% CO₂. After one-hour 1 mL of complete media was added. After 24 hours scaffolds were moved into fresh 48 well plates with fresh 1 mL of media to remove non-adhered cells. Cell proliferation was assessed at 1, 4 and 7 days following

MPC seeding by AlamarBlue® assay (section 2.3.2.1) with some adaptations as described below. For controls, AlamarBlue® was added to media only wells and media containing polyHIPE scaffolds. Before adding AlamarBlue® to the scaffold, scaffolds were placed in fresh wells with 1 mL of complete media. AlamarBlue® was added to the wells that previously contained the scaffolds, and to the fresh wells containing the scaffolds. This was to determine if the reduction of AlamarBlue® was from cells within the scaffold or cells in the surrounding area of the scaffold.

2.5.4 Assessment of PolyHIPE Scaffolds for Ad[CE1A] Treatment.

To assess whether Ad[CE1A] can cause oncolysis in MPCs cultured in polyHIPE scaffolds, 3×10^4 U266 cells were seeded onto polyHIPE scaffolds as described above, and cultured alone for 7 days. After 7 days MPCs were treated with Ad[CE1A] at an MOI 20 (based on the original 3×10^4 cells seeded, as cell counts on polyHIPE scaffolds are difficult), 2.5 nM of BTZ or treated in combination. After 72 hours, cell viability was determined by an AlamarBlue® assay (section 2.3.2.1.).

2.5.5 Assessment of Ad[CE1A] against Dormant Human Myeloma Cell Lines

Human MPC lines JJN-3-GFP, U266-GFP and OPM-2-GFP cells were stained with Vybrant™ DID (section 2.3.3). After 14 days culture in complete RPMI medium, 1×10^5 cells were treated in triplicate with Ad[CE1A] at MOI 2, 10 or 20. After a further 72 hours, cell death in DID stained cells was assessed by flow cytometry (section 2.3.4).

2.6 Animals

All animal experiments were performed in the University of Sheffield Biological Service Unit (registered facility license number: X57506C3D). All animal experiments were approved by the University of Sheffield animal ethics committee and the appropriate UK Home Office Project License (License holder: Dr Munitta Muthana 70/8670) and personal license (IBE55FEBE) authority, in strict compliance with the animal (Scientific Procedures) Act 1986. Mice were tail marked with a non-toxic permanent marker for identification and housed in groups of 4-5 in individually ventilated cages with constant access to standard diet and tap water, in a temperature and humidity-controlled room on a 12-hour light/dark cycle. Animal numbers ($n = 8/\text{group}$ for xenograft model or $n=10/\text{group}$ for syngeneic model) were calculated prospectively using power calculations and from previous experience with these models. Animals were allocated to treatment groups randomly by cage based on weight and/or tumour load depending on experimental conditions. Animals were monitored daily, any mice exhibiting hind limb paralysis (a clear indicator of high tumour load), hunched posture, reduced activity levels, >20% weight loss, difficulty breathing, skin ulceration, or other distress were removed and euthanized via cervical dislocation.

2.6.1 Animal Models

2.6.1.1 *In vivo* Xenograft Murine Myeloma Models

Non-obese diabetic (NOD) severely combined immunodeficiency (SCID) gamma (NOD.Cg-Prkdc^{scid} Il2rg^{tm1Wjl}/SzJ, NSG) models of MM have several advantages over other models of MM, such as better I.V tumour engraftment to the BM compared to SCID and NOD/SCID strains, where dissemination of tumour cells was found in skeletal and extra-skeletal sites (338). NSG models also reliably recapitulate many of the clinical features of MM, such as paraplegia, paraprotein in the serum, osteolytic lesions and loss of trabecular bone (339). Therefore, the NSG model has proven a valuable tool for testing antitumour and bone modulating drugs to target MM *in vivo* (340,341). Hence the choice of use of U266-NSG model in this thesis. The systemic xenograft model of MM was generated by injecting U266-GFP-Luc labelled cells ($1 \times 10^6/100 \mu\text{L}$) I.V into the tail vein of female, 8-week-old NSG mice (Charles

River Laboratories, Margate, UK), features of NSG mice are listed in Table 2.16. The U266-NSG model is a moderately aggressive with a disease course lasting 9-10 weeks before mice develop humane endpoint symptoms as discussed above. In NSG mice, U266 cells specifically colonise the BM after I.V injection with no extramedullary growth resulting in bone disease (338).

Table 2.16: Features of NSG Model

Name & Stock Number	NOD.Cg-Prkdc^{scid}Il2rg^{tm1Wjl}/SzJ (005557)
Branded or Common Name	NSG™ (Branded Name) NOD <i>scid</i> gamma
Mature B Cells	Absent
Mature T Cells	Absent
Dendritic Cells	Defective
Macrophages	Defective
Natural Killer Cells	Absent
Complement	Absent
Leakiness	Negligible
Irradiation Tolerance	Low
Lymphoma Incidence	Low

2.6.1.1.1 Efficacy of Ad[CE1A] in U266-NSG in vivo Xenograft Low Tumour Burden Model of Multiple Myeloma

1x10⁶ U266-GFP-Luc cells (in 100 µL PBS) were injected into the tail vein of 6–8-week-old female NSG mice (n=40). Mice were imaged by *in vivo* bioluminescent imaging from week 5 onwards throughout the experiment as described in section 2.5.2. From 6 weeks, when high tumour burden was established, mice were grouped randomly into treatment groups as previously described (n=8), two mice did not develop tumour, and were removed from the BTZ only treated group (n=6). Figure 2.5 illustrates the study design. At 6 weeks mice were treated with either vehicle (100 µL PBS I.V 1x/wk/100 µL PBS I.P 1x/2wk) or Ad[CE1A] (2x10⁷ ifu/100 µL 1x/wk). All other groups were treated with an initial induction dose of BTZ at 1mg/kg I.P 1x/2wk, after the induction dose, the BTZ dose was dropped to 0.75mg/kg I.P 1x/2wk. The control group received BTZ only for 8 weeks (4 doses) and the experimental groups either received BTZ and Ad[CE1A] (2x10⁷ ifu/100 µL 1x/wk) from week 6 for 8 weeks to test the hypothesis whether Ad[CE1A] can eradicate/control MRD and result in a survival advantage. The last group received BTZ for 4 weeks (2 doses) when tumour was relapsing, mice were

then treated with Ad[CE1A] (2×10^7 ifu/100 μ L 1x/wk) and continued BTZ treatment for a further 8 weeks. Each mouse was euthanised when humane endpoints were reached, and survival was tracked.

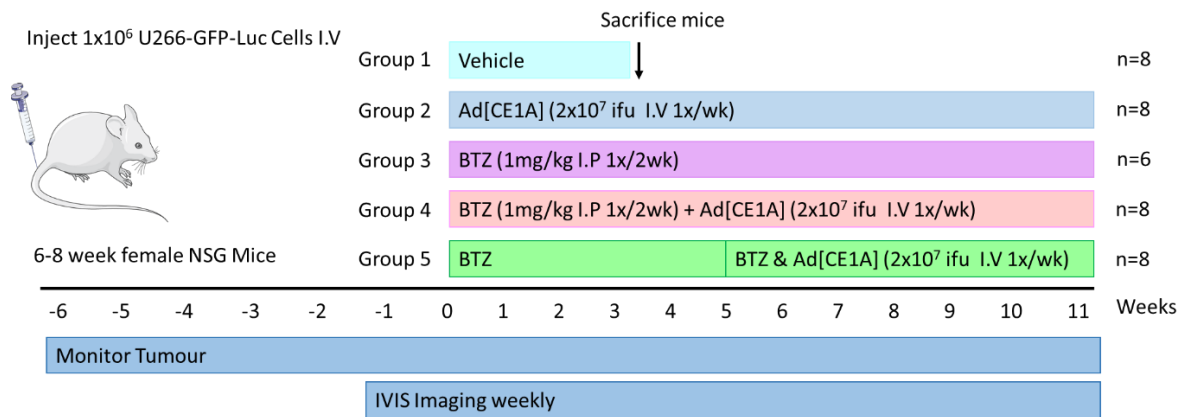


Figure 2.5: Schematic of study design of Ad[CE1A] survival study in U266 xenograft low tumour burden model of myeloma.

2.6.1.2 *In vivo* Syngeneic Murine Myeloma Models

The 5T series originated spontaneously in 0.5% of 2-year-old C57BL/KaLwRij mice, first reported by Radl *et al.*, in the late 1970s (342). To maintain these models, 5T cells are isolated from the BM of tumour bearing mice and re-implanted into young syngeneic recipient C57BL/KaLwRij mice, where cells typically home to the BM. Several different MM cell sub-lines have been isolated from these mice with the 5T2MM, 5T33MM and 5TGM1 being the most used and well-characterised models to-date (339).

The 5TGM1 model, was produced by continual *in vivo* passage of the 5T33MM cells (343). Unlike the 5T2MM cells, the 5TGM1 cells are able to grow *in vitro* and have been transduced with GFP (344,345) and Luc (346). The systemic syngeneic model of MM was generated by injecting 5TGM1-Luc labelled cells ($2 \times 10^6/100 \mu$ L) I.V into the tail vein of male, 6-8-week-old C57BL/KaLwRij (Envigo, Venray, Netherlands). Upon I.V injection 5TGM1 cells specifically colonise the bone and spleen, which results in trabecular bone loss with some cortical lesion formation (347). The 5TGM1 is an aggressive model with a disease course lasting 3-5 weeks before mice develop humane endpoint symptoms as discussed

above (348). The 5TGM1 model has advantages as it is a syngeneic model, therefore the interaction of the immune system on tumour and/or experimental drugs can be assessed.

5TGM1-Luc cells were a kind gift from Dr Oyajobi (University of Texas, San Antonio, USA), via Dr Ryan Bishop (Moffitt Cancer Centre, Tampa, Florida, USA). Before tumour injection, Luc expression and CD138 expression was tested *in vitro*. Figure 5.1 shows Luc expression by bioluminescent imaging and CD138 expression by flow cytometry (Figure 2.6).

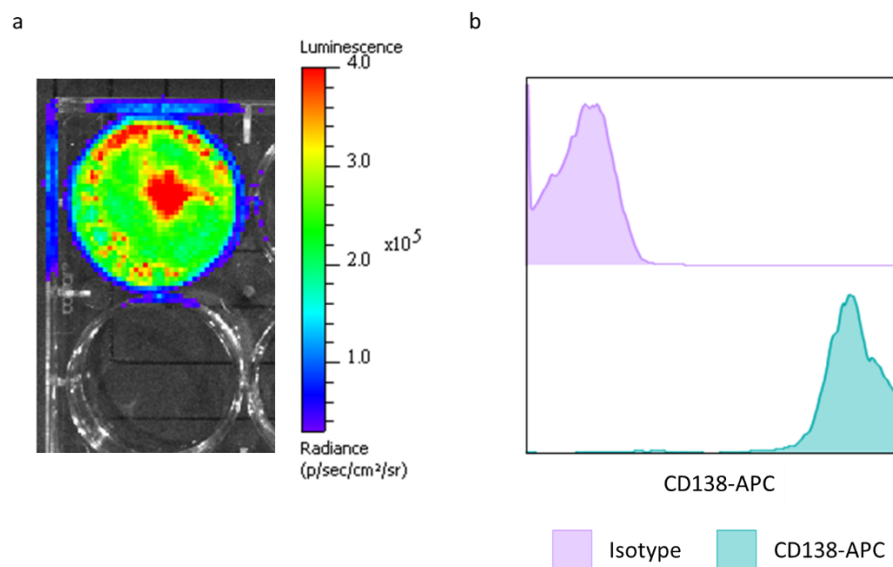


Figure 2.6: Expression of Luc and CD138 in 5TGM1-Luc cells.

(a) Luc expression in 5TGM1-Luc cells after addition of luciferin, detected in a well plate by the bioluminescent *in vivo* imaging system and **(b)** CD138 expression in 5TGM1-Luc cells determined by flow cytometry.

2.6.1.2.1 Proof of Concept Study: Ad[CE1A] Efficacy in 5TGM1-Luc Syngeneic Model.

2×10^6 5TGM1-Luc cells were injected into tail vein of 6-8 week old male C57BL/KaLwRij mice (n=40).

Mice were imaged biweekly by *in vivo* bioluminescent imaging from day 3 post tumour inoculation as described in section 2.5.2. From day 3 mice were randomised into treatment groups as previously described (n=10). Figure 2.7 illustrates the study design. At day 3, mice were treated with either vehicle (100 μ L PBS I.V 2x/wk/100 μ L PBS I.P 2x/wk), Ad[CE1A] low dose I.V (1×10^7 ifu/100 μ L 2x/wk), Ad[CE1A] high dose I.V (1×10^8 ifu/100 μ L 2x/wk) and we included a group that was treated with high dose Ad[CE1A] but via I.P (1×10^8 ifu/100 μ L 2x/wk). The I.P group was included to determine if I.P injection would be efficacious as I.P injections are easier than I.V injections that can result in tail vein

collapse and scaring. Mice were euthanised 28 days post tumour inoculation. Tumour burden was assessed by *in vivo* bioluminescent imaging, *ex vivo* flow cytometry and IHC as described in sections 2.6.2, 2.3.4 and 2.7.2 respectively.

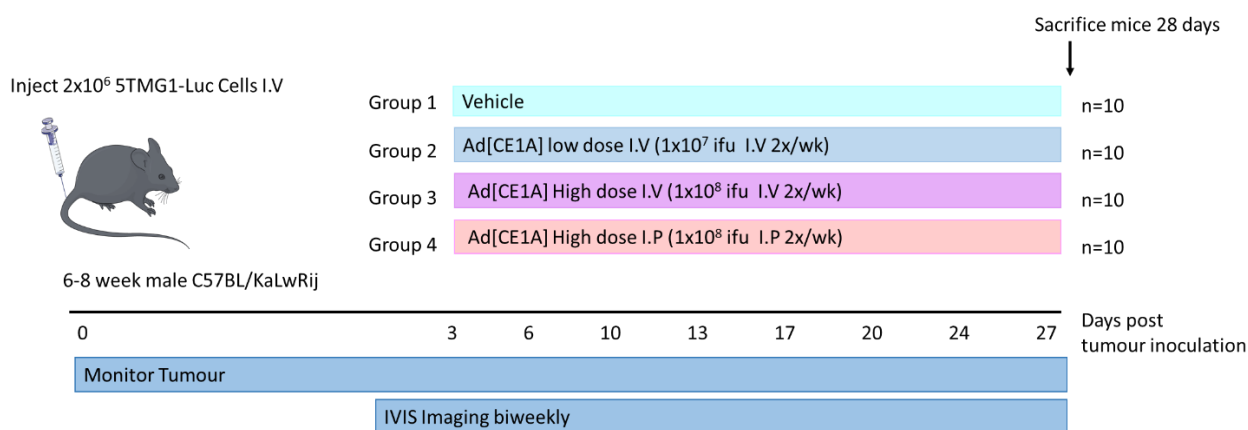


Figure 2.7: Schematic of study design of Ad[CE1A] proof of concept study in 5TGM1 model.

2.6.2 *In vivo* Imaging of Tumour

2.6.2.1 Bioluminescence *in vivo* Imaging System Methodology

To track *in vivo* tumour burden with Luc tagged MM cells bioluminescent *in vivo* imaging system (IVIS) was used. Mice were subcutaneously injected with 100 μ L D-luciferin 30mg/kg (Thermo Scientific Pierce) and anaesthetised with isoflurane by inhalation using an anaesthetic machine (5% induction; 1-2% maintenance). Five minutes after D-luciferin injection, mice were transferred to the anaesthetic nose cones inside the IVIS Lumia II imaging system (Perkin Elmer). Images were taken with exposure settings set at auto and posterior and anterior sides were imaged. Living image (v4.0) software was used to quantify the emission of bioluminescence.

2.6.2.3 *In vivo* Imaging System Quantification

IVIS images were opened with Living image software. The minimum and maximum radiance exposure was determined so the image was not oversaturated. These values are used for all images at all time points, so images are on the same luminescent scale. Regions of interest (ROI) were drawn over indicated tumour areas and total flux [p/s] was quantified. Figure 2.8 shows representative images of

a ROI drawn over tumour in hind limbs in anterior view, and tumour in vertebra and calvaria in posterior view.

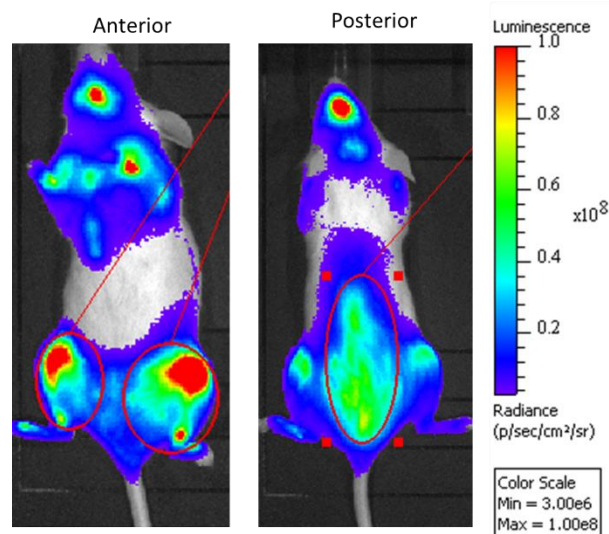


Figure 2.8: Representative bioluminescent images showing ROI analysis in hind limbs (anterior) and vertebra (posterior) in Living image software.

2.6.3 Primary Animal Cells and Tissues *ex vivo*

2.6.3.1 BM Isolation for Flow Cytometry

Flow cytometry was used to quantify tumour burden *ex vivo*. Mice were euthanised at the end of the study via cardiac bleed terminal procedure followed by cervical dislocation. The hind limbs were carefully dissected free of soft tissue and the femora and tibiae were separated at the knee joint. The proximal and distal ends of one femur (left) were cut using a scalpel to expose the BM. To isolate the BM, the femur was flushed using a sterile needle (27 Gauge) containing 500 μ L of PBS into a 1.5 mL Eppendorf and immediately stored on ice in the dark. Cells were prepared for flow cytometry as described in section 2.3.4. For U266-NSG models, tumour burden was analysed by GFP expression, for 5TGM1 model, the BM sample was divided in two and the tumour burden was determined by staining with a mouse anti-CD138 antibody or dose matched isotype control.

2.6.3.2 BM Isolation for RNA Extraction

BM was isolated as described in section 2.5.3.1, except the femur (right) was flushed using a sterile needle (27 Gauge) containing 500 μ L of RNA protect cell reagent (Qiagen) into a 1.5 mL RNase and DNase free Eppendorf. The samples were stored at 4°C for no more than 48 hours until RNA was extracted from samples as described in section 2.4.1 and stored at -80°C until needed. qPCR to assess *E1A* expression was performed as described in section 2.4.

2.6.3.3 Serum Isolation from Whole Blood

Blood was extracted from isoflurane-sedated mice via cardiac puncture using a sterile needle (27 Gauge). The blood was transferred into 1.5 mL Eppendorf's and placed on ice. Blood was left to coagulate for 30-60 minutes and then centrifuged at 4°C 800g for 10 minutes. Serum was removed and aliquoted at 50 μ L in 0.5 mL Eppendorf's and stored at -80°C until needed.

2.7 Histology

2.7.1 Preparation of Soft Tissue and Bones

Soft tissue including liver, spleen and ovary were dissected from mice and placed in labelled tissue processor cassettes. The soft tissues were fixed in 4% PFA at 4°C for 24 hours and stored in 70% ethanol at 4°C. Tibiae were dissected free of soft tissue from mice and placed in labelled tissue processor cassettes. The bones were fixed in 4% PFA at 4°C for 24 hours and stored in 70% ethanol at 4°C until micro-computed tomography (μ CT) scans were performed. The tibias were then decalcified in 0.4 M EDTA pH 8.0 containing 0.5% PFA for 2 weeks, changing the solution every other day. The bones were washed in PBS for one hour for a total of 3 times, this was to remove residual EDTA. The bones and soft tissues were placed into the Leica TP2010 processor to dehydrate the tissues and infiltrate them with wax, this was performed by the skelet-AL Lab, University of Sheffield.

After processing, the bones and soft tissue were embedded into wax, for the tibias, they were embedded in a specific orientation which was the same for each tibia. The wax blocks were trimmed using a Leica microtome to expose the length of the organ/BM, and 3 μ m sections were cut in serial,

put onto a 45°C water bath to ‘float-out’ for 30 minutes. They were then attached to super-frost positively charged slides and placed onto a hot plate to remove residual creases. Finally, they were placed in an oven at 37°C to fully adhere to the slides overnight before they were used for immunohistochemistry.

2.7.2 Immunohistochemistry Staining

2.7.2.1 Principles of Immunohistochemistry Staining

IHC techniques were used to visualise the expression of molecules of interest *ex vivo*. A ‘sandwich’ IHC system was optimised to visualise the presence of Lambda (U266) and Kappa (5TGM1) IgGs in BM and soft tissue histological sections taken from mice. The basic IHC method is displayed in Figure 2.9.

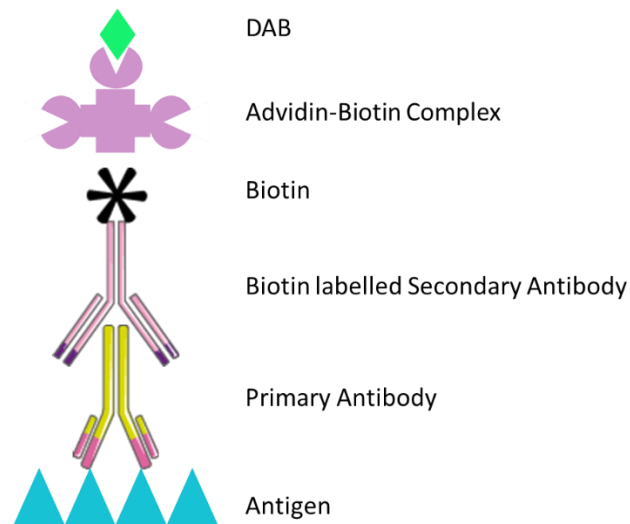


Figure 2.9: A schematic diagram demonstrating a sandwich IHC technique.

Primary antibody binds to the antigen of interest, followed by the binding of a biotinylated secondary antibody which is raised in a species complementary to the primary antibody species. The biotin on the secondary antibody then binds to the avidin-biotin complex, which then binds to peroxidase substrate 3'-Diaminobenzidine (DAB) creating a brown colour. This can be visualised using light microscopy.

2.7.2.2 IHC Methodology for Lamba/Kappa.

On the day of staining IHC buffers were made up as described in Table 2.17. Sections were deparaffinised twice in xylene for 5 minutes, followed by rehydration through a series of alcohol (99%, 99%, 95%, and 70% industrial methylated spirits (IMS) for 5 minutes each. The sections were washed in tap water for 5 minutes and PBS tween (PBST) for a further 5 minutes. Antigen retrieval was performed using x1 citrate buffer pH 6.0 (Abcam) in a coplin jar which was placed in an 80°C water bath. Sections were placed in the citrate buffer for 20 minutes. The sections in the coplin jar were removed from the water bath and left to cool to room temperature. The sections were then washed in PBST, with agitation twice for 3 minutes each. To block endogenous peroxidase, 200 µL of 3% hydrogen peroxidase (H₂O₂) was added to each slide for 30 minutes at room temperature, followed by washing twice in PBST for 3 minutes each with gentle agitation. To reduce non-specific staining, the sections were blocked by adding 200 µL of 10% casein to each slide for 20 minutes at room temperature. The block was tapped off and the slides were then incubated for 90 minutes with 200 µL of primary or concentration matched isotype control. The sections were then washed in PBST, with agitation twice for 3 minutes each. 200 µL of appropriate biotinylated secondary antibody was added to the slides for 20 minutes at room temperature and the slides were subsequently washed twice with PBST. To amplify the signal, the sections were then incubated in 200 µL of Avidin-Biotin Complex (ABC) for 20 minutes at room temperature. The sections were then washed in PBST, with agitation twice for 3 minutes each. Finally, the peroxidase reagent was used. 200 µL of Immupact DAB was added to the slides for up to 10 minutes at room temperature. The sections were then washed in tap water to remove excess DAB for 5 minutes with gentle agitation. Sections were then counterstained in Gill's haematoxylin for 10 seconds to visualise the nuclei. The slides were then left to 'blue' in running tap water for 3 minutes after which they were dehydrated through a series of alcohols (70%, 95%, 99%, 99%) for 10 seconds in 70% and 95% and 30 seconds in 99%. This was followed by two xylene washes, the first for 1 minute and the second for a further 3 minutes. The slides were then cover slipped using

22 x 22(mm) cover slips with Di-N-Butyl Phthalate in Xylene (DPX). Staining was visualised by scanning the slides using an Aperio scan scope scanner and images were captured.

2.7.3.3 Optimisation of Adenoviral Hexon/E1A Staining

Staining was performed as described in section 2.7.3.2, however in addition to citrate-heat mediated antigen retrieval other methods were also used, such as trypsin and pepsin. For trypsin antigen retrieval, trypsin was diluted 1 in 4 with buffer provided in the kit (Menarini Diagnostics Cat# MP-955-K25) and left to reach room temperature. 200 µL of Trypsin was added per slide and left for 10 minutes. For pepsin antigen retrieval (Sigma Cat# R2283), pepsin was aliquoted out of the bottle into a bijou to warm to room temperature. 200 µL of pepsin was added per slide and left for 20 minutes. Additionally, optimisation of the length of time blocking non-specific binding with casein and staining with primary antibody was performed.

Table 2.17: Buffers, reagents and antibodies used in IHC

Buffer	Buffer contents	Supplier
Wash Buffer: PSBT	PBS with 0.1% Tween 20	
Antigen Retrieval: Citrate buffer pH 6.0	100x citrate buffer diluted 1:100 in dH ₂ O	Abcam
Antigen Retrieval: Trypsin	Dilution 1:4 with buffer provided	
Antigen Retrieval: Pepsin	N/A	
Endogenous peroxidase block: 3% H ₂ O ₂	30% H ₂ O ₂ diluted 1:10 in PBS	VWR
Serum Block: 10% Casein	Casein diluted 1:10 in PBST	Vector
Antibody diluent: 1% Casein	Casein diluted 1:100 in PBST	Vector
Primary Lambda/Kappa antibody: Human/Mouse IgG Light Chain (Kappa) antibody raised in rabbit/ Human IgG Light Chain (Lambda) antibody raised in rabbit	IgG Light Chain (Kappa) antibody diluted 1:300 in 1% casein/ IgG Light Chain (Lambda) antibody diluted 1:2000 in 1% casein	ProteinTech®
Isotype control antibody for Lambda/Kappa: Rabbit IgG Isotype Control	Diluted 1:100 in 1% casein	Dako
Secondary Antibody for Lambda/Kappa: Biotinylated Goat anti-Rabbit	Diluted 1:200 in 1% casein	Vector
Primary hexon Antibody: anti-Ad5 antibody raised in goat	Diluted 1:200 in 1% casein	Merck
Isotype control antibody for hexon: Goat IgG Isotype Control	Diluted 1:200 in 1% casein	Dako
Secondary Antibody for hexon: Biotinylated Horse anti-Goat	Diluted 1:200 in 1% casein	Vector
Primary E1A Antibody: anti Ad5 E1A raised in Rabbit	Diluted 1:100-1:200 in 1% casein	Bioss Antibodies
Isotype control antibody for E1A: Rabbit IgG Isotype Control	Diluted 1:100-1:200 in 1% casein	Dako
Secondary Antibody for E1A : Biotinylated Goat anti-Rabbit	Diluted 1:200 in 1% casein	Vector
Enzyme: ABC Kit	1 drop of A and 1 drop of B in 2.5 mL of PBS	Vector
Substrate: Imm pact DAB	1 drop of DAB in 1 mL of diluent	Vector

2.7.2.4 IHC Staining Quantification

To quantify staining in tumour-bearing bone sections, an Aperio Scan Scope slide scanner and QuPath software were used (v0.2.3)(349). An image of an example of a tibia stained with Kappa light chain which has been analysed using QuPath software is shown in Figure 2.10. For analysis of tumour burden in tibiae, the total area of BM space was selected, only the cellular BM space was required, so the area of trabecular bone was subtracted from the total BM area. The total area of the tumour was then divided by the cellular BM area and multiplied by 100.

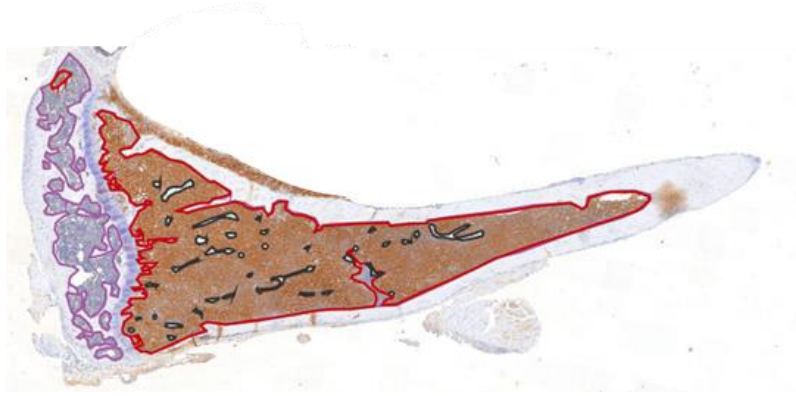


Figure 2.10: An example image using the Aperio Scan Scope slide scanner and analysis of tumour burden using QuPath software.

A representative section of tibia infiltrated with 5TGM1-Luc cells stained with anti-Kappa antibody (brown). QuPath software was used to measure tumour burden (red outline) the marrow space (purple outline) and bone (black outline).

2.8 Bone Parameter Analysis

2.8.1 *Ex vivo* Micro-computed Tomography

2.8.1.1 Principles of Micro-computed Tomography

To determine any differences between the bone parameters in the mice, μ CT was used. μ CT is a non-invasive and non-destructive technique using X-rays. X-ray photons are generated by accelerated electrons in the X-ray source which strikes the tungsten within the source. X-rays are emitted as a polychromatic beam, which pass through a sample which rotates within the machine. Depending on the density of the sample, X-rays are either absorbed or scattered, dense samples such as calcium containing bone cause X-ray absorption whilst soft tissues result in x-ray scattering. The images are detected and projected as 2D image slices, which can be reconstructed to produce 3D images. Many parameters can be analysed using μ CT such as trabecular bone volume normalised to tissue volume (BV/TV%), trabecular thickness (Tb. th./mm), trabecular number (Tb. N. /mm⁻¹) and trabecular separation (Tb. sp/mm)

2.8.1.2 Micro-computed Tomography Methodology

Mice tibias were fixed in 4% PFA prior to scanning. Bones were then scanned using a SkyScan 1172 at 50 kilo volts (Kv), 200 microamperes (μA), using an aluminium filter of 0.5mm and pixel size of $4.3 \mu\text{m}^2$ and images were then reconstructed using N-Recon software. Trabecular bone, 0.2 mm below the growth plate, was analysed using Ct-an and Batman software to provide data for bone parameters. BV/TV, trabecular number, trabecular thickness, cortical thickness was assessed. 3D models of trabecular bone were created using ParaView Software (Clifton Park, NY, USA).

2.9 Proteome Profiler Mouse Cytokine array

To assess cytokine expression from serum obtained from terminal cardiac bleeds, a semi-quantitative membrane-based sandwich immunoassay detecting 40 mouse proinflammatory cytokines and chemokines was used (Proteome profiler mouse cytokine array kit, panel A R&D systems Cat# ARY006). 50 μL of serum from four representative mice in each treatment group (closest to average tumour for the group) were pooled within their respective treatment group. 200 μL of this serum was used to assess cytokine expression following manufacturer's instructions. The microarray membranes were imaged on a BioRad ChemiDoc™ for 10 minutes, taking an image every 30 seconds. Images were analysed via densitometry on BioRad Image Lab software (v6.1). Each spot from each treatment group was compared relatively to vehicle control which were all normalised from background.

2.10 Statistics

Interactions between Ad[CE1A] and anti-MM drugs for each cell line was determined by calculating the CI using the Chou-Talalay equation produced using the computer software CompuSyn® v.1.0. Chou Talalay is the most widely used method for studying drug interactions between two modalities *in vitro*. GraphPad Prism version 9.0 (GraphPad Software, San Diego, USA) was used to generate sigmoid dose response curves to calculate the inhibitory dose 50 (IC_{50}) which describes the dose that is required to inhibit 50% of cell viability. An R^2 of <0.9 was not accepted and repeated as this represents a higher degree of variance.

All statistical analysis was performed using GraphPad Prism. The statistical tests used are stated in each case in the results figure. Unpaired T-tests were performed when comparing two conditions alone. One-way ANOVA was performed when comparing a set of means within a single group. Multiple comparison tests with the appropriate correction method were used to control the type I error rate. When all means in a set were compared with each other, Tukey's correction was used; when every mean was compared with one control, Dunnett's correction was used; for any other selected subset of means were compared, Šidák's correction was used. Two-way ANOVA was used to compare two or more groups of data. In all cases, cut offs for statistical significance were as follows * $p < 0.05$, ** $p < 0.01$, *** $p < 0.001$ and **** $p < 0.0001$.

If two sets of data were correlated, correlation coefficients were determined using Pearson's test, denoted by R. Linear regressions were also performed to display line of best fit. Values for R were interpreted as follows: 0, no linear relationship; ± 0.3 , a weak linear relationship; ± 0.5 , a moderate linear relationship; ± 0.7 , a strong linear relationship; ± 1 , a perfect linear relationship.



Chapter 3 : Efficacy and Cell Death Mechanisms of Ad[CE1A] in Human Multiple Myeloma



3.1 Introduction

3.1.1 Adenovirus in Multiple Myeloma

A range of potential OV's have shown therapeutic potential in MM and other cancers as discussed in throughout Chapter 1. Ads contain features that make them suitable for oncolytic virotherapy, especially Ad5, which have been tested in many models of pre-clinical research where they have shown promising anticancer activity (205,350), have a good safety record in phase I/II clinical trials and have shown efficacy in some trials (351–353). However, oncolytic adenoviral therapy has had less interest for haematological cancers, unless a chimeric Ad is used, due to the long-held belief that Ad5 requires CAR expression for viral infection, and that cells of haematological origin have less to no CAR expression compared to other cell types (354–356). This chapter details the expression of adenoviral entry receptors in MPCs, and the infection efficiency of Ad5 in MPCs.

Ad5, unlike naturally occurring pathogenically benign OV's, such as RV, can cause clinical disease, which commonly presents with mild gastrointestinal symptoms, respiratory symptoms or a combination of both (158,161). Most of these occur in children younger than 5 years of age and are generally self-limiting. Because of Ad5's potential for clinical disease, to improve their safety they are genetically modified to prevent replication in healthy tissue. There are several methods to genetically modify Ad5's, the method used for Ad[CE1A] in this thesis was to transcriptionally control viral replication using a tumour/tissue specific promoter. For MM, the promoter for *SLAMF7* also known as CS1 was chosen to restrict viral replication to CS1 expressing cells. CS1 is upregulated in MM, and is already an approved target for immunotherapy, with the approval of Elotuzumab, a mAb against CS1 for MM therapy (357–359). This chapter details CS1 expression in a range of MPC lines and primary patient-derived MM cells compared to control cancer cell lines or control patient-derived BMMCs, and whether CS1 expression correlates to viral replication and oncolysis.

Ad5's, along with a number of other OV's have become of significant interest, due to their ability to infect, replicate and selectively lyse cancer cells. A growing amount of preclinical data reviewed in the main introduction to this thesis (section 1.4) demonstrates the efficacy of Ad5's in a number of

settings, but predominantly solid malignancies. Some work has been conducted on Ad5 in MM to date, which have shown WT and genetically modified Ad5s are capable of *in vitro* lysis of MPC lines (125,127,129,265), and previous to this work, Ad[CE1A]'s efficacy was tested as a monotherapy in a few MPC lines and *in vivo* in a xenograft model (unpublished data, personal communication). This chapter details the efficacy of Ad[CE1A] replication and oncolysis in a larger panel of MPC lines, with differing expression of CS1.

Most importantly, this chapter details the efficacy of Ad[CE1A] in primary patient-derived MM cells, healthy plasma cells and their corresponding BMMCs. As mentioned in the introduction, most studies assessing OV's in primary MM cells only use small numbers of patient samples (n=1-3). Therefore, studying the efficacy of Ad[CE1A] in a larger set of patient samples would be more thorough and give a better insight into the efficacy of Ad[CE1A] in a heterogeneous population. Unfortunately, 40-70% of European or American adults are seropositive for Ads and even higher in other regions (90% Africa; 95% Thailand) (360). It has been shown preclinically in murine models that there is a dose dependence between neutralising Ad antibodies and adenoviral efficacy in a variety of settings (361,362). However, MM patients have compromised B cell function and hypogammaglobulinemia, thus commonly have depressed antibody titres to common infectious pathogens (363,364). Therefore it is important to test Ad[CE1A] efficacy against primary MM cells in the presence of their autologous serum to determine the impact of neutralising antibodies on Ad[CE1A] efficacy.

The precise mechanism by which conditionally replicating Ads kill tumour cells is unclear. Ads have complex infrastructure in which viral genes produce numerous proteins that prevent host cell death early after infection and other proteins that promote cell death at later stages (365–368). There are several encoded proapoptotic and antiapoptotic proteins known to maintain temporal control of Ads on the host cell. Because of this WT Ad-induced cell death was long presumed to be classical apoptosis in normal cells (369–371). However, several papers suggest different mechanisms of oncolytic cell death against cancer cells including programmed necrosis (necroptosis) (366), autophagy (372) and

novel adenoviral programmed cell death (61). These differences could be due to the use of different genetic modifications in the oncolytic Ad, and in different cancer cell types. Because Ad[CE1A] has deletions in *E1* and *E3* to make capacity for *SLAMF7* promoter insertion, investigations to determine if Ad[CE1A]-induced cell death resembles WT Ad5 induced apoptosis or if other cell death mechanisms are involved are needed. Therefore, this chapter attempts to determine if apoptosis and other cell death mechanisms are involved in Ad[CE1A]-induced cell death in MM cells.

Lastly, as discussed in the introduction to this thesis, it is now widely accepted that OV (including Ads), as well as having direct antitumour effects, can also cause ICD which generates antitumour immune responses critical for their efficacy (373–375). ICD generally describes any type of death that induces some form of adaptive immune response. However, ICD has recently been defined by The Nomenclature Committee on Cell Death as ‘a form of regulated cell death that is sufficient to activate an adaptive immune response in immunocompetent hosts’ (62,376). This adaptive immune response is either specific for endogenous (cellular) or exogenous (viral) antigens expressed by dying cells. A relatively restricted set of stimuli can initiate ICD, these include viral infection, some chemotherapeutics (e.g anthracyclines, BTZ, Melph), photodynamic therapy and specific forms of radiation therapy (377). These agents stimulate the release of a series of DAMPs and/or PAMPs, where they are recognised by pathogen recognition receptors (PRRs) expressed by innate and adaptive components of the immune system. This warns the host of danger, resulting in the induction of an immune response, usually associated with the formation of immunological memory (377). These processes help to retarget the adaptive immune system toward tumour, lifting local immunosuppression via cytotoxic CD8⁺ T cells and helper CD4⁺ T cells (64,378). Additionally, ICD reveals multiple TAAs for presentation to the immune system via activated mature DCs (65). Therefore, this chapter attempts to determine if MPCs release classical DAMPs involved in ICD following Ad[CE1A] treatment and whether antigen presentation via MHC class I and II are upregulated following Ad[CE1A] treatment.

3.1.2 Hypothesis, Aims and Objectives

3.1.2.1 Hypothesis and Aims

In this chapter, further assessment of the potential of Ad[CE1A] for MM therapy is performed. To do this, the following hypothesis will be tested 'Ad[CE1A] infects, replicates and induces cell death specifically in CS1-expressing MPC lines and primary MM cells'. An Additional aim is to determine what cell death mechanisms are involved in MPCs following Ad[CE1A] infection.

3.1.2.2 Objectives

The hypothesis was tested by the following objectives

1. Determine the expression of Ad5 infection receptors, CAR, $\alpha\beta_5$ and $\alpha\beta_3$ in MPC lines and control cell lines.
2. Determine the infection efficiency of Ad5 in MPC lines.
3. Assess CS1 (*SLAMF7*) expression in MPC lines and control cell lines.
4. Assess Ad[CE1A] replication in MPC lines
5. Investigate the efficacy of Ad[CE1A] on cell death and proliferation in MPC lines and control cell lines.
6. Determine CS1 expression in primary MM cells, healthy plasma cells and their corresponding BMMCs *ex vivo*.
7. Investigate the efficacy of Ad[CE1A] on cell death in primary MM cells, healthy plasma cells and their corresponding BMMCs *ex vivo*.
8. Investigate the involvement of apoptosis or other cell death mechanisms in Ad[CE1A]-induced cell death.
9. Determine the expression of ICD markers in Ad[CE1A]-induced cell death.

3.2 Results

3.2.1 Human Myeloma Cell Lines Express Primary and Secondary Adenovirus Entry Receptors

CAR is known to be the primary cell surface receptor for Ad5. Secondary Ad5 receptors include integrins $\alpha\beta_5$ and $\alpha\beta_3$. Therefore, the expression of CAR, $\alpha\beta_5$ and $\alpha\beta_3$ proteins on the surface of human MPC lines was initially evaluated compared to Ad5 susceptible cells HEK293A. A panel of human MPC lines and control HEK293A cells were stained with either fluorophore-conjugated antibody against integrins $\alpha\beta_5$, $\alpha\beta_3$ or CAR antibody (or with an isotype-matched control antibody), and then assessed for expression of this protein by flow cytometry (Figure 3.1). A high proportion of human MPC lines and HEK293A cells express cell surface CAR receptor (~75-85%). There was no significant difference in CAR expression in MPC lines and HEK293A cells, except for U266 and NCI-H929 which had significantly higher expression than HEK293A cells, and KMS-12-BM which had significantly lower expression (Figure 3.1.c). A proportion of all MPC lines express $\alpha\beta_5$, JIN-3, OMP-2, RPMI-8266, and KMS-11 cells had similar levels of $\alpha\beta_5$ expression compared to HEK293A cells, whilst L363, U266, NCI-H929 and KMS-12 had significantly lower expression levels (Figure 3.1.d). A low proportion of human MPCs and HEK293A cells expressed cell surface $\alpha\beta_3$, however all MPC lines had significantly lower expression than HEK293A cells (Figure 3.1.e).

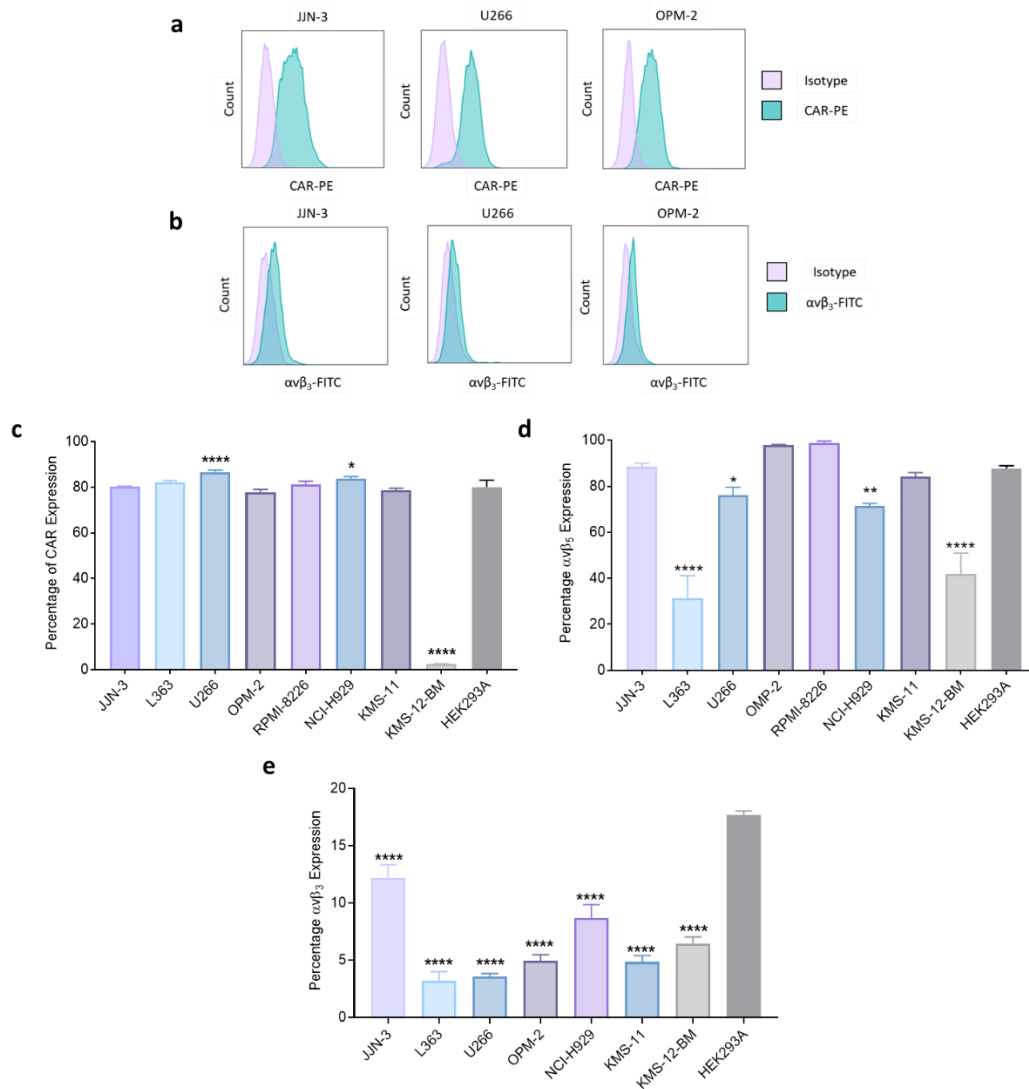


Figure 3.1: Flow cytometric analysis of CAR, $\alpha v\beta_5$ and $\alpha v\beta_3$ expression in human MPC lines compared to Ad5 susceptible cell line HEK293A:

Human MPC lines (JIN-3, L-363, U266, OPM-2, RPMI-8266, NCI-H929, KMS-11 and KMS-12-BM) and control cell line HEK293A were stained with a PE conjugated anti-human CAR antibody, APC conjugated $\alpha v\beta_5$ or FITC conjugated anti-human $\alpha v\beta_3$ integrin antibody and compared to respective isotype controls and analysed by flow cytometry. Viable cells were determined by gating on the PI negative population and only the viable cells used in the analysis. Representative histogram plots of MFI of (a) CAR, (b) $\alpha v\beta_5$ and (c) $\alpha v\beta_3$ integrin compared to respective isotype control in MPC lines JIN-3, U266 and OPM-2. (d) Percentage of MPC lines with surface expression of CAR or (d) $\alpha v\beta_5$ (e) $\alpha v\beta_3$ integrin compared to Ad5 susceptible cell line HEK293A. n=3 Data is the mean \pm SD. p values are for one-way ANOVA with multiple comparisons compared to control HEK293A cells with Dunnett's correction, where * p<0.05; ** p<0.01, *** p<0.001, **** p<0.0001.

3.2.2 Human Myeloma Cell Lines have Increased CS1 Expression Compared to Non-myeloma cells

Ad[CE1A] utilises CS1 for transcriptional control of the replication essential gene *E1A*. Therefore, it was essential to confirm if human MPC lines expressed CS1 at the protein and gene levels. Cell surface protein expression of CS1 on MPC lines were evaluated first. A panel of MPC lines, and negative control cell lines LNCaP, a prostate cancer cell line and HEK293A cells were stained with a PE-conjugated antibody against CS1 (or with an isotype-matched control antibody) and then protein expression was assessed by flow cytometry (Figure 3.2). A proportion of all MPC lines tested were found to express CS1 protein, and 6 out of 7 MPC lines had significantly higher CS1 protein expression levels compared to the control cell line HEK293A. A range of expression levels were observed- OPM-2, L363 and NCI-H929 expressed CS1 on 80% to ~100% of the cells, whereas JJN-3, KMS11 demonstrated low level expression (~30%) with intermediate results seen in the U266 cell line (~50%). Importantly, LNCaP cells did not express CS1 and HEK293 cells were ~4% positive. KMS-12-BM showed no significant increase in CS1 expression compared to HEK293 cells (~9%).

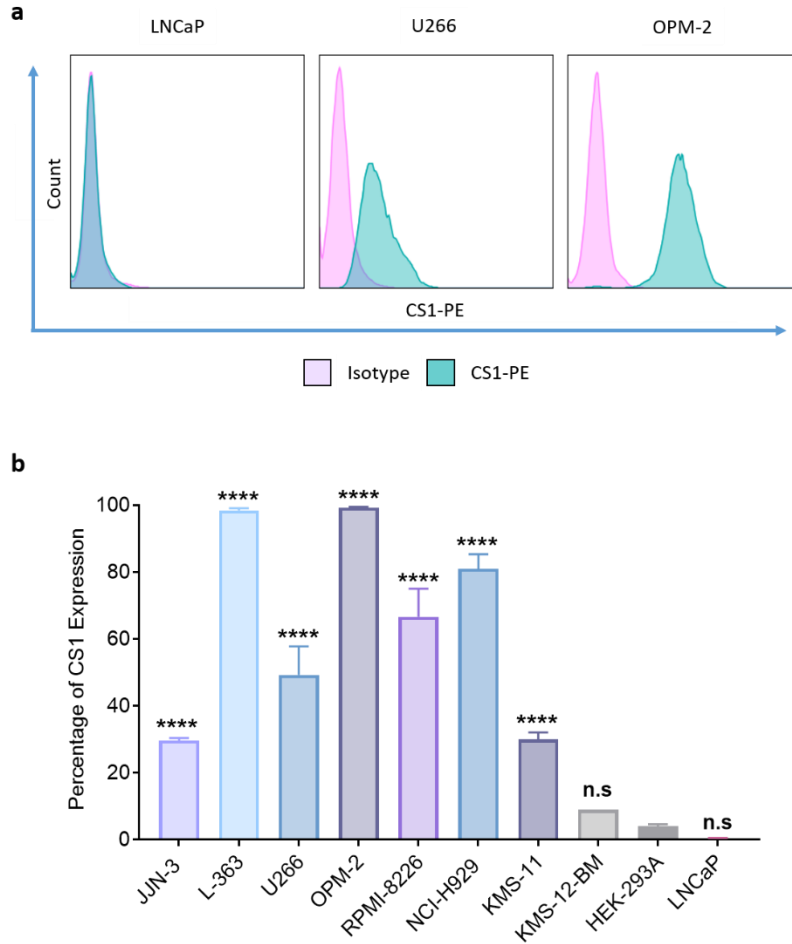


Figure 3.2: Flow cytometric analysis of CS1 cell surface expression in human MPC lines compared to control non-MM cells:

Human MPC lines (JUN-3, L-363, U266, OPM-2, NCI-H929, RPMI-8266, KMS-11 and KMS-12-BM) and control cell lines HEK293A and LNcaP were stained with a PE conjugated anti-human CS1 antibody and compared to respective isotype controls and analysed by flow cytometry. **(a)** Representative histogram plots of MFI of CS1 in LNcaP, U266 and OPM-2 cells. **(b)** Percentage of cells with surface expression of CS1 compared to non-cancer cell line HEK293A. n=3 Data is the mean ±SD. p values are for one-way ANOVA with multiple comparisons compared to control HEK293A cells with Dunnett's correction, where **** p<0.0001.

SLAMF7 (CS1) mRNA expression was then assessed at the gene level by RT-qPCR. Total RNA was extracted from a panel of human MPC lines, the LNcaP cell line and the HEK293A cell line. Total RNA was synthesised by reverse transcription to cDNA and RT-qPCR was performed using Taqman™ primers for *SLAMF7* (Figure 3.3). All human MPC lines tested showed significant levels of CS1 mRNA expression compared to the control cell line HEK293A. LNcaP cells did not express *SLAMF7* at mRNA level. A range of expression levels were seen- OPM-2, L363 and NCI-H929 having the highest relative

expression ($\sim 1 \times 10^4$ - 3×10^4), whereas JJN-3, KMS11 and KMS-12-BM demonstrated lower-level expression (~ 2 -300) with intermediate results seen in U266 and RPMI-8226 cells ($\sim 1 \times 10^3$ - 9×10^3).

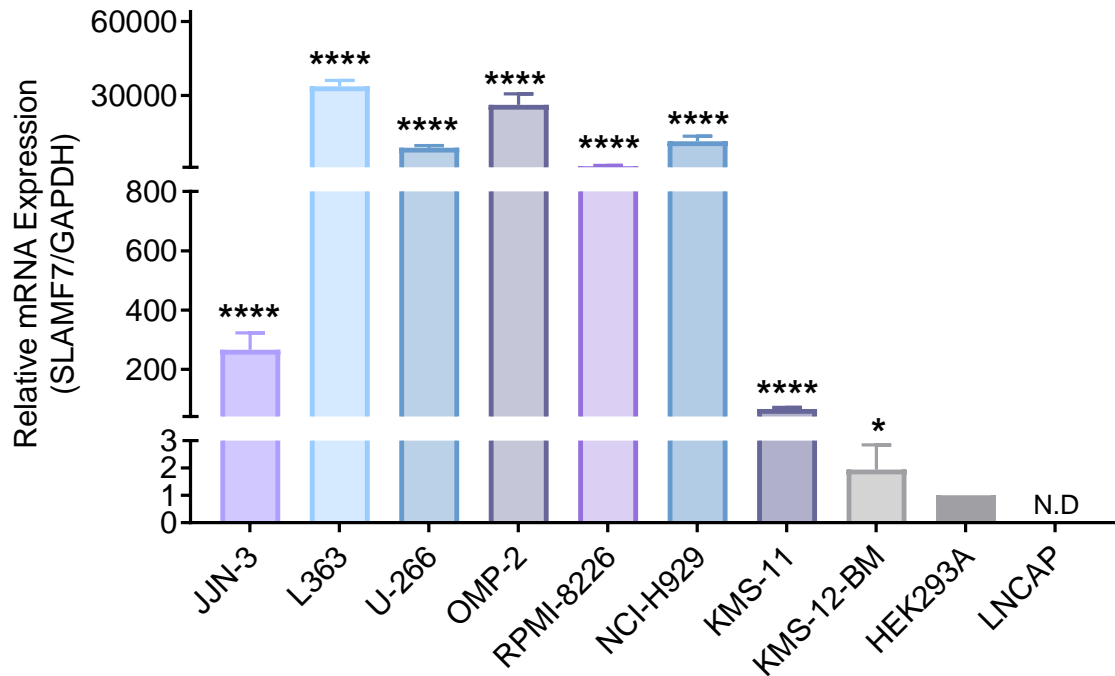


Figure 3.3: *SLAMF7* mRNA Expression in human MPC cell lines:

Relative *SLAMF7* (CS1) mRNA expression in a panel of human MPC lines JJN-3, L363, U266, OPM-2, RPMI-8226, NCI-H929, KMS-11 and KMS-12-BM compared to control HEK293A cells by RT-qPCR. n=3 Data is the mean \pm SD. p values are for one-way ANOVA with multiple comparisons compared to control HEK293A cells with Dunnett's correction, where * $p < 0.05$; **** $p < 0.0001$.

The correlation between CS1 mRNA and protein expression in all cell lines was determined (Figure 3.4). The mean percentage of cell surface CS1 expression plotted against the mean relative fold CS1 mRNA expression showed a strong positive correlation between mRNA expression and protein expression with a significance of $p < 0.01$ and an R^2 of 0.7118.

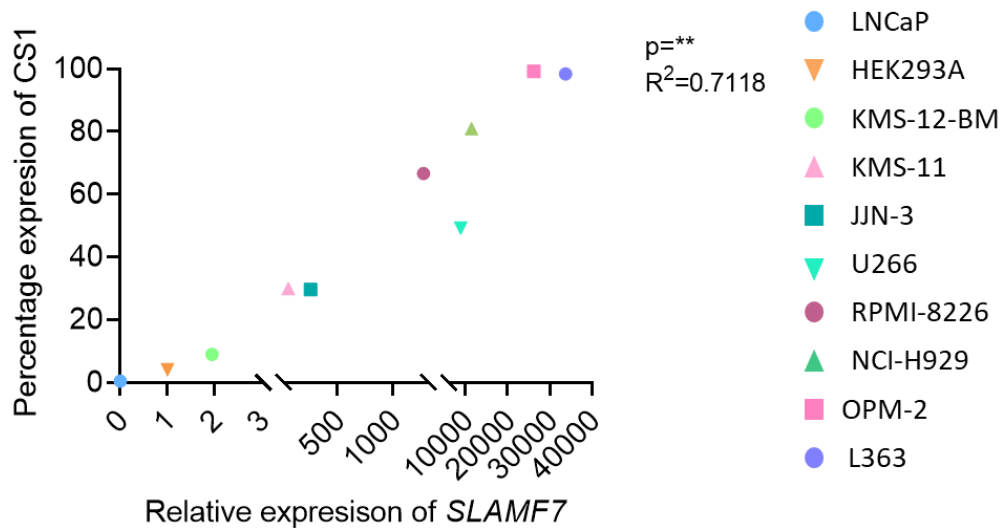


Figure 3.4: Correlation between CS1 cell surface protein expression and mRNA expression:

Percentage of cell surface CS1 expression, as determined by flow cytometry, was plotted against CS1 (*SLAMF7*) mRNA expression, as determined by RT-qPCR for control cell lines (LNCaP and HEK293A) and MPC lines (KMS-12-BM, KMS-11, JJN-3, U266, RPMI-8226, NCI-H929, L363 and OPM-2). Data shows the mean percentage of CS1 surface expression and mRNA expression from n=3 independent experiments. Statistical analysis was determined by Pearson's test with resulting R^2 values deemed to show a correlation if they were close to 1 and p values showing statistical significance of the trend where $** p < 0.01$. R^2 of 0.0-0.3 = weak positive correlation; R^2 of 0.3-0.7 moderate positive correlation; R^2 of 0.7-1.0 = strong positive correlation.

3.2.3 Human Myeloma Cell Lines have High Adenovirus Infection Efficiency

One way to measure infection efficiencies in cells is by using an E1A-deleted, non-replicative Ad5, Ad-GFP. Ad-GFP contains a CMV promoter which drives the expression of GFP. Ad-GFP was added at MOIs of 2 and 20 to human MPC lines. 24 and 48 hours after, infectivity was visualised qualitatively by fluorescent microscopy (Figure 3.5) and quantitatively as the percentage of GFP-positive cells using flow cytometry (Figure 3.6). Human MPC lines all expressed GFP at both 24 and 48 hours and at both doses MOI 2 and MOI 20. There was a significant dose response in GFP positivity between the two doses at both time points. At 24 hours, no statistical difference was seen between MPC lines GFP positivity between doses, except that KMS-12-BM had statistically lower GFP expression at MOI 2 (~2%) (Figure 3.6.b). By 48 hours, there was statistical differences between MPC lines GFP positivity between doses (Figure 3.6.c). JJN-3, L-363, U266 and OPM-2 have the highest GFP positivity at 48

hours (MOI 2 ~60-80%; MOI 20 ~95—100%), NCI-H929 had intermediate GFP positivity (MOI 2 ~65; MOI 20 ~75%), whilst KMS-11 and KMS-12 had the lowest (MOI 2 ~11-34%; MOI 20 ~80%).

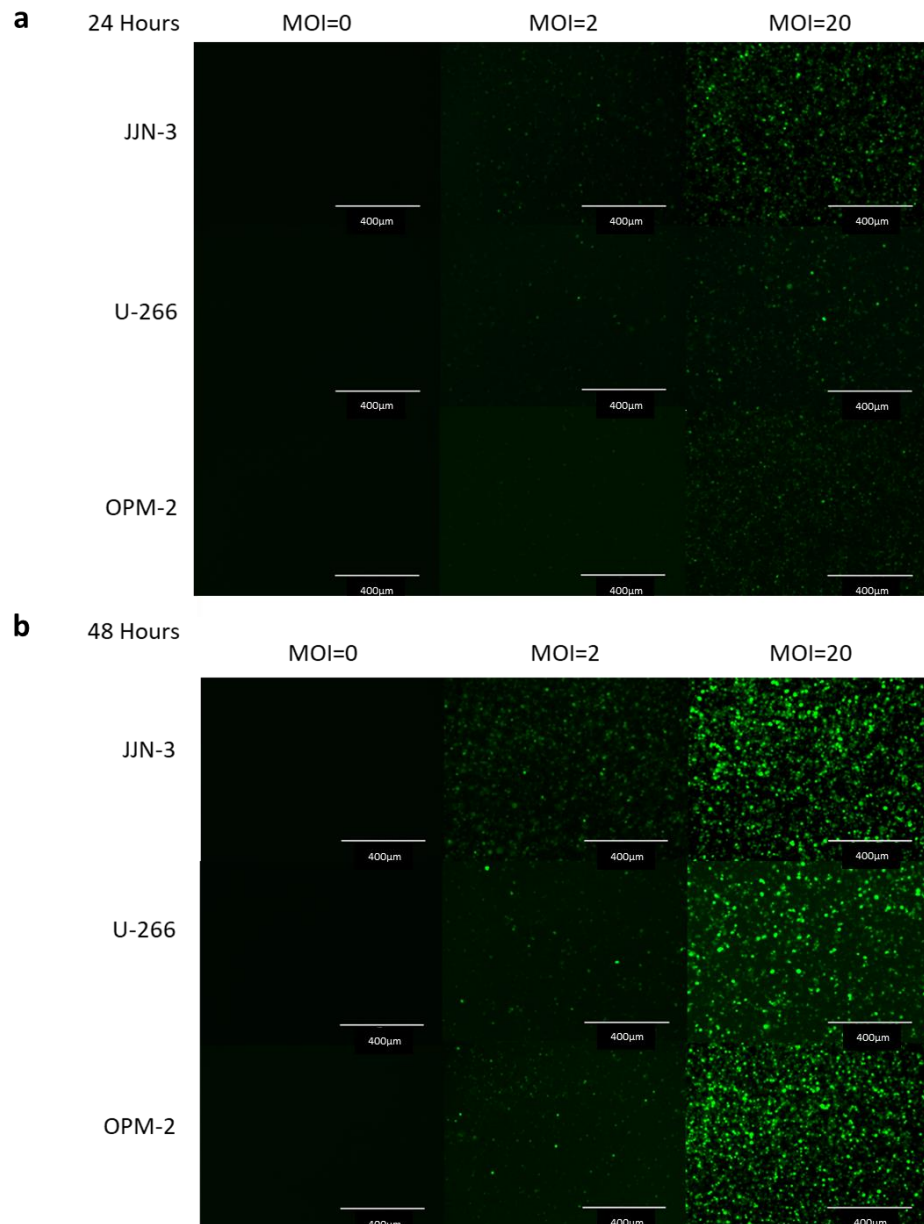


Figure 3.5: Representative images of live fluorescent microscopy of Ad-GFP expression in human MPC lines:

JJN-3, U266 and OPM-2 cells were infected with Ad-GFP at MOI 2 or 20 or PBS control. Fluorescent images taken at (a) 24 and (b) 48 hours after infection (Scale bar 400 µm) n=3.

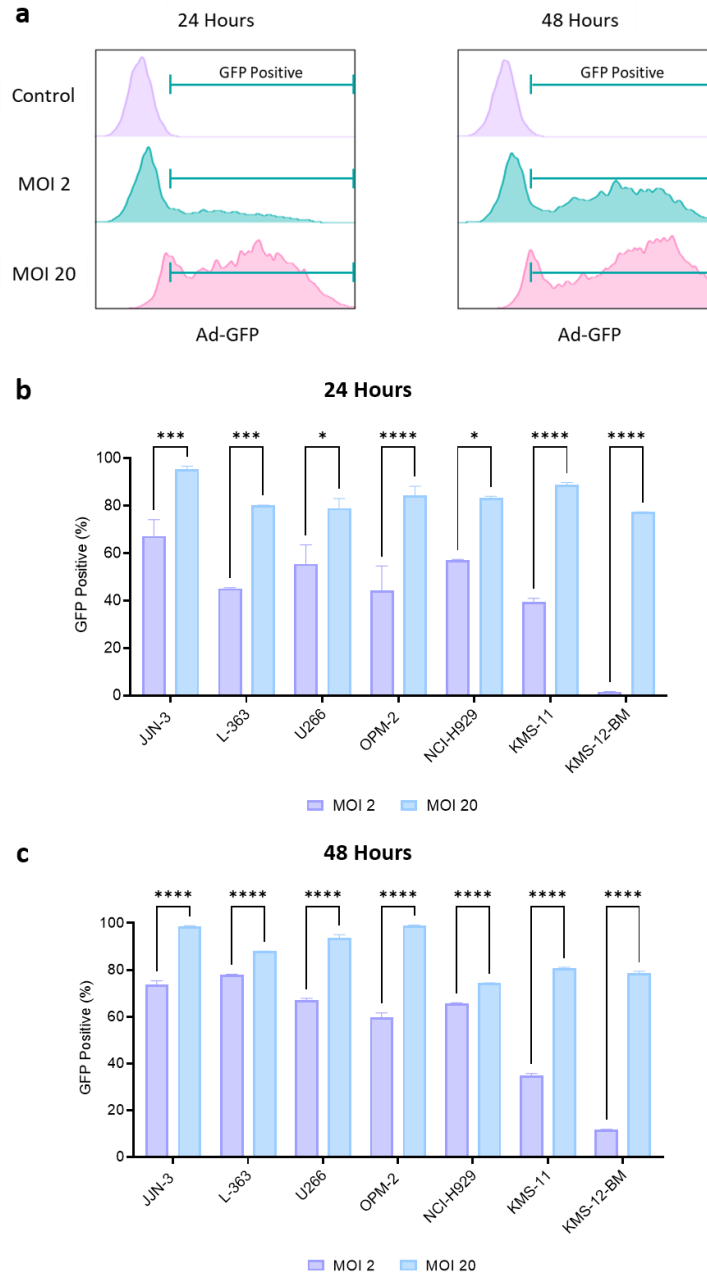


Figure 3.6: Flow cytometric analysis of the percentage of human MPC lines infected with Ad-GFP after 24 and 48 hours:

Human MPC lines (JLN-3, L-363, U266, OPM-2, NCI-H929, KMS-11 and KMS-12-BM) were infected with Ad-GFP MOI 2 or 20. After 24 and 48 hours GFP expression was determined using flow cytometry. **(a)** Representative histogram plots of MFI of Ad-GFP expression after 24 and 48 hours after infection of Ad-GFP at MOI 2 and 20 in JLN-3 cells. Percentage of cells with GFP expression shown at **(b)** 24 hours and **(c)** 48 hours. $n=3 \pm SD$. p values are for 2-way ANOVA with multiple comparisons with Šidák's correction where * $p < 0.05$; ** $p < 0.01$; *** $p < 0.001$; **** $p < 0.0001$.

3.2.4 Ad[CE1A] Replicates in Human Myeloma Cell Lines

Given that the MPC lines tested express CS1 at different levels, which may affect Ad[CE1A] replication, it was important to determine the differences in Ad[CE1A] replication between the different human MPC lines. To do this the essential viral replication gene *E1A* can be assessed by RT-qPCR and the ability of human MPC lines to generate intact infectious virions can be determined. Firstly, *E1A* mRNA expression was determined by RT-qPCR. MPC lines were treated ± Ad[CE1A] MOI 20. After 4- and 24-hours total RNA was extracted from cells, which was then reverse transcribed to cDNA and assessed by RT-qPCR using SYBR™ green primers for *E1A* (Figure 3.7). *E1A* expression increased in all human MPCs over time, however in the KMS-12-BM cell line, this increase did not reach significance. At 24 hours, OPM-2 and L-363 cell lines showed the highest *E1A* expression ($\sim 1.3 \times 10^5$ - 2.3×10^5), whereas JJN-3, U266 RPMI, NCI-H929 and KMS-11 all had intermediate expression ($\sim 3.5 \times 10^4$ - 7.2×10^4).

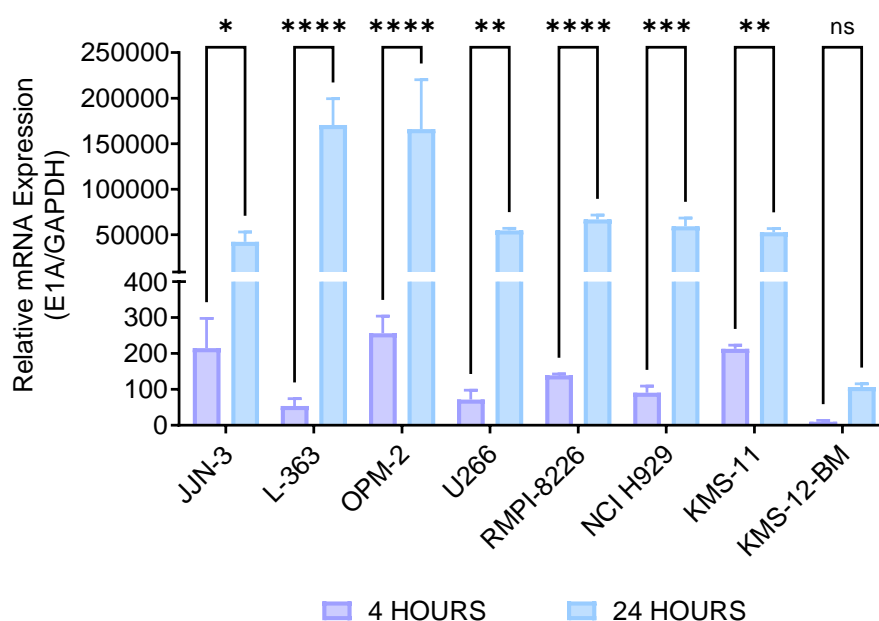


Figure 3.7: *E1A* mRNA expression in MPC lines at 4 and 24 hours:

Relative *E1A* mRNA expression in a panel of human MPC lines (JJN-3, L363, U266, OPM-2, RPMI-8226, NCI-H929, KMS-11 and KMS-12-BM) relative to untreated controls by RT-qPCR at 4 and 24 hours post Ad[CE1A] infection (MOI 20). n=3 Date is the mean ±SD. p values are for 2-way ANOVA with multiple comparisons with Šidák's correction where * p<0.05; ** p<0.01, *** p<0.001, **** p<0.0001.

The correlation between CS1 (*SLAMF7*) mRNA expression and *E1A* mRNA expression in all cell lines was tested (Figure 3.8). A strong positive correlation was found between *SLAMF7* expression and *E1A* expression with a significance of $p < 0.001$ and an R^2 of 0.8581.

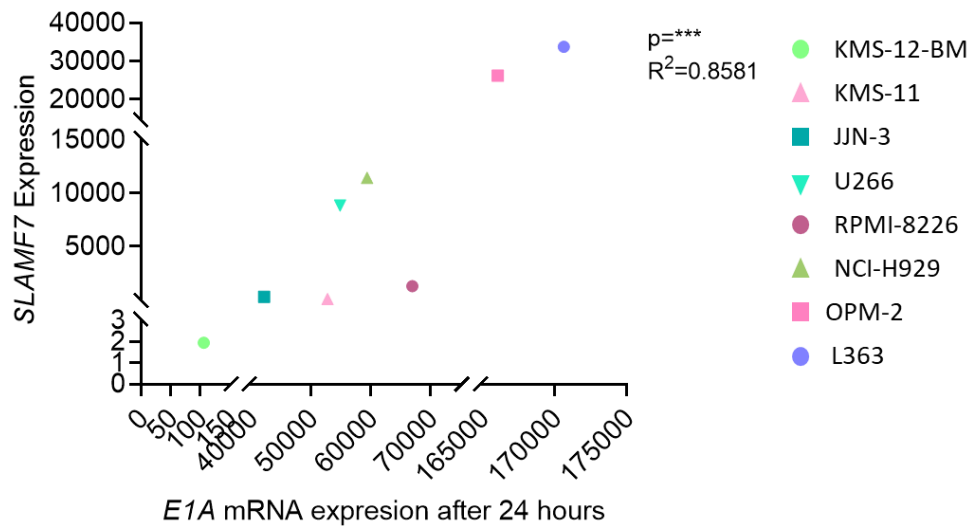


Figure 3.8: Correlation between *SLAMF7* mRNA expression and *E1A* mRNA expression:

Relative *SLAMF7* mRNA expression of human MPCs compared to control HEK293A cell line was determined by RT-qPCR, this was plotted against *E1A* mRNA expression after 24 hours of infection with Ad[CE1A] MOI 20 compared to untreated controls, as determined by RT-qPCR in KMS-12-BM, KMS-11, JJN-3, U266, RPMI-8226, NCI-H929, OPM-2 and L363 cells. Data shows mean from $n=3$ independent experiments. Statistical analysis was determined by Pearson's test with resulting R^2 values deemed to show a correlation if they were close to 1 and p values showing statistical significance of the trend where *** $p=0.001$. R^2 of 0.0-0.3 = weak positive correlation; R^2 of 0.3-0.7 moderate positive correlation; R^2 of 0.7-1.0 = strong positive correlation.

Next the ability of MPC lines to produce infectious viral progeny was assessed. Human MPC lines were infected with Ad[CE1A] at an MOI of 2, and after 72 hours, virus was harvested and viral titre assessed using the Adeno-X™ rapid titre kit (Figure 3.9). All human MPC lines tested showed the ability to produce infectious virions. A range of infectious virions was seen- OPM-2 showed the highest ifu/mL ($\sim 2.5 \times 10^6$), KMS-11 showed the lowest ifu/mL ($\sim 7.5 \times 10^5$) with JJN-3, U266 NCI-H929 and RPMI-8226 having intermediate ifu/mL ($\sim 1.4 \times 10^6$ - 2×10^6).

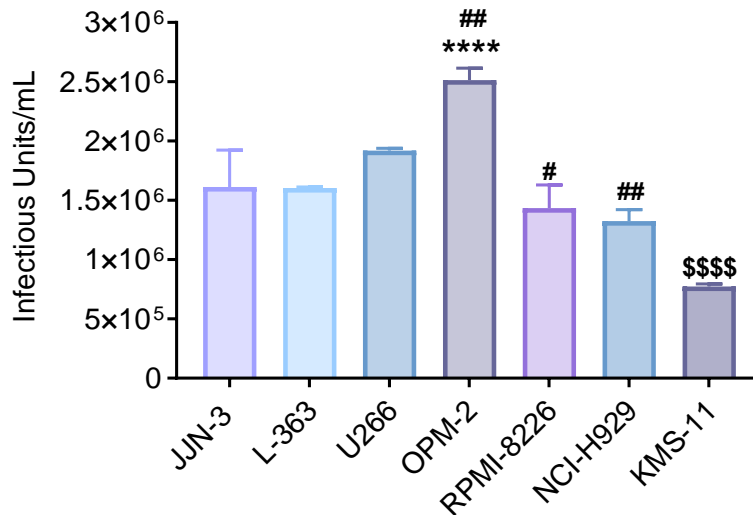


Figure 3.9: Infectious virion production in human MPCs lines:

Human MPC lines (JJN-3, L-363, U266, OPM-2, RPMI-8266, NCI-H929 and KMS-11) were infected with Ad[CE1A] at an MOI of 2 for 24 hours. After 24 hours exogenous Ad[CE1A] was removed, and MPC lines were resuspended in fresh medium. After 72 hours, cells were collected in CM and the cells were lysed to collect viral particles within the cells. Viral titres were determined by Adeno-X™ rapid titre viral quantification kit. n=3 Data is the mean ±SD. p values are for one-way ANOVA with multiple comparisons with Tukey’s correction, where * p<0.05; ** p<0.01, *** p<0.001, **** p<0.0001 * denotes significant difference from all cells except U266, # denotes significant difference from U266, \$ denotes significant difference from all cells.

3.2.4 Ad[CE1A] Causes Oncolysis in Human Myeloma Cell Lines.

To test the oncolytic activity of Ad[CE1A] in human MPC lines, a dose and time response assay was performed. JJN-3 and U266 cells were treated with vehicle control (PBS) or Ad[CE1A] at an MOI of 2, 10 and 20, and cell death (necrosis) was determined by PI staining and flow cytometric analysis at 24, 48 and 72 hours post infection (Figure 3.10). JJN-3 and U266 cells showed a significant dose and time response to Ad[CE1A] treatment, with the highest level of cell death seen at 72 hours for all doses, with MOI 20 causing the highest level of cell death (~80-100%).

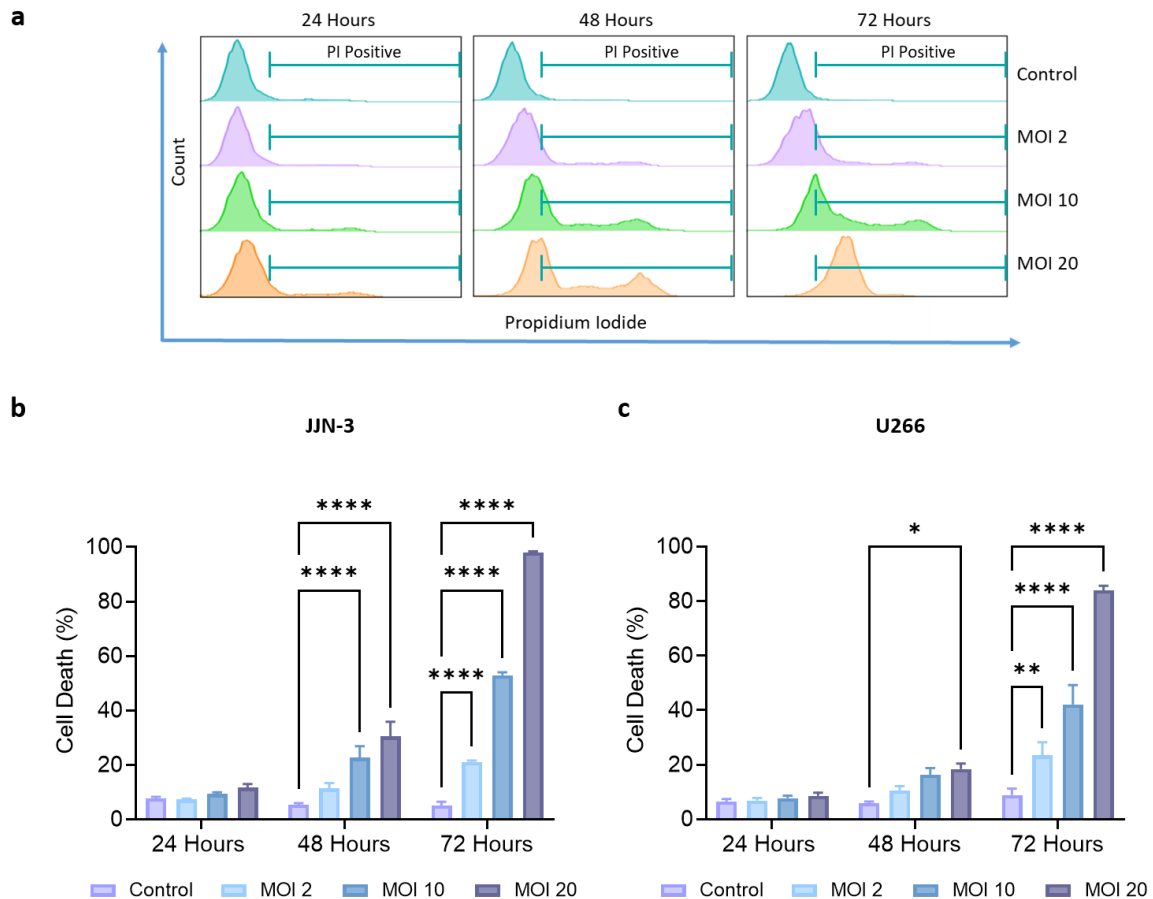


Figure 3.10: Dose and time response Ad[CE1A] toxicity in human MPCs:

(a) Representative histogram plots of PI MFI in JJN-3 cells after Ad[CE1A] treatment at indicated doses and time points. (b) Percentage of JJN-3 and (c) U266 cells dead after incubation with Ad[CE1A] at a range of multiplicities of infection (MOI) or vehicle control for the duration shown, as determined by PI staining using flow cytometry. $n=3$ Data is the mean \pm SD. p values are for 2-way ANOVA with multiple comparisons compared to vehicle control with Dunnett's correction, where * $p<0.05$; ** $p<0.01$; **** $p<0.0001$.

Next in order to confirm that it was the replication of Ad[CE1A] driven by the CS1 promoter that caused cell death and not just the viral infection and initial viral load, an Ad5 virus that has the prostate specific antigen promoter to transcriptionally control viral replication (Ad[PSA]) was used as a control. Human MPC lines (JJN-3, U-266 and OMP-2) were treated with Ad[CE1A] or Ad[PSA] at a concentration of MOI 2, 10 and 20. After 72 hours cell death was determined by PI staining using flow cytometry (Figure 3.11). In all MPC lines, there was a significant dose response to Ad[CE1A], however, this did not reach significance between MOI 10 and 20. Importantly, Ad[PSA] caused no significant increase in cell death at any dose compared to the untreated control.

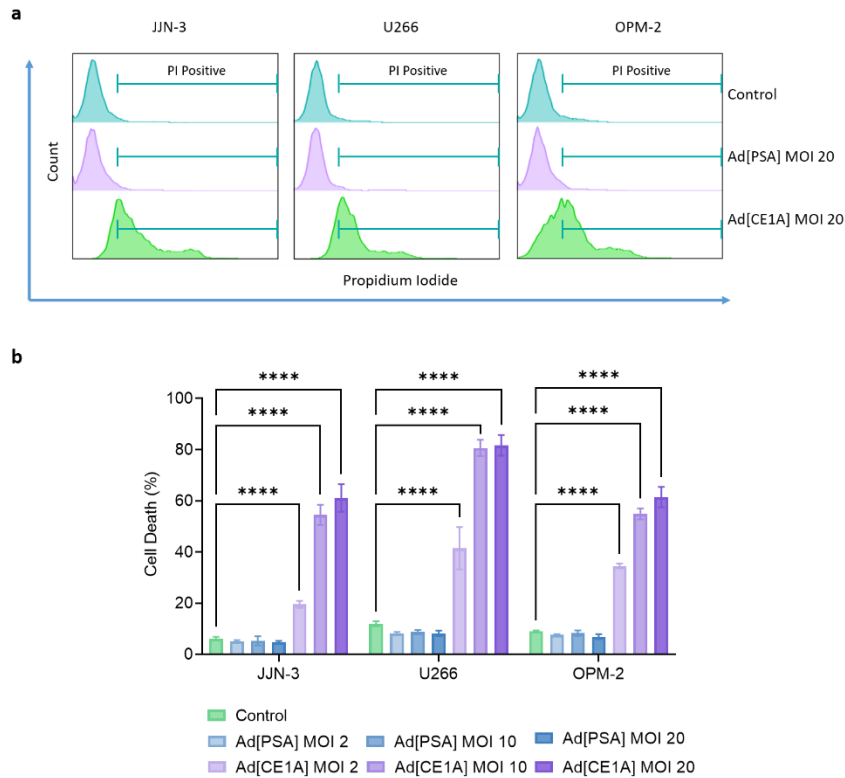


Figure 3.11: Cytotoxicity of Ad[CE1A] compared to Ad[PSA] in human MPCs:

Human MPC lines (JJN-3, U266 and OPM-2) were treated with Ad[CE1A] or Ad[PSA] at an MOI of 2, 10 or 20 or vehicle control and cell death determined by PI staining using flow cytometry after 72 hours. **(a)** Representative histogram plots of PI MFI in JJN-3, U266 and OPM-2 cells after Ad[PSA] or Ad[CE1A] MOI 20 treatment at 72 hours. **(b)** Percentage of human MPCs dead after Ad[CE1A] or Ad[PSA] treatment. n=3 Data is the mean \pm SD. p values are for 2-way ANOVA with multiple comparisons compared to vehicle control with Dunnett's correction, where **** p<0.0001.

To determine the ability of Ad[CE1A] to cause specific oncolysis to MPC, a panel of human MPC lines and LNCaP cells (negative control) were treated with Ad[CE1A] at an MOI of 20 for 72 hours based on previous data (Figure 3.10 & 3.11). Cell death was determined by PI staining using flow cytometry (Figure 3.13). All MPC lines had significant levels (~20-80%) of cell death compared to untreated controls. However, KMS-11 had intermediate levels of cell death (~40%) with KMS-12-BM showing low levels of cell death (~20%). LNCaP cells as predicted had no significant difference in cell death compared to control.

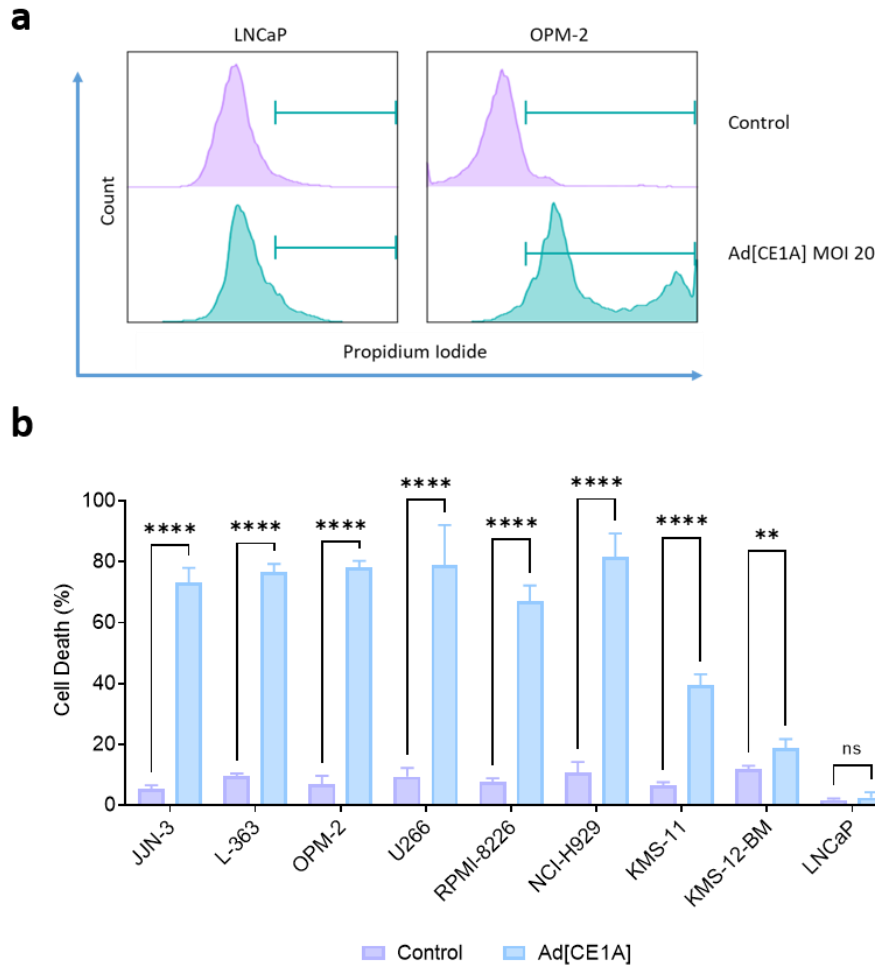


Figure 3.12: Cytotoxicity of Ad[CE1A] in human MPC lines compared to control cancer cell lines:

A panel of human MPC lines (JUN-3, L363, U266, OPM-2, RPMI-8226, NCI-H929, KMS-11 and KMS-12-BM) or control human prostate cancer cell line LNCaP were treated with Ad[CE1A] MOI 20 and cell death determined by PI staining using flow cytometry after 72 hours. (a) Representative histogram plots of PI MFI in control human prostate cancer cell line LNCaP and MPC line OPM-2 after Ad[CE1A] MOI 20 treatment at 72 hours. (b) Percentage of cells dead after Ad[CE1A] treatment. $n=3$ Data is the mean \pm SD. p values are for 2-way ANOVA with multiple comparisons with Šidák's correction, where ** $p<0.01$, **** $p<0.0001$.

The correlation between CS1 cell surface expression and cell death after Ad[CE1A] treatment in all cell lines was tested (Figure 3.13). Mean CS1 cell surface protein expression plotted against the mean cell death showed a moderate positive correlation, with a significance of $p<0.01$ and an R^2 of 0.6736.

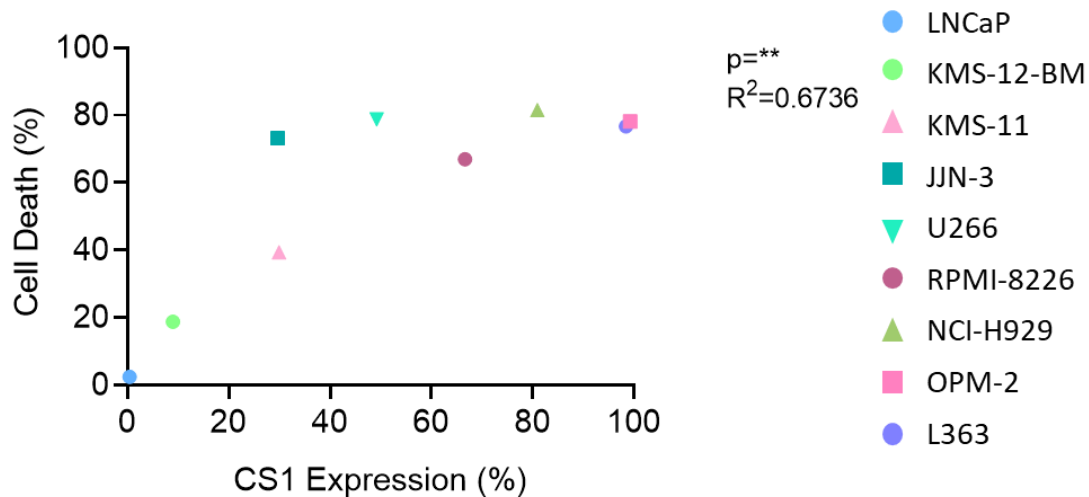


Figure 3.13: Correlation between CS1 cell surface expression and cell death after Ad[CE1A] treatment:

CS1 cell surface expression, as determined by flow cytometry, was plotted against cell death after 72 hours of Ad[CE1A] (MOI 20) treatment, as determined by PI staining using flow cytometry in LNCaP control prostate cancer cells line and KMS-12-BM, KMS-11, JJN-3, U266, RPMI-8226, NCI-H929, OPM-2 and L363 MPC lines. Data shows mean from n=3 independent experiments. Statistical analysis was determined by Pearson's test with resulting R^2 values deemed to show a correlation if they were close to 1 and p values showing statistical significance of the trend where $** p < 0.01$.

To determine whether Ad[CE1A] has an effect on MM cell proliferation, KI-67 expression was investigated. KI-67 is a nuclear cell proliferation-associated antigen that is expressed in the cell cycle phases G1, S, G2 and M but is absent in G0. JJN-3 and OPM-2 cells were incubated with Ad[CE1A] at MOIs of 2, 10 or 20. After 24 and 48 hours, cells were stained with an APC-conjugated antibody against KI-67 (or with a matched isotype control antibody) and then assessed for expression of this protein by flow cytometry (Figure 3.14). Untreated cells highly express KI-67, however, after Ad[CE1A] treatment the fold change of MFI significantly decreases in a dose-dependent manner compared to untreated controls at both 24 and 48 hours, with the highest dose having the largest fold decrease at the later time point (~ 0.1 for JJN-3 and ~ 0.03 for OPM-2).

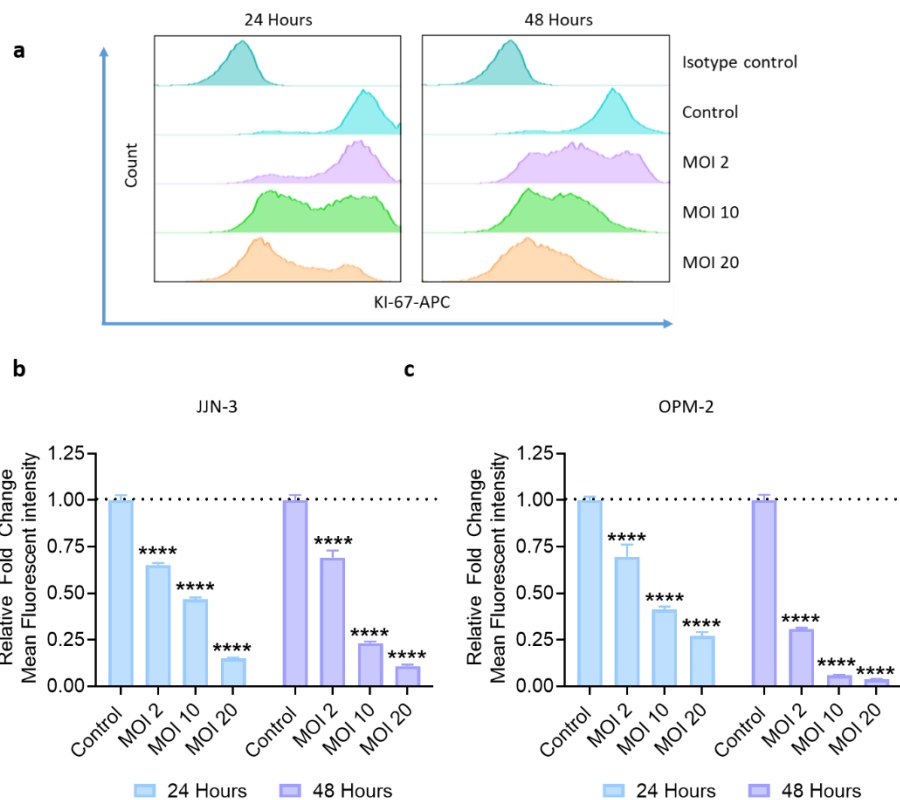


Figure 3.14: Flow cytometric analysis of KI-67 expression after Ad[CE1A] treatment at 24 and 48 hours in JIN-3 and OPM-2 cell lines:

JIN-3 and OPM-2 cells were incubated with Ad[CE1A] at doses of MOI 2, 10 and 20. KI-67 expression was determined by flow cytometry at 24 and 48 hours post treatment. **(a)** Viable cells were selected based on FSC and SSC parameters and representative histogram plots of MFI of KI-67 are shown in JIN-3 cells after incubation with Ad[CE1A] at indicated doses at 24 and 48 hours compared to control. **(b)** Relative KI-67 MFI in viable cells compared to untreated control shown. n=3 Data is the mean \pm SD. p values are for 2-way ANOVA with multiple comparisons compared to control with Dunnett's correction, where **** p<0.0001.

3.2.5 Ad[CE1A] Oncolysis in Myeloma Cell Lines when Cocultured with BMSC

A recent study found that coculture with BMSC cell lines protected MPC lines from RV oncolysis (147), similar to the protection conferred to MPCs against cytotoxic agents (379–381). Therefore, it was important to investigate if the same were true for Ad[CE1A]. To evaluate the susceptibility of MPCs lines to Ad[CE1A] in the context of the BM microenvironment, a MPC:BM coculture was employed using HS-5 human BMSC line. GFP-tagged Vybrant™ DID labelled MM cells were cultured either alone or on a basal layer of BMSCs (HS-5 cells) at a 1:1 ratio. Cultures were treated with Ad[CE1A] at an MOI of 2 or 10. Cell death was evaluated by flow cytometry after 48 hours using PI staining (Figure 3.15). GFP⁺DID⁺ MM cells were gates away from HS-5 BMSCs and then percentage PI was determined based

on the GFP⁺DID⁺ MM cell population There was no significant difference in Ad[CE1A] cytotoxicity in human MPC lines between monocultures and BMSC cocultures at both Ad[CE1A] doses, suggesting HS-5 BMSCs were not able to protect MM cells from Ad[CE1A] oncolysis.

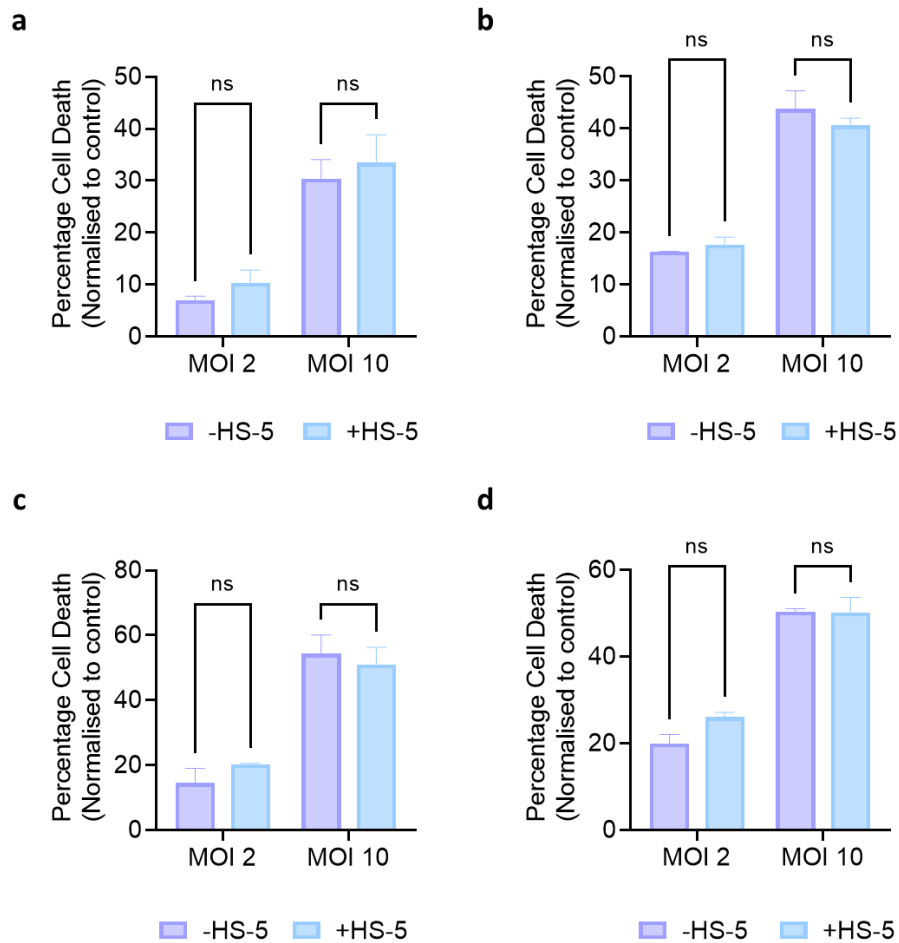


Figure 3.15: Cytotoxicity of Ad[CE1A] in JIN-3, U266 and OPM-2 cells in the presence or absence of BMSC line HS-5:

Vybrant™ DiD labelled (a) JIN-3-GFP, (b) U266-GFP, (c) OPM-2-GFP and (d) RPMI-8226-GFP cells were incubated with Ad[CE1A] at a MOI of 2 or 10 when cultured with or without the BMSC line, HS-5, at a 1:1 ratio. After 48 hours, the percentage of MPCs dead was determined by PI staining after gating on GFP⁺DID⁺ MM cells. n=3 Data is the mean ±SD. p values are for 2-way ANOVA with multiple comparisons with Šidák's correction.

3.2.6 Patient-derived Primary Multiple Myeloma Cells Highly Express Primary and Secondary Adenovirus Receptors

The expression of CAR, $\alpha\beta_5$ and $\alpha\beta_3$ proteins on the surface of patient-derived PCL cells (CB1 and ADC1) were evaluated. CB1 and ADC1 cells were stained with either fluorophore-conjugated antibody against integrins $\alpha\beta_5$, $\alpha\beta_3$ or CAR antibody (or with an isotype-matched control antibody), and then assessed for expression of these proteins by flow cytometry (Figure 3.16). Patient derived PCL cells show high-moderate expression of CAR and $\alpha\beta_5$ (~55-85% and ~40-60% respectively), and low expression of $\alpha\beta_3$ (~3-10%). This pattern of adenoviral receptor expression matches the majority of MPC lines.

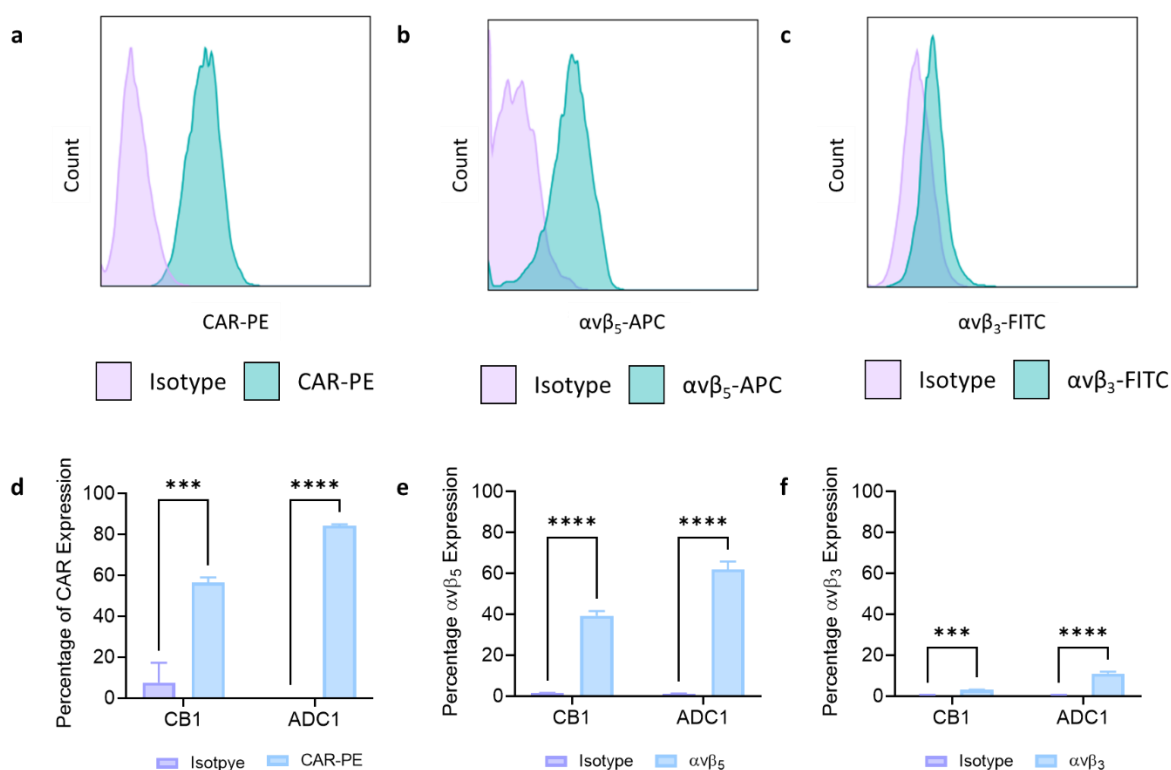


Figure 3.16: Flow cytometric analysis of CAR, $\alpha\beta_5$ and $\alpha\beta_3$ expression in patient derived PCL cells:

Patient derived PCL cells (CB1 and ADC1) were stained with a PE conjugated anti-human CAR antibody, APC conjugated $\alpha\beta_5$ or FITC conjugated anti-human $\alpha\beta_3$ integrin antibody and compared to respective isotype controls and analysed by flow cytometry. Representative histogram plots of MFI of CAR (a), $\alpha\beta_5$ integrin (b) $\alpha\beta_3$ (c) compared to respective isotype control on ADC1 cells. (d) Percentage of cells with surface expression of CAR or (e) $\alpha\beta_5$ (f) $\alpha\beta_3$ integrin. n=3 Data is the mean \pm SD. p values are for two-way ANOVA with multiple comparisons with Šidák's correction, where *** $p \leq 0.001$, **** $p \leq 0.0001$.

3.2.7 Patient-derived Primary Multiple Myeloma Cells Highly Express CS1 Compared to Healthy Donor Plasma Cells and BMMC *Ex vivo*

CS1 cell surface expression and *SLAMF7* mRNA expression were determined in primary CD138⁺ MM cells, HD CD138⁺ plasma cells, and their corresponding CD138⁻ BMMCs. For cell surface expression, each sample population of cells were stained with PE-conjugated antibody against CS1 (or with an isotype-matched control antibody) and then assessed for CS1 protein expression by flow cytometry (Figure 3.17.a & 3.17.b). For *SLAMF7* mRNA expression, total RNA was extracted from each sample population of cells and synthesised by reverse transcription to cDNA and RT-qPCR was performed using Taqman™ primers for *SLAMF7* (Figure 3.17.c). HD CD138⁺ cells could not be included in *SLAMF7* mRNA expression studies as the amount of CD138⁺ cells extracted from HD was never enough for RNA extractions. As expected, MM CD138⁺ cells showed significantly higher levels of CS1 protein (~80%) and mRNA expression (~28-fold change) compared to healthy control plasma cells (~35%) and/or BMMCs (~10% and ~1 fold change). It is important to note that there was some detection of CS1 protein in HD CD138⁺ plasma cells and protein and mRNA detection in CD138⁻ BMMCs from MM and HD samples cells which could potentially cause off-target effects. This could also be due to contaminating CD138⁺ cells in the CD138⁻ population, from our experience, there is ~5% of contaminating CD138⁺ cells in the CD138⁻ population (Section 2.1.3.3, Figure 2.1).

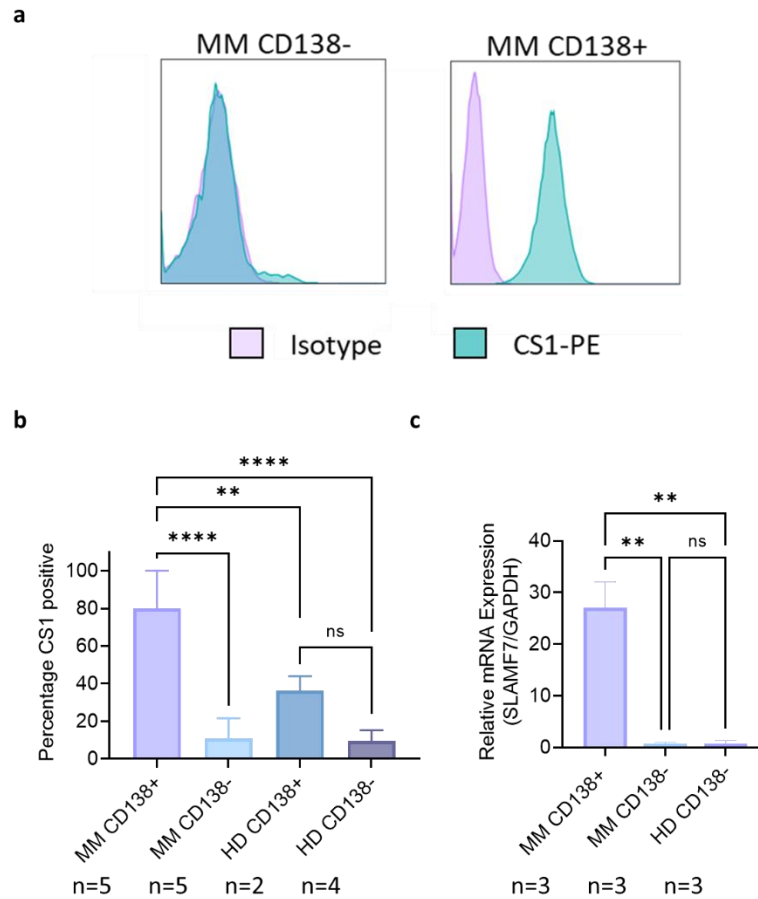


Figure 3.17: CS1 expression in primary cells *ex vivo*:

(a) Representative histogram plots of MFI of CS1 compared to isotype control in one MM patients CD138⁻ and CD138⁺ cell populations. **(b)** Percentage of CS1 cell surface expression in CD138⁺ and CD138⁻ cells from MM patients and healthy donors (HD). MM CD138⁺ (n=5), MM CD138⁻ (n=7), HD CD138⁺ (n=2) and HD CD138⁻ (n=4). Cells were stained with PE conjugated anti-human CS1 or isotype control and analysed by flow cytometry. p values are for one-way ANOVA with multiple comparisons with Tukey's correction, where ** p < 0.01; **** p < 0.0001. **(c)** Relative *SLAMF7* (CS1) mRNA expression in MM CD138⁺ plasma cells (n=3) and CD138⁻ BMMCs from MM patients (n=3) or HDs (n=3) Data is the mean ±SD. p values are for one-way ANOVA with multiple comparisons with Tukey's correction, where ** p < 0.01.

3.2.8 Oncolysis of Ad[CE1A] in Patient-derived Primary Multiple Myeloma Cells *ex vivo*

After assessing the ability of Ad[CE1A] to infect, replicate and lyse human MPCs was established, next was to determine the oncolytic efficacy of Ad[CE1A] by direct cytotoxicity in primary patient-derived MM cells and HD samples. Both the CD138⁺ and CD138⁻ populations were subject to Ad[CE1A] treatment (MOI 20). After 96 hours, cell death was determined by PI staining using flow cytometry (Figure 3.18). MM and PCL CD138⁺ cells showed variable levels of cell death in response to Ad[CE1A], but these levels of cell death were significant compared to untreated controls. However, Ad[CE1A] did not cause any statistically significant amounts of cell death in non-malignant CD138⁺ cells from MGUS patients or HDs. In non-malignant CD138⁻ populations from MM, MGUS and HDs, Ad[CE1A] did not cause any statistically significant amounts of cell death compared to untreated controls.

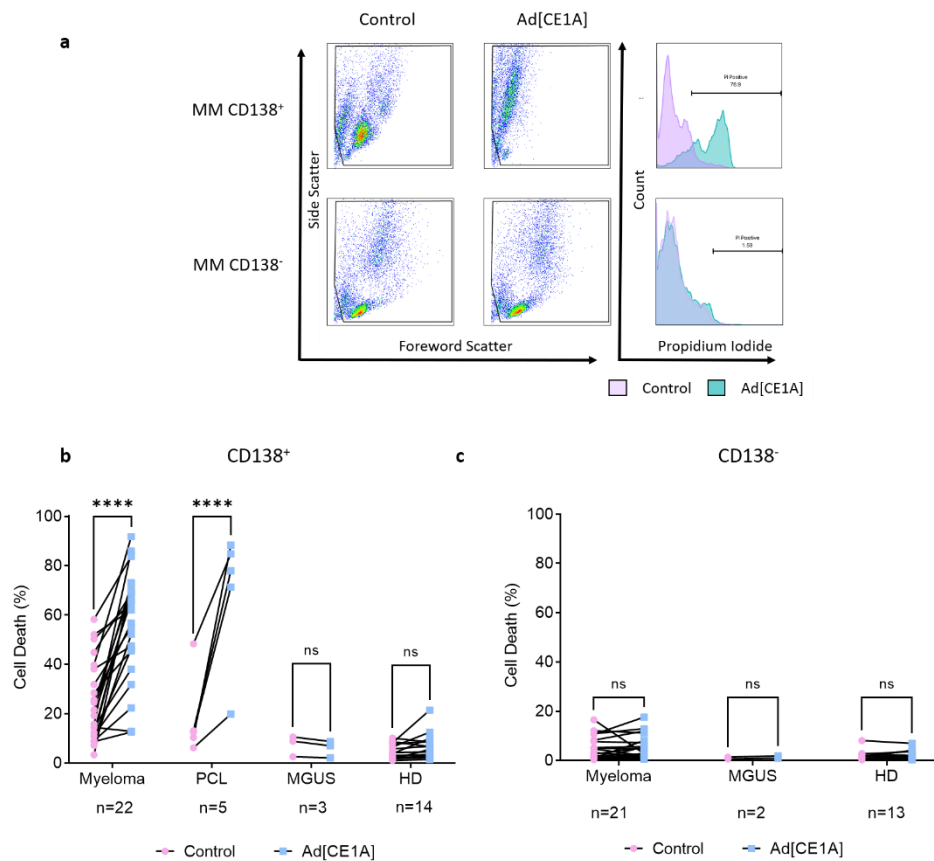


Figure 3.18: Cytotoxicity of Ad[CE1A] in patient-derived MM cells compared to non-malignant cell populations:

(a) Representative scatter and histogram plots of PI staining in MM and HD CD138⁺ and CD138⁻ populations after 96 hours of Ad[CE1A] MOI 20 treatment in the presence 10% autologous serum. Newly diagnosed MM, PCL, MGUS, HD, CD138⁺ plasma cells **(b)** and CD138⁻ cells **(c)** were treated with Ad[CE1A] MOI 20 in the presence of 10% autologous serum. Percentage cell death determined by PI staining using flow cytometry. p values are for 2-way ANOVA with multiple comparisons with Šidák's correction, where **** p<0.0001.

3.2.9 Adenovirus Infection in Patient-derived Primary MM Cells and Healthy Donor CD138⁻ BMMCs

A small percentage of MM and HD CD138⁻ BMMCs express CS1, which may drive viral replication and induce cell death, despite this there was no significant increase in cell death in this population. Therefore, it was important to determine Ad5 infection efficiency in HD derived BMMCs compared to patient-derived primary PCL cells (ADC1 and CB1), because if this population of cells are not greatly infected by Ad5, this could be an explanation to why there was no significant increase in cell death. Primary BMMCs from HD and CD138⁺ patient-derived primary MM cells were incubated with Ad-GFP at MOIs of 2 and 20. After 24 and 48 hours GFP expression was visualised qualitatively by fluorescent microscopy (Figure 3.19.a & 3.19.b) and quantitatively as the percentage of GFP-positive cells using flow cytometry (Figure 3.19.c). Primary HD BMMCs were infected by Ad-GFP at ~1.5% for MOI 2 and ~18% for MOI 20 at 24 hours, whereas CD138⁺ MM cells were significantly more infected at ~15% for MOI 2 and 63% for MOI 20 at 24 hours. At 48 hours GFP positivity was ~7% for MOI 2 and ~19% for MOI 20, whereas CD138⁺ MM cells were significantly more infected at ~37% for MOI 2 and ~78% for MOI 20 at 48 hours. There was no significant increase in GFP expression for MOI 2 and 20 between 24 and 48 hours for HD CD138⁻ BMMCs suggesting that cells were maximally infected at 24 hours. Whereas CD138⁺ MM cells had a significant increase in GFP expression in both MOI 2 and 20 between 24 and 48 hours.

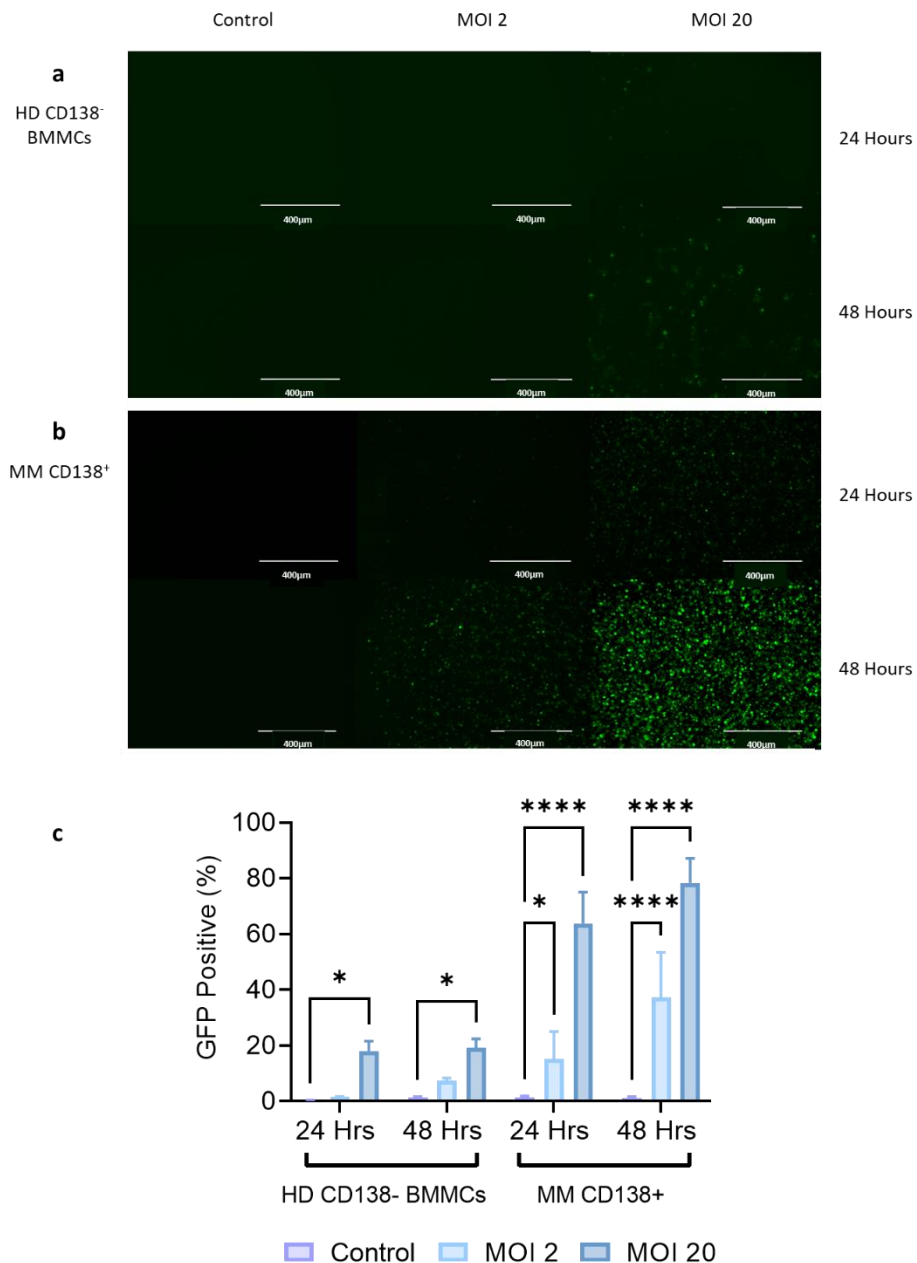


Figure 3.19: Percentage of patient-derived primary MM CD138⁺ cells and primary HD CD138⁻ BMMC infected with Ad-GFP after 24 and 48 hours:

Patient-derived primary MM CD138⁺ cells and HD CD138⁻ BMMCs were infected with Ad-GFP MOI 2 or 20. After 24 hours and 48 hours, GFP expression visualised qualitatively using fluorescent microscopy and quantitatively using flow cytometry. Representative images of live fluorescent microscopy in **(a)** HD CD138⁻ BMMCs or **(b)** MM CD138⁺ cells. **(c)** Percentage of Ad-GFP expression in HD CD138⁻ BMMCs and MM CD138⁺ cells at 24 and 48 hours. n=3 for MM; n=1 for HD Data is the mean ±SD. p values are for 2-way ANOVA with multiple comparisons compared to control with Dunnett's correction, where * p<0.05; **** p<0.0001.

3.2.10 The Involvement of Apoptosis in Ad[CE1A] Cytotoxicity

It is unclear in the literature how oncolytic Ad5 induce cell death, and whether it is purely passive (lysis) or whether some active cell death mechanisms are involved, such as apoptosis. To try to determine how Ad[CE1A] induces cell death in MPC lines apoptosis was investigated.

3.2.10.1 Annexin V Assay

MPC lines JJN-3 and U266 cells were treated with Ad[CE1A] MOI 20. At 6 and 24 hours after treatment cells were stained with Annexin-V-FITC and PI and assessed by flow cytometry (Figure 3.20). JJN-3 and U266 cells showed significant increase in Annexin V⁺ TO-PRO-3⁻ expression at 24 hours compared to untreated controls and Ad[CE1A] treatment at 6 hours (~30-50% Annexin V). This was also performed in a PCL patient and the same trend with a significant increase in Annexin V⁺ and TO-PRO-3⁻ at both time points (Appendix Figure 8.4).

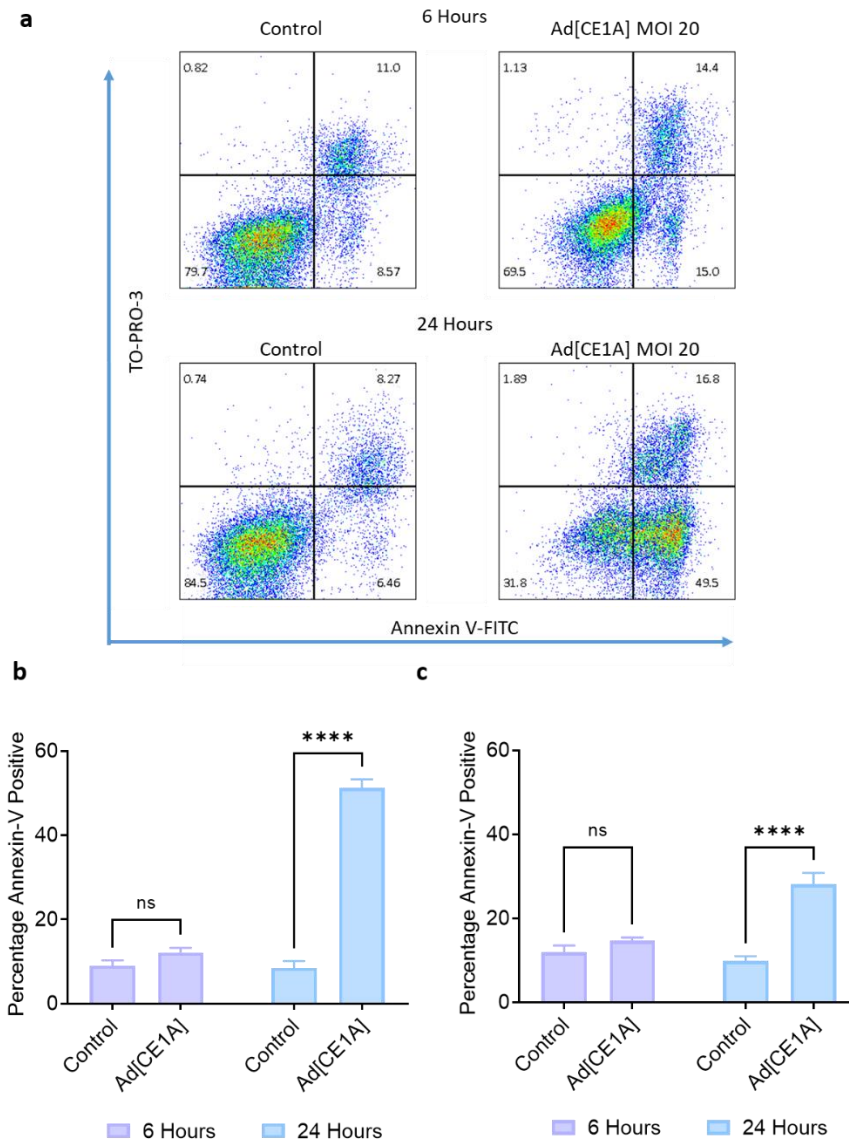


Figure 3.20: Percentage Annexin V⁺ TO-PRO-3⁻ after Ad[CE1A] treatment:

(a) Representative scatter plots of Annexin V against TO-PRO-3 in JLN-3 cells after Ad[CE1A] MOI 20 treatment at indicated time points compared to control. JLN-3 (b) and U266 (c) cells were incubated with Ad[CE1A] MOI 20. Annexin V expression was determined by flow cytometry at 6 and 24 hours post treatment. Percentage of annexin V⁺ and TO-PRO-3⁻ compared to untreated controls shown. n=3 Data is the mean ±SD. p values are for 2-way ANOVA with multiple comparisons with Šidák's correction where **** p<0.0001.

3.2.10.2 Apoptotic gene expression

Since increased Annexin V expression following Ad[CE1A] treatment was detected, next gene expression of apoptotic markers following Ad[CE1A] treatment was assessed in JJN-3 cells treated with Ad[CE1A] at MOI 20 after 6 and 24 hours by RT-qPCR compared to untreated control (Figure 3.21). There was no reliably significant upregulation of any of the apoptotic genes, and none of these genes significantly increased over time.

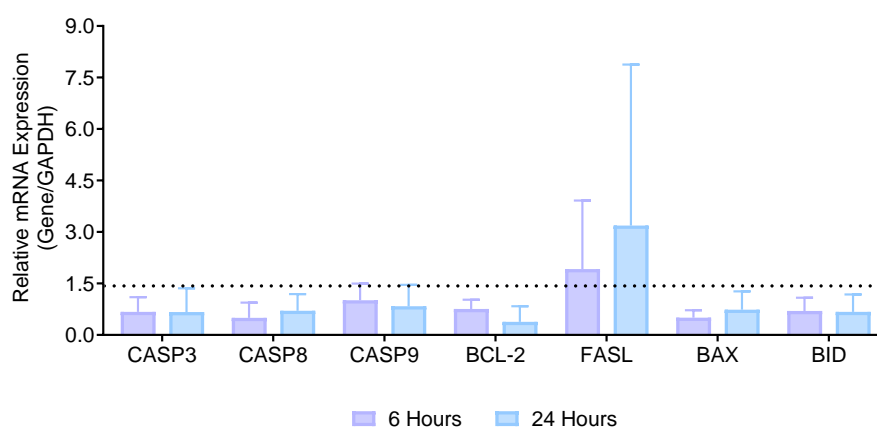


Figure 3.21: mRNA expression of apoptotic markers in JJN-3 after Ad[CE1A] incubation at indicated times:

Relative mRNA expression of caspase 3, caspase 8, caspase 9, BCL2, FAS ligand, BAX and BID relative to untreated controls in JJN-3 cells by RT-qPCR at 6 and 24 hours post Ad[CE1A] infection (MOI 20). $n=3 \pm SD$. p values are for 2-way ANOVA with multiple comparisons with Šidák's correction compared to the 6-hour time point.

3.2.10.3 Pharmacological inhibition of caspases

It has long been thought that PS exposure was a unique feature of apoptotic cell death. However, recent findings have found PS exposure in non-apoptotic forms of regulated inflammatory cell death, such as necroptosis (382). Therefore it was important to determine if pharmacologically blocking caspases would prevent Ad[CE1A] cytotoxicity, and if so, caspase-dependent apoptosis is likely the mechanism of cell death. To determine if caspases were involved in Ad[CE1A] cytotoxicity, MPC lines were treated with Ad[CE1A] \pm the cell permeable irreversible pan-caspase inhibitor Z-VAD-FMK (50 μM). JJN-3 and OPM2 cells were treated with Ad[CE1A] (0.1-1000 MOI) \pm 50 μM Z-VAD-FMK. After 72 hours, cell viability was determined by AlamarBlue[®] assay. Additionally, JJN-3 U266 and OPM-2 cells

were treated with Ad[CE1A] MOI 10 ± 50 μM Z-VAD-FMK. After 72 hours the percentage of dead cells were analysed by PI staining using flow cytometry (Figure 3.22). Addition of Z-VAD-FMK did not significantly alter dose response to Ad[CE1A] (Figure 3.22a-b) or significantly increase or decrease Ad[CE1A] induced cell death (Figure 3.22c-e).

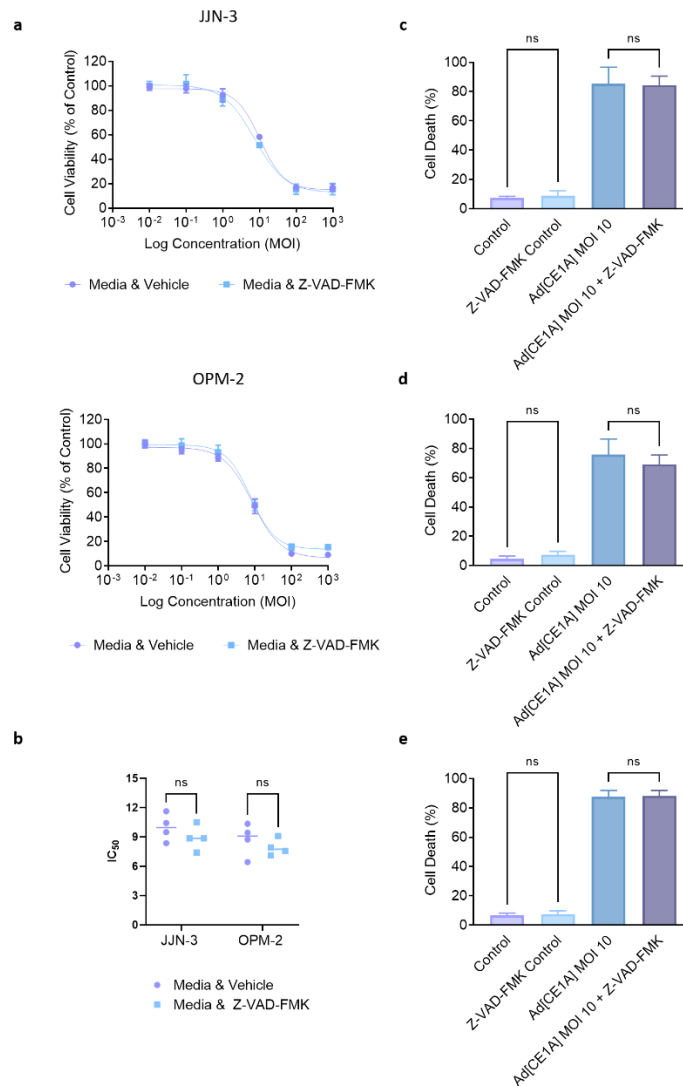


Figure 3.22: Ad[CE1A] response in MPCs in the presence of the pan caspase inhibitor Z-VAD-FMK:

(a) Dose response of Ad[CE1A] in JJN-3 and OPM-2 cells after 72 hours ± 50 μM Z-VAD-FMK. JJN-3 and OPM-2 cells were treated with Ad[CE1A] (0.1, 1, 10, 100, 1000 MOI) with or without the addition of 50 μM Z-VAD-FMK. After 72 hours, cell viability was determined by AlamarBlue® assay. Dose response to Ad[CE1A] ± 50 μM of Z-VAD-FMK. **(b)** IC₅₀ values for Ad[CE1A] ± 50 μM of Z-VAD-FMK determined by sigmoidal dose response curves from 4 independent repeats. n=4 ±SD. p values are for unpaired T test. Percentage of cells dead after incubation with Ad[CE1A] MOI 10 ± 50 μM Z-VAD-FMK. **(c)** JJN-3, **(d)** OPM-2, **(e)** OPM-2 cells were incubated with Ad[CE1A] MOI 10 ± 50 μM Z-VAD-FMK. After 72 hours, percentage of cell death was determined by PI staining using flow cytometry. n=3 Data is the mean ±SD. p values are for one-way ANOVA with multiple comparisons with Tukey's correction.

3.2.11 The Involvement Necroptosis in Ad[CE1A] Cytotoxicity

The results presented above give evidence that Ad[CE1A]-induced cytotoxicity is caspase-independent. Therefore, investigation into other regulated cell death pathways was warranted. Necroptosis is a form of regulated cell death that is caspase independent which generally manifests with a necrotic morphotype. Initiation of necroptosis is mediated by death receptors or pathogen recognition receptors (PRRs) which leads to activation of receptor-interacting serine/threonine-protein kinase 1 (RIPK1) which forms a functional heterodimer complex with receptor-interacting serine/threonine-protein kinase 3 (RIPK3) called the necrosome complex. The necrosome complex phosphorylates mixed lineage kinase domain-like protein (MLKL), which translocates into the inner leaflet of the plasma membrane and disturbs the integrity of the cell in the formation of a pore, which allows the release of DAMPs which stimulate an inflammatory response (383). Therefore, to assess whether necroptosis is a cell death mechanism involved in Ad[CE1A]-induced cytotoxicity, pharmacological inhibition of three of the main proteins involved in the pathway, RIPK1, RIPK3 and MLKL was investigated

3.2.11.1 Pharmacological Inhibition of RIPK1

Firstly, pharmacological inhibition of RIPK1 was investigated to determine whether it could alter Ad[CE1A]-induced cytotoxicity by using an inhibitor for RIPK1, Necrostatin-1 (Nec-1). MPC lines JJN-3, U266 and OPM-2 cells were treated with Ad[CE1A] (0.1-1000 MOI) \pm 50 μ M Nec-1 (non-toxic dose determined by dose response curves Appendix Figure 8.5) and cell viability was determined by AlamarBlue[®] assay after 72 hours. Additionally, JJN-3, U266 and OPM-2 cells were treated with Ad[CE1A] MOI 10 \pm 50 μ M Nec-1 and cell death was determined by PI staining using flow cytometry (Figure 3.23).

The addition of Nec-1 to Ad[CE1A]-treated cells showed no significant effect on the ability of Ad[CE1A] to induce cell death in JJN-3 and OPM2 cells both by AlamarBlue® assay and by flow cytometry. However, Nec-1 significantly affected the ability of Ad[CE1A] to decrease U266 cell viability by AlamarBlue® assay, which had a significantly higher Ad[CE1A] IC₅₀ value following Nec-1 treatment (3.8 fold change). However, by flow cytometry, there was no significant difference with the addition of Nec-1, therefore, this may have been due to an effect on proliferation and not cell death.

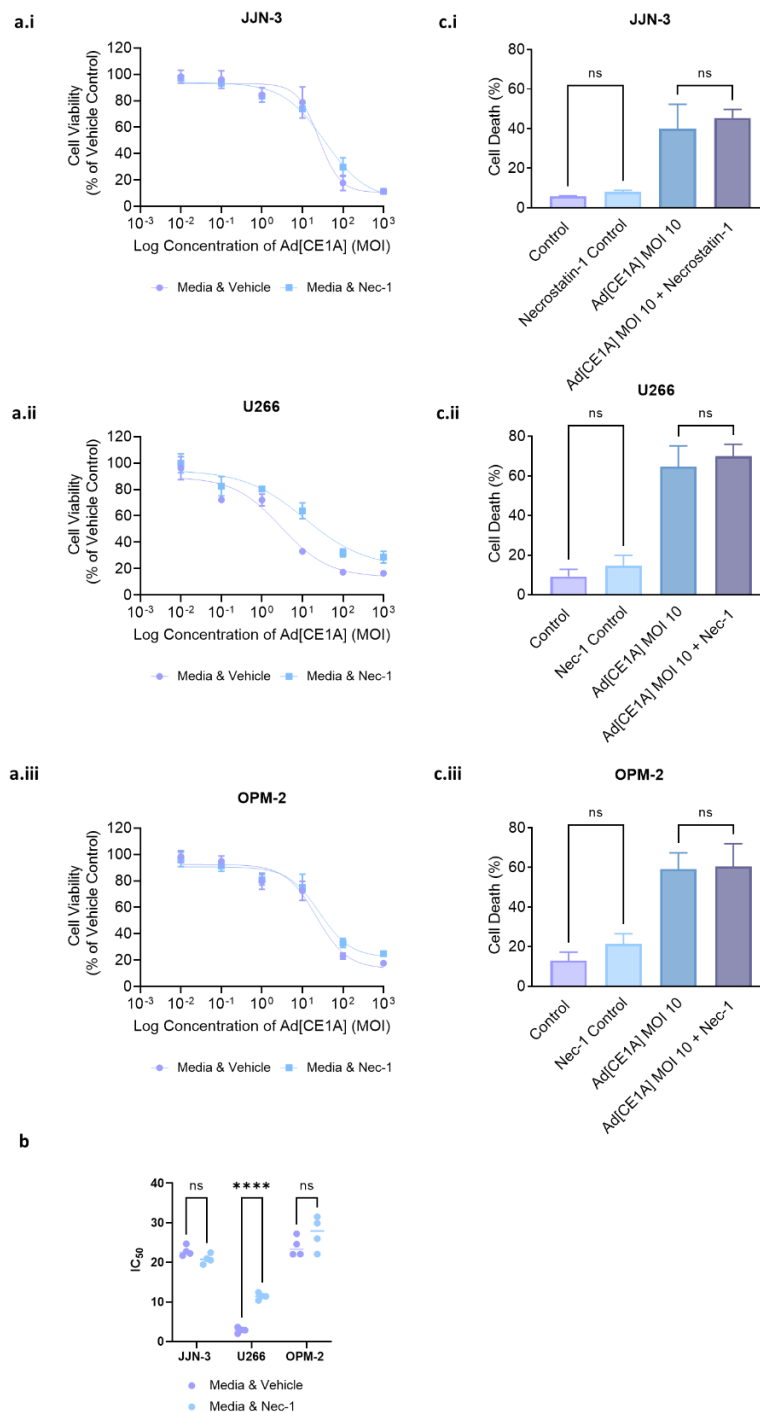


Figure 3.23 Ad[CE1A] response in MPCs in the presence of the RIPK1 inhibitor Nec-1.

(a) Dose response of Ad[CE1A] (0.1, 1, 10, 100, 1000 MOI) in (a.i) JYN-3, (a.ii) U266 and (a.iii) OPM-2 cells after 72 hours \pm 50 μ M Nec-1. After 72 hours, cell viability was determined by AlamarBlue[®] assay. (b) IC₅₀ values for Ad[CE1A] \pm 50 μ M of Nec-1 determined by sigmoidal dose response curves from 4 independent repeats. n=4 \pm SD, p values are for 2-way ANOVA with Šidák's correction. (c) Percentage of cell death after incubation with Ad[CE1A] MOI 10 \pm Nec-1 in (c.i) JYN-3, (c.ii) U266 and (c.iii) OPM-2 cells. After 72 hours, the percentage of cell death was determined by PI staining using flow cytometry. n=3 Data is the mean \pm SD. p values are for one-way ANOVA with multiple comparisons with Tukey's correction.

3.2.11.2 Pharmacological Inhibition of RIPK3

Secondly, pharmacological inhibition of RIPK3 was investigated to determine whether it could alter Ad[CE1A]-induced cytotoxicity by using an inhibitor for RIPK3, GSK-872. MPC lines JJN-3, U266 and OPM-2 cells were treated with Ad[CE1A] (0.1-1000 MOI) \pm 5 μ M GSK-872 (non-toxic dose determined by dose response curves Appendix Figure 8.6) and cell viability was determined by AlamarBlue[®] assay after 72 hours. Additionally, JJN-3, U266 and OPM-2 cells were treated with Ad[CE1A] MOI 10 \pm 5 μ M GSK-872 and cell death was determined by PI staining using flow cytometry (Figure 3.24).

The addition of GSK-872 to Ad[CE1A]-treated cells showed no significant effect on the ability of Ad[CE1A] to induce cell death in JJN-3, U266 and OPM2 cells both by AlamarBlue[®] assay and by flow cytometry. Ad[CE1A] IC₅₀ was not significantly different with the addition of GSK-872, IC₅₀ could not be determined for U266 because of the slope of the curve, but the dose response curve of Ad[CE1A] plus GSK-872 overlaps Ad[CE1A] minus GSK-872. Additionally, no protection from Ad[CE1A]-induced cell death was observed by flow cytometry for all three MPC lines.

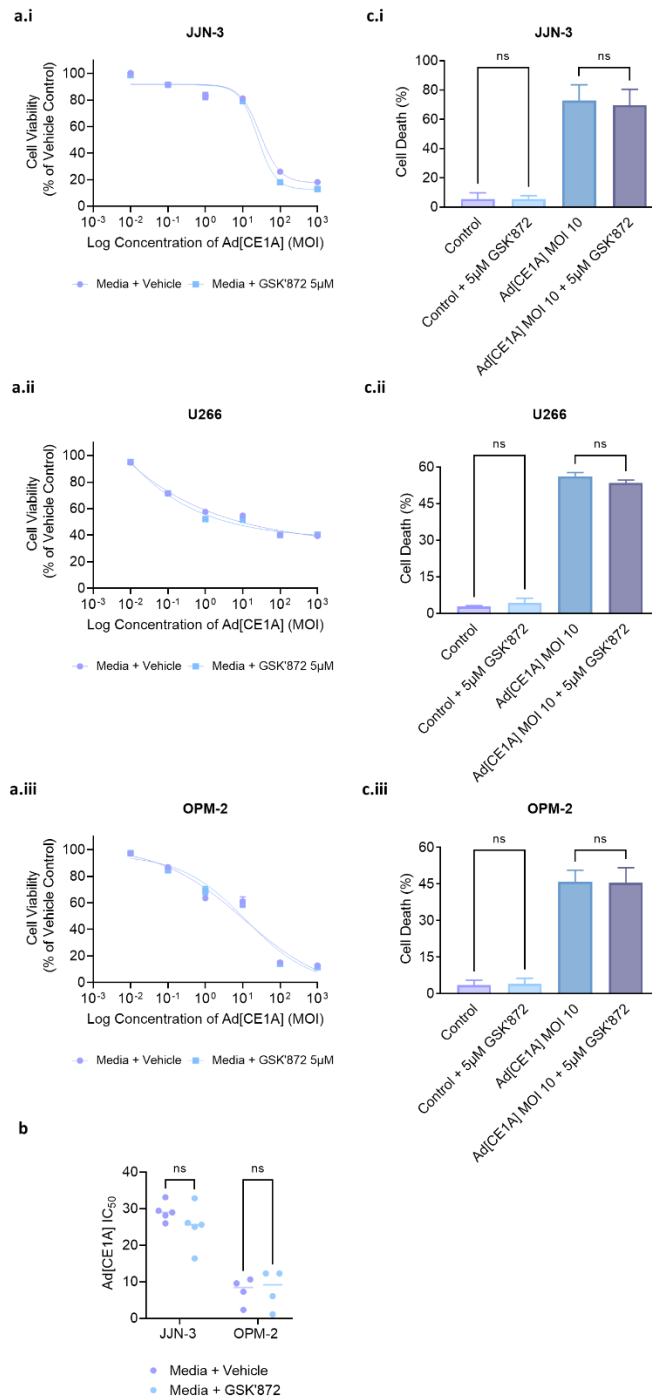


Figure 3.24 Ad[CE1A] response in MPCs in the presence of the RIPK3 inhibitor GSK-872:

(a) Dose response of Ad[CE1A] (0.1, 1, 10, 100, 1000 MOI) in (a.i) JJN-3, (a.ii) U266 and (a.iii) OPM-2 cells after 72 hours \pm 5 μ M GSK-872. After 72 hours, cell viability was determined by AlamarBlue[®] assay. (b) IC₅₀ values for Ad[CE1A] \pm 5 μ M GSK-872 determined by sigmoidal dose response curves from 5 independent repeats. n=5 \pm SD, p values are for 2-way ANOVA with Šidák's correction. (c) Percentage of cells death after incubation with Ad[CE1A] MOI 10 \pm 5 μ M GSK-872 in (c.i) JJN-3, (c.ii) U266 and (c.iii) OPM-2 cells. After 72 hours, the percentage of cell death was determined by PI staining using flow cytometry. n=3 Data is the mean \pm SD. p values are for one-way ANOVA with multiple comparisons with Tukey's correction.

3.2.11.3 Pharmacological Inhibition of MLKL

Thirdly, pharmacological inhibition of MLKL was investigated to determine whether it could alter Ad[CE1A]-induced cytotoxicity by using an inhibitor for MLKL, Necrosulfonamide (NSA). MPC lines JJN-3, U266 and OPM-2 cells were treated with Ad[CE1A] (0.1-1000 MOI) \pm 1 μ M NSA (non-toxic dose determined by dose response curves Appendix Figure 8.7) and cell viability was determined by AlamarBlue[®] assay after 72 hours. Additionally, JJN-3, U266 and OPM-2 cells were treated with Ad[CE1A] MOI 10 \pm 1 μ M NSA and cell death was determined by PI staining using flow cytometry (Figure 3.25).

The addition of NSA to Ad[CE1A]-treated cells showed a significant effect on the ability of Ad[CE1A] to induce cell death in JJN-3, U266 and OPM2 cells. Ad[CE1A] IC₅₀ significantly increased in JJN-3 cells following the addition of NSA, whilst in OPM-2 cells there was an increase observed, but this was not significant. Ad[CE1A] IC₅₀ could not be determined for U266 because of the slope of the curve, but Ad[CE1A] plus NSA suppressed Ad[CE1A]'s ability to reduce U266 cell viability. Additionally, NSA protected all three MPCs from Ad[CE1A]-induced cell death as there was a significantly lower percentage of dead cells with the addition of NSA.

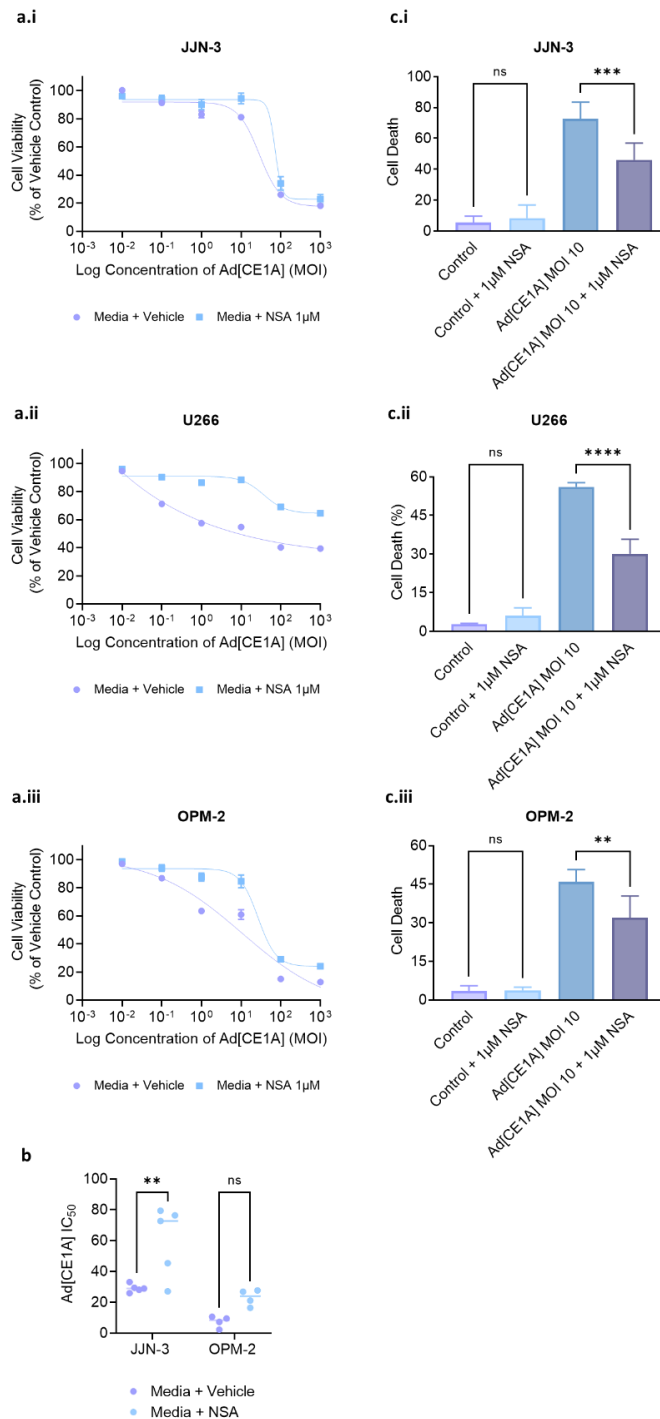


Figure 3.25 Ad[CE1A] response in MPCs in the presence of the MLKL inhibitor NSA:

(a) Dose response of Ad[CE1A] (0.1, 1, 10, 100, 1000 MOI) in **(a.i)** JLN-3, **(a.ii)** U266 and **(a.iii)** OPM-2 cells after 72 hours \pm 1 μ M NSA. After 72 hours, cell viability was determined by AlamarBlue[®] assay. **(b)** IC₅₀ values for Ad[CE1A] \pm 1 μ M NSA determined by sigmoidal dose response curves from 5 independent repeats. $n=5 \pm$ SD, p values are for 2-way ANOVA with Šidák's correction. **(c)** Percentage of cell death after incubation with Ad[CE1A] MOI 10 \pm 1 μ M NSA in **(c.i)** JLN-3, **(c.ii)** U266 and **(c.iii)** OPM-2 cells. After 72 hours, percentage of cell death was determined by PI staining using flow cytometry. $n=3$ Data is the mean \pm SD. p values are for one-way ANOVA with multiple comparisons with Tukey's correction, ** $p < 0.01$, *** $p < 0.001$, **** $p < 0.0001$.

3.2.12 The Expression of Immunogenic Cell Death Markers following Ad[CE1A] Treatment.

Next the expression of ICD markers following Ad[CE1A] treatment was investigated. There were two reasons for this line of investigation, the first reason was discussed in the chapter introduction (section 3.1.1) and involved the fact that previous research on OV's including Ads have shown oncolysis to be highly immunogenic, the second reason was based off the previous results that MLKL is involved in Ad[CE1A] induced cell death (Figure 3.25). MLKLs function is to form pores that release DAMPs therefore, investigation into the release of DAMPs following Ad[CE1A] infection was explored. The release of DAMPs occurs in synchrony with cell death signalling. There are six DAMPs that have been mechanistically linked to the perception of regulated cell death as immunogenic, these include CALR, ATP, HMGB1, type I IFN, cancer cell-derived nucleic acids and Annexin A1 (377). However, more recently several more DAMPs and cytokines have been mechanistically linked to ICD (376).

3.2.12.1 Cell Surface Calreticulin Exposure

CALR is the most abundant protein in the ER lumen, where it is involved in Ca^{2+} homeostasis. In ICD, CALR translocates to the outer leaflet of the plasma membrane where it functions as an 'eat me' signal for phagocytosis by macrophages, neutrophils, and DCs, which is required for subsequent antigen cross-presentation to cytotoxic T cells; and as a trigger for T_H17 cell priming. CALR exposure happens early in ICD-related cell death which is mediated (at least for chemotherapy-driven ICD) by three sequential signal transduction modules: (1) an ER stress module, which involves phosphorylation of eIF2 α to a block in protein synthesis; (2) an apoptotic module, which involves the CASP8-dependent cleavage of B-cell receptor-associated protein 31 (BCAP31), BAX, and BAK; and (3) an exocytosis module (377). Extracellular CALR can be detected by staining non-permeabilised cells and analysing using flow cytometry.

To determine whether CALR is exposed following Ad[CE1A] treatment, JIN-3, U266 and OMP-2 cells were treated with vehicle or Ad[CE1A] (MOI 2, 10 and 20). After 24 hours cells were stained with a primary polyclonal anti-CALR antibody and subsequently a secondary FITC conjugated antibody and

analysed using flow cytometry compared to vehicle control in PI negative viable cells (Figure 3.26). After 24 hours a dose-response increase in CALR exposure was seen, which reaches significance at an MOI 10 and 20 in all cell lines. Baseline levels of CALR were higher in JJJN-3 and U266 cells than in OPM-2 cells (MFI 89, 62 and 37), OPM-2 cells also showed the greatest relative increase in CALR compared to JJJN-3 and U266 cells (2.2 fold change, 1.7 fold change and 1.5 fold change respectively), whether this was due to OPM-2 cells having a lower CALR baseline can only be speculated.

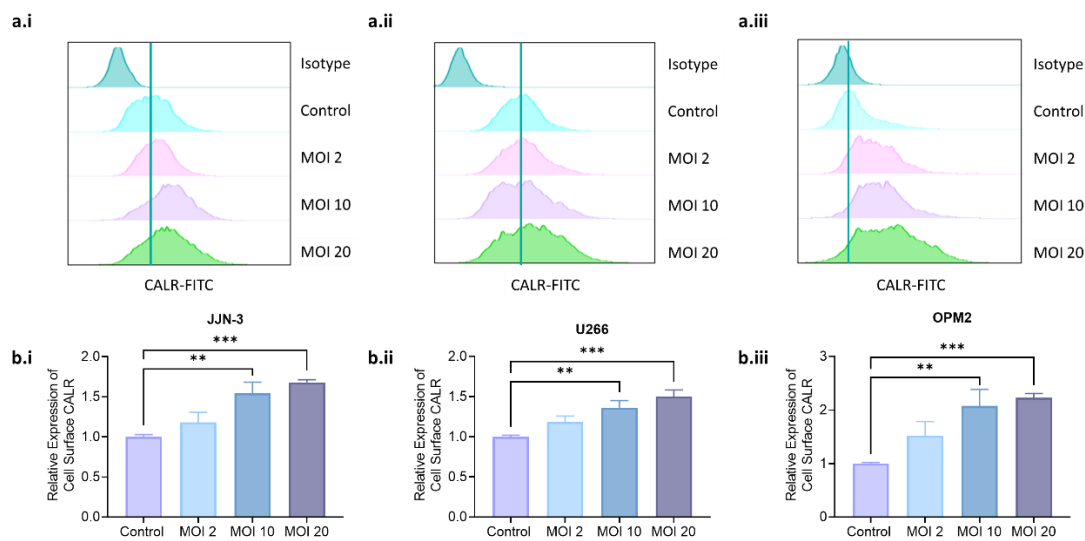


Figure 3.26: Cell surface calreticulin exposure in MPCs following Ad[CE1A] treatment:

JJJN-3, U266 and OPM-2 cells were treated with vehicle control or Ad[CE1A] at an MOI of 2, 10 or 20. After 24 hours, cells were stained with a polyclonal anti-CALR antibody and a FITC fluorescently labelled secondary antibody and TO-PRO-3 and then analysed by flow cytometry. Representative histogram plots of CALR in viable cells following Ad[CE1A] treatment in **(a.i)** JJJN-3, **(a.ii)** U266 and **(a.iii)** OPM2 cells. Non-permeabilised cells were gated (TO-PRO-3 negative) and relative MFI compared to vehicle control was determined in **(b.i)** JJJN-3, **(b.ii)** U266 and **(b.iii)** in OPM2. n=3 Data is the mean \pm SD. p values are for one-way ANOVA with multiple comparisons compared to control with Dunnett's correction, where ** p<0.01; *** p<0.001.

3.2.12.2 Cell Surface CD47 Expression

CD47 is an antiphagocytic molecule, and it is overexpressed in many cancer cell types allowing them to escape immunosurveillance. CD47 binds to signal regulatory protein alpha (SIRP α) on the surface of myeloid cells, which inhibits macrophage phagocytosis (384). CD47 has been shown to have high expression in a murine MM cell line 5T33vt, treatment with epigenetic-modulating compounds decreased CD47 expression (385). There is a balance to maintain between tolerogenic CD47 expression and immunogenic CALR expression, as CALR is antagonised by CD47 (377). Therefore it was important to determine whether Ad[CE1A] could alter CD47 expression in MM cells.

To determine whether CD47 expression was altered following Ad[CE1A] treatment, JJN-3, U266 and OMP-2 cells were treated with vehicle or Ad[CE1A] (MOI 2, 10 and 20). After 24- and 48-hours, cells were stained with an APC-conjugated anti-human CD47 antibody and analysed using flow cytometry compared to vehicle control in non-permeabilised cells (Figure 3.27). A dose and time response decrease in CD47 was observed. At 24 hours in JJN-3 cells, there was a trend for a dose response decrease, but it did not reach significance, however, at 48 hours there was a significant difference at MOI 10 and 20 (Figure 3.27 b.i & d.i). At 24 hours in U266 and OPM-2 cells there was a significant decrease in CD47 expression compared to control at MOI 10 and 20 (Figure 3.27 b.ii and b.iii), but at 48 hours there was a significant decrease in all three concentrations (Figure 3.27 d.ii and d.iii). It is important to note that all three MPCs tested showed a high level of CD47 expression, giving evidence that these MPCs are good at shielding from macrophage phagocytosis.

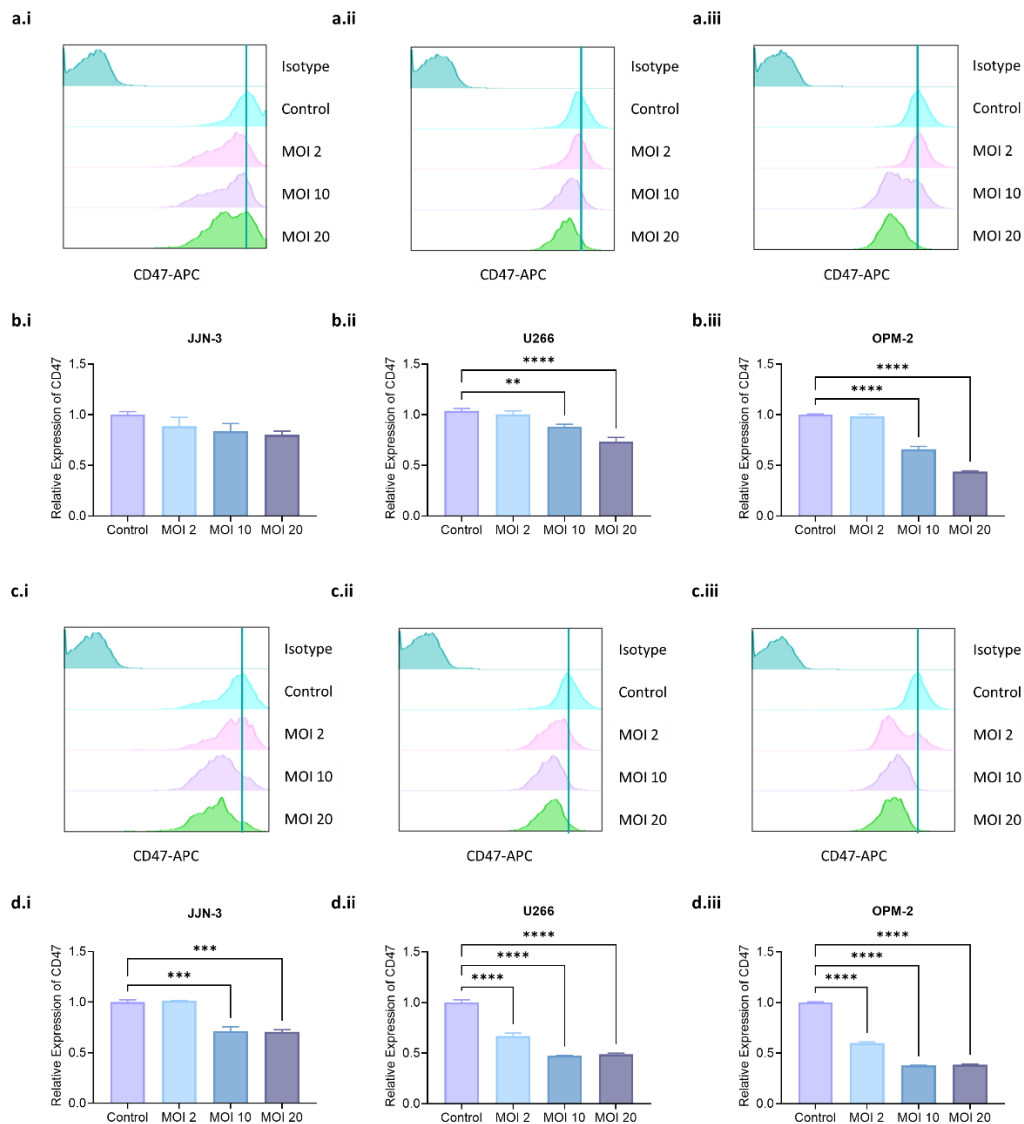


Figure 3.27: Cell surface CD47 expression in MPCs following Ad[CE1A] treatment:

JYN-3, U266 and OPM-2 cells were treated with vehicle control or Ad[CE1A] at an MOI of 2, 10 or 20. After 24 or 48 hours, cells were stained with a APC-conjugated anti-human CD47 antibody and TO-PRO-3 and then analysed using flow cytometry. Representative histogram plots of CD47 in viable cells following Ad[CE1A] treatment after 24 or 48 hours respectively in **(a.i; c.i)** JYN-3, **(a.ii; c.ii)** U266 and **(a.iii; c.iii)** OPM2 cells. Non-permeabilised cells were gated (TO-PRO-3 negative) and relative MFI compared to vehicle control was determined after 24 and 48 hours respectively in **(b.i; d.i)** JYN3, **(b.ii; d.ii)** U266 and **(b.iii; d.iii)** OPM-2 cells. n=3 Data is the mean \pm SD. p values are for one-way ANOVA with multiple comparisons compared to control with Dunnett's correction, where ** $p < 0.01$; *** $p < 0.001$, **** $p < 0.0001$.

3.2.12.3 Extracellular ATP Release

Extracellular ATP release is a major DAMP associated with ICD. ATP, along with other nucleotides, are also commonly associated with non-specific release following necrosis. Extracellular ATP acts as a ‘find me’ signal which promotes the migration of inflammatory cells such as macrophages and DC precursors. Extracellular ATP acts as a danger signal through binding to purinergic type 2 receptors, such as P2X7 on these immune cell types (386).

To determine if ATP was secreted following Ad[CE1A] treatment, JJN-3, U266 and OPM-2 cells were treated with vehicle control or Ad[CE1A] MOI 2, 10 or 20. After 24 hours supernatant was collected from cells and ATP concentration (nM) was determined by the ENLITEN® ATP assay, which is a luminescence-based assay which relies on the chemical reaction of ATP with D-luciferin (Figure 3.28). In JJN-3 cells, there was a significant increase in extracellular ATP at all concentrations, but there was no dose-response increase (Figure 3.28 a.i). In U266 and OPM-2 there was a dose-response increase in extracellular ATP, which reached significance at an MOI of 10 and 20 (Figure 3.28 a.ii & a.iii). It is important to note that OPM-2 cells had a much larger increase in extracellular ATP compared to control than the other cell lines.

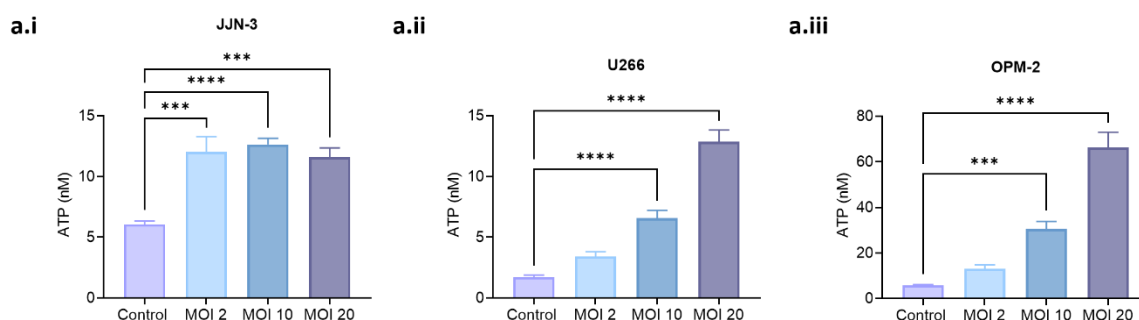


Figure 3.28: Extracellular release of ATP in MPCs following Ad[CE1A] treatment:

(a.i) JJN-3 (a.ii) U266 and (a.iii) OPM-2 cells were treated with vehicle control or Ad[CE1A] at an MOI of 2, 10 or 20. After 24 hours cell supernatant was collected and ATP concentration was determined using the ENLITEN® ATP assay using an ATP standard curve. n=3 Data is the mean \pm SD. P values are for one-way ANOVA with multiple comparisons compared to control with Dunnett's correction, where *** p < 0.001; **** p < 0.0001.

3.2.12.4 Expression of MHC Class I and II on MPC lines in response to Ad[CE1A]

MPCs are derived from germinal centre B cells so can express markers for antigen presentation including MHC class I and II (387). Investigation into whether MHC class I and II were upregulated following Ad[CE1A] treatment was explored, as upregulation of MHC may enable better antigen presentation by MPCs and subsequent T cell stimulation. To determine if MHC class I was upregulated following Ad[CE1A] treatment, JJN-3, U266 and OPM-2 cells were treated with Ad[CE1A] at MOI 2, 10 and 20 or vehicle (PBS) control. After 48 hours cells were stained with an HLA-ABC antibody (class I) (Figure 3.29) and analysed using flow cytometry compared to vehicle control in non-permeabilised cells.

Ad[CE1A] was able to induce a dose-response increase in MHC-Class I HLA-ABC expression in all three MPC lines. In JJN-3 cells, this was only significant at a high MOI (MOI 20) with a 1.4-fold change in expression (Figure 3.29 b.i). In U266 cells this was significant at all MOIs with the highest fold change observed at MOI 20 (1.6-fold change) (Figure 3.29 b.ii). In OPM-2 this was significant at MOI 10 and 20 with fold changes of 1.4 and 1.5 respectively (Figure 3.29 b.iii).

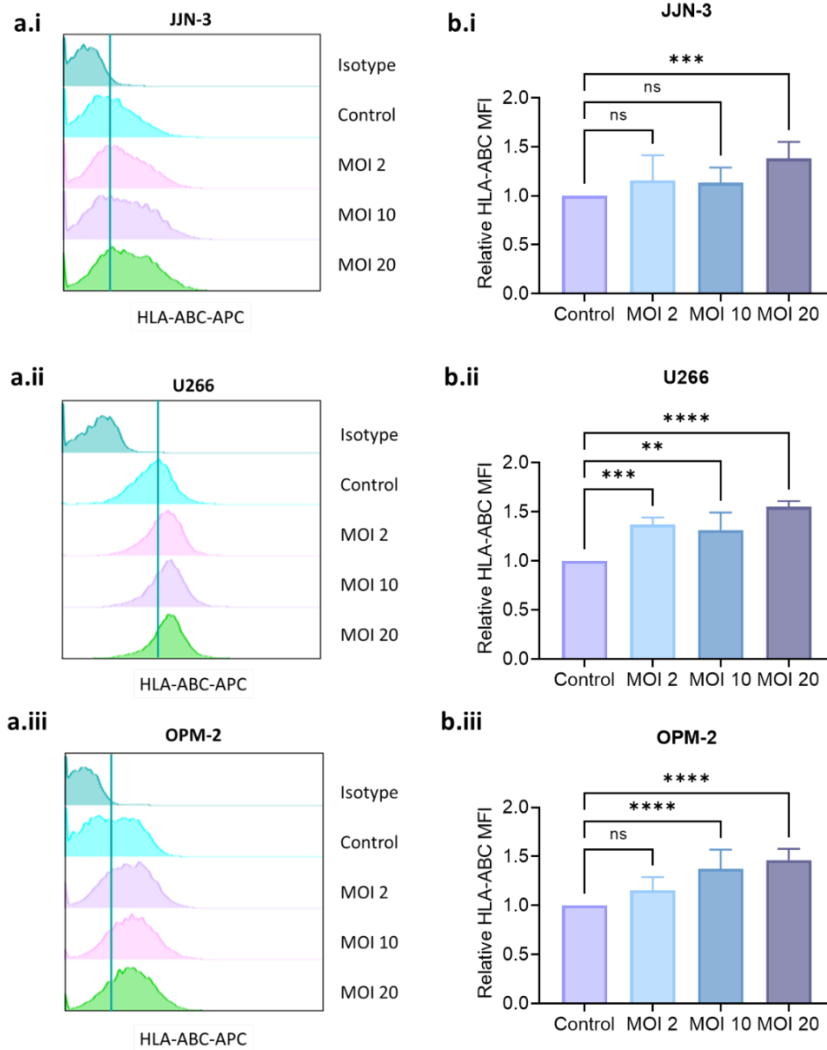


Figure 3.29 Cell surface HLA-ABC expression in MPCs following Ad[CE1A] treatment:

JJJN-3, U266 and OPM-2 cells were treated with vehicle control or Ad[CE1A] at an MOI of 2, 10 or 20. After 48 hours, cells were stained with an APC-conjugated anti-human HLA-ABC antibody and PI and then analysed using flow cytometry. Representative histogram plots of HLA-ABC in viable cells following Ad[CE1A] treatment after 48 hours in (a.i) JJJN-3, (a.ii) U266 and (a.iii) OPM2 cells. Non-permeabilised cells were gated (PI negative) and relative MFI compared to vehicle control was determined after 48 hours in (b.i) JJJN3, (b.ii) U266 and (b.iii) OPM-2 cells. n=3 Data is the mean \pm SD. P values are for one-way ANOVA with multiple comparisons compared to control with Dunnett's correction, where ** $p < 0.01$; *** $p < 0.001$ **** $p < 0.0001$.

To determine if MHC class II is upregulated following Ad[CE1A] infection, JJJN-3 and OPM-2 cells were treated with Ad[CE1A] at MOI 2, 10 and 20 or with vehicle (PBS) control. After 48 hours cells were stained with an HLA-DR antibody (class II) and analysed using flow cytometry compared to vehicle control in non-permeabilised cells (Figure 3.30). Ad[CE1A] was able to induce a dose-response increase in MHC-Class II HLA-DR expression in JJJN-3 and OPM-2 MPC lines (Figure 3.30 b.i & b.ii respectively).

It is important to note that OPM-2 cells had little HLA-DR expression over isotype control but Ad[CE1A] was still able to increase HLA-DR expression (Figure 3.30 b.ii).

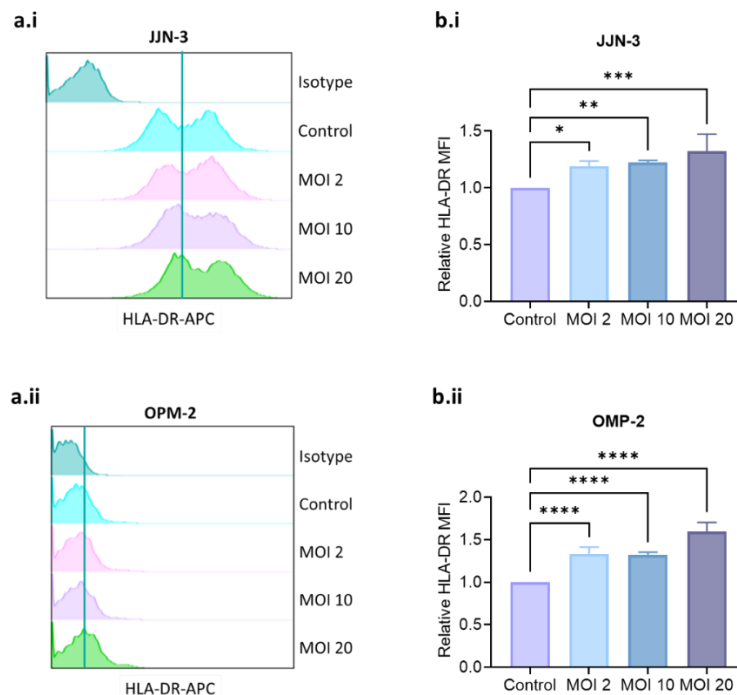


Figure 3.3.30 Cell surface HLA-DR expression in MPCs following Ad[CE1A] treatment:

JUN-3 and OPM-2 cells were treated with vehicle control or Ad[CE1A] at an MOI of 2, 10 or 20. After 48 hours, cells were stained with an APC-conjugated anti-human HLA-DR antibody and PI and then analysed by flow cytometry. Representative histogram plots of HLA-DR in viable cells following Ad[CE1A] treatment after 48 hours in **(a.i)** JUN-3 and **(a.ii)** OPM2 cells. Non-permeabilised cells were gated (PI negative) and relative MFI compared to vehicle control was determined after 48 hours in **(b.i)** JUN3 and **(b.ii)** OPM-2 cells. n=3 Data is the mean \pm SD. P values are for one-way ANOVA with multiple comparisons compared to control with Dunnett's correction, where ** $p < 0.01$; *** $p < 0.001$.

3.2.12.5 Bystander Cytokine Killing

Because of the finding that Ad[CE1A] can induce markers of ICD and increase MHC class I and II cell surface expression in MPC lines, investigation into whether Ad[CE1A] could induce BMMCs to release cytotoxic cytokines that result in bystander cytokine killing of MPC lines was also explored.

To investigate this, CM from BMMCs from HDs and MM patients were harvested after 48 hours of Ad[CE1A] treatment. MPC lines were then cultured in the CM (diluted 1:1 in fresh media) for 96 hours before evaluation of cell viability by AlamarBlue® assay. In an attempt to neutralise the direct cytotoxic effect of Ad[CE1A] the CM was UV-irradiated to neutralise virus particles followed by filter sterilisation which deactivated Ad[CE1A] particles (Appendix Figure 8.3).

The UV-inactivated Ad[CE1A]-CM was able to significantly reduce cell viability compared to control CM (Figure 3.31). This was significant in all three MPC lines from HD (Figure 3.31a), however, Ad[CE1A]-CM from MM BMMCs was only significant in JJN-3 cells (Figure 3.31b). It is clear that Ad[CE1A]-CM from MM patients has a more varied effect, likely due to differential immunogenic potential between the patients. Possibly if more n numbers were used this may reach significance for the other two cell lines.

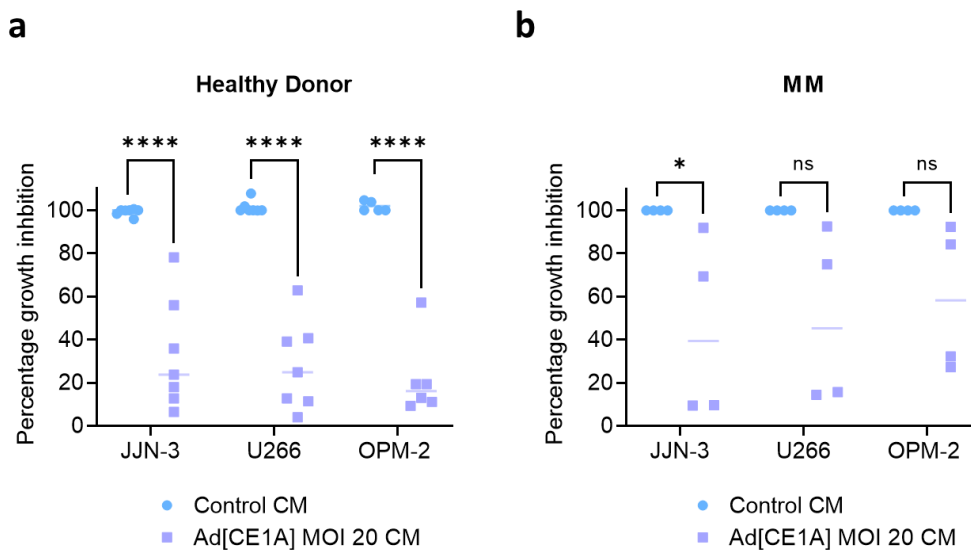


Figure 3.31 Cytokine-induced bystander killing of MM cells:

MPC lines JJN-3, U266 and OPM-2 were cultured in UV inactivated CM (1:1) from BMMCs from either (a) HD (HD) (n=7) or from (b) MM patients (n=4) that have been exposed to Ad[CE1A] for 48 hours. MPCs were cultured in this UV inactivated CM for 96 hours before cell viability was determined by AlamarBlue® assay. p values are for 2-way ANOVA with multiple comparisons with Šidák's correction, where * p<0.05; **** p<0.0001.

3.3 Discussion

The aim of this chapter was to determine the efficacy of Ad[CE1A] in MPC lines and patient-derived MM cells. Additionally the aim of this chapter was to determine what mechanism(s) may be involved in Ad[CE1A]-induced cell death, with the goal that the mechanism(s) could potentially be exploited to enhance Ad[CE1A]-induced cell death with other agents.

Firstly, human MPC lines were found to express CAR, the primary entry receptor for Ad5, to the same extent as the control Ad5 susceptible cell line, HEK293A, or significantly higher in the case of the U266 and NCI H929 cell lines (~75-85% for human MPCs; 80% for HEK293A). This is important as CAR has been found to be lowly expressed or absent on many haematological cells, including MM (260,261,388,389), with Drouin *et al.*, finding L363, RPMI-8226 and U266 cell lines to have lower CAR expression (~20%, ~45% and ~18% CAR expression, respectively) (261) compared to my findings which showed these cell lines to have higher CAR expression (82%, 81%, 86% CAR expression, respectively). However, others have also found other human MPC lines to have high CAR expression (60.9-97.67%) (125), including RPMI-8266 and U266 cell lines having CAR expression at 95.8% and 97.67% respectively, which is more comparable to my findings. Primary PCL cells CB1 and ADC1 also showed high CAR expression (56% and 84% respectively), whilst there has been no previous research assessing CAR expression in patient-derived primary MM cells, the percentage of expression is similar to the percentage that this study and other studies have found in MPC lines.

Integrin expression ($\alpha\beta_{3/5}$) was also investigated, as $\alpha\beta_{3/5}$ integrins are thought to be secondary receptors for Ad5 (390). All human MPC lines tested expressed $\alpha\beta_5$, with the majority of MPC lines demonstrating high expression (71-99%), this is in agreement with Beauvais *et al.*, who found MPC lines (RPMI-8226, U266, CAG and MM.1R) highly express $\alpha\beta_5$ (391). $\alpha\beta_5$ expression is thought to be the primary receptor for Ad5 in cells that have little to no expression of CAR. An early study showed that some cancer cells, with no expression of CAR, can be highly infected with Ad5, and this was found to be due to $\alpha\beta_5$. For example, MDA-MB-435 cells showed no CAR expression and yet had ~80% Ad-GFP transduction efficiency but they did express $\alpha\beta_5$ (94.8%). When $\alpha\beta_5$ was blocked, they were able

to significantly decrease Ad binding (263). Primary PCL cells CB1 and ADC1 also showed high expression levels of $\alpha\beta_5$ (40% and 62% respectively). However, only a small percentage of human MPC lines expressed $\alpha\beta_3$, interestingly, $\alpha\upsilon$ and β_3 individual subunit expression has been found to be high (45-91% and 67-100% expression respectively), particularly in MM patients with skeletal involvement, (392), assessment using an antibody that binds to the full $\alpha\beta_3$ integrin was not determined by these authors. However, Beauvais *et al.*, found MPC lines (RMPI-8226, U266, CAG and MM.1R) express little or no $\alpha\beta_3$ integrin (391). This low-level expression of $\alpha\beta_3$ was also found in primary PCL cells CB1 and ADC1 (3% and 11%, respectively). Furthermore, adenoviral susceptible cell line HEK293A only had 17% expression of $\alpha\beta_3$ integrin, therefore $\alpha\beta_3$ may only play a role in Ad attachment in the absence of CAR and/or $\alpha\beta_5$. There are also other receptors that may be involved in Ad5 infection, such as heparin sulphate glycosaminoglycan, MHC-1 and/or VCAM-1, but these have not been investigated in this thesis.

Next, investigation into whether human MPCs could be infected by Ad5, what the infection efficiencies were, and if there were any differences between the cell lines was explored. Human MPCs showed high infection efficiencies using an Ad-GFP reporter virus after 24 and 48 hours, with MOI 20 showing the highest infection rate (80-95% and 75-99%, respectively), compared to MOI 2 (1.6-67% and 11%-74%, respectively), which agrees with previous research which reported high Ad5 infection efficiencies in MPC lines (125,261). In this chapter KMS-12-BM had the lowest Ad-GFP infection at MOI 2 at both time points compared to other cell lines, whilst JJN-3 cells had the highest Ad-GFP infection for both doses at both time points (MOI 2: 67% MOI 20: 95%; MOI 2:74% MOI 20: 99%, respectively). JJN-3 cells showed high CAR expression, high $\alpha\beta_5$ expression and had the highest $\alpha\beta_3$ expression. Whilst KMS-12-BM showed lower CAR and $\alpha\beta_5$ expression compared to JJN-3 cells and other cell lines (2% CAR expression 42% $\alpha\beta_5$). However, this low CAR and $\alpha\beta_5$ expression only affected the low dose of Ad-GFP and not the high dose.

CS1 cell surface protein expression and mRNA expression were found to be significantly expressed in the majority of MPC lines compared to control cell line HEK293A. Cell surface protein expression was found to have strong positive correlation with mRNA expression. A range of CS1/*SLAMF7* expression levels were seen, OPM-2, L363 and NCI-H929 showed high expression, RPMI-8226, JIN-3 and KMS-11 showed intermediate expression and KMS-12-BM had low expression. This is in agreement with the literature that showed the majority of MPC lines/patient-derived MM cells to express CS1/*SLAMF7* (393,394). Importantly, the prostate cancer cell line, LNCaP, showed no protein or mRNA CS1 expression. Critically, patient-derived MPCs expressed CS1 at both protein and mRNA level at significantly higher levels than HD plasma cells or BMMCs from either HD or MM patients, again this is in agreement with what is known in the literature (277).

All MPC lines tested demonstrated Ad[CE1A] replication as evidenced by *E1A* mRNA expression and production of infectious viral progeny. The MPC lines that showed high CS1 expression (OPM-2, L363) showed the highest *E1A* expression after 24 hours, KMS-12-BM had the lowest *E1A* expression, which correlates with the CS1 data. *E1A* mRNA expression showed a strong positive correlation with *SLAMF7* expression, providing evidence that CS1 promoter activation is driving *E1A* expression. Additionally, MPC lines tested were able to produce intact infectious virions that are capable of infecting neighbouring cells.

Ad[CE1A] efficacy against MPCs was next investigated. Firstly, investigation into Ad[CE1A]-induced cell death in two human MPCs at different doses and time points was performed to determine the best dose and time which gave the best efficacy. Ad[CE1A] induced both a dose and time dependent levels of cell death, with the best efficacy at MOI 20 after 72 hours. Subsequently, to provide evidence that oncolysis was due to replication and not due to viral infection or viral load in cells, MPC lines were treated with Ad[CE1A] or a prostate specific antigen *E1A* driven Ad5 (Ad[PSA]) at three different doses. Ad[PSA] was not able to induce significant levels of cell death compared to untreated controls in any of the three doses tested, providing evidence that it was CS1-driven replication resulting in oncolysis.

Consequently, Ad[CE1A] efficacy against a panel of MPC lines using the dose and time point previously determined (MOI 20, 72 hours) was investigated. Ad[CE1A] induced significant levels of oncolysis in all MPC lines compared to untreated controls. The amount of cell death showed a moderate positive correlation with CS1 expression, and the CS1^{negative} cell line LNCaP showed no significant levels of cell death compared to control. Whilst the CS1^{low} cell line KMS-12-BM showed a significant increase in cell death compared to control, although this increase in cell death was much lower compared to CS1^{high} expressing cells. This provides further evidence that Ad[CE1A] oncolysis is due to CS1-promoter driven oncolysis and is promising that the CS1 modification to Ad5 has not affected its ability to induce oncolysis, as WT Ad5 and other genetically modified Ads have shown similar therapeutic benefit to MPCs (127,129,260,264).

BM niches have been commonly found to offer protection and induce chemotherapy resistance in MM, including resistance against BTZ, Melph and Dexamethasone (379–381). This resistance can be induced by the secretion of soluble factors and by direct cell contact (381). A recent paper showed that direct coculture with BMSC lines (HS-5 and HS-27) could protect MPC lines from RV direct oncolysis, which was not due to altered expression of RV entry receptor JAM-1 (147). Therefore, investigation into whether the BMSC line HS-5 could induce resistance to Ad[CE1A] was explored. Coculture of MPCs with BMSCs HS-5 did not protect MPC lines against Ad[CE1A] oncolysis. Whilst only one BMSC line (HS-5) was used in this thesis, the above paper found HS-5 cells only protected H929 and JIM3 cells from RV oncolysis, they did not protect U266 cells from RV oncolysis. Therefore, there could be some cell line dependencies on whether the cells will be protected or not. Additionally, the difference in OV used is more than likely to play a part as the virus biology is completely different, and it was not stated in the paper how BMSCs protect MPC lines from direct RV oncolysis (147). Investigation into whether MPCs changed CAR entry receptor expression following coculture with BMSCs was not investigated in this thesis, but because there was no significant difference in Ad[CE1A]-induced cell death between monoculture and coculture, it is unlikely that BMSC line HS-5 changed CAR expression in MPCs. In addition, it should be noted that the coculture model used in this chapter

is a simple 2D model and not entirely representative of the complexity of the BM microenvironment, therefore it can be assumed that other BM niches or as mentioned other BMSCs may provide a protective effect against direct oncolysis of Ad[CE1A].

The next step was to determine Ad[CE1A] cytotoxicity in primary patient derived and HD samples. Human primary CD138⁺ and CD138⁻ cells from MM, PCL, MGUS and HDs were infected with Ad[CE1A]. Ad[CE1A] was able to induce significant levels of cell death compared to untreated controls in CD138⁺ cells from MM and PCL populations only. Whilst the levels of cell death between patients varied and some patients seem to be non-responders, it demonstrates the heterogeneity of MM patients. An encouraging finding was that all primary cells were cultured in 10% of the patient's autologous serum, consequently, if the patient's serum contained any neutralising anti-adenoviral antibodies, which is likely as the majority of the population has harboured an Ad5 infection (as previously discussed), then Ad[CE1A] would have been neutralised by these antibodies. Promisingly, Ad[CE1A] had no effect on CD138⁺ cells isolated from HDs, MGUS patients or CD138⁻ cells from MM patients, MGUS patients and HDs. These findings are encouraging for successful translation of Ad[CE1A] into clinical practice as any inhibition by neutralising antibodies could potentially limit its success.

An interesting finding was that *CS1/SLAMF7* was expressed in HD CD138⁺ plasma cells and in CD138⁻ BMMC populations, but to a significantly lesser extent than in primary MM cells. Despite this, Ad[CE1A] did not induce significant levels of cell death. An explanation for this could be that these cell populations are not infected with Ad5 as much as primary MM cells. Whilst we have not looked at infection efficiency in HD CD138⁺ cells for reasons discussed below, infection efficiency was determined to be around ~18% in BMMCs from HDs. Again, it is unknown whether this percentage of cells are the same percentage of cells expressing CS1 in these populations. There may also be other factors in play, such as healthy plasma and BMMCs having functioning intact anti-viral mechanisms such as intact IFN signalling, which would prevent Ad[CE1A] replication and cell death in this population. Nevertheless, the use of B cell therapies with off-target effects are still widely used, such

as Rituximab, a CD20 mAb. CD20 is expressed on almost every B cell (excluding early B cells or plasma cells), which has not limited its use as a treatment for lymphoma and autoimmune diseases (395).

Another explanation as to why CD138⁺ cells showed differences in sensitivity to Ad[CE1A] was that there may have been differing levels of neutralising anti-adenoviral antibodies in autologous serum between patients. A further explanation may be that they express different levels of adenoviral receptors and/or CS1, as discussed earlier. Mechanistically speaking, those patient's cells that had better responses must have allowed for easier viral infection and replication. Unfortunately, there are a few technical and physiological problems when culturing primary CD138⁺ cells *ex vivo* from MM patients. Firstly, primary CD138⁺ cells lose their viability quickly once outside their normal BM microenvironment, hence in some patients there were high levels of cell death in the controls. Thus, primary CD138⁺ cells are fragile, relative to other leukocytes (396,397), and are likely to lyse easily during the numerous centrifugations in the isolation protocol. This could account for the high amount of cell death seen in the untreated controls in some patient samples. Secondly, low numbers of CD138⁺ cells are obtained from BM aspirates. This could be caused by haemodilution by sequential BM aspirates. I obtained second pass aspirates, whilst the first pass goes to the diagnostic labs, haemodilution occurs with every subsequent BM aspirate, consequently, there is a larger amount of blood mixed in with the cells resident in the marrow (397–399). Additionally, the amount of BM aspirate obtained varied from patient to patient. Lastly, in our research groups experience, CD138⁺ cells *ex vivo* are not proliferative and are not very metabolically active (personal communication, data not published), because of this, viral replication may be slower as the cells are not actively proliferating. For these reasons, several papers have been published on the maintenance of primary MM CD138⁺ cells *ex vivo*, this has mainly been performed either through 3D tissue culture methods, such as optimising the osteoblastic niche by using a microfluidic osteoblast-derived 3D tissue culture scaffold (301), or by using a formulated extracellular matrix to recapitulate the microenvironment of the human BM (400), or by coculture methods combined with a concoction of cytokines (401). These are long-winded, complicated, and expensive methods that are hard to optimise and repeat.

Therefore, it is for these reasons that further follow up experiments to address the above issues of patient sensitivity were not performed

Oncolytic Ads cause cell death by passive lysis, but it is unclear whether oncolytic Ads also use more active cell death processes such as apoptosis. Pathogenically, viruses modulate the apoptotic process by induction or suppression to increase viral survival and spread (402,403). Ad5 encodes several inhibitors of apoptosis, but it has also been shown that several adenoviral proteins have been implicated in the induction of apoptosis to facilitate cell lysis and release of viral progeny, such as E4 (404,405) and E3 (406). Ad[CE1A] was shown to increase PS externalisation by Annexin V staining using flow cytometry, which is a marker of apoptosis. However, common apoptosis genes were not upregulated when assessed by RT-qPCR. When cells were treated with Ad[CE1A] ± the pan caspase inhibitor Z-VAD-FMK, the presence of Z-VAD-FMK did not prevent Ad[CE1A]-induced cell death, therefore, Ad[CE1A]-induced cell death is caspase-independent. PS externalisation is not an absolute marker for apoptosis and may indicate different mechanisms of cell death. PS can occur independently of apoptosis, such as calcium dependent lipid scramblase (TMEM16) (407), or as a part of regulated inflammatory cell death such as necroptosis (408).

Therefore, investigation into necroptosis involvement in Ad[CE1A]-induced cell death was conducted. As mentioned earlier, necroptosis is a form of regulated cell death that is caspase-independent which generally manifests with a necrotic morphotype. Therefore, pharmacological inhibition of proteins involved in the necroptotic pathway, RIPK1, RIPK3 and MLKL were performed. RIPK1 and RIPK3 form the necrosome complex with RIPK1 initiating the process by activating RIPK3. Inhibiting RIPK1 and RIPK3 did not protect MPC lines from Ad[CE1A] induced cell death. However inhibiting MLKL did inhibit Ad[CE1A] induced cell death in all MPC lines.

MLKL is the critical final mediator of necroptosis. MLKL is phosphorylated by the necrosome complex which then translocated to the plasma membrane to form pore, which allows the release of DAMPs. One study using ovarian cancer cell lines found that inhibiting RIPK1 did not prevent oncolytic Ad

(dl922-947) mediated cell death, but inhibition of MLKL did induce a small but significant reduction in oncolytic Ad-induced cell death. However, the authors did not detect any MLKL phosphorylation following infection (similar to my findings), and MLKL knockdown by siRNA showed no significant effect on oncolytic Ad efficacy, therefore, the authors concluded MLKL is not an absolute requirement for oncolytic Ad-induced cell death. The study also found that expression of RIPK3 in HeLa cells following retroviral transduction increased sensitivity to oncolytic Ad cytotoxicity and WT Ad5. This enhanced sensitivity could be reversed by the addition of a RIPK3 inhibitor, but not by the addition of a RIPK1 or MLKL inhibitor. Expression of RIPK3 in transduced HeLa cells did not alter the expression of other core necroptosis proteins and it did not increase viral protein expression or viral replication. Additionally, when caspase-8 was inhibited, induction of necroptosis was observed that enhanced oncolytic Ad activity which was RIPK3 and MLKL dependent (409). Caspase-8 deactivates necroptosis by inhibiting the activity of RIPK3 and RIPK1, therefore elimination or inhibition of Caspase-8 results in necroptosis (383). Interestingly, the adenoviral protein E3 14.7 kDa is a known caspase-8 inhibitor, which is normally deleted in oncolytic Ads to increase apoptosis (410). The oncolytic Ad used in this study has deletions in E3, but it is not stated whether E3 14.7 kDa is deleted. The authors conclude that group C Ad-induced death differs from the classical pathway of necroptosis and does not absolutely require RIPK1, RIPK3 and MLKL and in the presence of caspase-8 inhibition, cell death can proceed down the necroptotic pathway in a RIPK3 and MLKL dependent manner (409). In support of this, another study investigated various mechanisms of cell death in a panel of different OVs, including WT Ad5. They showed WT Ad5 to induce necroptosis, inflammasome activation and autophagy before tumour cells died by Ad-mediated lysis (411). Regarding necroptosis, the study found increased p-RIP3 and increased pMLKL in A549 and HOS cells (lung carcinoma and osteosarcoma cell line respectively). Several other studies have also reported Ads at inducing necroptosis in other cancers (ovarian, breast and liver cancer cell lines) (60,173,412).

Whilst RIPK3 inhibition did not affect Ad[CE1A]-induced cell death which disagrees with the above studies, MLKL inhibition did significantly reduce Ad[CE1A]-induced cell death and this is in agreement with the above studies (409,413). Further work needs to be performed to fully understand the molecular mechanism, such as knocking down/out or overexpressing RIPK1/3 and MLKL, but the results presented here are the groundwork for future research into this area (section 3.2.12). In contrast, one study found no phosphorylated MLKL following infection with a range of group B oncolytic Ads (374), therefore the induction of necroptosis may not be the same across Ad serotypes. Essentially, it remains unclear if Ad infection induces necroptosis or necrosis, but it has been argued that necroptosis is a more appropriate mechanism in the context of Ad-induced cell death because necrosis typically occurs as a result of external injury, whilst necroptosis is the result of an intracellular mechanism initiated by internal changes like viral infections (414).

Finally, investigation into whether Ad[CE1A] induces ICD in MPCs was conducted. As mentioned in this chapter's introduction, OV oncolysis is highly immunogenic and several OVs including Ads have been shown to activate an anti-tumour immune response. ICD can initiate adaptive immune responses due to emission of DAMPs/PAMPS. Additionally, necroptosis/necrosis cell death associated changes result in the leakage of the cell content into the surrounding tissue, subsequently releasing DAMP molecules, which may initiate antitumour immune responses (414). Therefore, levels of key DAMPs in response to Ad[CE1A] were investigated, which may result in increased recruitment and activation of immune cells. Firstly, CALR exposure was assessed, CALR translocates to the outer leaflet of the plasma membrane and functions as a pro-phagocytotic signal. CALR exposure was increased in a dose-dependent manner 24 hours after Ad[CE1A] infection. Next, CD47, an antiphagocytic molecule, was assessed. CD47 is overexpressed on many cancer types allowing them to escape immunosurveillance. There is a balance between CALR exposure and CD47, as CALR is antagonised by CD47. CD47 cell surface expression decreased following Ad[CE1A] treatment in a time and dose-dependent manner. Next, extracellular ATP release was assessed, a major DAMP associated with ICD, which operates as

a 'find me' signal for macrophages and DC precursors. Extracellular ATP increased in a dose dependent manner following Ad[CE1A] treatment.

There have been several studies that have investigated ICD following oncolytic Ad therapy which are in agreement with the results presented here. One study found ATP and HMBG1 secretion and CALR and HSP90 exposure increased following WT Ad5 infection in HOS and A549 cells. Additionally, they also found WT Ad5 to increase phagocytosis of virally infected cells, this was significant in A549 cells, but not in HOS cells. The study also found that Ad-infected tumour cells were partly able to stimulate DCs to release Th1 cytokines and activation status of DCs. When DCs were cocultured with WT Ad5 infected tumour cells (A549 or HOS) increased CD83 in both A549 and HOS DC cocultures was found, whilst increased CD86 was found in HOS DC coculture and increased CD40 in A549 DC coculture, suggesting DC activation markers were cell line dependent (413). Another study reported that oncolytic Ad (dl922-947) was able to increase exposure of CALR, decreased intracellular ATP (implying its secretion) and an increase intracellular HMGB1 (secretion was pharmacologically blocked by brefeldin A, implying HMGB1 build up) in mesothelioma cell lines (373). Another study also found increases in HMGB1 and ATP secretion following oncolytic Ad therapy (Ad881), although this effect was only observed at very high MOIs (415). The release of ICD markers is also observed following treatment with oncolytic Ads from group B and WT Ad5. Extracellular release of HSP70 and CALR exposure increased following Ad infection, which was greater in the group B oncolytic Ad than WT Ad5. Release of TNF- α and IL-6 was also observed when cultures of freshly sliced resected patient-derived colorectal cancer liver metastasis were treated with oncolytic Ads *ex vivo*, again, this effect was greater in group B oncolytic Ad than WT Ad5. Coculture of DCs with group B oncolytic Ad-infected cancer cells significantly increased HLA-DR, CD80 and CD86 and increased CD4⁺ T cells in a mixed tumour-leukocyte reaction *in vitro* (374).

My findings and the studies discussed above indicate that oncolytic Ads are able to induce ICD DAMP release which may potentially be able to trigger an anticancer immune response, as has been shown

in some of the studies. Future work would be to assess if DAMP release following Ad[CE1A] infection in MPCs results in antitumour immune activation.

Next, investigation into MHC class I and II expression following Ad[CE1A] treatment was conducted. Ad[CE1A] was able to significantly increase the expression of both HLA-ABC and HLA-DR following 48 hours of Ad[CE1A] treatment. Not many studies have investigated class I and II expression following OV infection, but a recent study using an oncolytic Ad (LoAD) in MM cells found a decrease in HLA-ABC and HLA-DR expression in MM cells following infection, which the authors speculated was due to virus replication competing for cell transcription machinery or due to the oncolysis process (129), as these markers were increased in other APCs (416). Upregulating HLA expression following OV infection is getting more recognition and has recently been reviewed (417). Dysregulation of HLA is recognised as a common mechanism to escape immunosurveillance or immunotherapy, and OVs have the potential to counter this by upregulating HLA expression. Many viruses express proteins, such as E3 19k in Ads, that corrupt antigen presentation in infected cells such as pulling HLA molecules away from the cell surface (417,418). Hence why E3 and other HLA blocking viral proteins are removed from OVs, with the former being deleted in Ad[CE1A], to make them more immunogenic and to accelerate viral clearance in normal tissue (419). However, there is a fine balance as one of the benefits to OVs is the ability to induce ICD and release of DAMPs, which could create a proinflammatory environment resulting in anticancer immune responses. In contrast, allowing virus antigens to be presented via HLA may result in T-cell mediated killing of infected cancer cells by caspase-mediated apoptosis, which is a less inflammatory and a less immunogenic form of cell death. Therefore, increased viral antigen presentation via HLA could be less effective at priming immune responses than virus mediated lysis with simultaneous presentation of PAMPs or DAMPs (417). Therefore future work needs to assess the role of the increased expression of HLA following Ad[CE1A] infection and whether this impacts the potential ability for ICD via DAMP exposure.

In addition to DAMP exposure, investigation to determine if Ad[CE1A] could induce cytotoxic cytokine secretion from BMMCs that would cause bystander cytokine killing in MPCs was explored. UV inactivated Ad[CE1A]-CM from HD BMMCs were able to significantly decrease MPC viability, UV inactivated Ad[CE1A]-CM from MM BMMCs was only able to significantly decrease MPC viability in JJN-3 cells. The spread of data within the small n numbers used in the MM group could be due to the heterogeneity within patients suggesting a stronger degree of immunosuppression in the patients that did not respond as well. In a recent study using oncolytic RV in MM, bystander cytokine killing was observed in MPC lines following treatment with RV-CM from HD PBMCs. It would be interesting to know if a difference in bystander killing would be observed if MM patient PBMCs were used instead of HDs. An investigation into cytokine secretion from HD PBMCs following RV showed induction of type I IFN- α , type II IFN- γ , TNF- α and TRAIL (147). Secretion of IFN- α , IFN- γ , TNF- α resulting in bystander killing has been described by several studies following OV treatment (420). The investigation into what cytokines are secreted following Ad[CE1A] treatment is needed, but this preliminary investigation is promising.

3.4 Chapter conclusion

In conclusion, the data presented in this chapter supports the hypothesis that Ad[CE1A] can infect, replicate and induce cell death in MPC lines and patient-derived MM cells. The data also supports the hypothesis that viral replication and subsequent cell death is linked to the level of CS1 expression. Additionally, Ad[CE1A] does not appear to cause cell death by classical apoptotic pathway as cell death was caspase independent, nor does it appear to cause cell death by classical necroptosis pathways as RIPK1 and RIPK3 were not needed to induce cell death, but interestingly inhibition of MLKL was found to rescue MPC lines from Ad[CE1A] induced oncolysis.

Ad[CE1A] induced ICD DAMP exposure in MPC lines, increased MHC class I and II expression and induced bystander cytokine killing. These results are promising as accumulatively they may induce anti-MM immune responses as well as direct MM killing, which may enhance anti-MM efficacy in the clinical setting. However, at this stage it is unknown if Ad[CE1A] is effective against chemotherapy resistant MPCs or MRD. Therefore, in the next chapter I aim to try to determine this.



Chapter 4 : Ad[CE1A] Treatment to Target Minimal Residual Disease and Prevent Relapse



4.1 Introduction

The work presented in chapter 3, and previous work (Section 1.4.5) has shown that Ad[CE1A] is capable of *in vitro* lysis of a wide panel of CS1 expressing human MPC lines, *ex vivo* patient samples and is able to reduce tumour burden in a high tumour burden U266 xenograft MM model (unpublished data).

It is currently unknown what MM clinical setting OV's will be the most useful for, whether that is in newly diagnosed, relapsed, maintenance or eradication of MRD. The majority of preclinical and clinical studies have investigated the use of OV's as a tumour debulking strategy, or as a purging ASCT strategy, but with the ability of viruses to repeatedly infect cancer cells carries the potential for eradicating MRD. There are a few papers suggesting some OV's can remove MM MRD, but these studies are problematic. The murine models used in these studies use mice that have aggressive disease, and in one paper a subcutaneous model was used. The problem with these studies is that they state they eradicate MRD, but are used in advanced disease, and/or not *in situ* of the normal systemic sites in the BM (118,136). Therefore, these studies do not allow for the question of whether OV's are capable of removing MRD within BM niches that are refractory to other standard of care therapies, as it is thought that specific BM niches contribute to dormancy/MRD (337).

First, this chapter details the efficacy of Ad[CE1A] at preventing MM regrowth following BTZ treatment and Ad[CE1A]'s efficacy against BTZ insensitive cells *in vitro*. This chapter then details the efficacy of Ad[CE1A] in a clinically relevant, low tumour burden model of MM, to overcome the issues seen in the previously mentioned studies. To do this, the low tumour burden model was employed, which mimics MM MRD within patients and was developed by post doctorate Dr Alana Green in our research group (340). The low tumour burden model is created by using a U266 xenograft model, once tumour burden is high, mice receive MM standard of care therapies BTZ and Len to initially debulk tumour but also as a maintenance. This reduces the tumour to almost undetectable levels by IVIS imaging, and serum immunoglobulin levels of IgE significantly drop. After around six weeks tumour starts to relapse and becomes detectable in the hindlimbs and vertebra, and serum IgE levels start to rise. This is clinically

similar to what happens in MM patients. Therefore our research question was whether Ad[CE1A] could eradicate the remaining MRD following chemotherapy. For this, only BTZ was used as the tumour debulking agent, as some evidence from our research group suggests BTZ alone is just as effective at reducing tumour burden. Additionally, it is also currently unknown what clinical setting Ad[CE1A] will be most effective in, newly diagnosed or relapsed patients. Therefore, assessment of whether Ad[CE1A] could remove tumour after immediately after BTZ treatment and the development of BTZ resistance/tumour relapse using the low tumour burden model of MM was investigated.

4.1.1 Hypothesis, Aims and Objectives

4.1.1.1 Hypothesis and Aims

This chapter aims to assess the potential of Ad[CE1A] at preventing disease relapse by eradicating/controlling MRD. To do this the following hypothesis was tested 'Ad[CE1A] alongside standard MM chemotherapy BTZ will be effective at removing/controlling MRD in the low tumour burden model of MM which will result in improved overall survival'.

4.1.1.2 Objectives

The hypothesis was tested by the following objectives:

1. Investigate if Ad[CE1A] could prevent cell line regrowth after BTZ treatment *in vitro*.
2. Investigate if Ad[CE1A] has efficacy in BTZ insensitive MPC lines *in vitro*.
3. To perform an *in vivo* study to investigate if Ad[CE1A] was effective at removing/controlling MRD in the *in vivo* U266 low tumour burden model and to determine if Ad[CE1A] was effective against relapse and whether this results in prolonged overall survival.

From the results obtained in the last objectives 1-3, two new objectives were also investigated:

4. To preliminary investigate *in vitro* dormancy/MRD in order to test Ad[CE1A] efficacy.
5. To preliminary investigate more advanced *in vitro* models which may be suitable to induce MM dormancy/MRD in order to test Ad[CE1A] efficacy.

4.2 Results

4.2.1 Ad[CE1A] Prevents Myeloma Cell Regrowth after Bortezomib Treatment.

A typical MM patients' clinical history is characterised by multiple disease relapses after different lines of treatment until becoming refractory. One of the main causes for disease relapse is drug resistance, which is dramatically associated with an unfavourable prognosis. BTZ, was the first proteasome inhibitor introduced for MM and it is a breakthrough treatment for patients as previously discussed (section 1.3.3). However, many patients' disease becomes resistant to BTZ, therefore, it was important to assess *in vitro* if Ad[CE1A] can prevent tumour regrowth after BTZ treatment. In a basic preliminary *in vitro* assay, JJN-3 and U266 cells were treated with 2.5 nM BTZ and 24 hours after cells were then treated with various doses of Ad[CE1A]. At days 1, 3, 7, 14, 18, 21, and 25 days post Ad[CE1A] and BTZ treatment cell viability was determined by PI staining using flow cytometry. OPM-2 cells were not used in this assay as they are resistant to BTZ *in vivo* despite being BTZ sensitive *in vitro*. Ad[CE1A] treatment after BTZ treatment prevented regrowth of JJN-3 and U266 cells over a 25-day period compared to the BTZ only treated group, where cell viability recovered to similar levels of the untreated controls (Figure 4.1). However, in JJN-3 cells at an MOI 1 at day 25, there was an increase in cell viability, but this remained significantly lower compared to untreated control and BTZ only treated group.

4.2.2 Ad[CE1A] Causes Oncolysis of Bortezomib Insensitive Cells.

Next it was important to determine if Ad[CE1A] was able to induce oncolysis in BTZ insensitive MPC lines compared to the parental sensitive MPC lines. First, JJN-3 and U266 cells were exposed to BTZ over several months, and BTZ sensitivity was determined by dose response curves after 72 hours (Figure 4.2.a). Both JJN-3 and U266 BTZ insensitive cells had increased BTZ IC_{50} values compared to parental controls, with a 30.8 and a 30.3-fold increase in IC_{50} values, respectively. Ad[CE1A] cytotoxicity was then assessed in the BTZ insensitive cells. JJN-3 and U266 BTZ insensitive and parental cell lines were treated with Ad[CE1A] MOI 10 and cell death was determined by PI staining using flow cytometry after 72 hours (Figure 4.2.b). No significant difference in Ad[CE1A]-induced cell death was observed between JJN-3 or U266 BTZ insensitive cells compared to their respective parental cell lines.

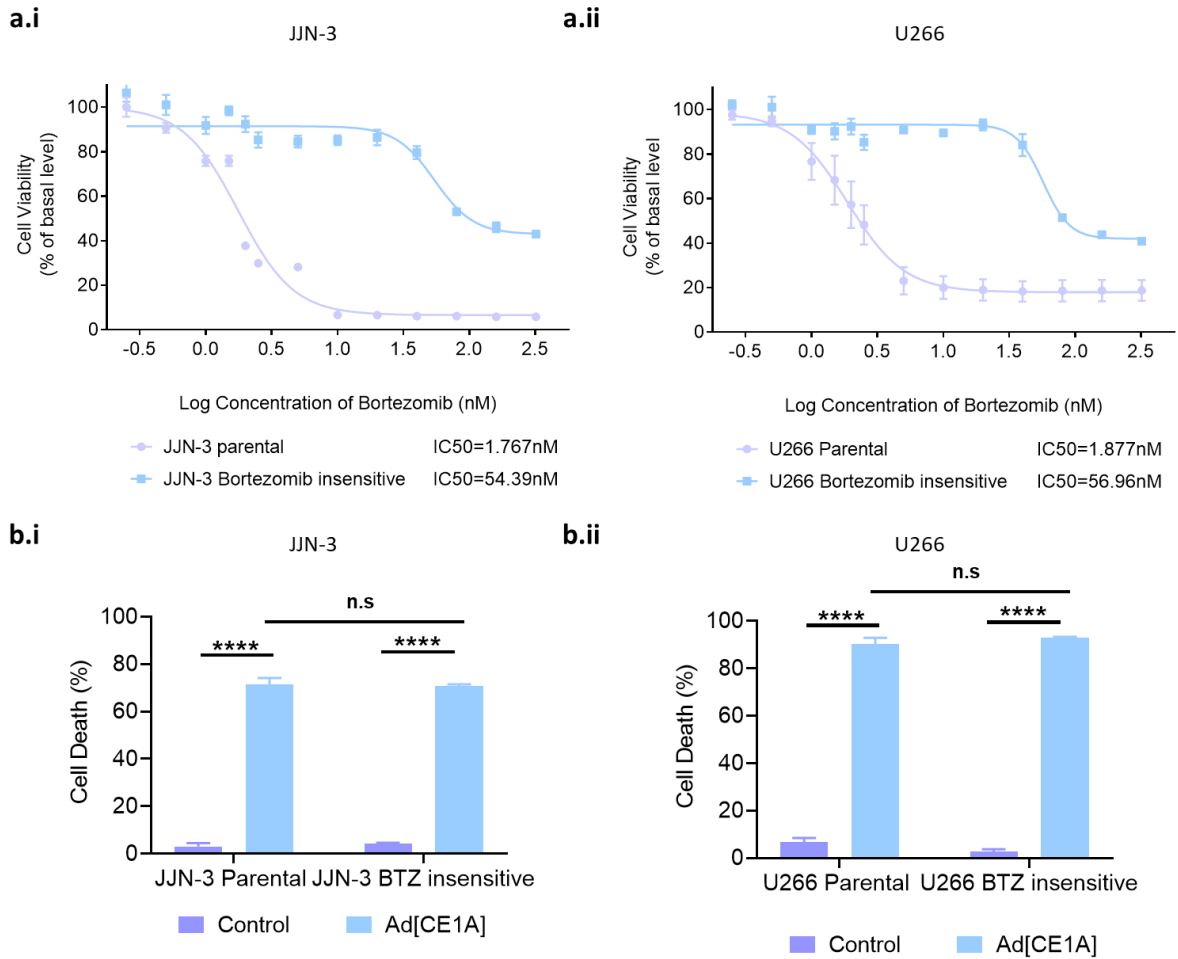


Figure 4.2: Percentage of JLN-3 and U266 BTZ insensitive and parental cells dead after Ad[CE1A] (MOI 10) incubation at 72 hours:

(a.i) JLN-3 and **(a.ii)** U266 BTZ insensitive and parental cell lines were treated with BTZ (0.5, 1.0, 1.5, 2.0, 2.5, 5.0, 10.0, 20.0, 40.0, 80.0, 160.0 and 320.0 nM). After 72 hours, cell viability was determined by an AlamarBlue® assay. n=3 Data is the mean ±SD. **(b.i)** JLN-3 and **(b.ii)** U266 BTZ insensitive and parental cell lines were treated with Ad[CE1A] MOI 10. After 72 hours, cell death was determined by PI staining using flow cytometry. n=3 Data is the mean ±SD. p values are for 2-way ANOVA with multiple comparisons with Šidák's correction where **** p<0.0001.

4.2.3 Efficacy of Ad[CE1A] Against MRD/relapse in the *in vivo* Low Tumour Burden Model.

The results presented above give evidence that Ad[CE1A] may be effective at eradicating/controlling MRD or effective against BTZ resistant/relapsed disease. Therefore the efficacy of Ad[CE1A] was tested in the U266 low tumour burden xenograft model. Ad[CE1A] was administered alone as a monotherapy (without tumour being debulked) compared to vehicle control, or combined with BTZ after tumour debulking (BTZ & Early Ad[CE1A]), or combined with BTZ when tumour started to relapse after initial tumour debulking (BTZ & Late Ad[CE1A]) compared to BTZ only treatment. Tumour was monitored by IVIS imaging weekly, and overall survival was monitored.

4.2.3.1 *In vivo* Tumour Burden

In vivo bioluminescence imaging was conducted weekly, and over time Ad[CE1A] showed no long-lasting significant reduction of tumour burden compared to the tumour control group, except for one time point (10 weeks post tumour injection) where Ad[CE1A] significantly reduced tumour burden compared to vehicle control (Figure 4.3). This was surprising as Ad[CE1A] previously showed efficacy as a monotherapy in this model (unpublished data), there are a few possible explanations for this which will be discussed later. In comparison, BTZ significantly reduced tumour burden for approximately 4 weeks before tumour started to relapse/increase. Ad[CE1A] was not able to control/eradicate MRD or prevent disease relapse for longer than the BTZ only treated mice; despite there being two time points (week 15 and week 18) where tumour burden was significantly lower than BTZ only treated group. Ad[CE1A] was also not effective at removing disease relapse after BTZ monotherapy treatment, despite there being two time points (week 15 and week 18) where tumour burden was significantly lower than BTZ only treated group.

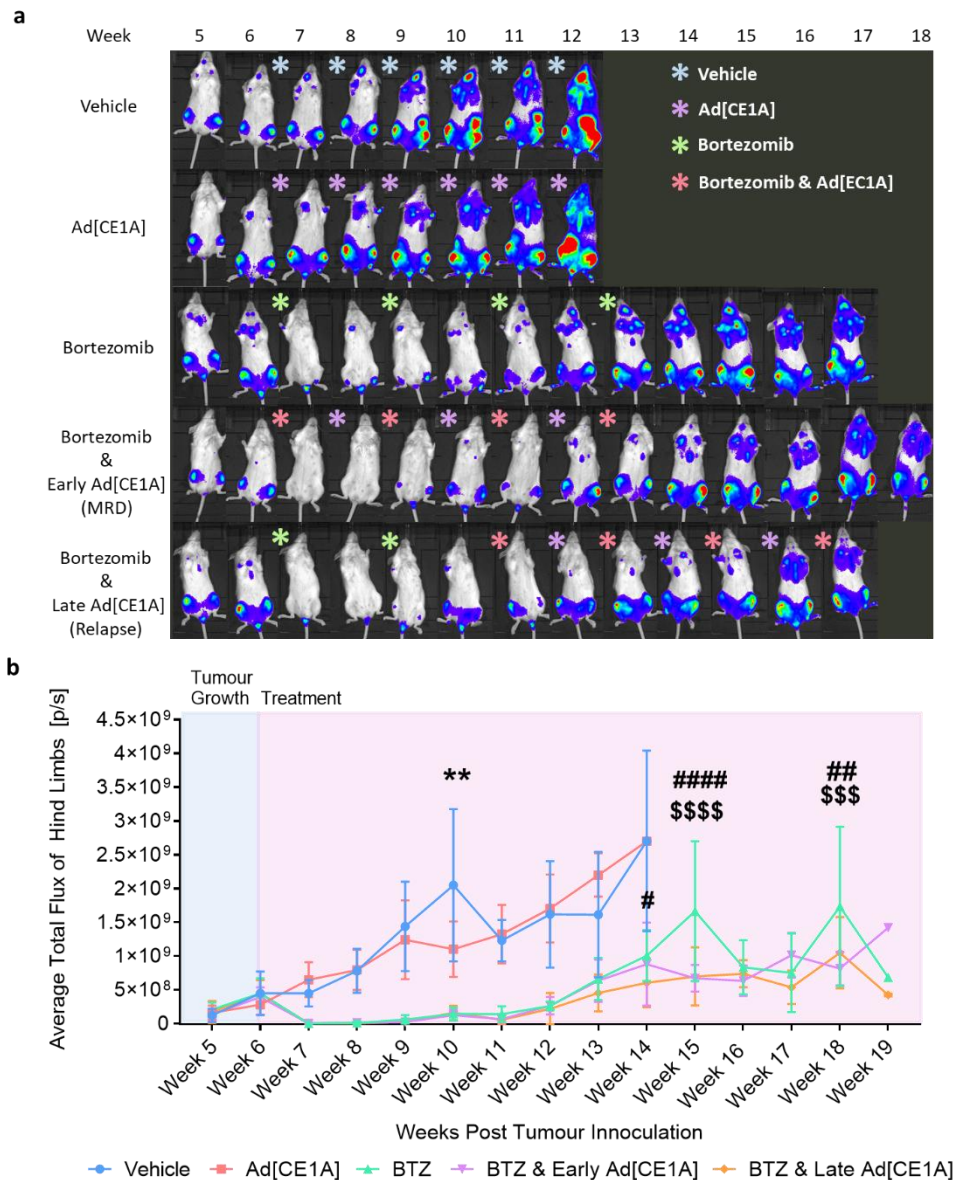


Figure 4.3: Analysis and quantification of *in vivo* tumour burden in U266 bearing NSG mice by bioluminescent imaging over time:

U266 bearing mice were IVIS imaged weekly from week 5. Treatment started at week 6. **(a)** Representative images of *in vivo* bioluminescence imaging over time of U266 bearing NSG mice treated with vehicle, Ad[CE1A], or with BTZ ± early Ad[CE1A] treatment to target MRD or late Ad[CE1A] treatment to target disease relapse. One representative mouse per group. Coloured asterisk represent treatment times and groups. **(b)** Quantification of bioluminescent signal in hind limbs over time. n=8 for all groups except BTZ where n=6. Data is the mean ±SD. p values are for 2-way ANOVA where vehicle and Ad[CE1A] monotherapy compared to each other and Šidák's correction was used and BTZ & early virus and BTZ & late virus compared to BTZ only where Tukey's correction was used. ** p<0.01; *** p<0.001; **** p<0.0001. * denotes significance between Vehicle control and Ad[CE1A], # denotes significance between BTZ and BTZ & Late Ad[CE1A], \$ denotes significance between BTZ & BTZ Early Ad[CE1A].

When mice were sacrificed, tumour burden at end point was determined by flow cytometry and GFP expression from tumour cells (Appendix Figure 8.8), this showed no significant difference in tumour burden between the groups, but because this was a survival study, no true comparisons can be made as mice were euthanised at different times.

It should also be noted that vehicle treated mice survived longer than usual (~14wk average) before losing more than 10% of their body mass and/or showing signs of end stage disease (Appendix Figure 8.9) such as hind limb paralysis. Additionally, the majority of mice in the vehicle (7/8) and some mice in the Ad[CE1A] group (4/8) were euthanised due to large solid tumour masses, that upon dissection, were tumours in the ovaries, as can be seen in the vehicle and Ad[CE1A] bioluminescent representative images in Figure 4.3. This could be explained by late-stage disease, as some mice sustained a high level of tumour burden for a time before tumour burden progressed severely to the extramedullary sites. However, ovarian tumours were detectable in IVIS imaging as early as week 7 post tumour injection. One mouse out of the BTZ treated group (depicted in Figure 4.3) and one mouse from the BTZ and late virus treated group also had ovarian tumours, but these tumours were small in comparison. The ovarian tumours were confirmed to be MM by staining for Lambda light chains by IHC (Appendix Figure 8.10). Our lab has never before observed the development of ovarian tumours in this model, so this was a new phenomenon, and one that will be discussed later.

4.2.3.2 Overall Survival

Given the *in vivo* tumour burden results above, it was not surprising that the addition of Ad[CE1A] as a monotherapy or the addition of Ad[CE1A] early to control/eradicate MRD or late to control/eradicate disease relapse did not result in any meaningful reduction of tumour burden, or that the addition of Ad[CE1A] did not translate into any significant survival advantage compared to the respective control groups (Figure 4.4). Ad[CE1A] as a monotherapy did not result in a significant increase in survival compared to vehicle control group. Additionally, Ad[CE1A] did not increase survival post BTZ treatment compared to BTZ only treated group.

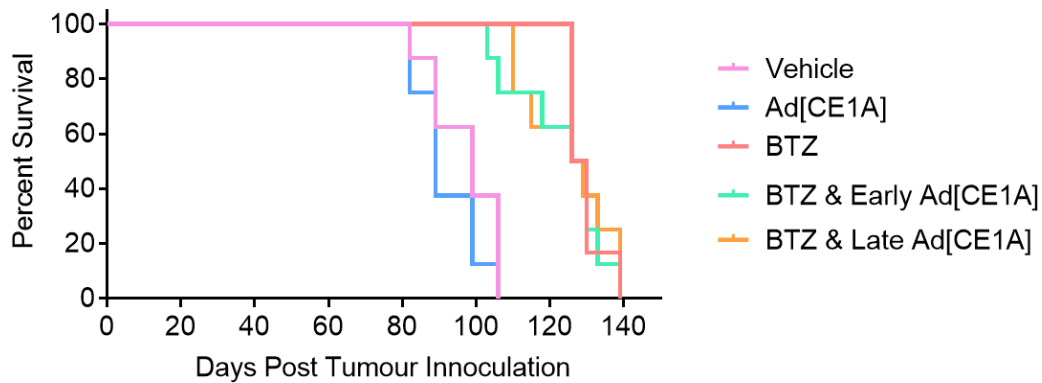


Figure 4.4: Kaplan-Meier survival curves of U266 bearing NSG mice treated with vehicle, Ad[CE1A], or with BTZ ± early Ad[CE1A] treatment to target MRD or late Ad[CE1A] treatment to target relapse:

Mice were monitored daily and euthanised when humane end points were reached. P values generated by Kaplan-Meier survival where vehicle and Ad[CE1A] monotherapy compared to each other and BTZ & early virus and BTZ late virus compared to BTZ only. $p < 0.05$.

4.2.4 Developing *in vitro* Models of MRD/dormancy

Given the disappointing results above, *in vitro* models of MRD/dormancy were of much interest as this would allow the investigation into the efficacy of Ad[CE1A] and other therapeutics against MRD/dormancy in a cheaper, quicker and more high throughput way. This method may also help us determine if Ad[CE1A] has any efficacy at all against these populations, or may help to better inform the design of other *in vivo* experiments in a low tumour burden model and would be in line with the 3Rs (reduction, replacement and refinement) guidelines.

It can be argued as to what is the cellular phenotype that makes up the cell population in MM MRD. One argument is that these cells are non-proliferative dormant cells (337,421). Previous work between our research group and Dr Peter Croucher's research group at the Garvan institute has shown preclinically in a murine syngeneic mouse model that dormant MM cells reside in osteoblast niches, and that when murine MM 5TGM1 cells are cultured in CM or cocultured with primary osteoblasts *in vitro*, their proliferation rate significantly decreases (337). Therefore, assessment of whether dormancy in human MPCs alone or in CM with osteoblast like cells Saos-2 or BMSC line HS-5 could be generated was investigated.

4.2.4.1 Basal Level of Dormancy in Human Myeloma Cell Lines

To determine the normal level of dormancy in human MPC lines, GFP expressing JIN-3, U266 and OPM-2 cells were labelled with Vybrant™ DID and cultured in normal conditions for 24 days. Flow cytometry was performed to assess DID levels at 0-, 3-, 7-, 10-, 14-, 17-, 21- and 24-days post staining (Figure 4.5). By day 24, 4.2% of viable JIN-3 cells, and 1.8% of viable U266 and OPM-2 cells were still brightly labelled with DID, demonstrating there was a small population of cells that were not proliferating and had full DID retention (Figure 4.6). It is interesting to note that the cells with lower GFP expression, retained vybrant™ DID for longer than cells with higher GFP expression.

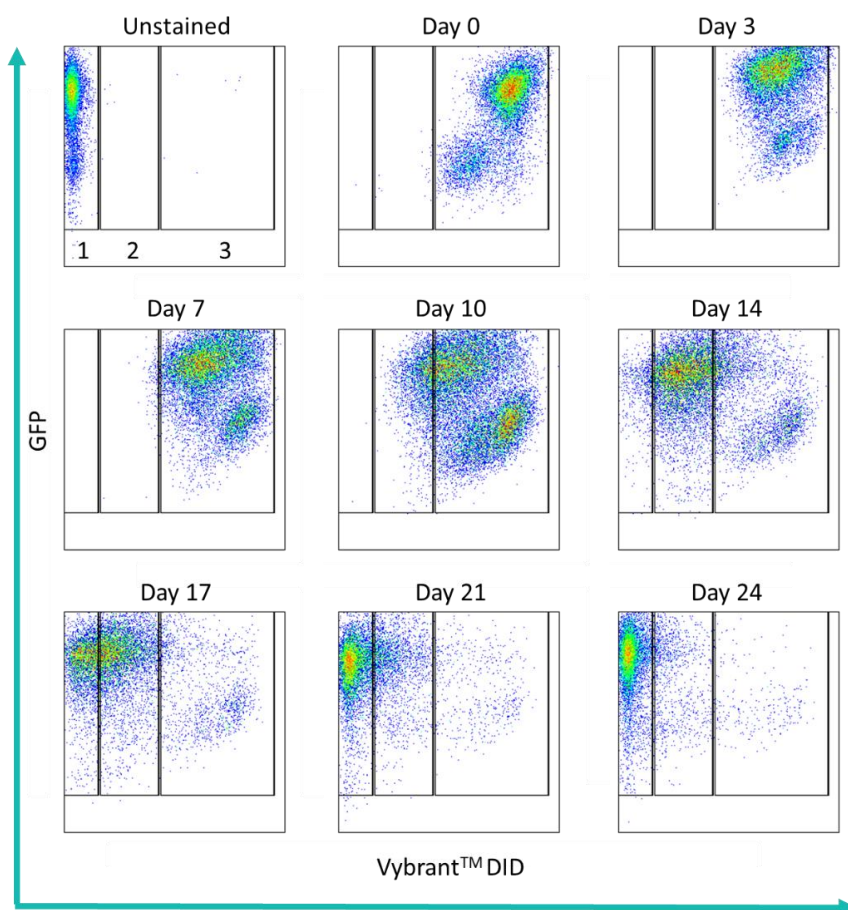


Figure 4.5: Representative flow cytometry dot plots over time of DID fluorescence in U266-GFP expressing cell lines:

U266-GFP cells were unstained or stained with DID on day 0. Unstained and DID Day 0 staining was used to determine the gating strategy after dead cells were gated out using PI. Gate 1= GFP^{positive} DID^{negative}; Gate 2=GFP^{positive} DID^{low}; Gate 3=GFP^{positive} DID^{High}.

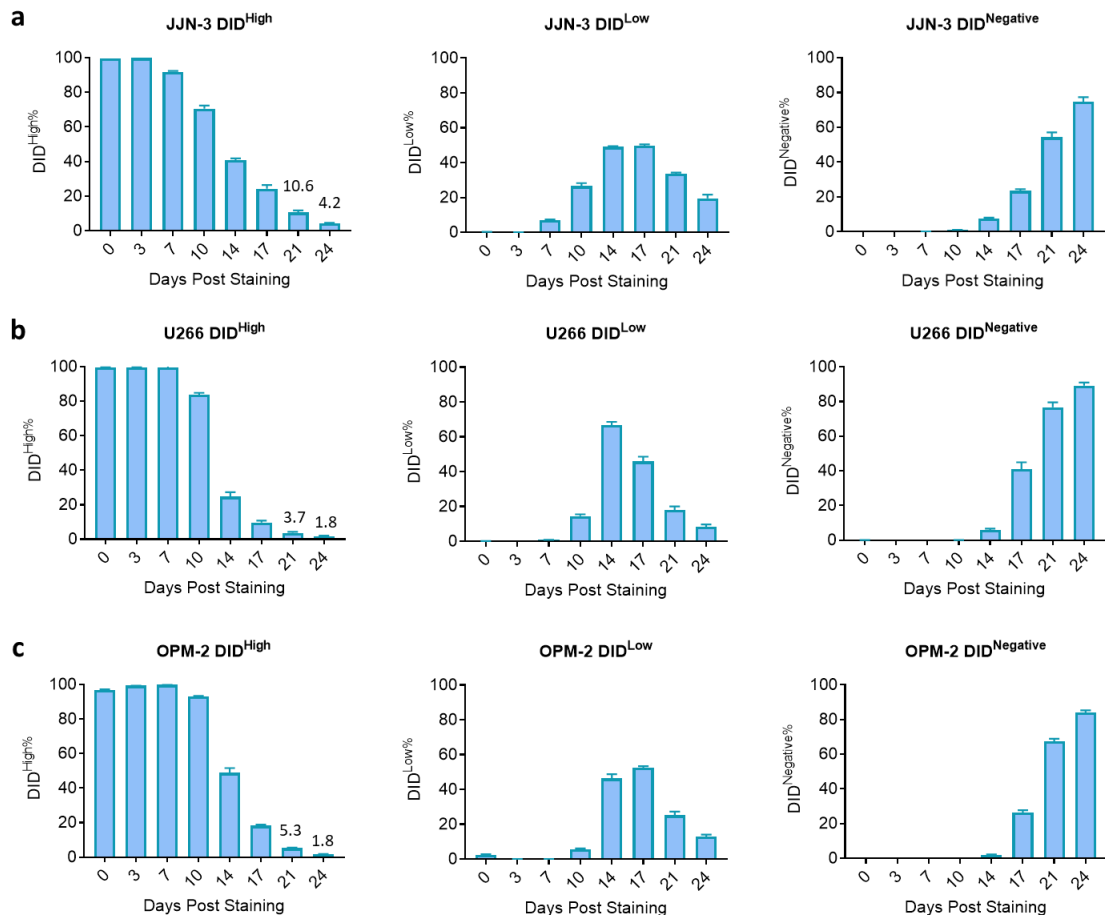


Figure 4.6: Percentage of Vybrant™ DID populations over time in JJJN-3, U266 and OPM-2 GFP expressing cell lines:

(a) JJJN-3, (b) U266, (c) OPM-2 GFP expressing cells were labelled with DID and fluorescence was tracked over time using flow cytometry. Percentage of DID^{High}, DID^{Low} and DID^{Negative} cells over time were plotted. n=3 Data is the mean ±SD.

4.2.4.2 Level of Dormancy after Culture in BMSC or Osteoblast-like Conditioned Media

After finding the basal level of dormant MM cells in normal culture conditions over time, next was to determine if dormancy could be induced by factors secreted by HS-5 BMSC lines or Saos-2 osteoblast-like cells. CM from Saos-2 or HS-5 was collected after 48 hours and sterile filtered to remove cellular debris. First, the volume of CM needed to keep the cells viable was determined to be 50% CM to 50% complete RPMI media (Appendix Figure 8.11). GFP expressing JJJN-3, U266 and OPM-2 cells were labelled with vybrant™ DID and then cultured in complete RPMI media, or for HS-5, RPMI:DMEM media or RPMI:HS-5 CM, or for Saos-2 RPMI:αMEM or RPMI:Saos-2 CM. Fluorescence (GFP and DID) was tracked over time by flow cytometry.

There was no significant increase in DID fluorescence at any time point in any MPC line in both HS-5 or Saos-2 compared to their respective controls (Figure 4.7 & 4.8). Interestingly, DMEM and α MEM controls showed significantly more DID retention at some time points (JIN-3 Day 14, 17 & 21 DMEM, Day 10, 17 & 21 α MEM; OMP-2 Day 10, 17 & 21 DMEM, Day 7, 14, 17 and 21), which highlighted the fact that the complete RPMI media was optimised for MM cell growth. This also highlighted the complexity of dormancy, and that these human MPCs may need to be in direct contact with stromal and/or osteoblastic cell types for dormancy to be induced.

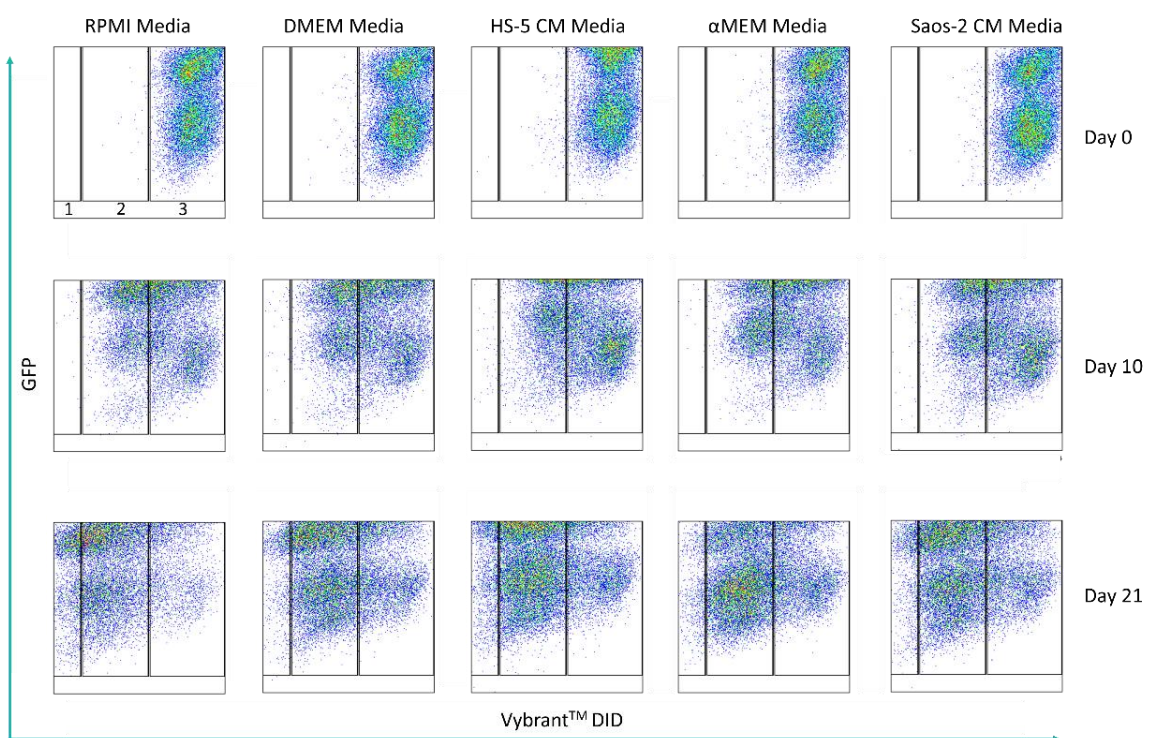


Figure 4.7: Representative flow cytometry plots of DID fluorescence in JIN-3 cells in cultured in HS-5 or Saos-2 conditioned media at Day 0, 10 and 21 post staining:

JIN3-GFP cells were unstained or stained with DID on day 0. JIN-3 cells were cultured in RPMI media, RPMI:DMEM media, RPMI:HS-5 CM, RPMI: α MEM media or RPMI:Saos-2 CM. Unstained and day 0 DID staining was used to determine gating strategy after dead cells were gated out using PI. Gate 1= GFP^{positive} DID^{negative}; Gate 2=GFP^{positive} DID^{low}; Gate 3=GFP^{positive} DID^{high}. Flow cytometry plots shown after day 0, 10 and 21 culture.

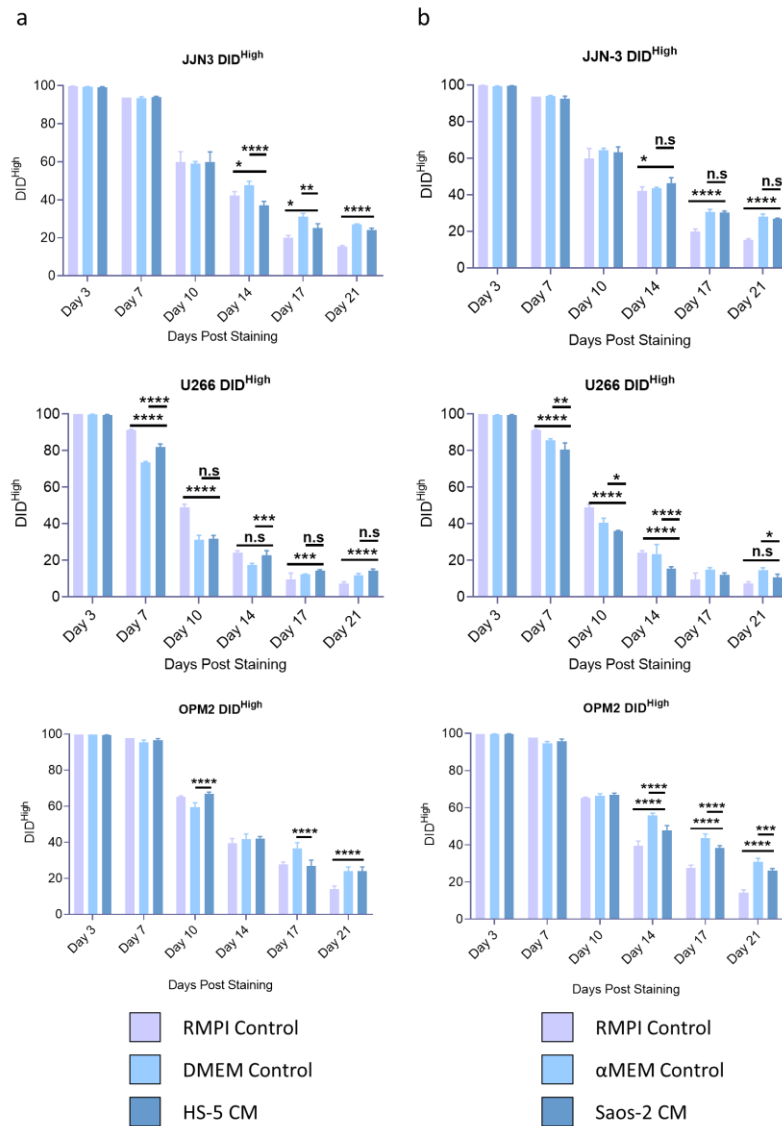


Figure 4.8: Percentage of Vybrant™ DID^{High} population over time in JN3, U266 and OPM2 GFP expressing cells after culture in HS-5 or Saos-2 CM compared to control:

JN3, U266, OPM2 GFP expressing cells were labelled with DID and cultured in **(a)** HS-5 or **(b)** Saos-2 CM or respective media controls. DID fluorescence was tracked over time used flow cytometry. $n=3 \pm SD$. P values are for 2-way ANOVA where * $p < 0.05$, ** $p < 0.01$, *** $p < 0.001$, **** $p < 0.0001$.

4.2.4.3 Investigation into 3D PolyHIPE Scaffolds for their Potential use for *in vitro* Dormancy Models.

As mentioned, MM cell dormancy is complex and hard to recapitulate *in vitro* in simple tissue culture flasks. Therefore, 3D models of MM alone or in coculture may be a better alternative. Prior to this thesis, I have had experience with culturing MPC lines in 3D sodium alginate models to investigate if cells become dormant and whether Ad[CE1A] and another oncolytic agent HSV1716, were able to kill proliferating and non-proliferative MM cells in 3D cell culture. Unfortunately, due to the pore size of the sodium alginate hydrogel, both viruses were not able to penetrate the hydrogel, therefore, could not be used for further investigation. Additionally, the 3D cell culture did not induce dormancy. The sodium alginate hydrogels do not greatly mimic the bone microenvironment. Therefore, in collaboration with Dr Frederick Claeys and his PhD student Betül Aldemir Dikici, the use of 3D polyHIPE scaffolds (4PCLMA) were investigated as they better mimic bone microenvironment with their porosity.

The ability of MPC lines and Saos-2 osteoblast like cells to proliferate alone or in coculture was assessed. Saos-2 cells were seeded onto polyHIPE scaffolds, for Saos-2 cocultures, MPCs U266 cells were seeded on to Saos-2 scaffolds 24 hours post Saos-2 seeding, for MPC monocultures, U266 cells were seeded onto fresh scaffolds. Prior to the addition of AlamarBlue®, scaffolds were moved into a fresh well plate with fresh media, AlamarBlue® was added to the wells containing the scaffold and to the media in the wells the scaffold was cultured in. This was to determine the amount of AlamarBlue® reduction that was coming from cells on/within the scaffold versus the number of unattached cells in the surrounding media or adhered to the bottom of the well. Scaffolds and media without cells were used as controls. AlamarBlue® analysis was performed on days 1, 4, and 7 post MPC seeding. U266, Saos-2 and the U266-Saos-2 coculture all proliferated on/within the scaffolds over time (Figure 4.9). The coculture had the highest proliferation at all time points. Scaffold cultured media from all three conditions had the similar RFU to scaffold blank and media blank, suggestive that the cells were residing within the scaffold and not the surrounding media/well. Additionally, Betül Aldemir Dikici

was kind enough to take scanning electron microscope images of the scaffold (Figure 4.10), where both U266 and Soas-2 were observed cells within the scaffold.

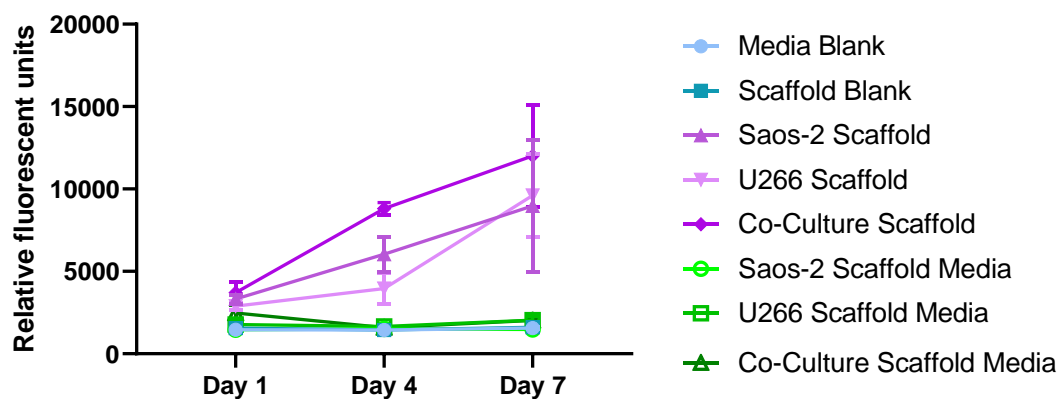


Figure 4.9: Proliferation of U266 MPCs, Saos-2 osteoblast like cells, and U266-Saos-2 cocultures in polyHIPE scaffolds:

U266 MPCs and Saos-2 osteoblast like cells were seeded on polyHIPE scaffolds in monoculture or coculture. Proliferation was assessed by AlamarBlue® in polyHIPE scaffolds and in the cultured media separately, to determine if reduction of AlamarBlue® was due to cells within the scaffold or cells in the surrounding media. Proliferation was assessed on Days 1, 4, and 7 post seeding. n=1.

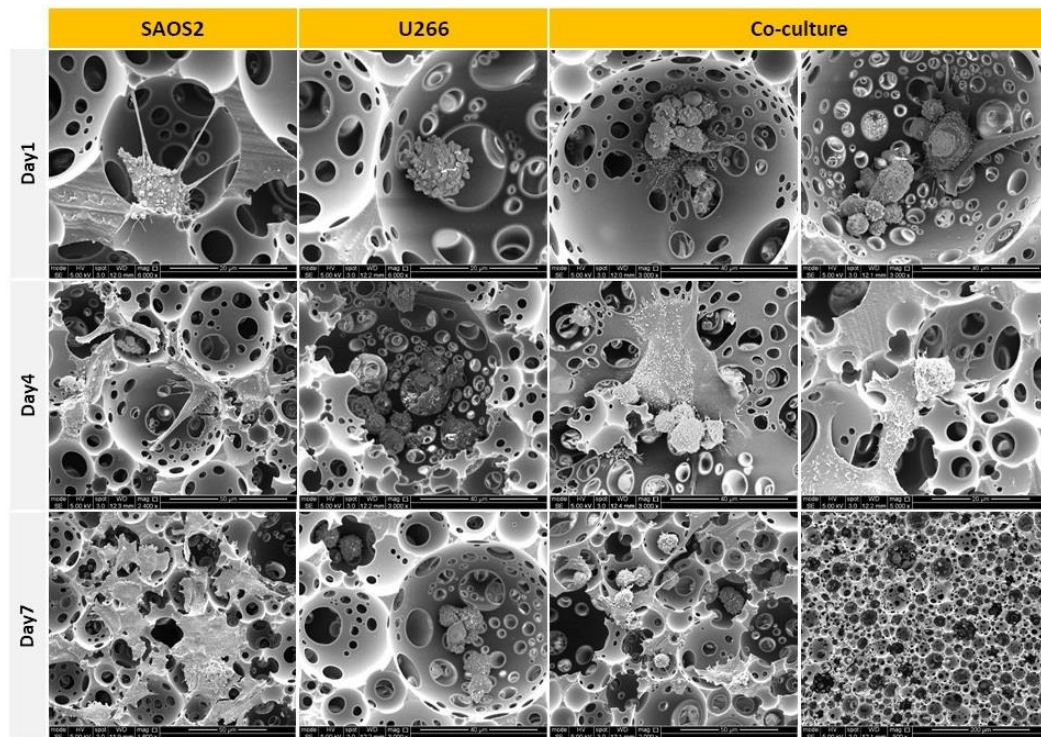


Figure 4.10 Scanning Electron Microscopy images of 3D polyHIPE scaffolds with MPC mono- or cocultures with Saos-2 Cells:

Images kindly taken and provided by Betül Aldemir Dikici showing U266 MPCs and Saos-2 osteoblast like cells cultured on polyHIPE scaffolds a monoculture or coculture at day 1, 4 and 7.

Next it was important to determine if Ad[CE1A] was able to penetrate the scaffolds and kill U266 cells within it, this was compared to BTZ which can penetrate the pores. U266 MPCs were cultured on scaffolds for 7 days. U266 polyHIPE scaffolds were treated with Ad[CE1A] at an MOI 20 (based off of the original seeding density, as cell counts could not be easily performed) or BTZ 2.5 nM or in combination. AlamarBlue® analysis was performed as previously described. Ad[CE1A] and BTZ were able to penetrate and kill MPCs within the scaffold compared to untreated controls (Figure 4.11). Whilst no statistics could be performed due to low n numbers (n=1), it is clear that Ad[CE1A] was able to penetrate the scaffolds and kill the MPC line. Therefore, PolyHIPE scaffolds may be a useful model to further investigate MM dormancy and Ad[CE1A] treatment.

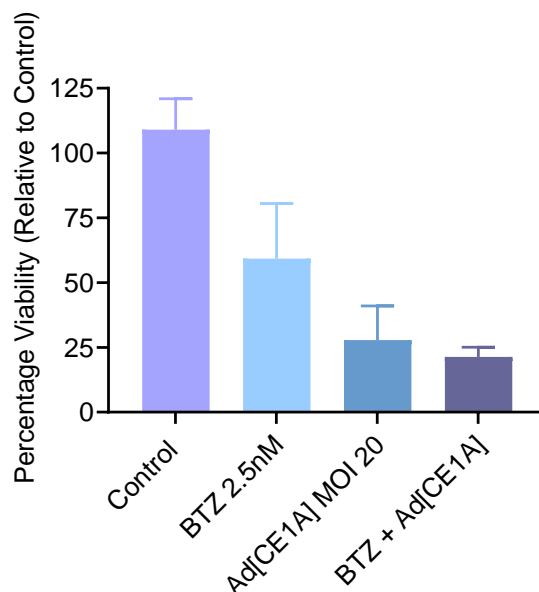


Figure 4.11: Cell viability of U266 cells after BTZ or Ad[CE1A] or combination treatment in polyHIPE scaffolds:

U266 cells were seeded on polyHIPE scaffolds for 7 days. U266 polyHIPE scaffolds were treated with BTZ 2.5 nM, Ad[CE1A] MOI 20, or the combination. Cell viability was determined by AlamarBlue® after 72 hours. n=1 Data are mean ±SD.

4.2.4.3 Ad[CE1A] Efficacy against MRD/Dormant Cells

To determine whether Ad[CE1A] can cause cell death in dormant MPCs, GFP expressing JJN-3, U266 and OMP-2 cells were labelled with Vybrant™ DID and cultured in normal 2D conditions for 14 days. After 14 days cells were treated with Ad[CE1A] at MOI 2, 10 and 20. After a further 3 days (Day 17) the percentage of DID^{High} cells that were viable/dead and the percentage of DID^{Low} cells that were viable/dead was determined by flow cytometry (Figure 4.7). Ad[CE1A] was able to significantly increase the amount of dead cells in the DID^{High} and DID^{Low} populations compared to vehicle (PBS) control. The opposite effect was observed in the viable cells, there was a significant decrease in the percentage viable in the DID^{Low} population for all 3 cell lines. It is difficult to determine whether Ad[CE1A] was targeting true dormant cells (DID^{High}), or whether it lowered their proliferation capacity further (of an already slightly slower proliferating cell population), which killed them resulting in an increase of dead DID^{High} cells; or whether the slightly slower proliferating DID^{High} cells, as well as the

faster proliferating DID^{Low} cells were able to proliferate in the vehicle control uninhibited, effecting the percentage of dead DID^{High} cells in the vehicle control.

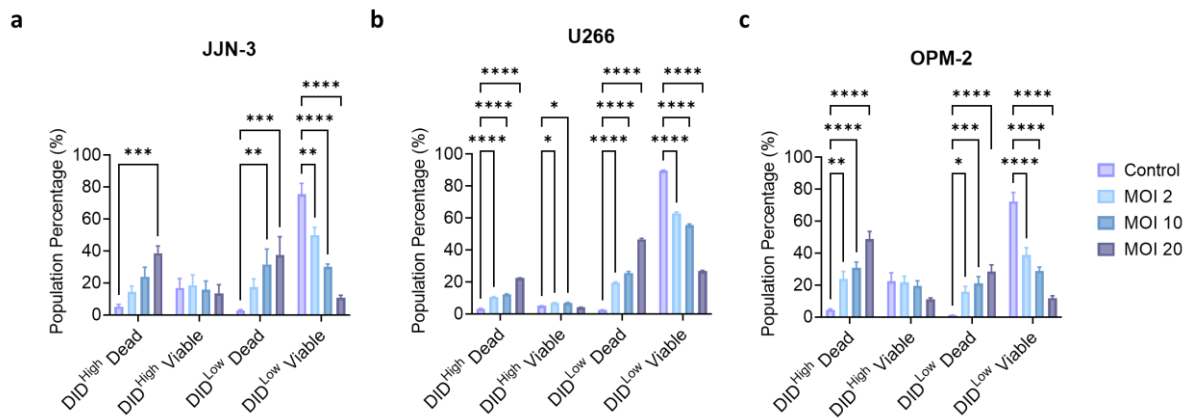


Figure 4.12 Percentage of Live/Dead Vybrant™ DID populations JJN-3, U266 and OPM-2 following Ad[CE1A] treatment:

JJN-3, U266 and OPM-2 GFP expressing cells were labelled with DID. After 14 days cells were treated with Ad[CE1A] MOI 2, 10 and 20. After 72 hours (17 days), the percentage of DID fluorescence and PI was assessed as DID^{High} dead, DID^{High} viable, DID^{Low} Dead and DID^{Low} viable cell populations. n=3 Data is the mean ±SD. P values are for 2-way ANOVA with multiple comparisons compared to control with Dunnett’s correction, where * p<0.05, ** p<0.01, *** p<0.001, **** p<0.0001.

4.3 Discussion

As discussed previously, MM patients clinically experience disease relapse due to MRD, disease can reoccur for many reasons, but one of the main reasons is chemotherapy resistance. Therefore, it was of importance to determine if Ad[CE1A] could prevent cell regrowth after MM standard of care treatment such as BTZ and to determine if Ad[CE1A] still had efficacy in treatment (BTZ) insensitive cells.

Firstly, Ad[CE1A] was able to prevent MPC line regrowth after BTZ treatment, whilst BTZ only treated MPC lines recovered viability back to the level of untreated control cells. This occurred even in low doses of Ad[CE1A], however, in JIN-3 cells by day 25, the cell viability started to recover in the lowest dose. This may be because the JIN-3 cells express CS1 at a lower level than other MPC lines, and they are more aggressive than the U266 cells. Additionally, there have been reports of cancer cells becoming resistant to OV6 (422,423), this has been observed in VSV in melanoma cells, an upregulation of APOBEC3 was thought to be the mechanism behind viral resistance (422). It has also been observed with oncolytic MVs, with the resistance thought to be due to strong IFIT1 expression after MV infection, which is a strong inducer of an active antiviral state in the host cells (423). In this study, it can only be speculated whether cell recovery at the lowest dose (MOI 1) in JIN-3 cells was due to viral resistance or a CS1-negative population recovering. Despite this, the results are encouraging as Ad[CE1A] may be able to prevent tumour regrowth in a clinical setting. Secondly, Ad[CE1A] was still effective at killing BTZ insensitive cells compared to parental cell line, suggesting Ad[CE1A] may be effective clinically in either a MRD setting or relapsed/refractory disease.

Because of this data, the efficacy of Ad[CE1A] in an *in vivo* low tumour burden model of MM was next investigated. Unfortunately, Ad[CE1A] as a monotherapy was not able to significantly reduce tumour burden at the majority of time points compared to control. This differs to what was previously shown before this project. However, the lack of reduction in tumour burden following Ad[CE1A] monotherapy could have been due to a slightly different dosing schedule compared to what was previously used. In the previous study, 1×10^7 ifu/100 μ l I.V 2x/wk was used, but in this study the dosing

schedule was changed to 2×10^7 ifu/100 μ l I.V 1x/wk. This was decided because mice were going to be treated for a longer period, and with every sequential I.V injection there is a chance of scaring and collapsing the tail vein making it harder to administer subsequent treatments. It is also interesting to note that week 10 post tumour injection, there was a significant difference in tumour burden between control and Ad[CE1A] monotherapy groups, however, the bioluminescent signal from the tumour decreased in the vehicle group at week 11 post tumour injection compared to the previous week (week 10) . This decrease in bioluminescence in the vehicle group was not from the euthanasia of mice with high tumour load (reducing the average bioluminescent signal and reducing the n numbers in the vehicle group), but from a decrease in tumour burden within individual mice from week 10 to week 11. The evidence for this is presented in Appendix Figure 8.12, but briefly, example images of the same mouse over the selected time points (week 10-13 post tumour inoculation) showed a clear loss of tumour burden within the same mouse between week 10 and 11 post tumour inoculation. When the bioluminescence data was plotted by last observation carried forward (whereby once a mouse is euthanised, the last data point received from that mouse is carried forward for the subsequent time points), the same drop in tumour burden is seen. This phenomenon was also seen in the BTZ only treated group between week 15 and 16 post tumour inoculation, also evidenced in Appendix Figure 8.12. An explanation for this could be as simple as the tumour growing more rapidly in vehicle and BTZ only treated groups until the tumour becomes necrotic, and hence a loss of signal.

It is not that surprising that given the Ad[CE1A] monotherapy results, that Ad[CE1A] was not able to eradicate MRD, prevent relapse, or be efficacious against disease relapse. Again, this could be due to the same reasons above. Nevertheless, even though the tumour in the BTZ only treated mice did drop bioluminescence signal from week 15 to 16 post tumour inoculation, Ad[CE1A] did not eradicate 'MRD' in these mice, but it can be speculated that if this phenomenon did not happen, then the addition of Ad[CE1A] either as a monotherapy or as in combination could have slowed disease progression.

Other notable issues to discuss include vehicle mice surviving longer than normal, the homing of U266 cells to the ovaries and a Rotavirus outbreak in the animal facility during this study. Firstly, as mentioned, vehicle mice survived on average an extra 5 weeks more compared to what we normally see in this model. Mice normally exhibit signs of HLP or loss of weight (>10%) by week 9 post tumour injection, but after week 10 is when the drop in bioluminescence signal was seen. It can be speculated that this drop in tumour signal could have accounted for the vehicle mice surviving longer than normal. On top of this, U266 cells homed to the ovaries which resulted in ovarian tumours, and was the primary reason most mice in the vehicle and Ad[CE1A] only treated group got euthanised. Ovary tumours in this model have never been experienced by our group before and a search of the literature yields no results of similar experiences in NSG models. As discussed earlier, NSG models have shown improved homing of MM cells to BM sites compared to NOD/SCID mice where tumour was commonly seen in skeletal and extra-skeletal sites. Clinically, extramedullary involvement is uncommon in MM, with 7-18% at diagnosis and ~20% at relapse. It has been reported to occur in the lymph nodes, skin, liver and spleen, and less frequently in the kidney, breast, testis and meninges (424–427). Therefore, MM ovarian involvement is extremely rare and has been reported in a few case studies (427,428). In patients, the mechanism of extramedullary disease is unknown, but thought to be related to alterations in adhesion molecules and chemokine receptors (424,426) or by haematogenous spread. However, in this study, it is unknown whether upon tumour cell injection, U266 cells homed to the ovary in first instance, or if they homed from BM sites to the ovary due to alterations in adhesion molecules or chemokine receptors or by haematogenous spread.

Another problem that occurred during this study, was an outbreak of murine Rotavirus within the University of Sheffield's animal facility. Rotavirus (Epizootic Diarrhoea of Infant Mice: EDIM) is a non-enveloped RNA virus that shows clinical signs (diarrhoea and distended abdomen) in young mice (<14 days old). Adult mice can be infected with Rotavirus but do not show clinical signs (429). Whilst adult mice do not show symptoms, an underlying viral infection could have a significant impact on virotherapy by upregulating antiviral immune responses which may clear

therapeutic virus more quickly or stimulate an antitumour immune response. However, the latter is less likely due to the mice being immunocompromised. One could only speculate that the mice in this study harboured Rotavirus infection which lead to lack of Ad[CE1A] efficacy.

Whilst the Rotavirus outbreak was ongoing, other lab groups and other studies within our own group were experiencing mice with ovarian tumours and sickness that was not related to the tumour load. These were in various mouse strains (immunocompetent and immunocompromised) and in various cancer models. Whilst the ovarian tumours others experienced, including another study in our group that was using the same cell line and mouse strain, were found to be of mouse origin and not of the injected cancer cells homing to ovary. There is nothing to suggest in the literature that Rotavirus causes cancer metastasis to any site let alone the ovaries. In fact, Rotavirus vaccines have been used as anticancer oncolytics and immunostimulatory agents (430). Whether these issues were caused by Rotavirus or another pathogenic organism is to be speculated, but these issues were widespread during the time of this *in vivo* study.

In conclusion, there are many variables that may have contributed to the lack of efficacy in this study, whether this was related to study design (dose schedule), factors outside our control or that Ad[CE1A] truly had no effect. Therefore, the results are inconclusive as the study may have been compromised by the factors discussed above. However, because mice studies are costly and time consuming, and without a clear defined reason as to what went wrong, it was decided that it would be irresponsible to repeat the study, as the same results may be seen. In order to conform to NC3R's guidelines, preliminary investigation into *in vitro* models of MM dormancy/MRD to try to better determine efficacy and to inform us to design better *in vivo* studies in the future.

As mentioned earlier, our research group published on osteoblasts inducing dormancy in the 5TGM1 syngeneic model of MM. In this study our research group found that dormant cells were found to be in osteoblastic niches *in vivo* and dormancy could be induced *in vitro* by culturing 5TGM1 cells in CM from either murine primary osteoblasts or MC3T3 murine osteoblast-like cell lines (337). Whilst this

has been investigated for murine MM, osteoblast induced dormancy has yet to be investigated for human MM cells.

First, investigation into the basal level of dormancy in GFP expressing MPC lines by tracking proliferation using label retention assays using Vybrant™ DID was performed. Human MPC lines exhibited a small population of DID^{High} cells by day 24 post cell labelling (4.2%-1.8%). This was a little higher than what was seen for the 5TGM1 cells which were <1% after 21 days (337). It was interesting to note that there were two noticeable populations of GFP expressing cells in all MPC lines tested, the dimmer GFP cells retained vybrant™ DID more than the brighter GFP expressing cells, this was probably due to slower proliferating cells transcribing and translating less GFP than faster proliferating cells.

Next, the potential of Saos-2 osteoblast-like cells and HS-5 BMSCs ability to induce dormancy in human MPCs was investigated. GFP expressing human MPCs were labelled with vybrant™ DID and were cultured in Saos-2 CM, HS-5 CM or their respective media controls. There was no increase in DID^{High} cells over their respective media controls. This was interesting because in the 5TGM1 cells CM from MC3T3 osteoblast-like cells induced a ten-fold increase in DID^{High} cells (337). Saos-2 cells may not be the best cell line to use for induction for MM dormancy, because the Saos-2 cells are derived from osteosarcoma tumour tissue, they can only be compared to osteoblasts to a limited extent. Also due to their cancer origin, it is likely that the majority of growth factors, cytokines/chemokines secreted increase the proliferative capacity rather than induce dormancy. However, the alternative is using primary patient osteoblasts, which can introduce issues such as a lack of standardisation between patients and the difficulty of harvesting and expanding primary osteoblasts, which can undergo de-differentiation, therefore have a finite lifespan (431,432).

It is unlikely that CM alone would induce MM dormancy, human MPCs may need direct contact with stromal and/or osteoblastic cell types in a more complex environment than tissue culture flasks. Therefore, in collaboration with Dr Frederick Claeys and his PhD student Betül Aldemir Dikici, the

use of 3D polyHIPE scaffolds (4PCLMA) were first investigated for their ability to allow MPCs to proliferate within the scaffold either alone or in culture with osteoblast like cells Saos-2; and whether Ad[CE1A] could penetrate the polyHIPE scaffolds. As discussed earlier, it was important to determine if Ad[CE1A] could penetrate the pores of the scaffold and kill MPCs. Previous experience prior to this project using sodium alginate hydrogel models to create 3D MPCs cultures, showed that Ad[CE1A] and another OV HSV1716, could not penetrate the pores of the hydrogel.

Whilst the data presented here is very preliminary and MM dormancy was not yet investigated, the results show that both Saos-2, U266 and the coculture of the two proliferate within the scaffold and stay adhered to the scaffold instead of detaching and proliferating within the surrounding media/well plate. Additionally, Ad[CE1A] was able to penetrate the scaffolds and decrease U266 viability within the scaffolds. The polyHIPE scaffolds seem like a promising avenue to investigate MM dormancy and interactions with other BM niche cells, and to test new therapies within a more complex environment than 2D tissue culture flasks.

Lastly, I wanted to determine if Ad[CE1A] could induce cell death in DID^{High} dormant MPC lines. DID labelled MPC lines were cultured in complete RMPI media and treated with Ad[CE1A] at various MOIs after 14 days. After a further 3 days (17 days in total) viability in DID^{High} and DID^{Low} populations were determined by flow cytometry. Ad[CE1A] was able to induce significant cell death in DID^{High} and DID^{Low} cells and oppositely significantly reduced cell viability in DID^{Low} cells. As mentioned in the results section, it is difficult to determine if Ad[CE1A] is targeting DID^{High} cells causing cell death or if Ad[CE1A] is slowing proliferation of already slightly slower proliferating cells causing cell death. Therefore, it is not clear if true dormant (DID^{High}) cells were targeted, or slightly slower proliferating cells. One way I could have assessed this was by culturing DID stained MPC lines until low levels of DID^{High} cells remained and then separate the DID^{High} cells from DID^{Low} cells by flow cytometry activated cell sorting. However, this would obtain a very low number of cells, and in our research group's experience, a substantial amount of cell death is observed following flow cytometry activated cell sorting.

Additionally, without performing this experiment there is no way of knowing whether once you separate the DID^{High} cells and culture them into new well plates that this might either 1) cause them to die as they are not amongst the high proliferating cells, or 2) they may start proliferating immediately, in which case you are no longer targeting 'dormant/quiescent' cells. An additional issue is that there aren't any defined markers of dormancy until recently, where AXL, a tyrosine kinase, has been shown to be highly expressed in dormant MM cells, and blocking AXL expression released the MM cells from dormancy (421).

4.4 Chapter Conclusion

As evidenced in this chapter, targeting MRD/dormant cells is complex and without *in vitro* models that have been properly assessed and optimised to test out such methods, translation *in vivo* is going to be difficult. Going forward from this thesis two PhD research students will be optimising the polyHIPE scaffold model and other 3D monoculture and coculture models with the aim of inducing dormancy in MPCs to target them with conventional or novel agents such as Ad[CE1A]. As discussed in the thesis introduction, OV's efficacy can rely on the presence of an active immune system, stimulating anti-MM immunological memory may be key to eliminate/control MRD effectively. The lack of a functional immune system used in this study could have also contributed to the lack of efficacy. Therefore in the next chapter Ad[CE1A] efficacy in a 5TGM1 immunocompetent syngeneic model of MM is investigated.



Chapter 5 : The Efficacy of Ad[CE1A] in 5TGM1 Murine Myeloma



5.1 Introduction

5.1.1 Adenovirus Serotype 5 in Murine Cells

The work presented in chapter 4 highlights the importance of developing better preclinical tumour models. As discussed in the introduction, current animal models used to evaluate the efficacy of oncolytic Ads rely on human tumour xenografts in immunodeficient murine models. Whilst these models do have their advantages such as growth of human tumour, their main disadvantage is the lack of a functional immune system. Ads, along with other OV, clearly have complex interactions with the host immune system. In the presence of an immune system, the oncolytic effects of Ads may be reduced due to immune responses against viral particles. This is an issue with xenograft models as the lack of functional immune responses in immunodeficient mice may overestimate the OV's efficacy preclinically, therefore hindering the accuracy of predicting clinical effects in human patients. On the other hand, the immune system may be recruited to sites of oncolytic activity, and induce tumour-killing by NK cells, cytokines, or tumour-specific cytotoxic T lymphocytes to enhance therapeutic outcome.

As discussed earlier, mice are considered poor model systems for therapy with replication competent human Ads because murine tumour cells are often not infected by human Ads and are generally unable to produce infectious viral progeny (268,270,433–436). However, a growing body of evidence has shown that oncolytic Ads can infect, replicate, and have antitumour efficacy in some murine tumour cells, such as ED-1 (cyclin E overexpressing lung adenocarcinoma) (437) ADS-12 (lung adenocarcinoma) (266), Pan02 (pancreatic), CT26 (colon), MB49 (bladder), 4T1 (breast), SAI (sarcoma) (438), and GL261 (glioma) (439) to name a few.

A recent literature review was published discussing the dogma that more viral replication and spread is correlated to better oncolytic efficacy, and that this is the 'dogma' of the oncolytic virotherapy field. But this review brings to light several examples that oppose the dogma (440). One study showed that several OV (HSV & VSV) showed clear differences in the replication and cytopathic effects *in vitro*. However, all had similar antitumour efficacy *in vivo* in immunocompetent mice, even when one virus

was given at a much greater dose than the other (441). This shows that *in vitro* replication and cytolytic properties can be poor prognostic indicators of *in vivo* antitumour activity. But again, direct comparisons between different species of virus against each other in the same model cannot be done as they differ in viral biology.

Another study found a negative correlation between *in vitro* replication and *in vivo* antitumour activity between two oncolytic HSV viruses. In this study they found that one HSV mutant had the 'lowest' oncolytic activity *in vitro* and was cleared the quickest *in vivo* but was the only HSV treatment to confer a significant survival benefit by increased ICD, increased HSP70 and elevated serum HMGB1, resulting in stimulation of specific CD8⁺ T cell responses (442). Again, highlighting the difference between *in vitro* and *in vivo* findings. Whilst these studies are mainly using HSV, it seems that initial viral infection leading to activation of antitumour immunity may be more important than virus replication and persistence causing direct tumour debulking. Therefore, oncolytic Ads, including Ad[CE1A] may still have efficacy in murine cells *in vivo*, even if they do not replicate well *in vitro*, or vice versa.

Additionally, the lack of efficacy Ad[CE1A] had as a monotherapy and as an agent to eradicate MRD (discussed in chapter 4) may be due to the fact a xenograft model was used. In order for Ad[CE1A] to be effective, particularly to eradicate MRD a functional immune system may need to be present, so that there is long lasting immunological memory. Therefore, it was important to investigate whether Ad[CE1A] has efficacy in murine MM.

This chapter details the efficacy of Ad[CE1A] against murine MM cells 5TGM1 *in vitro* and *in vivo*. As discussed in section 2.6, the 5TGM1 model is one of the most well-characterised syngeneic models, alongside the 5T2MM and 5T33MM models, the latter of which is where the 5TGM1 model derived from. The advantage of 5TGM1 cells is that they can proliferate *in vitro*, whilst the 5T2MM do not grow outside the BM microenvironment. Additionally, the 5TGM1 cells have been transfected with GFP and Luc. For these reasons the 5TGM1 cells were selected for our *in vitro* and *in vivo* studies.

5.1.2 Hypothesis, Aims and Objectives

5.1.2.1 Hypothesis and Aims

This chapter aimed to assess the potential of Ad[CE1A] efficacy in murine MM 5TGM1 cells. To do this the following hypothesis will be tested 'Ad[CE1A] will have oncolytic efficacy against murine 5TGM1 cells *in vitro* and *in vivo*'.

5.1.2.2 Objectives

The hypothesis was tested by the following objectives:

1. Determine CS1 expression in the murine 5TGM1 cell line
2. Determine the infection and replication efficiency of Ad[CE1A] in the murine 5TGM1 cell line.
3. Investigate the efficacy of Ad[CE1A] in the murine 5TGM1 cell line
4. Determine the Ad[CE1A] cell death mechanism in the murine 5TGM1 cell line.
5. Determine the expression of immunogenic cell death markers in 5TGM1 cell line following infection
6. Investigate the efficacy of Ad[CE1A] *in vivo* in the 5TGM1 syngeneic model.

5.2 Results

5.2.1 The 5TGM1 Murine Myeloma Cell Line Expresses CS1

Ad[CE1A] utilises CS1 for transcriptional control of the replication of essential gene *E1A*. Therefore, it was essential to test our murine MM cell line 5TGM1 for CS1 expression at the protein level. Cell surface protein expression of 5TGM1 cells were evaluated by anti-mouse CS1 antibody using flow cytometry. Almost all 5TGM1 cells highly expressed CS1 on the cell surface (99%) (Figure 5.1).

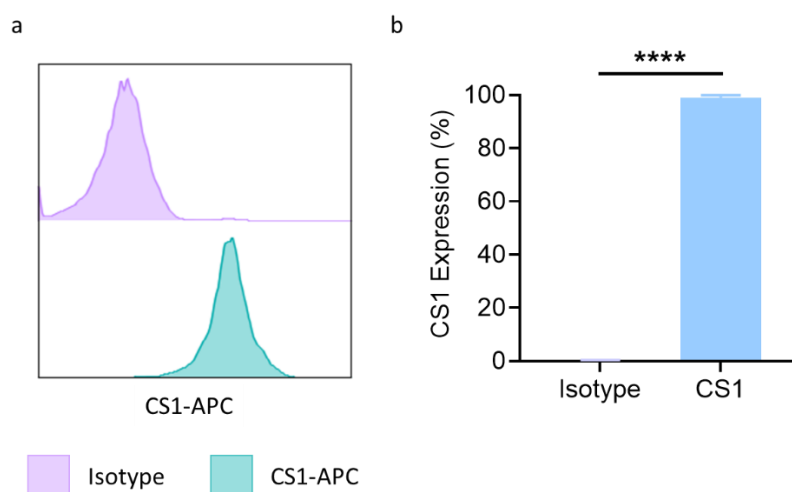


Figure 5.1: CS1 cell surface protein expression in 5TGM1 cells:

(a) Representative histogram plots of MFI of CS1 compared to isotype control in 5TGM1 cells. (b) Percentage of 5TGM1 cells with surface expression of CS1. n=3 Data is the mean \pm SD. P values are for unpaired students T test where **** $p < 0.0001$.

5.2.2 The 5TGM1 Murine Myeloma Cell Line has High Adenovirus Infection Efficiency.

As mentioned in chapter 3, one way to measure infection efficiencies in cells is by using an E1A-deleted, non-replicative GFP-expressing Ad5 vector (Ad-GFP). Ad-GFP contains a CMV promoter which drives the expression of GFP. Ad-GFP was added at a MOI of 2 and 20 to 5TGM1 cells. After 24 and 48 hours, infectivity was determined as the percentage of GFP-positive cells using fluorescence and flow cytometry (Figure 5.2). 5TGM1 cells expressed GFP after 24 hours (Figure 5.2a-c), there was a significant increase in GFP expression between time points (Figure 5.2c). There was a significant difference between MOI 2 and 20 at 24 hours (53% MOI 2, 82% MOI 20), but by 48 hours there was

no significant difference in MOIs (90% MOI2, 99% MOI 20) suggesting maximum infection rates occur after 24 hours (Figure 5.2c).

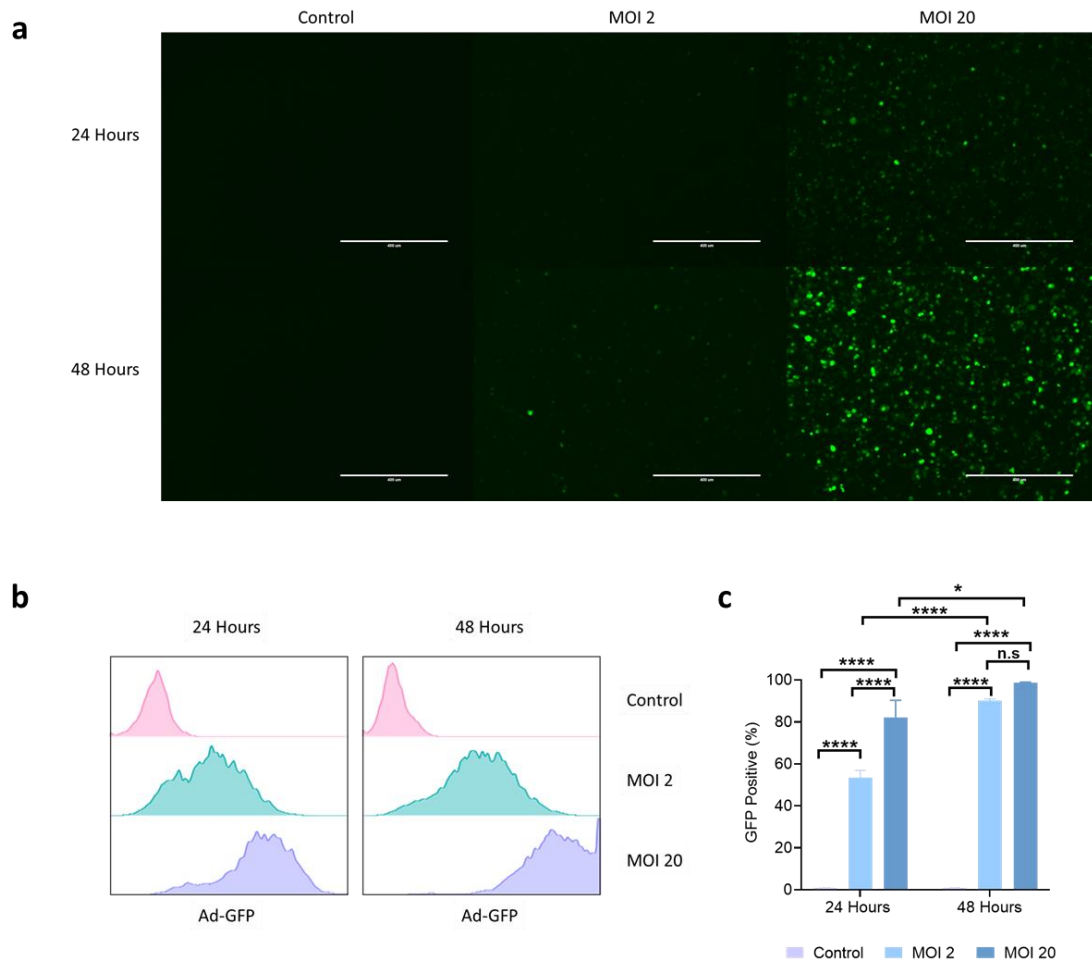


Figure 5.2 Percentage of 5TGM1 cells infected with Ad-GFP:

(a) Representative images of live fluorescent microscopy of Ad-GFP expression in 5TGM1 cell line at 24 and 48 hours after infection of Ad-GFP at MOI 2 or 20. **(b)** Representative histogram plots of MFI of Ad-GFP expression after 24 and 48 hours after infection of Ad-GFP at MOI 2 and 20. **(c)** 5TGM1 cells were infected with Ad-GFP MOI 2 or 20 or vehicle (PBS) control. After 24 and 48 hours GFP expression was determined using flow cytometry. Percentage of cells with GFP expression shown. n=3 Data is the mean \pm SD. P values are for 2-way ANOVA with multiple comparisons with Šidák's correction, where * p<0.05; **** p<0.0001.

5.2.3 Ad[CE1A] Replicates in the 5TGM1 Murine Myeloma Cell Line.

Given that the 5TGM1 cell line expresses CS1, it is important to determine if Ad[CE1A] can express *E1A* using the human CS1 promoter in 5TGM1 cells, and whether this results in viral progeny. To do this the essential viral replication gene *E1A* was assessed by RT-qPCR, then the ability of 5TGM1 cells to generate intact infectious virions was assessed. Firstly, *E1A* mRNA expression was determined by RT-qPCR in 5TGM1 cells compared to human MPC lines J2N-3 and U266. 5TGM1, J2N-3 and U266 cells were treated \pm Ad[CE1A] MOI 20. After 4- and 24-hours total RNA was extracted from the cells, which was then reverse transcribed to cDNA and assessed by RT-QPCR using SYBR™ green primers for *E1A*. Figure 5.3 shows relative *E1A* expression over time in J2N-3, U266 and 5TGM1 (n=3). *E1A* expression increased over time in the 5TGM1 cells and in the human MPCs J2N-3 and U266. After 24 hours, *E1A* expression was significantly higher in the U266 cells than in the 5TGM1 cells, but there was no significant difference between 5TGM1 and J2N-3 at 24 hours.

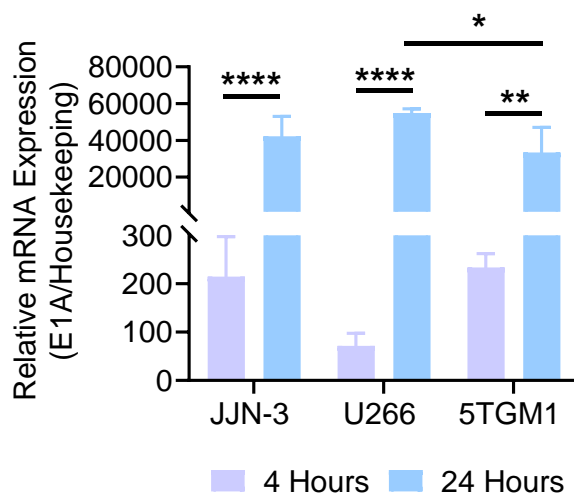


Figure 5.3: *E1A* mRNA expression in 5TGM1 cell lines compared to J2N-3 and U266 human MPCs:

Relative *E1A* mRNA expression in 5TGM1, J2N-3 and U266 cells relative to untreated control by RT-qPCR at 4 and 24 hours post Ad[CE1A] infection (MOI 20). Housekeeping gene for J2N-3 and U266 was GAPDH, for 5TGM1, the housekeeping gene was B2M. n=3 Data is the mean \pm SD. P values are for 2-way ANOVA with multiple comparisons with Šidák's correction, where * $p < 0.05$; ** $p < 0.01$, **** $p < 0.0001$.

Next, the ability of the 5TGM1 cells to produce infectious viral progeny compared to human MPC lines JJN-3 and U266 was assessed. 5TGM1, JJN-3 and U266 cells were infected with Ad[CE1A] MOI 2. After 24 hours any exogenous Ads in culture medium was removed by centrifugation and cells resuspended in fresh complete medium. 48 hours after this (72 hours after initial infection) cells were lysed by freeze/thaw cycles to release virus. Viral lysate was harvested, and viral titre was assessed using the Adeno-X™ Rapid titre viral quantification kit. There was no significant difference in the amount of infectious viral progeny between 5TGM1 cells and human MPC lines JJN-3 and U266 (Figure 5.4).

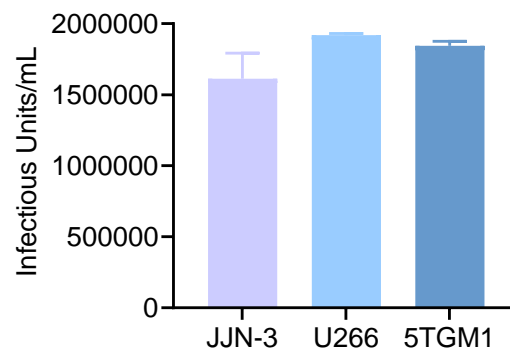


Figure 5.4: Infectious virion production in 5TGM1 cells compared to JJN-3 and U266 cells:

5TGM1, JJN-3 and U266 cells were infected with Ad[CE1A] (MOI 2) for 24 hours. After 24 hours exogenous Ad[CE1A] was removed, and MPCs were resuspended in fresh medium. After 72 hours, cells were collected in CM and the cells were lysed to collect viral particles withing the cells. Viral titres were determined by Adeno-X™ rapid titre viral quantification kit. n=3 Data is the mean ±SD.

5.2.4 Ad[CE1A] Causes Oncolysis in the 5TGM1 Murine Myeloma Cell Lines.

To test the oncolytic activity of Ad[CE1A] in the 5TGM1 cells, a dose and time response assay was performed. 5TGM1 cells were treated with an MOI of 2, 10 and 20 and cell death was determined by PI staining using flow cytometric analysis at 24, 48 and 72 hours post infection. 5TGM1 cells showed a significant dose and time response to Ad[CE1A] treatment (Figure 5.5). With the highest amount of cell death seen at 72 hours for all doses with MOI 20 having the biggest response. The dose and time response to Ad[CE1A] in the 5TGM1 cells was similar, if not better, to what was seen in JJN-3 and U266 cells discussed in chapter 3, (Figure 3.10).

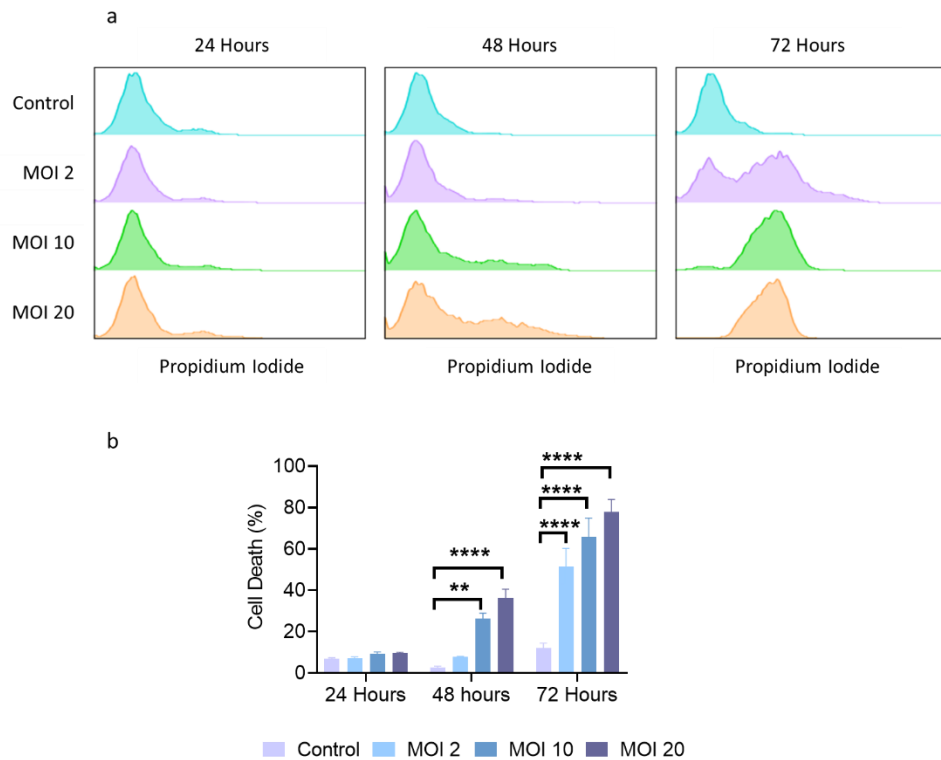


Figure 5.5: Percentage of 5TGM1 cells dead after incubation with Ad[CE1A]:

5TGM1 cells were treated with Ad[CE1A] at MOI 2, 10 and 20. Cell death was determined by PI staining using flow cytometric analysis after 24, 48 and 72 hours. **(a)** Representative histogram plots of PI MFI in 5TGM1 cells after Ad[CE1A] treatment at indicated doses and time points. **(b)** Percentage of cell death in 5TGM1 cells after Ad[CE1A] treatment. n=3 Data is the mean \pm SD. P values are for 2-way ANOVA with multiple comparisons compared to control with Dunnett's correction, where ** $p < 0.01$; **** $p < 0.0001$.

5.2.5 The Involvement of Apoptosis in Ad[CE1A]-induced Cytotoxicity in the 5TGM1 Cell Line

5.2.5.1 Annexin V Assay

As discussed in chapter 3, it appears Ad[CE1A] does not induce caspase dependent apoptosis in human MPC lines, therefore, it was important to find out if this was also the case for 5TGM1 murine MM cells. 5TGM1 cells were treated with Ad[CE1A] MOI 20. At 6 and 24 hours after treatment cells were stained with Annexin-V-FITC and PI and assessed by flow cytometry. At 6 hours, there was no significant difference in Annexin V positivity between control and Ad[CE1A] treated, however by 24 hours there was a significant increase in Annexin V positivity (Figure 5.6). This raise in Annexin V expression after 24 hours was similar to what was seen in human MPC lines (Chapter 3 Figure 3.20).

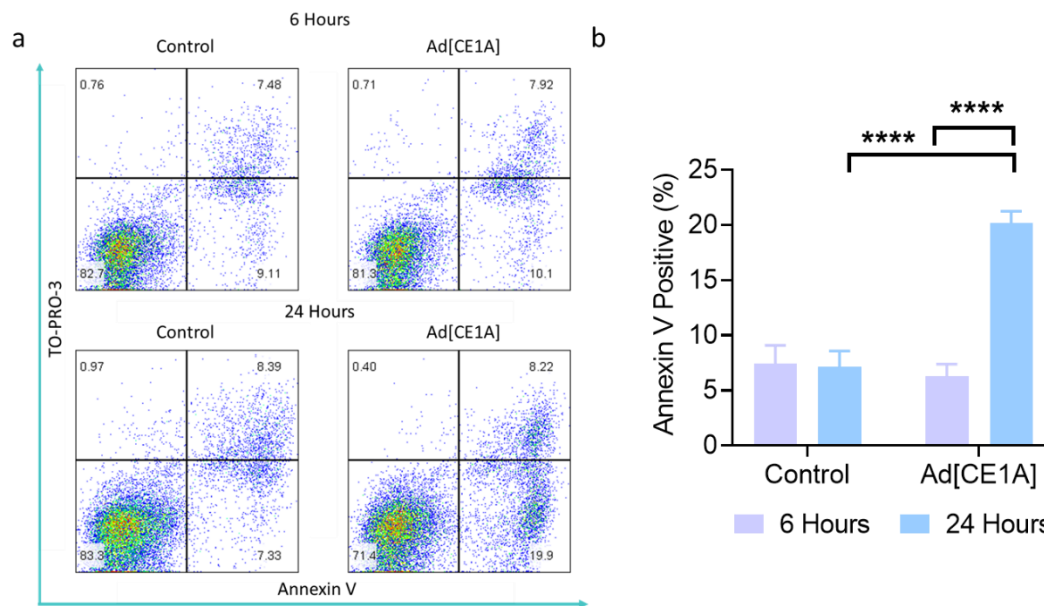


Figure 5.6: Percentage Annexin V positive 5TGM1 cells after Ad[CE1A] treatment:

5TGM1 cells were incubated with Ad[CE1A] MOI 20. Annexin V expression was determined by flow cytometry at 6 and 24 hours post treatment. **(a)** Representative scatter plots of Annexin V against TO-PRO-3 after Ad[CE1A] treatment at indicated time points compared to controls. **(b)** Percentage of Annexin V expression after Ad[CE1A] treatment compared to untreated controls. n=3 Data is the mean \pm SD. P values are for 2-way ANOVA with multiple comparisons with Šidák's correction, where * $p < 0.05$; ** $p < 0.01$, **** $p < 0.0001$.

5.2.5.2 Pharmacological Inhibition of Caspases

Because a significant increase in Annexin V staining was detected, similar human MPCs, next was to determine if whether blocking caspase activity had an effect on Ad[CE1A]-induced cell death. To determine whether caspases were involved in Ad[CE1A] cytotoxicity, 5TGM1 cells were treated with Ad[CE1A] MOI 10 \pm the cell permeable irreversible pan-caspase inhibitor Z-VAD-FMK (50 μ M) or respective controls. After 72 hours the percentage of dead cells were analysed by PI staining using flow cytometry (Figure 5.7). Addition of Z-VAD-FMK did not significantly alter Ad[CE1A]-induced cell death, this is in agreement with what was observed in human MPCs (Chapter 3 Figure 3.22).

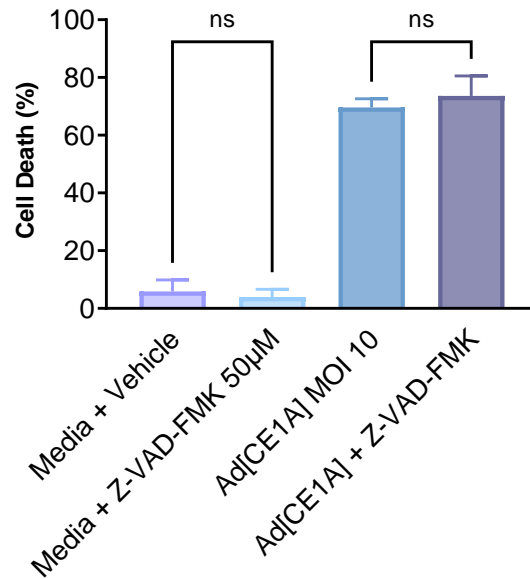


Figure 5.7 Ad[CE1A] response in 5TGM1 cells in the presence of the pan caspase inhibitor Z-VAD-FMK:

5TGM1 cells were incubated with Ad[CE1A] MOI 10 ± 50 µM Z-VAD-FMK. After 72 hours, the percentage of cell death was determined by PI staining using flow cytometry. n=3 Data is the mean ±SD. P values are for one-way ANOVA with multiple comparisons with Tukey's correction.

5.2.6 The Involvement Necroptosis in Ad[CE1A] Cytotoxicity in 5TGM1 Cell Line

The results presented above give evidence that Ad[CE1A]-induced cytotoxicity is caspase-independent, as was observed in the human MPCs. Therefore, investigation into other mechanisms of regulated cell death were performed. As mentioned in the section 3.2.11, necroptosis is a form of regulated cell death that is caspase independent which generally manifests with a necrotic morphotype. Therefore to assess whether necroptosis was a cell death mechanism involved in Ad[CE1A]-induced cytotoxicity in 5TGM1 cells, pharmacological inhibition of two of the main proteins involved in this pathway, RIPK1 and RIPK3 was performed. For similar studies in the human MPC lines, inhibition of a third protein was performed, MLKL. However, this could not be assessed in the 5TGM1 cells as the commercially available MLKL inhibitor NSA does not inhibit murine MLKL.

5.2.6.1 Pharmacological Inhibition of RIPK1

Firstly, investigation into whether blocking RIPK1 could alter Ad[CE1A]-induced cytotoxicity by using an inhibitor for RIPK1, Nec-1, was conducted. 5TGM1 cells were treated with Ad[CE1A] (0.1-1000 MOI) \pm 10 μ M Nec-1 (non-toxic dose determined by dose response curves Appendix Figure 8.5) and cell viability was determined by an AlamarBlue[®] assay after 72 hours. Additionally, 5TGM1 cells were treated with Ad[CE1A] MOI 10 \pm 10 μ M Nec-1 and cell death was determined by PI staining using flow cytometry (Figure 5.8). Addition of Nec-1 did not alter Ad[CE1A]-induced cell death in 5TGM1 cells, similar to what was observed in human MPC lines (Chapter 3, Figure 3.23).

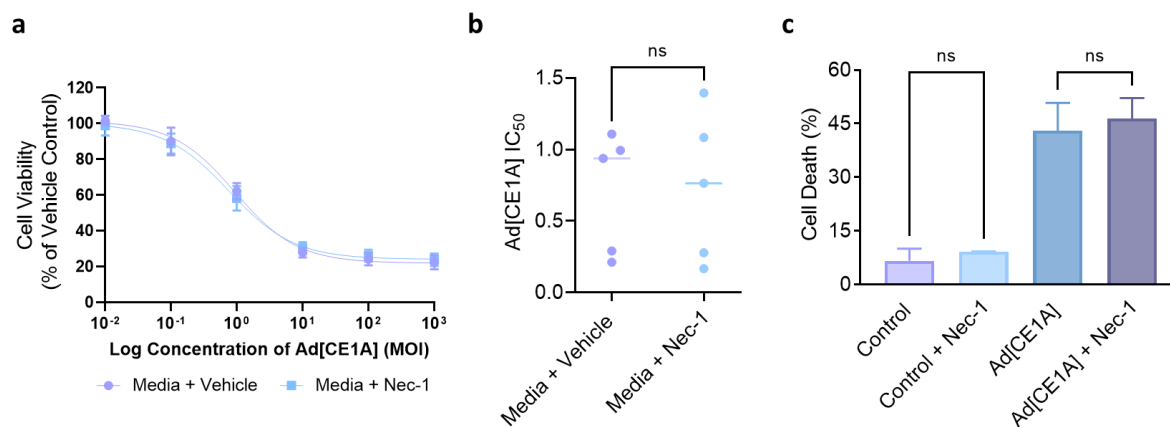


Figure 5.8 Ad[CE1A] response in 5TGM1 cells in the presence of RIPK1 inhibitor Nec-1:

(a) Dose response of Ad[CE1A] (0.1, 1, 10, 100, 1000 MOI) in 5TGM1 cells after 72 hours \pm 10 μ M Nec-1. Cell viability was determined by AlamarBlue[®] assay. **(b)** IC₅₀ values for Ad[CE1A] \pm 10 μ M of Nec-1 determined by sigmoidal dose response curves from 5 independent repeats. $n=5 \pm$ SD, p values are for 2-way ANOVA with Šidák's correction. **(c)** Percentage of 5TGM1 cell death after incubation with Ad[CE1A] MOI 10 \pm Nec-1 in 5TGM1 cells. After 72 hours, the percentage of cell death was determined by PI staining using flow cytometry. $n=3$ Data is the mean \pm SD. P values are for one-way ANOVA with multiple comparisons with Tukey's correction.

5.2.6.2 Pharmacological Inhibition of RIPK3

Secondly, investigation into whether blocking RIPK3 could alter Ad[CE1A]-induced cytotoxicity by using an inhibitor for RIPK3, GSK-872, was conducted. 5TGM1 cells were treated with Ad[CE1A] (0.1-1000 MOI) \pm 1 μ M GSK-872 (non-toxic dose determined by dose response curves Appendix Figure 8.13) and cell viability was determined by an AlamarBlue[®] assay after 72 hours. Additionally, 5TGM1 cells were treated with Ad[CE1A] MOI 10 \pm 1 μ M GSK-872 and cell death was determined by PI staining

using flow cytometry (Figure 5.9). Addition of GSK-872 did not alter Ad[CE1A]-induced cell death in 5TGM1 cells, similar to what was observed in human MPC lines (Chapter 3 Figure 3.24).

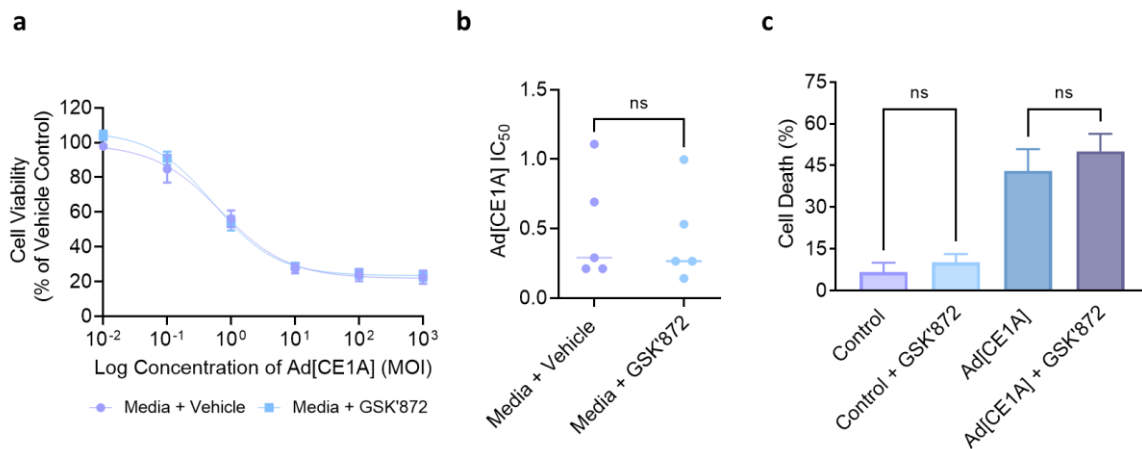


Figure 5.9 Ad[CE1A] response in 5TGM1 cells the presence of the RIPK3 inhibitor GSK-872:

(a) Dose response of Ad[CE1A] (0.1, 1, 10, 100, 1000 MOI) in 5TGM1 cells after 72 hours \pm 1 μ M GSK-872. Cell viability was determined by AlamarBlue[®] assay. **(b)** IC₅₀ values for Ad[CE1A] \pm 1 μ M of GSK-872 determined by sigmoidal dose response curves from 5 independent repeats. n=5 \pm SD, p values are for 2-way ANOVA with Šidák's correction. **(c)** Percentage of 5TGM1 cell death after incubation with Ad[CE1A] MOI 10 \pm GSK-872 1 μ M in 5TGM1 cells. After 72 hours, the percentage of cell death was determined by PI staining using flow cytometry. n=3 Data is the mean \pm SD. P values are for one-way ANOVA with multiple comparisons with Tukey's correction.

5.2.7 The Expression of Immunogenic Cell Death Markers in Ad[CE1A] Infection.

Next, investigation into the expression levels of ICD markers in Ad[CE1A] infected in 5TGM1 cells was explored. This is particularly important as expression of these markers may increase antitumour immune responses towards 5TGM1 cells *in vivo* when using the syngeneic model.

5.2.7.1 Cell Surface Calreticulin Exposure

As mentioned in chapter 3 (section 3.2.12.1), CALR translocates to the cell surface following ICD where it functions as a pro-phagocytotic signal. Therefore, to determine whether CALR is exposed following Ad[CE1A] treatment, 5TGM1 cells were treated with vehicle or Ad[CE1A] (MOI 2, 10 and 20). After 24 hours cells were stained with a primary polyclonal anti-CALR antibody and subsequently a secondary FITC conjugated antibody and analysed by flow cytometry, infected 5TGM1 cells were compared to vehicle control in non-permeabilised cells (Figure 5.10). After 24 hours, CALR exposure was only significantly increased at MOI of 20, this effect was similar to what was observed in human MPC lines (Figure 3.26), except significance was also reached at the MOI 10 and 20 in human MPCs.

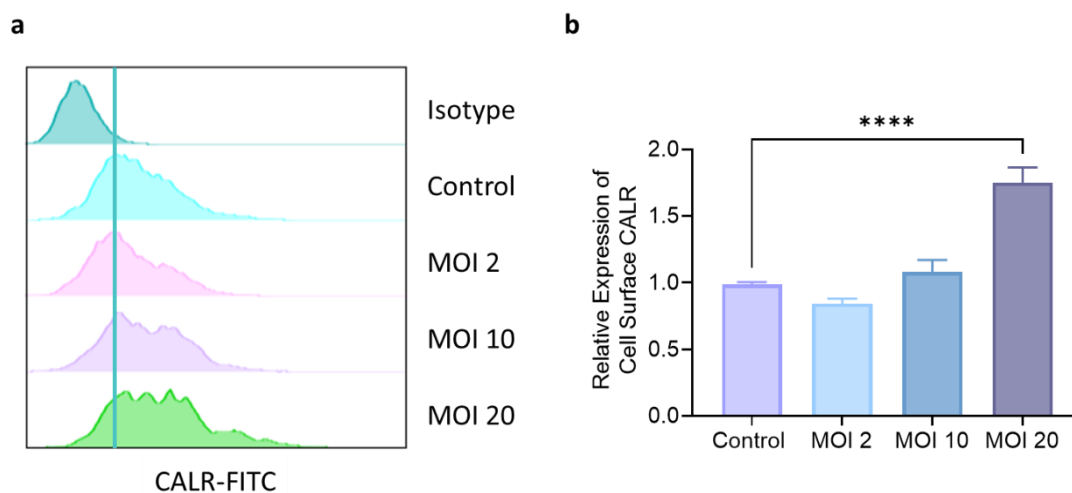


Figure 5.10 Cell surface calreticulin exposure following Ad[CE1A] treatment in 5TGM1 cells:

5TGM1 cells were treated with vehicle control or Ad[CE1A] at an MOI of 2, 10 or 20. After 24 hours, cells were stained with a polyclonal anti-CALR antibody and a FITC fluorescently labelled secondary antibody and TO-PRO-3 and then analysed by flow cytometry. **(a)** Representative histogram plots of CALR in viable 5TGM1 cells following Ad[CE1A] treatment. **(b)** Non-permeabilised cells were gated (TO-PRO-3 negative) and relative MFI compared to vehicle control was determined. $n=3$ Data is the mean \pm SD. P values are for one-way ANOVA with multiple comparisons compared to control with Dunnett's correction, where **** $p < 0.0001$.

5.2.7.2 Extracellular ATP Release

As mentioned in chapter 3 (section 3.2.12.3), ATP release is a major DAMP associated with ICD. To determine if ATP is secreted following Ad[CE1A] infection, 5TGM1 cells were treated with vehicle control or Ad[CE1A] MOI 2, 10 or 20. After 24 hours supernatant was collected from cells and ATP was determined by the ENLITEN® ATP assay, which is a luminescence-based assay which relies on the chemical reaction of ATP with D-luciferin (Figure 5.11). In 5TGM1 cells, there was a dose response increase in extracellular ATP, but this only reached significance at MOI 20, this dose-response effect was similar to what was observed in human MPC lines (Figure 3.28), except significance was also reached at the MOI 2, 10 and 20 (for JJN-3) or MOI 10 and 20 (for U266 and OPM-2).

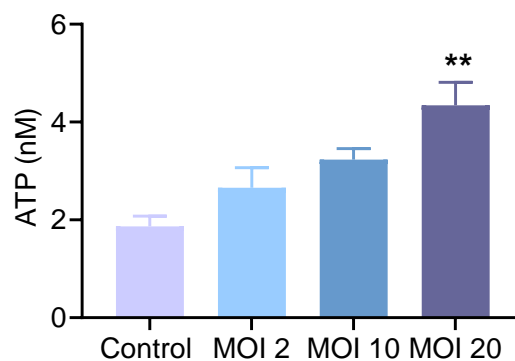


Figure 5.11 Extracellular release of ATP following Ad[CE1A] treatment in 5TGM1 cells:

5TGM1 cells were treated with vehicle control or Ad[CE1A] at an MOI of 2, 10 or 20. After 24 hours cell supernatant was collected and ATP concentration was determined using the ENLITEN® ATP assay using an ATP standard curve. n=3 Data is the mean \pm SD. P values are for one-way ANOVA with multiple comparisons compared to control with Dunnett's correction, where ** $p < 0.01$.

5.2.8 Efficacy of Ad[CE1A] against 5TGM1 in a Syngeneic Model.

As Ad[CE1A] showed similar efficacy in 5TGM1 cells compared to human MPCs, Ad[CE1A] efficacy was next tested *in vivo* in the 5TGM1 C57BL/KaLwRij model. Ad[CE1A] efficacy was tested at two doses, low dose (1×10^7 ifu/100 μ l) and high dose (1×10^8 ifu/100 μ l) by I.V injection, or high dose by I.P injection compared to tumour vehicle control (PBS). This was a proof of principle study, so Ad[CE1A] treatment started before tumour was detected at 3 days post tumour inoculation. Mice were treated

twice/week for a total of 4 weeks before sacrifice. Tumour was monitored over time by *in vivo* bioluminescent imaging and at end stage by *ex vivo* flow cytometry and Kappa IHC.

5.2.8.1 *In vivo* Tumour Bioluminescent Imaging

Mice were imaged twice weekly for 4 weeks by bioluminescent imaging. Figure 5.12a shows *in vivo* bioluminescent images of one representative mouse over time. Average hind limb bioluminescence over time showed that by day 24, mice treated with low dose I.V or high dose I.P had significantly lower tumour burden than vehicle control, and by day 27, all Ad[CE1A] treated mice had significantly lower tumour burden than vehicle control, despite a large SD in the vehicle treated mice (Figure 5.12b). When plotting average hind limb bioluminescence at day 27 (Figure 5.12c), a large variability in vehicle tumour burden was seen. Despite this, all Ad[CE1A] treatment groups had significantly lower tumour burden than vehicle control. The number of individual bioluminescent signals were counted as the number of disseminated tumour sites (Figure 5.12d). All Ad[CE1A] treatment groups resulted in significantly less tumour sites than vehicle control. Interestingly, in all these parameters (average bioluminescence in hind limbs over time, average bioluminescence in hind limbs at end point and number of disseminated tumour sites), low dose I.V and high dose I.P showed higher significance than high dose I.V compared to vehicle control, but there was no significance difference between the Ad[CE1A] groups.

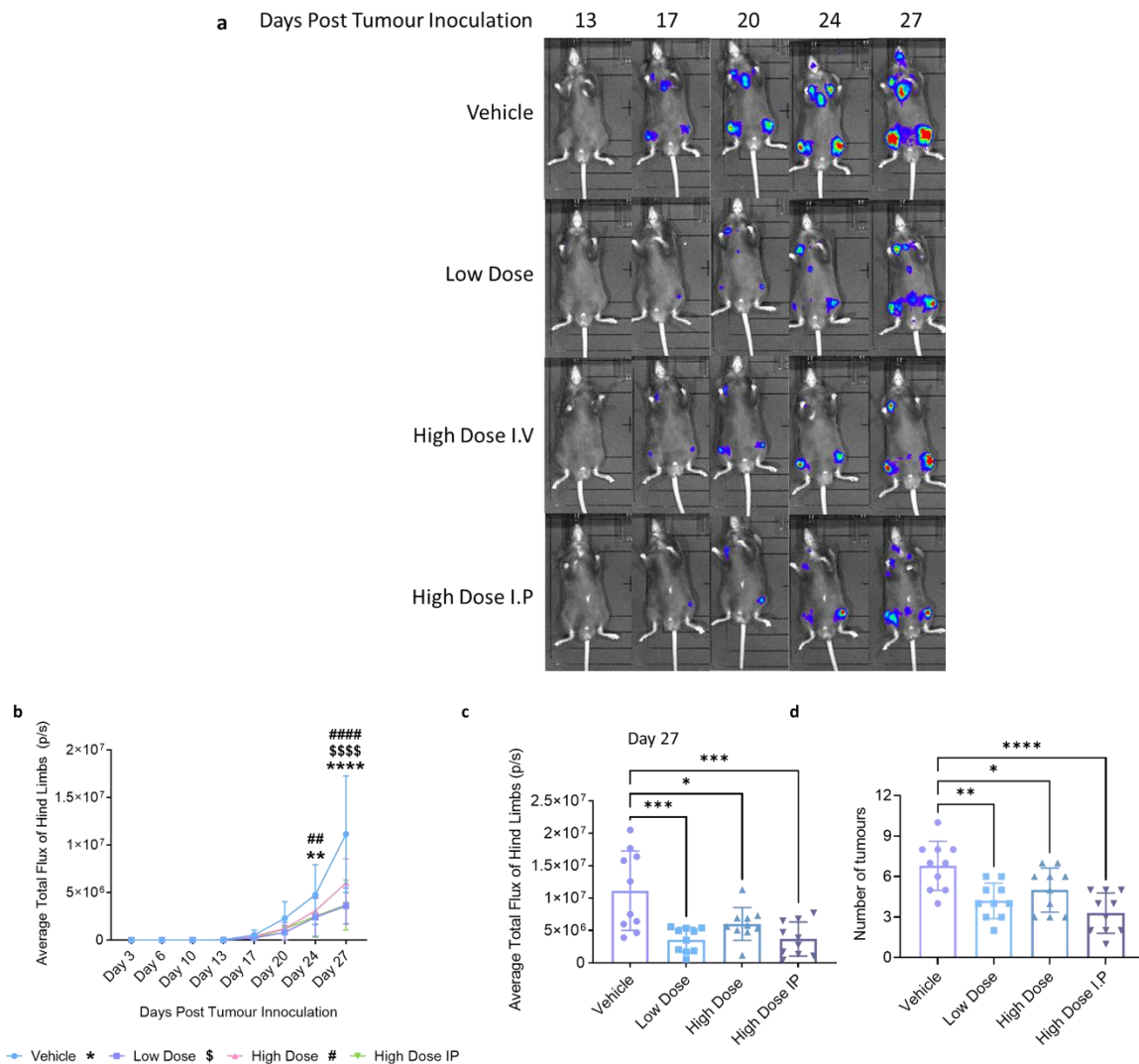


Figure 5.12: Analysis and quantification of *in vivo* tumour burden in 5TGM1 bearing C57BL/KaLwRij mice treated with vehicle or Ad[CE1A] at two doses by two routes of admission:

5TGM1 bearing mice were IVIS imaged 2x/week from day 3 post tumour inoculation. Treatment started at a day 3 post tumour inoculation. **(a)** Representative images of *in vivo* bioluminescence imaging over time of 5TGM1 bearing C57B/KaLwRij mice treated with vehicle or Ad[CE1A] at either low dose I.V, high dose I.V, or high dose I.P. One representative mouse per group. **(b)** Average total flux of hind limbs over time. N=10 Data is the mean \pm SD. P values are for 2-way ANOVA with multiple comparisons with Tukey's correction, where ** $p < 0.01$, **** $p < 0.0001$. * Denotes significance between vehicle and low dose I.V, \$ denotes significance between vehicle and high dose I.V and # denotes significance between vehicle and high dose I.P. **(c)** Average total flux of hind limbs at day 27. n=10 Data is the mean \pm SD. P values are for one-way ANOVA with multiple comparisons compared to vehicle control with Dunnett's correction, where * $p < 0.05$; *** $p < 0.001$. **(d)** Number of disseminated tumour sites at day 27. n=10 Data is the mean \pm SD. P values are for one-way ANOVA with multiple comparisons compared to vehicle control with Dunnett's correction, where * $p < 0.05$; ** $p < 0.01$ *** $p < 0.001$.

5.2.8.2 *Ex vivo* Tumour Burden Analysis by CD138 Staining using Flow Cytometry.

After sacrifice the BM was flushed from the left femora and stained with CD138-APC or isotype matched control and analysed using flow cytometry. Figure 5.13a shows representative flow cytometry scatter plots of CD138 positive staining from one representative mouse per group; figure 5.14(b) shows percent of CD138 positive cells. Figure 5.13b shows a reduction of tumour in the low dose and high dose I.P group, however this did not reach significance. It is important to note that tumour burden was not high in the femora in the vehicle group, as over half the mice had MGUS levels of BM infiltration (<10% CD138⁺ cells) in the femora by flow cytometric examination (Figure 5.13.b). This corresponds with the bioluminescence images (Figure 12a), as the signal appears to be mainly in the anatomical area of the tibia and fibula. Despite this not reaching significance, it follows the same trend as the bioluminescent analysis, where there was a trend that low dose Ad[CE1A] and high dose Ad[CE1A] I.P had a lower tumour burden than high dose I.V. Ad[CE1A].

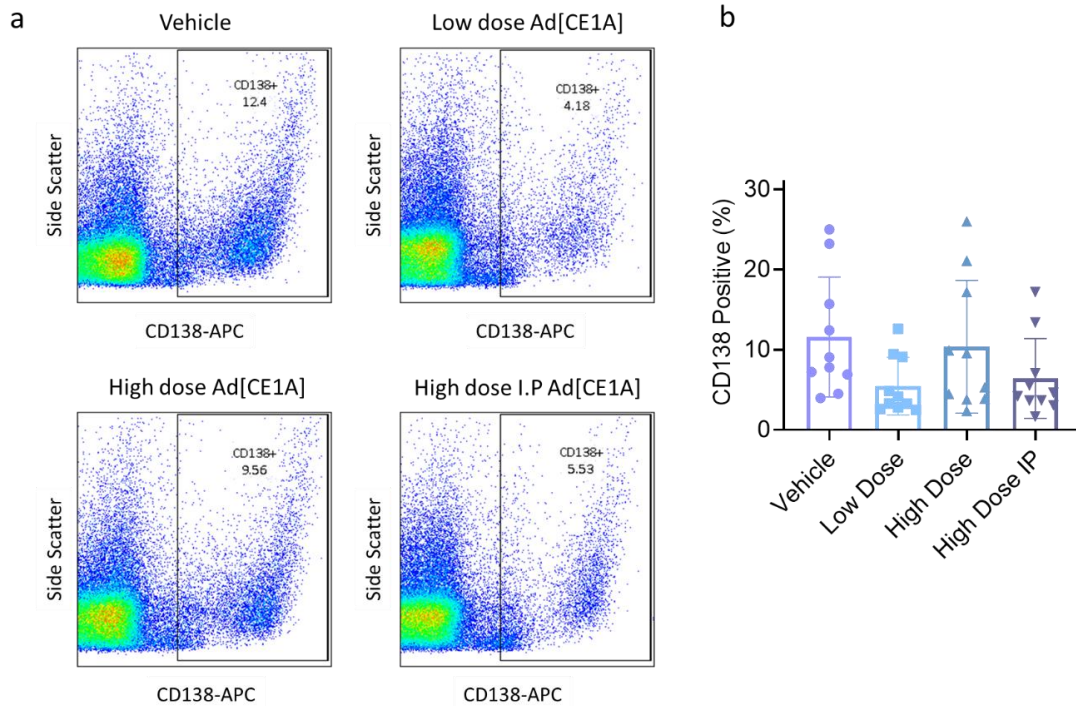


Figure 5.13: Percentage of BM cells expressing CD138 in 5TGM1 bearing C57BL/KaLwRij mice following treatment with vehicle or Ad[CE1A] at two doses by two routes of admission:

5TGM1 bearing mice were treated with vehicle (PBS) or Ad[CE1A] at either low dose I.V, high dose I.V, or high dose I.P 2x/week. After 4 weeks mice were sacrificed and the BM from left femora was flushed, and cells were stained with an anti-mouse CD138 APC conjugated antibody. **(a)** Representative flow cytometry plots of CD138 staining from one representative mouse per group. **(b)** Percentage of CD138⁺ cells were gated on viable BM marrow cells (PI) and fluorescence was assessed by flow cytometry. n=10 Data is the mean \pm SD. P values are for one-way ANOVA with multiple comparisons compared to vehicle control with Dunnett's correction.

5.2.8.3 *Ex vivo* Tumour Burden Analysis by Immunohistochemistry.

Both left and right tibias were formalin fixed, paraffin embedded, sectioned, and stained with an anti-Kappa antibody to detect Kappa light chain secreting 5TGM1 cells (Figure 5.14). All Ad[CE1A] treatment groups significantly reduced tumour burden compared to vehicle control. Similar to the *in vivo* bioluminescent data (Figure 5.12), low dose I.V and high dose I.P Ad[CE1A] treatment reduced tumour burden more significantly than high dose I.V Ad[CE1A] compared to vehicle control, but there was no significant difference between the three treatment groups. The vehicle tibias showed much higher BM infiltration than in the femurs, where the average BM infiltration of total cellular BM space was approximately 60%.

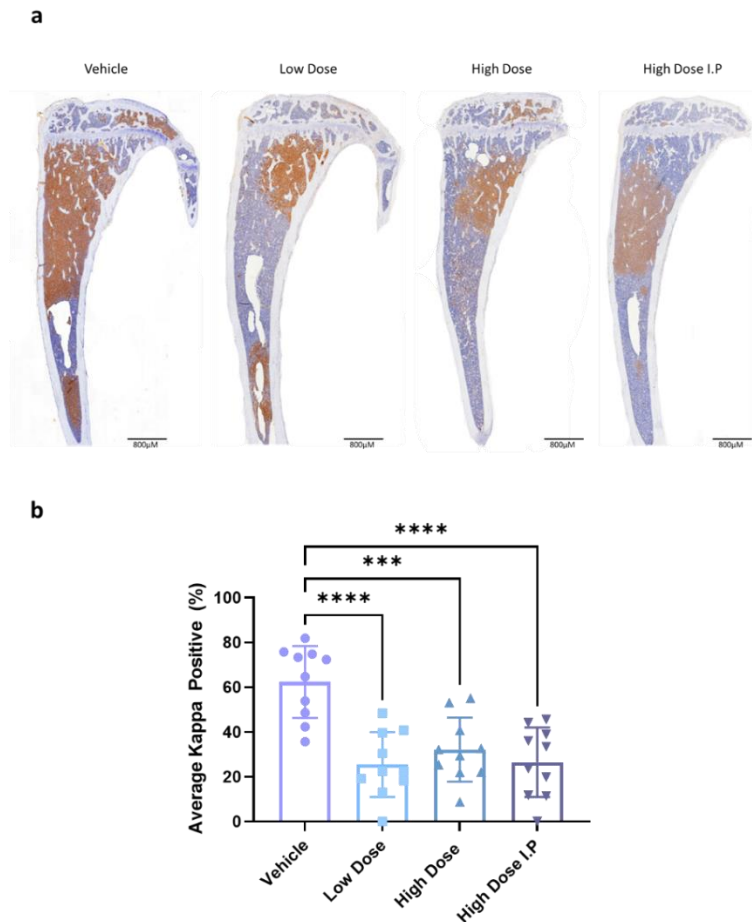


Figure 5.14: Kappa IHC staining in the tibiae of 5TGM1 bearing C57BL/KaLwRij mice following treatment with vehicle or Ad[CE1A] at two doses by two routes of admission:

5TGM1 bearing mice were treated with vehicle (PBS) or Ad[CE1A] at either low dose I.V, high dose I.V, or high dose I.P 2x/week. After 4 weeks mice were sacrificed, left and right tibiae were stained *ex vivo* for Kappa light chains by IHC. **(a)** Representative images of the left tibia in one representative mouse per group. Images taken on QuPath software from slide scanned images. **(b)** Average percentage of Kappa positive cells within the total cellular BM space from both left and right tibiae per mouse per group. n=10 Data is the mean ±SD. P values are for one-way ANOVA with multiple comparisons compared to vehicle control with Dunnett's correction, where *** $p < 0.001$, **** $p < 0.0001$.

5.2.8.4 *Ex Vivo* Micro-CT Analysis of Trabecular Bone Loss

The percentage trabecular bone volume was also assessed following Ad[CE1A] treatment, as reducing tumour burden can decrease MM-associated bone disease. Left and right tibiae were scanned by micro-CT and analysis of trabecular bone volume, number, thickness and separation were analysed (Figure 5.15). Analysis of these parameters showed no significant difference compared to vehicle control tibiae. It is important to note that no bone disease was observed in vehicle treated mice at time of sacrifice.

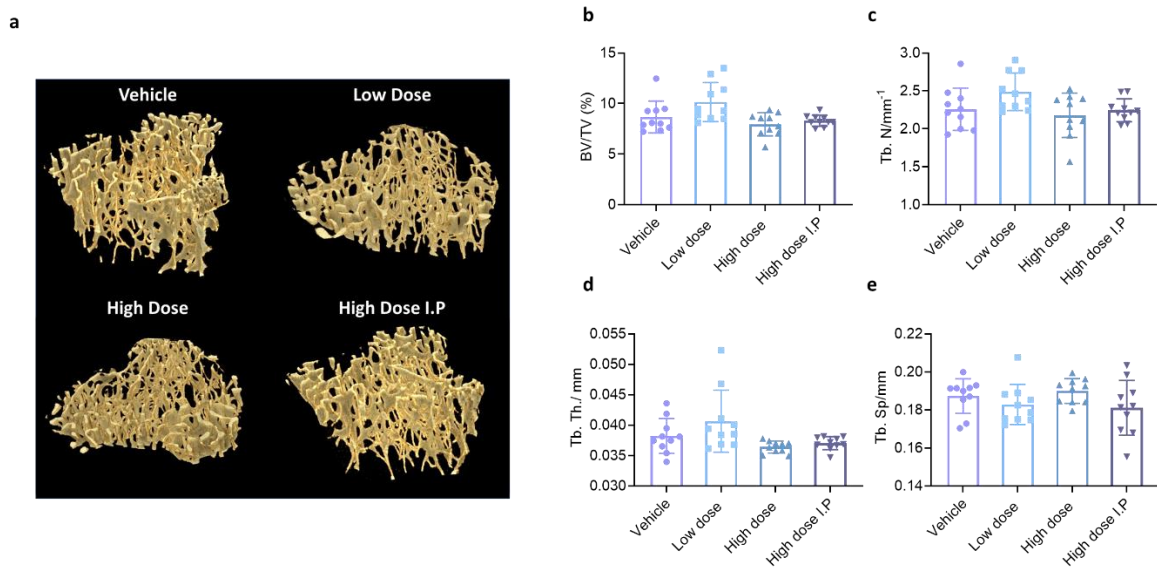


Figure 5.15 Micro-CT analysis of tibias in 5TGM1 bearing C57BL/KaLwRij mice following treatment with vehicle or Ad[CE1A] at two doses by two routes of admission:

5TGM1 bearing mice were treated with vehicle (PBS) or Ad[CE1A] at either low dose I.V, high dose I.V, or high dose I.P 2x/week. After 4 weeks mice were sacrificed, left and right tibiae were assessed for bone disease using micro-CT. **(a)** Micro-CT images in 5TGM1-bearing mice after treatment with vehicle or Ad[CE1A] low dose I.V, high dose I.V or high dose I.P. Analysis of trabecular **(b)** bone volume (BV/TV%), **(c)** number (Tb.N/mm³), **(d)** thickness (Tb.Th./mm) and **(e)** separation (Tb.Sp/mm) in tibias in 5TGM1-bearing mice after treatment with vehicle or Ad[CE1A] low dose I.V, high dose I.V or high dose I.P. n=10 Data is mean \pm SD. P values are for one-way ANOVA with multiple comparisons compared to vehicle control with Dunnett's correction.

5.2.8.5 *Ex vivo* Analysis of Presence of Ad[CE1A]

The presence of Ad[CE1A] in the BM of 5TGM1 mice was assessed *ex vivo* by RT-qPCR assessing expression levels of *E1A*. Mice were sacrificed the day after final treatment, yet no expression of *E1A* could be detected in the BM at that time, CT values were above the CT cut off threshold of 35 or undetermined by the machine (Figure 5.16). This could indicate that the Ad[CE1A] was cleared quickly after treatment due to increased anti-viral immune clearance following repeated treatments, or that Ad[CE1A] was not able to reach the tumour site in large enough amounts for other reasons, such as dilution via the blood or by poor escape from the vasculature. Additionally, the RNA was extracted from the right femora, as discussed in section 5.2.8.3, 5TGM1-bearing mice had little to no tumour in their left femora as determined by CD138 staining using flow cytometry, most tumour was located in the tibias evidenced by the bioluminescence images and the anatomical position of the mice.

Therefore, expression of *E1A* in the femora would be expected to be low/absent. However, when staining mice tibias with either an antibody detecting Ad hexon or *E1A*, no specific virus staining could be observed either, and/or background staining could not be completely eliminated from tibias. When staining the liver to determine if the liver was clearing the virus, no specific staining could be observed and there was little to no background staining (Appendix Figure 8.14). Therefore, at the point of sacrifice presence of Ad[CE1A] could not be detected.

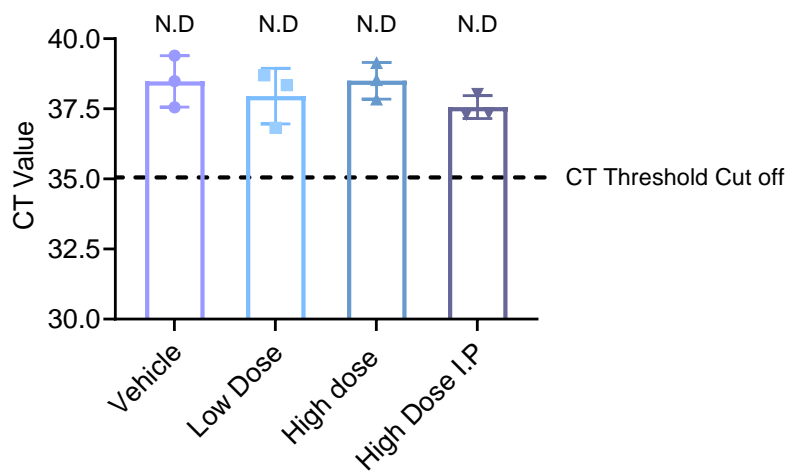


Figure 5.16 Analysis of *E1A* expression in 5TGM1-bearing C57BL/KaLwRij mice following treatment with vehicle or Ad[CE1A] at two doses by two routes of admission:

5TGM1 bearing mice were treated with vehicle (PBS) or Ad[CE1A] at either low dose I.V, high dose I.V, or high dose I.P 2x/week. After 4 weeks mice were sacrificed, and total RNA was extracted from right femora of 5TGM1-bearing mice and *E1A* was assessed by RT-qPCR. CT values of *E1A* were plotted. n=3 Data is the mean \pm SD.

5.2.8.6 Proinflammatory Cytokine Secretion from 5TGM1 Bearing Mice

Next, determination into whether there was an immune mediated response following Ad[CE1A] treatment in 5TGM1 bearing mice was investigated. In section 5.2.7 there was an increased exposure of CALR and extracellular ATP in the 5TGM1 cells in response to Ad[CE1A] and in Chapter 3 I observed bystander cytokine killing from BMMCs, therefore, investigation to determine whether any proinflammatory cytokines were secreted in response to Ad[CE1A] was performed, which may inform future research decisions and experiments.

Serum samples from 5TGM1 bearing mice were taken from terminal cardiac bleeds at sacrifice. 200 μ L of serum were pooled together from 4 individual mice from each group and analysed via a membrane-based sandwich immunoassay which detected an array of proinflammatory mouse cytokines (Figure 5.17). Following image analysis and the quantification of pixel intensity for each spot, 8 cytokines were detected in the serum (CXCL13, C5/C5a, IFN- γ , IL-17, CXCL1, M-CSF, CXCL12 and TIMP-1). The pixel density for each spot in the treatment groups were determined relative to vehicle. A cut off of ≥ 1.5 -fold increase or ≤ 0.65 -fold decrease was deemed to be significant and measurable as per the literature. Variation was observed amongst relative cytokine secretion within the different Ad[CE1A] treatment groups, however no cytokine expression was increased over 1.5, but cytokines IL-16 and CXCL12 were decreased below the ≤ 0.65 -fold in mice treated with Ad[CE1A] high dose I.V and high dose I.P.

Expression of CXCL12 and its receptors subsequently excite the downstream signalling pathways to affect tumour angiogenesis, proliferation and chemoresistance, therefore CXCL12 is a target for therapy which will be discussed later (see chapter discussion 5.3) (443). Therefore, reducing CXCL12 expression may be beneficial due to reducing CXCL12 protumour effects. IL-16 is a chemoattractant, growth factor and differentiation factor for CD4 cells and has implications in the development of inflammation, however, more recently IL-16 has been associated with the onset and progression of haematopoietic cancers, including MM (448), which will be discussed later (see chapter discussion section 5.3). Therefore, reducing IL-16 expression may be beneficial due reducing MM progression.

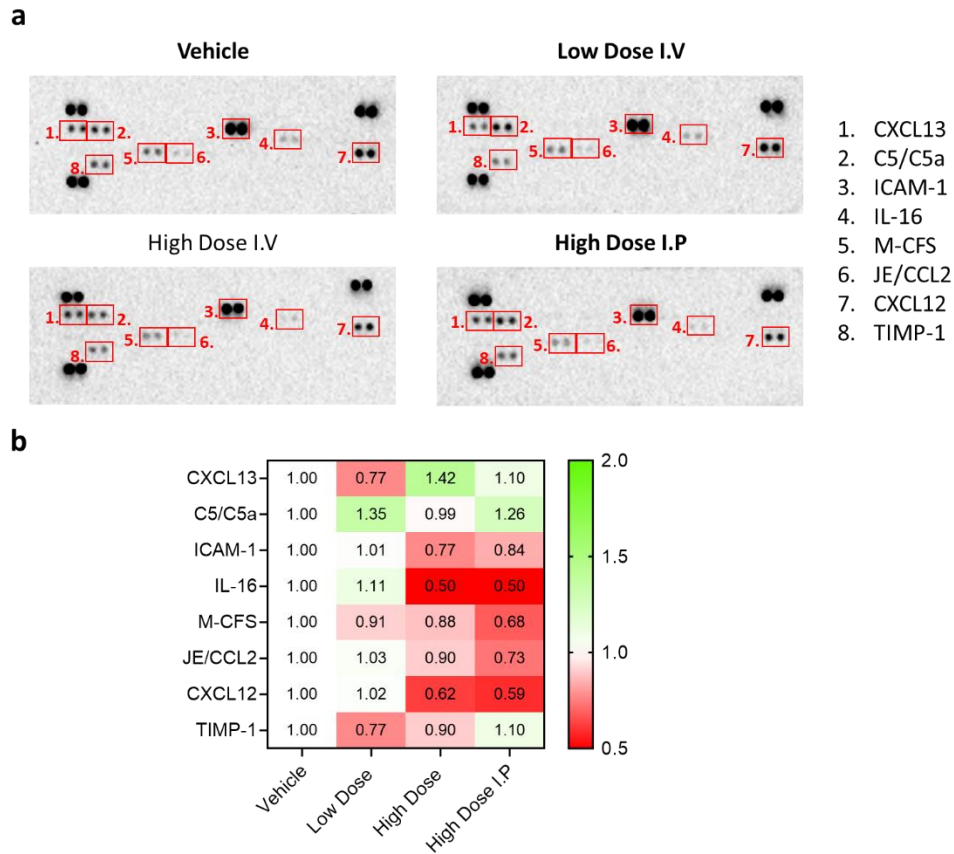


Figure 5.17 Proinflammatory cytokine secretion from serum in 5TGM1 bearing C57BL/KaLwRij mice following treatment with vehicle or Ad[CE1A] at two doses by two routes of admission:

5TGM1 bearing mice were treated with vehicle (PBS) or Ad[CE1A] at either low dose I.V, high dose I.V, or high dose I.P 2x/week. After 4 weeks mice were sacrificed, and serum was collected from whole blood samples from terminal cardiac bleeds. 50 μ L of serum from four mice per group (with average representative tumour burden) were pooled together and assessed using a sandwich-based immunoassay **(a)** Images obtained from sandwich-based immunoassay used for densitometry analysis with an annotated numbered key corresponding to each cytokine. **(b)** Heatmap showing fold-change differences compared to vehicle treated mice. n=1 for each group.

5.3 Discussion

The assessment of novel biological therapies in immunocompetent models is very important. This is especially true for OVAs, given how the immune system response may have potential importance to overall efficacy. As discussed in the introduction (section 3.1.2), Ad replication is species specific with serotype 5 being specific to humans, which has limited their preclinical testing in xenograft mouse models.

Murine MM 5TGM1 cells showed similar infection and replication kinetics *in vitro* to human MPC lines. As discussed previously, recent research implies that human Ads can infect and replicate in some murine cancer cells, resulting in significant oncolysis. In contrast, one paper states infection and viral gene transcription of Ad5 in murine ovarian cancer cells is efficient, however, there is a profound failure of productive virion production with late protein expression being poor (445). The authors stated this to be down to lack of viral mRNA loading onto ribosomes, therefore, cannot be translated. This does not appear to be the case for 5TGM1 cells as they had the same amount of infectious virion progeny (as indicated by viral titre assays) as the human MPC lines. Therefore, it appears that 5TGM1 cells can be infected by Ad[CE1A], leading to virus transcription and translation resulting in virus progeny and 5TGM1 cell oncolysis. This highlights the differences between cell types of different origin and possibly viral biology as the virus used in this paper was E1A-CR2 deleted (pRb binding site). To also confirm 5TGM1 cell death was due to lytic viral replication rather than apoptotic shut down due to viral infection, Annexin V staining was performed, which showed a significant increase in Annexin V positivity after 24 hours, this was similar to the levels seen in human cells as discussed in chapter 3 (section 3.2.10). 5TGM1 cells appeared to undergo cell death in a similar manner to human MPCs as addition of inhibitors of caspases, RIPK1 and RIPK3 had no effect on Ad[CE1A]-induced cytotoxicity. Additionally, 5TGM1 cells expressed markers of ICD, similar to human MPC lines, but required higher MOIs to reach significance at the same time point. Possibly if these markers were assessed at later time points, a significant difference may have been observed at the lower MOIs. Unfortunately, I was unable to assess whether inhibiting MLKL had any effect on Ad[CE1A] induced cytotoxicity in 5TGM1

cells, but as was discussed in chapter 3 further work is needed to try to fully elucidate the mechanism(s) involved in Ad[CE1A]-induced cytotoxicity in MM cells.

Furthermore, it would be ideal to test Ad[CE1A] efficacy on multiple murine MM cells, but as discussed earlier (section 5.1) other murine MM cells in the 5T series do not proliferate *ex vivo* and it would be a risk to jump straight to other 5T *in vivo* models without previous *in vitro* experimentation.

Another issue is that Ad[CE1A] uses the human CS1 (hCS1) promoter. As discussed earlier (section 1.4.5.3), the major regulatory unit of *SLAMF7* promoter contains an atypical TATA box and putative-binding sites for BLIMP-1/PRDM1 and C/EBPs, with BLIMP-1 being identified as a pivotal transcriptional activator. Deletion of this region decreased *SLAMF7* promoter activity in healthy NK and B cells (292). However, the promoter segment contains three putative-binding sites for Ikaros family flanking the BLIMP-1-binding site. The authors found that when MPC lines were treated with Len, which targets Ikaros, it decreased *SLAMF7* transcription which was strongly correlated to expression levels of Ikaros. Whilst BLIMP-1 expression was not consistently associated with Len-induced changes in *SLAMF7* expression levels. The authors then went on to show, using ChIP assays, that Ikaros bound downstream of the IKZF-binding site (290). These results suggest *SLAMF7* transactivation is mostly driven by Ikaros in human MM cells, unlike NK and B cells. The murine CS1 (mCS1) promoter was found to be regulated by YY1 in B cells (291). However, the mCS1 promoter region also contains four IKZF putative binding sites, therefore it is likely that IKZF-binding transactivates the CS1 promoter in human and murine cells infected with Ad[CE1A]. Nevertheless, it is clear that at least some of the regulatory mechanisms in the hCS1 and mCS1 promoters are distinct based on previous research (292). Despite the apparent distinct regulatory mechanisms, the hCS1 promoter can efficiently use mouse transcription machinery, as evidenced by similar *E1A* levels between human and murine MPCs.

Due to Ad[CE1A] showing similar efficacy in 5TGM1 cells compared to human MPC lines, Ad[CE1A] was tested in the 5TGM1 syngeneic murine model. Ad[CE1A] was administered 3 days post tumour inoculation for maximum effect, as normally this model is aggressive (~3 weeks) and a longer treatment window was wanted. Ad[CE1A] was administered twice a week, two doses were administered I.V, low dose (used in previous studies) and high dose to determine if there was a dose response. The treatment schedule was selected at 2x/week, as this schedule showed efficacy in the U266 xenograft model that was performed prior to this PhD, whilst 1x/week showed no efficacy in the same U266 model. Ad[CE1A] was also administered at high dose I.P, this was performed to see if this route of administration had efficacy, as I.V administration is technically more difficult, and can result in venous collapse and scaring to the tail vein making subsequent repeat administrations increasingly difficult. Interestingly, when conducting the study, tumour growth with 5TGM1-luc cells were much slower than what is normally seen/expected with this model when using WT-5TGM1 cells and GFP-expressing 5TGM1 cells (3 weeks). Mice were culled at 4 weeks, despite not having extremely high bioluminescence signal (comparatively to NSG models by end point) or displaying signs of end stage disease. This was done as a precaution because I was unaware if the Luc expression was weak in the cells or if all cells were expressing Luc which could account for a decreased signal. Additionally, the fur on the mice hind limbs was not shaved, so the black fur could have blocked some bioluminescent signal.

Despite this, all Ad[CE1A] treatment groups resulted in significant reduction in tumour compared to vehicle control by bioluminescent imaging and immunohistochemistry in the tibia. However, flow cytometry showed a trend for lower tumour burden in the low dose and high dose I.P group but this did not reach significance. Although as discussed earlier, levels of tumour in the femur in the vehicle group were predominantly at MGUS levels, therefore 5TGM1 cells had not sufficiently infiltrated the BM of the femora. There did not appear to be a dose-response, and high dose I.V Ad[CE1A] showed less significance from vehicle than low dose I.V and high dose I.P Ad[CE1A]. An explanation for this could be that high dose I.V Ad[CE1A] may elicit a stronger anti-viral immune response so may be

cleared quicker than low dose I.V or high dose I.P. What is interesting is that high dose I.P treatment showed efficacy. One study using HSV-1 in peritoneal carcinomas showed that I.P injection resulted in better tumour targeting than I.V injection (due to the tumour being in the peritoneum), additionally, I.P administration restricted systemic delivery compared to I.V, which resulted in the lethal dose 50 (LD₅₀) being higher in the I.P treated group as they were less off target toxicity (446). Similar antitumour efficacy has been found with an oncolytic Ad administered I.P to treat peritoneal cancers (447,448). I.P injected agents are obviously ideal for abdominal cancers, however, I.P injected agents are absorbed slower than agents delivered by I.V injection. Therefore it would be interesting to do biodistribution studies with Ad[CE1A] and different routes of administration.

There was also no detection of bioluminescent signal in the spine, upon dissection, mice did not appear to have splenomegaly, and no MM-related bone disease was observed by micro-CT analysis. As mentioned, the 5TGM1-luc transfected cells appear to grow slower in C57BL/KawLRij mice, and this has been observed anecdotally with other groups (personal communication, Dr Ryan Bishop). Therefore, mice were either sacrificed early before MM bone disease and splenomegaly could occur or the 5TGM1-luc cells do not home to the spleen or cause bone disease compared to WT-5TGM1 and 5TGM1-GFP.

Disappointingly, I was unable to detect the presence of Ad[CE1A] in the BM by RT-qPCR and IHC or in the liver by IHC. As discussed in the results, this could indicate increased viral clearance, or the inability of Ad[CE1A] to reach the tumour sites, however, because Ad[CE1A] showed a therapeutic effect it is unlikely to be the latter.

Encouragingly, the results from the microarray suggest that Ad[CE1A] may modulate the BM microenvironment as a decreased expression in CXCL12 and IL-16 was observed after both I.V and I.P high dose Ad[CE1A] treatments. As discussed in section 5.2.8.6, IL-16 and CXCL12 both mediate pro-MM effects. CXCL12 is constitutively expressed by stromal cells, fibroblasts and epithelial cells in the tumour microenvironment, signalling the proliferation of CXCR4 positive tumour cells in a paracrine

manner (443). In MM BMSC cocultures, CXCL12 downstream signalling (CXCR4 and CXCR7) were pharmacologically blocked which resulted in re-sensitisation of MPC cells to anti-MM agents (Vorinostat, Pom, BTZ and Carfilzomib) (449). The CXCR4/CXCL12 axis has been shown to regulate homing, adhesion, invasion, migration and mobilisation of MM cells out of the BM (450). High expression levels of CXCR4 alongside high integrin and adhesion molecule expression have been observed in chemo-resistant MRD MM plasma cell clones (451). Abrogating the CXCR4/CXCL12 pathway has been shown to deregulate haematopoietic cells from colonising the BM (452). Therefore, reducing CXCL12 expression by Ad[CE1A] may be beneficial as it may enhance MPCs chemosensitivity and reduce further MPC BM colonisation.

Researchers have previously tried to target CXCL12/CXCR4 axis by OV. Several OVs have been investigated alongside CXCR4 targeting either by genetically manipulating them to express CXCR4 antagonists or genetically manipulating them to target CXCR4/7 (453–455). Oncolytic VV expressing CXCR4 antagonist in triple-negative 4T1 breast syngeneic model resulted in higher intertumoral VV concentration and increased efficacy than other unarmed VVs. Additionally, reduced metastasis was observed after primary tumour resection and increased overall survival (453), a similar effect was also observed in ovarian cancer models by the same research group (454). One study retargeted an oncolytic Ad to CXCR4 and CXCR7, which was tested in breast cancer cells. The modified Ad infected breast cancer cells more efficiently than WT Ad. Additionally, the retargeting modification did not interfere with the viruses oncolytic ability (455).

IL-16 is an emerging factor in cancer pathogenesis. Increased levels of IL-16 have been correlated to the onset and progression of various cancers (e.g., renal, breast, lung), including MM (448). For MM, elevated serum IL-16 levels correlated with increased disease severity, which were found to decrease following chemotherapy (460,461). Overexpression of IL-16 in MM patients has been found to be directly attributed to the tumour cells, where it acts as a growth factor for CD4 and/or CD9-expressing MPCs. Inhibiting IL-16 with either siRNA or antibodies resulted in >80% reduction in cell proliferation

(462). Therefore reducing IL-16 expression by Ad[CE1A] may be beneficial as it may further reduce MM proliferation.

5.4 Chapter Conclusion

The results presented in this chapter give evidence that Ad[CE1A] has efficacy in 5TGM1 cells *in vitro* and *in vivo*, therefore, the 5TGM1 syngeneic immunocompetent model can be used in future research to assess Ad[CE1A]. For the future *in vivo* studies in this model, Ad[CE1A] treatment will be delayed until mice have sufficient disseminated tumour, as this is more clinically relevant. Most importantly, like in previous *in vivo* models investigating Ad[CE1A] treatment, not all tumour was eradicated following Ad[CE1A] monotherapy in the 5TGM1 syngeneic model, therefore, combination treatments might be required to potentiate the effect of Ad[CE1A] to induce a complete and sustained anti-MM response. This line of investigation will be explored in the next chapter.



Chapter 6 : Preclinical Investigation of Ad[CE1A] in Combination with Anti- myeloma Therapies



6.1 Introduction

6.1.1 Adenovirus in combination in Multiple Myeloma

OVs are promising new treatments for cancer patients, with some patients, including MM patients, already appreciating the benefits from their development (135,458). As discussed previously, the mechanisms for OVs to cause antitumour responses happens through a multitude of events, from causing simple oncolysis to the more complex modification of tumour micro and macro-environment and modulation of the immune response (310). Despite the multi-mechanistic therapeutic activity, most viruses, including Ads, demonstrate low to moderate response rates in clinical trials as a monotherapy in solid cancers (459). This is also what has been observed pre-clinically in our research group with Ad[CE1A] *in vivo* (Chapter 1, 4 & 5) . Only two phase I trials have been published with OVs (MVs and RV) in MM and these have had a focus on safety rather than efficacy, so it remains to be seen how effective OVs are in clinic (68,105). Despite this, and as discussed previously (section 1.3.6) one MM patient receiving MV therapy had an outstanding clinical response (105).

For OVs to be curative as a monotherapy in MM, they would either have to directly infect and kill the vast majority (if not all) MM cells, and/or induce a potent systemic antitumour immune response, making it unlikely that OVs as a monotherapy will completely eradicate widespread disseminated disease in the majority of patients. Therefore, strategies to potentiate OVs or sensitise MM cells to their killing will be important if larger cohorts of patients are to benefit. While initial clinical investigation with Ad[CE1A] will likely be as a single agent in heavily advanced MM disease, future trials may explore combinations with current standard of care therapies in a wider cohort of patients. Results from the first completed clinical trial utilizing oncolytic RV in MM support the need for combinational treatment to enhance antitumour responses (464), which has resulted in a phase Ib clinical trial with RV in combination with Len or Pom (MUK eleven; NCT03015922), which is underway in MM with the results yet to be published. However, pending the results of an Ad[CE1A] single agent phase I trial in MM, it is likely that combination therapy trials will be initiated. Combining OVs with

approved therapies have the added benefit that there is a known safety profile, which helps when determining possible adverse interactions.

At present, very little is known about oncolytic Ad interactions with anti-MM standard of care drugs/drug classes in MM, including Ad[CE1A]. To design trials with greater chance of success, it is necessary to better understand the interactions between these treatments. Preclinical investigations can provide insight into optimal timing, dose and route of administration, as well as any potential toxicities related to the combination. Therefore, drugs from four different drug classes used as MM standard of care treatments were chosen for use in this chapter. BTZ (Velcade[®]), a proteasome inhibitor, Melph (Alkeran[™]), a nitrogen mustard alkylating agent, Pan (Farydak[®]), a pan HDACI and Pom (Imnovid[®]), an IMiD. The rationale for choosing these drugs is discussed in section 1.6, but briefly, these drugs/drug classes were chosen due to either their common use in MM and/or there being previous research with the drug in combination with other OV's resulting in improved outcomes in MM or other cancers.

Therefore this chapter aims to explore whether Ad[CE1A] in combination with MM standard of care results in enhanced anti-MM effects (synergy), and if so, is the mechanism due to the MM standard of care drugs enhancing the viral lifecycle (infection & replication). Additionally, BTZ and Melph are one of the few drugs that are inducers of ICD, there's also evidence that Pan and Pom also enhance ICD. Therefore it would be interesting to see if combining Ad[CE1A] with these drugs results in enhanced DAMP release. Overall this chapter will contribute to the understanding of how these drug classes may interact with Ad[CE1A], and this will help guide Ad[CE1A] combinations in MM clinical trials.

6.1.7 Hypothesis, Aims and Objectives

6.1.7.1 Hypothesis and Aims

In this chapter the goal is to identify whether anti-MM drugs, or classes of drugs are synergistic with Ad[CE1A]. To do this I will test the hypothesis that 'Ad[CE1A] will have synergistic interactions with the chosen anti-MM chemotherapies (BTZ, Melph, Pan or Pom) which will result in increased anti-MM effects'. This chapter also aimed to investigate the mechanisms behind any synergism or antagonism effect observed, by investigation into drug-induced augmentation of Ad[CE1A] life cycle.

6.1.7.2 Objectives

The hypothesis was tested by the following objectives

1. Investigate synergistic interactions between Ad[CE1A] and chosen anti-MM therapies in human and murine MPC lines using AlamarBlue® assays and synergy software (CompuSyn)
2. Validate the effects seen in objective 1 by apoptosis and cell death assays (Annexin V TO-PRO-3 assays)
3. Investigate if viral infection was increased following chosen anti-MM therapies by investigation into CAR expression and viral infection following treatment
4. Investigate if viral replication was increased following chosen anti-MM therapies by investigation into CS1 expression, *E1A* mRNA expression and viral titre following treatment.
5. Determine if Ad[CE1A] combination therapy increased ICD markers

6.2 Results

6.2.1 Dose Response to Ad[CE1A] and Anti-myeloma Chemotherapies.

To determine the appropriate concentration of Ad[CE1A] or drug, MPC lines JJN-3, U266, OPM-2 and 5TGM1 cells were treated with increasing concentrations of either Ad[CE1A] or BTZ, Melph, Pan or Len or Pom. After 72 hours, cell viability was assessed using an AlamarBlue® assay and dose response curves were generated to determine IC₅₀ (Figure 6.1). For IMiDs, Pom was chosen over Len as initial early IC₅₀ experiments showed Len to have no dose response in JJN-3 and U266 cells even at high concentrations (1mM) (Appendix Figure 8.15).

MPC lines showed similar dose responses to Ad[CE1A] and chemotherapies with similar IC₅₀ concentrations (Figure 6.1). Table 6.1 shows the suboptimal doses chosen for synergy experiments based on the dose response curves. Pom doses were chosen at a lower concentration, as Pom did not affect MPC lines as a monotherapy *in vitro* unless used at high concentrations which contained a higher DMSO concentration which may affect cell viability.

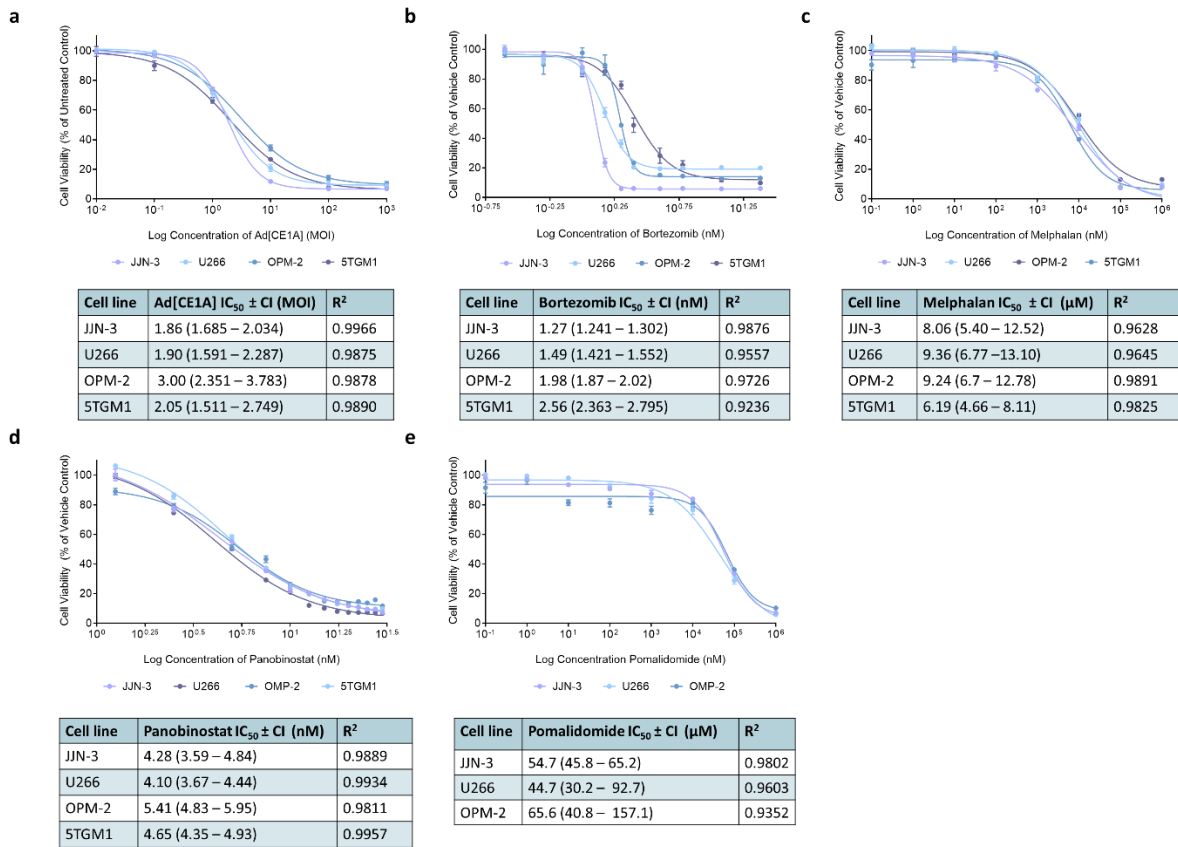


Figure 6.1: Dose response curves of Ad[CE1A] and anti-MM chemotherapies in MPC lines:

MPC lines JJN-3, U266, OPM-2 and 5TGM1 were treated with increasing concentrations of **(a)** Ad[CE1A]; **(b)** BTZ; **(c)** Melph; **(d)** Pan or Pom. 72 hours after incubation, cell viability was assessed using the AlamarBlue® assay. Data are mean the of 3 experiments ± SD. IC₅₀ values ± confidence interval (CI) was determined by using sigmoidal, non-linear fit curve with an R² of above 0.9.

Table 6.1: Suboptimal dose range for synergy experiments

Drug	Dose range
Ad[CE1A]	0 – 2 MOI
Melphalan	0-10 μM
Panobinostat	0 – 5 nM
Pomalidomide	0 – 320 nm
Bortezomib	
For JJN-3, U266 and OPM2	0 – 2.4 nM
For 5TGM1	0 – 4.3 nM

6.2.2 Augmenting Ad[CE1A] Suppression of MPC Line Viability with Anti-Myeloma Chemotherapies

6.2.2.1 Ad[CE1A] in Combination with Bortezomib

To determine whether Ad[CE1A] had antagonistic or synergistic effects with the proteasome inhibitor BTZ, JJN-3, U266, OPM-2 and 5TGM1 cells were treated with BTZ alone at indicated doses (0-2.4 nM) or treated with Ad[CE1A] at indicated doses (0-2 MOI) or treated with a combination of BTZ and Ad[CE1A] at increasing doses. After 72 hours incubation, cell viability was assessed by an AlamarBlue® assay (Figure 6.2) and synergy was determined by CI calculated by CompuSyn software (Figure 6.3).

The combination of Ad[CE1A] and BTZ induced the highest loss of cell viability in all cell lines at higher concentrations. There were only a few doses that showed significant differences between both monotherapies and combination therapy in the human cell lines (JJN-3 1.5 nM + 1.25 MOI and 1.8 nM + 1.5 MOI; U266 1.8 nM + 1.5 MOI; OPM-2 0.6 nM + 0.5 MOI). However, in the 5TGM1 cell line, all doses showed a significant difference between both monotherapies and combination therapies.

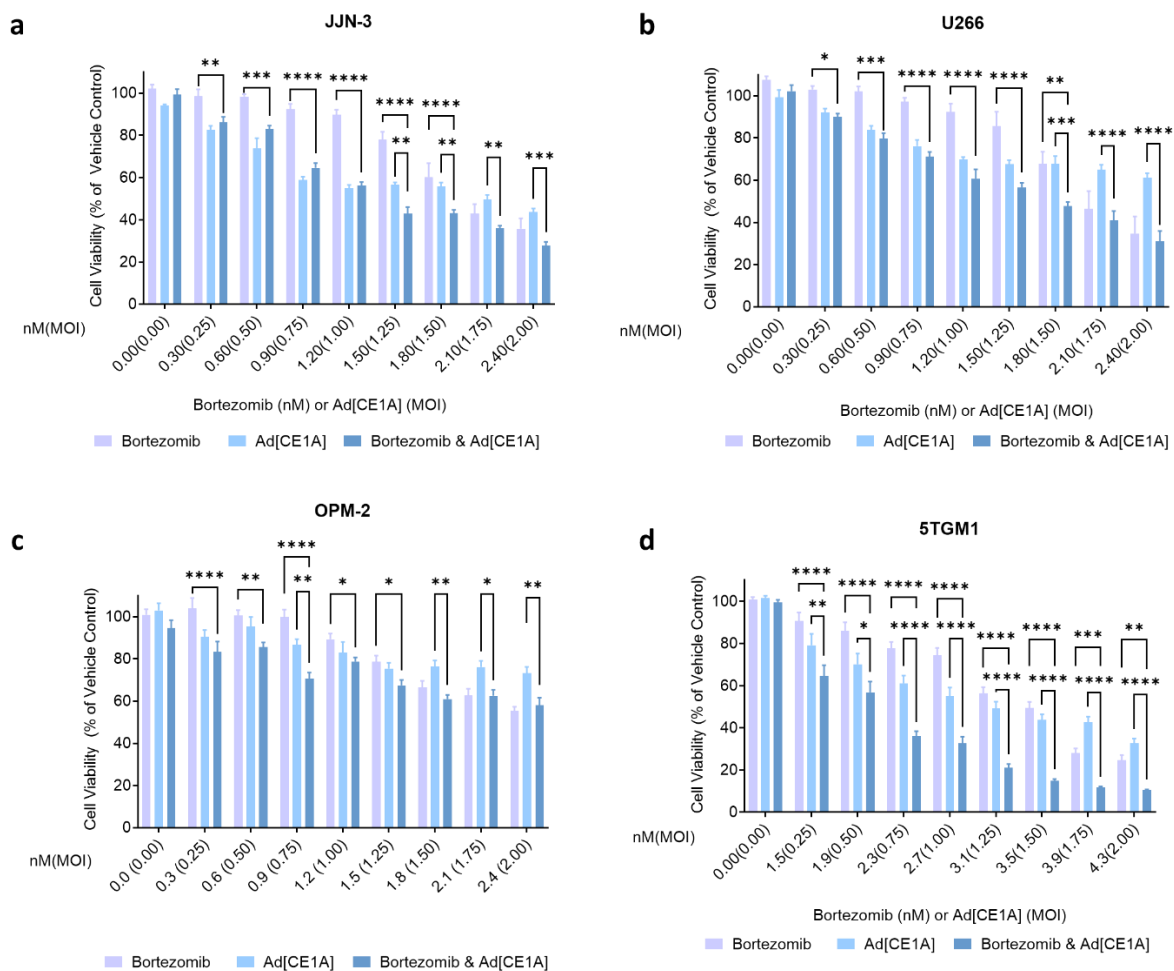


Figure 6.2: Ad[CE1A] in combination with BTZ in MPCs cell lines:

Cell viability of Ad[CE1A] and BTZ combination therapy compared to monotherapies in **(a)** JYN-3, **(b)** U266, **(c)** OPM-2 and **(d)** 5TGM1 cells as determined AlamarBlue® after 72 hours. Concentration of BTZ (nM) on x axis denoted first, concentration of Ad[CE1A] (MOI) denoted second in brackets, BTZ,nM(Ad[CE1A],MOI). n=3 Data is the mean ±SD. P values are for 2-way ANOVA with multiple comparisons with Tukey's correction where * p<0.05; ** p<0.01; *** p<0.001 **** p<0.0001.

Dose-response parameters were used to determine CI by CompuSyn software. CI was plotted in a heatmap, with the shading referring to the level of synergism/antagonism (Figure 6.3). In JYN-3 cells the CI ranged from 2.74-1.10, with antagonistic and additive interactions observed. However, the majority of the doses showed either antagonistic (3/8) or slight antagonistic (3/8) interactions. Therefore, it was determined that Ad[CE1A] in combination with BTZ is antagonistic in JYN-3 cells. In U266 cells the CI ranged from 1.19-0.92, with additive and slight antagonistic interactions observed. Half of the doses showed additive interactions (4/8) mainly at higher doses, whilst the other half showed antagonistic interactions (4/8) mainly at lower doses. Therefore it was determined that

Ad[CE1A] in combination with BTZ is additive at higher doses and antagonistic at lower doses in U266 cells. In OPM-2 cells the CI ranged from 3.42-0.66, with moderate synergistic, synergistic, additive or antagonistic interactions observed. Half of the doses showed either moderate synergistic (3/8) or synergistic (1/8) interactions, whilst the other half showed either additive (2/8) or antagonistic (2/8) interactions. Therefore, it was determined that Ad[CE1A] in combination with BTZ is synergistic-additive in OPM-2 cells. Interestingly, OPM-2 cells showed more synergism than JLN-3 or U266 cells. OPM-2 cells, in our research groups experience, are resistant to BTZ *in vivo* in NSG mice [data unpublished]. It would be interesting to investigate if Ad[CE1A] could re-sensitise OPM-2 cells to BTZ *in vivo*. In 5TGM1 cells, which showed less sensitivity to BTZ by dose response compared to human MPC lines, had a CI range of 1.14-0.64, with synergistic, moderate synergistic, additive, and slight antagonistic interactions observed. The majority of the combinations had moderate synergistic (3/8) or synergistic (3/8) interactions with these being seen at higher concentrations. Therefore, it was determined that Ad[CE1A] in combination with BTZ is synergistic in 5TGM1 cells.

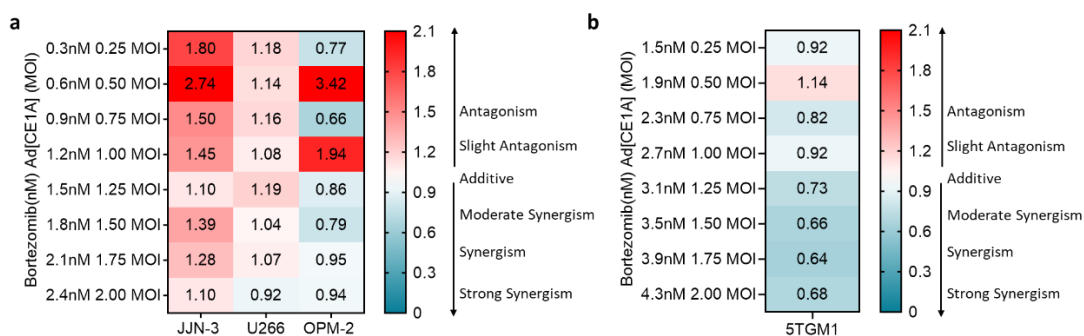


Figure 6.3: Heatmap of CI of Ad[CE1A] in combination with BTZ in MPC lines:

The mean cell viability for Ad[CE1A] and BTZ monotherapies and combination therapy obtained from the previous AlamarBlue[®] assay was input into CompuSyn software which determines the dose-effect parameters of each drug alone as well as in combination. CI was determined by the median-effect analysis equation. CI= <0.3 strong synergism; CI=0.3-0.7 synergism; CI=0.7-0.9 moderate synergism; CI=0.9-1.1 additive; CI=1.1-1.45 slight antagonism; 1.45-2 antagonism in **(a)** human MPC lines and **(b)** mouse 5TGM1 cell line.

6.2.2.2 Ad[CE1A] in Combination with Melphalan

To determine whether Ad[CE1A] had antagonistic or synergistic effects with the nitrogen mustard alkylating agent, Melph, JJN-3, U266 and OPM-2 cell lines were treated with Melph alone at indicated doses (0-10 μ M) or with Ad[CE1A] at indicated doses (0-2 MOI) or with a combination of Melph and Ad[CE1A] at increasing doses. After 72 hours incubation, cell viability was assessed by an AlamarBlue[®] assay (Figure 6.4) and CI calculated by CompuSyn software (Figure 6.5).

The combination of Ad[CE1A] and Melph induced the highest loss of cell viability in all cell lines at higher concentrations. For the JJN-3, and U266 cells there was a significant difference between combination therapy and both monotherapies at all doses used. For 5TGM1 cells there was a significant difference between combination therapy and both monotherapies in all doses except for the lowest dose combination. For OPM-2 cells, there was only a significant difference between combination therapy and both monotherapies at 4 doses (2.50 μ M + 0.50 MOI; 3.75 μ M + 0.75 MOI; 6.25 μ M + 1.25 MOI; 10.00 μ M + 2.00 MOI).

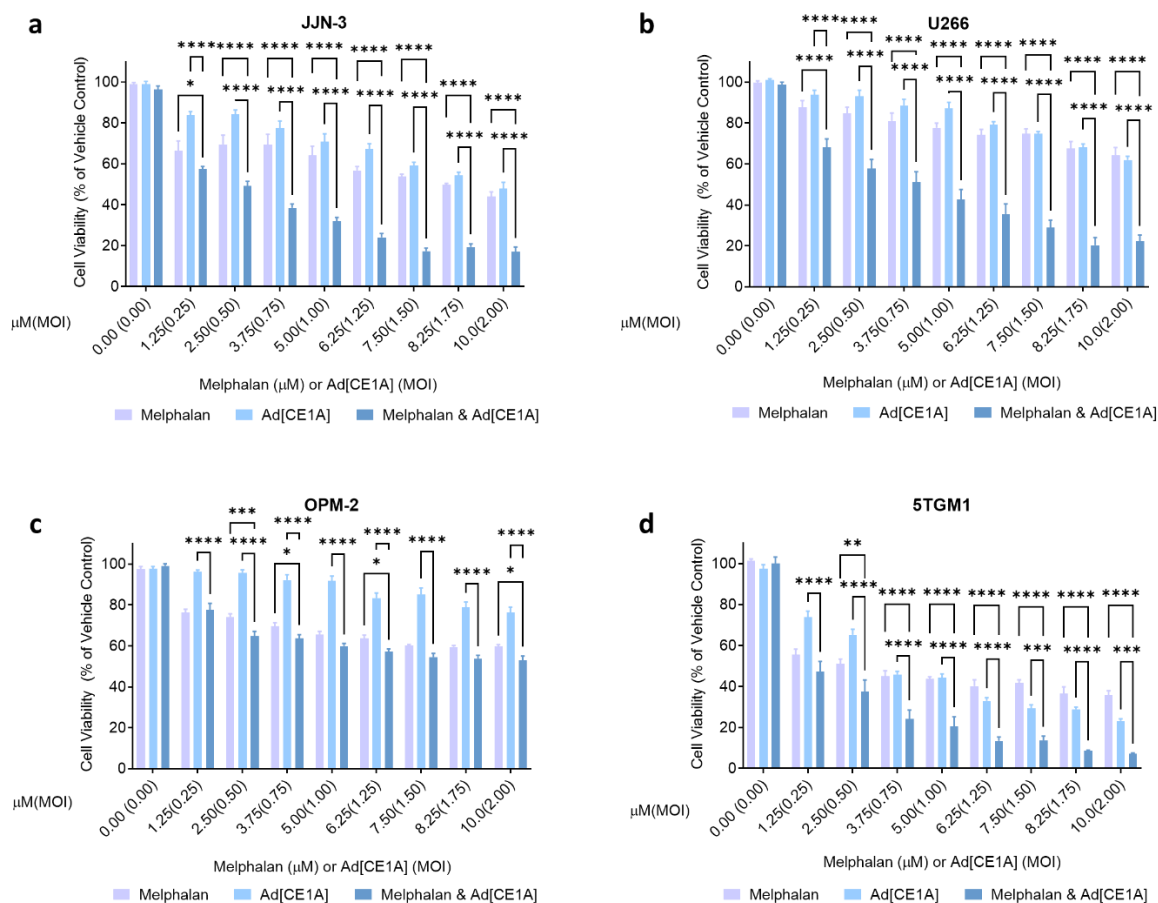


Figure 6.4: Ad[CE1A] in combination with Melph in MPC cell lines:

Cell viability of Ad[CE1A] and Melph combination therapy compared to monotherapies in **(a)** JLN-3, **(b)** U266, **(c)** OPM-2 and **(d)** 5TGM1 cells as determined by AlamarBlue® after 72 hours. Concentration of Melph (μM) on x axis denoted first, concentration of Ad[CE1A] (MOI) denoted second in brackets, Melph,μM(Ad[CE1A],MOI). n=3 Data is the mean ±SD. P values are for 2-way ANOVA with multiple comparisons with Tukey's correction where * p<0.05; ** p<0.01; *** p<0.001 **** p<0.0001.

Dose-response parameters were used to determine CI index by CompuSyn software. CI index was plotted in a heatmap, with the shading referring to the level of synergism/antagonism (Figure 6.5). In JLN-3 cells the CI ranged from 0.41-0.12 with strong synergistic (5/8) and synergistic (3/8) interactions observed. Therefore, it was determined that Ad[CE1A] in combination with Melph is strongly synergistic in JLN-3 cells. In U266 cells, the CI ranged from 0.32-0.16 with strong synergistic (7/8) and synergistic (1/8) interactions observed. Therefore, it was determined that Ad[CE1A] in combination with Melph is strongly synergistic in U266 cells. In OPM-2 cells, the CI ranged from 1.19-0.58 with slight antagonistic, moderate synergistic and synergistic interactions observed. The majority of the doses showed moderate synergistic (6/8) or synergistic (1/8) interactions. Therefore, it was

determined that Ad[CE1A] in combination with Melph is synergistic in OPM-2 cells. In 5TGM1 cells the CI ranged from 0.68-0.28, with synergistic to strong synergistic interactions observed. The majority of doses showed synergistic interactions (7/8). Therefore, it was determined that Ad[CE1A] in combination with Melph is synergistic in 5TGM1 cells.

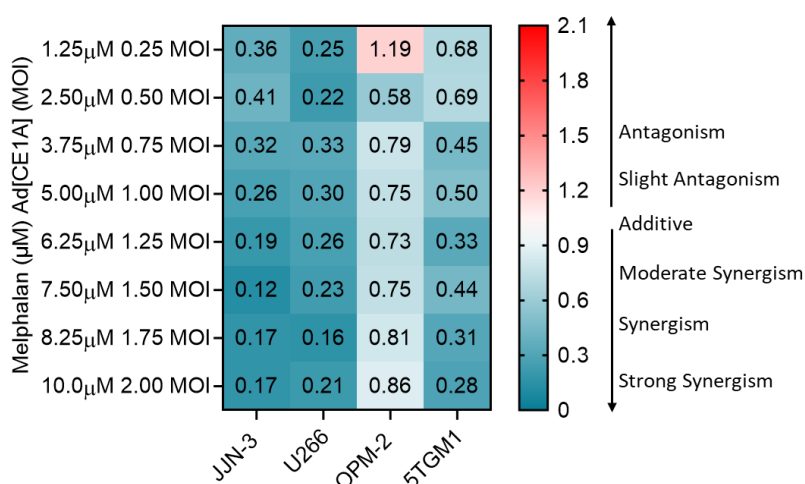


Figure 6.5: Heatmap of CI of Ad[CE1A] in combination with Melph in MPC lines:

The mean cell viability for Ad[CE1A] and Melph monotherapies and combination therapy obtained from the previous AlamarBlue® assay was input into CompuSyn software which determines the dose-effect parameters of each drug alone as well as in combination. CI was determined by the median-effect analysis equation. CI= <0.3 strong synergism; CI=0.3-0.7 synergism; CI=0.7-0.9 moderate synergism; CI=0.9-1.1 additive; CI=1.1-1.45 slight antagonism; 1.45-2 antagonism.

6.3.2.3 Ad[CE1A] in Combination with Panobinostat

To determine whether Ad[CE1A] had antagonistic or synergistic effects with the pan-histone deacetylase inhibitor Pan, JJN-3, U266, OPM-2 and 5TGM1 cell lines were treated with Pan alone at indicated doses (0-5 nM) or with Ad[CE1A] at indicated doses (0-2 MOI) or with a combination of Pan and Ad[CE1A]. After 72 hours incubation, cell viability was assessed by an AlamarBlue® assay (Figure 6.6) and CI calculated by CompuSyn software (Figure 6.7).

The combination of Ad[CE1A] and Pan induced the highest loss of cell viability in all cell lines at every concentration combination compared to monotherapies. For JJN-3, U266 and 5TGM1 cells there was a significant difference between combination therapy and both monotherapies at all doses, except for three doses in JJN-3 (0.625 nM + 0.25 MOI; 1.25 nM + 0.5 MOI; 1.875 nM + 0.75 MOI), two doses in

5TGM1 (0.625 nM + 0.25 MOI; 1.25 nM + 0.5 MOI) and one dose in U266 (0.625 nM + 0.25 MOI). In OPM-2 cells there were less combination doses that were significantly different from both monotherapies, with only three doses being significant (3.125 nM + 1.25 MOI; 3.75 nM + 1.50 MOI; 4.375 nM + 1.75 MOI).

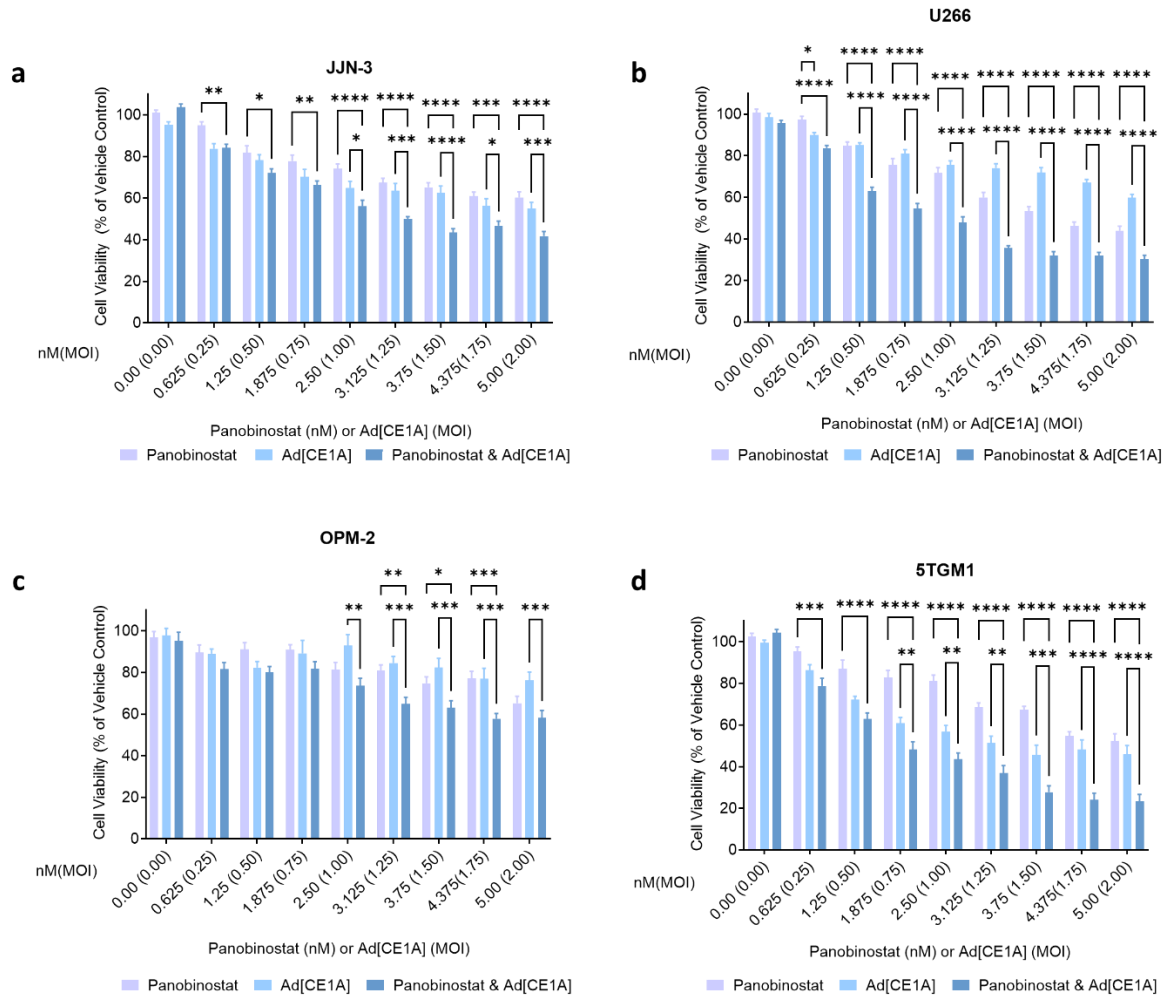


Figure 6.6: Ad[CE1A] in combination with Pan in MPC lines:

Cell viability of Ad[CE1A] and Pan combination therapy compared to monotherapies in **(a)** JN-3, **(b)** U266, **(c)** OPM-2 and **(d)** 5TGM1 cells as determined by AlamarBlue® after 72 hours. Concentration of Pan (nM) on x axis denoted first, concentration of Ad[CE1A] (MOI) denoted second in brackets, Pan,nM(Ad[CE1A],MOI). N=3 Data is the mean ±SD. P values are for 2-way ANOVA with multiple comparisons with Tukey's correction where * p<0.05; ** p<0.01; *** p<0.001 **** p<0.0001.

Dose-response parameters were used to determine CI index by CompuSyn software. CI index was plotted in a heatmap, with the shading referring to the level of synergism/antagonism (Figure 6.7). In JIN-3 cells the CI ranged from 1.4-0.88, with moderate synergistic, additive, and slight antagonistic interactions observed. Half of the combination doses showed slight antagonistic interactions (4/8), which was seen mainly at lower doses whilst the other half showed an additive (3/8) or moderate synergistic interaction (1/8). Therefore, it was determined that Ad[CE1A] in combination with Pan is additive-slightly antagonistic in JIN-3 cells. In U266 cells, the CI ranged from 0.94-0.65, with additive, moderate synergistic and synergistic interactions observed. The majority of the doses showed moderate synergistic (5/8) or synergistic (2/8) interactions. Therefore, it was determined that Ad[CE1A] in combination with Pan is synergistic in U266 cells. In OPM-2 cells, the CI ranged from 2.00-0.54, with antagonistic, additive, and synergistic interactions observed. The majority of the doses showed synergistic (5/8) or additive interactions (2/8). Therefore, it was determined that Ad[CE1A] in combination with Pan is synergistic-additive in OPM-2 cells. In 5TGM1 cells, the CI ranged from 0.96-0.71, with additive and moderate synergistic interactions observed. Half of the dose combinations showed moderate synergistic interactions, whilst the other half showed additive interactions. Therefore, it was determined that Ad[CE1A] in combination with Pan is synergistic/additive in 5TGM1 cells.

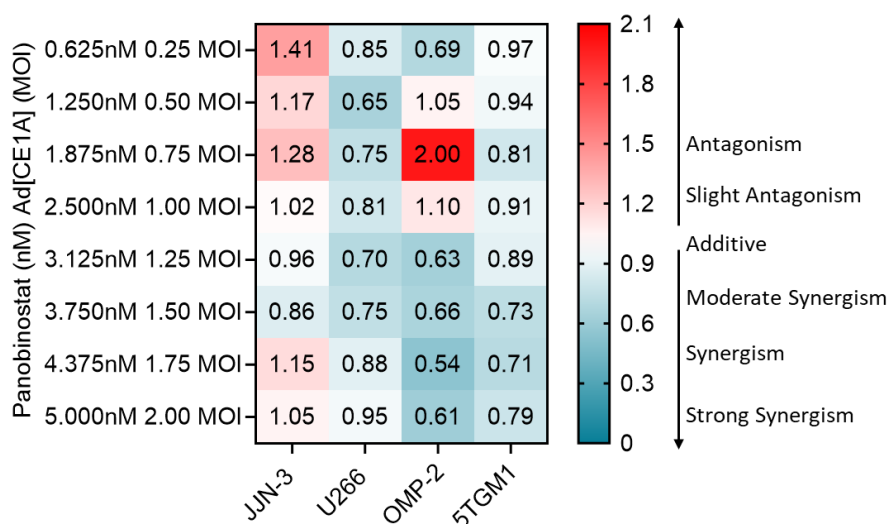


Figure 6.7: Heatmap of CI of Ad[CE1A] in combination with Pan in MPC lines:

The mean cell viability for Ad[CE1A] and Pan monotherapies and combination therapy obtained from the previous AlamarBlue[®] assay was input into CompuSyn software which determines the dose-effect parameters of each drug alone as well as in combination. CI was determined by the median-effect analysis equation. CI= <0.3 strong synergism; CI=0.3-0.7 synergism; CI=0.7-0.9 moderate synergism; CI=0.9-1.1 additive; CI=1.1-1.45 slight antagonism; 1.45-2 antagonism.

6.3.2.4 Ad[CE1A] in Combination with Pomalidomide

To determine whether Ad[CE1A] had antagonistic or synergistic effects with the IMiD, Pom, JLN-3, U266, OPM-2 and 5TGM1 cell lines were treated with Pom alone at indicated doses (0-320 nM) or with Ad[CE1A] at indicated doses (0-2 MOI) or with a combination of Pom and Ad[CE1A]. After 72 hours incubation, cell viability was assessed by an AlamarBlue[™] assay (Figure 6.8), and CI calculated by CompuSyn software (Figure 6.9).

The combination of Ad[CE1A] and Pom induced the highest loss of cell viability in all cell lines at every concentration combination compared to monotherapies. For JLN-3, there was a significant difference between combination therapy and monotherapy in the highest 4 combination doses. For U266, there was a significant difference in between combination therapy and monotherapy in all doses except for the lowest dose. For OPM-2 and 5TGM1, there was a significant difference between combination therapy compared to monotherapy in all doses except for the lowest two doses.

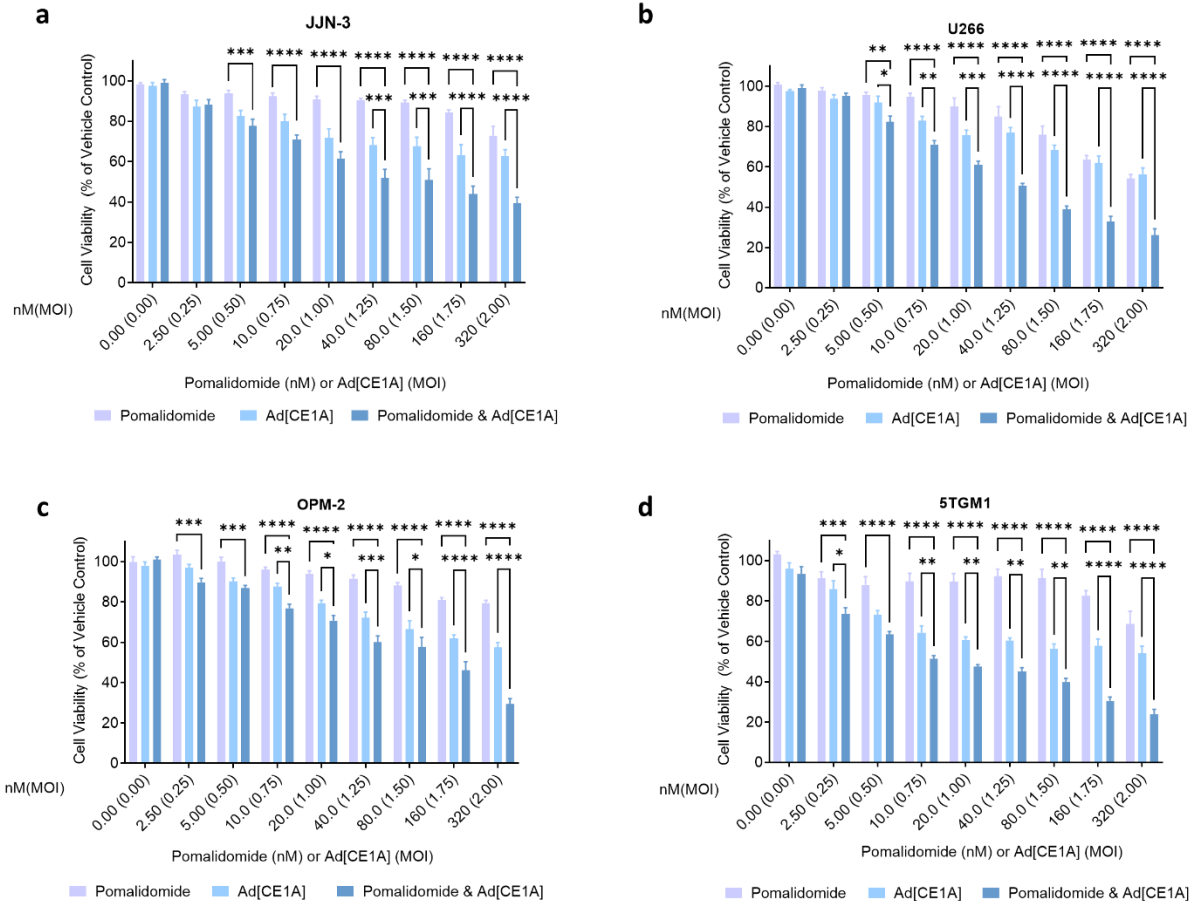


Figure 6.8: Ad[CE1A] in combination with Pom in MPC lines:

Cell viability of Ad[CE1A] and Pom combination therapy compared to monotherapies in **(a)** JYN-3, **(b)** U266, **(c)** OPM-2 and **(d)** 5TGM1 cells as determined by AlamarBlue® after 72 hours. Concentration of Pom (nM) on x axis denoted first, concentration of Ad[CE1A] (MOI) denoted second in brackets, Pom,nM(Ad[CE1A],MOI). n=3 Data is the mean ±SD. P values are for 2-way ANOVA with multiple comparisons with Tukey's correction where * p<0.05; ** p<0.01; *** p<0.001 **** p<0.0001

Dose-response parameters were used to determine CI index by CompuSyn software. CI index was plotted in a heatmap, with the shading refereeing to the level of synergism/antagonism (Figure 6.9).

In JYN-3 cells the CI ranged from 0.27-1.08, with strong synergistic, synergistic, moderate synergistic and additive interactions observed. The majority of the doses showed synergistic (5/8 dose), strong synergistic (1/8 doses) or moderate synergistic (1/8 doses) interactions. Therefore, it was determined that Ad[CE1A] in combination with Ad[CE1A] is synergistic in JYN-3 cells. In U266 cells the CI ranged from 0.55-0.96, with synergistic, moderate synergistic and additive interactions observed. The majority of the doses showed synergistic (6/8 doses), or moderate synergistic (1/8) interactions,

therefore, it was determined that Ad[CE1A] in combination with Pom is synergistic in U266 cells. In OPM-2 cells the CI ranged from 0.50-1.28, with synergistic, moderate synergistic and slight antagonistic interactions observed. The majority of the doses showed moderate synergistic (5/8 doses), or synergistic (2/8) interactions. Therefore, it was determined that Ad[CE1A] in combination with Pom was synergistic in OPM2- cells. In 5TGM1 cells the CI ranged from 0.48-0.24, with synergistic and strong synergistic interactions observed. Therefore, it was determined that Ad[CE1A] in combination with Pom is synergistic in 5TGM1 cells.

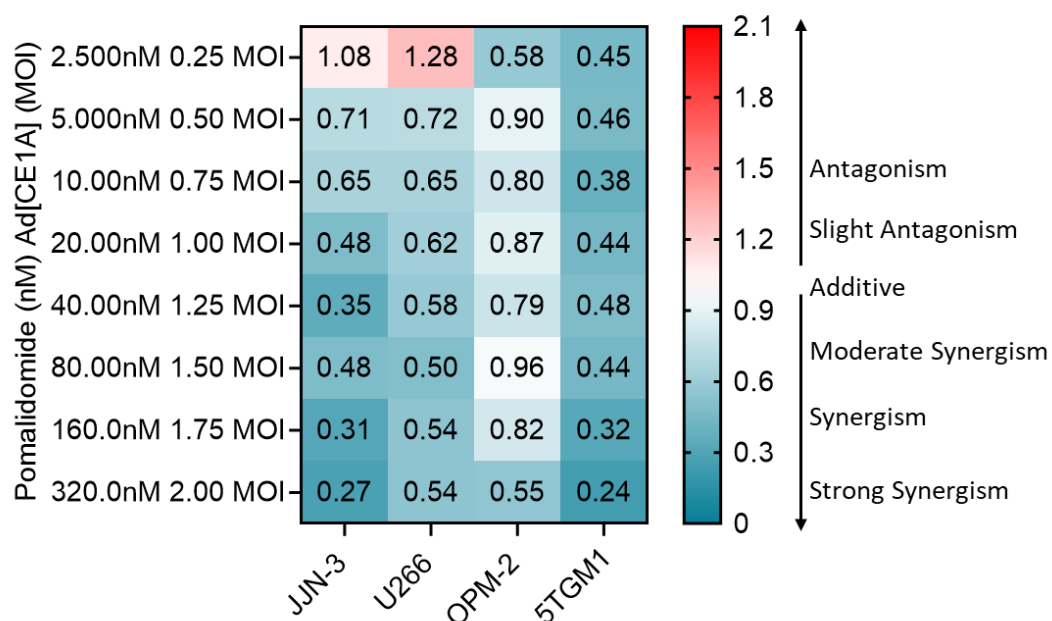


Figure 6.9: Heatmap of CI of Ad[CE1A] in combination with Pom in MPC lines:

The mean cell viability for Ad[CE1A] and Pom monotherapies and combination therapy obtained from the previous AlamarBlue® assay was input into CompuSyn software which determines the dose-effect parameters of each drug alone as well as in combination. CI was determined by the median-effect analysis equation. CI= <0.3 strong synergism; CI=0.3-0.7 synergism; CI=0.7-0.9 moderate synergism; CI=0.9-1.1 additive; CI=1.1-1.45 slight antagonism; 1.45-2 antagonism.

6.2.2.5 Summary of Combination Cell Viability Experiments in MPC Lines

Ad[CE1A] in combination with anti-MM chemotherapies appears promising, especially with Melph which showed the greatest synergistic interactions and was consistent in all four cell lines. Table 6.2 summarises CI data in all cell lines for Ad[CE1A] and anti-MM combination therapies. Interestingly, 5TGM1 cells responded better to Ad[CE1A] and BTZ combinations showing synergistic interactions compared to human MPC lines, which were additive/synergistic in some cell lines (U266 and OPM2) and antagonistic in others (JJN-3).

Table 6.2: Summary of CI data from cell viability experiments in MPC lines

Drug	Cell Line			
	JJN-3	U266	OPM-2	5TGM1
Bortezomib	Antagonism	Additive/ Antagonism	Synergism/ Additive	Synergism
Melphalan	Strong Synergism	Strong Synergism	Synergism	Synergism
Panobinostat	Additive/ Slightly Antagonism	Synergism	Synergism/ Additive	Synergism/Additive
Pomalidomide	Synergism	Synergism	Synergism	Synergism

6.2.3 Augmenting Ad[CE1A]-induced MPC Cytotoxicity with Anti-myeloma Chemotherapies

As the above results were promising, it was important to test the Ad[CE1A] drug combinations on cell death and apoptosis. The above results were obtained from AlamarBlue® assays, which strictly speaking, is an assay of metabolic health, an indicator of cell viability. The AlamarBlue® test does not directly test cytotoxicity. Therefore, the effects seen may just be growth inhibitory effects and not actual cytotoxicity. Therefore apoptosis and cell death after Ad[CE1A] and anti-MM therapy combinations at 72 hours was assessed in human MPC lines JJN-3, U266 and OPM2.

For logistical reasons one dose combination was chosen per cell line, so the highest combination dose was initially chosen as this generally showed the best synergistic effect (Table 6.3). However, initial experiments showed doses of drug and Ad[CE1A] caused more or less cell death by flow cytometry than by AlamarBlue® assays. Therefore, drug doses were adjusted. Melph and BTZ doses were adjusted slightly as they caused too much cell death, Ad[CE1A] and Pom doses were adjusted as they caused a lower amount of cell death than expected. For the former this variation could be due to increased sensitivity of flow cytometry, or the extra washes or mechanical forces the cells must undergo before and during flow cytometry which could result in more cell death seen by flow cytometry than AlamarBlue®. Additionally, the AlamarBlue® does not specifically detect apoptotic cells, which could still reduce resazurin in the AlamarBlue® assay, leading to more cell death seen by flow cytometry than AlamarBlue®. For the latter, this may be due to Ad[CE1A] having a faster effect on cell metabolism before cell death occurs, so a lower dose is needed to see an effect in AlamarBlue® assays than by flow cytometry. For Pom a larger dose was chosen as Pom had little effect on cell viability in the AlamarBlue® assays and by flow cytometry.

Table 6.3: Summary of CI data for highest dose concentration

Drug	Dose (Drug/Ad[CE1A])	Cell Line			Amended Dose (Drug/Ad[CE1A])
		JJN-3	U266	OPM-2	
Bortezomib	2.4 nM/2.0 MOI	Additive	Additive	Additive	1.5 nM/10 MOI
Melphalan	10 µM/2.0 MOI	Strong Synergism	Strong Synergism	Moderate Synergism	5 µM/10 MOI
Panobinostat	5 nM/2.0 MOI	Additive	Additive	Synergism	5 nM/10 MOI
Pomalidomide	320 nM/2.0 MOI	Strong Synergism	Synergism	Synergism	10 µM/10 MOI

All Ad[CE1A] combination therapies induced significantly higher total cell death (Annexin V⁺ TO-PRO⁻ 3⁻ and Annexin V⁺ TO-PRO⁺) than monotherapies (Figure 6.10). However, in JJN-3 cells only Melph significantly increased Annexin-V⁺ To-PRO-3⁻ cells compared to monotherapies whilst in U266 only BTZ and Pom resulted in significantly increased Annexin-V⁺ To-PRO-3⁻ cells, suggesting only in those cell lines in those combinations is apoptosis increased (Appendix Figure 8.16) rather than just necrosis in the other cell lines. Some of these findings show better responses in some of the combinations than were observed in AlamarBlue[®] assays. This could be due to the change in dosages or as discussed because apoptotic/permeabilised cells could still be reducing resazurin in the AlamarBlue[®] assay but the flow cytometry assay is detecting these cells therefore is more sensitive.

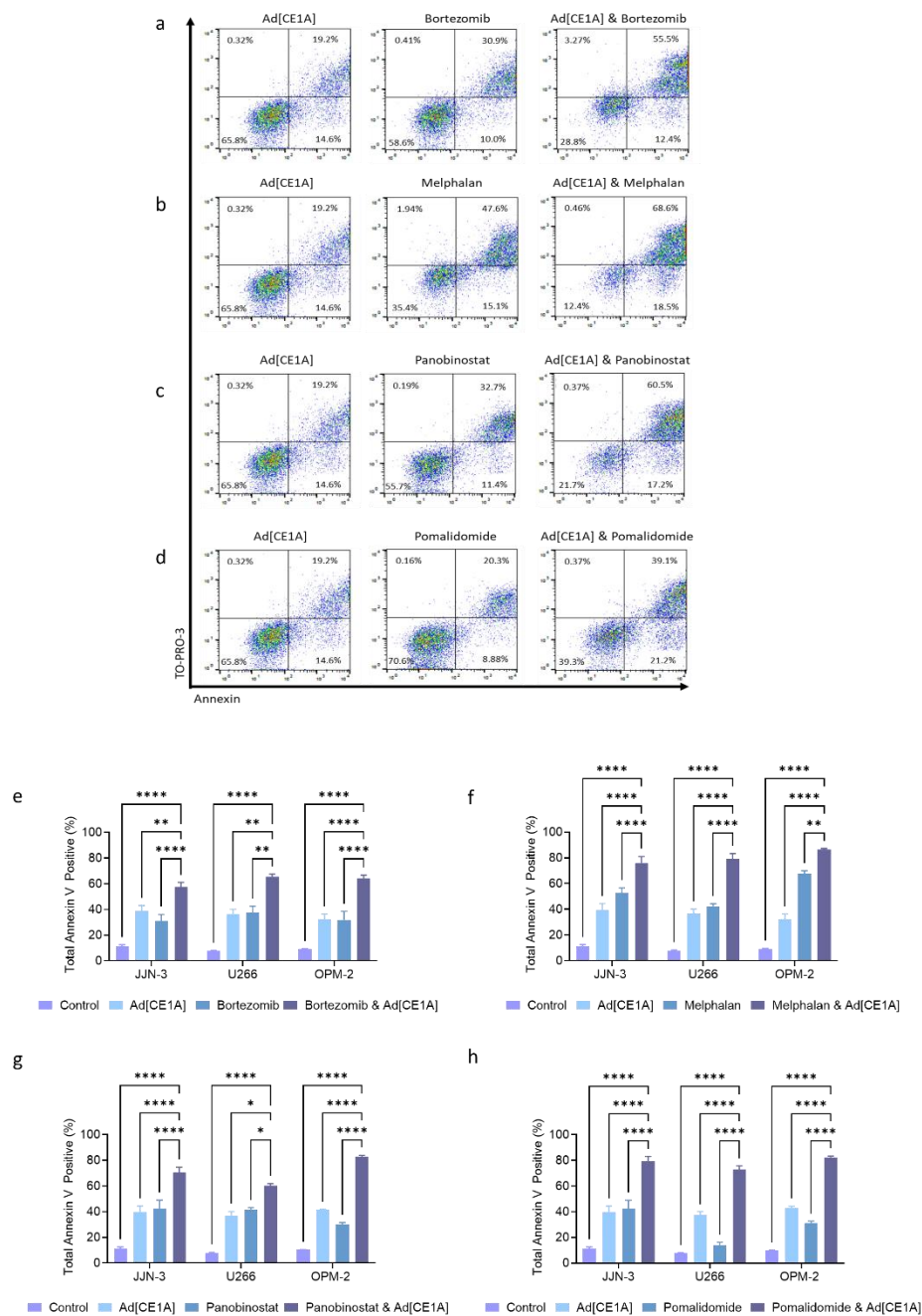


Figure 6.10: Percentage of total Annexin V positive cells after A[CE1A] and anti-MM chemotherapy combination therapy in MPC lines:

Representative dot plots of Annexin V TO-PRO-3 in JUN-3 cells after Ad[CE1A] (MOI 10) treatment after 72 hours. **(a)** BTZ (1.5 nM); **(b)**, Melph (5 μ M); **(c)** Pan (5 nM) or **(d)** Pom (10 μ M) or in combination. JUN-3, U266 and OPM-2 cells were incubated with Ad[CE1A] (MOI 10) or **(e)** BTZ (1.5 nM); **(f)** Melph (5 μ M); **(g)** Pan (5 nM) or **(h)** Pom (10 μ M) or combination. Percentage of total Annexin V expression (Annexin V positive and Annexin V and TO-PRO-3 positive) was determined by flow cytometry at 72 hours post treatment. N=3 Data is the mean \pm SD. P values are for 2-way ANOVA with multiple comparisons with Tukey's correction where * $p < 0.05$; ** $p < 0.01$; *** $p < 0.001$ **** $p < 0.0001$.

6.2.4 Mechanisms of Synergy

As discussed in the chapter introduction the anti-MM chemotherapies and the drug classes they belong to, have been found to augment different stages of various OV's life cycle, including Ads.

Therefore, it was important to investigate if they could augment Ad[CE1A]'s life cycle in MPCs.

6.2.4.1 Augmenting Coxsackie Adenovirus Receptor Expression after Anti-myeloma Chemotherapies.

In order to try and determine some of the mechanisms behind additive/synergistic interactions in MPC lines in Ad[CE1A] and anti-MM chemotherapy combinations, expression of CAR after chemotherapy treatment was explored. CAR is the main receptor of Ad5 and its upregulation has been shown to be a mechanism of synergy in other cancers with other drugs (555,556). The proposed hypothesis is that the upregulation of CAR expression results in increased viral infection, which results in additive or synergistic interactions. Human MPC lines JJN-3, U266 and OPM-2 cells were treated with indicated doses of BTZ, Melph, Pan or Pom. Doses were kept the same as the previous flow cytometry experiment. After 48 hours cells were stained with a CAR antibody, and cell surface CAR expression was determined by flow cytometry on viable cells (Figure 6.11). Whilst murine cells do express a murine CAR (m/CAR) (557), there are no commercial antibodies available to detect m/CAR available for flow cytometric analysis, so 5TGM1 cells were omitted from this investigation.

BTZ was able to significantly increase CAR expression in all three cell lines, with U266 having the greatest relative fold change compared to control at 1.6 average fold increase. Melph was able to significantly increase CAR expression in all three cell lines, with JJN-3 and OPM-2 cells having above ~1.5 average fold change and U266 having a 1.9-fold change compared to control. Pan was able to significantly increase CAR expression in all three cell lines with OPM-2 cells having the greatest relative fold change compared to control at 1.9 with U266 and JJN-3 cells having a relative fold change of 1.4 and 1.3 respectively. Pom was able to significantly increase CAR expression in OPM-2 cells with a relative fold change of 1.2. However, CAR expression was significantly decreased following Pom treatment in JJN-3 and U266 cells with relative fold change of 0.7 and 0.9, respectively.

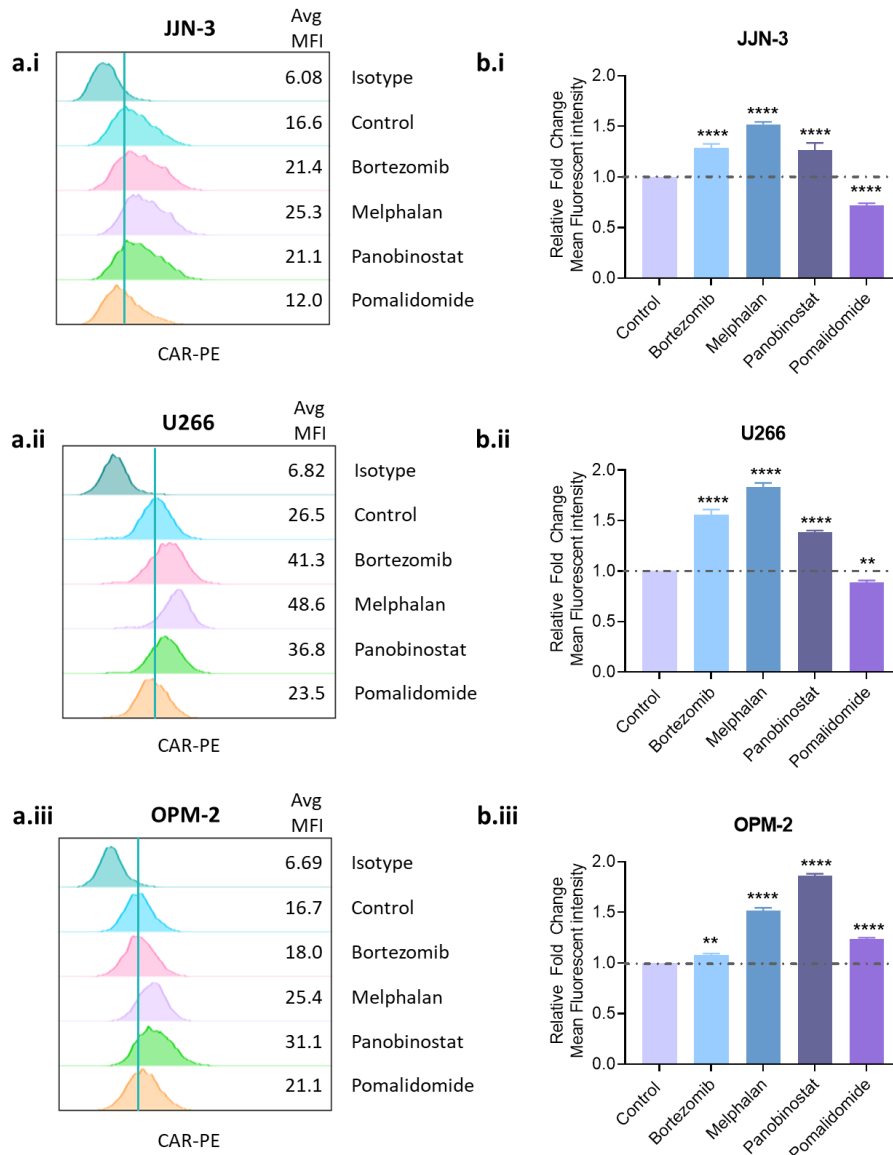


Figure 6.11: CAR expression after 48 hours of anti-MM chemotherapy treatment:

Representative histogram plots of MFI of CAR after 48 hours treatment with anti-MM chemotherapies (BTZ 1.5 nM, Melph 5 μ M, Pan 5 nM or Pom 10 μ M) in **(a.i)** JYN-3, **(a.ii)** U266 and **(a.iii)** OPM2. Viable cells only included in analysis, TO-PRO-3 positive dead cells were gated out. Relative fold change of CAR MFI after anti-MM chemotherapies compared to untreated control in **(b.i)** JYN-3, **(b.ii)** U266 **(b.iii)** OPM2. n=3 Data is the mean \pm SD. P values are for one-way ANOVA with multiple comparisons compared to control with Dunnett's correction where ** $p < 0.01$; **** $p < 0.0001$.

CAR expression data was correlated with CI data from cell viability assays (Appendix Figure 8.17). There is no correlation between CAR expression and CI scores for BTZ, Melph and Pom. However, there was a significant negative correlation with Pan with a value of $p=0.0178$ and an R^2 0.9992, therefore the higher the fold change of CAR correlated with the lower CI.

6.2.4.2 Augmenting Adenovirus Infection after Anti-Myeloma Chemotherapy

After identifying that anti-MM chemotherapies significantly upregulated or downregulated CAR receptor expression, it was important to determine if this affected Ad infection. Therefore, JJN-3, U266, OMP-2 and 5TGM1 cells were treated with Ad-GFP MOI 2 \pm anti-MM chemotherapies at indicated doses. Doses were kept the same as previous flow cytometry experiments. After 24 and 48 hours, GFP expression was determined by flow cytometry (Figure 6.12).

Surprisingly, despite the significant changes in CAR expression, there was no significant difference in percentage of cells infected by Ad-GFP at 24 and 48 hours compared to untreated controls in all the human MPC lines (Figure 6.12 b.i-b.ii). In 5TGM1 cells, Pan was able to significantly increase Ad-GFP infection at 24 hours, however, there was no difference by 48 hours (Figure 6.12 b.iv). These results could be because upregulation of CAR does not result in increased Ad infection, or it could be because of the treatment schedule. If treatment with chemotherapy was given before Ad-GFP infection, rather than at the same time, an increase in infection may be observed. CAR expression was assessed at 48 hours (Figure 6.11), whether CAR is upregulated/downregulated earlier has not been tested. However, in drug combination assays, treatment was given at the same time, but assessed after 72 hours, by which point Ad infection may have increased. It is also important to note that whilst percentage of infected cells was not increased in the majority of cases, GFP MFI was significantly increased in some cases. In U266 cells at 48 hours Pan and Pom significantly increased GFP MFI, and in OPM-2 and 5TGM1 cells, Pan significantly increased MFI after 48 hours (Appendix Figure 8.18). This could be due to the Pom and Pan increasing GFP transgene expression by the cytomegalovirus promoter in the already infected cell lines rather than increasing infection. This has been observed with other HDACis

(558). Therefore, it would be interesting to investigate if these drugs also increase *E1A* driven by CS1 like it has with adenoviral vectors with GFP driven by the CMV promoter.

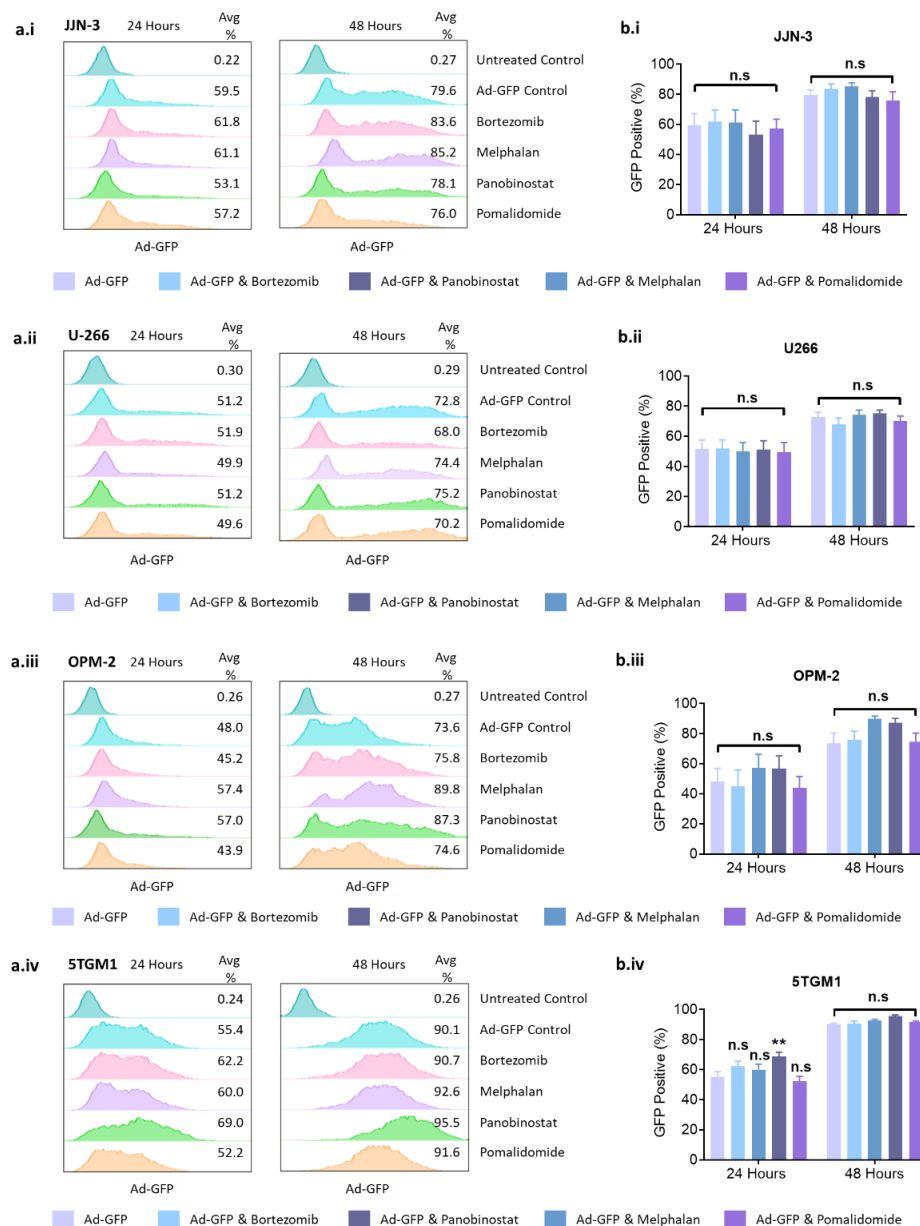


Figure 6.12: Percentage of Ad-GFP expression after anti-MM therapies compared to untreated control:

JJN-3, U266, OPM-2 and 5TGM1 cells were treated with Ad-GFP (MOI 2) ± anti-MM chemotherapies (BTZ 1.5 nM, Melph 5 µM, Pan 5 nM or Pom 10 µM). GFP expression was determined by flow cytometry after 24 and 48 hours. Representative histogram plots of GFP expression of Ad-GFP after anti-MM chemotherapies after 24 and 48 hours in (a.i) JJN-3, (a.ii) U266, (a.iii) OPM-2 and (a.iv) 5TGM1 cell lines. Percentage GFP expression after anti-MM chemotherapies compared to untreated control plotted in (b.i) JJN-3, (b.ii) U266, (b.iii) OPM-2 (b.iv). n=3 Data is the mean ±SD. P values are for 2-way ANOVA with multiple comparisons compared to Ad-GFP control for each time point with Dunnett's correction where ** p<0.01.

Because CAR expression was tested 48 hours after chemotherapy treatment, MPC lines were next treated with chemotherapy first for 24 hours, then infected with Ad-GFP for 24 hours and assessed for GFP expression (Figure 6.13). This time two doses of Ad-GFP (0.2 MOI and 2 MOI) were used.

At a lower MOI of 0.2, percentage of GFP expression was increased by Melph in all four cell lines (JJN-3 30% vs 15% control; U266 27% vs 20% control; OPM2 35% vs 19% control; 5TGM1 18% vs 10% control) (Figure 6.13 b.i-iv), BTZ increased GFP expression in OPM-2 (32% vs 19% control) (figure 6.13 b.iii), Pan increased GFP expression in U266 (31% vs 20% control) (Figure 6.13 b.ii) and Pom increased GFP expression in OPM-2 and 5TGM1 (28% vs 19% control, 18% vs 10% control, respectively) (Figure 6.13 b.iii-iv). However, at a higher dose of MOI 2 there was no significant difference in JJN-3 or U266 (Figure 6.13 b.i-ii), although a similar nonsignificant trend is observed in JJN-3. For OPM-2 cells, there was a significant difference in Melph (91% vs 73% control) and BTZ (83% vs 73% control) similar to what is observed at the lower concentration, however there was no significant difference in pom (Figure 6.13 b.iii). In 5TGM1 cells, there was a significant difference in Pom (52% vs 44%) similar to what is observed at the lower concentration, however, there was no significant difference in Melph but there was a significant difference by Pan (59% vs 44%) (Figure 6.13 b.iv). The significant increase in GFP following Pan in 5TGM1 cells does match the previous experiment where the cells were treated with virus at the same time. It is also important to note that whilst percentage of infected cells was not increased in the majority of cases, GFP MFI was significantly increased in some cases (Appendix Figure 8.19).

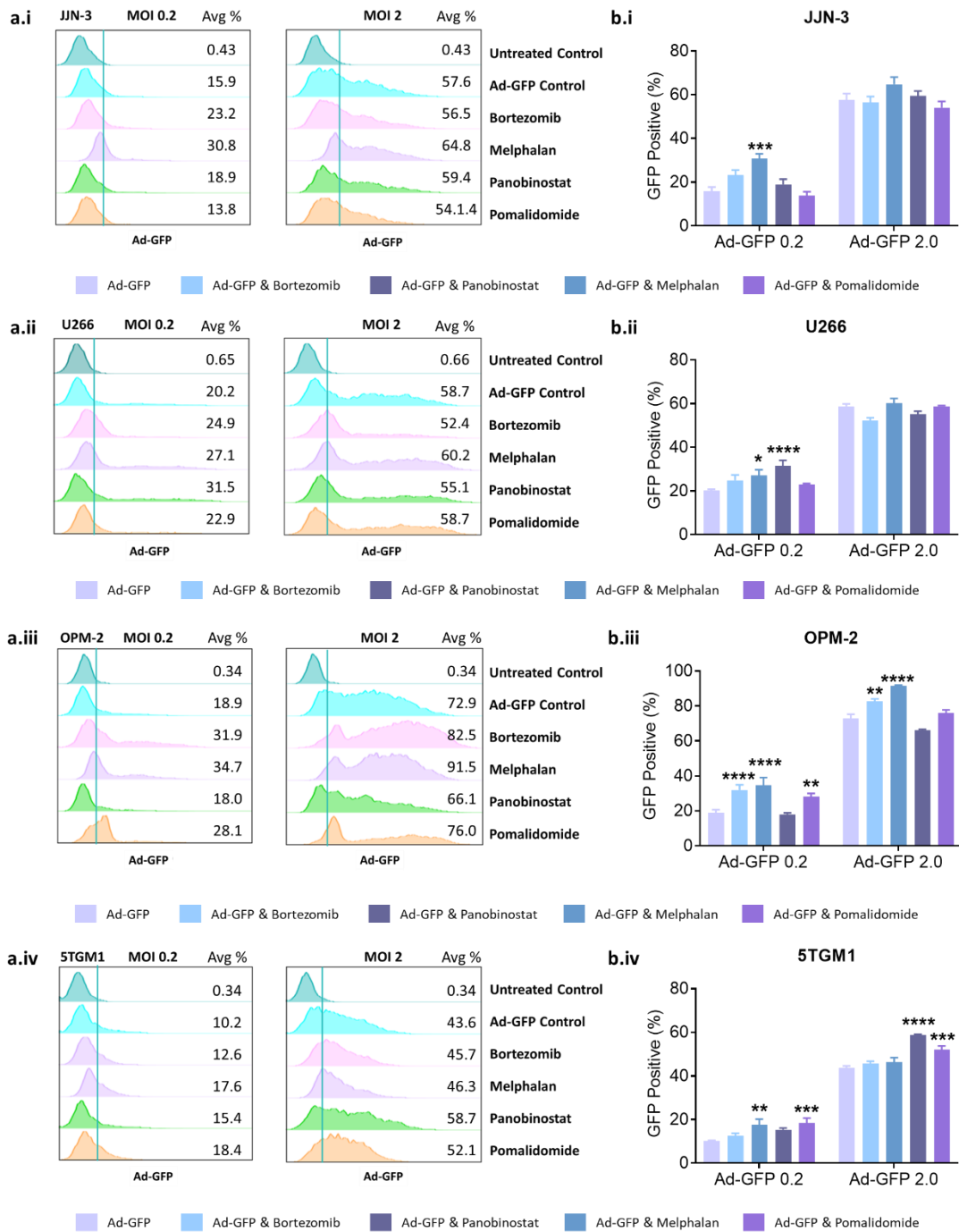


Figure 6.13: Percentage of Ad-GFP expression after anti-MM therapies compared to untreated control:

JJJN-3, U266, OPM-2 and 5TGM1 cells were treated with anti-MM chemotherapies (BTZ 1.5 nM, Melph 5 μ M, Pan 5 nM or Pom 10 μ M). After 24 hours cells were infected with Ad-GFP (MOI 0.2 or 2). GFP expression was determined by flow cytometry after 24 hours. Representative histogram plots of GFP expression of Ad-GFP after anti-MM chemotherapies at MOI 0.2 and MOI 2 in (a.i) JJJN-3, (a.ii) U266, (a.iii) OPM-2 and (a.iv) 5TGM1 cell lines. Percentage GFP expression after anti-MM chemotherapies compared to untreated control plotted in (b.i) JJJN-3, (b.ii) U266, (b.iii) OPM-2 (b.iv). n=3 Data is the mean \pm SD. P values are for 2-way ANOVA with multiple comparisons compared to Ad-GFP only for each MOI with Dunnett's correction where ** p<0.01.

A summary table shows current data on viral infection following chemotherapy (Table 6.4). With the current data, it is hard to determine whether anti-MM chemotherapy increases Ad-GFP expression by increasing cell surface CAR expression, Melph was the only consistent chemotherapy that increased CAR expression and increased Ad-GFP expression but only after pre-treatment with chemotherapy and only at the lower dose of Ad-GFP. Therefore, for Melph and the other chemotherapies, the synergistic/ additive interactions observed are unlikely to be caused by increased viral infection.

Table 6.4: Summary of viral infection data following anti-MM chemotherapies.

Drug	Cell Line	CAR	Ad[CE1A] Concurrent treatment		Anti-MM therapy first treatment	
			24 Hours	48 Hours	0.2 MOI	2 MOI
Bortezomib	JJN-3	**** ↑	NSD	NSD	NSD	NSD
	U266	**** ↑	NSD	NSD	NSD	NSD
	OPM2	** ↑	NSD	NSD	**** ↑	** ↑
	5TGM1	ND	NSD	NSD	NSD	NSD
Melphalan	JJN-3	**** ↑	NSD	NSD	*** ↑	NSD
	U266	**** ↑	NSD	NSD	* ↑	NSD
	OPM2	**** ↑	NSD	NSD	**** ↑	**** ↑
	5TGM1	ND	NSD	NSD	** ↑	NSD
Panobinostat	JJN-3	**** ↑	NSD	NSD	NSD	NSD
	U266	**** ↑	NSD	NSD	**** ↑	NSD
	OPM2	**** ↑	NSD	NSD	NSD	NSD
	5TGM1	ND	** ↑ 2	NSD	NSD	**** ↑
Pomalidomide	JJN-3	**** ↓	NSD	NSD	NSD	NSD
	U266	** ↓	NSD	NSD	NSD	NSD
	OPM2	**** ↑	NSD	NSD	** ↑	NSD
	5TGM1	NSD	NSD	NSD	*** ↑	*** ↑

NSD= No significant difference; * ↑ = Significant increase; * ↓ = Significant decrease

6.2.4.3 Augmenting CS1 Receptor Expression after Anti-Myeloma Chemotherapies.

As it remains to be determined if anti-MM chemotherapies result in increased infection leading to increased oncolysis, therefore, another mechanism was explored. Investigation into whether Ad[CE1A] replication was augmented following treatment with anti-MM chemotherapies was examined. The proposed hypothesis was that the upregulation of CS1 by anti-MM chemotherapies will result in increased/decreased viral replication (by increased CS1 driven *E1A* expression), which results in enhanced anti-MM efficacy. Therefore, expression of CS1 cell surface protein after anti-MM chemotherapies was investigated. MPC lines JJN-3, U266, OPM-2 and 5TGM1 were treated with indicated doses of BTZ, Melph, Pan or Pom. Doses were kept the same as previous experiments. After 48 hours cells were stained with a CS1 antibody, and cell surface CS1 expression was determined by flow cytometry on viable cells (Figure 6.14).

BTZ was able to significantly increase CS1 expression in U266 and 5TGM1 cells (1.9- and 1.1-fold change respectively) (Figure 6.14 b.ii & b.iv), but there was no significant difference in CS1 expression in JJN-3 and OPM-2 cells (Figure 6.14 b.i & b.iv). Melph was able to significantly increase CS1 expression in all cell lines compared to untreated control, with 5TGM1 cells having the greatest fold change at 1.7 (Figure 6.14 b.i-b.iv). Pan significantly increased CS1 expression in JJN-3 cells but decreased CS1 expression in 5TGM1 cells (1.5- and 0.7-fold change respectively) (Figure 6.14 b.i & b.iv). U266 and OPM2 cells showed no significant difference in CS1 expression compared to untreated controls (Figure 6.14 b.ii-b.iii). Pom significantly decreased CS1 expression in OPM-2 and 5TGM1 cells (0.6- and 0.9-fold change respectively) (Figure 6.14 b.iii-b.iv), whilst there was no significant difference in JJN-3 and U266 compared to untreated controls (Figure 6.14 b.i-b.ii). The data here shows that the expression of CS1 in response to these anti-MM chemotherapies seems to be cell line dependent, with only Melph consistently resulting in a significant increase fold change in CS1 across all MPC lines tested. Melph also consistently resulted in synergy with Ad[CE1A] in cell viability experiments,

however, there was no correlation between relative CS1 expression and CI scores (Appendix Figure 8.20) .

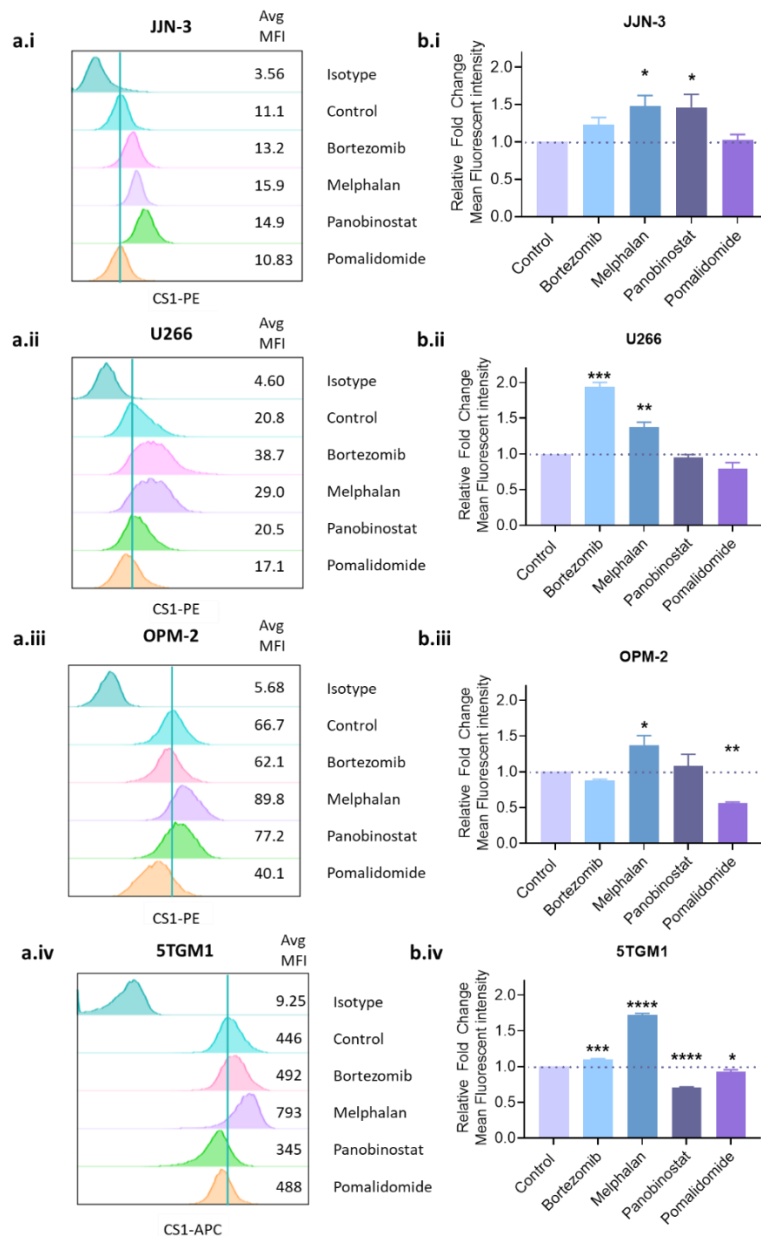


Figure 6.14: CS1 receptor expression after 48 hours of anti-MM chemotherapy treatment:

JJN-3, U266, OPM-2 and 5TGM1 cells were treated with \pm anti-MM chemotherapies (BTZ 1.5 nM, Melph 5 μ M, Pan 5 nM or Pom 10 μ M). After 48 hours cells were stained with an APC-conjugated CS1 antibody and fluorescence was measured by flow cytometry. Representative histograms plots of MFI of CS1 receptor after 48 hours treatment with anti-MM chemotherapies in (a.i) JJN3 (a.ii) U266 (a.iii) OPM2 (a.iv) 5TGM1. Viable cells only were included in analysis, PI positive dead cells were gated out prior to analysis. Relative fold change of CAR MFI after anti-MM chemotherapies compared to untreated control in (b.i) JJN-3, (b.ii) U266, (b.iii) OPM-2 and (b.iv) 5TGM1. n=3 Data is the mean \pm SD. P values are for one-way ANOVA with multiple comparisons compared to untreated control with Dunnett's correction, where * $p < 0.05$; ** $p < 0.01$; *** $p < 0.001$; **** $p < 0.0001$.

6.2.4.4 Augmenting Ad[CE1A] E1A Expression after Anti-Myeloma Chemotherapies.

As there were changes in CS1 expression following anti-MM drugs this may result in changes in Ad[CE1A] genome replication, therefore, it was important to test whether Ad[CE1A] in combination with anti-MM chemotherapy resulted in significant changes in *E1A* expression, and whether this was a mechanism for the synergistic interactions observed. To investigate this, MPC lines were treated with Ad[CE1A] MOI 10 ± anti-MM chemotherapies (BTZ 1.5 nM, Melph 5 µM, Pan 5 nM and Pom 10 µM). After 24 hours, total RNA was extracted and converted to cDNA, and RT-qPCR was performed using primers for *E1A* and *GAPDH* (housekeeping gene for human) of *B2M* (housekeeping gene for murine) (Figure 6.15).

BTZ did not significantly increase *E1A* expression in any cell line. Melph significantly increased *E1A* expression in JJN-3, OMP-2 and 5TGM1 cell lines (2.4-fold, 4.2-fold, and 4.2-fold change respectively) (Figure 6.15 a-d). Pan significantly decreased *E1A* expression in U266 cells (0.25-fold), but significantly increased *E1A* expression in OMP-2 cells (2.1-fold) (Figure 6.15 b & c). Pom significantly increased *E1A* expression in JJN-3 cells (1.7-fold) (Figure 6.15 a).

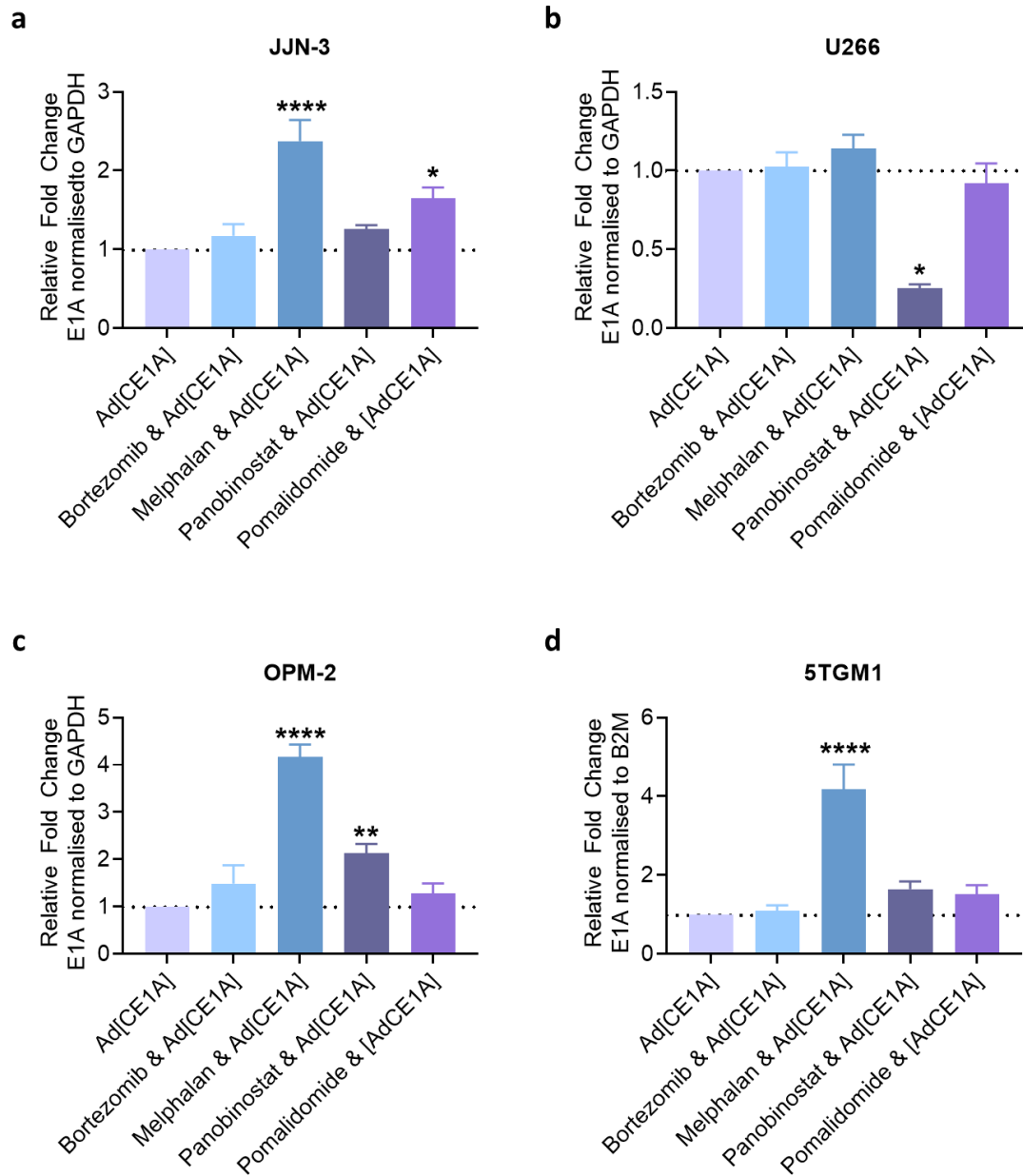


Figure 6.15 *E1A* expression after 24 hours of anti-MM chemotherapy treatment:

(a) JLN-3, (b) U266, (c) OPM-2 and (d) 5TGM1 cells were treated with Ad[CE1A] MOI 10 ± anti-MM chemotherapies, BTZ 1.5 nM, Melph 5 µM, Pan 5 nM or Pom 10 µM. After 24 hours total RNA was extracted, and RT-qPCR was performed using *E1A* primers and *GAPDH* (for human) or *B2M* (for mouse) was used as a housekeeping gene. Relative *E1A* mRNA expression compared to Ad[CE1A] alone was plotted. n=3 Data is the mean ±Sd. p values are for one-way ANOVA with multiple comparisons compared to Ad[CE1A] only treated cells with Dunnett's correction, where * p<0.05; ** p<0.01; *** p<0.001; **** p<0.0001.

6.2.4.5 Augmenting Ad[CE1A] Viral Progeny Production after Anti-myeloma Chemotherapies.

It was also important to determine if any of the anti-MM drugs increase/decrease viral progeny production. This could be linked to the increase/decrease of CS1 but may happen independently as the anti-MM therapies may upregulate/interact with the viral protein production machinery. MPC lines (JJN-3, U266, OMP-2 and 5TGM1) were treated with Ad[CE1A] at an MOI of 2 ± anti-MM chemotherapies (BTZ 1.5 nM; Melph 5 µM; Pan 5 nM or Pom 10 µM). After 72 hours virus was harvested from CM and cell lysate and viral titre was determined by Adeno-X™ Rapid titre kit (Figure 6.16)

BTZ significantly increased viral titre in U266 and OMP-2 cells (~1.5-fold change for both cell lines). Melph significantly increased viral titre in all MPC lines (~1.5-1.8-fold change). Pan only increased viral titre in U266 cells (1.3-fold change). Lastly, Pom did not significantly increase viral titre in any cell line.

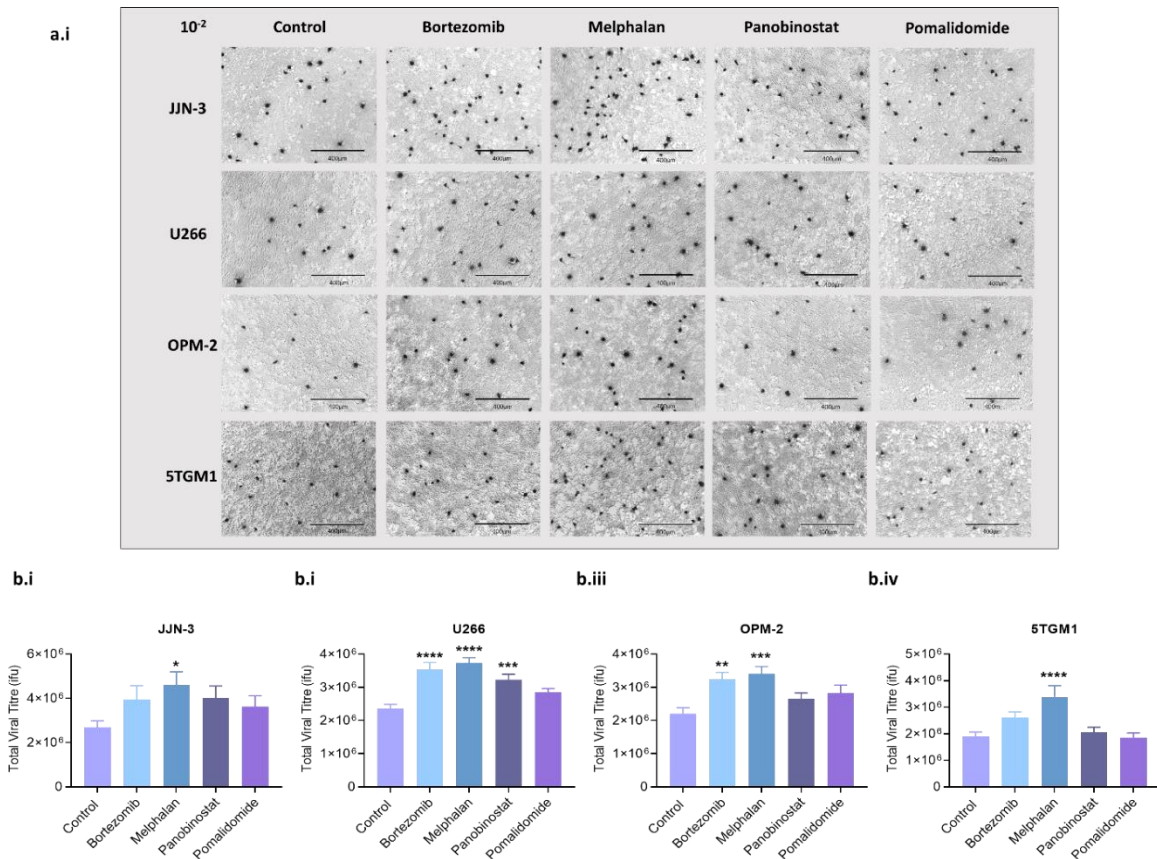


Figure 6.16 Anti-MM chemotherapies increase viral titre in MPC lines:

MPC lines (JJN-3, U266, OPM-2 and 5TGM1 cells) were treated with Ad[CE1A] (MOI 2) ± anti-MM chemotherapies, BTZ 1.5 nM, Melph 5 µM, Pan 5 nM or Pom 10 µM. After 72 hours viral titre was determined by Adeno-X™ rapid titre viral quantification kit. **(a.i)** Representative images of Adeno-X™ rapid titre staining at 10⁻² dilution factor. Scale bar 400 µm. Quantification of viral titre in **(b.i)** JJN-3, **(b.ii)** U266, **(b.iii)** OPM-2 and **(b.iv)** 5TGM1 after 72 hour anti-MM therapy. n=3 Data is the mean ±SD. P values are for one-way ANOVA with multiple comparisons compared with Ad[CE1A] only control with Dunnett's correction, where * p<0.05; ** p<0.01; *** p<0.001; **** p<0.0001.

A summary table shows current data on viral replication following anti-MM chemotherapy (Table 6.5).

With the current data, it is hard to determine whether anti-MM chemotherapy increases Ad[CE1A] replication consistently, which will be discussed later. However, Melph did consistently increase CS1 expression, E1A expression and viral titre so it is likely that the synergistic interactions seen in MPC lines following Ad[CE1A] and Melph treatment may be due to increased Ad[CE1A] replication.

Table 6.5 Summary of viral replication data following anti-MM chemotherapies.

Drug	Cell line	CS1 Expression	E1A mRNA Expression	Viral Titre
Bortezomib	JJN-3	NSD	NSD	NSD
	U266	***↑	NSD	****↑
	OPM-2	NSD	NSD	**↑
	5TGM1	***↑	NSD	NSD
Melphalan	JJN-3	*↑	****↑	*↑
	U266	**↑	NSD	****↑
	OPM-2	*↑	****↑	****↑
	5TGM1	****↑	****↑	****↑
Panobinostat	JJN-3	*↑	NSD	NSD
	U266	NSD	****↓	***↑
	OPM-2	NSD	**↑	NSD
	5TGM1	****↓	NSD	NSD
Pomalidomide	JJN-3	NSD	*↑	NSD
	U266	NSD	NSD	NSD
	OPM-2	**↓	NSD	NSD
	5TGM1	*↓	NSD	NSD

NSD= No significant difference; *↑= Significant increase; *↓= Significant decrease

6.2.5.6 Augmenting ICD following Ad[CE1A] in Combination with Anti-myeloma Therapies.

It was important to determine if any of the anti-MM drugs augment markers of ICD as this may result in improved MM cell killing *in vivo*. The proposed hypothesis behind this line of investigation was that, as discussed, BTZ and Melph are one of the few drugs that are classified as ICD inducers (reviewed in (559), and Pom is a IMiD drug and studies have shown HDACIs to induce ICD to some degree. Firstly, MPC lines JIN-3 and OPM-2 were treated with Ad[CE1A] at an MOI of 2 or anti-MM chemotherapies (BTZ 1.5 nM; Melph 5 μ M; Pan 5 nM or Pom 10 μ M) or in combination. After 24 hours cells were stained with an anti-CALR antibody followed by a fluorescently conjugated secondary antibody and cell surface CALR was determined on viable cells by flow cytometry (Figure 6.17).

Ad[CE1A] in combination with BTZ did not significantly increase cell surface CALR expression compared to both monotherapies in JIN-3 cells with a fold change of 1.5, however in OPM-2 cells, there was a significant increase in cell surface CALR expression between both monotherapies and the combination therapy with a fold change of 2.2 (Figure 6.17 a.i & b.i). Ad[CE1A] in combination with Melph significantly increased cell surface CALR expression between both monotherapies in both JIN-3 and OPM-2 cells with a fold change of 1.5 and 1.7, respectively (Figure 6.17 a.ii & b.ii). Ad[CE1A] in combination with Pan did not significantly increase cell surface CALR expression compared to both monotherapies in JIN-3 cells with a fold change of 1.8. In OPM-2 cells, Ad[CE1A] in combination with Pan significantly decreased cell surface CALR expression compared to both monotherapies with a fold change of 0.6 (Figure 6.17 a.iii & b.iii). Ad[CE1A] in combination with Pom did not significantly increase cell surface CALR expression compared to both monotherapies in both JIN-3 and OPM-2 cells with a fold change of 1.2 and 1.3, respectively (Figure 6.17 a.iv & b.iv).

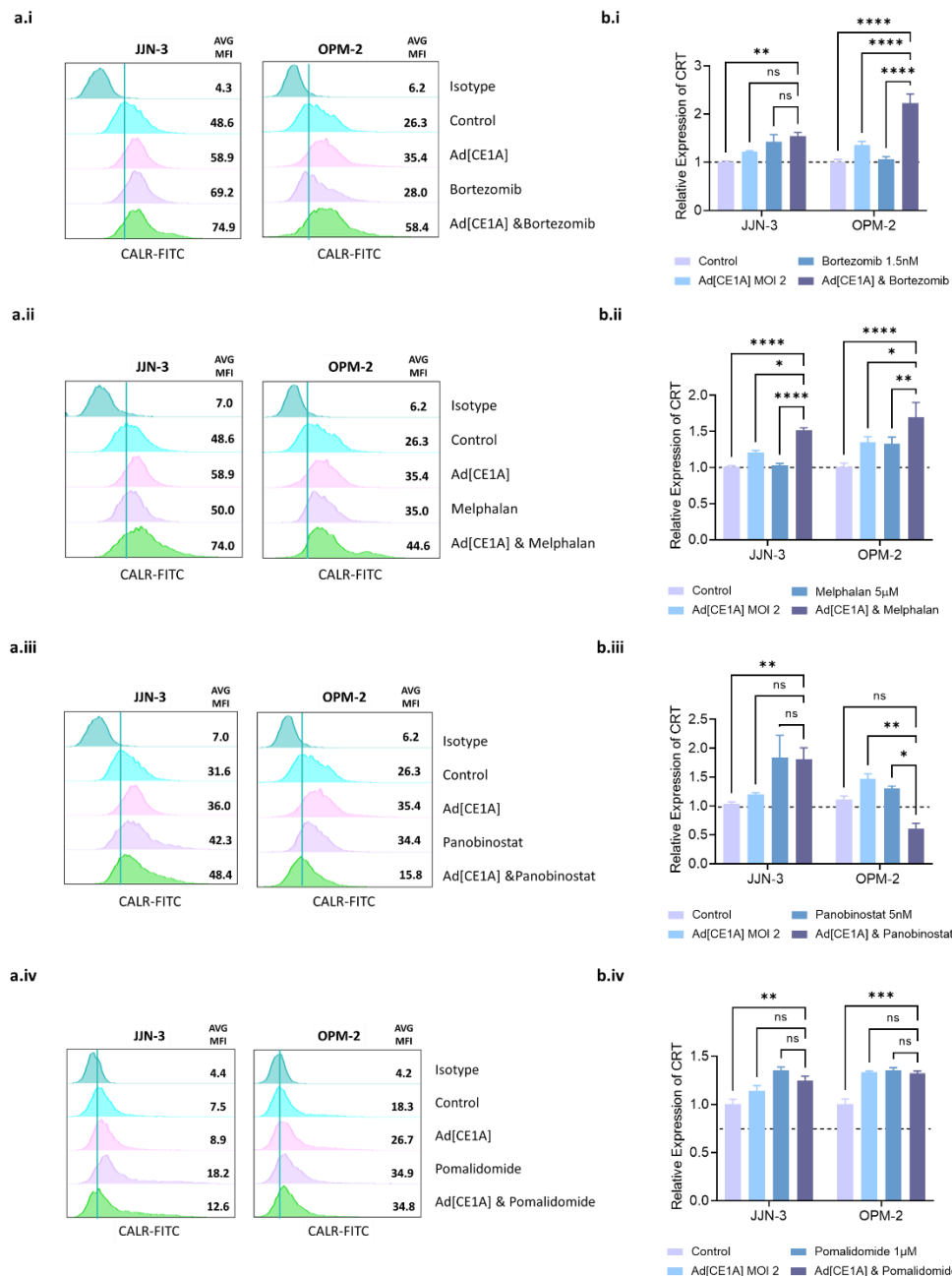


Figure 6.17: Cell surface CALR expression after 24 hour treatment of Ad[CE1A] ± anti-MM chemotherapy:

JJN-3, and OPM-2 cells were treated with Ad[CE1A] MOI 2 ± anti-MM chemotherapies, BTZ 1.5 nM, Melph 5 µM, Pan 5 nM and Pom 10 µM. After 24 hours cells were stained with a primary CALR antibody and FITC conjugated secondary antibody, and fluorescence was measured by flow cytometry. Viable cells only were used in analysis, TO-PRO-3 positive dead cells were gated out prior to analysis. Representative histograms plots of MFI of cell surface CALR expression in viable JJN-3 or OPM-2 cells 24 hours after treatment with Ad[CE1A] MOI 2 ± anti-MM chemotherapies (**a.i**) BTZ, (**a.ii**) Melph, (**a.iii**) Pan or (**a.iv**) Pom. Relative fold change of cell surface CALR MFI in JJN-3 and OPM-2 cells after anti-MM chemotherapies compared to untreated control (**b.i**) BTZ, (**b.ii**) Melph, (**b.iii**) Pan or (**b.iv**) Pom. n=3 Data is the mean ±SD. P values are for two-way ANOVA with multiple comparisons with Tukey's correction, where * p<0.05; ** p<0.01; *** p<0.001; **** p<0.0001.

Next, it was important to determine if any of the anti-MM drugs augment extracellular ATP release. Firstly, MPC lines JJN-3 and OPM-2 were treated with Ad[CE1A] at an MOI of 2 or anti-MM chemotherapies (BTZ 1.5 nM; Melph 5 μ M; Pan 5 nM or Pom 10 μ M) or in combination. After 24 hours supernatant was collected from cells and ATP was determined by the ENLITEN[®] ATP assay, which is a luminescence-based assay which relies on the chemical reaction of ATP with D-luciferin (Figure 6.16). Ad[CE1A] in combination with BTZ had significantly higher concentration of extracellular ATP than both monotherapies in both JJN-3 and OPM-2 cells (Figure 6.18 a). Ad[CE1A] in combination with Melph had significantly higher concentration of extracellular ATP than both monotherapies in both JJN-3 OPM-2 cells (Figure 6.18 b) Ad[CE1A] in combination with Pan had significantly higher concentration of extracellular ATP than both monotherapies in OPM-2 cell only (Figure 6.18 c). Ad[CE1A] in combination with Pom did not have a significantly higher concentration than both monotherapies in both JJN-3 and OPM-2 cells (Figure 6.18 d).

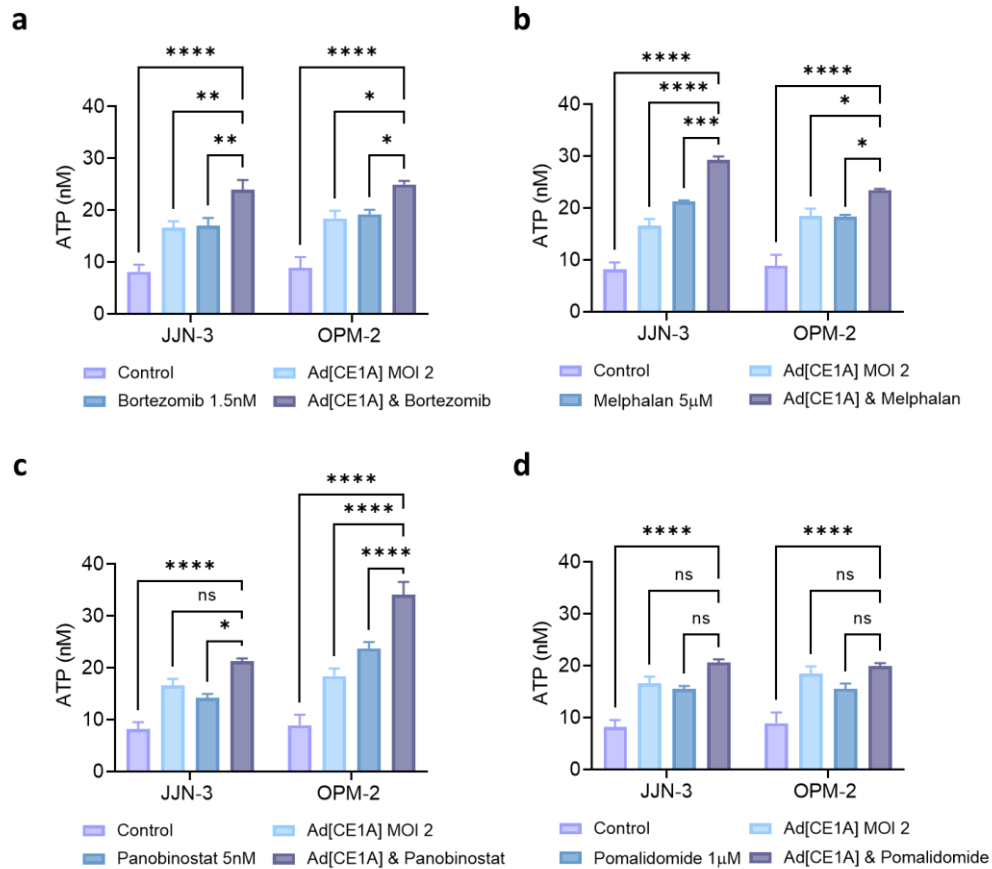


Figure 6.18: Extracellular release of ATP following 24 hour treatment of Ad[CE1A] ± anti-MM chemotherapy:

JJN-3, and OPM-2 cells were treated with Ad[CE1A] MOI 2 ± anti-MM chemotherapies, **(a)** BTZ 1.5 nM, **(b)** Melph 5 μM, **(c)** Pan 5 nM and **(d)** Pom 10 μM. After 24 hours supernatant was collected from cells and ATP concentration was determined by the ENLITEN® ATP assay using an ATP standard curve. n=3 Data is the mean ±SD. P values are for one-way ANOVA with multiple comparisons with Tukey's correction, where * p<0.05; ** p<0.01; *** p<0.001; **** p<0.0001.

6.3 Discussion

The overall aim of this chapter was to determine the efficacy of Ad[CE1A] in combination with different classes of approved anti-MM drugs and to determine how they potentiate Ad[CE1A]. As mentioned in the chapter introduction, there were two reasons to investigate this. Firstly, it was critical to determine oncolytic virotherapy in the context of other MM therapies, typically patients clinically receive three or more different therapies (chemotherapy, targeted therapy, IMiDs, steroids etc) in their treatment regimens, so clinically, Ad[CE1A] will be used in conjunction with other therapies. Secondly, previous clinical trials with other OV's including Ads have displayed limited efficacy in clinical trials as a monotherapy and the vast majority of OV trials are now used in combination with other therapies. To make the discussion easier, I have separated each anti-MM chemotherapy in combination with Ad[CE1A] into their own section.

6.3.1 Bortezomib

Before the main discussion, the results of BTZ in combination with Ad[CE1A] have been recapped in table format for easier referencing (Table 6.6). The first aim was to determine synergistic interactions between Ad[CE1A] and BTZ in human and murine MPCs. The results in section 6.2.2 show the complex and cell line dependent responses of these combinations.

Table 6.6 Summary of Bortezomib in combination with Ad[CE1A].

Drug		Cell Line			
		JJN-3	U266	OPM-2	5TGM1
Bortezomib	Overall CI index	Antagonism	Additive/ synergism	Synergism/ Additive	Synergism
	Dose Specific CI Index	Additive	Additive	Additive	Synergism
	CAR expression	****↑	****↑	**↑	-
	Infection rate concurrent treatment	NSD	NSD	NSD	NSD
	Infection rate drug first treatment	NSD	NSD	****↑ MOI 0.2 **↑ MOI 2	NSD
	CS1 expression	NSD	***↑	NSD	***↑
	E1A Expression	NSD	NSD	NSD	NSD
	Viral Titre	NSD	****↑	**↑	NSD
	CALR Expression	n.s BTZ n.s Ad[CE1A]	-	****↑ BTZ ****↑ Ad[CE1A]	-
	Extra-cellular ATP	**↑ BTZ **↑ Ad[CE1A]	-	*↑ BTZ *↑ Ad[CE1A]	-

NSD= No significant difference; *↑= Significant increase; *↓= Significant decrease; *↑BTZ/Ad[CE1A]= Significant increase between BTZ/Ad[CE1A] monotherapy and BTZ & Ad[CE1A] combination;

Firstly, the results in section 6.2.2 showed that BTZ and Ad[EC1A] in JJN-3 cells was antagonistic whilst in U-266 cells, the combination was antagonistic at lower concentrations but additive at higher concentrations. However, in OPM-2 cells the combination was synergistic/additive and in 5TGM1 cells the combinations were found to be synergistic. This suggests that there are differences in the way the cells respond to both treatments within MPC lines.

In agreement with the results found in OPM-2 and 5TGM1 cells, previous studies have shown beneficial outcomes when oncolytic Ads are used in combination with proteasome inhibitors. When BTZ was used in combination with an hTERT-Ad, enhanced oncolysis *in vitro* and *in vivo* was observed via ER stress and enhanced apoptosis in HCC (472). When proteasome inhibitor MG132 was used in combination with an oncolytic Ad (rAd-p53), the combination increased oncolysis in colon cancer cells due to increased CAR expression and subsequent viral infection (470). Proteasome inhibition in combination with other OV's have resulted in synergistic oncolysis, for example BTZ in combination with oHSV-1 resulted in synergistic oncolysis via enhanced viral replication, necroptosis and ER stress in ovarian, head and neck, glioma, and malignant peripheral nerve sheath tumour cells (473). Possibly the synergistic interactions seen in OPM-2 and 5TGM1 cells may be due to their sensitivity to ER stress over the JJN-3 and U266 cells and/or upregulation of CAR in these cells in response to BTZ.

In contrast, JJN-3 cells showed antagonistic effects, proteasome inhibition by either BTZ or PS-341 has been shown to result in antagonistic interactions with VSV in MM (119) and lung adenocarcinoma A549 cells (474), respectively. With BTZ inhibiting VSV replication in MM, however *in vivo* the combination resulted in improved antitumour efficacy compared to monotherapy (119). There does appear to be opposing interactions when combining OV's with proteasome inhibitors, however due to these studies being performed with different OV's, in different tumours and with different proteasome inhibitors, it is hard to compare and correlate as some differences will solely be due to differences in viral/tumour/proteasome inhibitor biology.

Secondly, in section 6.2.3, when assessing apoptosis and taking into account the drug dosages were changed to reflect the difference between AlamarBlue® and Annexin V and PI/TO-PRO-3 staining, the results were in agreement with the AlamarBlue® assays for U266 and OPM-2 as enhanced total cell death was detected compared to AlamarBlue® assays, However, U266 cells had significantly more apoptotic cells, which may not have been detected by AlamarBlue® assay which may be why BTZ and Ad[CE1A] combinations in this cell line were only additive at best as determined by AlamarBlue®. In

contrast JLN-3 cells oncolysis was enhanced compared to AlamarBlue® which were found to be antagonistic in AlamarBlue® assays. However, this increase wasn't due to increased apoptosis as by 72 hours most of the cells were necrotic. Whilst only U266 cells showed a significant increase in Annexin V⁺ only cells, whether apoptosis was increased at an earlier time point in the other cell lines was not investigated. The combination of an oncolytic ad (hTERT-Ad) with BTZ enhanced apoptosis by increased Annexin V staining, caspase 3 activity and pro-apoptotic proteins in HCC (472). The studies discussed above, whilst in different cancers and with different OV's and in most cases with different proteasome inhibitors are in agreement with the results presented in 6.2.2 and 6.2.3, that BTZ and Ad[CE1A] combinations increased cytotoxicity to either additive or synergistic level in MPC lines at certain doses.

Next it was important to determine if viral infection is increased following BTZ therapy. BTZ significantly increased CAR expression in all three human MPC lines tested. The results here are in agreement with previous studies, as proteasome inhibitors have been found to enhance viral infection by upregulation of CAR (359). As discussed in chapter 1 section 1.6.1, blocking the proteasome may affect how CAR expression is regulated as it is known to associate with an E3-ubiquitin ligase (LN3) (364) and other Ad receptors (Ad pVI) require ubiquitin ligases (Nedd4) to traffic Ad to the nucleus (365). Therefore, blocking the proteasome may prevent CAR degradation by the proteasome.

Despite this upregulation of CAR, there was no difference in Ad infection when MPCs were treated with BTZ and Ad-GFP concurrently, when cells were treated with BTZ first followed by Ad-GFP 24 hours later, there was only a significant increase in GFP expression in OPM-2 cells at both MOIs, which was interesting as OPM-2 cells had the lowest significant CAR fold change compared to JLN-3 and U266 cells. When looking at GFP MFI rather than percentage of GFP positive, there was no significant difference in MFI when cells were treated with BTZ and Ad-GFP concurrently. However, when BTZ was administered 24 hours before Ad-GFP, increases in GFP MFI were observed in OPM-2 cells at the higher MOI, but in U266 and 5TGM1 cells there was a significant decrease in GFP MFI at the higher

MOI. This effect may be due to BTZ altering the CMV promoter activity that controls GFP in Ad-GFP in infected MPC lines. One paper found that proteasome inhibition increases reporter proteins due to up-regulation of the CMV promoter by proteasome inhibitors (560), whilst this could be the case for OPM-2 cells which had an increase in GFP MFI, this does not explain the decrease seen in U266 and 5TGM1. Additionally, inhibiting the proteasome could lead to increases of GFP due to no proteasome degradation of GFP, which could also account for the increase in GFP MFI in OPM-2 cells.

Next was to determine if viral replication was increased following BTZ treatment. Firstly, investigation into whether BTZ altered CS1 expression was explored, as this may result in increased *E1A* expression. BTZ was able to significantly increase CS1 cell surface expression in U266 and 5TGM1 cells, but not in JJN-3 or OPM-2 cells. U266 cells had a much greater fold change in CS1 expression compared to 5TGM1 cells (1.9-fold vs 1.1-fold respectively), this may be because 5TGM1 cells have much higher basal CS1 expression than U266 cells. There is little research on whether proteasome inhibition alters CS1 expression, but one study found that BTZ did not significantly increase CS1 cell surface expression in different MPC lines. It is also important to note that at the time CS1 mRNA expression has not yet been investigated following anti-MM chemotherapy, so it is unknown whether CS1 mRNA expression is also increased, but the same study found that BTZ did not increase CS1 (*SLAMF7*) mRNA expression (290). The increases in cell surface CS1 expression could be due to excess CS1 not being degraded by the proteasome or as a survival mechanism following BTZ treatment as CS1 has been shown to be a growth factor for MM cells, as discussed in thesis introduction (section 1.4.5), and not by an increase in CS1 (*SLAMF7*) gene expression. Therefore, there are differences in BTZ's ability to increase CS1 expression, and it is likely to be cell line dependent.

Secondly, investigation into whether BTZ altered *E1A* mRNA expression was explored, either because of altered CS1 expression or by other mechanisms. BTZ did not significantly alter *E1A* mRNA expression in any of the MPC lines, even in U266 cells which had a significant increase in CS1 expression. This discrepancy may be due to assessing *E1A* expression after 24 hours, whilst CS1 expression was

assessed after 48 hours, so it may have been too early to see the effects. There is little to no previous research on whether proteasome inhibition alters Ad replication by directly altering some part of the Ad replication cycle, including *E1A*. As discussed in chapter 1 section 1.6.1 most research into proteasome inhibitors effects on increased viral replication was mainly found to be via indirect methods such as decreasing innate and adaptive immunity *in vivo* by blocking NF- κ B, allowing increased viral replication.

However, some research has been conducted which has found that the Ad protein E4-34kDa (which promotes viral replication and late gene expression) was found to be depended on functional proteasomes. The ability of E4-34kDa relies on target proteasome degradation which is important for efficient transition of infected cells to the late phase. However, when proteasome inhibitor MG132 was used, it did not dramatically affect late gene expression (561), therefore, E4-34kDa might not be needed for viral replication as originally thought. On the other hand, other OVs, such as HSV, have shown increased viral replication in combination with BTZ, due to BTZ-increased HSP90 expression supporting increased viral replication via enhanced nuclear location of the viral polymerase (471). HSP90 has also been found to play a major role in Ad5 replication. When a HSP90 chaperone inhibitor was used (17-AAG), Ad5 replication decreased by 95%. 17-AAG inhibited the transcription of early and late genes, replication of viral DNA, and expression of viral proteins (562). It would be of interest to test late gene expression to determine if there is an increase due to increase HSP90 expression or a decrease due to lowered E4-34kDa function.

Finally, investigation into whether BTZ increased viral titre was explored, either because of altered *E1A* expression, late gene expression, or other effects on viral life cycle. BTZ was able to significantly increase viral titre in U266 and OPM-2 cell lines, but this was not due to increased *E1A* expression, but may be due to increased viral infection in OPM-2 cells as they had increased GFP expression when cells were treated with BTZ before Ad-GFP. For U266 cell this could be due to increased CS1 expression following BTZ treatment, which did not increase *E1A* after 24 hours, but by 72 hours, when viral titre

was assessed, an increase in viral replication by *E1A* mRNA expression may have occurred. Or alternatively these increases in viral titre following BTZ could be due to increased late viral gene expression by HSP90 (562). Another possible explanation for increased viral titre could be due to loss of proteasome degradation of Ad proteins, therefore, more Ad protein available for transcription, and viral virion production.

The results presented here suggest the additive/synergistic interactions between Ad[CE1A] and BTZ in MPC lines may be due in part to increased viral production, but was most likely not due to increased *E1A* expression, but may be due to other factors, such as late viral gene expression and viral protein production and/or assembly, but was more likely to be due to enhanced cytotoxic effects via some specific cell death mechanism.

Lastly, investigation into whether BTZ increased Ad[CE1A]-induced markers of ICD was explored. As discussed in chapter 1 section 1.6.1, BTZ is a bona fide inducer of ICD. BTZ/Carfilzomib has been shown to upregulate CALR exposure, DC uptake and induce an adaptive immune response. Therefore, it was of interest to determine if BTZ in combination would enhance Ad[CE1A]-induced ICD marker expression.

Firstly, investigation into whether CALR exposure was increased following Ad[CE1A] in combination with BTZ after 24 hours was conducted. The combination significantly increased expression of cell surface CALR compared to monotherapies in both OPM-2 cells but not in JIN-3 cells, which showed no significant increase. Subsequently, investigation into whether extracellular ATP was increased following Ad[CE1A] in combination with anti-MM chemotherapy after 24 hours was conducted. The combination was able to significantly increase extracellular ATP concentration more than monotherapies in both JIN-3 and OPM-2 cells, this is in agreement with previous studies, as BTZ has been shown to increase ICD markers in either MM or other cancers, as discussed in section 1.6.1. This form of cell death could further enhance the synergy/additivity of the combinations *in vivo*.

6.3.2 Melphalan

Before the main discussion, the results of Melph in combination with Ad[CE1A] have been recapped in table format for easier referencing (Table 6.7). The first aim was to determine synergistic interactions between Ad[CE1A] and Melph in human and murine MPCs.

Table 6.7 Summary of Melphalan in combination with Ad[CE1A].

Drug		Cell Line			
		JJN-3	U266	OPM-2	5TGM1
Melphalan	Overall CI index	Strong Synergism	Strong Synergism	Synergism	Synergism
	Dose Specific CI Index	Strong Synergism	Strong synergism	Moderate Synergism	Synergism
	CAR Expression	**** ↑	**** ↑	**** ↑	-
	Infection rate concurrent treatment	NSD	NSD	NSD	NSD
	Infection rate drug first treatment	*** ↑ MOI 0.2	* ↑ MOI 0.2	**** ↑ MOI 0.2 **** ↑ MOI 2	** ↑ MOI 0.2
	CS1 expression	* ↑	** ↑	* ↑	**** ↑
	E1A Expression	**** ↑	NSD	**** ↑	**** ↑
	Viral Titre	* ↑	**** ↑	*** ↑	**** ↑
	CALR Expression	**** ↑ Melph * ↑ Ad[CE1A]	-	** ↑ Melph * ↑ Ad[CE1A]	-
	Extra-cellular ATP	**** ↑ Melph **** ↑ Ad[CE1A]	-	**** ↑ Melph **** ↑ Ad[CE1A]	-

NSD= No significant difference; * ↑= Significant increase; * ↓= Significant decrease; * ↑ Melph/Ad[CE1A]= Significant increase between Melph/Ad[CE1A] monotherapy and Melph & Ad[CE1A] combination;

Firstly, the results in section 6.2.2 showed that Melph and Ad[EC1A] in all cell lines were synergistic, with strong synergism observed in JJN-3 and U266 cells. This suggests that there are similarities in the way the cells respond to both treatments within MPC lines.

Previously minimal studies have been performed on OV_s in combination with Melph. There has been a small preclinical *in vitro* study combining oncolytic Ad (ONYX-015) with Melph in a squamous cell carcinoma cell line and a colon cancer cell line (505). The study found Melph synergised with ONYX-015 and upregulated CAR expression. The rest of the studies involving Melph and OV_s have predominately been in soft tissue sarcoma as a standard of care alongside TNF α via isolated limb perfusion alongside oncolytic VV (502), \pm various therapies such as radiotherapy and surgery (503) or PD-L1 (504). In each study, the full combination including oncolytic VV and Melph, showed the best treatment/disease control. However as discussed at length in the section 1.6.2, other alkylating agents have synergised with OV_s including Ads in other cancers. Whilst most research is investigating immunomodulatory effects *in vivo*, alkylating agents have been found to increase direct cytotoxicity in combination with OV_s. For example, increased cytotoxicity of an oncolytic Ad in combination with TMZ was observed in glioma and lung cancer (490), (491).

Secondly, in section 6.2.3, when assessing apoptosis and considering the drug dosages were changed to reflect the difference between AlamarBlue[®] and Annexin V and PI/TO-PRO-3 staining, the results were in agreement with the AlamarBlue[®] assays. Enhanced total cell death was found in JJN-3 U266 and OPM-2 cells similar to AlamarBlue[®] assays, however only in JJN-3 cells were there significant levels of Annexin V⁺ only cells compared to monotherapies, whilst the combination in the other cell lines were mainly necrotic. Whether apoptosis was increased at an earlier time point in the other cell lines was not investigated. The studies discussed above, whilst in different cancers and with different OV_s and in most cases with different alkylating agents are in agreement with the results presented in 6.2.2 and 6.2.3, that Melph and Ad[CE1A] combinations increased cytotoxicity in MPC lines.

Next was to determine if viral infection is increased following Melph treatment. Melph was found to significantly enhance CAR expression in all three human MPC lines tested. There is minimal previous research regarding whether alkylating agents increase CAR expression, as discussed in chapter 1 section 1.6.2 one study found that Melph did increase CAR expression and synergise with oncolytic Ad (dl1520) in a squamous cell carcinoma and colon cancer cell line (505). However, one study found that alkylating agent TMZ in combination with an E1B-deleted Ad did not result in increased CAR expression but did result in enhanced oncolysis, virus replication, apoptosis, autophagy and transduction efficacy in three murine cancer cells (563). However, the differences in CAR expression could be due to species differences, regarding the latter paper, alkylating agent differences, and tumour biology differences.

Despite the upregulation of CAR presented here, there was no difference in Ad infection when MPCs were treated with Melph and Ad-GFP concurrently, when cells were treated with Melph first followed by Ad-GFP 24 hours later, Melph significantly increased in GFP expression in all cell lines at the lower MOI 0.2 and in OMP-2 cells lines at MOI 2. When looking at GFP MFI rather than percentage of GFP positive, there was so significant difference in MFI when cells were treated with Melph and Ad-GFP concurrently. However, when Melph was administered 24 hours before Ad-GFP increases in GFP MFI were observed in JIN-3 cells at both MOIs, and U266 and OMP2 cells at the higher MOI, however in 5TGM1 cells at higher dose the MFI was significantly lower. This effect may be due to Melph altering the CMV promoter activity that controls GFP in Ad-GFP in the MPC lines. Alkylating agents have been shown to change gene expression as measured by CMV regulated Luc activity. Alkylating agents that bind to the major groove increased CMV-Luc activity, whilst minor groove binders decreased CMV-Luc activity (564). Melph can bind to both major and minor grooves (guanine N7 and adenine N3 respectively) (565), which may account for the varied effects amongst human and murine cell lines.

Next was to determine if viral replication was increased following Melph treatment. Firstly, investigation into whether Melph altered CS1 expression was explored, as this may result in increased *E1A* expression. Melph was able to significantly increase CS1 cell surface expression in all cell lines.

Again, there is little research on whether alkylating agents alter CS1 expression, but one study investigated whether Melph increased CS1 expression. The results were varied across the MM cell lines they used, but they did see an increase in CS1 expression following Melph treatment in MPC lines KMS-12-BM and RPMI-8226 by roughly a 1.5-fold change (290), which was a similar fold change seen in the MPC lines tested here (1.4-1.7 fold change). They also saw the same pattern looking at CS1 (*SLAMF7*) mRNA expression. Therefore, Melph's ability to increase CS1 expression was cell line dependent. The mechanism behind Melph increasing CS1 expression is unknown, but as discussed for BTZ it may be a survival mechanism in response to Melph.

Secondly, investigation into whether Melph altered *E1A* mRNA expression was explored, either because of altered CS1 expression or by other mechanisms. Melph significantly increased *E1A* expression in JJN-3, OPM-2 and 5TGM1 MPC lines (2.4-4.2-fold). This may be due to increased CS1 expression, which was increased in all cell lines following Melph treatment, but could be also due to increased infection, as increased GFP positive cells were found in JJN-3, U266, OPM-2 and 5TGM1 cells when cells were treated with Melph before Ad-GFP. Whilst U266 cells didn't have a significant fold change in *E1A* expression they did have an increase in *E1A* (1.15-fold change) but this did not reach significance, therefore the effects of increasing CS1 expression and/or infection had a smaller effect on increasing *E1A* expression in U266 cell lines. As discussed in chapter 1 section 1.6.2 minimal studies have investigated whether Melph, or other alkylating agents increase *E1A* expression or adenoviral replication. TMZ in combination with an oncolytic Ad (Adhz60) in lung cancer increased E1A protein as detected by western blot, but they did not look at *E1A* mRNA expression. They also observed an increase in viral titre *in vitro* and Ad Hexon *in vivo* (491), therefore no one has previously assessed adenoviral gene expression/replication in combination with alkylating agents.

Finally, investigation into whether Melph increased viral titre was explored, either as a result of altered *E1A* expression, late gene expression, or other effects on viral life cycle. Melph increased viral titre in all MPC lines tested. This was probably due to the increase in CS1 expression and increase in *E1A*

mRNA expression, but as mentioned could also be in a small part due to increased infection. It would be interesting to investigate if Melph alters other viral genes to see if similar effects are observed

The results presented here suggest the synergy between Ad[CE1A] and Melph in MPC lines was due to increased viral replication, which was consistent in all MPC lines tested.

Lastly, investigation into whether Melph increased Ad[CE1A]-induced markers of ICD was conducted. As discussed in chapter 1 section 1.6.2, Melph is a bone fide inducer of ICD. Melph has been shown to increase CALR exposure HMGB1 release and has many immune-related effects, such as depletion of T-regs, type I IFN induction etc. In MM, Melph induced MPC exosome release which stimulated NK cell IFN- γ production in a HSP70-dependent manner (508). Therefore, it was of interest to determine if these drugs in combination would enhance Ad[CE1A]-induced ICD marker expression.

Firstly, investigation into whether CALR exposure was increased following Ad[CE1A] in combination with Melph after 24 hours was conducted. Ad[CE1A] in combination with Melph had significantly higher levels of CALR exposure compared to monotherapies in both JJN-3 and OPM-2 cells. Subsequently, investigation into whether extracellular ATP concentration was increased following Ad[CE1A] in combination with Melph after 24 hours was conducted. Ad[CE1A] in combination with Melph was able to significantly increase extracellular ATP more than monotherapies in JJN-3 and OPM-2 cells, this is in agreement with previous studies, as Melph has been shown to increase ICD markers in either MM or other cancers. This form of cell death could further enhance the synergy of the combinations *in vivo*.

6.3.3 Panobinostat

Before the main discussion, the results of Pan in combination with Ad[CE1A] have been recapped in table format for easier referencing (Table 6.8). The first aim was to determine synergistic interactions between Ad[CE1A] and Pan in human and murine MPCs. The results in section 6.2.2 show the complex and cell line dependent responses of these combinations.

Table 6.8 Summary of Panobinostat in combination with Ad[CE1A].

Drug		Cell Line			
		JJN-3	U266	OPM-2	5TGM1
Panobinostat	Overall CI index	Additive/ Slightly antagonism	Synergism	Synergism/ Additive	Synergism/ Additive
	Dose Specific CI Index	Additive	Additive	Synergism	Synergism/ Additive
	CAR expression	****↑	****↑	****↑	-
	Infection rate concurrent treatment	NSD	NSD	NSD	**↑ at 24 hours
	Infection rate drug first treatment	****↑ MOI 0.2	NSD	NSD	****↑ MOI 2
	CS1 expression	*↑	NSD	NSD	****↓
	E1A expression	NSD	*↓	NSD	**↑
	Viral Titre	NSD	****↑	NSD	NSD
	CALR Expression	NSD Pan NSD Ad[CE1A]	-	* ↓Pan ** ↓ Ad[CE1A]	-
	Extra-cellular ATP	*↑Pan NSD Ad[CE1A]	-	****↑ Pan ****↑ Ad[CE1A]	-

NSD= No significant difference; *↑= Significant increase; *↓= Significant decrease; *↑/↓Pan/Ad[CE1A]= Significant increase/decrease between Pan/Ad[CE1A] monotherapy and Pan & Ad[CE1A] combination; NSDPan/Ad[CE1A]= No significant difference between Pan/Ad[CE1A] monotherapy and Pan & Ad[CE1A] combination.

Firstly, the results in section 6.2.2 showed that Pan and Ad[EC1A] in JJN-3 cells were additive/antagonistic, additive/synergistic in OPM-2 and 5TGM1 and synergistic in U266 cells. This suggests that there are similarities in the way the cells respond to both treatments within MPC lines, but some of these cell lines are more sensitive to the combinations than others.

In agreement with the results stated here, and as discussed in chapter 1 section 1.6.3, several groups have explored the use of HDACIs with OVAs and have seen beneficial antitumour effects. HDACIs have been combined with OVAs including Ads in other cancers which has resulted in enhanced cytotoxicity *in vitro* and *in vivo* in several tumour types, via upregulated CAR expression (526,527,529) or $\alpha v\beta_3$ integrin expression (528), apoptosis (528,532) and/or cycle growth arrest (532) following HDACI treatment. This resulted in increased infection and in some instances increased replication (526,527), but in some instances decreased viral replication was observed despite enhanced cytotoxicity and apoptosis (528) however, in one case the combination of HDACI and oncolytic Ad was antagonistic *in vivo* despite increased CAR expression and Ad transduction *in vitro* (529). The latter study found that the timing of HDACI was important, if HDACI were given after the oncolytic Ad, this suppressed replication, which agrees with the former study as they also found decreased viral replication, however they did see improvements in antitumour responses with the combination, and HDACI was given at the same time as the oncolytic Ad. We also treated cells with combination treatments concurrently, so Pan may not have suppressed Ad replication, resulting in the synergistic/additive interactions observed.

Secondly, in section 6.2.3, when assessing apoptosis and taking into account the drug dosages were changed to reflect the difference between AlamarBlue® and Annexin V and PI/TO-PRO-3 staining, the results were in agreement with the AlamarBlue® assay as enhanced total cell death was found in JJN-3 U266 and OPM-2 cells similar to AlamarBlue® assays, this was mainly a necrosis effect as there was no significant increase in Annexin V⁺ only cells compared to monotherapies. Similar to the other anti-MM chemotherapies discussed, whether apoptosis was increased at an earlier time point was not investigated. The studies discussed above, whilst in different cancers and with different OVAs and in most cases with different HDACIs are in the most part in agreement with the results presented in 6.2.2 and 6.23 that Ad[CE1A] in combination with HDACI Pan increased cytotoxicity of MPC lines.

Next was to determine if viral infection increased following Pan treatment. Pan was found to significantly increase CAR expression in all three human MPC lines tested. This is in agreement with other research that HDACs upregulate CAR (526,527,529,530), and $\alpha\beta_3$ integrins (528) as discussed in chapter 1 section 1.6.3. For example, HDACI FR901228 upregulated CAR expression in human lung cancer cell lines which increased infection efficiency of oncolytic Ad OBP-301. The combination also resulted in a synergistic antitumour effect *in vitro* (526). The mechanism behind the increase in CAR expression following HDACs is thought to be due to altered transcriptional regulation of CAR. (566). One issue with upregulation of CAR could be the off-target effects of the HDACs increasing CAR expression in normal tissues, one study however found that the upregulation of CAR was only seen in bladder cancer cells following HDACs TSA and sodium phenylbutyrate and not in normal urothelial cells and CAR-positive papilloma cells. Additionally, cancer cells that are CAR-negative did not show increased CAR expression or Ad transduction (567). In further support of HDACI increasing Ad infection and as discussed in section 1.6.3, one study found HDACs increased $\alpha\beta_3$ expression resulting in enhanced infection (528), unfortunately we did not test $\alpha\beta_3$ expression following Pan treatment in this study.

Despite this upregulation of CAR, there was only a significant increase in GFP expression in 5TGM1 cells after 24 hours when they were treated with Pan and Ad-GFP concurrently. When cells were treated with Pan first followed by Ad-GFP 24 hours later there was a significant increase in GFP expression in U266 cells when treated at the lower MOI 0.2 and a significant increase in 5TGM1 cell when treated at the higher MOI 2. When looking at MFI rather than percentage of GFP positive, there was a significant increase observed in GFP MFI in U266, OMP2 and 5TGM1 cells after 48 hours when cells were treated with Pan and Ad-GFP concurrently. Additionally, when Pan was administered 24 hours before Ad-GFP increases in GFP MFI were observed in JJN-3, U266 and OPM-2 cells at the higher MOIs, and 5TGM1 cells at both MOIs. This effect may be due to Pan augmenting the CMV promoter activity that controls GFP in Ad-GFP in the MPC lines. HDACs have been previously shown to enhance

transcriptional activity of the CMV promoter in bladder cancer *in vitro* and *in vivo* (568) and in prostate cancer (569).

Next was to determine if viral replication was increased following Pan treatment. Firstly, investigation into whether Pan altered CS1 expression was explored, as this may result in increased *E1A* expression. Pan was able to significantly increase CS1 cell surface expression in JJN-3 cells, but significantly decreased cell surface expression in 5TGM1 cells. Again, little research has been conducted on whether HDACs alter CS1 expression, however in one study, Pan was shown to not significantly increase CS1 cell surface expression in different MPC lines (~0.8-1 fold change) however, CS1 (*SLAMF7*) mRNA expression was upregulated in the KMS-12-BM cell line (~1.5 fold) (290). HDACs have been shown to increase other cell surface immunogenic proteins in MM, such as CD38, which was increased in response to Ricolinostat (protein and mRNA) due to more acetylation in histone 3 lysine 27 in the CD38 promoter (570), this may explain why we saw an increase in CS1 expression in JJN-3 cells but does not explain the decrease we saw in 5TGM1 cells. Therefore, Pan's ability to increase CS1 expression is cell line dependent.

Secondly, investigation into whether Pan altered *E1A* mRNA expression was explored, either because of altered CS1 expression or by other mechanisms. Pan significantly decreased *E1A* expression in U266 cell lines but significantly increased it in OPM-2 cells, whilst in JJN-3 and 5TGM1 cells there was a slight increase in *E1A* expression, but this did not reach significance (1.25 fold and 1.64 fold respectively). There are a few studies regarding HDACs effects on Ad replication as discussed in chapter 1 section 1.6.3, one study found that HDACs increased late viral gene expression (as assessed by GFP expression controlled by the *E3* promoter), but decreased viral titre in glioblastoma stem cells (528). In another study HDACs were found to decrease Ad replication as measured by viral titre assays, which resulted in antagonistic effects. This was due HDAC-induced increase in p21. When p21 was suppressed by siRNA, it reversed the HDAC-induced suppression of Ad replication. However, if HDACs were given prior to Ad administration, synergy was observed, this was probably due HDACs not suppressing Ad

replication (529). p21 has been implicated as a mechanism for decreasing viral replication following HDACi in other cancers (prostate) and with other HDACi. In this study HDACi increased E1A and E1B protein production but decreased Ad protein production late in the viral life cycle. p21 expression limited viral replication in different cancer cell models (as determined by overexpression and knockout experiments), therefore, suggesting that p21-induced increases in E1A result in dysfunctional E1A or that p21 inhibits downstream effectors of E1A action (530). Whilst only *E1A* expression was investigated following Pan treatment in this thesis, it would be interesting to investigate late viral gene expression following Pan as the studies here have contradictory results, as one found increased late viral gene expression, whilst one found decreased late viral gene expression. Additionally, it would have been interesting to stagger treatment schedules to see if that would influence viral replication. Whilst one study did observe an increase in E1A protein, my results seem to be cell line dependent as U266 cells had significantly less *E1A* expression following Pan treatment.

Finally, investigation into whether Pan increased viral titre was explored, either because of altered *E1A* expression, late gene expression, or other effects on viral life cycle. Pan only significantly increased viral titre in U266 cells, but in JJN-3 and OPM-2 there were increases in viral titre, but it did not reach significance. The significant increase in viral titre in U266 cells was in stark contrast to the significant decrease in *E1A* expression. The increase in viral titre could be due to several mechanisms not investigated as part of this thesis, such as late viral gene expression, epigenetic regulation of other viral or host cell genes increasing viral titre that are not *E1A*-dependent. A small part of this increased viral titre could be due to Pan significantly increasing Ad infection when administered 24 hours prior to Ad-GFP in U266 cells.

The results presented here suggest the synergistic interactions between Ad[CE1A] and Pan in MPC lines may be due in part to increased viral production, but was most likely not due to increased *E1A* expression, but may be due to other factors, such as late viral gene expression, epigenetic regulation,

viral protein production and/or assembly, but was more likely to be due to enhanced cytotoxic effects via some specific cell death mechanism.

Lastly, investigation into whether Pan increased Ad[CE1A]-induced markers of ICD was explored. As discussed in chapter 1 section 1.6.3, HDACIs have been shown to induce ICD in MM and other cancers (197,540–544). HDACI Quisinostat has been shown to increase CALR exposure and decrease CD47 expression, increased DC maturation, and number of memory and Naïve T cells in the BM in 5T33MM models of MM. However, in *in vivo* vaccination assays, Quisinostat did not provide 100% protection (545). Therefore it was of interest to determine if these drugs in combination would enhance Ad[CE1A]-induced ICD marker expression.

Firstly, investigation into whether CALR exposure was increased following Ad[CE1A] in combination with Pan after 24 hours was conducted. Pan failed to enhance CALR exposure compared to monotherapies. Subsequently, investigation into whether extracellular ATP was increased following Ad[CE1A] in combination with Pan after 24 hours was conducted. Ad[CE1A] in combination with pan Pan was able to significantly increase extracellular ATP concentration compared to monotherapies in OPM-2 cells but not in JIN-3 cells, where there no significant difference between combination and monotherapies. This is in agreement with previous studies HDACIs have all been shown to increase ICD markers in either MM or other cancers, but it appears that Pan does not always enhance Ad[CE1A] release of DAMPs. However, this is still promising as Pan could still further enhance the synergy of the combinations *in vivo* by inducing greater ICD.

6.3.4 Pomalidomide

Before the main discussion, the results of Pom in combination with Ad[CE1A] have been recapped in table format for easier referencing (Table 6.9). The first aim was to determine synergistic interactions between Ad[CE1A] and Pom in human and murine MPCs. The results in section 6.2.2 show the complex and cell line dependent responses of these combinations.

Table 6.9 Summary of Pomalidomide in combination with Ad[CE1A].

Drug		Cell Line			
		JJN-3	U266	OPM-2	5TGM1
Pom	Overall CI index	Synergistic	Synergistic	Synergistic	Synergism
	Dose Specific CI Index	Strong Synergism	Synergism	Synergism	Synergism
	CAR Expression	****↓	**↓	****↑	-
	Infection rate concurrent treatment	NSD	NSD	NSD	NSD
	Infection rate drug first treatment	NSD	NSD	**↑ MOI 0.2	***↑ MOI 0.2 ***↑ MOI 2
	CS1 expression	NSD	NSD	**↓	*↓
	E1A Expression	*↑	NSD	NSD	NSD
	Viral Titre	NSD	NSD	NSD	NSD
	CALR Expression	n.s Pom n.s Ad[CE1A]	-	n.s Pom n.s Ad[CE1A]	-
	Extra-cellular ATP	n.s Pom n.s Ad[CE1A]	-	n.s Pom n.s Ad[CE1A]	-

NSD= No significant difference; *↑= Significant increase; *↓= Significant decrease; NSDPom/Ad[CE1A]= No significant difference between Pom/Ad[CE1A] monotherapy and Pom & Ad[CE1A] combination.

Firstly, the results in section 6.2.2 showed that Pom and Ad[EC1A] in all cell lines were synergistic. This suggests that there are similarities in the way the cells respond to both treatments within MPC lines.

In agreement with the results stated here, the use of IMiDs with OV_s has been minimally explored but beneficial anti-MM effects have been observed. As discussed in chapter 1 section 1.6.4, thalidomide in combination with oHSV-1 was able to decrease primary breast cancer in syngeneic mouse models and decrease lung metastasis (552), whilst Len in combination with oHSV-1 in MM was able to enhance cytotoxicity and suppress subcutaneous MM tumour growth *in xenograft mice* (553). Len in combination with oncolytic RV augmented antitumour efficacy in *ex vivo* primary patient MM cells and MPC lines (554).

Secondly, in section 6.2.3, when assessing apoptosis and taking into account the drug dosages were changed to reflect the difference between AlamarBlue[®] and Annexin V and PI/TO-PRO-3 staining, the results were in agreement with the AlamarBlue[®] assay as enhanced total cell death was found in JLN-3 U266 and OPM-2 cells similar to AlamarBlue[®] assays, this was mainly a necrosis effect, however in U266 cells there was a significant increase in Annexin V⁺ only cells compared to monotherapies. Again, similar to the other anti-MM chemotherapies discussed, whether apoptosis was increased in the other cell lines at an earlier time point was not investigated. The studies discussed above, whilst for the slight majority were in MM but were with different OV_s and with different IMiDs are in the agreement with the results presented in 6.2.2 and 6.23 that Ad[CE1A] in combination with IMiD Pom increased cytotoxicity of MPC lines.

Next was to determine if viral infection increased following Pom treatment. Pom was found to decrease CAR expression in JLN-3 cells and U266 cells, but it increased CAR expression in OPM-2 cells. There is no prior research on the effects of IMiDs on CAR expression, however, IMiDs have been shown to downregulate adhesion molecules such as VCAM-1, ICAM-1, E-selectin and L-selectin which disrupts adhesion of MM cells to BMSCs suppressing adhesion mediated cell signalling and secretion of cytokines that supports MM cell growth, survival, and development of drug resistance (571,572). Additionally, IMiDs have been shown to modulate several other cell surface antigens such as CD38, CD56, CD20 and CD180 (290,573,574). Obviously, the effect of Pom on CAR was cell line dependent

as there was an increase in CAR expression in OMP-2 cells compared to JIN-3 and U266. Despite Pom altering CAR expression, there was no significant difference in Ad infection in MPC lines following concurrent treatment of Pom and Ad-GFP. However, when Pom was administered 24 hours before Ad-GFP there was a significant increase in Ad-GFP in OMP-2 and 5TGM1 cells at the lower MOI of 0.2 and in the 5TGM1 cells at the higher MOI 2. When looking at MFI rather than percentage of GFP positive, there was a significant increase in GFP MFI in U266 cells after 48-hour treatment when Pom and Ad-GFP was administered concurrently. Additionally, when Pom was administered 24 hours before Ad-GFP, an increase in GFP MFI was observed in U266 and OPM-2 cells at the higher MOI, but a significant decrease in GFP MFI was observed in JIN3 cells at a higher MOI. This effect may be due to Pom altering the CMV promoter activity that controls GFP in Ad-GFP in the MPC lines. There is no literature stating the effects of IMiDs on CMV transcriptional activity.

As discussed at length in the introduction of this chapter and my third objective, was to determine if viral replication was increased following Pom treatment. Firstly, investigation into whether Pom altered CS1 expression was explored, as this may result in increased *E1A* expression. Pom was able to significantly decrease CS1 expression in OMP-2 cells and 5TGM1 cells. Again, little research has been conducted on whether IMiDs alter CS1 expression, however one study found IMiDs Len and Pom downregulated CS1 protein and mRNA expression (290), as discussed in the thesis introduction (section 1.4.5.3). This was due to a decrease in the transcription factor Ikaros (IKZF1) which are the targets of Len and Pom, which was found to transcriptionally control CS1 in MM cells. Therefore, the decreases in OMP-2 cells and 5TGM1 cells agree with this study.

Secondly, investigation into whether Pom altered *E1A* mRNA expression was explored, either because of altered CS1 expression or by other mechanisms. Pom only significantly increased *E1A* expression in JIN-3 cells. This was not due to an increase in CS1 expression or viral infection. The mechanism of increased *E1A* expression in JIN-3 cells is unknown, but similar to Pan, IMiDs (Len and Pom) have been shown to increase p21. Len has been shown to increase p21 epigenetically, by reducing histone

methylation and increasing histone acetylation in the p21 promoter (575,576). As discussed in section 6.3.3.3, p21 was upregulated following HDACI, and was shown to increase E1A but decrease late adenoviral production. The authors conclude that p21-induced increases in E1A result in dysfunctional E1A or that p21 inhibits downstream effectors of E1A action (530), this could be a mechanism why there was increased *E1A* expression following Pom treatment. It's interesting that the decrease in CS1 expression seen following Pom treatment in OMP-2 and 5TGM1 cells did not result in a significant decrease in *E1A* expression. This may be because we investigated *E1A* expression after 24 hours and not 48 hours, which was when CS1 expression was assessed following Pom.

Finally, investigation into whether Pom increased viral titre was explored, either because of altered *E1A* expression, late gene expression, or other effects on viral life cycle. Pom did not significantly increase viral titre in any MPC line. It is interesting that the significant increase in *E1A* expression in JJN-3 cells did not result in a significant increase in viral titre, however there was a non-significant increase in viral titre in JJN-3, U266 and OMP-2 cells.

The results presented here suggest the synergistic interactions between Ad[CE1A] and Pom in MPC lines was not likely to be solely due to increased viral replication via increased CS1 expression, *E1A* expression or viral titre, but was more likely to be due to enhanced cytotoxic effects via some specific cell death mechanism.

Lastly, investigation into whether Pom increased Ad[CE1A]-induced markers of ICD was explored. As discussed in the introduction to this chapter, Pom is an IMiD, and can stimulate and suppress various immune cells via upregulation and downregulation of costimulatory or inhibitory molecules. Therefore it was of interest to determine if these drugs in combination would enhance Ad[CE1A]-induced ICD marker expression.

Firstly, investigation into whether CALR exposure was increased following Ad[CE1A] in combination with Pom after 24 hours was conducted. Ad[CE1A] in combination with Pom failed to enhance CALR exposure compared to monotherapies. Subsequently, investigation into whether extracellular ATP concentration was increased following Ad[CE1A] in combination with Pom after 24 hours was conducted. Ad[CE1A] in combination with Pom, however, failed to enhance extracellular ATP release compared to monotherapies. Whilst Pom did not enhance these particular DAMPs, Pom could still enhance ICD in combination with Ad[CE1A] by upregulation of costimulatory molecules and down regulation of immune inhibitory molecules enhancing the synergy of the combination *in vivo*.

6.3.5 Summary

The results presented and discussed regarding augmenting Ad[CE1A] following anti-MM chemotherapy are quite complex. Clearly there are differences in the way the MPCs respond to anti-MM chemotherapies, however, it is promising that there are additive/synergistic interactions seen with all drugs in at least one of the MPC lines, if we are able determine the mechanism of these additive/synergistic interactions we may be able to enhance the effect in cells lines that did not respond as well.

Whilst the results of CAR expression appeared promising, particularly following BTZ, Melph and Pan treatment in human MPC lines, the adenoviral infection results appeared less promising, there was only one anti-MM therapy that increased Ad-GFP significantly in all cell lines, and that was Melph, when administered before Ad-GFP, but only when Ad-GFP was given at a low dose. Some of the other drugs also significantly increased Ad-GFP at a lower dose when administered 24 hours prior. Speculatively, the increased CAR expression may only enhance adenoviral infection when there are fewer virions, the more virions available may not benefit from the increased CAR expression. Therefore, it is unlikely that increased Ad infection alone contributes solely to the additive/synergistic interactions but may contribute slightly. Additionally, I have not investigated whether other secondary Ad receptors are altered following anti-MM chemotherapies, CAR expression may be increased but $\alpha\beta_{5/3}$ may be decreased, which may balance out the effect of increased CAR expression.

The results presented and discussed regarding viral replication following anti-MM chemotherapy are quite complex. For BTZ and Pan, there were increases in viral titre, but this did not correspond to increases in *E1A* expression or vice versa, therefore, it is difficult to conclude whether these drugs increase viral replication as we could have missed the time point in which to see the effects. Additionally other factors may be involved, as discussed, such as late viral gene expression, p21 and effects on viral protein production. For Melph, it was clear that Melph increased viral replication by increasing CS1, *E1A* expression and viral titre in almost all the MPC lines. Whether the increase in CS1 was the cause of the increase in *E1A* expression is unknown. For Pom, it does not appear to increase viral replication resulting in increased viral progeny, but interestingly the decrease in CS1 did not negatively affect *E1A* expression, so the two may be independent of each other. Encouragingly, BTZ and Melph and to an extent Pan enhanced expression of ICD DAMPs, which could further enhance anti-MM immune response *in vivo* and in a clinical setting.

6.4 Chapter Conclusion

Results presented earlier in this thesis (chapter 4 & 5) evidenced that Ad[CE1A] as a single agent in MM *in vivo* murine models was safe, but did not eradicate all tumour burden. Results presented in this chapter show that Ad[CE1A] can be enhanced with the addition of anti-MM drugs. For Melph it was clear that it enhanced viral replication causing increased oncolysis. For the other agents it was less clear how they were able to improve anti-MM cell killing. The results show that within MPCs there are differences to how Ad[CE1A] and anti-MM chemotherapies interact, and how those anti-MM chemotherapies affect Ad life cycle. However, future work can build on the data presented in this chapter. Of particular interest would be to investigate ER stress and necroptosis in response to Ad[CE1A] & anti-MM chemotherapies, but more importantly, is to investigate if these combinations enhance anti-MM activity *in vivo* either against established disease or in a MRD setting. Additionally, the drugs used in combination with Ad[CE1A] is not an exhaustive list, it would be of interest to test Ad[CE1A] with other drugs in the same drug class (carfilzomib, Len), but also other anti-MM drugs such as some of mAbs or PD-L1 inhibitors.



Chapter 7 : Final Conclusions and Future Directions



7.1 Final Conclusions

The results presented within this research have demonstrated Ad[CE1A] efficacy against MM. Chapter 3 focused on the potential for the use of Ad[CE1A] for MM treatment in MPC lines and patient-derived MM cells. To investigate this, this chapter aimed to determine whether Ad[CE1A] could infect, replicate and kill MM cells, and to determine the mechanism(s) behind Ad[CE1A] induced cell death. Contrary to the long-held belief, MPCs were shown to express Ad5 receptors and were efficiently infected with Ad5. Ad[CE1A] also replicated efficiently resulting in significant oncolysis in a large panel of MPCs and in multiple MM patients, but not in any of the control cells used, demonstrating its specificity for MPCs. Experiments were conducted to try to deduce Ad[CE1A]'s cell death mechanism, which was found not to be caspase-dependent, but may involve MLKL-dependent necroptosis. To explore further the cell-death inducing properties of Ad[CE1A], ICD was investigated. Encouragingly, Ad[CE1A] was able to cause ICD DAMP expression in MPCs, which may result in enhanced anti-MM immune cell killing in patients or *in vivo*. Additionally, Ad[CE1A] was able to increase MHC class I and II expression and cause bystander cytokine killing. Further understanding of how Ad[CE1A] kills MM can only help to design studies to maximise the effects of Ad[CE1A] either alone or in combination with other anti-MM chemotherapies.

Following this was to assess Ad[CE1A] *in vivo* against MRD in chapter 4. To investigate this, the chapter aimed to determine whether Ad[CE1A] could prevent MPC regrowth *in vitro*, whether Ad[CE1A] had equal efficacy against BTZ insensitive cells compared to BTZ sensitive cells, and to determine if Ad[CE1A] was able control/eradicate MRD *in vivo* in the low tumour burden model of myeloma. Firstly, preliminary *in vitro* assays demonstrated that Ad[CE1A] was able to reduce MPC viability over 25 days following BTZ treatment, whilst BTZ-only treated cells recovered viability to that of controls. Additionally Ad[CE1A] was just as effective at killing BTZ-insensitive cell lines as parental BTZ sensitive cell lines. Disappointingly, these results did not translate *in vivo*. Ad[CE1A] had no effect as a monotherapy in established disease or after tumour debulking with BTZ. As discussed in the chapter

4 discussion, there were many complex reasons that could have accounted for the lack of efficacy, it was clear that the study was inconclusive as there were many confounding factors for this reason, preliminarily investigation into dormancy *in vitro* was conducted. It appears culturing human MPCs alone or with CM from osteoblast-like cells or BMSCs does not produce/induce high levels of dormancy, like what is observed in 5TGM1 cells following osteoblast CM media (337). Preliminary investigations of 3D cocultures with polyHIPE scaffolds appear promising, MPCs and Saos-2 cells were able to proliferate on/within the scaffolds and Ad[CE1A] was able to penetrate the pores and cause MPC lysis. Ad[CE1A] was able to induce cell death in DID^{High} and DID^{Low} cells but it was difficult to determine if these cells were true non-proliferative dormant cells.

As Ads are species specific, it was long thought human Ad5 could not be tested in murine syngeneic models, limiting the ability to test the efficacy of oncolytic Ads in immunocompetent models, which as discussed, may be essential for efficacy, particularly for long-term disease control. With multiple reports of Ad5 infecting, replicating and causing oncolysis in murine cancer cells, chapter 5 focussed on the efficacy of Ad[CE1A] in the 5TGM1 syngeneic model. To investigate this, this chapter aimed to determine whether, Ad[CE1A] could infect, replicate and kill MPC cells *in vitro* and *in vivo*. Ad[CE1A] was able to infect, replicate and kill 5TGM1 cells to a similar level of human MPCs, therefore Ad[CE1A] efficacy was tested *in vivo* in a 5TGM1 study. Ad[CE1A] was able to reduce tumour burden in 5TGM1-bearing mice, but did not eradicate all tumour. There did not appear to be a dose response to Ad[CE1A] and disappointingly, Ad[CE1A] could not be detected at gene or protein level. Encouragingly, cytokine microarray results show that Ad[CE1A] may alter the microenvironment as reduced CXCL12 and IL-17 was observed following two of the three treatment groups.

Lastly in chapter 6, Ad[CE1A] was assessed in combination with anti-MM chemotherapies BTZ, Melph, Pan or Pom. This was investigated as it was clear from the previous work presented that Ad[CE1A] alone could not eradicate all tumour burden. The aim of this chapter was to investigate if Ad[CE1A] had enhanced anti-MM efficacy in combination with anti-MM chemotherapies, and to investigate if

these drug combinations augmented Ad[CE1A] life cycle. Ad[CE1A] showed additive/synergistic interactions in combination with anti-MM chemotherapies in MPCs, but this was not always consistent between cell lines or within them, except for Melph. After assessing how the anti-MM chemotherapies augment Ad life cycle, it was clear that Melph enhanced viral replication resulting in increased cell death, as this was consistent in all cell lines. For the other agents it was less clear how they were able to augment Ad life cycle and whether augmenting Ad life cycle was the cause of the enhanced cytotoxicity, or whether the combination caused enhanced cytotoxicity through complementary cell death mechanisms.

To conclude, the data presented here on Ad[CE1A] are extremely exciting and indicate a potential novel therapy for MM. Particularly exciting is the fact Ad[CE1A] killed patient derived MM cells, which has promise for their clinical efficacy. Disappointingly, I was unable to determine if Ad[CE1A] was effective against MRD, but now we know that Ad[CE1A] has efficacy in the 5TGM1 immunocompetent model of myeloma, we can use that model in the future for the same research question, which may yield better results. Additionally, we now know anti-MM chemotherapies in combination with Ad[CE1A] can increase anti-MM cell death, and it appears the mechanism for this for Melph is by increasing viral replication, therefore, we could experiment with combining Ad[CE1A] and these anti-MM chemotherapies in models of MRD.

7.2 Future directions

Further preclinical work will now be undertaken by myself and new PhD students to help further understand Ad[CE1A]-induced cytotoxicity. Further experiments need to be performed to assess necroptosis in molecular detail. The results presented in this thesis show that MLKL plays a role in Ad[CE1A]-induced cytotoxicity, so experiments to overexpress/knockout MLKL and other necroptosis proteins may help to better understand Ad[CE1A]-induced cell death in MPC cells.

After inconclusive results using Ad[CE1A] in the U266 murine low tumour burden model of MM, *in vitro* models are going to be developed to generate dormant cells that mimic the cells that remain in

MRD. Preliminary investigation presented in this thesis with the polyHIPE scaffolds alongside other 3D cell culture methods I have helped our research lab get preliminary results for which do not appear in this thesis, appear encouraging. This preliminary work contributed to a successful NC3Rs studentship application, therefore, a new PhD student will be taking this work forward and developing the models with the long-term goal of using the models to test Ad[CE1A] efficacy and the efficacy of other drugs in models of dormancy/MRD.

To further develop Ad[CE1A] work, *in vivo* scheduling, dose of Ad[CE1A] and route of administration requires more work to fully understand the best Ad[CE1A] treatment strategy. Based off the experiments performed in this study, Ad[CE1A] did not show a dose response when a tenfold higher dose was used, additionally, the U266 MRD model may not have shown efficacy as treatment was administered once per week over twice per week. However, interestingly, Ad[CE1A] did show efficacy via I.P administration, which was the same if not better than I.V administration of the same dose. Therefore, it would be worthwhile to perform some dose escalation and biodistribution studies to try to determine the best treatment schedule.

Ad[CE1A] showed additive/synergistic interactions in combination with anti-MM chemotherapies, this was particularly clear in Melph combinations. Mechanistically, it was clear that Melph increased viral replication, but if/how the other anti-MM chemotherapies augmented Ad life cycle was less clear and more work needs to be performed trying to understand the additive/synergistic mechanisms. One avenue of interest would be to assess complementary cell death mechanisms like necroptosis or ER stress following combination therapy. Unfortunately, I was unable to assess the combinations *in vivo* to determine whether this translates to better anti-MM efficacy within this thesis, but there is work planned immediately after my PhD to do so. I will be assessing Ad[CE1A] in combination with either Melph or BTZ in the 5TGM1 syngeneic MM model with the primary objective assessing anti-tumour responses, but with some secondary objectives assessing immune responses. As previously mentioned, the work presented here with Ad[CE1A] in combination with the anti-MM therapies is not

an exhaustive list. It would be of interest to assess other drugs within the same drug class (Carfilzomib, Len, Vorinostat), but also other anti-MM drugs such as mAbs or PD-L1 inhibitors.

Lastly, the field of OV therapy has grown increasingly to investigate immune responses over basic oncolysis. The results presented in this thesis show Ad[CE1A] is able to induce ICD DAMP expression in MPCs, induce bystander cytokine killing, and may modulate the tumour microenvironment, therefore it needs to be investigated if this results in enhanced anti-MM immune responses in *ex vivo* patient samples and in the 5TGM1 syngeneic mouse model. Additionally, it needs to be further investigated if anti-MM chemotherapies can potentiate Ad[CE1A]-induced immune effects.

7.3 Overall Conclusion

This work has demonstrated that Ad[CE1A] could play a role in the treatment of MM, and could enhance anti-MM responses alongside standard chemotherapies. The results presented in this thesis provide a solid foundation for the development of Ad[CE1A] in combination with complementary therapies for translation to clinical trials and patient benefit.



Chapter 8 : Appendices



Appendix Table 8.1:STR profile of human cell lines.

A cell line is considered authentic when the STR profile is >80% match to its original derivative cell line.

		THO1	D21S11	D5S818	D13S317	D7S820	D16S539	CSFIPO	AMEL	vWA	TPOX
Tested Cell Line	JJN-3 WT	9,9	28,33.2	11,12	9,9	8,9	11,12	12,12	X,X	15,15	8,10
	JJN-3 GFP	9,9	28,33.2	11,12	9,9	8,9	11,12	12,12	X,X	15,15	8,10
Cell line	Match										
JJN-3	18/18	9,9		11,12	9,9	8,9	11,12	12,12	X,X	15,15	8,10

		THO1	D21S11	D5S818	D13S317	D7S820	D16S539	CSFIPO	AMEL	vWA	TPOX
Tested Cell Line	U266	5,7	28,29	11,12	12,12	11,12	10,10	12,13	X,Y	17,17	8,8
	U266-GFP-LUC	5,7	28,29	11,12	12,12	11,12	10,10	12,13	X,Y	17,17	8,8
Cell line	Match										
U-266	18/18	5,7		11,12	12,12	11,12	10,10	12,13	X,Y	17,17	8,8

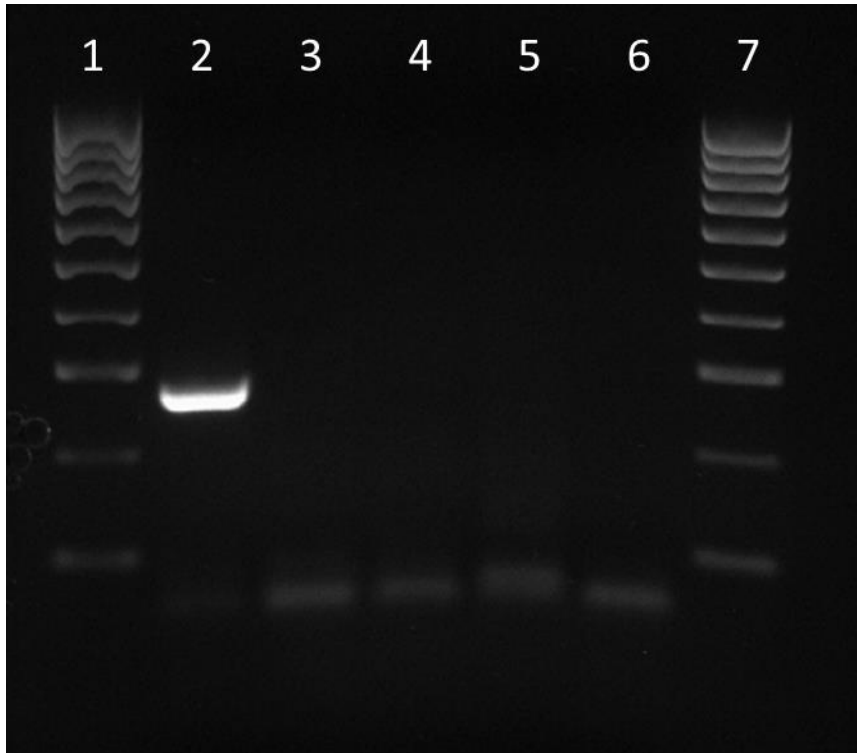
		THO1	D21S11	D5S818	D13S317	D7S820	D16S539	CSFIPO	AMEL	vWA	TPOX
Tested Cell Line	OPM-2	6,7	30,33.2	13,13	11,11	12,12	9,13	12,12	X,X	14,17	8,8
Cell line	Match										
OPM-2	17,18	6,7		13,13	11,11	12,12	9,13	12,13	X,X	14,17	8,8

		THO1	D21S11	D5S818	D13S317	D7S820	D16S539	CSFIPO	AMEL	vWA	TPOX
Tested Cell Line	NCI-H929	9.3,9.3	28,29	11,12	12,12	10,12	9,13	11,11	X,X	14,15	8,11
Cell line	Match										
NCI-H929	18/18	9.3,9.3		11,12	12,12	10,12	9,13	11,11	X,X	14,15	8,11

		THO1	D21S11	D5S818	D13S317	D7S820	D16S539	CSFIPO	AMEL	vWA	TPOX
Tested Cell Line	KMS-11	6,9	28,30	12,12	12,12	11,12	9,13	13,13	X,X	17,18	12,12
Cell line	Match										
KMS-11	17,18	6,9		10,12	12,12	11,12	9,13	13,13	X,X	17,18	12,12

		THO1	D21S11	D5S818	D13S317	D7S820	D16S539	CSFIPO	AMEL	vWA	TPOX
Tested Cell Line	L-363	6,9.3	30,32.2	11,12	12,12	9,11	10,12	10,10	X,X	16,19	8,12
Cell line	Match										
L-363	18/18	6,9.3		11,12	12,12	9,11	10,12	10,10	X,X	16,19	8,12

		THO1	D21S11	D5S818	D13S317	D7S820	D16S539	CSFIPO	AMEL	vWA	TPOX
Tested Cell Line	RPMI-8226	8,8	28,29	11,13	11,11	9,10	9,9	12,12	X,X	16,16	8,11
Cell line	Match										
RPMI-8226	17/18	8,8		11,13	11,11	9,10	9,9	12,12	X,Y	16,16	8,11



Appendix Figure 8.1: Example of results from Mycoplasma PCR kit.

Lane 1 and 7: 100bp ladder; lane 2: positive control; lane 3: HEK293A; lane 4: JJN-3 WT; lane 5: U266 WT; lane 6 negative control

Patient information Sheet

INFORMATION SHEET

Studies into the mechanisms and management of multiple myeloma, myeloma bone disease and related paraproteinaemia associated conditions Version 7, 12/09/2019 (REC number: 05/Q2305/96)

You are invited to take part in a research study. Before you decide, it is important for you to understand why the research is being done and what it would involve. Please take time to read the following information carefully and discuss it with friends, relatives and your General Practitioner if you wish. Ask us if there is anything that is not clear or if you would like more information. Take time to decide whether or not you wish to take part. Thank you for reading this.

What is the purpose of the study?

Multiple myeloma is a disease in which an increased number of plasma cells are found in the bone marrow. Patients with multiple myeloma can develop different complications, such as problems with the kidneys, nerves and bones. The bone disease seen in myeloma patients can cause thinning of the bones, which can cause pain and problems with fractures.

It is unclear why some people develop myeloma, whilst other people do not. Additionally, we do not know why some patients develop problems with their bones (or other complications) whilst other patients with myeloma or related conditions are not affected. We want to learn more about multiple myeloma (and related conditions), how and why the disease develops, and identify factors in our genetic make-up that are associated with myeloma.

The purpose of this study is to better our understanding about the mechanisms behind multiple myeloma and related conditions (e.g. MGUS, amyloidosis), as well as investigating new and more effective treatments for myeloma. We also want to learn more about related conditions such as myeloma bone disease, myeloma associated pain and neuropathy, as well as exploring new ways to improve the ways these complications are treated in the future (including chemotherapies, oncolytic viral therapy and immunotherapy etc).

Why have I been chosen?

We are inviting patients undergoing investigations for multiple myeloma, or related conditions to participate in this study. If you are a patient under investigation, at this stage we may not be sure whether you have myeloma or a related condition; however, we would like to collect samples before you begin treatment, should this be required, as current treatments can influence our research.

Do I have to take part?

It is up to you to decide whether or not to take part. If you do decide to take part, you would be given this information sheet to keep and be asked to sign a consent form. If you decide to take part, you are still free to withdraw at any time and without giving a reason. This would not affect the standard of care you receive.

What would happen if I take part?

If you agree to take part in this study you will be asked to donate a blood sample, up to 30 mls. (6 teaspoons), and you may also be asked to donate a bone marrow sample. The bone marrow sample is taken as part of the tests you will be having for your diagnosis and treatment, you will be asked for an extra sample up to 15mls (three teaspoons) of bone marrow at the same time for research purposes. A portion of the bone marrow trephine, or core biopsy, taken as a routine part of the bone marrow biopsy will also be forwarded to the research team for analysis. You may be asked to donate a second bone marrow trephine, or core biopsy, which would involve an additional biopsy needle to be used during the procedure (this is optional).

You may also be asked for additional samples of your blood and bone marrow but, where possible, we would try and take these samples from you at a time when the samples would be taken anyway. At the most we would ask for up to 5 samples of blood and 3 samples of bone marrow, but it is more likely to be fewer than this.

In rarer cases, patients may need biopsies taken from other areas of their body as part of their standard care (e.g their back (vertebrae) or lung (pleural) fluid. We may ask if you would be willing to donate some of the biopsy sample for this research (this may require taking additional biopsy material during the procedure). Donation of further samples would be optional and you could decide at the time.

If we do ask for extra samples, this would cause the same amount of pain and inconvenience experienced when other samples are taken, but will slightly prolong the procedure. You should be aware that once you have given your consent you have also given up your rights of ownership of the samples once they have been taken from you.

What are the possible benefits of taking part?

The information we get from this study may help us to better treat future patients with multiple myeloma and related conditions.

Would my taking part in this study be kept confidential?

All participant information is stored on a password protected computer database or in locked filing cabinets. You will be allocated a study number and staff not directly involved in your clinical care will only see this code. When the results of the study are reported, individuals who have taken part will not be identified in any way.

The Royal Hallamshire Hospital will use your name, NHS number and contact details to contact you about the research study and make sure that relevant information about the study is recorded for your care, and to oversee the quality of the study. The only people in RHH with access to information that identifies you will be people who need to contact you for the study or audit the data collection process. RHH will keep identifiable information about you until the study finishes. RHH will then archive the study anonymously for 15 years.

Sheffield Teaching Hospital NHSFT (STH NHSFT) is the sponsor for this study based in the United Kingdom. Anonymised data will be transferred from RHH to STH NHSFT along with information collected from you and/or your medical records. We will be using this information in order to analyse the study and will act as the data controller for this study. This means that we are responsible for looking after your information and using it properly. The people who analyse the information will not be able to identify you and will not be able to find out your name, NHS number or contact details.

Your rights to access, change or move your information are limited, as we need to manage your information in specific ways in order for the research to be reliable and accurate. If you withdraw from the study, we will keep the information about you that we have already obtained. To safeguard your rights, we will use the minimum personally-identifiable information possible. You can find out more about how we use your information at <http://www.sth.nhs.uk/NHS/InformationGovernance/>

All information collected during this study will be kept confidential. However, authorised representatives from the hospital research office or UK regulatory authorities might perform an audit of the study and review the study data and your medical records to check the accuracy of the study.

The information will only be used for the purpose of research and cannot be used to contact you or affect your care. It will not be used to make decisions about future services available to you, such as insurance

What would happen to samples at the end of the study?

We anticipate that the majority of samples that you give would be used in the course of this study. However, should any material not be used, with your consent, this would be retained and may be used for further studies in the future. This material would only be used for studies of the biological basis and treatment of multiple myeloma and related conditions and the associated bone disease. Although such studies would be undertaken by Dr. A.D. Chantry, these samples would be important and therefore other researchers may also like to work with them. However, if you so wish, we would limit the use of this material to this study only. All information would remain confidential.

Would these samples be used for genetic research?

The samples that you give may be used in genetic studies to investigate factors that may influence the development of multiple myeloma and related conditions and the associated bone disease. This genetic information will be kept confidential and will not be traced back to individuals.

What would happen to the results of the research study?

The results of this study would be published in a medical journal; however, participants in this research would not be identified in any report or publication in any way.

Who is funding this research?

This research is being funded by Bloodwise (formerly known as Leukaemia and Lymphoma Research).

Who has reviewed this study?

The study has been reviewed by the Sheffield Research Ethics Committee.

Contact for further information:

If you require any further information, please feel free to contact Dr A Chantry or Prof Snowden at the following addresses:

Dr A.D. Chantry, Senior Lecturer in Haematology
Dept of Oncology and Metabolism
Medical School
Beech Hill Road
SHEFFIELD, S10 2RX
Tel: 0114 2159003

Prof J.A. Snowden
Consultant Haematologist
Royal Hallamshire Hospital
Glossop Road
SHEFFIELD, S10 2JF
Tel: 0114 271 3411

If anything happens during the course of this study that I am not happy about, who should I complain to?

If you have any complaints, these should be addressed to the Patient Services Team:

Patient Services Team
B Floor, Royal Hallamshire Hospital
Glossop Road
Sheffield, S10 2JF
Tel 0114 2712400

Email PST@sth.nhs.uk

Patient Consent Form

PATIENT CONSENT FORM

Studies into the mechanisms and management of multiple myeloma, myeloma bone disease and related paraproteinaemia associated conditions
Version 7, 12/09/2019 (REC number: 05/Q2305/96)

Researchers: Dr. A.D. Chantry, Prof. J.A. Snowden

Patient Identification Number.....

Please initial each box adjacent to the following statements.

1. I confirm that I have read and understand the information sheet version 7, dated 21 st May 2019, for the above study and have had the opportunity to ask questions. I understand why the research is being done and any risks involved.	
2. I agree to give samples of blood and bone marrow aspirate and trephine for this research.	
3. I understand I may be asked to give further samples of blood (up to 5) and bone marrow (up to 3) for this research, but I can refuse to do so if I don't want to donate more.	
4. I understand that sections of my medical notes may be looked at by researchers involved in this project where it is relevant to my taking part in this research. I give permission for these individuals to have access to my records.	
5. I understand that my doctor will be informed of my participation in this study and if any of the results of this research are important for my health.	
6. I understand that I will not benefit financially if this research leads to the development of any new treatment or medical test.	
7. I know how to contact the research team if I need to.	
8. I understand and give permission for analysis of my DNA (the substance my genes are made of) in this project and possible future projects using the samples I have donated.	
9. I give consent for the storage of clinical information about me on a computer database. I understand that the data held will be labelled with a code number and that no other personal information will be held with it (it will not have my name and address on it). I understand that the coded data may be shared with other research partners.	
10. I understand that my participation is voluntary and that I am free to withdraw at any time without giving any reason, without my medical care or legal rights being affected.	
11. I agree that the samples I have given and the information gathered, can be stored by Drs. Chantry and Snowden for possible use in future projects. I understand that some of these projects may be carried out by researchers other than Drs.Chantry and Snowden including researchers working for commercial companies. I understand that I give up my rights to ownership of these samples.	
12. I agree to take part in this study.	
13. I agree to the storage and future use of my samples.	
14. If my healthcare provider refers me for a biopsy of a different part of my body (e.g. my back (vertebrae)) as part of my routine care and investigations, I agree to additional biopsy material being collected at the same time and donated to this research study (<i>optional</i>).	

 Name of Patient

 Date

 Signature

 Researcher

 Date

 Signature

Healthy Donor information sheet

HEALTHY VOLUNTEER INFORMATION SHEET Studies into the mechanisms and management of multiple myeloma, myeloma bone disease and related paraproteinaemia associated conditions Version 7, 12/09/2019 (REC number: 05/Q2305/96)

You are invited to take part in a research study. Before you decide, it is important for you to understand why the research is being done and what it would involve. Please take time to read the following information carefully and discuss it with friends, relatives and your General Practitioner if you wish. Ask us if there is anything that is not clear or if you would like more information. Take time to decide whether or not you wish to take part. Thank you for reading this.

What is the purpose of the study?

Multiple myeloma is a disease in which an increased number of plasma cells are found in the bone marrow. Patients with multiple myeloma can develop different complications, such as problems with the kidneys, nerves and bones. The bone disease seen in myeloma patients can cause thinning of the bones, which can cause pain and problems with fractures.

It is unclear why some people develop myeloma, whilst other people do not. Additionally, we do not know why some patients develop problems with their bones (or other complications) whilst other patients with myeloma or related conditions are not affected. We want to learn more about multiple myeloma (and related conditions), how and why the disease develops, and identify factors in our genetic make-up that are associated with myeloma.

The purpose of this study is to better our understanding about the mechanisms behind multiple myeloma and related conditions (e.g. MGUS, amyloidosis), as well as investigating new and more effective treatments for myeloma. We also want to learn more about related conditions such as myeloma bone disease, myeloma associated pain and neuropathy, as well as exploring new ways to improve the ways these complications are treated in the future (including new chemotherapies, oncolytic viral therapy and immunotherapy etc).

Why have I been chosen?

We are recruiting healthy bone marrow donors to take part in these studies. After your bone marrow has been harvested from your pelvis, your precious bone marrow is sealed in a specially designed collection bag and taken to the National Blood Service laboratories for processing and extraction of stem cells. The collection funnel and double filter is cut away from the collection bag and usually thrown away and destroyed. We are asking for your permission, instead of it being thrown away and destroyed, to take this collection funnel and double filter to the Medical School laboratories and extract the few remaining stem cells that remain in the collection funnel and double filter. We are not proposing to take any of the precious cells collected for your bone marrow recipient. We will compare your healthy bone marrow cells with those of patients with myeloma which will help us identify key differences and give us greater understanding of why some patients develop myeloma and why those patients develop bone disease.

Do I have to take part?

It is up to you to decide whether or not to take part. If you do decide to take part, you would be given this information sheet to keep and be asked to sign a consent form. If you decide to take part, you are still free to withdraw at any time and without giving a reason. This would not affect the standard of care you receive.

What would happen if I take part?

If you agree to take part in this study you will be asked to donate a blood sample, up to 10 mls. (4 teaspoons). After your bone marrow harvest, the collection funnel and double filter

normally cut away from the collection bag and thrown away, will be taken by researchers to laboratories in the Medical School. Stem cells and other bone marrow cells will be extracted and used for research as part of this study.

People with myeloma undergo a second biopsy, called a core biopsy, which removes a small portion of the bone marrow called a trephine. To do this, a hollow needle is inserted in the same site of the bone marrow harvest site. It would be very useful for us to have samples of bone marrow trephine from patients who do not have myeloma, for scientific comparison. If you would be willing to donate a bone marrow trephine sample, it would involve your stem cell harvest procedure being an additional 1-3 minutes in length. We do not expect any additional discomfort arising from having this biopsy. Donating a trephine sample would be entirely optional.

You should be aware that once you have given your consent you have also given up your rights of ownership of the samples once they have been taken from you.

What are the possible benefits of taking part?

The information we get from this study may help us to better treat future patients with multiple myeloma and related conditions.

Would my taking part in this study be kept confidential?

All participant information is stored on a password protected computer database or in locked filing cabinets. You will be allocated a study number and staff not directly involved in your clinical care will only see this code. When the results of the study are reported, individuals who have taken part will not be identified in any way.

The Royal Hallamshire Hospital will use your name, NHS number and contact details to contact you about the research study and make sure that relevant information about the study is recorded for your care, and to oversee the quality of the study. The only people in RHH with access to information that identifies you will be people who need to contact you for the study or audit the data collection process. RHH will keep identifiable information about you until the study finishes. RHH will then archive the study anonymously for 15 years.

Sheffield Teaching Hospital NHSFT (STH NHSFT) is the sponsor for this study based in the United Kingdom. Anonymised data will be transferred from RHH to STH NHSFT along with information collected from you and/or your medical records. We will be using this information in order to analyse the study and will act as the data controller for this study. This means that we are responsible for looking after your information and using it properly. The people who analyse the information will not be able to identify you and will not be able to find out your name, NHS number or contact details.

Your rights to access, change or move your information are limited, as we need to manage your information in specific ways in order for the research to be reliable and accurate. If you withdraw from the study, we will keep the information about you that we have already obtained. To safeguard your rights, we will use the minimum personally-identifiable information possible. You can find out more about how we use your information at <http://www.sth.nhs.uk/NHS/InformationGovernance/>

All information collected during this study will be kept confidential. However, authorised representatives from the hospital research office or UK regulatory authorities might perform an audit of the study and review the study data and your medical records to check the accuracy of the study.

The information will only be used for the purpose of research and cannot be used to contact you or affect your care. It will not be used to make decisions about future services available to you, such as insurance

What would happen to samples at the end of the study?

We anticipate that the majority of samples that you give would be used in the course of this study. However, should any material not be used, with your consent, this would be retained and may be used for further studies in the future. This material would only be used for studies of the biological basis and treatment of multiple myeloma and related conditions and the associated bone disease. Although such studies would be undertaken by Dr A.D. Chantry, these samples would be important and therefore other researchers may also like to work with them. However, if you so wish, we would limit the use of this material to this study only. All information would remain confidential.

Would these samples be used for genetic research?

The samples that you give may be used in genetic studies to investigate factors that may influence the development of multiple myeloma and related conditions and the associated bone disease. This genetic information will be kept confidential and will not be traced back to individuals.

What would happen to the results of the research study?

The results of this study would be published in a medical journal; however, participants in this research would not be identified in any report or publication in any way.

Who is funding this research?

This research is being funded by Bloodwise (formerly known as Leukaemia and Lymphome Research).

Who has reviewed this study?

The study has been reviewed by the Sheffield Research Ethics Committee.

Contact for further information:

If you require any further information, please feel free to contact Dr A Chantry or Prof Snowden at the following addresses:

Dr A.D. Chantry, Senior Lecturer in Haematology
Dept of Oncology and Metabolism
Medical School
Beech Hill Road
SHEFFIELD, S10 2RX
Tel: 0114 2159003

Prof J.A. Snowden
Consultant Haematologist
Royal Hallamshire Hospital
Glossop Road
SHEFFIELD, S10 2JF
Tel: 0114 271 3411

If anything happens during the course of this study that I am not happy about, who should I complain to?

If you have any complaints, these should be addressed to the Patient Services Team at::

Patient Services Team
B Floor, Royal Hallamshire Hospital
Glossop Road
Sheffield, S10 2JF
Tel 0114 2712400

Email PST@sth.nhs.uk

Healthy Donor Consent Form

HEALTHY VOLUNTEER CONSENT FORM
Studies into the mechanisms and management of multiple myeloma, myeloma bone disease and related paraproteinaemia associated conditions
Version 7, 12/09/2019 (REC number: 05/Q2305/96)

Researchers: Dr. A.D. Chantry, Prof. J.A. Snowden

Volunteer Identification Number.....

Please initial each box adjacent to the following statements.

1. I confirm that I have read and understand the information sheet version 6, dated 12 th August 2016, for the above study and have had the opportunity to ask questions. I understand why the research is being done and any risks involved.	
2. I agree to give samples of blood and bone marrow aspirate and trephine for this research.	
3. I understand that sections of my medical notes may be looked at by researchers involved in this project where it is relevant to my taking part in this research. I give permission for these individuals to have access to my records.	
4. I understand that I will not benefit financially if this research leads to the development of any new treatment or medical test.	
5. I know how to contact the research team if I need to.	
6. I understand and give permission for analysis of my DNA (the substance my genes are made of) in this project and possible future projects using the samples I have donated.	
7. I give consent for the storage of clinical information about me on a computer database. I understand that the data held will be labelled with a code number and that no other personal information will be held with it (it will not have my name and address on it). I understand that the coded data may be shared with other research partners.	
8. I understand that my participation is voluntary and that I am free to withdraw at any time without giving any reason, without my medical care or legal rights being affected.	
9. I agree that the samples I have given and the information gathered, can be stored by Drs. Chantry and Snowden for possible use in future projects. I understand that some of these projects may be carried out by researchers other than Drs. Chantry and Snowden including researchers working for commercial companies. I understand that I give up my rights to ownership of these samples.	
10. I agree to take part in this study.	
11. I agree to the storage and future use of my samples.	

Name of Patient

Date

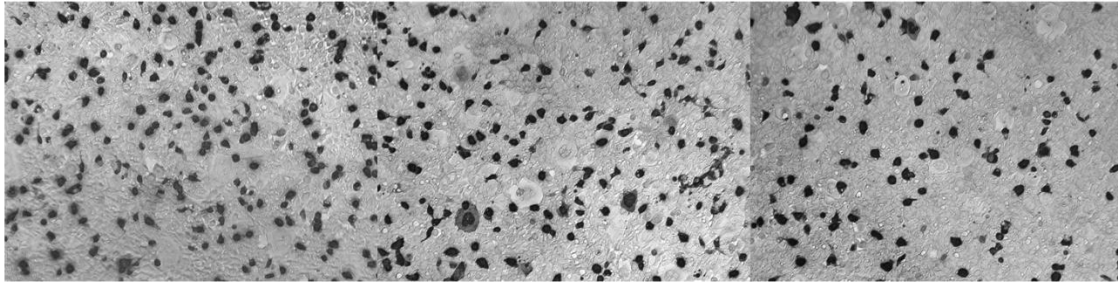
Signature

Researcher

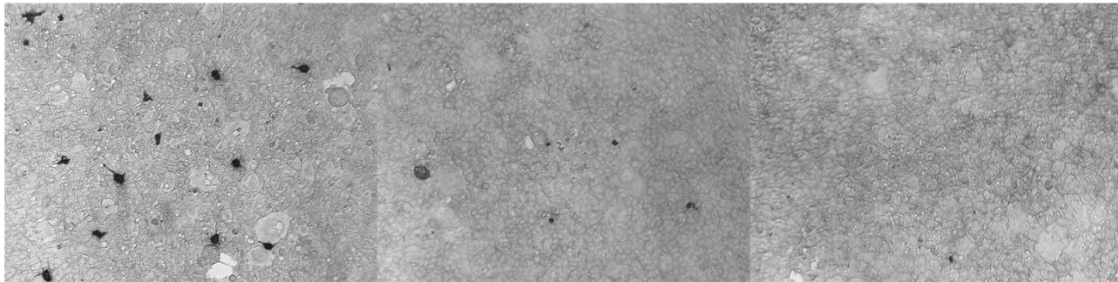
Date

Signature

10⁻¹ Control Sterile Filtered only 5 minutes UV + Sterile Filtered

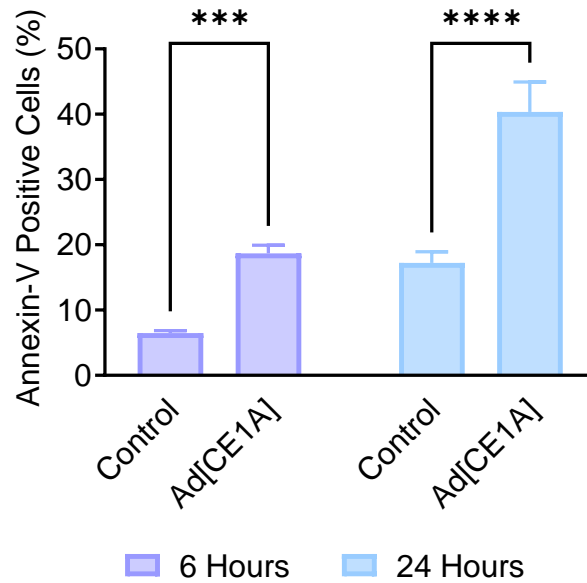


10 minutes UV + Sterile Filtered 30 minutes UV + Sterile Filtered 60 minutes UV + Sterile Filtered



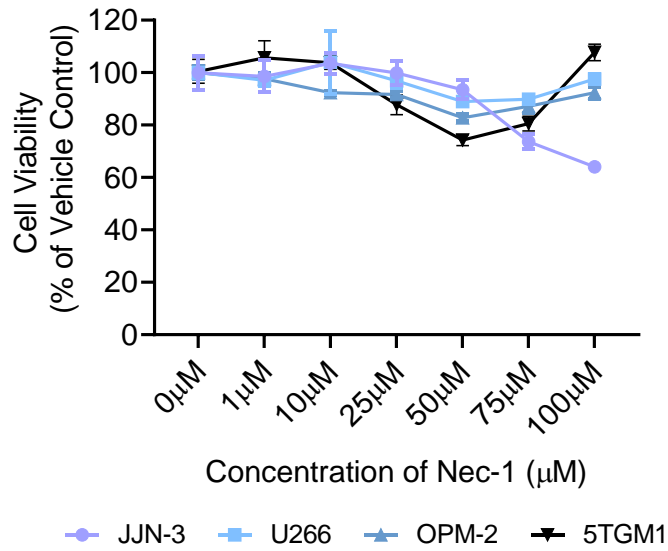
Appendix Figure 8.3 Time required to UV inactivate Ad[CE1A] in CM.

Images taken on EVOS microscope at x10 magnification.



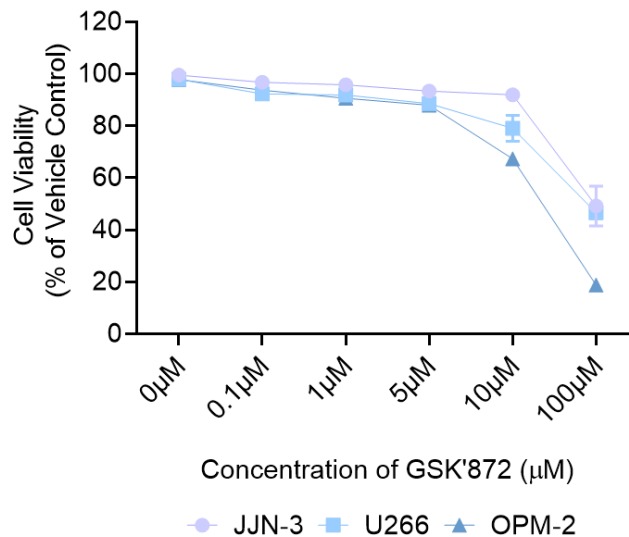
Appendix Figure 8.4 Percentage Annexin V positive after Ad[CE1A] treatment in a primary patient-derived PCL cells, CB1.

Primary patient derived PCL cells, CB1, were incubated with Ad[CE1A] MOI 20. Annexin V expression was determined by flow cytometry at 6 and 24 hours post treatment. Percentage of annexin V expression compared to untreated controls shown. n=3 Data is the mean \pm SD. P values are for 2-way ANOVA with multiple comparisons with Šidák's correction where **** p<0.0001.



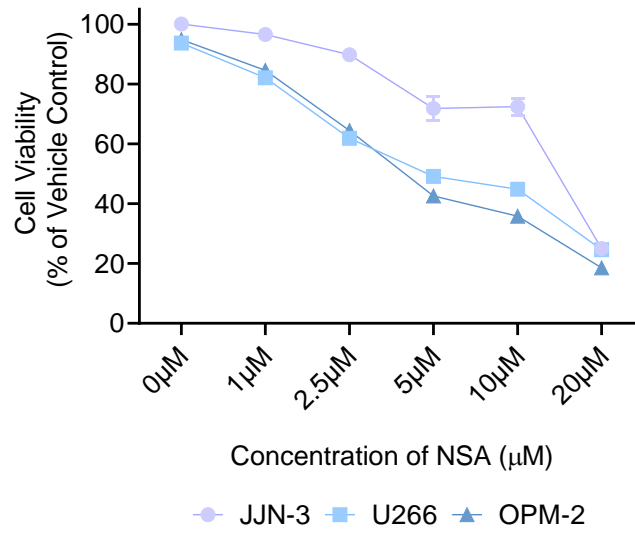
Appendix Figure 8.5 Dose response to Nec-1 to determine non-toxic dose.

MPC lines JYN-3, U266, OPM-2 and 5TGM1 cells were treated with Nec-1 at indicated doses. After 72 hours, cell viability was determined by AlamarBlue® assay. n=3 Data is the mean ±SD.



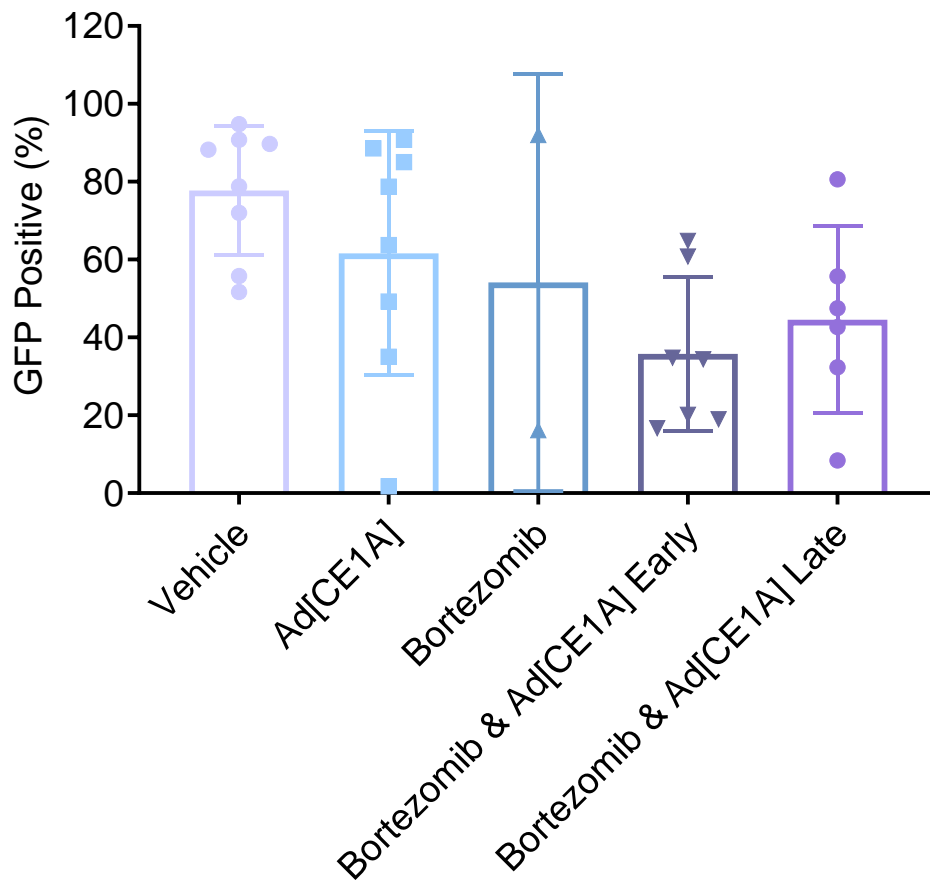
Appendix Figure 8.6 Dose response to GSK-872 to determine non-toxic dose.

MPC lines JYN-3, U266 and OPM-2 cells were treated with GSK'872 at indicated doses. After 72 hours, cell viability was determined by AlamarBlue® assay. n=3 Data is the mean ±SD.



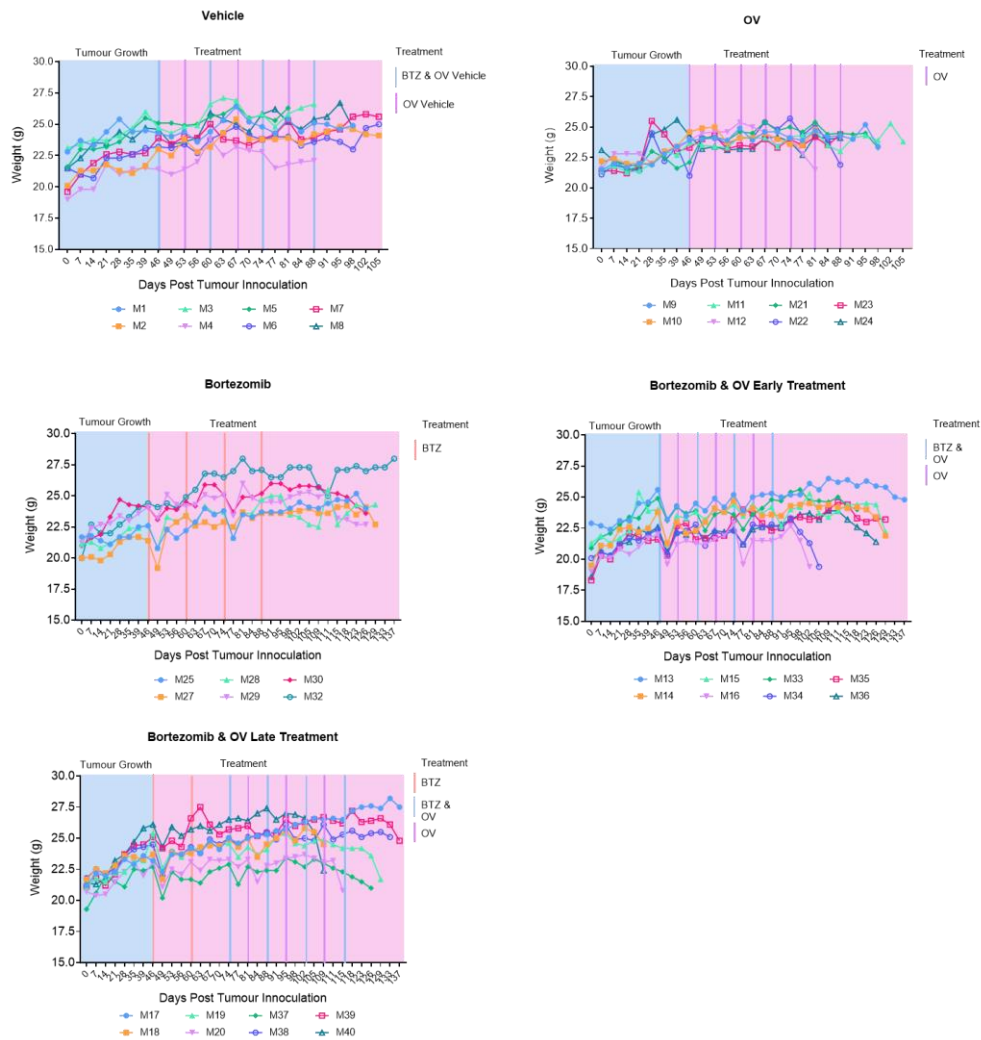
Appendix Figure 8.7 Dose response to NSA to determine non-toxic dose.

MPC lines JYN-3, U266 and OPM-2 cells were treated with NSA at indicated doses. After 72 hours, cell viability was determined by AlamarBlue® assay. n=3 Data is the mean ±SD.



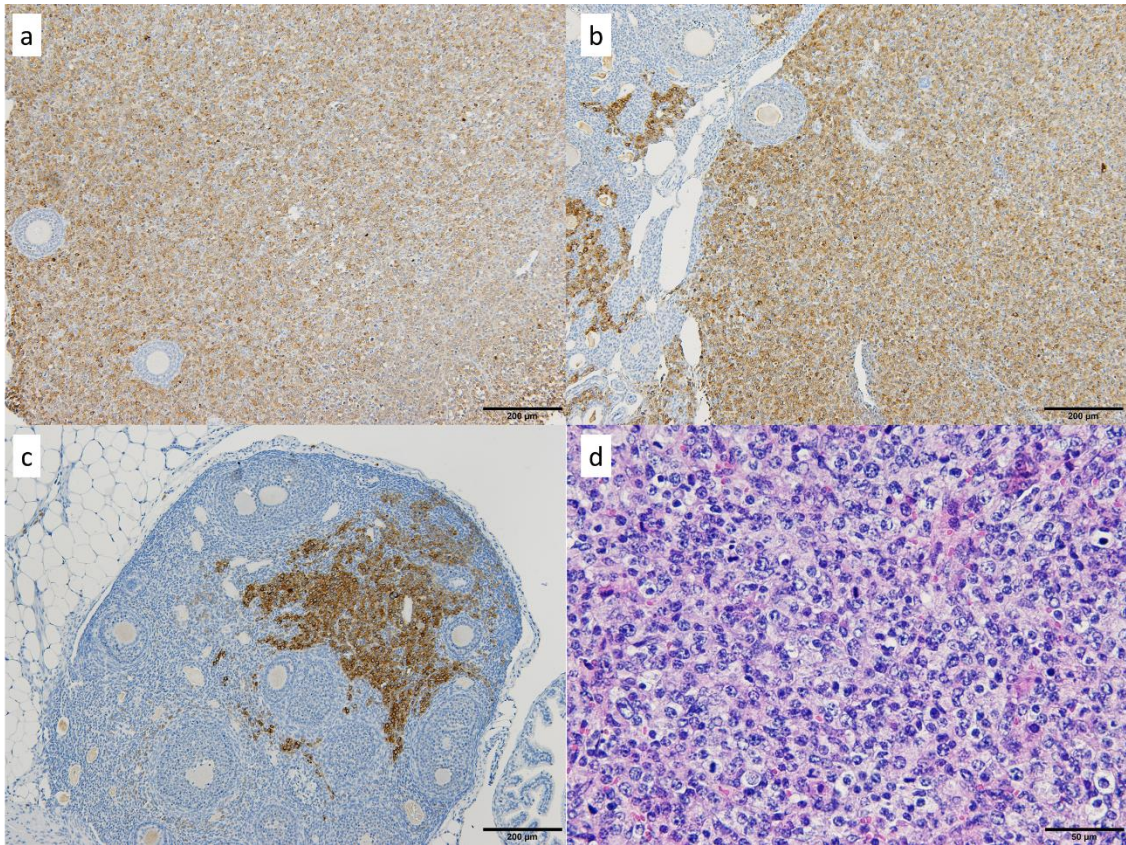
Appendix Figure 8.8 Percentage of GFP positive U266 cells from BM flush of left femora in U266 low tumour burden model of myeloma.

At time of sacrifice, mouse BM was flushed from left femora and analysed for GFP expression in viable cells (TO-PRO-3) using flow cytometry. Not all mice could be included, because the BM in some mice, particularly in the BTZ group, were no longer viable when flow cytometry was performed.



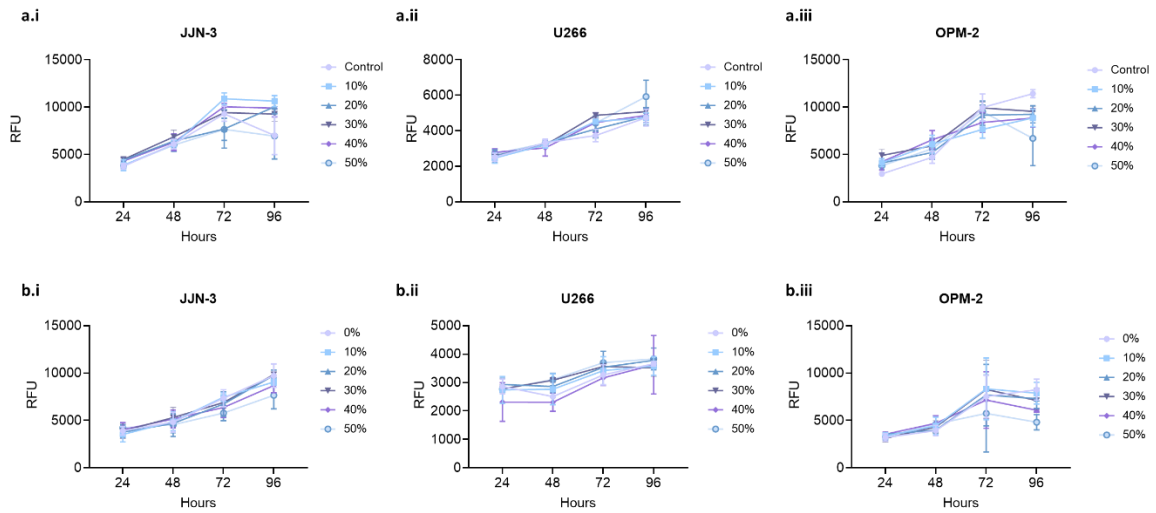
Appendix Figure 8.9 Body weight of mice in U266 low tumour burden model over time.

U266 bearing mice were weighed twice weekly post tumour inoculation. Treatment started at week 6. U266 bearing NSG mice treated with vehicle, Ad[CE1A] (1x/wk), or with BTZ (1x/2wk) ± early Ad[CE1A] treatment to target MRD or BTZ ± late Ad[CE1A] treatment to target disease relapse.



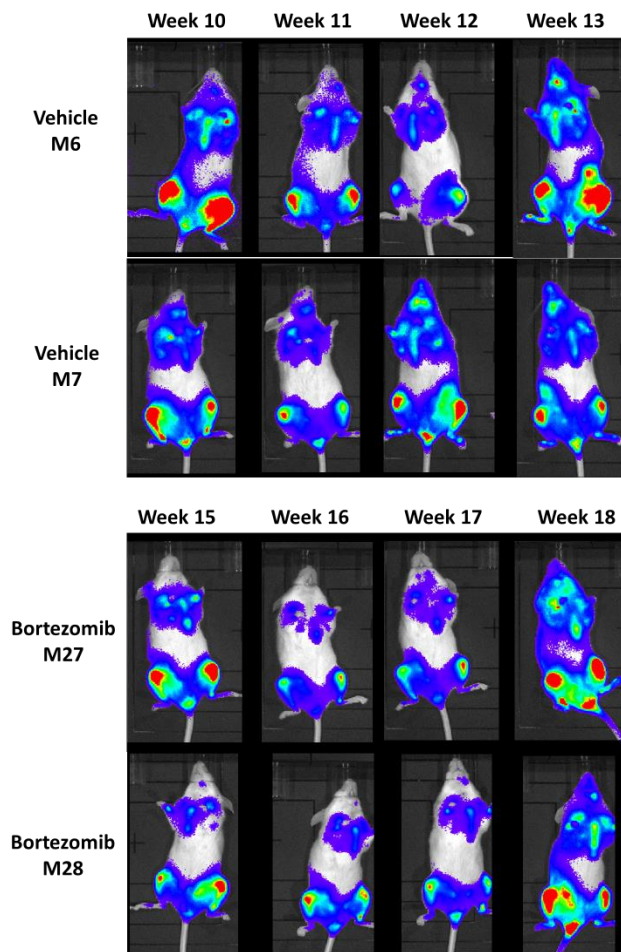
Appendix Figure 8.10 U266 cells within the ovary of NSG mice in the U266 low tumour burden model of MM.

(a-c) Histological images of positive lambda staining in the ovary of three different mouse ovarian tumour sections. Scale bar 200 μm . **(d)** Close up image of plasma cells within the ovary by H&E staining. Scale bar 50 μm .



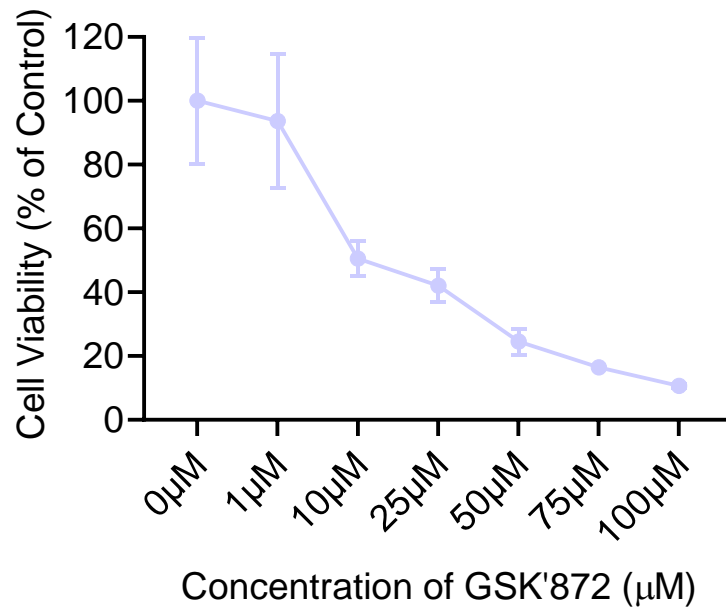
Appendix Figure 8.11 Proliferation of MPCs following different percentages of CM from either HS-5 cells or Saos-2 cells

(a.i-a.iii) 1×10^4 JYN-3, U266 and OPM-2 cells were cultured in CM from HS-5 cells at 10%, 20%, 30%, 40%, or 50%. Proliferation was tracked by AlamarBlue[®] after 24, 48, 72 and 96 hours. **(b.i-b.iii)** JYN-3, U266 and OPM-2 cells were cultured in CM from Saos-2 cells at 10%, 20%, 30%, 40%, or 50%. Proliferation was tracked by AlamarBlue[®] after 24, 48, 72 and 96 hours.



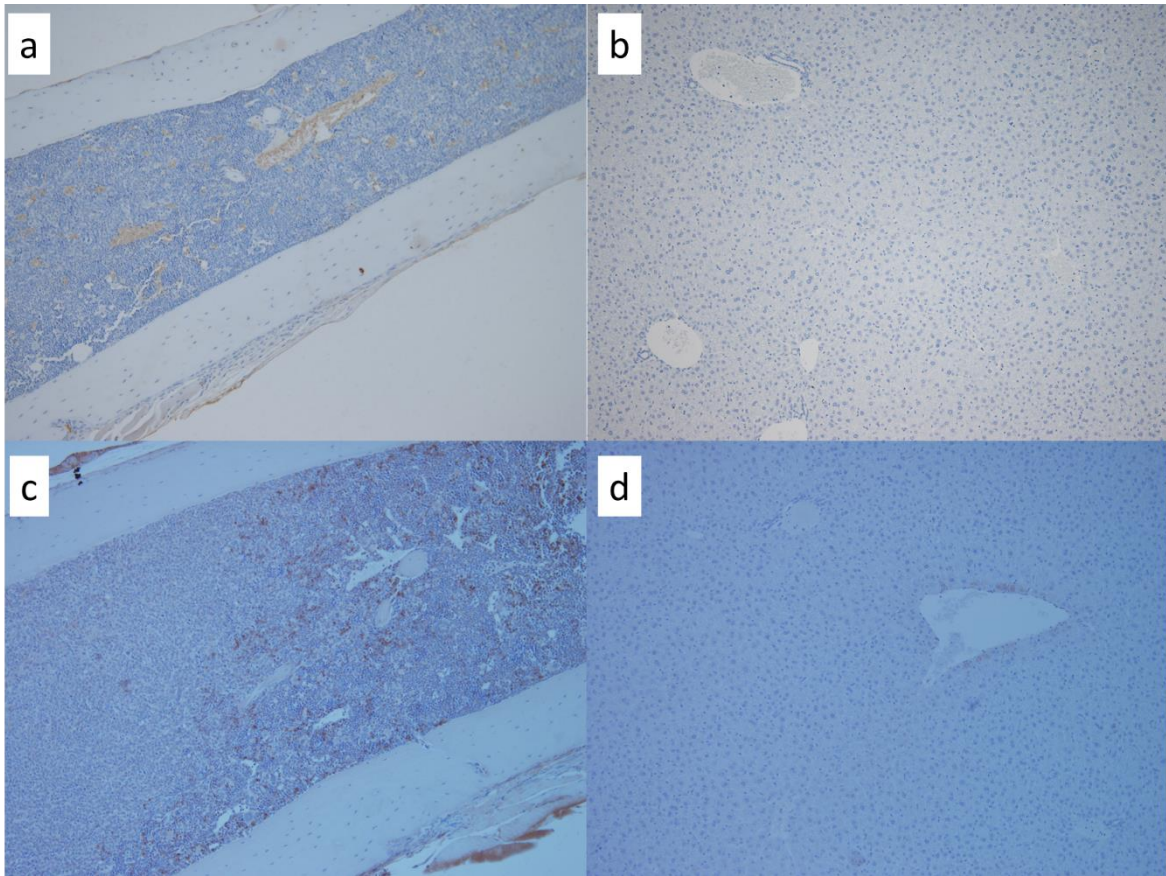
Appendix Figure 8.12 Examples of bioluminescent signal fluctuating over time in two vehicle treated mice and two BTZ treated mice in the U266 low tumour burden model of MM.

U266 bearing mice were IVIS imaged weekly from week 5. Treatment started at week 6. Representative images of *in vivo* bioluminescence imaging in two vehicle mice and two BTZ treated mice from week 10 to week 13 post tumour inoculation in vehicle mice and from week 15 to week 18 in BTZ treated mice evidencing tumour burden fluctuating in the same mouse over time.



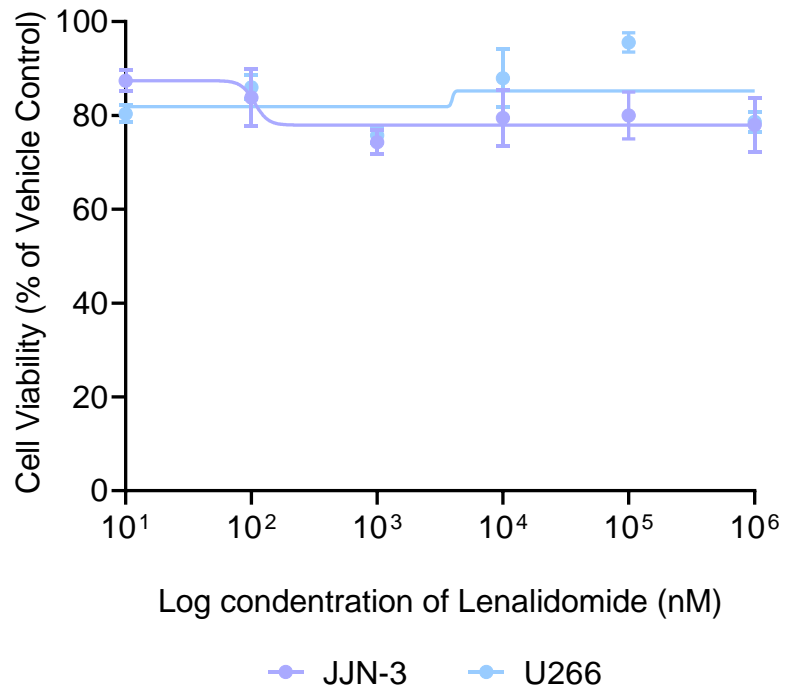
Appendix Figure 8.13 Dose response to GSK-872 to determine non-toxic dose in 5TGM1 cells.

5TGM1 cells were treated with GSK'872 at indicated doses. After 72 hours, cell viability was determined by AlamarBlue® assay. n=3 Data is the mean ±SD.



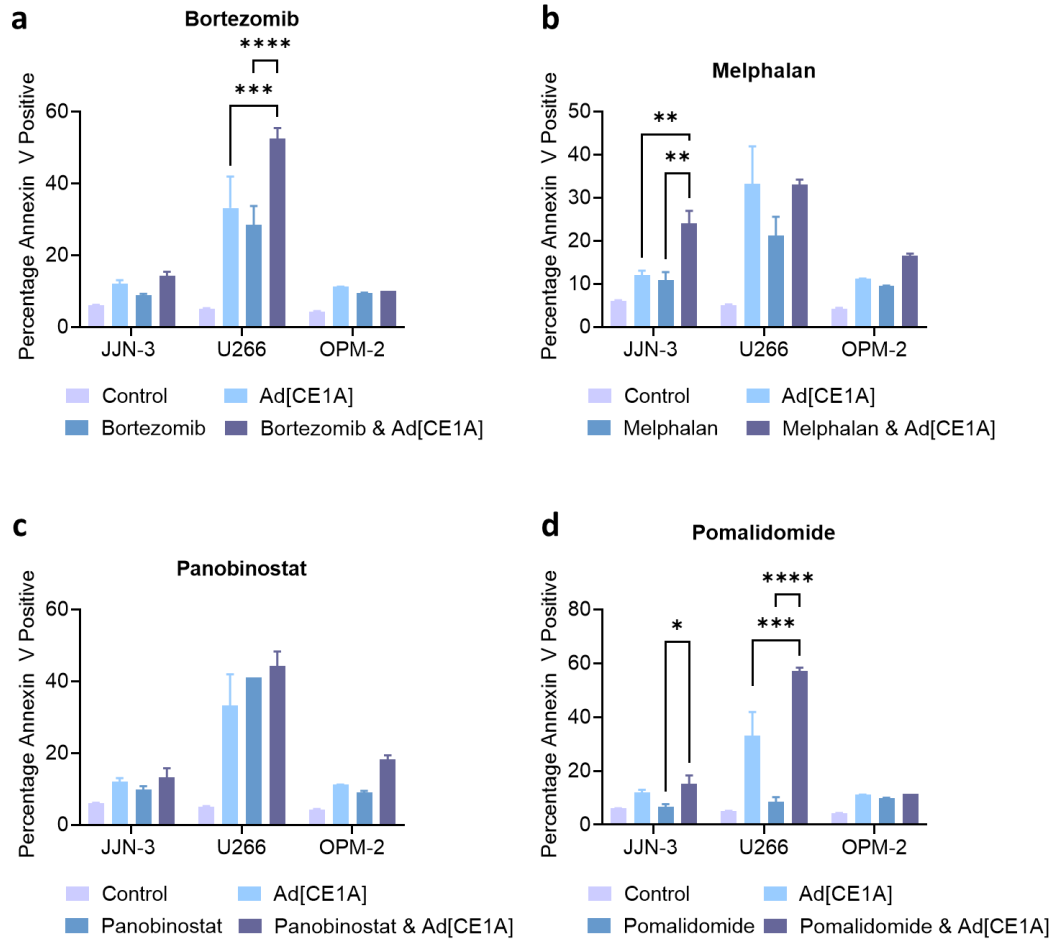
Appendix Figure 8.14 Histological analysis of Ad hexon or E1A staining from Ad[CE1A] treated 5TGM1-bearing mice.

Mice **(a)** tibia or **(b)** liver were stained with an anti-adenoviral anti-hexon antibody. Images taken at x10. Mice **(c)** tibia or **(d)** liver were stained with an anti-adenoviral anti-E1A antibody. Images taken at x10.



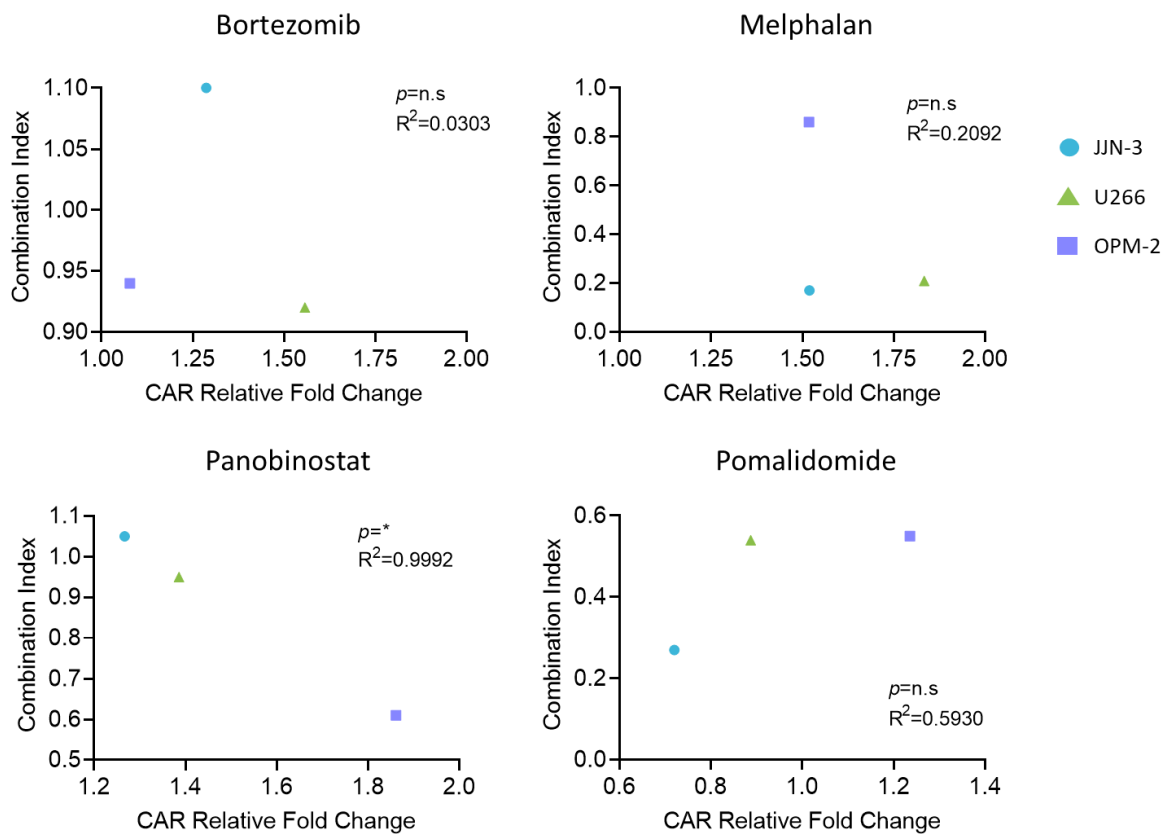
Appendix Figure 8.15 Dose response to Len.

JJN-3 and U266 MPCs were treated with Len at indicated doses. After 72 hours, cell viability was determined by AlamarBlue® assay. n=3 ±SD.



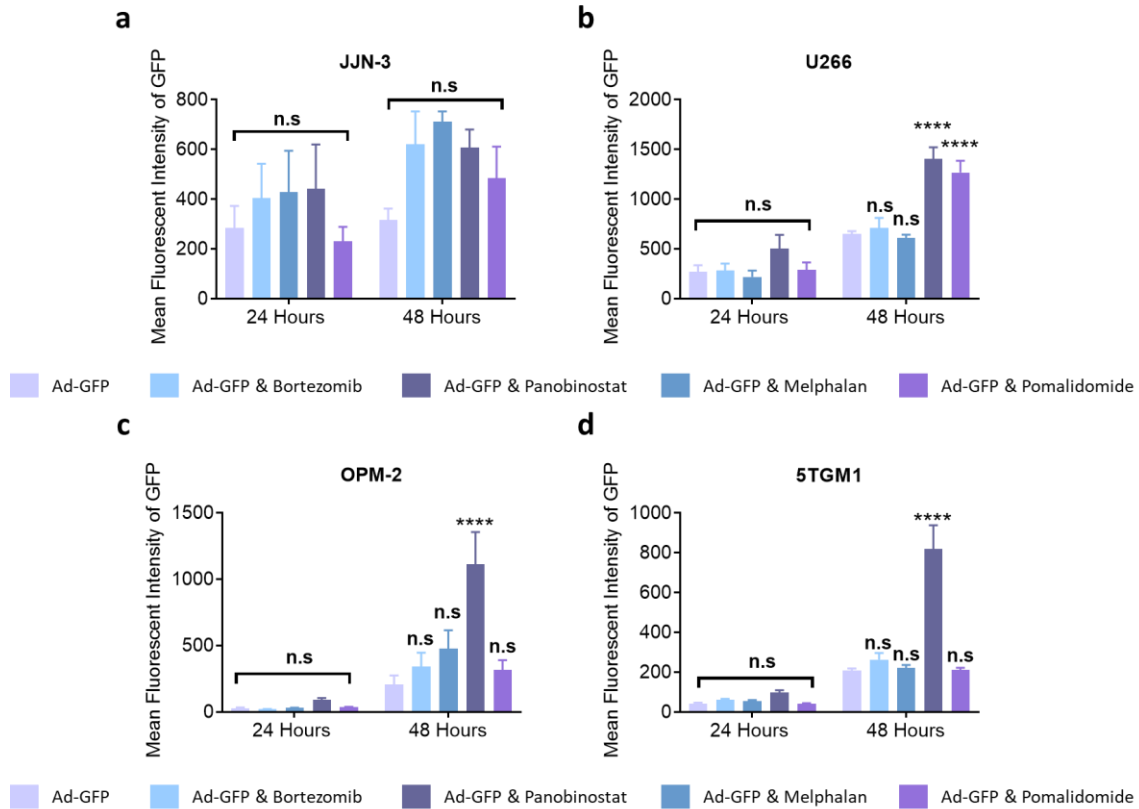
Appendix Figure 8.16 Percentage of Annexin V positive cells after A[CE1A] and anti-MM chemotherapy combination therapy in MPC lines.

JJN-3, U266 and OPM-2 cells were incubated with Ad[CE1A] or (a) BTZ; (b) Melph; (c) Pan and (d) Pom or combination. Percentage of Annexin V expression was determined by flow cytometry at 72 hours post treatment. n=3 Data is the mean \pm SD. P values are for 2-way ANOVA with multiple comparisons with Tukey's correction where * $p < 0.05$; ** $p < 0.01$; *** $p < 0.001$ **** $p < 0.0001$.



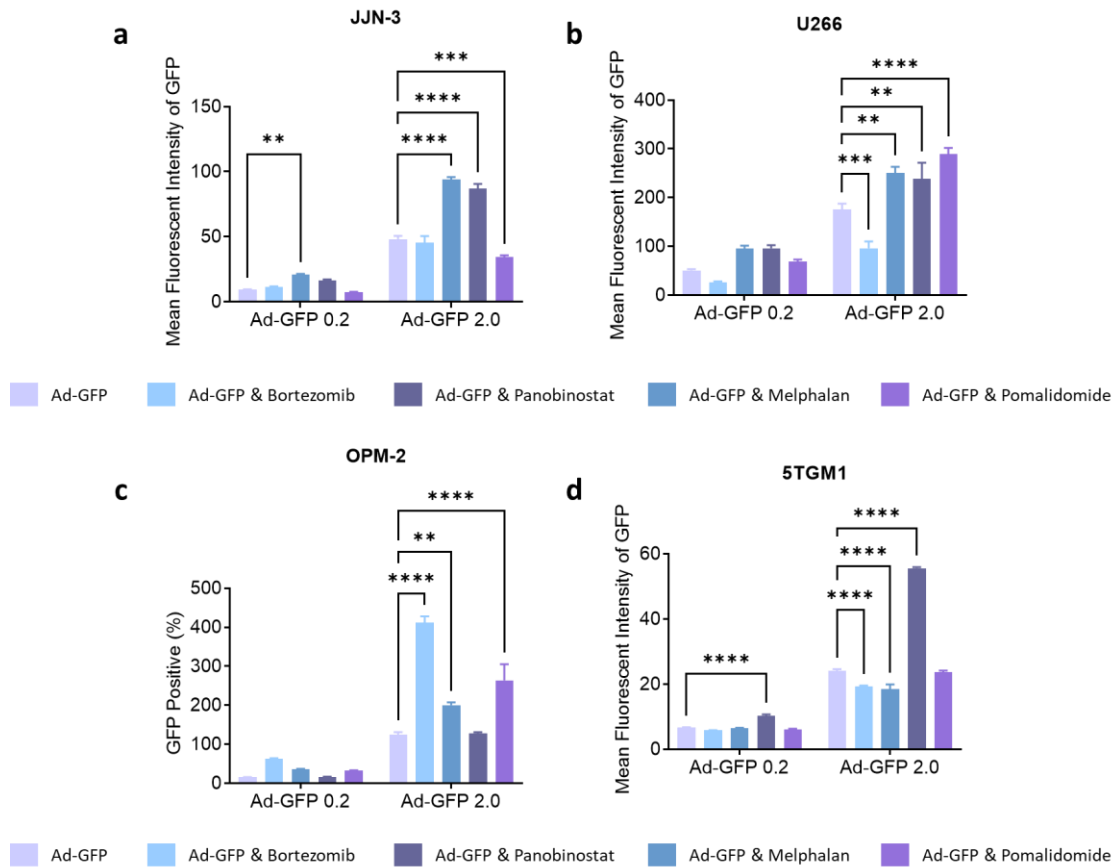
Appendix Figure 8.17 Correlation between CAR relative fold change after treatment and synergy CI score.

Relative CAR fold change after treatment as determined by flow cytometry was plotted against CI as determined by CompuSyn software from input from cell viability experiments in JJN-3, U266 and OPM-2 cells. Data shows mean from n=3 independent experiments. Statistical analysis was determined by Pearson's test with resulting R^2 values deemed to show a correlation if they were close to 1 and p values showing statistical significance of the trend where $p < 0.05$.



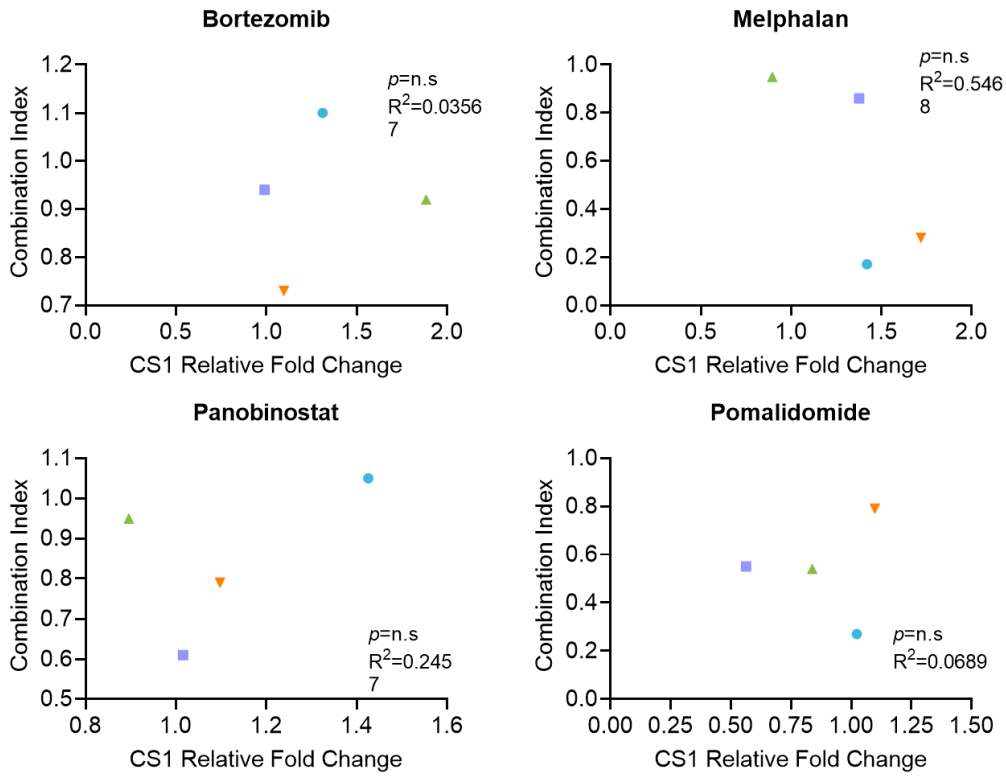
Appendix Figure 8.18 Mean fluorescent intensity of Ad-GFP in combination anti-MM therapies compared to untreated control.

JJN-3, U266, OPM-2 and 5TGM1 cells were treated with Ad-GFP (MOI 2) ± anti-MM chemotherapies. GFP MFI was determined by flow cytometry after 24 and 48 hours. MFI of GFP after anti-MM chemotherapies compared to untreated control plotted in (a) JJN-3, (b) U266, (c) OPM-2 (d). n=3 Data is the mean ±SD. P values are for 2-way ANOVA with multiple comparisons compared to Ad-GFP alone with Dunnett's correction where ** p<0.01.



Appendix Figure 8.19 Mean fluorescent intensity of Ad-GFP after anti-MM therapies compared to untreated control.

JLN-3, U266, OPM-2 and 5TGM1 cells were treated with anti-MM chemotherapies, after 24 hours cells were infected with Ad-GFP (MOI 0.2 or 2). GFP MFI was determined by flow cytometry after a further 24 hours. MFI of GFP after anti-MM chemotherapies compared to untreated control plotted in (a) JLN-3, (b) U266, (c) OPM-2 (d). n=3 Data is the mean \pm SD. P values are for 2-way ANOVA with multiple comparisons compared to Ad-GFP alone with Dunnett's correction where ** p<0.01.



Appendix Figure 8.20 Correlation between CS1 relative fold change after treatment and synergy CI score.

Relative CS1 fold change after treatment as determined by flow cytometry was plotted against CI as determined by CompuSyn software from input from cell viability experiments in JJN-3, U266 and OPM-2 cells. Data shows mean from n=3 independent experiments. Statistical analysis was determined by Pearson's test with resulting R² values deemed to show a correlation if they were close to 1 and p values showing statistical significance of the trend where p<0.05.



References



1. UK CR. Myeloma incidence statistics | Cancer Research UK [Internet]. Myeloma Incidence Statistics. 2016 [cited 2020 Sep 21]. Available from: <https://www.cancerresearchuk.org/health-professional/cancer-statistics/statistics-by-cancer-type/myeloma/incidence#ref->
2. Marinac CR, Ghobrial IM, Birmann BM, Soiffer J, Rebbeck TR. Dissecting racial disparities in multiple myeloma. Vol. 10, *Blood Cancer Journal*. Springer Nature; 2020. p. 1–8.
3. Stenehjem JS, Kjærheim K, Bråtveit M, Samuelsen SO, Barone-Adesi F, Rothman N, et al. Benzene exposure and risk of lymphohaematopoietic cancers in 25 000 offshore oil industry workers. *British Journal of Cancer*. 2015 Apr 28;112(9):1603–12.
4. Antoine-Pepeljugin C, Braunstein MJ. Management of Newly Diagnosed Elderly Multiple Myeloma Patients [Internet]. Vol. 21, *Current Oncology Reports*. Current Medicine Group LLC 1; 2019 [cited 2020 Sep 21]. p. 1–11. Available from: <https://doi.org/10.1007/s11912-019-0804-4>
5. King AJ, Gooding S, Ramasamy K. Managing multiple myeloma in the over 70s: A review. *Maturitas* [Internet]. 2015 Feb 1 [cited 2018 Jul 19];80(2):148–54. Available from: <https://www.sciencedirect.com/science/article/pii/S0378512214003831>
6. Rosenberg PS, Barker KA, Anderson WF. Future distribution of multiple myeloma in the United States by sex, age, and race/ethnicity. *Blood* [Internet]. 2015 Aug 8 [cited 2020 Sep 21];125(2):410–2. Available from: <https://www.ncbi.nlm.nih.gov/pmc/articles/PMC4287646/>
7. Kumar SK, Rajkumar V, Kyle RA, van Duin M, Sonneveld P, Mateos MV, et al. Multiple myeloma. *Nature Reviews Disease Primers* [Internet]. 2017 [cited 2018 Jan 2];3. Available from: <https://www.nature.com/articles/nrdp201746.pdf>
8. Berenson JR, Anderson KC, Audell RA, Boccia R v., Coleman M, Dimopoulos MA, et al. Monoclonal gammopathy of undetermined significance: A consensus statement: Guideline [Internet]. Vol. 150, *British Journal of Haematology*. Blackwell Publishing Ltd; 2010 [cited 2018 Jan 2]. p. 28–38. Available from: <http://doi.wiley.com/10.1111/j.1365-2141.2010.08207.x>
9. Kyle RA, Gertz MA, Witzig TE, Lust JA, Lacy MQ, Dispenzieri A, et al. Review of 1027 Patients With Newly Diagnosed Multiple Myeloma. *Mayo Clinic Proceedings* [Internet]. 2003 Jan [cited 2018 Jan 15];78(1):21–33. Available from: <http://www.ncbi.nlm.nih.gov/pubmed/12528874>
10. Dispenzieri A, Katzmann JA, Kyle RA, Larson DR, Melton LJ, Colby CL, et al. Prevalence and risk of progression of light-chain monoclonal gammopathy of undetermined significance: a retrospective population-based cohort study. *The Lancet* [Internet]. 2010 [cited 2020 Sep 21];375(9727):1721–8. Available from: </pmc/articles/PMC2904571/?report=abstract>
11. Weinhold N, Johnson DC, Rawstron AC, Försti A, Doughty C, Vijayakrishnan J, et al. Inherited genetic susceptibility to monoclonal gammopathy of unknown significance. *Blood*. 2014 Apr 17;123(16):2513–7.
12. Grammatico S, Scalzulli E, Petrucci MT. Solitary Plasmacytoma. *Mediterr J Hematol Infect Dis*. 2017;9(1):e2017052.

13. Dispenzieri A, Kyle RA, Katzmann JA, Therneau TM, Larson D, Benson J, et al. Immunoglobulin free light chain ratio is an independent risk factor for progression of smoldering (asymptomatic) multiple myeloma. *Blood*. 2008 Jan 15;111(2):785–9.
14. Drayson M, Tang LX, Drew R, Mead GP, Carr-Smith H, Bradwell AR. Serum free light-chain measurements for identifying and monitoring patients with nonsecretory multiple myeloma. *Blood*. 2001 May 1;97(9):2900–2.
15. Ring ES, Lawson MA, Snowden JA, Jolley I, Chantry AD. New agents in the Treatment of Myeloma Bone Disease. *Calcified Tissue International*. 2017 Nov 2;
16. Panaroni C, Yee AJ, Raje NS. Myeloma and Bone Disease. *Current Osteoporosis Reports*. 2017 Oct 31;15(5):483–98.
17. Rajkumar SV, Dimopoulos MA, Palumbo A, Blade J, Merlini G, Mateos MV, et al. International Myeloma Working Group updated criteria for the diagnosis of multiple myeloma. Vol. 15, *The Lancet Oncology*. Lancet Publishing Group; 2014. p. e538–48.
18. Group IMW. Updated International Myeloma Working Group Criteria Diagnostic Challenges - The ASCO Post [Internet]. Updated International Myeloma Working Group Criteria Diagnostic Challenges. 2019 [cited 2020 Sep 21]. Available from: <https://ascopost.com/issues/april-25-2018/updated-international-myeloma-working-group-criteria-diagnostic-challenges/>
19. Manier S, Salem KZ, Park J, Landau DA, Getz G, Ghobrial IM. Genomic complexity of multiple myeloma and its clinical implications. *Nature Reviews Clinical Oncology*. 2016 Aug 17;14(2):100–13.
20. Fonseca R, Debes-Marun CS, Picken EB, Dewald GW, Bryant SC, Winkler JM, et al. The recurrent IgH translocations are highly associated with nonhyperdiploid variant multiple myeloma. *Blood* [Internet]. 2003 Oct 1 [cited 2022 Jan 27];102(7):2562–7. Available from: <https://pubmed.ncbi.nlm.nih.gov/12805059/>
21. Onodera N, McCab NR, Nachman JB, Leonard Johnson F, le Beau MM, Rowley JD, et al. Hyperdiploidy arising from near-haploidy in childhood acute lymphoblastic leukemia. *Genes, Chromosomes and Cancer*. 1992;4(4):331–6.
22. Morgan GJ, Walker BA, Davies FE. The genetic architecture of multiple myeloma. *Nature Reviews Cancer* 2012 12:5 [Internet]. 2012 Apr 12 [cited 2022 Mar 10];12(5):335–48. Available from: <https://www.nature.com/articles/nrc3257>
23. Barwick BG, Gupta VA, Vertino PM, Boise LH. Cell of origin and genetic alterations in the pathogenesis of multiple myeloma. *Frontiers in Immunology*. 2019;10(MAY):1121.
24. Fonseca R, Bergsagel PL, Drach J, Shaughnessy J, Gutierrez N, Stewart AK, et al. International Myeloma Working Group molecular classification of multiple myeloma: spotlight review. *Leukemia* [Internet]. 2009 [cited 2022 Jan 30];23(12):2210–21. Available from: <https://pubmed.ncbi.nlm.nih.gov/19798094/>
25. Caers J, Garderet L, Kortüm KM, O’dwyer ME, van de Donk NWCJ, Binder M, et al. European Myeloma Network recommendations on tools for the diagnosis and monitoring of multiple myeloma: what to use and when. *Haematologica* [Internet]. 2018 Nov 1 [cited 2022 Jan 30];103(11):1772–84. Available from: <https://haematologica.org/article/view/8655>

26. Cardona-benavides IJ, de Ramón C, Gutiérrez NC. Genetic Abnormalities in Multiple Myeloma: Prognostic and Therapeutic Implications. *Cells* [Internet]. 2021 Feb 1 [cited 2022 Jan 30];10(2):1–28. Available from: [/pmc/articles/PMC7914805/](https://pubmed.ncbi.nlm.nih.gov/348014805/)
27. Jagannath S, Richardson PG, Sonneveld P, Schuster MW, Irwin D, Stadtmauer EA, et al. Bortezomib appears to overcome the poor prognosis conferred by chromosome 13 deletion in phase 2 and 3 trials. *Leukemia* [Internet]. 2007 [cited 2022 Jan 30];21(1):151–7. Available from: <https://pubmed.ncbi.nlm.nih.gov/17096017/>
28. Walker BA, Leone PE, Chiecchio L, Dickens NJ, Jenner MW, Boyd KD, et al. A compendium of myeloma-associated chromosomal copy number abnormalities and their prognostic value. *Blood* [Internet]. 2010 Oct 14 [cited 2022 Jan 30];116(15). Available from: <https://pubmed.ncbi.nlm.nih.gov/20616218/>
29. Fonseca R, van Wier SA, Chng WJ, Ketterling R, Lacy MQ, Dispenzieri A, et al. Prognostic value of chromosome 1q21 gain by fluorescent in situ hybridization and increase CKS1B expression in myeloma. *Leukemia* [Internet]. 2006 [cited 2022 Jan 30];20(11):2034–40. Available from: <https://pubmed.ncbi.nlm.nih.gov/17024118/>
30. Walker BA, Mavrommatis K, Wardell CP, Ashby TC, Bauer M, Davies F, et al. A high-risk, Double-Hit, group of newly diagnosed myeloma identified by genomic analysis. *Leukemia* 2018 33:1 [Internet]. 2018 Jul 2 [cited 2022 Jan 30];33(1):159–70. Available from: <https://www.nature.com/articles/s41375-018-0196-8>
31. Shaughnessy JD, Zhan F, Burington BE, Huang Y, Colla S, Hanamura I, et al. A validated gene expression model of high-risk multiple myeloma is defined by deregulated expression of genes mapping to chromosome 1. *Blood* [Internet]. 2007 Mar 15 [cited 2022 Jan 30];109(6):2276–84. Available from: <https://pubmed.ncbi.nlm.nih.gov/17105813/>
32. Smadja NV, Bastard C, Brigaudeau C, Leroux D, Fruchart C. Hypodiploidy is a major prognostic factor in multiple myeloma. *Blood* [Internet]. 2001 Oct 1 [cited 2022 Jan 30];98(7):2229–38. Available from: <https://ashpublications.org/blood/article/98/7/2229/107083/Hypodiploidy-is-a-major-prognostic-factor-in>
33. Ghobrial IM, Landgren O. How I treat smoldering multiple myeloma. *Blood*. 2014 Nov 27;124(23):3380–8.
34. Barteel E. Potential of oncolytic viruses in the treatment of multiple myeloma. *Oncolytic Virother* [Internet]. 2017 [cited 2018 Jul 22];7:1–12. Available from: <http://www.ncbi.nlm.nih.gov/pubmed/29503813>
35. Zhan F, Huang Y, Colla S, Stewart JP, Hanamura I, Gupta S, et al. The molecular classification of multiple myeloma. *Blood*. 2006 Sep 15;108(6):2020–8.
36. Bolli N, Avet-Loiseau H, Wedge DC, Van Loo P, Alexandrov LB, Martincorena I, et al. Heterogeneity of genomic evolution and mutational profiles in multiple myeloma. *Nature Communications*. 2014 Dec 16;5(1):2997.
37. Lohr JG, Stojanov P, Carter SL, Cruz-Gordillo P, Lawrence MS, Auclair D, et al. Widespread Genetic Heterogeneity in Multiple Myeloma: Implications for Targeted Therapy. *Cancer Cell* [Internet]. 2014 Jan 13 [cited 2018 Jul 19];25(1):91–101. Available from: <http://www.ncbi.nlm.nih.gov/pubmed/24434212>

38. Chaidos A, Barnes CP, Cowan G, May PC, Melo V, Hatjiharissi E, et al. Clinical drug resistance linked to interconvertible phenotypic and functional states of tumor-propagating cells in multiple myeloma. *Blood*. 2013 Jan 10;121(2):318–28.
39. Hajek R, Okubote SA, Svachova H. Myeloma stem cell concepts, heterogeneity and plasticity of multiple myeloma. *British Journal of Haematology*. 2013 Dec;163(5):551–64.
40. Kim D, Park CY, Medeiros BC, Weissman IL. CD19- CD45low/- CD38high/CD138+ plasma cells enrich for human tumorigenic myeloma cells. *Leukemia*. 2012 Dec 30;26(12):2530–7.
41. Matsui W, Huff CA, Wang Q, Malehorn MT, Barber J, Tanhehco Y, et al. Characterization of clonogenic multiple myeloma cells. *Blood*. 2004 Mar 15;103(6):2332–6.
42. Matsui W, Wang Q, Barber JP, Brennan S, Smith BD, Borrello I, et al. Clonogenic multiple myeloma progenitors, stem cell properties, and drug resistance. *Cancer Res*. 2008 Jan 1;68(1):190–7.
43. Boucher K, Parquet N, Widen R, Shain K, Baz R, Alsina M, et al. Stemness of B-cell progenitors in multiple myeloma bone marrow. *Clin Cancer Res*. 2012 Nov 15;18(22):6155–68.
44. McDonald MM, Fairfield H, Falank C, Reagan MR. Adipose, Bone, and Myeloma: Contributions from the Microenvironment. *Calcified Tissue International*. 2017 May 24;100(5):433–48.
45. Selby P, Zulian G, Forgeson G, Nandi A, Milan S, Meldrum M, et al. The development of high dose melphalan and of autologous bone marrow transplantation in the treatment of multiple myeloma: Royal Marsden and St Bartholomew's Hospital studies. *Hematol Oncol* [Internet]. 1998 [cited 2018 Jul 19];6(2):173–9. Available from: <http://www.ncbi.nlm.nih.gov/pubmed/3292375>
46. Al Hamed R, Bazarbachi AH, Malard F, Harousseau JL, Mohty M. Current status of autologous stem cell transplantation for multiple myeloma. Vol. 9, *Blood Cancer Journal*. Nature Publishing Group; 2019. p. 44.
47. Bourhis JH, Bouko Y, Koscielny S, Bakkus M, Greinix H, Derigs G, et al. Relapse risk after autologous transplantation in patients with newly diagnosed myeloma is not related with infused tumor cell load and the outcome is not improved by CD34+ cell selection: long term follow-up of an EBMT phase III randomized study. *Haematologica* [Internet]. 2007 Aug [cited 2018 Jul 19];92(8):1083–90. Available from: <http://www.ncbi.nlm.nih.gov/pubmed/17640853>
48. Dyson P, Horvath N, Joshua D, Barrow L, van Holst N, Brown R, et al. CD34+ selection of autologous peripheral blood stem cells for transplantation following sequential cycles of high-dose therapy and mobilisation in multiple myeloma. *Bone Marrow Transplantation* [Internet]. 2000 Jun 5 [cited 2018 Jul 19];25(11):1175–84. Available from: <http://www.nature.com/articles/1702408>
49. Vogel W, Kopp HG, Kanz L, Einsele H. Myeloma cell contamination of peripheral blood stem-cell grafts can predict the outcome in multiple myeloma patients after high-dose chemotherapy and autologous stem-cell transplantation. *Journal of Cancer Research and Clinical Oncology*. 2005 Apr 23;131(4):214–8.

50. UK CR. Myeloma survival statistics | Cancer Research UK [Internet]. 2017 [cited 2021 Sep 7]. Available from: <https://www.cancerresearchuk.org/health-professional/cancer-statistics/statistics-by-cancer-type/myeloma/survival#heading-Zero>
51. van de Donk NW, Lokhorst HM. New developments in the management and treatment of newly diagnosed and relapsed/refractory multiple myeloma patients. Expert Opinion on Pharmacotherapy [Internet]. 2013 Aug 31 [cited 2018 Jan 2];14(12):1569–73. Available from: <http://www.ncbi.nlm.nih.gov/pubmed/23721099>
52. UK CR. Breast cancer statistics | Cancer Research UK [Internet]. Breast Cancer Statistics. 2017 [cited 2020 Sep 21]. Available from: <https://www.cancerresearchuk.org/health-professional/cancer-statistics/statistics-by-cancer-type/breast-cancer#heading-Three>
53. Avet-Loiseau H, Fonseca R, Siegel D, Dimopoulos MA, pi ka I, Masszi T, et al. Carfilzomib significantly improves the progression-free survival of high-risk patients in multiple myeloma. Blood [Internet]. 2016 Sep 1 [cited 2018 Jul 19];128(9):1174–80. Available from: <http://www.ncbi.nlm.nih.gov/pubmed/27439911>
54. Miguel JS, Weisel K, Moreau P, Lacy M, Song K, Delforge M, et al. Pomalidomide plus low-dose dexamethasone versus high-dose dexamethasone alone for patients with relapsed and refractory multiple myeloma (MM-003): a randomised, open-label, phase 3 trial. The Lancet Oncology. 2013 Oct;14(11):1055–66.
55. San-Miguel JF, Hungria VTM, Yoon SS, Beksac M, Dimopoulos MA, Elghandour A, et al. Panobinostat plus bortezomib and dexamethasone versus placebo plus bortezomib and dexamethasone in patients with relapsed or relapsed and refractory multiple myeloma: a multicentre, randomised, double-blind phase 3 trial. The Lancet Oncology. 2014 Oct;15(11):1195–206.
56. Chari A, Suvannasankha A, Fay JW, Arnulf B, Kaufman JL, Ifthikharuddin JJ, et al. Daratumumab plus pomalidomide and dexamethasone in relapsed and/or refractory multiple myeloma. Blood [Internet]. 2017 Aug 24 [cited 2018 Jul 19];130(8):974–81. Available from: <http://www.ncbi.nlm.nih.gov/pubmed/28637662>
57. JE F. Isatuximab: A Review of Its Use in Multiple Myeloma. Target Oncol [Internet]. 2021 [cited 2021 Sep 7]; Available from: <https://pubmed.ncbi.nlm.nih.gov/34351561/>
58. Moreau P, Masszi T, Grzasko N, Bahlis NJ, Hansson M, Pour L, et al. Oral Ixazomib, Lenalidomide, and Dexamethasone for Multiple Myeloma. New England Journal of Medicine [Internet]. 2016 Apr 28 [cited 2018 Jul 19];374(17):1621–34. Available from: <http://www.nejm.org/doi/10.1056/NEJMoa1516282>
59. NS J, YT T, KC A, S L. Novel Approaches to Treating Relapsed and Refractory Multiple Myeloma with a Focus on Recent Approvals of Belantamab Mafodotin and Selinexor. Clin Pharmacol [Internet]. 2021 Aug [cited 2021 Sep 7];13:169–80. Available from: <https://pubmed.ncbi.nlm.nih.gov/34434061/>
60. Lonial S, Lee HC, Badros A, Trudel S, Nooka AK, Chari A, et al. Belantamab mafodotin for relapsed or refractory multiple myeloma (DREAMM-2): a two-arm, randomised, open-label, phase 2 study. The Lancet Oncology [Internet]. 2020 Feb 1 [cited 2020 Sep 23];21(2):207–21. Available from: <http://www.thelancet.com/article/S1470204519307880/fulltext>

61. Munshi NC, Larry D. Anderson Jr, Shah N, Madduri D, Berdeja J, Lonial S, et al. Idecabtagene Vicleucel in Relapsed and Refractory Multiple Myeloma. <https://doi.org/10.1056/NEJMoa2024850> [Internet]. 2021 Feb 24 [cited 2021 Sep 7];384(8):705–16. Available from: <https://www.nejm.org/doi/10.1056/NEJMoa2024850>
62. Jung SH, Lee HJ, Vo MC, Kim HJ, Lee JJ. Immunotherapy for the treatment of multiple myeloma. *Critical Reviews in Oncology/Hematology* [Internet]. 2017 Mar [cited 2018 Jan 2];111:87–93. Available from: <http://www.ncbi.nlm.nih.gov/pubmed/28259300>
63. Bluming AZ, Ziegler JL. REGRESSION OF BURKITT'S LYMPHOMA IN ASSOCIATION WITH MEASLES INFECTION. Vol. 298, *The Lancet*. 1971. p. 105–6.
64. Taqi AM, Abdurrahman MB, Yakubu AM, Fleming AF. Regression of Hodgkin's disease after measles. *Lancet*. 1981 May 16;1(8229):1112.
65. Kawa A, Arakawa S. The effect of attenuated vaccinia virus AS strain on multiple myeloma; a case report. *Jpn J Exp Med*. 1987 Feb;57(1):79–81.
66. Russell SJ, Peng KW. Oncolytic Virotherapy: A Contest between Apples and Oranges. *Molecular Therapy* [Internet]. 2017 May 3 [cited 2018 Jan 2];25(5):1107–16. Available from: <http://www.ncbi.nlm.nih.gov/pubmed/28392162>
67. Hanahan D, Weinberg RA. Hallmarks of Cancer: The Next Generation. *Cell*. 2011 Mar 4;144(5):646–74.
68. Oliva S, Gambella M, Boccadoro M, Bringhen S. Systemic virotherapy for multiple myeloma. *Expert Opinion on Biological Therapy*. 2017 Aug 10;17(11):1–13.
69. Singh PK, Doley J, Ravi Kumar G, Sahoo AP, Tiwari AK. Oncolytic viruses & their specific targeting to tumour cells. *The Indian Journal of Medical Research* [Internet]. 2012 Oct [cited 2022 Mar 10];136(4):571. Available from: </pmc/articles/PMC3516024/>
70. Guo ZS, Liu Z, Bartlett DL. Oncolytic Immunotherapy: Dying the Right Way is a Key to Eliciting Potent Antitumor Immunity. *Front Oncol*. 2014;4:74.
71. Seymour LW, Fisher KD. Oncolytic viruses: finally delivering. *British Journal of Cancer*. 2016 Feb 16;114(4):357–61.
72. Cary ZD, Willingham MC, Lyles DS. Oncolytic vesicular stomatitis virus induces apoptosis in U87 glioblastoma cells by a type II death receptor mechanism and induces cell death and tumor clearance in vivo. *J Virol*. 2011 Jun;85(12):5708–17.
73. Felt SA, Moerdyk-Schauwecker MJ, Grdzlishvili VZ. Induction of apoptosis in pancreatic cancer cells by vesicular stomatitis virus. *Virology*. 2015 Jan 1;474:163–73.
74. Baird SK, Aerts JL, Eddaoudi A, Lockley M, Lemoine NR, McNeish IA. Oncolytic adenoviral mutants induce a novel mode of programmed cell death in ovarian cancer. *Oncogene*. 2008 May;27(22):3081–90.
75. Whilding LM, Archibald KM, Kulbe H, Balkwill FR, Öberg D, McNeish IA. Vaccinia Virus Induces Programmed Necrosis in Ovarian Cancer Cells. *Molecular Therapy*. 2013 Nov;21(11):2074–86.

76. Galluzzi L, Buqué A, Kepp O, Zitvogel L, Kroemer G. Immunogenic cell death in cancer and infectious disease. *Nature Reviews Immunology* 2016 17:2 [Internet]. 2016 Oct 17 [cited 2021 Sep 7];17(2):97–111. Available from: <https://www.nature.com/articles/nri.2016.107>
77. CM O, HJ C, C K. Combination Immunotherapy Using Oncolytic Virus for the Treatment of Advanced Solid Tumors. *Int J Mol Sci.* 2020 Oct 2;21(20):1–16.
78. Hemminki O, Santos JM dos, Hemminki A, Dos Santos JM, Hemminki A. Oncolytic viruses for cancer immunotherapy. *BioMed Central*; Jun 29, 2020.
79. Chon HJ, Lee WS, Yang H, Kong SJ, Lee NK, Moon ES, et al. Tumor Microenvironment Remodeling by Intratumoral Oncolytic Vaccinia Virus Enhances the Efficacy of Immune-Checkpoint Blockade. *Clinical Cancer Research.* 2019 Mar 1;25(5):1612–23.
80. Fukuhara H, Ino Y, Todo T. Oncolytic virus therapy: A new era of cancer treatment at dawn. *Cancer Science.* 2016 Oct;107(10):1373–9.
81. Aurelian L. Oncolytic virotherapy: the questions and the promise. *Oncolytic Virotherapy.* 2013 Jun;2:19.
82. Sborov DW, Nuovo GJ, Stiff A, Mace T, Lesinski GB, Benson DM, et al. A Phase I Trial of Single-Agent Reolysin in Patients with Relapsed Multiple Myeloma. *Clinical Cancer Research.* 2014 Dec 1;20(23):5946–55.
83. Kicielinski KP, Chiocca EA, Yu JS, Gill GM, Coffey M, Markert JM. Phase 1 Clinical Trial of Intratumoral Reovirus Infusion for the Treatment of Recurrent Malignant Gliomas in Adults. *Molecular Therapy.* 2014 May;22(5):1056–62.
84. Gollamudi R, Ghalib MH, Desai KK, Chaudhary I, Wong B, Einstein M, et al. Intravenous administration of Reolysin®, a live replication competent RNA virus is safe in patients with advanced solid tumors. *Investigational New Drugs.* 2010 Oct 2;28(5):641–9.
85. Galanis E, Markovic SN, Suman VJ, Nuovo GJ, Vile RG, Kottke TJ, et al. Phase II Trial of Intravenous Administration of Reolysin® (Reovirus Serotype-3-dearing Strain) in Patients with Metastatic Melanoma. *Molecular Therapy.* 2012 Oct;20(10):1998–2003.
86. Kolb E. A, Sampson V, Stabley D, Walter A, Sol-Church K, Cripe T, et al. A phase I trial and viral clearance study of reovirus (Reolysin) in children with relapsed or refractory extra-cranial solid tumors: A Children’s Oncology Group Phase I Consortium report. *Pediatric Blood & Cancer.* 2015 May;62(5):751–8.
87. Morris DG, Feng X, DiFrancesco LM, Fonseca K, Forsyth PA, Paterson AH, et al. REO-001: A phase I trial of percutaneous intralesional administration of reovirus type 3 dearing (Reolysin®) in patients with advanced solid tumors. *Investigational New Drugs.* 2013 Jun 12;31(3):696–706.
88. Bai Y, Hui P, Du X, Su X. Updates to the antitumor mechanism of oncolytic virus. Vol. 10, *Thoracic Cancer.* John Wiley and Sons Inc.; 2019. p. 1031–5.
89. Turnbull S, West EJ, Scott KJ, Appleton E, Melcher A, Ralph C. Evidence for oncolytic virotherapy: Where have we got to and where are we going? Vol. 7, *Viruses.* MDPI AG; 2015. p. 6291–312.

90. Breitbach CJ, Lichty BD, Bell JC. Oncolytic Viruses: Therapeutics With an Identity Crisis. Vol. 9, *EBioMedicine*. Elsevier B.V.; 2016. p. 31–6.
91. Parato KA, Breitbach CJ, Le Boeuf F, Wang J, Storbeck C, Ilkow C, et al. The Oncolytic Poxvirus JX-594 Selectively Replicates in and Destroys Cancer Cells Driven by Genetic Pathways Commonly Activated in Cancers. *Molecular Therapy*. 2012 Apr;20(4):749–58.
92. M M, J H, HC L, WY T, Y C, SW P, et al. Vaccinia-based oncolytic immunotherapy Pexastimogene Devacirepvec in patients with advanced hepatocellular carcinoma after sorafenib failure: a randomized multicenter Phase IIb trial (TRAVERSE). *Oncoimmunology*. 2019;8(8).
93. Patel MR, Kratzke RA. Oncolytic virus therapy for cancer: the first wave of translational clinical trials. *Translational Research*. 2013 Apr;161(4):355–64.
94. Park BH, Hwang T, Liu TC, Sze DY, Kim JS, Kwon HC, et al. Use of a targeted oncolytic poxvirus, JX-594, in patients with refractory primary or metastatic liver cancer: a phase I trial. *The Lancet Oncology* [Internet]. 2008 Jun [cited 2018 Jul 19];9(6):533–42. Available from: <http://www.ncbi.nlm.nih.gov/pubmed/18495536>
95. Duffy MR, Fisher KD, Seymour LW. Making Oncolytic Virotherapy a Clinical Reality: The European Contribution. *Human Gene Therapy*. 2017 Nov 1;28(11):1033–46.
96. Matsuda T, Karube H, Aruga A. A Comparative Safety Profile Assessment of Oncolytic Virus Therapy Based on Clinical Trials. *Therapeutic Innovation and Regulatory Science*. 2018 Jul 1;52(4):430–7.
97. Varghese S, Newsome JT, Rabkin SD, McGeagh K, Mahoney D, Nielsen P, et al. Preclinical safety evaluation of G207, a replication-competent herpes simplex virus type 1, inoculated intraprostatically in mice and nonhuman primates. *Human Gene Therapy*. 2001;12(8):999–1010.
98. Chesney J, Awasthi S, Curti B, Hutchins L, Linette G, Triozzi P, et al. Phase IIIb safety results from an expanded-access protocol of talimogene laherparepvec for patients with unresected, stage IIIB-IVM1c melanoma. *Melanoma Research*. 2018;28(1):44–51.
99. Gangi A, Zager JS. The safety of talimogene laherparepvec for the treatment of advanced melanoma. *Expert Opinion on Drug Safety*. 2017 Feb 1;16(2):265–9.
100. Cripe TP, Ngo MC, Geller JI, Louis CU, Currier MA, Racadio JM, et al. Phase 1 study of intratumoral Pexa-Vec (JX-594), an oncolytic and immunotherapeutic vaccinia virus, in pediatric cancer patients. *Molecular Therapy*. 2015 Mar 5;23(3):602–8.
101. Galanis E, Hartmann LC, Cliby WA, Long HJ, Peethambaram PP, Barrette BA, et al. Phase I trial of intraperitoneal administration of an oncolytic measles virus strain engineered to express carcinoembryonic antigen for recurrent ovarian cancer. *Cancer Research*. 2010 Feb 1;70(3):875–82.
102. Hu JCC, Coffin RS, Davis CJ, Graham NJ, Groves N, Guest PJ, et al. A phase I study of OncoVEXGM-CSF, a second-generation oncolytic herpes simplex virus expressing granulocyte macrophage colony-stimulating factor. *Clinical Cancer Research*. 2006 Nov 15;12(22):6737–47.

103. Rui-Hua Xu, Zhong-Yu Yuan, Zhong-Zhen Guan, Ye Cao, Hua-Qing Wang, Xiao-Hua Hu, Ji-Feng Feng, Yang Zhang, Fang Li, Zheng-Tang Chen, Jie-Jun Wang, Jian-Jin Huang, Qing-Hua Zhou, San-Tai Song Rui-Hua Xu 1, Zhong-Yu Yuan, Zhong-Zhen Guan, Ye Cao, Hua-Qing Wan STS. Phase II clinical study of intratumoral H101, an E1B deleted adenovirus, in combination with chemotherapy in patients with cancer. *Chinese Journal of Cancer*. 2003;22(12):1307–10.
104. Beierle E, Waters AM, Friedman GK, Ring EK. Oncolytic virotherapy for pediatric malignancies: future prospects. *Oncolytic Virotherapy*. 2016 Aug;Volume 5:73–80.
105. Comins C, Spicer J, Protheroe A, Roulstone V, Twigger K, White CM, et al. REO-10: A phase I study of intravenous reovirus and docetaxel in patients with advanced cancer. *Clinical Cancer Research*. 2010 Nov 15;16(22):5564–72.
106. Zhong-Jun Xia, Jian-Hua Chang, Li Zhang, Wen-Qi Jiang, Zhong-Zhen Guan, Ji-Wei Liu, Yang Zhang, Xiao-Hua Hu, Guo-Hua Wu, Hua-Qing Wang, Zheng-Chang Chen, Jian-Chao Chen, Qing-Hua Zhou, Jian-Wei Lu, Qing-Xia Fan, Jian-Jin Huang XZ. Phase III randomized clinical trial of intratumoral injection of E1B gene-deleted adenovirus (H101) combined with cisplatin-based chemotherapy in treating squamous cell cancer of head and neck or esophagus. *Chinese Journal of Cancer*. 2004;23(12):1666–70.
107. Li L, Liu S, Han D, Tang B, Ma J. Delivery and Biosafety of Oncolytic Virotherapy. Vol. 10, *Frontiers in Oncology*. Frontiers Media S.A.; 2020.
108. Todo T, Feigenbaum F, Rabkin SD, Lakeman F, Newsome JT, Johnson PA, et al. Viral shedding and biodistribution of G207, a multimutated, conditionally replicating herpes simplex virus type 1, after intracerebral inoculation in Aotus. *Molecular Therapy*. 2000;2(6):588–95.
109. Corrigan PA, Beaulieu C, Patel RB, Lowe DK. Talimogene Laherparepvec: An Oncolytic Virus Therapy for Melanoma. Vol. 51, *Annals of Pharmacotherapy*. SAGE Publications Inc.; 2017. p. 675–81.
110. Harrington KJ, Michielin O, Malvey J, Pezzani Grüter I, Grove L, Frauchiger AL, et al. A practical guide to the handling and administration of talimogene laherparepvec in Europe. Vol. 10, *OncoTargets and Therapy*. Dove Medical Press Ltd.; 2017. p. 3867–80.
111. Streby KA, Geller JI, Currier MA, Warren PS, Racadio JM, Towbin AJ, et al. Intratumoral injection of HSV1716, an oncolytic herpes virus, is safe and shows evidence of immune response and viral replication in young cancer patients. *Clinical Cancer Research*. 2017 Jul 15;23(14):3566–74.
112. Hu JCC, Coffin RS, Davis CJ, Graham NJ, Groves N, Guest PJ, et al. A phase I study of OncoVEXGM-CSF, a second-generation oncolytic herpes simplex virus expressing granulocyte macrophage colony-stimulating factor. *Clinical Cancer Research*. 2006 Nov 15;12(22):6737–47.
113. García M, Moreno R, Gil-Martin M, Cascallò M, De Olza MO, Cuadra C, et al. A Phase 1 trial of oncolytic adenovirus ICOVIR-5 administered intravenously to cutaneous and uveal melanoma patients. *Human Gene Therapy*. 2019 Mar 1;30(3):352–64.
114. Kim KH, Ryan MJ, Estep JE, Miniard BM, Rudge TL, Peggins JO, et al. A new generation of serotype chimeric infectivity-enhanced conditionally replicative adenovirals: The safety profile of Ad5/3-Δ24 in advance of a phase i clinical trial in ovarian cancer patients. *Human Gene Therapy*. 2011 Jul 1;22(7):821–8.

115. Kimball KJ, Preuss MA, Barnes MN, Wang M, Siegal GP, Wan W, et al. A phase I study of a tropism-modified conditionally replicative adenovirus for recurrent malignant gynecologic diseases. *Clinical Cancer Research*. 2010 Nov 1;16(21):5277–87.
116. Zeh HJ, Downs-Canner S, McCart JA, Guo ZS, Rao UNM, Ramalingam L, et al. First-in-man study of western reserve strain oncolytic vaccinia virus: Safety, systemic spread, and antitumor activity. *Molecular Therapy*. 2015 Jan 10;23(1):202–14.
117. Downs-Canner S, Guo ZS, Ravindranathan R, Breitbach CJ, O’Malley ME, Jones HL, et al. Phase 1 Study of Intravenous Oncolytic Poxvirus (vvDD) in Patients with Advanced Solid Cancers. *Molecular Therapy*. 2016 Aug 1;24(8):1492–501.
118. Park SH, Breitbach CJ, Lee J, Park JO, Lim HY, Kang WK, et al. Phase 1b Trial of Biweekly Intravenous Pexa-Vec (JX-594), an Oncolytic and Immunotherapeutic Vaccinia Virus in Colorectal Cancer. *Molecular Therapy*. 2015 Sep 3;23(9):1532–40.
119. Cohn DE, Sill MW, Walker JL, O’Malley D, Nagel CI, Rutledge TL, et al. Randomized phase IIB evaluation of weekly paclitaxel versus weekly paclitaxel with oncolytic reovirus (Reolysin®) in recurrent ovarian, tubal, or peritoneal cancer: An NRG Oncology/Gynecologic Oncology Group study. *Gynecologic Oncology*. 2017 Sep 1;146(3):477–83.
120. Dispenzieri A, Tong C, Laplant B, Lacy MQ, Laumann K, Dingli D, et al. Phase I trial of systemic administration of edmonston strain of measles virus genetically engineered to express the sodium iodide symporter in patients with recurrent or refractory multiple myeloma. *Leukemia*. 2017;31(12):2791–8.
121. R R, G C, V P, J N, D H, D B, et al. Toxicity evaluation of replication-competent herpes simplex virus (ICP 34.5 null mutant 1716) in patients with recurrent malignant glioma. *Gene Ther* [Internet]. 2000 [cited 2021 Sep 7];7(10):859–66. Available from: <https://pubmed.ncbi.nlm.nih.gov/10845724/>
122. Russell SJ, Maroun J, Muñoz-Alfía M, Ammayappan A, Schulze A, Peng KW, et al. Designing and building oncolytic viruses. *Future Virol*. 2017;12(4):193–213.
123. Garber K. China Approves World’s First Oncolytic Virus Therapy For Cancer Treatment. *JNCI: Journal of the National Cancer Institute*. 2006 Mar 1;98(5):298–300.
124. KW P, GJ A, LP, PR G, RC, SJ R, et al. Systemic therapy of myeloma xenografts by an attenuated measles virus. *Blood*. 2001 Oct 1;98(7):2002–7.
125. Ong HT, Timm MM, Greipp PR, Witzig TE, Dispenzieri A, Russell SJ, et al. Oncolytic measles virus targets high CD46 expression on multiple myeloma cells. *Experimental Hematology*. 2006 Jun;34(6):713–20.
126. Dingli D, Peng KW, Harvey ME, Greipp PR, O’Connor MK, Cattaneo R, et al. Image-guided radiovirotherapy for multiple myeloma using a recombinant measles virus expressing the thyroidal sodium iodide symporter. *Blood*. 2004 Mar 1;103(5):1641–6.
127. Liu C, Russell SJ, Peng KW. Systemic therapy of disseminated myeloma in passively immunized mice using measles virus-infected cell carriers. *Mol Ther*. 2010 Jun;18(6):1155–64.
128. Lok A, Descamps G, Tessoulin B, Chiron D, Eveillard M, Godon C, et al. P53 regulates CD46 expression and measles virus infection in myeloma cells. *Blood Advances*. 2018 Dec 11;2(23):3492–505.

129. McGowan JJ, Wagner RR. Inhibition of cellular DNA synthesis by vesicular stomatitis virus. *Journal of Virology*. 1981;38(1):356–67.
130. Lichty BD, Stojdl DF, Taylor RA, Miller L, Frenkel I, Atkins H, et al. Vesicular stomatitis virus: A potential therapeutic virus for the treatment of hematologic malignancy. *Human Gene Therapy*. 2004 Sep;15(9):821–31.
131. Goel A, Carlson SK, Classic KL, Greiner S, Naik S, Power AT, et al. Radioiodide imaging and radiovirotherapy of multiple myeloma using VSV(Δ 51)-NIS, an attenuated vesicular stomatitis virus encoding the sodium iodide symporter gene. *Blood*. 2007 Oct 1;110(7):2342–50.
132. Naik S, Nace R, Federspiel MJ, Barber GN, Peng KWW, Russell SJ, et al. Curative one-shot systemic virotherapy in murine myeloma. *Leukemia*. 2012 Aug 19;26(8):1870–8.
133. Naik S, Nace R, Barber GN, Russell SJ. Potent systemic therapy of multiple myeloma utilizing oncolytic vesicular stomatitis virus coding for interferon- β . *Cancer Gene Therapy*. 2012 Jul;19(7):443–50.
134. Yarde DN, Nace RA, Russell SJ. Oncolytic vesicular stomatitis virus and bortezomib are antagonistic against myeloma cells in vitro but have additive anti-myeloma activity in vivo. *Exp Hematol*. 2013 Dec;41(12):1038–49.
135. Thirukkumaran CM, Shi ZQ, Luider J, Kopciuk K, Gao H, Bahlis N, et al. Reovirus modulates autophagy during oncolysis of multiple myeloma. *Autophagy*. 2013;9(3):413–4.
136. Thirukkumaran CM, Shi ZQ, Luider J, Kopciuk K, Gao H, Bahlis N, et al. Reovirus as a viable therapeutic option for the treatment of multiple myeloma. *Clinical Cancer Research*. 2012 Sep 15;18(18):4962–72.
137. Thirukkumaran CM, Shi ZQ, Luider J, Kopciuk K, Bahlis N, Neri P, et al. Reovirus as a successful ex vivo purging modality for multiple myeloma. *Bone Marrow Transplantation*. 2014;49(1):80–6.
138. Kelly KR, Espitia CM, Zhao W, Wendlandt E, Tricot G, Zhan F, et al. Junctional adhesion molecule-A is overexpressed in advanced multiple myeloma and determines response to oncolytic reovirus. *Oncotarget*. 2015;6(38):41275–89.
139. Thirukkumaran CM, Shi ZQ, Nuovo GJ, Luider J, Kopciuk KA, Dong Y, et al. Oncolytic immunotherapy and bortezomib synergy improves survival of refractory multiple myeloma in a preclinical model. *Blood Advances*. 2019 Mar 12;3(5):797–812.
140. Senac JS, Doronin K, Russell SJ, Jelinek DF, Greipp PR, Barry MA. Infection and Killing of Multiple Myeloma by Adenoviruses. *Human Gene Therapy [Internet]*. 2010 Feb [cited 2018 Jan 2];21(2):179–90. Available from: <http://www.ncbi.nlm.nih.gov/pubmed/19788385>
141. Chen CY, Senac JS, Weaver EA, May SM, Jelinek DF, Greipp P, et al. Species D adenoviruses as oncolytics against B-cell cancers. *Clin Cancer Res*. 2011 Nov 1;17(21):6712–22.
142. Fernandes MS, Gomes EM, Butcher LD, Hernandez-Alcoceba R, Chang D, Kansopon J, et al. Growth Inhibition of Human Multiple Myeloma Cells by an Oncolytic Adenovirus Carrying the CD40 Ligand Transgene. *Clinical Cancer Research [Internet]*. 2009 Aug 1 [cited 2018 Jan 11];15(15):4847–56. Available from: <http://www.ncbi.nlm.nih.gov/pubmed/19622582>

143. Tong Y, Zhu W, Huang X, You L, Han X, Yang C, et al. PI3K inhibitor LY294002 inhibits activation of the Akt/mTOR pathway induced by an oncolytic adenovirus expressing TRAIL and sensitizes multiple myeloma cells to the oncolytic virus. *Oncology Reports*. 2014;31(4):1581–8.
144. Wenthe J, Naseri S, Hellström AC, Wiklund HJ, Eriksson E, Loskog A. Immunostimulatory oncolytic virotherapy for multiple myeloma targeting 4-1BB and/or CD40. *Cancer Gene Therapy* [Internet]. 2020 [cited 2020 Oct 1];27(12). Available from: <https://pubmed.ncbi.nlm.nih.gov/32355275/>
145. Futami M, Sato K, Miyazaki K, Suzuki K, Nakamura T, Tojo A. Efficacy and Safety of Doubly-Regulated Vaccinia Virus in a Mouse Xenograft Model of Multiple Myeloma. *Molecular Therapy - Oncolytics*. 2017 Sep 15;6:57–68.
146. Deng H, Tang N, Stief AE, Mehta N, Baig E, Head R, et al. Oncolytic virotherapy for multiple myeloma using a tumour-specific double-deleted vaccinia virus. *Nature Publishing Group*; May 29, 2008 p. 2261–4.
147. Lei W, Wang S, Yang C, Huang X, Chen Z, He W, et al. Combined expression of miR-34a and Smac mediated by oncolytic vaccinia virus synergistically promote anti-tumor effects in Multiple Myeloma. *Scientific Reports*. 2016 Aug 24;6.
148. Lei W, Wang S, Xu N, Chen Y, Wu G, Zhang A, et al. Enhancing therapeutic efficacy of oncolytic vaccinia virus armed with Beclin-1, an autophagic Gene in leukemia and myeloma. *Biomedicine and Pharmacotherapy*. 2020 May 1;125:110030.
149. Bartee MY, Dunlap KM, Bartee E. Myxoma Virus Induces Ligand Independent Extrinsic Apoptosis in Human Myeloma Cells. *Clinical Lymphoma, Myeloma and Leukemia*. 2016 Apr 1;16(4):203–12.
150. Bartee E, Bartee MY, Bogen B, Yu XZZ. Systemic therapy with oncolytic myxoma virus cures established residual multiple myeloma in mice. *Molecular Therapy — Oncolytics* [Internet]. 2016 Dec 7 [cited 2020 Jun 4];3(October):16032. Available from: <http://www.ncbi.nlm.nih.gov/pubmed/27933316><http://www.nature.com/articles/mto201632>
151. Bartee, Dunlap K, Bartee M. Myxoma virus attenuates expression of activating transcription factor 4 (ATF4) which has implications for the treatment of proteasome inhibitor-resistant multiple myeloma. *Oncolytic Virotherapy*. 2015 Jan;4:1.
152. Bartee E, Chan WM, Moreb JS, Cogle CR, McFadden G. Selective Purging of Human Multiple Myeloma Cells from Autologous Stem Cell Transplantation Grafts using Oncolytic Myxoma Virus. *Biology of Blood and Marrow Transplantation*. 2012 Oct;18(10):1540–51.
153. Lilly CL, Villa NY, Lemos de Matos A, Ali HM, Dhillon JKS, Hofland T, et al. Ex Vivo Oncolytic Virotherapy with Myxoma Virus Arms Multiple Allogeneic Bone Marrow Transplant Leukocytes to Enhance Graft versus Tumor. *Molecular Therapy - Oncolytics*. 2017 Mar 1;4(March):31–40.
154. Villa NY, Rahman MM, Mamola J, D'Isabella J, Goras E, Kilbourne J, et al. Autologous Transplantation Using Donor Leukocytes Loaded Ex Vivo with Oncolytic Myxoma Virus Can Eliminate Residual Multiple Myeloma. *Molecular Therapy - Oncolytics*. 2020 Sep 25;18:171–88.

155. Marchica V, Franceschi V, Vescovini R, Storti P, Vicario E, Toscani D, et al. Bovine pestivirus is a new alternative virus for multiple myeloma oncolytic virotherapy. *Journal of Hematology and Oncology*. 2020 Jul 11;13(1).
156. Guerrero RA, Guerrero CA, Guzmán F, Acosta O. Assessing the oncolytic potential of rotavirus on mouse myeloma cell line Sp2/O-Ag14. *Biomedica*. 2020;40(2):362.
157. Bais S, Bartee E, Rahman MM, McFadden G, Cogle CR. Oncolytic virotherapy for hematological malignancies. *Advances in Virology*. 2012 Oct 29;2012:1–8.
158. Thirukkumaran CM, Shi ZQ, Luider J, Kopciuk K, Morris D. Abstract 1779: Selective oncolysis of multiple myeloma cells by reovirus is mediated through apoptosis. *Cancer Research*. 2011 Apr 15;71(8 Supplement):1779–1779.
159. Thirukkumaran CM, Shi ZQ, Luider J, Stewart D, Kopciuk KA, Gao H, et al. Abstract 396: Reovirus successfully purges multiple myeloma ex vivo and does not affect human CD34+ cell engraftment in a murine transplantation model. *Cancer Research*. 2010 Apr 15;70(8 Supplement):396–396.
160. Kelly KR, Espitia CM, Mahalingam D, Oyajobi BO, Coffey M, Giles FJ, et al. Reovirus therapy stimulates endoplasmic reticular stress, NOXA induction, and augments bortezomib-mediated apoptosis in multiple myeloma. *Oncogene*. 2012 Jun;31(25):3023–38.
161. Kelly KR, Espitia CM, Zhao W, Wu K, Visconte V, Anwer F, et al. Oncolytic reovirus sensitizes multiple myeloma cells to anti-PD-L1 therapy. *Leukemia* Jan 1, 2018.
162. Müller LME, Migneco G, Scott GB, Down J, King S, Askar B, et al. Reovirus-induced cell-mediated immunity for the treatment of multiple myeloma within the resistant bone marrow niche. *Journal for ImmunoTherapy of Cancer*. 2021 Mar;9(3):e001803.
163. Russell SJ, Peng KW. Measles virus for cancer therapy. *Curr Top Microbiol Immunol*. 2009;330:213–41.
164. Hummel HD, Kuntz G, Nakamura T, Greiner A, Russell SJ, Einsele H, et al. Fully Retargeted Oncolytic Measles Virus for Multiple Myeloma Therapy. *Blood*. 2006 Nov 16;108(11):5474.
165. Calton CM, Kelly KR, Anwer F, Carew JS, Nawrocki ST. Oncolytic Viruses for Multiple Myeloma Therapy. *Cancers (Basel)*. 2018 Jun 14;10(6).
166. A G, SK C, KL C, S G, S N, AT P, et al. Radioiodide imaging and radiovirotherapy of multiple myeloma using VSV(Delta51)-NIS, an attenuated vesicular stomatitis virus encoding the sodium iodide symporter gene. *Blood*. 2007 Oct 1;110(7):2342–50.
167. S N, R N, GN B, SJ R. Potent systemic therapy of multiple myeloma utilizing oncolytic vesicular stomatitis virus coding for interferon- β . *Cancer Gene Ther*. 2012 Jul;19(7):443–50.
168. Stiff A, Caserta E, Sborov DW, Nuovo GJ, Mo X, Schlotter SY, et al. Histone deacetylase inhibitors enhance the therapeutic potential of reovirus in multiple myeloma. *Molecular Cancer Therapeutics*. 2016 May 1;15(5):830–41.
169. Kelly KR, Wu K, Tsao-Wei D, Groshen S, Triche TJ, Mohrbacher A, et al. Oncolytic Reovirus Immune Priming: A Phase 1b Study of Reolysin with Bortezomib and Dexamethasone in Patients with Relapsed/Refractory Multiple Myeloma. *Blood*. 2016 Dec 2;128(22):4507–4507.

170. Packiriswamy N, Upreti D, Zhou Y, Khan R, Miller A, Diaz RM, et al. Oncolytic measles virus therapy enhances tumor antigen-specific T-cell responses in patients with multiple myeloma. *Leukemia*. 2020 Dec 1;34(12):3310.
171. ROWE WP, HUEBNER RJ, GILMORE LK, PARROTT RH, WARD TG. Isolation of a cytopathogenic agent from human adenoids undergoing spontaneous degeneration in tissue culture. *Proc Soc Exp Biol Med*. 1953 Dec;84(3):570–3.
172. Davison AJ, Benko M, Harrach B. Genetic content and evolution of adenoviruses. *Journal of General Virology*. 2003 Nov 1;84(11):2895–908.
173. Ghebremedhin B. Human adenovirus: Viral pathogen with increasing importance. *Eur J Microbiol Immunol (Bp)*. 2014 Mar;4(1):26–33.
174. Larson C, Oronsky B, Scicinski J, Fanger GR, Stirn M, Oronsky A, et al. Going viral: a review of replication-selective oncolytic adenoviruses. *Oncotarget*. 2015 Aug 21;6(24):19976–89.
175. Alemany R. Oncolytic Adenoviruses in Cancer Treatment. *Biomedicines*. 2014 Feb 21;2(1):36–49.
176. Kunz AN, Ottolini M. The Role of Adenovirus in Respiratory Tract Infections. *Current Infectious Disease Reports*. 2010 Mar 24;12(2):81–7.
177. Na HN, Nam JH. Infectobesity: a New Area for Microbiological and Virological Research. *Journal of Bacteriology and Virology*. 2011;41(2):65.
178. Russell WC. Update on adenovirus and its vectors. *Journal of General Virology*. 2000 Nov 1;81(11):2573–604.
179. RUSSELL WC, LAVER WG, SANDERSON PJ. Internal Components of Adenovirus. *Nature*. 1968 Sep 14;219(5159):1127–30.
180. Milavetz BI, Balakrishnan L. Viral Epigenetics. In: *Methods in molecular biology (Clifton, NJ)*. 2015. p. 569–96.
181. Russell WC. Adenoviruses: update on structure and function. *Journal of General Virology*. 2009 Jan 1;90(1):1–20.
182. De Jong JC, Wermenbol AG, Verweij-Uijterwaal MW, Slaterus KW, Wertheim-Van Dillen P, Van Doornum GJ, et al. Adenoviruses from human immunodeficiency virus-infected individuals, including two strains that represent new candidate serotypes Ad50 and Ad51 of species B1 and D, respectively. *J Clin Microbiol*. 1999 Dec;37(12):3940–5.
183. Stewart PL, Burnett RM, Cyrklaff M, Fuller SD. Image reconstruction reveals the complex molecular organization of adenovirus. *Cell*. 1991 Oct 4;67(1):145–54.
184. Rosewell A, Vetrini F, Ng P. Helper-Dependent Adenoviral Vectors. *J Genet Syndr Gene Ther*. 2011 Oct 29;Suppl 5.
185. Gonçalves MAF V., de Vries AAF. Adenovirus: from foe to friend. *Reviews in Medical Virology*. 2006 May;16(3):167–86.
186. Bergelson JM, Cunningham JA, Droguett G, Kurt-Jones EA, Krithivas A, Hong JS, et al. Isolation of a common receptor for Coxsackie B viruses and adenoviruses 2 and 5. *Science*. 1997 Feb 28;275(5304):1320–3.

187. Nemerow GR, Pache L, Reddy V, Stewart PL. Insights into adenovirus host cell interactions from structural studies. *Virology*. 2009 Feb 20;384(2):380–8.
188. LEOPOLD P, CRYSTAL R. Intracellular trafficking of adenovirus: Many means to many ends☆. *Advanced Drug Delivery Reviews*. 2007 Aug 10;59(8):810–21.
189. Dehecchi MC, Melotti P, Bonizzato A, Santacatterina M, Chilosi M, Cabrini G. Heparan sulfate glycosaminoglycans are receptors sufficient to mediate the initial binding of adenovirus types 2 and 5. *J Virol*. 2001 Sep;75(18):8772–80.
190. Leopold PL, Pfister KK. Viral Strategies for Intracellular Trafficking: Motors and Microtubules. *Traffic*. 2006 May;7(5):516–23.
191. Le Sage V, Mouland AJ. Viral subversion of the nuclear pore complex. *Viruses*. 2013 Aug 16;5(8):2019–42.
192. Strunze S, Engelke MF, Wang IH, Puntener D, Boucke K, Schleich S, et al. Kinesin-1-Mediated Capsid Disassembly and Disruption of the Nuclear Pore Complex Promote Virus Infection. *Cell Host & Microbe*. 2011 Sep 15;10(3):210–23.
193. Tollefson AE, Scaria A, Hermiston TW, Ryerse JS, Wold LJ, Wold WS. The adenovirus death protein (E3-11.6K) is required at very late stages of infection for efficient cell lysis and release of adenovirus from infected cells. *J Virol*. 1996;70(4):2296–306.
194. Sato-Dahlman M, Larocca CJ, Yanagiba C, Yamamoto M. Adenovirus and immunotherapy: Advancing cancer treatment by combination. *Cancers (Basel)*. 2020 May 1;12(5).
195. Medina-Kauwe LK. Endocytosis of adenovirus and adenovirus capsid proteins. *Adv Drug Deliv Rev*. 2003 Nov 14;55(11):1485–96.
196. Ying B, Tollefson AE, Wold WSM. Identification of a Previously Unrecognized Promoter That Drives Expression of the UXP Transcription Unit in the Human Adenovirus Type 5 Genome. *Journal of Virology*. 2010 Nov 1;84(21):11470–8.
197. Gallimore PH, Turnell AS. Adenovirus E1A: remodelling the host cell, a life or death experience. *Oncogene*. 2001 Nov 28;20(54):7824–35.
198. Weitzman MD, Ornelles DA. Inactivating intracellular antiviral responses during adenovirus infection. *Oncogene*. 2005 Nov 21;24(52):7686–96.
199. White E. Mechanisms of apoptosis regulation by viral oncogenes in infection and tumorigenesis. *Cell Death & Differentiation*. 2006 Aug 5;13(8):1371–7.
200. White E. Regulation of the cell cycle and apoptosis by the oncogenes of adenovirus. *Oncogene*. 2001 Nov 28;20(54):7836–46.
201. Gros A, Guedan S. Adenovirus Release from the Infected Cell as a Key Factor for Adenovirus Oncolysis. *The Open Gene Therapy Journal*. 2010;3:24–30.
202. Horwitz MS. Function of adenovirus E3 proteins and their interactions with immunoregulatory cell proteins. *The Journal of Gene Medicine*. 2004 Feb;6(S1):S172–83.
203. McSharry BP, Burgert HG, Owen DP, Stanton RJ, Prod'homme V, Sester M, et al. Adenovirus E3/19K promotes evasion of NK cell recognition by intracellular sequestration of the NKG2D

- ligands major histocompatibility complex class I chain-related proteins A and B. *J Virol.* 2008 May 1;82(9):4585–94.
204. Wilson-Rawls J, Deutscher SL, Wold WSM. The Signal-Anchored Domain of Adenovirus E3-6.7K, a Type III Integral Membrane Protein, Can Direct Adenovirus E3-gp19K, a Type I Integral Membrane Protein, into the Membrane of the Endoplasmic Reticulum. *Virology.* 1994 May 15;201(1):66–76.
 205. Lichtenstein DL, Toth K, Doronin K, Tollefson AE, Wold WSM. Functions and mechanisms of action of the adenovirus E3 proteins. *Int Rev Immunol.* 23(1–2):75–111.
 206. Lichtenstein DL, Doronin K, Toth K, Kuppuswamy M, Wold WSM, Tollefson AE. Adenovirus E3-6.7K Protein Is Required in Conjunction with the E3-RID Protein Complex for the Internalization and Degradation of TRAIL Receptor 2. *Journal of Virology.* 2004 Nov 15;78(22):12297–307.
 207. Garnett CT, Talekar G, Mahr JA, Huang W, Zhang Y, Ornelles DA, et al. Latent Species C Adenoviruses in Human Tonsil Tissues. *Journal of Virology.* 2009 Mar 15;83(6):2417–28.
 208. Garnett CT, Erdman D, Xu W, Gooding LR. Prevalence and Quantitation of Species C Adenovirus DNA in Human Mucosal Lymphocytes. *Journal of Virology.* 2002 Nov 1;76(21):10608–16.
 209. Fox JP, Hall CE, Cooney MK. The seattle virus watch: VII. Observations of adenovirus infections. *American Journal of Epidemiology.* 1977;105(4):362–86.
 210. Zhang Y, Huang W, Ornelles DA, Gooding LR. Modeling Adenovirus Latency in Human Lymphocyte Cell Lines. *Journal of Virology.* 2010 Sep 1;84(17):8799–810.
 211. Flomenberg P, Piaskowski V, Harb J, Segura A, Casper JT. Spontaneous, persistent infection of a B-cell lymphoma with adenovirus. *Journal of Medical Virology.* 1996 Mar 1;48(3):267–72.
 212. VK M, DA O, LR G, HT W, W H, AE T, et al. Adenovirus death protein (ADP) is required for lytic infection of human lymphocytes. *J Virol.* 2014;88(2).
 213. Choi JW, Lee JS, Kim SW, Yun CO. Evolution of oncolytic adenovirus for cancer treatment. *Advanced Drug Delivery Reviews.* 2012 Jun 1;64(8):720–9.
 214. Garcia-Moure M, Martinez-Vélez N, Patiño-García A, Alonso MM. Oncolytic adenoviruses as a therapeutic approach for osteosarcoma: A new hope. *Journal of Bone Oncology.* 2017 Nov 1;9:41–7.
 215. Cripe TP, Wang PY, Marcato P, Mahller YY, Lee PW. Targeting cancer-initiating cells with oncolytic viruses. *Mol Ther.* 2009 Oct 1;17(10):1677–82.
 216. Whyte P, Buchkovich KJ, Horowitz JM, Friend SH, Raybuck M, Weinberg RA, et al. Association between an oncogene and an anti-oncogene: the adenovirus E1A proteins bind to the retinoblastoma gene product. *Nature.* 1988 Jul 14;334(6178):124–9.
 217. Tripodi L, Vitale M, Cerullo V, Pastore L. Oncolytic Adenoviruses for Cancer Therapy. *International Journal of Molecular Sciences* 2021, Vol 22, Page 2517. 2021 Mar 3;22(5):2517.
 218. Dormond E, Kamen AA. Manufacturing of adenovirus vectors: production and purification of helper dependent adenovirus. *Methods Mol Biol.* 2011;737:139–56.

219. Bischoff JR, Kirn DH, Williams A, Heise C, Horn S, Muna M, et al. An adenovirus mutant that replicates selectively in p53-deficient human tumor cells. *Science*. 1996 Oct 18;274(5286):373–6.
220. Niemann J, Kühnel F. Oncolytic viruses: adenoviruses. *Virus Genes*. 2017 Oct;53(5):1–7.
221. Dix BR, O’Carroll SJ, Myers CJ, Edwards SJ, Braithwaite AW. Efficient induction of cell death by adenoviruses requires binding of E1B55k and p53. *Cancer Res*. 2000 May 15;60(10):2666–72.
222. Rivlin N, Brosh R, Oren M, Rotter V. Mutations in the p53 Tumor Suppressor Gene: Important Milestones at the Various Steps of Tumorigenesis. *Genes & Cancer*. 2011 Apr 1;2(4):466–74.
223. Peller S, Rotter V. TP53 in hematological cancer: Low incidence of mutations with significant clinical relevance. *Human Mutation*. 2003 Mar;21(3):277–84.
224. Ahmed AA, Etemadmoghadam D, Temple J, Lynch AG, Riad M, Sharma R, et al. Driver mutations in TP53 are ubiquitous in high grade serous carcinoma of the ovary. *J Pathol*. 2010 May;221(1):49–56.
225. Chng WJ, Price-Troska T, Gonzalez-Paz N, Van Wier S, Jacobus S, Blood E, et al. Clinical significance of TP53 mutation in myeloma. *Leukemia*. 2007 Mar 11;21(3):582–4.
226. Lode L, Eveillard M, Trichet V, Soussi T, Wuilleme S, Richebourg S, et al. Mutations in TP53 are exclusively associated with del(17p) in multiple myeloma. *Haematologica*. 2010 Nov 1;95(11):1973–6.
227. Drach J, Ackermann J, Fritz E, Krömer E, Schuster R, Gisslinger H, et al. Presence of a p53 gene deletion in patients with multiple myeloma predicts for short survival after conventional-dose chemotherapy. *Blood*. 1998 Aug 1;92(3):802–9.
228. Boyd KD, Ross FM, Tapper WJ, Chiecchio L, Dagrada G, Konn ZJ, et al. The clinical impact and molecular biology of del(17p) in multiple myeloma treated with conventional or thalidomide-based therapy. *Genes Chromosomes Cancer*. 2011;50(10):765–74.
229. Teoh PJ, Chng WJ. p53 abnormalities and potential therapeutic targeting in multiple myeloma. *Biomed Res Int*. 2014 Jun 17;2014:717919.
230. Harada JN, Berk AJ. p53-Independent and -dependent requirements for E1B-55K in adenovirus type 5 replication. *J Virol*. 1999 Jul;73(7):5333–44.
231. Rothmann T, Hengstermann A, Whitaker NJ, Scheffner M, zur Hausen H. Replication of ONYX-015, a potential anticancer adenovirus, is independent of p53 status in tumor cells. *J Virol*. 1998 Dec;72(12):9470–8.
232. O’Shea CC, Johnson L, Bagus B, Choi S, Nicholas C, Shen A, et al. Late viral RNA export, rather than p53 inactivation, determines ONYX-015 tumor selectivity. *Cancer Cell*. 2004 Dec;6(6):611–23.
233. Fueyo J, Gomez-Manzano C, Alemany R, Lee PS, McDonnell TJ, Mitlianga P, et al. A mutant oncolytic adenovirus targeting the Rb pathway produces anti-glioma effect in vivo. *Oncogene*. 2000 Jan 6;19(1):2–12.

234. Engel BE, Cress WD, Santiago-Cardona PG. THE RETINOBLASTOMA PROTEIN: A MASTER TUMOR SUPPRESSOR ACTS AS A LINK BETWEEN CELL CYCLE AND CELL ADHESION. *Cell Health Cytoskelet.* 2015;7:1–10.
235. McCormick F. Cancer gene therapy: fringe or cutting edge? *Nature Reviews Cancer.* 2001 Nov 1;1(2):130–41.
236. A G, J MQ, C P, S G, DG M, R A, et al. Bioselection of a gain of function mutation that enhances adenovirus 5 release and improves its antitumoral potency. *Cancer Res.* 2008 Nov 1;68(21):8928–37.
237. Cunliffe TG, Bates EA, Parker AL. Hitting the Target but Missing the Point: Recent Progress towards Adenovirus-Based Precision Virotherapies. *Cancers* 2020, Vol 12, Page 3327. 2020 Nov 11;12(11):3327.
238. W D, JW van G, KY A, R A, JJ M, VW van B. ORCA-010, a novel potency-enhanced oncolytic adenovirus, exerts strong antitumor activity in preclinical models. *Hum Gene Ther.* 2014 Oct 1;25(10):897–904.
239. Baker AT, Aguirre-Hernández C, Halldén G, Parker AL. No Title [Internet]. *Cancers* Jun 14, 2018. Available from: [/pmc/articles/PMC6025169/?report=abstract](https://pubmed.ncbi.nlm.nih.gov/30000000/)
240. Hardcastle J, Kurozumi K, Chiocca EA, Kaur B. Oncolytic viruses driven by tumor-specific promoters. *Curr Cancer Drug Targets.* 2007 Mar;7(2):181–9.
241. Zhang KJ, Zhang J, Wu YM, Qian J, Liu XJ, Yan LC, et al. Complete eradication of hepatomas using an oncolytic adenovirus containing AFP promoter controlling E1A and an E1B deletion to drive IL-24 expression. *Cancer Gene Therapy.* 2012 Sep 13;19(9):619–29.
242. DeWeese TL, van der Poel H, Li S, Mikhak B, Drew R, Goemann M, et al. A phase I trial of CV706, a replication-competent, PSA selective oncolytic adenovirus, for the treatment of locally recurrent prostate cancer following radiation therapy. *Cancer Res.* 2001 Oct 15;61(20):7464–72.
243. Muthana M, Giannoudis A, Scott SD, Fang HY, Coffelt SB, Morrow FJ, et al. Use of Macrophages to Target Therapeutic Adenovirus to Human Prostate Tumors. *Cancer Research.* 2011 Mar 1;71(5):1805–15.
244. Rodriguez R, Schuur ER, Lim HY, Henderson GA, Simons JW, Henderson DR. Prostate attenuated replication competent adenovirus (ARCA) CN706: a selective cytotoxic for prostate-specific antigen-positive prostate cancer cells. *Cancer Res.* 1997 Jul 1;57(13):2559–63.
245. Kurihara T, Brough DE, Kovesdi I, Kufe DW. Selectivity of a replication-competent adenovirus for human breast carcinoma cells expressing the MUC1 antigen. *Journal of Clinical Investigation.* 2000 Sep 15;106(6):763–71.
246. Hashimoto Y, Tazawa H, Teraishi F, Kojima T, Watanabe Y, Uno F, et al. The hTERT promoter enhances the antitumor activity of an oncolytic adenovirus under a hypoxic microenvironment. *PLoS One.* 2012;7(6):e39292.
247. He XY, Zheng YM, Lan J, Wu YH, Yan J, He XN, et al. Recombinant adenovirus-mediated human telomerase reverse transcriptase gene can stimulate cell proliferation and maintain

- primitive characteristics in bovine mammary gland epithelial cells. *Development, Growth & Differentiation*. 2011 Apr 1;53(3):312–22.
248. Huang TG, Savontaus MJ, Shinozaki K, Sauter B V, Woo SLC. Telomerase-dependent oncolytic adenovirus for cancer treatment. *Gene Therapy*. 2003 Aug 14;10(15):1241–7.
 249. Kim M, Sumerel LA, Belousova N, Lyons GR, Carey DE, Krasnykh V, et al. The coxsackievirus and adenovirus receptor acts as a tumour suppressor in malignant glioma cells. *British Journal of Cancer*. 2003 May 29;88(9):1411–6.
 250. Shay JW, Wright WE. Role of telomeres and telomerase in cancer. *Semin Cancer Biol*. 2011 Dec;21(6):349–53.
 251. Stewart SA, Bertuch AA. The Role of Telomeres and Telomerase in Cancer Research. *Cancer Research*. 2010 Oct 1;70(19):7365–71.
 252. Shirakawa T, Hamada K, Zhang Z, Okada H, Tagawa M, Kamidono S, et al. A Cox-2 Promoter-Based Replication-Selective Adenoviral Vector to Target the Cox-2-Expressing Human Bladder Cancer Cells. *Clinical Cancer Research*. 2004 Jul 1;10(13):4342–8.
 253. Bortolanza S, Bunuales M, Otano I, Gonzalez-Aseguinolaza G, Ortiz-de-Solorzano C, Perez D, et al. Treatment of pancreatic cancer with an oncolytic adenovirus expressing interleukin-12 in Syrian hamsters. *Mol Ther*. 2009 Apr;17(4):614–22.
 254. Hernandez-Alcoceba R, Pihajla M, Qian D, Clarke MF. New Oncolytic Adenoviruses with Hypoxia- and Estrogen Receptor-Regulated Replication. *Human Gene Therapy*. 2002 Sep 20;13(14):1737–50.
 255. Post DE, Van Meir EG. A novel hypoxia-inducible factor (HIF) activated oncolytic adenovirus for cancer therapy. *Oncogene*. 2003 Apr 10;22(14):2065–72.
 256. Gürlevik E, Woller N, Strüver N, Schache P, Kloos A, Manns MP, et al. Selectivity of oncolytic viral replication prevents antiviral immune response and toxicity, but does not improve antitumoral immunity. *Mol Ther*. 2010 Nov;18(11):1972–82.
 257. Kemp V, Dautzenberg IJC, Cramer SJ, Hoeben RC, van den Wollenberg DJM. Characterization of a replicating expanded tropism oncolytic reovirus carrying the adenovirus E4orf4 gene. *Gene Therapy* 2018 25:5 [Internet]. 2018 Jul 16 [cited 2022 Jan 5];25(5):331–44. Available from: <https://www.nature.com/articles/s41434-018-0032-9>
 258. van den Wollenberg DJM, Dautzenberg IJC, Ros W, Lipińska AD, van den Hengel SK, Hoeben RC. Replicating reoviruses with a transgene replacing the codons for the head domain of the viral spike. *Gene Therapy* 2015 22:3 [Internet]. 2015 Jan 15 [cited 2022 Jan 5];22(3):267–79. Available from: <https://www.nature.com/articles/gt2014126>
 259. Farrera-Sal M, Fillat C, Alemany R. Effect of transgene location, transcriptional control elements and transgene features in armed oncolytic adenoviruses. Vol. 12, *Cancers*. MDPI AG; 2020.
 260. Hajeri PB, Sharma NS, Yamamoto M. Oncolytic adenoviruses: Strategies for improved targeting and specificity. Vol. 12, *Cancers*. MDPI AG; 2020. p. 1–26.

261. Ganly I, Kirn D, Eckhardt G, Rodriguez GI, Soutar DS, Otto R, et al. A phase I study of Onyx-015, an E1B attenuated adenovirus, administered intratumorally to patients with recurrent head and neck cancer. *Clin Cancer Res*. 2000 Mar;6(3):798–806.
262. Nemunaitis J, Khuri F, Ganly I, Arseneau J, Posner M, Vokes E, et al. Phase II Trial of Intratumoral Administration of ONYX-015, a Replication-Selective Adenovirus, in Patients With Refractory Head and Neck Cancer. *Journal of Clinical Oncology*. 2001 Jan 15;19(2):289–98.
263. Khuri FR, Nemunaitis J, Ganly I, Arseneau J, Tannock IF, Romel L, et al. a controlled trial of intratumoral ONYX-015, a selectively-replicating adenovirus, in combination with cisplatin and 5-fluorouracil in patients with recurrent head and neck cancer. *Nature Medicine*. 2000 Aug 1;6(8):879–85.
264. Vasey PA, Shulman LN, Campos S, Davis J, Gore M, Johnston S, et al. Phase I Trial of Intraperitoneal Injection of the *E1B* -55-kd-Gene-Deleted Adenovirus ONYX-015 (dl1520) Given on Days 1 Through 5 Every 3 Weeks in Patients With Recurrent/Refractory Epithelial Ovarian Cancer. *Journal of Clinical Oncology*. 2002 Mar 15;20(6):1562–9.
265. Rogulski KR, Freytag SO, Zhang K, Gilbert JD, Paielli DL, Kim JH, et al. In vivo antitumor activity of ONYX-015 is influenced by p53 status and is augmented by radiotherapy. *Cancer Res*. 2000 Mar 1;60(5):1193–6.
266. Dmitriev I, Kashentseva E, Rogers BE, Krasnykh V, Curiel DT. Ectodomain of coxsackievirus and adenovirus receptor genetically fused to epidermal growth factor mediates adenovirus targeting to epidermal growth factor receptor-positive cells. *J Virol*. 2000 Aug 1;74(15):6875–84.
267. Doronin K, Shashkova E V, May SM, Hofherr SE, Barry MA. Chemical modification with high molecular weight polyethylene glycol reduces transduction of hepatocytes and increases efficacy of intravenously delivered oncolytic adenovirus. *Hum Gene Ther*. 2009 Sep;20(9):975–88.
268. Nwanegbo E, Vardas E, Gao W, Whittle H, Sun H, Rowe D, et al. Prevalence of Neutralizing Antibodies to Adenoviral Serotypes 5 and 35 in the Adult Populations of The Gambia, South Africa, and the United States. *Clinical and Diagnostic Laboratory Immunology*. 2004 Mar;11(2):351–7.
269. Krasnykh V, Dmitriev I, Mikheeva G, Miller CR, Belousova N, Curiel DT. Characterization of an adenovirus vector containing a heterologous peptide epitope in the HI loop of the fiber knob. *J Virol*. 1998 Mar;72(3):1844–52.
270. Yamamoto M, Davydova J, Wang M, Siegal GP, Krasnykh V, Vickers SM, et al. Infectivity enhanced, cyclooxygenase-2 promoter-based conditionally replicative adenovirus for pancreatic cancer. *Gastroenterology*. 2003 Oct;125(4):1203–18.
271. Xia ZJ, Chang JH, Zhang L, Jiang WQ, Guan ZZ, Liu JW, et al. [Phase III randomized clinical trial of intratumoral injection of E1B gene-deleted adenovirus (H101) combined with cisplatin-based chemotherapy in treating squamous cell cancer of head and neck or esophagus]. *Ai Zheng*. 2004 Dec;23(12):1666–70.
272. Chen SH, Pan PY, Eisenstein S. Immune cells: more than simple carriers for systemic delivery of oncolytic viruses. *Oncolytic Virotherapy*. 2014 Nov 6;3:83.

273. Nemunaitis J, Tong AW, Nemunaitis M, Senzer N, Phadke AP, Bedell C, et al. A Phase I Study of Telomerase-specific Replication Competent Oncolytic Adenovirus (Telomelysin) for Various Solid Tumors. *Molecular Therapy*. 2010 Feb;18(2):429–34.
274. Hemminki A. Oncolytic immunotherapy: where are we clinically? *Scientifica (Cairo)*. 2014;2014:862925.
275. Teoh G, Chen L, Urashima M, Tai YT, Celi LA, Chen D, et al. Adenovirus vector-based purging of multiple myeloma cells. *Blood*. 1998 Dec 15;92(12):4591–601.
276. Raus S, Coin S, Monsurrò V. Adenovirus as a new agent for multiple myeloma therapies: Opportunities and restrictions. *Korean J Hematol*. 2011 Dec;46(4):229–38.
277. Chen CY, Senac JS, Weaver EA, May SM, Jelinek DF, Greipp P, et al. Species D adenoviruses as oncolytics against B-cell cancers. *Clinical Cancer Research*. 2011 Nov 1;17(21):6712–22.
278. Drouin M, Cayer MP, Jung D. Adenovirus 5 and chimeric adenovirus 5/F35 employ distinct B-lymphocyte intracellular trafficking routes that are independent of their cognate cell surface receptor. *Virology*. 2010 Jun 5;401(2):305–13.
279. Shayakhmetov DM, Li ZY, Ternovoi V, Gaggar A, Gharwan H, Lieber A. The interaction between the fiber knob domain and the cellular attachment receptor determines the intracellular trafficking route of adenoviruses. *J Virol*. 2003 Mar;77(6):3712–23.
280. Lyle C, McCormick F. Integrin alphavbeta5 is a primary receptor for adenovirus in CAR-negative cells. *Virol J*. 2010 Jul 8;7:148.
281. Lavery D, Fu SM, Lufkin T, Chen-Kiang S. Productive infection of cultured human lymphoid cells by adenovirus. *J Virol*. 1987 May;61(5):1466–72.
282. Lavery DJ, Chen-Kiang S. Adenovirus E1A and E1B genes are regulated posttranscriptionally in human lymphoid cells. *J Virol* [Internet]. 1990 Nov [cited 2018 Jan 2];64(11):5349–59. Available from: <http://www.ncbi.nlm.nih.gov/pubmed/2145444>
283. Zhang L, Hedjran F, Larson C, Perez GL, Reid T. A novel immunocompetent murine model for replicating oncolytic adenoviral therapy. *Cancer Gene Ther*. 2015 Jan;22(1):17–22.
284. Duncan SJ, Gordon FCA, Gregory DW, McPhie JL, Postlethwaite R, White R, et al. Infection of Mouse Liver by Human Adenovirus Type 5. *Journal of General Virology*. 1978 Jul 1;40(1):45–61.
285. Young AM, Archibald KM, Tookman LA, Pool A, Dudek K, Jones C, et al. Failure of translation of human adenovirus mRNA in murine cancer cells can be partially overcome by L4-100K expression in vitro and in vivo. *Mol Ther*. 2012 Sep;20(9):1676–88.
286. Ferguson MS, Lemoine NR, Wang Y. Systemic delivery of oncolytic viruses: Hopes and hurdles. *Advances in Virology*. 2012;2012.
287. Ginsberg HS, Moldawer LL, Sehgal PB, Redington M, Kilian PL, Chanock RM, et al. A mouse model for investigating the molecular pathogenesis of adenovirus pneumonia. *Proc Natl Acad Sci U S A*. 1991 Mar 1;88(5):1651–5.
288. Thomas MA, Spencer JF, Wold WSM. Use of the Syrian hamster as an animal model for oncolytic adenovirus vectors. *Methods Mol Med*. 2007;130:169–83.

289. Kleijn A, Kloezeman J, Treffers-Westerlaken E, Fulci G, Leenstra S, Dirven C, et al. The In Vivo Therapeutic Efficacy of the Oncolytic Adenovirus Delta24-RGD Is Mediated by Tumor-Specific Immunity. Castro MG, editor. PLoS ONE. 2014 May 27;9(5):e97495.
290. Wu C, Öberg D, Rashid A, Gupta R, Mignardi M, Johansson S, et al. A mouse mammary epithelial cell line permissive for highly efficient human adenovirus growth. *Virology*. 2013 Jan 20;435(2):363–71.
291. Tai YT, Dillon M, Song W, Leiba M, Li XF, Burger P, et al. Anti-CSI humanized monoclonal antibody HuLuc63 inhibits myeloma cell adhesion and induces antibody-dependent cellular cytotoxicity in the bone marrow milieu. *Blood*. 2008 Aug 15;112(4):1329–37.
292. Hsi ED, Steinle R, Balasa B, Szmania S, Draksharapu A, Shum BP, et al. CS1, a potential new therapeutic antibody target for the treatment of multiple myeloma. *Clinical Cancer Research*. 2008 May 1;14(9):2775–84.
293. van de Donk NWCJ, Moreau P, Plesner T, Palumbo A, Gay F, Laubach JP, et al. Clinical efficacy and management of monoclonal antibodies targeting CD38 and SLAMF7 in multiple myeloma. *Blood*. 2016 Feb 11;127(6):681–95.
294. Ashour R, Ri M, Aly SS, Yoshida T, Tachita T, Kanamori T, et al. Expression analysis of two SLAM family receptors, SLAMF2 and SLAMF7, in patients with multiple myeloma. *International Journal of Hematology* [Internet]. 2019 Jul 1 [cited 2020 Oct 2];110(1):69–76. Available from: <https://pubmed.ncbi.nlm.nih.gov/31115879/>
295. Xie Z, Gunaratne J, Cheong LL, Liu SC, Koh TL, Huang G, et al. Plasma membrane proteomics identifies biomarkers associated with MMSET overexpression in t(4;14) multiple myeloma. *Oncotarget* [Internet]. 2013 [cited 2020 Oct 2];4(7):1008–18. Available from: <https://pubmed.ncbi.nlm.nih.gov/23900284/>
296. Chen J, Zhong MC, Guo H, Davidson D, Mishel S, Lu Y, et al. SLAMF7 is critical for phagocytosis of haematopoietic tumour cells via Mac-1 integrin. *Nature*. 2017 Apr 27;544(7651):493–7.
297. Pazina T, James AM, MacFarlane AW, Bezman NA, Henning KA, Bee C, et al. The anti-SLAMF7 antibody elotuzumab mediates NK cell activation through both CD16-dependent and – independent mechanisms. *Oncolmmunology*. 2017 Sep 2;6(9).
298. Bouchon A, Cella M, Grierson HL, Cohen JL, Colonna M. Cutting Edge: Activation of NK Cell-Mediated Cytotoxicity by a SAP-Independent Receptor of the CD2 Family. *The Journal of Immunology*. 2001 Nov 15;167(10):5517–21.
299. Murphy JJ, Hobby P, Vilarino-Varela J, Bishop B, Iordanidou P, Sutton BJ, et al. A novel immunoglobulin superfamily receptor (19A) related to CD2 is expressed on activated lymphocytes and promotes homotypic B-cell adhesion. *Biochemical Journal*. 2002 Feb 1;361(3):431–6.
300. Krämer B, Kobschull M, Nowak M, Demmer RT, Haupt M, Körner C, et al. Role of the NK cell-activating receptor CRACC in periodontitis. *Infection and Immunity*. 2013 Mar;81(3):690–6.
301. Lee JK, Mathew SO, Vaidya S V., Kumaresan PR, Mathew PA. CS1 (CRACC, CD319) Induces Proliferation and Autocrine Cytokine Expression on Human B Lymphocytes. *The Journal of Immunology*. 2007 Oct 1;179(7):4672–8.

302. Kumaresan PR, Lai WC, Chuang SS, Bennett M, Mathew PA. CS1, a novel member of the CD2 family, is homophilic and regulates NK cell function. *Molecular Immunology*. 2002 Sep 15;39(1-2):1-8.
303. Lee JK, Boles KS, Mathew PA. Molecular and functional characterization of a CS1 (CRACC) splice variant expressed in human NK cells that does not contain immunoreceptor tyrosine-based switch motifs. *European Journal of Immunology*. 2004 Oct;34(10):2791-9.
304. Cruz-Munoz ME, Dong Z, Shi X, Zhang S, Veillette A. Influence of CRACC, a SLAM family receptor coupled to the adaptor EAT-2, on natural killer cell function. *Nature Immunology*. 2009;10(3):297-305.
305. Guo H, Cruz-Munoz ME, Wu N, Robbins M, Veillette A. Immune Cell Inhibition by SLAMF7 Is Mediated by a Mechanism Requiring Src Kinases, CD45, and SHIP-1 That Is Defective in Multiple Myeloma Cells. *Molecular and Cellular Biology*. 2015 Jan 1;35(1):41-51.
306. Tai YT, Dillon M, Song W, Leiba M, Li XF, Burger P, et al. Anti-CS1 humanized monoclonal antibody HuLuc63 inhibits myeloma cell adhesion and induces antibody-dependent cellular cytotoxicity in the bone marrow milieu. *Blood*. 2008 May 13;112(4):1329-37.
307. Kikuchi J, Hori M, Iha H, Toyama-Sorimachi N, Hagiwara S, Kuroda Y, et al. Soluble SLAMF7 promotes the growth of myeloma cells via homophilic interaction with surface SLAMF7. *Leukemia*. 2020 Jan 1;34(1):180-95.
308. Dongre P, Mathew S, Akopova I, Gryczynski I, Mathew P. YY1 and a unique DNA repeat element regulates the transcription of mouse CS1 (CD319, SLAMF7) gene. *Molecular Immunology*. 2013 Jul 1;54(3-4):254-63.
309. Kim JR, Mathew SO, Mathew PA. Blimp-1/PRDM1 regulates the transcription of human CS1 (SLAMF7) gene in NK and B cells. *Immunobiology [Internet]*. 2016 Jan 1 [cited 2020 Jul 1];221(1):31-9. Available from: <https://pubmed.ncbi.nlm.nih.gov/26310579/>
310. Taniwaki M, Yoshida M, Matsumoto Y, Shimura K, Kuroda J, Kaneko H. Elotuzumab for the treatment of relapsed or refractory multiple myeloma, with special reference to its modes of action and SLAMF7 signaling. Vol. 10, *Mediterranean Journal of Hematology and Infectious Diseases*. Universita Cattolica del Sacro Cuore; 2018. p. 2018014.
311. Collins SM, Bakan CE, Swartzel GD, Hofmeister CC, Efebera YA, Kwon H, et al. Elotuzumab directly enhances NK cell cytotoxicity against myeloma via CS1 ligation: Evidence for augmented NK cell function complementing ADCC. *Cancer Immunology, Immunotherapy*. 2013 Dec;62(12):1841-9.
312. Woo J, Vierboom MPM, Kwon H, Chao D, Ye S, Li J, et al. PDL241, a novel humanized monoclonal antibody, reveals CD319 as a therapeutic target for rheumatoid arthritis. *Arthritis Research and Therapy*. 2013 Dec 4;15(6).
313. Vij R, Nath R, Afar DEH, Mateos MV, Berdeja JG, Raab MS, et al. First-in-Human Phase I Study of ABBV-838, an Antibody-Drug Conjugate Targeting SLAMF7/CS1 in Patients with Relapsed and Refractory Multiple Myeloma. *Clinical Cancer Research*. 2020 May 15;26(10):2308-17.
314. Chu J, He S, Deng Y, Zhang J, Peng Y, Hughes T, et al. Genetic modification of T cells redirected toward CS1 enhances eradication of myeloma cells. *Clinical Cancer Research*. 2014 Aug 1;20(15):3989-4000.

315. Gogishvili T, Danhof S, Prommersberger S, Rydzek J, Schreder M, Brede C, et al. SLAMF7-CAR T cells eliminate myeloma and confer selective fratricide of SLAMF7+ normal lymphocytes. *Blood*. 2017 Dec 28;130(26):2838–47.
316. HR E, T K, MA L, RE W, W H, C F, et al. Osteolytica: An automated image analysis software package that rapidly measures cancer-induced osteolytic lesions in in vivo models with greater reproducibility compared to other commonly used methods. *Bone*. 2016 Feb 1;83:9–16.
317. Bam R, Khan S, Ling W, Randal SS, Li X, Barlogie B, et al. Primary myeloma interaction and growth in coculture with healthy donor hematopoietic bone marrow. *BMC Cancer*. 2015 Dec 6;15(1):864.
318. Zhang W, Gu Y, Sun Q, Siegel DS, Tolias P, Yang Z, et al. Ex vivo maintenance of primary human multiple myeloma cells through the optimization of the osteoblastic niche. *PLoS ONE*. 2015;10(5):1–19.
319. Zlei M, Egert S, Wider D, Ihorst G, Wäsch R, Engelhardt M. Characterization of in vitro growth of multiple myeloma cells. *Experimental Hematology*. 2007 Oct;35(10):1550–61.
320. Carlisle RC, Di Y, Cerny AM, Sonnen AFP, Sim RB, Green NK, et al. Human erythrocytes bind and inactivate type 5 adenovirus by presenting Coxsackie virus-adenovirus receptor and complement receptor 1. *Blood*. 2009 Feb 26;113(9):1909–18.
321. Russell SJ, Peng KW, Bell JC. Oncolytic virotherapy. *Nat Biotechnol*. 2012 Jul 10;30(7):658–70.
322. Fisher K. Striking out at disseminated metastases: the systemic delivery of oncolytic viruses. *Curr Opin Mol Ther*. 2006 Aug;8(4):301–13.
323. Evgin L, Acuna SA, Tanese de Souza C, Marguerie M, Lemay CG, Ilkow CS, et al. Complement Inhibition Prevents Oncolytic Vaccinia Virus Neutralization in Immune Humans and Cynomolgus Macaques. *Molecular Therapy*. 2015 Jun;23(6):1066–76.
324. Magge D, Guo ZS, O'Malley ME, Francis L, Ravindranathan R, Bartlett DL. Inhibitors of C5 complement enhance vaccinia virus oncolysis. *Cancer Gene Therapy*. 2013 Jun 10;20(6):342–50.
325. Peng KWW, Dogan A, Vrana J, Liu C, Ong HT, Kumar S, et al. Tumor-associated macrophages infiltrate plasmacytomas and can serve as cell carriers for oncolytic measles virotherapy of disseminated myeloma. *American Journal of Hematology*. 2009 Jul 1;84(7):401–7.
326. Bartee E. Potential of oncolytic viruses in the treatment of multiple myeloma. *Oncolytic Virotherapy*. 2018 Feb;Volume 7:1–12.
327. Melcher A, Parato K, Rooney CM, Bell JC. Thunder and Lightning: Immunotherapy and Oncolytic Viruses Collide. *Molecular Therapy*. 2011 Jun;19(6):1008–16.
328. Meyers DE, Thakur S, Thirukkumaran CM, Morris DG. Oncolytic virotherapy as an immunotherapeutic strategy for multiple myeloma. *Blood Cancer Journal [Internet]*. 2017 Dec 5 [cited 2018 Jan 11];7(12):640. Available from: <http://www.ncbi.nlm.nih.gov/pubmed/29208938>

329. Romano A, Conticello C, Cavalli M, Vetro C, La Fauci A, Parrinello NL, et al. Immunological Dysregulation in Multiple Myeloma Microenvironment. *BioMed Research International*. 2014;2014:1–10.
330. Ohno S, Ono N, Seki F, Takeda M, Kura S, Tsuzuki T, et al. Measles Virus Infection of SLAM (CD150) Knockin Mice Reproduces Tropism and Immunosuppression in Human Infection. *Journal of Virology*. 2007 Feb 15;81(4):1650–9.
331. Fulci G, Breyman L, Gianni D, Kurozumi K, Rhee SS, Yu J, et al. Cyclophosphamide enhances glioma virotherapy by inhibiting innate immune responses. *Proceedings of the National Academy of Sciences*. 2006 Aug 22;103(34):12873–8.
332. Han J, Chen X, Chu J, Xu B, Meisen WH, Chen L, et al. TGF Treatment Enhances Glioblastoma Virotherapy by Inhibiting the Innate Immune Response. *Cancer Research*. 2015 Dec 15;75(24):5273–82.
333. Kurozumi K, Hardcastle J, Thakur R, Yang M, Christoforidis G, Fulci G, et al. Effect of Tumor Microenvironment Modulation on the Efficacy of Oncolytic Virus Therapy. *JNCI: Journal of the National Cancer Institute*. 2007 Dec 5;99(23):1768–81.
334. Cerullo V, Diaconu I, Kangasniemi L, Rajecki M, Escutenaire S, Koski A, et al. Immunological Effects of Low-dose Cyclophosphamide in Cancer Patients Treated With Oncolytic Adenovirus. *Molecular Therapy*. 2011 Sep;19(9).
335. Dhar D, Spencer JF, Toth K, Wold WSM. Effect of preexisting immunity on oncolytic adenovirus vector INGN 007 antitumor efficacy in immunocompetent and immunosuppressed Syrian hamsters. *J Virol*. 2009 Mar 1;83(5):2130–9.
336. Wakimoto H, Fulci G, Tyminski E, Antonio Chiocca E. Altered expression of antiviral cytokine mRNAs associated with cyclophosphamide's enhancement of viral oncolysis. *Gene Therapy*. 2004 Jan 8;11(2):214–23.
337. Tesfay MZ, Kirk AC, Hadac EM, Griesmann GE, Federspiel MJ, Barber GN, et al. PEGylation of vesicular stomatitis virus extends virus persistence in blood circulation of passively immunized mice. *J Virol*. 2013 Apr;87(7):3752–9.
338. Nguyen T V, Heller GJ, Barry ME, Crosby CM, Turner MA, Barry MA. Evaluation of polymer shielding for adenovirus serotype 6 (Ad6) for systemic virotherapy against human prostate cancers. *Molecular Therapy - Oncolytics*. 2016 Jan 1;3.
339. Prill JM, Šubr V, Pasquarelli N, Engler T, Hoffmeister A, Kochanek S, et al. Traceless Bioresponsive Shielding of Adenovirus Hexon with HEMA Copolymers Maintains Transduction Capacity In Vitro and In Vivo. Hong SS, editor. *PLoS ONE*. 2014 Jan 27;9(1):e82716.
340. Aoyama K, Kuroda S, Morihiro T, Kanaya N, Kubota T, Kakiuchi Y, et al. Liposome-encapsulated plasmid DNA of telomerase-specific oncolytic adenovirus with stealth effect on the immune system. *Scientific Reports*. 2017 Dec 26;7(1):14177.
341. Roy DG, Bell JC, Roy DG. Cell carriers for oncolytic viruses: current challenges and future directions. *Oncolytic Virotherapy*. 2013 Oct;2:47.
342. Baker AT, Aguirre-Hernández C, Halldén G, Parker AL. Designer oncolytic adenovirus: Coming of age [Internet]. Vol. 10, *Cancers*. MDPI AG; 2018 [cited 2020 Oct 1]. Available from: /pmc/articles/PMC6025169/?report=abstract

343. Sborov DW, Nuovo GJ, Stiff A, Mace T, Lesinski GB, Benson DM, et al. A phase I trial of single-agent reolysin in patients with relapsed multiple myeloma. *Clin Cancer Res.* 2014 Dec 1;20(23):5946–55.
344. Freytag SO, Stricker H, Pegg J, Paielli D, Pradhan DG, Peabody J, et al. Phase I study of replication-competent adenovirus-mediated double-suicide gene therapy in combination with conventional-dose three-dimensional conformal radiation therapy for the treatment of newly diagnosed, intermediate- to high-risk prostate cancer. *Cancer Res.* 2003 Nov 1;63(21):7497–506.
345. Galanis E, Okuno SH, Nascimento AG, Lewis BD, Lee RA, Oliveira AM, et al. Phase I–II trial of ONYX-015 in combination with MAP chemotherapy in patients with advanced sarcomas. *Gene Therapy.* 2005 Mar 13;12(5):437–45.
346. Karapanagiotou EM, Roulstone V, Twigger K, Ball M, Tanay M, Nutting C, et al. Phase I/II Trial of Carboplatin and Paclitaxel Chemotherapy in Combination with Intravenous Oncolytic Reovirus in Patients with Advanced Malignancies. *Clinical Cancer Research.* 2012 Apr 1;18(7):2080–9.
347. Ranki T, Pesonen S, Hemminki A, Partanen K, Kairemo K, Alanko T, et al. Phase I study with ONCOS-102 for the treatment of solid tumors – an evaluation of clinical response and exploratory analyses of immune markers. *Journal for ImmunoTherapy of Cancer.* 2016 Dec 15;4(1):17.
348. Malogolovkin A, Gasanov N, Egorov A, Weener M, Ivanov R, Karabelsky A. Combinatorial Approaches for Cancer Treatment Using Oncolytic Viruses: Projecting the Perspectives through Clinical Trials Outcomes. *Viruses.* 2021 Jun 29;13(7):1271.
349. Chesney J, Puzanov I, Collichio F, Singh P, Milhem MM, Glaspy J, et al. Randomized, open-label phase II study evaluating the efficacy and safety of talimogene laherparepvec in combination with ipilimumab versus ipilimumab alone in patients with advanced, unresectable melanoma. *Journal of Clinical Oncology.* 2018 Jun 10;36(17):1658–67.
350. Mahalingam D, Fountzilas C, Moseley J, Noronha N, Tran H, Chakrabarty R, et al. A phase II study of REOLYSIN® (pelareorep) in combination with carboplatin and paclitaxel for patients with advanced malignant melanoma. *Cancer Chemotherapy and Pharmacology.* 2017 Apr 1;79(4):697–703.
351. Roulstone V, Khan K, Pandha HS, Rudman S, Coffey M, Gill GM, et al. Phase I Trial of Cyclophosphamide as an Immune Modulator for Optimizing Oncolytic Reovirus Delivery to Solid Tumors. *Clinical Cancer Research.* 2015 Mar 15;21(6):1305–12.
352. Field-Smith A, Morgan GJ, Davies FE. Bortezomib (Velcade[®]) in the Treatment of Multiple Myeloma. *Ther Clin Risk Manag.* 2006 Sep;2(3):271–9.
353. Hideshima T, Richardson P, Chauhan D, Palombella VJ, Elliott PJ, Adams J, et al. The proteasome inhibitor PS-341 inhibits growth, induces apoptosis, and overcomes drug resistance in human multiple myeloma cells. *Cancer Res.* 2001 Apr 1;61(7):3071–6.
354. Adams J. The development of proteasome inhibitors as anticancer drugs. *Cancer Cell.* 2004 May;5(5):417–21.

355. Ling YH, Liebes L, Zou Y, Perez-Soler R. Reactive Oxygen Species Generation and Mitochondrial Dysfunction in the Apoptotic Response to Bortezomib, a Novel Proteasome Inhibitor, in Human H460 Non-small Cell Lung Cancer Cells. *Journal of Biological Chemistry*. 2003 Sep 5;278(36):33714–23.
356. R S, A C, A M, DH V, S J, MV D. Bortezomib enhances dendritic cell (DC)-mediated induction of immunity to human myeloma via exposure of cell surface heat shock protein 90 on dying tumor cells: therapeutic implications. *Blood*. 2007 Jun 1;109(11):4839–45.
357. V J, P J, O G, D de M, A RL, L ML, et al. Inhibition of autophagy with chloroquine potentiates carfilzomib-induced apoptosis in myeloma cells in vitro and in vivo. *Cancer Lett*. 2016 Nov 1;382(1):1–10.
358. Malfitano AM, Di Somma S, Iannuzzi CA, Pentimalli F, Portella G. Virotherapy: From single agents to combinatorial treatments. *Biochemical Pharmacology*. 2020 Jul 1;177:113986.
359. Zhang NH, Song LB, Wu XJ, Li RP, Zeng MS, Zhu XF, et al. Cell Cycle Proteasome inhibitor MG-132 modifies coxsackie and adenovirus receptor expression in colon cancer cell line Iovo. *Cell Cycle [Internet]*. 2008 [cited 2020 Jul 2];7(7):925–33. Available from: <https://www.tandfonline.com/action/journalInformation?journalCode=kccy20>
360. Yoo JY, Hurwitz BS, Bolyard C, Yu JG, Zhang J, Selvendiran K, et al. Bortezomib-induced unfolded protein response increases oncolytic HSV-1 replication resulting in synergistic, anti-tumor effects. *Clin Cancer Res*. 2014 Jul 15;20(14):3787.
361. Boozari B, Mundt B, Woller N, Strüver N, Gürlevik E, Schache P, et al. Antitumoural immunity by virus-mediated immunogenic apoptosis inhibits metastatic growth of hepatocellular carcinoma. *Gut*. 2010 Oct 1;59(10):1416–26.
362. Yoo JY, Jaime-Ramirez AC, Bolyard C, Dai H, Nallanagulagari T, Wojton J, et al. Bortezomib treatment sensitizes oncolytic HSV-1-treated tumors to NK cell immunotherapy. *Clinical Cancer Research*. 2016 Nov 1;22(21):5265–76.
363. Dudek SE, Luig C, Pauli EK, Schubert U, Ludwig S. The Clinically Approved Proteasome Inhibitor PS-341 Efficiently Blocks Influenza A Virus and Vesicular Stomatitis Virus Propagation by Establishing an Antiviral State. *Journal of Virology*. 2010 Sep 15;84(18):9439.
364. K S, E R, M M, U E, L P, PO L, et al. The Coxsackievirus and adenovirus receptor (CAR) forms a complex with the PDZ domain-containing protein ligand-of-numb protein-X (LNx). *J Biol Chem [Internet]*. 2003 Feb 28 [cited 2021 Aug 4];278(9):7439–44. Available from: <https://pubmed.ncbi.nlm.nih.gov/12468544/>
365. Wodrich H, Henaff D, Jammart B, Segura-Morales C, Seelmeir S, Coux O, et al. A Capsid-Encoded PPxY-Motif Facilitates Adenovirus Entry. *PLoS Pathogens [Internet]*. 2010 [cited 2021 Aug 4];6(3):1000808. Available from: </pmc/articles/PMC2841620/>
366. Spiesschaert B, Angerer K, Park J, Wollmann G. Combining Oncolytic Viruses and Small Molecule Therapeutics: Mutual Benefits. *Cancers (Basel) [Internet]*. 2021 Jul 2 [cited 2021 Aug 4];13(14). Available from: </pmc/articles/PMC8306439/>
367. AS L, LM H. ER stress and cancer. *Cancer Biol Ther*. 2006;5(7):721–2.
368. H Y. ER stress and diseases. *FEBS J*. 2007 Feb;274(3):630–58.

369. H Z, K L, Y L, F X, X X, J C, et al. Targeting VCP enhances anticancer activity of oncolytic virus M1 in hepatocellular carcinoma. *Sci Transl Med*. 2017 Aug 23;9(404).
370. Prasad V, Suomalainen M, Pennauer M, Yakimovich A, Andriasyan V, Hemmi S, et al. Chemical Induction of Unfolded Protein Response Enhances Cancer Cell Killing through Lytic Virus Infection. *Journal of Virology*. 2014 Nov 15;88(22):13086.
371. WK T, EJ J, J C, B C, AW P, JC P, et al. Calcium Influx Caused by ER Stress Inducers Enhances Oncolytic Adenovirus Enadenotucirev Replication and Killing through PKC α Activation. *Mol Ther Oncolytics*. 2019 Dec 20;15:117–30.
372. Esma F, Salvini M, Troia R, Boccadoro M, Larocca A, Pautasso C. Melphalan hydrochloride for the treatment of multiple myeloma. *Expert Opinion on Pharmacotherapy*. 2017 Jul 24;18(11):1127–36.
373. Kuczma M, Ding ZC, Zhou G. Immunostimulatory Effects of Melphalan and Usefulness in Adoptive Cell Therapy with Antitumor CD4⁺ T Cells. *Crit Rev Immunol*. 2016;36(2):179–91.
374. Mutlu P, Ural AU, Gündüz U. Different types of cell cycle- and apoptosis-related gene expressions alter in corticosteroid-, vincristine-, and melphalan-resistant u-266 multiple myeloma cell lines. *Turk J Haematol*. 2014 Sep 5;31(3):231–8.
375. Park GB, Kim YS, Kim D, Kim S, Lee HK, Cho DH, et al. Melphalan-Induced Apoptosis of EBV-Transformed B Cells through Upregulation of TAp73 and XAF1 and Nuclear Import of XPA. *The Journal of Immunology*. 2013 Dec 15;191(12):6281–91.
376. Lu X, Ding ZC, Cao Y, Liu C, Habtetsion T, Yu M, et al. Alkylating Agent Melphalan Augments the Efficacy of Adoptive Immunotherapy Using Tumor-Specific CD4⁺ T Cells. *The Journal of Immunology*. 2015 Feb 15;194(4):2011–21.
377. Kaliberova L, Krendelchtchikova V, Harmon D, Stockard C, Petersen A, Markert J, et al. CRAAdRGDflt-IL24 virotherapy in combination with chemotherapy of experimental glioma. *Cancer Gene Ther*. 2009 Oct;16(10):794.
378. Gomez-Gutierrez JG, Nitz J, Sharma R, Wechman SL, Riedinger E, Martinez-Jaramillo E, et al. Combined therapy of oncolytic adenovirus and temozolomide enhances lung cancer virotherapy in vitro and in vivo. *Virology*. 2016 Jan 1;487:249–59.
379. Bai Y, Chen Y, Hong X, Liu X, Su X, Li S, et al. Newcastle disease virus enhances the growth-inhibiting and proapoptotic effects of temozolomide on glioblastoma cells in vitro and in vivo. *Scientific Reports* 2018 8:1. 2018 Jul 31;8(1):1–12.
380. Pisklakova A, McKenzie B, Zemp F, Lun X, Kenchappa RS, Etame AB, et al. M011L-deficient oncolytic myxoma virus induces apoptosis in brain tumor-initiating cells and enhances survival in a novel immunocompetent mouse model of glioblastoma. *Neuro-Oncology*. 2016 Aug 1;18(8):1088.
381. Lun XQ, Jang JH, Tang N, Deng H, Head R, Bell JC, et al. Efficacy of Systemically Administered Oncolytic Vaccinia Virotherapy for Malignant Gliomas Is Enhanced by Combination Therapy with Rapamycin or Cyclophosphamide. *Clinical Cancer Research*. 2009 Apr;15(8):2777–88.
382. Fulci G, Breyman L, Gianni D, Kurozumi K, Rhee SS, Yu J, et al. Cyclophosphamide enhances glioma virotherapy by inhibiting innate immune responses. *Proc Natl Acad Sci U S A*. 2006 Aug 22;103(34):12873.

383. Peng KW, Myers R, Greenslade A, Mader E, Greiner S, Federspiel MJ, et al. Using clinically approved cyclophosphamide regimens to control the humoral immune response to oncolytic viruses. *Gene Therapy*. 2013 Mar;20(3):255–61.
384. Thomas MA, Spencer JF, Toth K, Sagartz JE, Phillips NJ, Wold WS. Immunosuppression Enhances Oncolytic Adenovirus Replication and Antitumor Efficacy in the Syrian Hamster Model. *Mol Ther*. 2008;16(10):1665.
385. Hofmann E, Weibel S, Szalay AA. Combination treatment with oncolytic Vaccinia virus and cyclophosphamide results in synergistic antitumor effects in human lung adenocarcinoma bearing mice. *Journal of Translational Medicine* 2014 12:1. 2014 Jul 17;12(1):1–14.
386. Roulstone V, Khan K, Pandha HS, Rudman S, Coffey M, Gill GM, et al. Phase I Trial of Cyclophosphamide as an Immune Modulator for Optimizing Oncolytic Reovirus Delivery to Solid Tumors. *Clin Cancer Res*. 2015 Mar 15;21(6):1305.
387. Burke MJ, Ahern C, Weigel BJ, Poirier JT, Rudin CM, Chen Y, et al. Phase I trial of Seneca Valley Virus (NTX-010) in children with relapsed/refractory solid tumors: A report of the Children's Oncology Group. *Pediatric Blood & Cancer*. 2015 May;62(5):743–50.
388. C W, RM D, P W, F G, T K, J T, et al. Vesicular stomatitis virus-induced immune suppressor cells generate antagonism between intratumoral oncolytic virus and cyclophosphamide. *Mol Ther*. 2011;19(1):140–9.
389. MJ W, HG S, TD P, DC M, J KC, AA K, et al. Isolated limb perfusion with biochemotherapy and oncolytic virotherapy combines with radiotherapy and surgery to overcome treatment resistance in an animal model of extremity soft tissue sarcoma. *Int J Cancer*. 2016 Sep 15;139(6):1414–22.
390. TD P, MJ W, DC M, AA K, R S, EM K, et al. Isolated limb perfusion with melphalan, tumour necrosis factor-alpha and oncolytic vaccinia virus improves tumour targeting and prolongs survival in a rat model of advanced extremity sarcoma. *Int J Cancer*. 2015 Feb 15;136(4):965–76.
391. Smith HG, Mansfield D, Roulstone V, Kyula-Currie JN, McLaughlin M, Patel RR, et al. PD-1 Blockade Following Isolated Limb Perfusion with Vaccinia Virus Prevents Local and Distant Relapse of Soft-tissue Sarcoma. *Clinical Cancer Research*. 2019 Jun 1;25(11):3443–54.
392. Ferguson PJ, Sykelyk A, Figueredo R, Koropatnick J. Synergistic Cytotoxicity against Human Tumor Cell Lines by Oncolytic Adenovirus dl1520 (ONYX-015) and Melphalan: <https://doi-org.sheffield.idm.oclc.org/105301/tj5000438>. 2015 Sep 30;102(1):31–9.
393. Post DE, Devi NS, Li Z, Brat DJ, Kaur B, Nicholson A, et al. Cancer Therapy with a Replicating Oncolytic Adenovirus Targeting the Hypoxic Microenvironment of Tumors. *Clinical Cancer Research*. 2004 Dec 15;10(24):8603–12.
394. KK B, S M. Regulation of the human O(6)-methylguanine-DNA methyltransferase gene by transcriptional coactivators cAMP response element-binding protein-binding protein and p300. *J Biol Chem*. 2000 Nov 3;275(44):34197–204.
395. Andreu-Vieyra C V, Berenson JR. The potential of panobinostat as a treatment option in patients with relapsed and refractory multiple myeloma. *Ther Adv Hematol*. 2014 Dec;5(6):197–210.

396. Moore D. Panobinostat (Farydak): A Novel Option for the Treatment of Relapsed Or Relapsed and Refractory Multiple Myeloma. *P T*. 2016 May;41(5):296–300.
397. Wolf JL, Siegel D, Goldschmidt H, Hazell K, Bourquelot PM, Bengoudifa BR, et al. Phase II trial of the pan-deacetylase inhibitor panobinostat as a single agent in advanced relapsed/refractory multiple myeloma. *Leukemia & Lymphoma*. 2012 Sep;53(9):1820–3.
398. Ocio EM, Vilanova D, Atadja P, Maiso P, Crusoe E, Fernandez-Lazaro D, et al. In vitro and in vivo rationale for the triple combination of panobinostat (LBH589) and dexamethasone with either bortezomib or lenalidomide in multiple myeloma. *Haematologica*. 2010 May 1;95(5):794–803.
399. Catley L, Weisberg E, Kiziltepe T, Tai YT, Hideshima T, Neri P, et al. Aggresome induction by proteasome inhibitor bortezomib and α -tubulin hyperacetylation by tubulin deacetylase (TDAC) inhibitor LBH589 are synergistic in myeloma cells. *Blood*. 2006 Nov 15;108(10):3441–9.
400. Chang HM, Paulson M, Holko M, Rice CM, Williams BRG, Marie I, et al. Induction of interferon-stimulated gene expression and antiviral responses require protein deacetylase activity. *Proceedings of the National Academy of Sciences*. 2004 Jun 29;101(26):9578–83.
401. Nusinzon I, Horvath CM. Interferon-stimulated transcription and innate antiviral immunity require deacetylase activity and histone deacetylase 1. *Proceedings of the National Academy of Sciences*. 2003 Dec 9;100(25):14742–7.
402. Tang X, Gao JS, Guan Y jie, McLane KE, Yuan ZL, Ramratnam B, et al. Acetylation-Dependent Signal Transduction for Type I Interferon Receptor. *Cell*. 2007 Oct 5;131(1):93–105.
403. Laengle J, Kabiljo J, Hunter L, Homola J, Prodinge S, Egger G, et al. Histone deacetylase inhibitors valproic acid and vorinostat enhance trastuzumab-mediated antibody-dependent cell-mediated phagocytosis. *Journal for ImmunoTherapy of Cancer*. 2020 Jan 1;8(1):e000195.
404. J S, S G, S B, S W, M S, JF B. The histone deacetylase inhibitor vorinostat induces calreticulin exposure in childhood brain tumour cells in vitro. *Cancer Chemother Pharmacol*. 2010 Aug;66(3):611–6.
405. F G, B B, C B, JF F, M R, M G, et al. Vaccination with epigenetically treated mesothelioma cells induces immunisation and blocks tumour growth. *Vaccine*. 2011 Jul 26;29(33):5534–43.
406. AC W, SR M, J S, LA C, AJ C, MJ S, et al. An intact immune system is required for the anticancer activities of histone deacetylase inhibitors. *Cancer Res*. 2013 Dec 15;73(24):7265–76.
407. Christiansen AJ, West A, Banks KM, Haynes NM, Teng MW, Smyth MJ, et al. Eradication of solid tumors using histone deacetylase inhibitors combined with immune-stimulating antibodies. *Proc Natl Acad Sci U S A*. 2011 Mar 8;108(10):4141.
408. L DB, S M, K DV, E M, E DB, K V, et al. Epigenetic treatment of multiple myeloma mediates tumor intrinsic and extrinsic immunomodulatory effects. *Oncoimmunology*. 2018 Oct 3;7(10).
409. Génin P, Morin P, Civas A. Impairment of Interferon-Induced IRF-7 Gene Expression due to Inhibition of ISGF3 Formation by Trichostatin A. *Journal of Virology*. 2003 Jun 15;77(12):7113.
410. I N, CM H. Positive and negative regulation of the innate antiviral response and beta interferon gene expression by deacetylation. *Mol Cell Biol*. 2006 Apr 15;26(8):3106–13.

411. HA B, R M, RJ V, AC van der M, S L, GR S, et al. Combinatorial association and abundance of components of interferon-stimulated gene factor 3 dictate the selectivity of interferon responses. *Proc Natl Acad Sci U S A*. 1995;92(12):5645–9.
412. M P, MF W, T A, JS D. Oncolytic Viruses on Drugs: Achieving Higher Therapeutic Efficacy. *ACS Infect Dis* [Internet]. 2018 Oct 12 [cited 2021 Aug 6];4(10):1448–67. Available from: <https://pubmed.ncbi.nlm.nih.gov/30152676/>
413. TL N, H A, M A, C B, S L, JS D, et al. Chemical targeting of the innate antiviral response by histone deacetylase inhibitors renders refractory cancers sensitive to viral oncolysis. *Proc Natl Acad Sci U S A*. 2008 Sep 30;105(39):14981–6.
414. MH D, R K, AM M, M S, N ES, HH S, et al. First-in-class small molecule potentiators of cancer virotherapy. *Sci Rep*. 2016 May 26;6.
415. S J, L P. Modifying chromatin and concepts of cancer. *Curr Opin Genet Dev*. 1999;9(2):175–84.
416. SY A, RA H. Histone acetylation and cancer. *Curr Opin Genet Dev*. 1999;9(2):171–4.
417. J G, SD G, JG H, MA C. The clinical application of targeting cancer through histone acetylation and hypomethylation. *Clin Cancer Res*. 2004 Jul 15;10(14):4589–96.
418. WATANABE T, HIOKI M, Fujiwara TT, Nishizaki M, KAGAWA S, TAKI M, et al. Histone deacetylase inhibitor FR901228 enhances the antitumor effect of telomerase-specific replication-selective adenoviral agent OBP-301 in human lung cancer cells. 312(3).
419. Bieler A, Mantwill K, Dravits T, Bernshausen A, Glockzin G, Köhler-Vargas N, et al. Novel Three-Pronged Strategy to Enhance Cancer Cell Killing in Glioblastoma Cell Lines: Histone Deacetylase Inhibitor, Chemotherapy, and Oncolytic Adenovirus dl520. <https://home.liebertpub.com/hum>. 2006 Jan 12;17(1):55–70.
420. Pont LMEB, Kleijn A, Kloezevan JJ, Bossche W van den, Kaufmann JK, Vrij J de, et al. The HDAC Inhibitors Scriptaid and LBH589 Combined with the Oncolytic Virus Delta24-RGD Exert Enhanced Anti-Tumor Efficacy in Patient-Derived Glioblastoma Cells. *PLoS ONE*. 2015 May 18;10(5).
421. Kim DR, Park MY, Lim HJ, Park JS, Cho YJ, Lee SW, et al. Combination therapy of conditionally replicating adenovirus and histone deacetylase inhibitors. *International Journal of Molecular Medicine*. 2012 Feb 1;29(2):218–24.
422. Höti N, Chowdhury W, Hsieh JT, Sachs MD, Lupold SE, Rodriguez R. Valproic Acid, a Histone Deacetylase Inhibitor, Is an Antagonist for Oncolytic Adenoviral Gene Therapy. *Molecular Therapy*. 2006 Dec 1;14(6):768–78.
423. Hulin-Curtis SL, Davies JA, Jones R, Hudson E, Hanna L, Chester JD, et al. Histone deacetylase inhibitor trichostatin A sensitises cisplatin-resistant ovarian cancer cells to oncolytic adenovirus. *Oncotarget*. 2018 May 29;9(41):26328.
424. Han X, Wang S, Zhou W, Li Y, Lei W, Lv W. Synergistic combination of histone deacetylase inhibitor suberoylanilide hydroxamic acid and oncolytic adenovirus ZD55-TRAIL as a therapy against cervical cancer. *Molecular Medicine Reports*. 2015 Jul 1;12(1):435–41.

425. Stiff A, Caserta E, Sborov DW, Nuovo GJ, Mo X, Schlotter SY, et al. Histone Deacetylase Inhibitors Enhance the Therapeutic Potential of Reovirus in Multiple Myeloma. *Molecular Cancer Therapeutics*. 2016 May 1;15(5):830–41.
426. CA AB, J Y, R P, M W, Y W, MO N, et al. The histone deacetylase inhibitor valproic acid lessens NK cell action against oncolytic virus-infected glioblastoma cells by inhibition of STAT5/T-BET signaling and generation of gamma interferon. *J Virol*. 2012 Apr 15;86(8):4566–77.
427. VA J, GB S, AMS R, KJ S, G M, B K, et al. Potentiating Oncolytic Virus-Induced Immune-Mediated Tumor Cell Killing Using Histone Deacetylase Inhibition. *Mol Ther*. 2019 Jun 5;27(6):1139–52.
428. Li J, Bonifati S, Hristov G, Marttila T, Valmary-Degano S, Stanzel S, et al. Synergistic combination of valproic acid and oncolytic parvovirus H-1PV as a potential therapy against cervical and pancreatic carcinomas. *EMBO Molecular Medicine*. 2013 Oct;5(10):1537.
429. Bridle BW, Chen L, Lemay CG, Diallo JS, Pol J, Nguyen A, et al. HDAC Inhibition Suppresses Primary Immune Responses, Enhances Secondary Immune Responses, and Abrogates Autoimmunity During Tumor Immunotherapy. *Molecular Therapy*. 2013;21(4):887.
430. RF P, EJ N, C G. HDAC inhibition prevents NF-kappa B activation by suppressing proteasome activity: down-regulation of proteasome subunit expression stabilizes I kappa B alpha. *Biochem Pharmacol*. 2005 Aug 1;70(3):394–406.
431. Shen L, Ciesielski M, Ramakrishnan S, Miles KM, Ellis L, Sotomayor P, et al. Class I Histone Deacetylase Inhibitor Entinostat Suppresses Regulatory T Cells and Enhances Immunotherapies in Renal and Prostate Cancer Models. *PLoS ONE*. 2012 Jan 27;7(1).
432. Moreau P, Attal M, Facon T. Frontline therapy of multiple myeloma. *Blood*. 2015 May 14;125(20):3076–84.
433. Haslett PA, Corral LG, Albert M, Kaplan G. Thalidomide costimulates primary human T lymphocytes, preferentially inducing proliferation, cytokine production, and cytotoxic responses in the CD8+ subset. *J Exp Med*. 1998 Jun 1;187(11):1885–92.
434. Davies FE, Raje N, Hideshima T, Lentzsch S, Young G, Tai YT, et al. Thalidomide and immunomodulatory derivatives augment natural killer cell cytotoxicity in multiple myeloma. *Blood*. 2001 Jul 1;98(1):210–6.
435. Galustian C, Meyer B, Labarthe MC, Dredge K, Klaschka D, Henry J, et al. The anti-cancer agents lenalidomide and pomalidomide inhibit the proliferation and function of T regulatory cells. *Cancer Immunology, Immunotherapy*. 2009 Jul 14;58(7):1033–45.
436. Luptakova K, Rosenblatt J, Glotzbecker B, Mills H, Stroopinsky D, Kufe T, et al. Lenalidomide enhances anti-myeloma cellular immunity. *Cancer Immunology, Immunotherapy*. 2013 Jan 24;62(1):39–49.
437. Sedlarikova L, Kubiczkova L, Sevcikova S, Hajek R. Mechanism of immunomodulatory drugs in multiple myeloma. *Leukemia Research*. 2012 Oct 1;36(10):1218–24.
438. Israyelyan A, Shannon EJ, Baghian A, Kearney MT, Kousoulas KG. Thalidomide suppressed the growth of 4T1 cells into solid tumors in Balb/c mice in a combination therapy with the oncolytic fusogenic HSV-1 OncdSyn. 2009;64(6):1201–10.

439. Oku M, Ishino R, Uchida S, Imataki O, Sugimoto N, Todo T, et al. Oncolytic herpes simplex virus type 1 (HSV-1) in combination with lenalidomide for plasma cell neoplasms. *British Journal of Haematology*. 2021 Jan 1;192(2):343–53.
440. Parrish C, Scott GB, Coffey M, Melcher A, Errington-Mais F, Cook G. Combination Therapy with Reovirus and Immunomodulatory Drugs Induces Direct Oncolytic and Immune-Mediated Killing of Multiple Myeloma Cells and Overcomes Stromal-Mediated Microenvironmental Protection. *Blood*. 2014;124(21).
441. Gooding RP, Bybee A, Cooke F, Little A, Marsh SGE, Coelho E, et al. Phenotypic and molecular analysis of six human cell lines derived from patients with plasma cell dyscrasia. *British Journal of Haematology*. 1999 Sep 1;106(3):669–81.
442. Lombardi L, Poretti G, Mattioli M, Fabris S, Agnelli L, Biciato S, et al. Molecular characterization of human multiple myeloma cell lines by integrative genomics: Insights into the biology of the disease. *Genes, Chromosomes and Cancer*. 2007 Mar 1;46(3):226–38.
443. Adamo A, Delfino P, Gatti A, Bonato A, Takam Kamga P, Bazzoni R, et al. HS-5 and HS-27A Stromal Cell Lines to Study Bone Marrow Mesenchymal Stromal Cell-Mediated Support to Cancer Development. *Frontiers in Cell and Developmental Biology* [Internet]. 2020 Nov 5 [cited 2022 Mar 9];8. Available from: [/pmc/articles/PMC7674674/](#)
444. Adamo A, Delfino P, Gatti A, Bonato A, Takam Kamga P, Bazzoni R, et al. HS-5 and HS-27A Stromal Cell Lines to Study Bone Marrow Mesenchymal Stromal Cell-Mediated Support to Cancer Development. *Frontiers in Cell and Developmental Biology*. 2020 Nov 5;8:1227.
445. Hayes J. Osteoblast models for matrix research. *European Cells and Materials*. 24(2012):1–17.
446. van Steenbrugge GJ, Groen M, van Dogen JW, Bolt J, van der Korput H, Trapman J, et al. The human prostatic carcinoma cell line LNCaP and its derivatives. An overview. *Urol Res* [Internet]. 1989 Mar [cited 2022 Mar 9];17(2):71–7. Available from: <https://pubmed.ncbi.nlm.nih.gov/2660395/>
447. Kovesdi I, Hedley SJ. Adenoviral Producer Cells. *Viruses* [Internet]. 2010 Aug [cited 2022 Mar 9];2(8):1681. Available from: [/pmc/articles/PMC3185730/](#)
448. Chou TC. Theoretical basis, experimental design, and computerized simulation of synergism and antagonism in drug combination studies. Vol. 58, *Pharmacological Reviews*. Pharmacol Rev; 2006. p. 621–81.
449. Sun X, Kaufman PD. Ki-67: more than a proliferation marker. Vol. 127, *Chromosoma*. Springer Science and Business Media Deutschland GmbH; 2018. p. 175–86.
450. Demchenko AP. Beyond annexin V: Fluorescence response of cellular membranes to apoptosis. Vol. 65, *Cytotechnology*. Springer; 2013. p. 157–72.
451. Lawson MA, McDonald MM, Kovacic N, Khoo WH, Terry RL, Down J, et al. Osteoclasts control reactivation of dormant myeloma cells by remodelling the endosteal niche. *Nature Communications*. 2015 Dec 3;6.
452. Lawson MA, Paton-Hough JM, Evans HR, Walker RE, Harris W, Ratnabalan D, et al. NOD/SCID-GAMMA mice are an ideal strain to assess the efficacy of therapeutic agents used in the treatment of myeloma bone disease. *PLoS ONE* [Internet]. 2015 Mar 13 [cited 2020 Apr 21];10(3). Available from: [/pmc/articles/PMC4358985/](#)

453. Paton-Hough J, Chantry AD, Lawson MA. A review of current murine models of multiple myeloma used to assess the efficacy of therapeutic agents on tumour growth and bone disease [Internet]. Vol. 77, Bone. Elsevier Inc.; 2015 [cited 2020 Apr 21]. p. 57–68. Available from: <http://www.ncbi.nlm.nih.gov/pubmed/25868800>
454. Green AC, Lath D, Hudson K, Walkley B, Down JM, Owen R, et al. TGF β Inhibition Stimulates Collagen Maturation to Enhance Bone Repair and Fracture Resistance in a Murine Myeloma Model. *Journal of Bone and Mineral Research*. 2019 Dec;34(12):2311–26.
455. Paton-Hough J, Tazzyman S, Evans H, Lath D, Down JM, Green AC, et al. Preventing and Repairing Myeloma Bone Disease by Combining Conventional Antiresorptive Treatment With a Bone Anabolic Agent in Murine Models. *Journal of Bone and Mineral Research*. 2019 May 1;34(5):783–96.
456. Radl J, De Glopper ED, Schuit HR, Zurcher C. Idiopathic paraproteinemia. II. Transplantation of the paraprotein-producing clone from old to young C57BL/KaLwRij mice. *J Immunol*. 1979 Feb;122(2):609–13.
457. Garrett IR, Dallas S, Radl J, Mundy GR. A murine model of human myeloma bone disease. *Bone*. 1997 Jun;20(6):515–20.
458. Hurchla MA, Garcia-Gomez A, Hornick MC, Ocio EM, Li A, Blanco JF, et al. The epoxyketone-based proteasome inhibitors carfilzomib and orally bioavailable oprozomib have anti-resorptive and bone-anabolic activity in addition to anti-myeloma effects. *Leukemia*. 2013 Feb;27(2):430–40.
459. Oyajobi BO, Muñoz S, Kakonen R, Williams PJ, Gupta A, Wideman CL, et al. Detection of myeloma in skeleton of mice by whole-body optical fluorescence imaging. *Molecular Cancer Therapeutics*. 2007 Jun 1;6(6):1701–8.
460. Bera S, Greiner S, Choudhury A, Dispenzieri A, Spitz DR, Russell SJ, et al. Dexamethasone-induced oxidative stress enhances myeloma cell radiosensitization while sparing normal bone marrow hematopoiesis. *Neoplasia*. 2010;12(12):980–92.
461. Lwin ST, Edwards CM, Silbermann R. Preclinical animal models of multiple myeloma. *BoneKEY Reports*. 2016 Feb 3;5:772.
462. Dallas SL, Garrett IR, Oyajobi BO, Dallas MR, Boyce BF, Bauss F, et al. Ibandronate reduces osteolytic lesions but not tumor burden in a murine model of myeloma bone disease. *Blood*. 1999 Mar 1;93(5):1697–706.
463. Bankhead P, Loughrey MB, Fernández JA, Dombrowski Y, McArt DG, Dunne PD, et al. QuPath: Open source software for digital pathology image analysis. *Scientific Reports*. 2017 Dec 1;7(1):1–7.
464. Fueyo J, Alemany R, Gomez-Manzano C, Fuller GN, Khan A, Conrad CA, et al. Preclinical Characterization of the Antiglioma Activity of a Tropism-Enhanced Adenovirus Targeted to the Retinoblastoma Pathway.
465. Lang FF, Conrad C, Gomez-Manzano C, Alfred Yung WK, Sawaya R, Weinberg JS, et al. Phase I study of DNX-2401 (delta-24-RGD) oncolytic adenovirus: replication and immunotherapeutic effects in recurrent malignant glioma. *Journal of Clinical Oncology*. 2018 May 10;36(14):1419–27.

466. Machiels JP, Salazar R, Rottey S, Duran I, Dirix L, Geboes K, et al. A phase 1 dose escalation study of the oncolytic adenovirus enadenotucirev, administered intravenously to patients with epithelial solid tumors (EVOLVE). *Journal for ImmunoTherapy of Cancer*. 2019 Jan 28;7(1).
467. Packiam VT, Lamm DL, Barocas DA, Trainer A, Fand B, Davis RL, et al. An open label, single-arm, phase II multicenter study of the safety and efficacy of CG0070 oncolytic vector regimen in patients with BCG-unresponsive non-muscle-invasive bladder cancer: Interim results. *Urologic Oncology: Seminars and Original Investigations*. 2018 Oct 1;36(10):440–7.
468. Chen CY, Senac JS, Weaver EA, May SM, Jelinek DF, Greipp P, et al. Species D adenoviruses as oncolytics against B-cell cancers. *Clinical Cancer Research*. 2011 Nov 1;17(21):6712–22.
469. Yotnda P, Onishi H, Heslop HE, Shayakhmetov D, Lieber A, Brenner M, et al. Efficient infection of primitive hematopoietic stem cells by modified adenovirus. *Gene Therapy*. 2001;8(12):930–7.
470. Lu ZZ, Ni F, Hu ZB, Wang L, Wang H, Zhang QW, et al. Efficient gene transfer into hematopoietic cells by a retargeting adenoviral vector system with a chimeric fiber of adenovirus serotype 5 and 11p. *Exp Hematol*. 2006 Sep;34(9):1171–82.
471. M. Fancher, PharmD, BCOP K, J. Bunk, PharmD E. Elotuzumab: The First Monoclonal Antibody for the Treatment of Multiple Myeloma. *Journal of the Advanced Practitioner in Oncology*. 2016 Aug 1;7(5):542.
472. Lonial S, Dimopoulos M, Palumbo A, White D, Grosicki S, Spicka I, et al. Elotuzumab Therapy for Relapsed or Refractory Multiple Myeloma. *New England Journal of Medicine*. 2015 Aug 13;373(7):621–31.
473. Mateos MV, Granell M, Oriol A, Martinez-Lopez J, Blade J, Hernandez MT, et al. Elotuzumab in combination with thalidomide and low-dose dexamethasone: a phase 2 single-arm safety study in patients with relapsed/refractory multiple myeloma. *British Journal of Haematology*. 2016 Nov 1;175(3):448–56.
474. Mast TC, Kierstead L, Gupta SB, Nikas AA, Kallas EG, Novitsky V, et al. International epidemiology of human pre-existing adenovirus (Ad) type-5, type-6, type-26 and type-36 neutralizing antibodies: Correlates of high Ad5 titers and implications for potential HIV vaccine trials. *Vaccine*. 2010 Jan 22;28(4):950–7.
475. Appaiahgari MB, Saini M, Rauthan M, Jyoti, Vrati S. Immunization with recombinant adenovirus synthesizing the secretory form of Japanese encephalitis virus envelope protein protects adenovirus-exposed mice against lethal encephalitis. *Microbes and Infection*. 2006 Jan;8(1):92–104.
476. Tsai V, Johnson DE, Rahman A, Wen SF, LaFace D, Philopena J, et al. Impact of human neutralizing antibodies on antitumor efficacy of an oncolytic adenovirus in a murine model. *Clinical Cancer Research*. 2004 Nov 1;10(21):7199–206.
477. Ludwig H, Boccadoro M, Moreau P, San-Miguel J, Cavo M, Pawlyn C, et al. Recommendations for vaccination in multiple myeloma: a consensus of the European Myeloma Network. *Leukemia*. Springer Nature; 2020.

478. Tete SM, Bijl M, Sahota SS, Bos NA. Immune defects in the risk of infection and response to vaccination in monoclonal gammopathy of undetermined significance and multiple myeloma. Vol. 5, *Frontiers in Immunology*. Frontiers Research Foundation; 2014.
479. McNees AL, Gooding LR. Adenoviral inhibitors of apoptotic cell death. Vol. 88, *Virus Research*. *Virus Res*; 2002. p. 87–101.
480. Abou El Hassan MAI, van der Meulen-Muileman I, Abbas S, Kruyt FAE. Conditionally Replicating Adenoviruses Kill Tumor Cells via a Basic Apoptotic Machinery-Independent Mechanism That Resembles Necrosis-Like Programmed Cell Death. *Journal of Virology*. 2004 Nov 15;78(22):12243–51.
481. Lichtenstein DL, Krajcsi P, Esteban DJ, Tollefson AE, Wold WSM. Adenovirus RID β Subunit Contains a Tyrosine Residue That Is Critical for RID-Mediated Receptor Internalization and Inhibition of Fas- and TRAIL-Induced Apoptosis. *Journal of Virology*. 2002 Nov 15;76(22):11329–42.
482. Braithwaite AW, Russell IA. Induction of cell death by adenoviruses. Vol. 6, *Apoptosis*. *Apoptosis*; 2001. p. 359–70.
483. Hall AR, Dix BR, O’Carroll SJ, Braithwaite AW. p53-dependent cell death/apoptosis is required for a productive adenovirus infection. *Nature Medicine*. 1998 Sep;4(9):1068–72.
484. Robert A, Miron MJ, Champagne C, Gingras MC, Branton PE, Lavoie JN. Distinct cell death pathways triggered by the adenovirus early region 4 ORF 4 protein. *Journal of Cell Biology*. 2002;158(3):519–28.
485. Rao L, Debbas M, Sabbatini P, Hockenbery D, Korsmeyer S, White E. The adenovirus E1A proteins induce apoptosis, which is inhibited by the E1B 19-kDa and Bcl-2 proteins. *Proc Natl Acad Sci U S A*. 1992;89(16):7742–6.
486. Ito H, Aoki H, Kühnel F, Kondo Y, Kubicka S, Wirth T, et al. Autophagic Cell Death of Malignant Glioma Cells Induced by a Conditionally Replicating Adenovirus. *J Natl Cancer Inst*. 2006;98(9).
487. Di Somma S, Iannuzzi CA, Passaro C, Forte IM, Iannone R, Gigantino V, et al. The Oncolytic Virus dl922-947 Triggers Immunogenic Cell Death in Mesothelioma and Reduces Xenograft Growth. *Frontiers in Oncology*. 2019 Jul;564.
488. Dyer A, Di Y, Calderon H, Illingworth S, Kueberuwa G, Tedcastle A, et al. Oncolytic Group B Adenovirus Enadenotucirev Mediates Non-apoptotic Cell Death with Membrane Disruption and Release of Inflammatory Mediators. 2017;
489. Kuryk L, Møller ASW, Garofalo M, Cerullo V, Pesonen S, Alemany R, et al. Antitumor-specific T-cell responses induced by oncolytic adenovirus ONCOS-102 (AdV5/3-D24-GM-CSF) in peritoneal mesothelioma mouse model. *Journal of Medical Virology*. 2018 Oct 1;90(10):1669–73.
490. Galluzzi L, Vitale I, Warren S, Adjemian S, Agostinis P, Martinez AB, et al. Consensus guidelines for the definition, detection and interpretation of immunogenic cell death [Internet]. Vol. 8, *Journal for ImmunoTherapy of Cancer*. BMJ Publishing Group; 2020 [cited 2021 Feb 17]. p. 70. Available from: <http://jitc.bmj.com/>

491. Galluzzi L, Vitale I, Aaronson SA, Abrams JM, Adam D, Agostinis P, et al. Molecular mechanisms of cell death: Recommendations of the Nomenclature Committee on Cell Death 2018 [Internet]. Vol. 25, Cell Death and Differentiation. Nature Publishing Group; 2018 [cited 2021 Feb 17]. p. 486–541. Available from: <https://pubmed.ncbi.nlm.nih.gov/29362479/>
492. T R, T J, E J, J K, C W, K K, et al. Local treatment of a pleural mesothelioma tumor with ONCOS-102 induces a systemic antitumor CD8 + T-cell response, prominent infiltration of CD8 + lymphocytes and Th1 type polarization. *Oncoimmunology*. 2014 Sep 1;3(10):e958937-1-e958937-4.
493. Tang J, Zhou H, Wang C, Fei X, Zhu L, Huang Y, et al. Cell adhesion downregulates the expression of Homer1b/c and contributes to drug resistance in multiple myeloma cells. *Oncology Reports*. 2016 Mar 1;35(3):1875–83.
494. Furukawa M, Ohkawara H, Ogawa K, Ikeda K, Ueda K, Shichishima-Nakamura A, et al. Autocrine and paracrine interactions between multiple myeloma cells and bone marrow stromal cells by growth arrest-specific gene 6 cross-talk with interleukin-6. *Journal of Biological Chemistry*. 2017 Mar 10;292(10):4280–92.
495. Xu X, Liu J, Shen C, Ding L, Zhong F, Ouyang Y, et al. The role of ubiquitin-specific protease 14 (USP14) in cell adhesion-mediated drug resistance (CAM-DR) of multiple myeloma cells. *European Journal of Haematology*. 2017 Jan 1;98(1):4–12.
496. Shlomovitz I, Speir M, Gerlic M. Flipping the dogma - Phosphatidylserine in non-apoptotic cell death. Vol. 17, Cell Communication and Signaling. BioMed Central Ltd.; 2019. p. 1–12.
497. Dhuriya YK, Sharma D. Necroptosis: a regulated inflammatory mode of cell death. *Journal of Neuroinflammation* 2018 15:1. 2018 Jul 6;15(1):1–9.
498. Folkes AS, Feng M, Zain JM, Abdulla F, Rosen ST, Querfeld C. Targeting CD47 as a cancer therapeutic strategy: The cutaneous T-cell lymphoma experience. Vol. 30, Current Opinion in Oncology. Lippincott Williams and Wilkins; 2018. p. 332–7.
499. Maes K, Breckpot K. Commentary: Immunogenic Cell Death and Immunotherapy of Multiple Myeloma. *Frontiers in Cell and Developmental Biology*. 2019 Jul 31;7(JULY):50.
500. Savio LEB, de Andrade Mello P, da Silva CG, Coutinho-Silva R. The P2X7 Receptor in Inflammatory Diseases: Angel or Demon? *Frontiers in Pharmacology*. 2018 Feb 6;9(FEB):52.
501. Walz S, Stickel JS, Kowalewski DJ, Schuster H, Weisel K, Backert L, et al. The antigenic landscape of multiple myeloma: mass spectrometry (re)defines targets for T-cell-based immunotherapy. *Blood*. 2015 Sep 3;126(10):1203.
502. Reeh M, Bockhorn M, Görgens D, Vieth M, Hoffmann T, Simon R, et al. Presence of the Coxsackievirus and Adenovirus Receptor (CAR) in human neoplasms: A multitumour array analysis. *British Journal of Cancer*. 2013 Oct 1;109(7):1848–58.
503. Ebbinghaus C, Al-Jaibaji A, Operschall E, Schöffel A, Peter I, Greber UF, et al. Functional and Selective Targeting of Adenovirus to High-Affinity Fcγ Receptor I-Positive Cells by Using a Bispecific Hybrid Adapter. *Journal of Virology*. 2001 Jan 1;75(1):480–9.
504. Zhang Y, Bergelson JM. Adenovirus Receptors. *Journal of Virology*. 2005 Oct 1;79(19):12125–31.

505. Beauvais DLM, Jung O, Yang Y, Sanderson RD, Rapraeger AC. Syndecan-1 (CD138) suppresses apoptosis in multiple myeloma by activating IGF1 receptor: Prevention by synstatin IGF1R inhibits tumor growth. *Cancer Research*. 2016 Sep 1;76(17):4981–93.
506. Tucci M, De Palma R, Lombardi L, Rodolico G, Berrino L, Dammacco F, et al. B 3 Integrin Subunit Mediates the Bone-Resorbing Function Exerted by Cultured Myeloma Plasma Cells. *Cancer Res*. 2009;69(16):6738–84.
507. Einsele H, Schreder M. Treatment of multiple myeloma with the immunostimulatory SLAMF7 antibody elotuzumab. *Therapeutic Advances in Hematology*. 2016 Oct 31;7(5):288–301.
508. Chu J, Deng Y, Benson DM, He S, Hughes T, Zhang J, et al. CS1-specific chimeric antigen receptor (CAR)-engineered natural killer cells enhance in vitro and in vivo antitumor activity against human multiple myeloma. *Leukemia*. 2014 Sep 26;28(4):917–27.
509. Feugier P. A review of rituximab, the first anti-CD20 monoclonal antibody used in the treatment of B non-Hodgkin's lymphomas. <http://dx.doi.org/10.2217/fon1557> [Internet]. 2015 May 8 [cited 2021 Sep 12];11(9):1327–42. Available from: <https://www.futuremedicine.com/doi/abs/10.2217/fon.15.57>
510. Braylan RC. Impact of flow cytometry on the diagnosis and characterization of lymphomas, chronic lymphoproliferative disorders and plasma cell neoplasias. *Cytometry*. 2004 Mar;58A(1):57–61.
511. Smock KJ, Perkins SL, Bahler DW. Quantitation of plasma cells in bone marrow aspirates by flow cytometric analysis compared with morphologic assessment. *Arch Pathol Lab Med*. 2007 Jun;131(6):951–5.
512. Bain BJ. Bone marrow aspiration. *J Clin Pathol*. 2001 Sep;54(9):657–63.
513. Loken MR, Chu SC, Fritschle W, Kalnoski M, Wells DA. Normalization of bone marrow aspirates for hemodilution in flow cytometric analyses. *Cytometry Part B: Clinical Cytometry*. 2009 Jan;76B(1):27–36.
514. Parikh MR, Belch AR, Pilarski LM, Kirshner J. A Three-dimensional Tissue Culture Model to Study Primary Human Bone Marrow and its Malignancies. *Journal of Visualized Experiments*. 2014 Mar 8;(85):1–8.
515. Cocco M, Stephenson S, Care MA, Newton D, Barnes NA, Davison A, et al. In Vitro Generation of Long-lived Human Plasma Cells. *The Journal of Immunology*. 2012 Dec 15;189(12):5773–85.
516. Singh PK, Doley J, Ravi Kumar G, Sahoo AP, Tiwari AK. Oncolytic viruses & their specific targeting to tumour cells. Vol. 136, *Indian Journal of Medical Research*. Wolters Kluwer -- Medknow Publications; 2012. p. 571–84.
517. Johnson DC, Huber MT. Directed Egress of Animal Viruses Promotes Cell-to-Cell Spread. *Journal of Virology*. 2002 Jan 1;76(1):1–8.
518. Marcellus RC, Lavoie JN, Boivin D, Shore GC, Ketner G, Branton PE. The early region 4 orf4 protein of human adenovirus type 5 induces p53-independent cell death by apoptosis. *J Virol*. 1998 Sep;72(9):7144–53.

519. Marcellus RC, Chan H, Paquette D, Thirlwell S, Boivin D, Branton PE. Induction of p53-independent apoptosis by the adenovirus E4orf4 protein requires binding to the Balph subunit of protein phosphatase 2A. *J Virol*. 2000 Sep 1;74(17):7869–77.
520. Benedict CA, Norris PS, Prigozy TI, Bodmer JL, Mahr JA, Garnett CT, et al. Three adenovirus E3 proteins cooperate to evade apoptosis by tumor necrosis factor-related apoptosis-inducing ligand receptor-1 and -2. *J Biol Chem*. 2001 Feb 2;276(5):3270–8.
521. Suzuki J, Umeda M, Sims PJ, Nagata S. Calcium-dependent phospholipid scrambling by TMEM16F. *Nature*. 2010 Dec 9;468(7325):834–40.
522. Zargarian S, Shlomovitz I, Erlich Z, Hourizadeh A, Ofir-Birin Y, Croker BA, et al. Phosphatidylserine externalization, “necroptotic bodies” release, and phagocytosis during necroptosis. Walczak H, editor. *PLOS Biology*. 2017 Jun 26;15(6):e2002711.
523. Weigert M, Binks A, Dowson S, Leung EYL, Athineos D, Yu X, et al. RIPK3 promotes adenovirus type 5 activity. *Cell Death & Disease* [Internet]. 2017 Dec 13 [cited 2018 Jul 19];8(12):3206. Available from: <http://www.ncbi.nlm.nih.gov/pubmed/29238045>
524. Mocarski ES, Upton JW, Kaiser WJ. Viral infection and the evolution of caspase 8-regulated apoptotic and necrotic death pathways. *Nat Rev Immunol*. 2012 Feb;12(2):79.
525. Zhou J, Wang G, Chen Y, Wang H, Hua Y, Cai Z. Immunogenic cell death in cancer therapy: Present and emerging inducers. Vol. 23, *Journal of Cellular and Molecular Medicine*. Blackwell Publishing Inc.; 2019. p. 4854–65.
526. Huang H, Xiao T, He L, Ji H, Liu XYY. Interferon- β -armed oncolytic adenovirus induces both apoptosis and necroptosis in cancer cells. *Acta Biochimica et Biophysica Sinica*. 2012 Sep 1;44(9):737–45.
527. Ma J, Ramachandran M, Jin C, Quijano-Rubio C, Martikainen M, Yu D, et al. Characterization of virus-mediated immunogenic cancer cell death and the consequences for oncolytic virus-based immunotherapy of cancer. *Cell Death and Disease*. 2020 Jan 1;11(1):1–15.
528. Laevskaya A, Borovjagin A, Timashev PS, Lesniak MS, Ulasov I. Metabolome-Driven Regulation of Adenovirus-Induced Cell Death. *International Journal of Molecular Sciences* 2021, Vol 22, Page 464. 2021 Jan 5;22(1):464.
529. Yamano T, Kubo S, Fukumoto M, Yano A, Mawatari-Furukawa Y, Okamura H, et al. Whole cell vaccination using immunogenic cell death by an oncolytic adenovirus is effective against a colorectal cancer model. 2016;
530. Eriksson E, Milenova I, Wenthe J, Ståhle M, Leja-Jarblad J, Ullenhag G, et al. Shaping the Tumor Stroma and Sparking Immune Activation by CD40 and 4-1BB Signaling Induced by an Armed Oncolytic Virus. *Clinical Cancer Research*. 2017 Oct 1;23(19):5846–57.
531. Fisher K, Hazini A, Seymour LW. Tackling HLA Deficiencies Head on with Oncolytic Viruses. *Cancers (Basel)*. 2021 Feb 2;13(4):1–14.
532. AP A, JC S, S S. Viral interference with MHC class I antigen presentation pathway: the battle continues. *Vet Immunol Immunopathol*. 2005 Aug 15;107(1–2):1–15.

533. S B, M B, P A, O L, R A, J P, et al. Deletion of the E3-6.7K/gp19K region reduces the persistence of wild-type adenovirus in a permissive tumor model in Syrian hamsters. *Cancer Gene Ther.* 2009 Sep 20;16(9):703–12.
534. Sprague L, Braidwood L, Conner J, Cassady KA, Benencia F, Cripe TP. Please stand by: how oncolytic viruses impact bystander cells. *Future Virology.* 2018;13(9):671.
535. Khoo WH, Ledergor G, Weiner A, Roden DL, Terry RL, McDonald MM, et al. A niche-dependent myeloid transcriptome signature defines dormant myeloma cells. *Blood.* 2019 Jul 4;134(1):30–43.
536. Huff AL, Wongthida P, Kottke T, Thompson JM, Driscoll CB, Schuelke M, et al. APOBEC3 Mediates Resistance to Oncolytic Viral Therapy. *Molecular Therapy - Oncolytics.* 2018 Dec 21;11:1–13.
537. Noll M, Berchtold S, Lampe J, Malek NP, Bitzer M, Lauer UM. Primary resistance phenomena to oncolytic measles vaccine viruses. *International Journal of Oncology.* 2013 Jul 1;43(1):103–12.
538. Bladé J, Fernández De Larrea C, Rosiñol L, Cibeira MT, Jiménez R, Powles R. Soft-tissue plasmacytomas in multiple myeloma: Incidence, mechanisms of extramedullary spread, and treatment approach. Vol. 29, *Journal of Clinical Oncology.* J Clin Oncol; 2011. p. 3805–12.
539. Fechtner K, Hillengass J, Delorme S, Heiss C, Neben K, Goldschmidt H, et al. Staging monoclonal plasma cell disease: Comparison of the Durie-Salmon and the Durie-Salmon PLUS staging systems. *Radiology.* 2010 Oct;257(1):195–204.
540. Kakati BR, Krishna K, Krishna SG, Sharma SG, Sanathkumar N, Rego RF. Extensive extramedullary disease involving the colon in multiple myeloma: A case report and review of literature. *Journal of Gastrointestinal Cancer.* 2012 Jun;43(2):379–81.
541. Kazeminezhad B, Zare-mirzaie A, Mirafsharieh A, Soleimantabar H, Zahedifard S. Bilateral ovarian involvement: A rare presentation of disseminated multiple myeloma. *Journal of Obstetrics and Gynaecology Research.* 2013 Jan 1;39(1):446–9.
542. Zhong Y ping, Zhang J jia, Huang X nan. Multiple myeloma with rupture of ovarian plasmacytoma. *Chinese Medical Journal.* 2012 Aug;125(16):2948–50.
543. Kordasti S, Istrate C, Banasaz M, Rottenberg M, Sjövall H, Lundgren O, et al. Rotavirus Infection Is Not Associated with Small Intestinal Fluid Secretion in the Adult Mouse. *Journal of Virology.* 2006 Nov 1;80(22):11355–61.
544. Shekarian T, Sivado E, Jallas AC, Depil S, Kielbassa J, Janoueix-Lerosey I, et al. Repurposing rotavirus vaccines for intratumoral immunotherapy can overcome resistance to immune checkpoint blockade. *Science Translational Medicine.* 2019 Oct 23;11(515).
545. McManus LL, Bonnier F, Burke GA, Meenan BJ, Boyd AR, Byrne HJ. Assessment of an osteoblast-like cell line as a model for human primary osteoblasts using Raman spectroscopy. *Analyst.* 2012 Apr 7;137(7):1559–69.
546. Wilkesmann S, Fellenberg J, Nawaz Q, Reible B, Moghaddam A, Boccaccini AR, et al. Primary osteoblasts, osteoblast precursor cells or osteoblast-like cell lines: Which human cell types are (most) suitable for characterizing 45S5-bioactive glass? *Journal of Biomedical Materials Research Part A.* 2020 Mar 4;108(3):663–74.

547. Duncan SJ, Gordon FCA, Gregory DW, McPhie JL, Postlethwaite R, White R, et al. Infection of mouse liver by human adenovirus type 5. *Journal of General Virology*. 1978 Jul 1;40(1):45–61.
548. Zhang L, Hedjran F, Larson C, Perez GL, Reid T. A novel immunocompetent murine model for replicating oncolytic adenoviral therapy. *Cancer Gene Therapy*. 2015 Jan 28;22(1):17–22.
549. Wang H, Wei F, Zhang J, Wang F, Li H, Chen X, et al. A novel immunocompetent murine tumor model for the evaluation of RCAd-enhanced RDAAd transduction efficacy.
550. Silverstein G, Strohl WA. Restricted replication of adenovirus type 2 in mouse balb/3T3 cells. *Archives of Virology*. 1986 Sep;87(3–4):241–64.
551. Cheng PHH, Rao XMM, Wechman SL, Li XFF, McMasters KM, Zhou HS. Oncolytic adenovirus targeting cyclin E overexpression repressed tumor growth in syngeneic immunocompetent mice. *BMC Cancer*. 2015;15(1):716.
552. Robinson M, Li B, Ge Y, Ko D, Yendluri S, Harding T, et al. Novel Immunocompetent Murine Tumor Model for Evaluation of Conditionally Replication-Competent (Oncolytic) Murine Adenoviral Vectors. *Journal of Virology*. 2009 Apr 15;83(8):3450–62.
553. Jiang H, Rivera-Molina Y, Gomez-Manzano C, Clise-Dwyer K, Bover L, Vence LM, et al. Oncolytic adenovirus and tumor-targeting immune modulatory therapy improve autologous cancer vaccination. *Cancer Research*. 2017;77(14):3894–907.
554. Davola ME, Mossman KL. *Oncolytic viruses: how “lytic” must they be for therapeutic efficacy?* Vol. 8, *Oncolimmunology*. Taylor and Francis Inc.; 2019.
555. Sobol PT, Boudreau JE, Stephenson K, Wan Y, Lichty BD, Mossman KL. Adaptive antiviral immunity is a determinant of the therapeutic success of oncolytic virotherapy. *Molecular Therapy*. 2011;19(2):335–44.
556. Workenhe ST, Mossman KL. *Oncolytic Virotherapy and Immunogenic Cancer Cell Death: Sharpening the Sword for Improved Cancer Treatment Strategies*. 2014;
557. Meng W, Xue S, Chen Y. The role of CXCL12 in tumor microenvironment. *Gene*. 2018 Jan 30;641:105–10.
558. Richmond J, Tuzova M, Cruikshank W, Center D. Regulation of Cellular Processes by Interleukin-16 in Homeostasis and Cancer. *Journal of Cellular Physiology* [Internet]. 2014 Feb 1 [cited 2022 Jan 11];229(2):139–47. Available from: <https://onlinelibrary.wiley.com/doi/full/10.1002/jcp.24441>
559. Young AM, Archibald KM, Tookman LA, Pool A, Dudek K, Jones C, et al. Failure of translation of human adenovirus mRNA in murine cancer cells can be partially overcome by L4-100K expression in vitro and in vivo. *Molecular Therapy*. 2012 Sep 1;20(9):1676–88.
560. Y K, JD D, D K, BC F, JM G, T F, et al. Comparison of intravenous versus intraperitoneal administration of oncolytic herpes simplex virus 1 for peritoneal carcinomatosis in mice. *Cancer Gene Ther*. 2009 Apr;16(4):291–7.
561. Ishikawa W, Kikuchi S, Ogawa T, Tabuchi M, Tazawa H, Kuroda S, et al. Boosting Replication and Penetration of Oncolytic Adenovirus by Paclitaxel Eradicate Peritoneal Metastasis of Gastric Cancer. *Molecular Therapy Oncolytics*. 2020 Sep 25;18:262.

562. Takakura M, Nakamura M, Kyo S, Hashimoto M, Mori N, Ikoma T, et al. Intraperitoneal administration of telomerase-specific oncolytic adenovirus sensitizes ovarian cancer cells to cisplatin and affects survival in a xenograft model with peritoneal dissemination. *Cancer Gene Therapy* 2010 17:1. 2009 Aug 7;17(1):11–9.
563. Waldschmidt JM, Simon A, Wider D, Müller SJ, Follo M, Ihorst G, et al. CXCL12 and CXCR7 are relevant targets to reverse cell adhesion-mediated drug resistance in multiple myeloma. *British Journal of Haematology*. 2017 Oct 1;179(1):36–49.
564. Alsayed Y, Ngo H, Runnels J, Leleu X, Singha UK, Pitsillides CM, et al. Mechanisms of regulation of CXCR4/SDF-1 (CXCL12)–dependent migration and homing in multiple myeloma. *Blood*. 2007 Apr 1;109(7):2708.
565. B P, LA C, MB V, N P, P M, I R, et al. Phenotypic and genomic analysis of multiple myeloma minimal residual disease tumor cells: a new model to understand chemoresistance. *Blood*. 2016 Apr 14;127(15):1896–906.
566. Ullah TR. The role of CXCR4 in multiple myeloma: Cells’ journey from bone marrow to beyond. *Journal of Bone Oncology*. 2019 Aug 1;17:100253.
567. M G, M S, MP K, SI A, D K. Targeting CXCL12/CXCR4 signaling with oncolytic virotherapy disrupts tumor vasculature and inhibits breast cancer metastases. *Proc Natl Acad Sci U S A*. 2013 Apr 2;110(14).
568. Gil M, Komorowski MP, Seshadri M, Rokita H, McGray AJR, Opyrchal M, et al. CXCL12/CXCR4 Blockade by Oncolytic Virotherapy Inhibits Ovarian Cancer Growth by Decreasing Immunosuppression and Targeting Cancer-Initiating Cells. *The Journal of Immunology*. 2014 Nov 15;193(10):5327–37.
569. Bhatia S, O’Byrne SM, Rivera AA, Curiel DT, Mathis JM. CXCL12 retargeting of an adenovirus vector to cancer cells using a bispecific adapter. *Oncolytic Virother*. 2016;5:99–113.
570. Allegra A, Alonci A, Bellomo G, Granata A, Tolomeo A, Penna G, et al. Serum levels of interleukin-16 in a multiple myeloma patient with cutaneous involvement. *Int J Dermatol* [Internet]. 2010 Apr [cited 2022 Jan 11];49(4):435–7. Available from: <https://pubmed.ncbi.nlm.nih.gov/20465701/>
571. Alexandrakis MG, Passam FH, Kyriakou DS, Christophoridou A v., Perisinakis K, Hatzivasili A, et al. Serum level of interleukin-16 in multiple myeloma patients and its relationship to disease activity. *Am J Hematol* [Internet]. 2004 Feb [cited 2022 Jan 11];75(2):101–6. Available from: <https://pubmed.ncbi.nlm.nih.gov/14755377/>
572. Atanackovic D, Hildebrandt Y, Templin J, Cao Y, Keller C, Panse J, et al. Role of interleukin 16 in multiple myeloma. *J Natl Cancer Inst* [Internet]. 2012 Jul 3 [cited 2022 Jan 11];104(13):1005–20. Available from: <https://pubmed.ncbi.nlm.nih.gov/22745469/>
573. Haitz K, Khosravi H, Lin JY, Menge T, Nambudiri VE. Review of talimogene laherparepvec: A first-in-class oncolytic viral treatment of advanced melanoma. *Journal of the American Academy of Dermatology*. Mosby Inc.; 2020.
574. Zheng M, Huang J, Tong A, Yang H. Oncolytic Viruses for Cancer Therapy: Barriers and Recent Advances. Vol. 15, *Molecular Therapy - Oncolytics*. Cell Press; 2019. p. 234–47.

575. Sborov DW, Nuovo GJ, Stiff A, Mace T, Lesinski GB, Benson DM, et al. A phase I trial of single-agent reolysin in patients with relapsed multiple myeloma. *Clinical Cancer Research*. 2014 Dec 1;20(23):5946–55.
576. Ali S, Liu Y, Ma L, Tahir M, Wang S, Zhang L, et al. Upregulation of coxsackie adenovirus receptor sensitizes cisplatin-resistant lung cancer cells to CRAd-induced inhibition. *J Cancer*. 2017;8(8):1425–32.
577. Zhang NH, Song LB, Wu XJ, Li RP, Zeng MS, Zhu XF, et al. Proteasome inhibitor MG-132 modifies coxsackie and adenovirus receptor expression in colon cancer cell line lovo. *Cell Cycle*. 2008 Apr 29;7(7):925–33.
578. Venkatraman G, Behrens M, Pyrski M, Margolis FL. Expression of Coxsackie-Adenovirus receptor (CAR) in the developing mouse olfactory system. *Journal of Neurocytology*. 2005 Sep;34(3–5):295–305.
579. Danielsson A, Dzovic H, Rashkova V, Cheng WS, Essand M. The HDAC Inhibitor FK228 Enhances Adenoviral Transgene Expression by a Transduction-Independent Mechanism but Does Not Increase Adenovirus Replication. Cheriya V, editor. *PLoS ONE*. 2011 Feb 17;6(2):e14700.
580. Serrano-del Valle A, Anel A, Naval J, Marzo I. Immunogenic cell death and immunotherapy of multiple myeloma. Vol. 7, *Frontiers in Cell and Developmental Biology*. Frontiers Media S.A.; 2019.
581. Alvarez-Castelao B, Martín-Guerrero I, García-Orad Á, Castaño JG. Cytomegalovirus Promoter Up-regulation Is the Major Cause of Increased Protein Levels of Unstable Reporter Proteins after Treatment of Living Cells with Proteasome Inhibitors. *The Journal of Biological Chemistry*. 2009 Oct 9;284(41):28253.
582. Corbin-Lickfett KA, Bridge E. Adenovirus E4-34kDa requires active proteasomes to promote late gene expression. *Virology*. 2003 Oct 10;315(1):234–44.
583. Dalidowska I, Gazi O, Sulejczak D, Przybylski M, Bieganowski P. Heat Shock Protein 90 Chaperones E1A Early Protein of Adenovirus 5 and Is Essential for Replication of the Virus. *International Journal of Molecular Sciences*. 2021 Feb 2;22(4):1–15.
584. Garza-Morales R, Yaddanapudi K, Perez-Hernandez R, Riedinger E, McMasters KM, Shirwan H, et al. Temozolomide renders murine cancer cells susceptible to oncolytic adenovirus replication and oncolysis. 2018 Mar 4;19(3).
585. MA G, C de B, P T, LR F, WA D. The effect of DNA-alkylating agents on gene expression from two integrated reporter genes in a mouse mammary tumor line. *Anticancer Drugs*. 2002;13(3):271–80.
586. Molphy Z, Montagner D, Bhat SS, Slator C, Long C, Erxleben A, et al. A phosphate-targeted dinuclear Cu(II) complex combining major groove binding and oxidative DNA cleavage. *Nucleic Acids Research*. 2018 Nov 2;46(19):9918.
587. E V, F C, R M, A S, C F, G P, et al. Genotoxic stress modulates the release of exosomes from multiple myeloma cells capable of activating NK cell cytokine production: Role of HSP70/TLR2/NF- κ B axis. *Oncoimmunology*. 2017 Mar 4;6(3).

588. Sachs MD, Ramamurthy M, Van Der Poel H, Wickham TJ, Lamfers M, Gerritsen W, et al. Histone deacetylase inhibitors upregulate expression of the coxsackie adenovirus receptor (CAR) preferentially in bladder cancer cells. *Cancer Res*. 2004;11(7):477–86.
589. Lai MD, Chen CS, Yang CR, Yuan SY, Tsai JJ, Tu CF, et al. An HDAC inhibitor enhances the antitumor activity of a CMV promoter-driven DNA vaccine. *Cancer Gene Therapy* 2010 17:3. 2009 Oct 23;17(3):203–11.
590. Kasman L, Onicescu G, Voelkel-Johnson C. Histone Deacetylase Inhibitors Restore Cell Surface Expression of the Coxsackie Adenovirus Receptor and Enhance CMV Promoter Activity in Castration-Resistant Prostate Cancer Cells. *Prostate Cancer*. 2012;2012:1–8.
591. García-Guerrero E, Götz R, Doose S, Sauer M, Rodríguez-Gil A, Nerreter T, et al. Upregulation of CD38 expression on multiple myeloma cells by novel HDAC6 inhibitors is a class effect and augments the efficacy of daratumumab. *Leukemia* 2020 35:1. 2020 Apr 29;35(1):201–14.
592. D G, SP T, Y S, T H, K P, YT T, et al. Adherence of multiple myeloma cells to bone marrow stromal cells upregulates vascular endothelial growth factor secretion: therapeutic applications. *Leukemia*. 2001;15(12):1950–61.
593. H G, S H, K Z. Thalidomide selectively modulates the density of cell surface molecules involved in the adhesion cascade. *Immunopharmacology*. 1996;31(2–3):213–21.
594. R L, B Y, G T, Q L, JP B, G L, et al. Lenalidomide down-regulates the CD20 antigen and antagonizes direct and antibody-dependent cellular cytotoxicity of rituximab on primary chronic lymphocytic leukemia cells. *Blood*. 2008 Dec 15;112(13):5180–9.
595. PL F, SN W, Y L, MS L, J R, DH S, et al. IMiDs prime myeloma cells for daratumumab-mediated cytotoxicity through loss of Ikaros and Aiolos. *Blood*. 2018 Nov 15;132(20):2166–78.
596. Martiniani R, Di Loreto V, Di Sano C, Lombardo A, Liberati AM. Biological activity of lenalidomide and its underlying therapeutic effects in multiple myeloma. *Advances in Hematology*. 2012;2012.
597. L EL, IL L, K JP, HA B, AK G, PH S, et al. Pomalidomide and lenalidomide induce p21 WAF-1 expression in both lymphoma and multiple myeloma through a LSD1-mediated epigenetic mechanism. *Cancer Res*. 2009;69(18):7347–56.